

УНИВЕРЗИТЕТ У БЕОГРАДУ
ГРАЂЕВИНСКИ ФАКУЛТЕТ

Јелена С. Драгаш

**ГРАНИЧНА НОСИВОСТ
АРМИРАНОБЕТОНСКИХ ГРЕДНИХ НОСАЧА
ОД БЕТОНА СА ВЕЛИКИМ САДРЖАЈЕМ
ЛЕТЕЋЕГ ПЕПЕЛА**

докторска дисертација

Београд, 2018

UNIVERSITY OF BELGRADE
FACULTY OF CIVIL ENGINEERING

Jelena S. Dragaš

**ULTIMATE CAPACITY OF HIGH VOLUME FLY
ASH REINFORCED CONCRETE BEAMS**

Doctoral Dissertation

Belgrade, 2018

Ментори: Др Снежана Маринковић, редовни професор
Грађевински факултет, Универзитет у Београду

Чланови комисије: Др Снежана Маринковић, редовни професор
Грађевински факултет, Универзитет у Београду

Др Иван Игњатовић, доцент
Грађевински факултет, Универзитет у Београду

Др Властимир Радоњанин, редовни професор
Факултет техничких наука, Универзитет у Новом Саду

Датум одбране:

Supervisors: Prof. Snežana Marinković, PhD civ. Eng.
University of Belgrade, Faculty of Civil Engineering

Members of the jury: Prof. Snežana Marinković, PhD civ. Eng.
University of Belgrade, Faculty of Civil Engineering

Assistant prof. Ivan Ignjatović, PhD civ. Eng.
University of Belgrade, Faculty of Civil Engineering

Prof. Vlastimir Radonjanin, PhD civ. Eng.
University of Novi Sad, Faculty of Technical Sciences

Defense date:

Acknowledgements

ACKNOWLEDGEMENTS

Firstly, I would like to express my sincere gratitude to my supervisor professor Snežana Marinković for the continuous support during my PhD studies and related research, for her guidance, motivation, and immense knowledge she unselfishly shared. She has been a true mentor that taught me how to think critically, work diligently and always put an honest research work as the primary goal.

Besides my supervisor, I would like to thank professor Ivan Ignjatović for his help during my research, for his support and motivation, good advice when needed, persistence he taught me, and for the hard questions that motivated me to widen my research from various perspectives. To professor Vlastimir Radonjanin I express my sincere appreciation for his insightful comments, encouragement, and positive thinking that motivated me in my work.

I wish to express my deepest gratitude to my colleagues Ivan Milićević, Nikola Tošić and Vedran Carević for being my biggest support during this journey. Nikola was along my side from the beginning of my research work helping me shape my thesis as an excellent copyeditor. I am particularly thankful to Vedran for working with me during my experimental work, for his advices during our stimulating discussions and always being willing to step in when needed. His patience, cheerful, and positive attitude helped me tremendously through the hard times. For that professional and emotional help I am extremely grateful.

This thesis could not be completed without the support of all my colleagues working at the Faculty of Civil Engineering, especially the ones from the Department of materials and structures. I sincerely thank my colleagues Mladen Jović, Veljko Koković, Nenad Brodić, Aleksandar Savić, Aleksandar Radević, and Savo Stavnjak for helping me in the experimental work carried out for the purpose of this thesis. I'm grateful not only for their time and professional help but, maybe even more, for always cheering for me during this whole process. I also wish to thank professor Zoran Mišković for providing me with the necessary testing equipment needed for my research and for his professional help. My special

Acknowledgements

gratitude goes to Marko Orešković and Marina Aškračić for giving me their sincere support and incentive to carry on.

This research was financially supported by the Ministry for Education, Science and Technological Development of the Republic of Serbia and the Swiss National Science Foundation. Also, I thank my colleagues working in the following institutions for providing important contributions: VV Čelik, Deneza M, Thermal power plant “Nikola Tesla B”, Institute of Technical Sciences of SASA, Institute for testing of materials-IMS, Mostogradnja, and Gradient. Their help is gratefully acknowledged. In particular, I would like to thank Stamenko Jovanović for finding the way to collect the fly ash necessary for this research.

My research and writing of this thesis would not be possible without the emotional support of some of my dearest people. I feel a strong need to acknowledge all of them because they helped in each step of this process and for that, I am eternally grateful.

My special thanks go to my friends Marko Pečenković, Damjan Milić, Milorad Pejanović, and Mladen Pešić. Their help during my experimental work showed me that research can be fun, but their unconditional belief in me is the value I appreciate the most.

I am most sincerely thankful for having great and strong women by my side along this journey. The emotional help and consistent support I got from Milica Vasić, Borka Čonjić, Nela Kolundžija, Marija Đokić, Ana Ostojić, Mira Vasić, Anka Rađenović, Jelena Ninković, and Sanja Arežina was my strongest motivation. A heartfelt gratitude I owe to Tijana Zorić, not only for dedicating her free time to do the proofreading of this thesis but also for being by my side for more than 20 years.

Last but not least, I would like to thank my family: my parents and my brother Mihajlo for always being there for me and for having the most patience when I had the least. This work is as much theirs as it is mine.

ГРАНИЧНА НОСИВОСТ АРМИРАНОБЕТОНСКИХ ГРЕДНИХ НОСАЧА ОД БЕТОНА СА ВЕЛИКИМ САДРЖАЈЕМ ЛЕТЕЋЕГ ПЕПЕЛА

Резиме:

Бетон је један од најчешће коришћених материјала данашњице. Међутим, током производње цемента, испушта се приближно једна тона CO_2 за сваку тону произведеног портланд цементног клинкера. До сада је уложено пуно труда у проналажење одрживих решења за бетон као конструкцијски материјал. Сви ови напори имају за циљ унапређења животне средине на исти начин: очувањем природних ресурса, смањењем емисије CO_2 и смањењем количине насталог отпада. Сви ови циљеви се могу постићи употребом летећег пепела као делимичне замене цемента у бетону: коришћењем отпада уместо природних ресурса за производњу бетона, смањењем емисије CO_2 кроз смањење коришћења портланд цемента и смањењем количине депонованог пепела. Управо из наведених разлога, данас је свеprisутна општа тежња замене већих количина портланд цемента у бетону различитим замењујућим цементним материјалима (ЦМ).

Бетон са великим садржајем летећег пепела (БВСЛП)—бетон са најмање 50% летећег пепела у укупној маси ЦМ—постао је једна од најперспективнијих одрживих алтернатива конвенционалном цементном бетону. Преглед постојеће литературе и расположивих извора показао је да се БВСЛП тренутно углавном користи као део темеља конструкција. Међутим, потребно је још доста истраживања да би са сигурношћу могао да се примењује у грађевинској индустрији као конструкцијски бетон. Већина истраживања спроведених до сада усмерена је на одређивање физичких и механичких својстава БВСЛП. Кроз ограничен број студија спроведено је тестирање конструктивних елемената у пуној величини произведених од БВСЛП како би се утврдила његова потенцијална употреба у армиранобетонским конструкцијама. Главна сврха овог истраживања била је процена могућности примене БВСЛП као бетона за примену у конструкцијама.

Резиме

Ова теза представља експериментални програм развијен у две фазе. У првој фази спроведено је експериментално истраживање како би се дефинисао процес добијања БВСЛП направљеног са летећим пепелом класе Ф из једне термоелектране из Србије, а који се може користити као конструкцијски бетон. Експериментални програм се састојао од седамнаест мешавина БВСЛП и две мешавине цементног бетона. Показано је да се може произвести БВСЛП који садржи више од 50% летећег пепела класе Ф у укупној маси ЦМ који има чврстоћу при притиску при старости од три дана већу од 20 МПа и чврстоћу при старости од 28 дана већу од 40 МПа уз адекватну уградљивост. Процена механичких карактеристика БВСЛП извршена је и на основу базе који чине одговарајући експериментални резултати БВСЛП пронађени у литератури. Такође је анализирана могућност примене постојећих смерница дефинисаних за механичке карактеристике цементних бетона на БВСЛП. Дошло се до закључка да се исти облик ових једначина може применити на БВСЛП, уз неопходне модификације. Дат је нови предлог фактора ефикасности летећег пепела као функције његовог хемијског састава и величине честица.

У другој фази експерименталног програма испитано је понашање при савијању и смицању армиранобетонских гредних носача распона 3.0 m, направљених од цементног бетона и БВСЛП. Понашање греда при савијању испитано је на две греде од БВСЛП (64% летећег пепела у укупној маси ЦМ) и две греде од цементног бетона направљене са различитим процентом армирања подужном арматуром (0.28% и 1.46%). Понашање греда при смицању испитано је на шест греда од БВСЛП (50% летећег пепела у укупној маси ЦМ) и шест греда од цементног бетона направљених са различитим процентом армирања попречног арматуром (0%, 0.14% и 0.28%). Анализирано је понашање греда, са фокусом на деформације настале услед краткотрајног оптерећења, дилатације у бетону и арматури, главне дилатације у бетону, прслине, врсту лома и чврстоћу при савијању и смицању. У наставку је анализирана могућност примене различитих стандарда који дефинишу чврстоћу при савијању и смицању

Резиме

армиранобетонских елемената направљених од цементних бетона на греде направљене од БВСЛП. Поређење и анализа понашања армиранобетонских греда од цементних бетона и БВСЛП извршена је на основу сопствених експерименталних резултата и базе резултата испитаних греда од БВСЛП из доступне литературе.

Добијени резултати указују на то да не постоје значајне разлике између граничне носивости при савијању и смицању греда направљених од цементних бетона и БВСЛП. Актуелни стандарди који дефинишу граничну носивост при савијању и смицању армиранобетонских елемената направљених од цементних бетона могу се применити у анализи елемената од БВСЛП са истом тачношћу.

Кључне речи: бетон, летећи пепео, бетони са великим садржајем летећег пепела, армиранобетонске греде, експериментално испитивање, савијање, смицање, краткотрајно оптерећење, одредбе стандарда

Научна област: Грађевинарство

Ужа научна област: Бетонске конструкције

УДК број: 624.012.45:624.071.2]:662.613.13(043.3)

ULTIMATE CAPACITY OF HIGH VOLUME FLY ASH REINFORCED CONCRETE BEAMS

Abstract:

Concrete is the most widely used construction material today. However, during cement production, approximately one ton of CO₂ is released for each ton of Portland cement clinker produced. So far, immense effort has been put into finding sustainable solutions for concrete as a structural material. All of these efforts aim at the same environmental improvements: preservation of natural resources, lowering of CO₂ emissions, and decreasing the amount of generated waste. With fly ash as a partial replacement of cement in concrete all these aims can be accomplished: using waste instead of natural resources for concrete production, lowering CO₂ emissions through the reduction of Portland cement use and decreasing the amount of deposited fly ash in landfills. It is for these reasons that today there is a general trend of replacing higher amounts of Portland cement in concrete with different supplementary cementitious materials (CM).

High volume fly ash concrete (HVFAC)—concrete with at least 50% of fly ash in total CM mass—has become one of the most promising sustainable alternatives to conventional concrete. Reviewing the existing literature and available sources revealed that HVFAC is currently mostly used on construction sites as a part of foundations. However, much more research is still needed for its safe application in the construction industry as structural concrete. Most research so far focused only on the evaluation of HVFAC physical and mechanical properties. Only a limited number of studies implemented full-scale testing of structural members produced with HVFAC to determine its potential use in reinforced concrete structures. The main purpose of this research was to evaluate HVFAC as concrete for structural application.

This thesis presents an experimental program developed in two phases. In the first phase, research was performed in order to define the process of developing structural-grade HVFAC mix design using a class F fly ash obtained from one power plant in Serbia. The experimental program consisted of seventeen HVFAC and two

Abstract

cement concrete mixtures. It was shown that HVFAC containing more than 50% of class F fly ash in total CM mass can be produced to have 3-day compressive strength greater than 20 MPa and 28-day strength greater than 40 MPa with adequate workability. The evaluation of HVFAC mechanical properties was also performed based on a database of all adequate HVFAC experimental results found in literature. The possible application of current guidelines defined for mechanical properties of cement concrete to HVFAC was also analyzed. It was concluded that the same form of these equations can be used on HVFAC with necessary modifications. The new proposal for fly ash efficiency factor as a function of its chemical composition and fineness was presented.

In the second phase of the experimental program, flexural and shear performance of simply supported reinforced concrete beams with a span of 3.0 m constructed with HVFAC and cement concrete was investigated. Flexural behavior was tested on two HVFAC (64% of fly ash in CM) and two cement concrete beams made with different longitudinal reinforcement ratios (0.28% and 1.46%). Shear behavior was tested on six HVFAC (50% of fly ash in CM mass) and six cement concrete beams made with different shear reinforcement ratios (0%, 0.14%, and 0.28%). The overall behavior of the beams was analyzed, with a focus on short-term deflections, concrete and steel strains, principal concrete strains, crack patterns, failure modes, and flexural and shear strength. Furthermore, the application of different design codes defining flexural and shear strength for reinforced cement concrete structures was evaluated for their applicability to HVFAC beams. The flexural and shear behavior of reinforced cement concrete and HVFAC beams was compared and discussed based on own experimental results and a database of collected results on HVFAC beams from available literature.

The obtained results indicate that there are no significant differences between reinforced cement concrete and HVFAC beam flexural and shear strengths. Available design code predictions defining the flexural and shear strength of reinforced cement concrete structural members can be applied to the design of reinforced HVFAC elements with the same accuracy.

Abstract

Keywords: *concrete, fly ash, high volume fly ash concrete, reinforced concrete beams, experimental tests, flexure, shear, short-term loading, code provisions*

Science field: *Civil Engineering*

Narrow science field: *Concrete Structures*

UDC number: *624.012.45:624.071.2]:662.613.13(043.3)*

Table of contents

TABLE OF CONTENTS

Acknowledgments	ii
Резиме	v
Abstract	viii
Table of Contents	xi
<i>Chapter 1. Introduction</i>	
1.1. Background	2
1.2. Objectives of the research	5
1.3. Methodology of the research.....	6
1.4. Thesis outline	6
<i>Chapter 2. Literature review</i>	
2.1. Introduction	10
2.2. Characterization of fly ash and its material properties	10
2.2.1. Physical properties of fly ash.....	10
2.2.2. Chemical and mineralogical properties of fly ash	12
2.2.3. Classification of fly ash.....	15
2.3. Fly ash in concrete.....	17
2.4. High volume fly ash concrete – HVFAC	21
2.4.1. Physical properties of HVFAC.....	23
2.4.2. Mechanical properties of HVFAC	27
2.4.3. Durability of HVFAC	34
2.5. Existing regulations on the use of fly ash in concrete	35
2.6. Structural applications of HVFAC.....	38
2.6.1. Bond strength of reinforcing steel in HVFAC	38

Table of contents

2.6.2. Flexural behavior of HVFAC beams.....	41
2.6.3. Shear behavior of HVFAC beams.....	45
2.7. Engineering applications of HVFAC.....	50
2.8. The role of fly ash in sustainable construction	52
2.9. Conclusions	54

Chapter 3. Flexural and shear strength of reinforced concrete beams - theory and standards

3.1. Introduction	57
3.2. Flexural strength of reinforced concrete beams	57
3.3. Code provisions – flexural behavior of reinforced concrete beams.....	58
3.3.1. Cracking moment	58
3.3.2. Modified compression field theory program Response-2000	61
3.4. Shear strength of reinforced concrete beams.....	61
3.4.1. Basic shear transfer mechanisms	61
3.4.2. Shear design models	69
3.5. Code provisions – shear behavior of reinforced concrete beams.....	73
3.5.1. Serbian standard for concrete and reinforced concrete - BAB '87	74
3.5.2. European Standard EN 1992-1-1: Design of concrete structures - Part 1-1: General rules and rules for buildings.....	75
3.5.3. <i>fib</i> Model Code 2010	78
3.5.4. American standard ACI 318	83

Chapter 4. Experimental program and results

4.1. Introduction	86
4.2. Testing of HVFAC physical and mechanical properties	87

Table of contents

4.2.1. Introduction	87
4.2.2. Component materials	87
4.2.2.1. Fly ash	87
4.2.2.2. Cement and chemical admixtures	90
4.2.2.3. Coarse and fine aggregate	91
4.2.3. Casting, curing and testing of specimens	92
4.2.4. The first phase of the HVFAC research	93
4.2.4.1. Concrete mixtures	93
4.2.4.2. Results and discussion	95
4.2.5. The second phase of the HVFAC research	98
4.2.5.1. Concrete mixtures	98
4.2.5.2. Results and discussion	99
4.2.6. Conclusions.....	102
4.3. Testing of reinforced concrete beams' flexural behavior	103
4.3.1. Introduction	103
4.3.2. Material properties.....	104
4.3.2.1. Concrete	104
4.3.2.2. Steel reinforcement	106
4.3.3. Preparation of beam elements.....	106
4.3.4. Test set-up	110
4.3.5. Instrumentation.....	111
4.3.5.1. Deflection measurements	111
4.3.5.2. Strain measurements.....	112
4.3.5.3. Crack measurements.....	115
4.3.6. Testing results of concrete and steel reinforcement properties	118
4.3.6.1. Fresh and hardened concrete properties.....	118

Table of contents

4.3.6.2.	Steel reinforcement properties.....	122
4.3.7.	Reinforced concrete beams' flexural behavior	124
4.3.7.1.	Overall behavior of beams tested for flexural behavior.....	124
4.3.8.	Deflection of beams.....	134
4.3.9.	Longitudinal reinforcement strains.....	138
4.3.10.	Concrete strains.....	151
4.3.10.1.	Distribution of strains.....	159
4.3.11.	Concrete cracks.....	160
4.3.12.	Conclusions.....	180
4.4.	Testing of reinforced concrete beams' shear behavior.....	184
4.4.1.	Introduction.....	184
4.4.2.	Material properties.....	185
4.4.2.1.	Concrete.....	185
4.4.2.2.	Steel reinforcement.....	186
4.4.3.	Preparation of beam elements.....	187
4.4.4.	Test set-up.....	190
4.4.5.	Instrumentation.....	191
4.4.5.1.	Deflection measurements.....	191
4.4.5.2.	Strain measurements.....	192
4.4.5.3.	Crack measurements.....	197
4.4.6.	Testing results of concrete and steel reinforcement properties	197
4.4.6.1.	Fresh and hardened concrete properties.....	197
4.4.6.2.	Steel reinforcement properties.....	201
4.4.7.	Overall behavior of beams tested for shear behavior.....	203
4.4.7.1.	Overall behavior of beams without shear reinforcement.....	205
4.4.7.2.	Overall behavior of beams with shear reinforcement.....	210

Table of contents

4.4.8. Deflection of beams	218
4.4.9. Longitudinal reinforcement strains.....	222
4.4.10. Shear reinforcement strains.....	227
4.4.11. Concrete strains	242
4.4.11.1. Distribution of strains.....	251
4.4.12. Concrete cracks	254
4.4.12.1. Concrete cracks in the OPC-1 and HVFAC-1 beams	256
4.4.12.2. Concrete cracks in the OPC-2 and HVFAC-2 beams	259
4.4.12.3. Concrete cracks in the OPC-3 and HVFAC-3 beams	263
4.4.13. Principal concrete strains	268
4.4.13.1. Principal strains in the OPC-1 and HVFAC-1 beams	271
4.4.13.2. Principal strains in the OPC-2 and HVFAC-2 beams	279
4.4.13.3. Principal strains in the OPC-3 and HVFAC-3 beams	287
4.4.14. Conclusions	295

Chapter 5. Analysis and discussion of results

5.1. Introduction	300
5.2. Analysis of HVFAC material properties.....	300
5.2.1. Analysis of HVFAC mechanical properties based on a literature review.....	301
5.2.1.1. Comparison of HVFAC and OPCC compressive strength	312
5.2.1.2. HVFAC 28-day compressive strength evaluation	315
5.2.1.3. Compressive strength development over time.....	338
5.2.1.4. Modulus of elasticity	348
5.2.1.5. Splitting tensile strength	354
5.2.2. Analysis of HVFAC mechanical properties based on own experimental results	356

Table of contents

5.2.2.1.	k-value concept	356
5.2.2.2.	Compressive strength development over time.....	358
5.2.2.3.	Modulus of elasticity	359
5.2.2.4.	Splitting tensile strength	361
5.2.3.	Conclusions.....	361
5.3.	Analysis of HVFAC structural properties.....	364
5.3.1.	Evaluation of HVFAC strength variation	365
5.3.2.	HVFAC beams flexural behavior – HVFAC beams database	370
5.3.2.1.	Application of standards on own flexural test results	376
5.3.2.1.1.	Cracking moment	376
5.3.2.1.2.	Ultimate bending moment.....	381
5.3.2.2.	Application of standards on flexural test results –HVFAC beams database.....	384
5.3.3.	HVFAC shear behavior – HVFAC beams database.....	387
5.3.3.1.	Database of HVFAC beams made without shear reinforcement.....	387
5.3.3.2.	Database of HVFAC beams made with shear reinforcement.....	390
5.3.3.3.	Application of standards on own shear test results.....	392
5.3.3.4.	Application of standards on shear test results – HVFAC beams database.....	396
5.3.3.4.1.	HVFAC beams made without shear reinforcement.....	396
5.3.3.4.2.	HVFAC beams made with shear reinforcement.....	400
5.3.3.5.	Application of standards on shear test results – Reineck database.....	405
5.3.3.5.1.	HVFAC and OPCC beams made without shear reinforcement.....	405
5.3.3.5.2.	HVFAC and OPCC beams made with shear reinforcement.....	414
5.3.4.	Conclusions.....	423

Table of contents

Chapter 6. Conclusions and recommendations for future research

6.1. Summary of presented thesis	428
6.1.1. Literature review	429
6.1.2. Testing of HVFAC physical and mechanical properties.....	430
6.1.3. Testing of reinforced concrete beams' flexural behavior.....	430
6.1.4. Testing of reinforced concrete beams' shear behavior	432
6.1.5. Analysis and discussion of results	434
6.2. Conclusions	442
6.3. Recommendations for future research	446
References	448
Appendix A	478
Appendix B	494
Curriculum vitae	501
Authorship Statement	502

1. INTRODUCTION

1. Introduction

1.1. BACKGROUND

In the modern age, a lot of human action is directed at the preservation of the environment and special attention is paid to large volumes of waste or by-products generated by different industries. The best option for a large reduction of these materials in many industries is their reuse or recycling. The construction industry is a potential beneficiary of this approach since large quantities of waste or by-products can be used in the development of new projects. Among various options, different pozzolanic waste materials are most widely used as supplementary cementitious materials (SCM) in concrete production making it more sustainable (Radonjanin et al. 2013). The pozzolanic material (natural pozzolana) was first found in the city of Pozzuoli near Naples, and got its name based on the chocolate-red volcanic earth of the area (Britannica 2016). It is usually defined as the material which will, in the presence of moisture, chemically react with calcium hydroxide $\text{Ca}(\text{OH})_2$ at ordinary temperatures to form compounds possessing cementitious properties. Some wastes and by-products have properties similar to natural pozzolana, such as coal FA, which is most commonly used in the production of concrete (ACI 2013). The coal FA, usually referred to as fly ash (FA), is a by-product of the combustion of pulverized coal in thermal power plants. Depending on the type and quality, FA consists of a different proportion of oxides—mostly silica, alumina and calcium—and can display pozzolanic activity. This allows it to be a substitution of cement and fine aggregate in concrete.

Besides FA, coal burning power plants also generate bottom ash (BA) which consists of coarse granular particles, collected at the bottom of coal furnaces. These particles are porous, irregular, rough-textured and lighter than the natural aggregate (Singh and Siddique 2013). The coal BA can be used in road bases, structural fills, drainage medians, masonry asphalt (Nikbin et al. 2016), and as fine or coarse aggregate replacement in concrete (Aggarwal and Siddique 2014; Kim 2015; Kim et al. 2012; Nikbin et al. 2016; Rafieizonooz et al. 2016; Siddique et al. 2012; Singh and Siddique 2013, 2014, 2015, 2016).

In addition to the large amount of FA and BA from power plants, a generation of municipal solid waste is rapidly increasing due to population growth. Since it

1. Introduction

presents a threat to public health and the environment, it is being incinerated. Municipal solid waste ash is a by-product from the combustion of municipal solid waste. The properties of ash generated in this way strongly depend on the solid waste type and the combustion process. This type of ash can be used in concrete as a partial cement or aggregate replacement having in mind the fact that it contains silica, alumina, and calcium oxides. The municipal solid waste ash also contains heavy metals and has high loss on ignition (LOI). Its use is still in an early phase of research, and scientists are testing its performance in concrete (Siddique 2010) and trying to reduce heavy metals (Aubert et al. 2004). Its possible application is mainly in construction materials, geotechnical and agricultural engineering (Ferreira et al. 2003).

Another by-product used in concrete is rice husk ash, obtained from the combustion of rice husk. This is a material with proven pozzolanic characteristics and it can be used as a partial cement replacement in concrete if properly treated. Properties of rice husk ash depend on the nature of husks and burning/cooling conditions, but if properly treated it can possess more than 90% of total silica (Antiohos et al. 2014). Research completed so far shows that this is one of the most promising SCMs with a high specific surface and a large amount of silica (Antiohos et al. 2014; Antiohos and Tsimas 2006; Ganesan et al. 2008; Givi et al. 2010; Kartini 2011; Malhotra 1993; Nehdi et al. 2003; Rodríguez De Sensale 2006; Safiuddin 2008; Van Tuan et al. 2011).

As the construction industry is developing, the need for sustainable construction materials is increasing and it is logical that research is oriented towards the development of these materials by using various waste and by-products. New materials that are being tested the most in the last decade as SCMs are: rice straw ash (Roselló et al. 2017), bamboo leaf ash (Villar-Cociña et al. 2011), palm oil residue ash (Tangchirapat et al. 2007), wood ash (Chowdhury et al. 2014), etc. In order for these materials to find practical commercial use, years of extensive research are needed for the construction industry to actually use them. This is the reason that, from all of the above mentioned pozzolanic ashes, only FA found its

1. Introduction

way into the construction industry but still requires more research for full determination in standards.

Large amounts of FA are still being generated worldwide. Despite the modernization efforts in many countries, the main energy source globally still remains coal combustion. In Serbia, for instance, there are six coal-burning power plants, and their working process has a major environmental consequence – 6 million tons of FA is produced per year, while 200 million tons of FA is already deposited in landfills (EPS 2011). At the moment, only 2.7% of the total FA production in Serbia is utilized by the construction industry (EPS 2011).

Since the 1930s, FA has been used as a partial replacement of clinker in Portland cement, or as an addition in concrete to improve the material's durability, while also limiting the amount of early heat generation. The important benefit from the utilization of FA as a cement replacement is the lowering of the carbon dioxide (CO₂) emissions from the Portland cement production. Approximately one ton of the greenhouse gas CO₂ is released for each ton of the Portland cement clinker (Bilodeau and Malhotra 2000), the gas originating from the combustion of carbon-based fuels and the calcination of limestone. A positive environmental effect is also obtained through the decrease of the amount of FA deposited in landfills and through the use of the waste material instead of natural resources for concrete production. It is for these reasons that today there is a general trend of replacing higher amounts of Portland cement in concrete. In 1985, the Advanced Concrete Technology Group at CANMENT, Canada, started a project to develop structural high volume FA concrete (HVFAC) (Bouzoubaâ et al. 2001; Bouzoubaa and Malhotra 2001; Malhotra and Mehta 2005). There are different definitions of HVFAC: Malhotra (1986) defined it as concrete with a large amount of FA between 40% and 60% of total CM mass; Ramme and Tharaniyil (ACI 2014) defined it as concrete with 37% or more of FA in total CM mass; Siddique (Siddique 2004) also considered concrete as HVFAC if FA constituted more than 50% of CM mass.

Despite the several decades-long use of FA in concrete, it is still a subject of much research. A great variety of FA physical and chemical properties made it difficult to draw general and unambiguous conclusions about its influence on concrete

1. Introduction

properties. Regardless of the fact that a lot of research has been done so far regarding the HVFAC material properties, a systematic analysis of research conducted to date cannot be found in literature. Furthermore, only a small number of studies analyzing the structural behavior of HVFAC members can be found in literature. It can be concluded that based on the conducted research and the analyses, no general conclusions regarding the HVFAC structural behavior can be made.

1.2. OBJECTIVES OF THE RESEARCH

The aim of the research presented in this thesis is to evaluate and promote the application of HVFAC as a structural concrete. The main objective is to evaluate the possible application of available code predictions defined for cement concrete on HVFAC. In order to achieve that, the following specific tasks were defined:

- In order to draw some general conclusions regarding the mechanical properties of HVFAC, a systematic analysis of the experimental results found in literature will be conducted. For that purpose, the database of all adequate experimental results found in literature will be made in order to analyze the possible application of available code predications defining the mechanical properties of concrete cement on HVFAC.
- Own experimental research will be conducted in order to design the structural grade HVFAC. Having in mind the heterogeneity of FA's physical and chemical properties and the lack of reliable predictions for HVFAC mechanical properties, extensive experimental research regarding physical and mechanical properties of HVFAC will be conducted.
- The flexural behavior testing of reinforced concrete beams will be analyzed on cement concrete and HVFAC beams with equally designed compressive strengths and different longitudinal reinforcement ratios.
- The shear behavior testing of reinforced concrete beams will be done on cement concrete and HVFAC beams with equally designed compressive strength and longitudinal reinforcement ratios but, different shear reinforcement.

1. Introduction

- The database of all available results regarding HVFAC structural behavior will be made. The evaluation of HVFAC beams flexural and shear behavior in comparison with the cement concrete beams will be done based on the collected results from literature and own experimental results obtained in this study.
- The possible application of available code predications defining the flexural and shear strength of cement concrete on HVFAC beams will be analyzed on available cement concrete beams database and collected HVFAC beams database.

1.3. METHODOLOGY OF THE RESEARCH

The methodology used to reach previously defined objectives is described in this section. A literature review analysis will be performed to obtain a current state-of-the-art on HVFAC physical, mechanical properties and structural behavior. Systematization, critical and statistical data analysis of the existing results in this field will be conducted. Based on the conclusions that will be obtained after the literature review analysis, the experimental program will be defined.

The experimental program that will be conducted in this research will be divided into three phases. In the first phase, experimental work regarding HVFAC physical and mechanical properties will be performed by testing the following: component materials properties (standard FA, cement, aggregate and reinforcement steel tests) and basic physical (fresh and hardened density of concrete, workability) and mechanical concrete properties (compressive strength, splitting tensile strength, flexural tensile strength, and modulus of elasticity). In the second and third phase of the experimental program, the flexural and shear behavior of beams will be tested on simply supported reinforced concrete beams with a span of 3.0 m in a four point bending test. The overall behavior of the beams will be analyzed, with a focus on short-term deflections, concrete and steel strains, principal concrete strains, crack patterns, failure modes, and flexural and shear strength. A comparative analysis will be carried out to compare the behavior of cement concrete and HVFAC.

1. Introduction

Finally, the application of different design codes defining flexural and shear strength for reinforced cement concrete structures will be evaluated for their applicability to HVFAC beams based on own experimental results and a database of collected results on HVFAC beams from available literature.

1.4. THESIS OUTLINE

The content of this thesis is organized in six chapters.

Chapter 1 is an introduction to the thesis. This introduction contains a brief background and motivation; it discusses the research objectives and gives the thesis outline.

Chapter 2 gives an overview of the FA material properties and its characterization and current standards. Possible application of FA in concrete is summarized and discussed. The main focus of this chapter is to summarize previous research on the HVFAC physical, mechanical, and durability properties as well as the structural application regarding flexural and shear behavior of HVFAC beams. At the end, the role of FA in sustainable construction is discussed.

Chapter 3 provides an overview of the basic flexural and shear transfer mechanisms in reinforced concrete beams. General assumptions and detailed design code provisions are presented. The design code evaluation is done using: Serbian standard for concrete and reinforced concrete – BAB '87 (Faculty of Civil Engineering 1995), European Standard EN 1992-1-1 (CEN 2004), *fib* Model Code 2010 (fib 2010) and American Standard ACI 318 (ACI 2008). The modified compression field theory is also used for flexural and shear strength calculation using the Response–2000 program.

Chapter 4 includes information about the experimental program and results. The experimental program consisted of ten tests performed on full-scale reinforced concrete beams, as well as the material and component testing to determine fresh and hardened concrete properties such as compressive strength, splitting tensile strength, flexural tensile strength, and modulus of elasticity. The testing of HVFAC material properties was done in order to design structural grade HVFAC with the

1. Introduction

maximum amount of FA on 17 different HVFAC mixtures. HVFAC mixtures with 50% and 64% of class F FA were selected for further testing on beam elements. The flexural and shear behavior of reinforced concrete beams was tested in the four point bending test on cement concrete and HVFAC beams with equally designed compressive strengths. This chapter describes the fabrication process, test set-up and the instrumentation for the full-scale beams. The test results obtained during testing are also presented. The overall behavior of the specimens is described, with a focus on deflection, concrete and steel strains, crack patterns, failure modes, and flexural and shear strength.

Chapter 5 presents the analysis of the HVFAC material properties and the full-scale beams tested in this study. The analysis of HVFAC material properties was done by comparing the HVFAC and OPCC mechanical properties and by analyzing the possible application of available code predications defined for OPCC on HVFAC. The database of available HVFAC mixtures tested for basic mechanical properties is made and analyzed. The application of code predictions defining the mechanical properties of cement concrete defined in EN 1992-1-1 is evaluated for HVFAC mixtures from the database. All proposals for modification of those predictions which were found in literature are re-evaluated using the collected HVFAC database. This analysis was also done on own experimental results.

In the second part of the analysis, evaluation of equations defined in BAB '87 (Faculty of Civil Engineering 1995), European Standard EN 1992-1-1 (CEN 2004), American Standard ACI 318 (ACI 2008) and *fib* Model Code 2010 (*fib* 2010b) in designing HVFAC beams was done. The variation of the HVFAC compressive strength based on the database of own experimental results of HVFAC samples was analyzed first. The analysis of the flexural and shear behavior of full-scale beams was done based on own experimental results and the HVFAC beams database collected from current literature. Finally, the application of available code predictions was analyzed on the cement concrete and HVFAC beams databases.

Chapter 6 gives the summary, main findings and conclusions of this study proposing future research.

2. LITERATURE REVIEW

2. Literature review

2.1. INTRODUCTION

This chapter gives an overview of the FA material properties, its characterization, and current standards. Having in mind the heterogeneity of FA physical and chemical properties and the lack of reliable predictions for HVFAC mechanical properties, a systematic analysis of the current results is needed. The main focus of this chapter is to summarize previous research on the HVFAC physical, mechanical, and durability properties as well as the structural application regarding flexural and shear behavior of HVFAC beams. At the end, the engineering application of HVFAC and the role of FA in sustainable construction are presented and discussed.

2.2. CHARACTERIZATION OF FLY ASH AND ITS MATERIAL PROPERTIES¹

FA is a by-product material and its physical, mineralogical and chemical properties strongly depend on the type and mineralogical composition of coal, processing conditions of the furnace, and the collection and storage of FA. These properties vary not only from one power plant to another but also within one plant, so large variations in the quality of FA are common. This is certainly one of the main obstacles for its commercial use, and a hard one to overcome. In order to improve FA's heterogeneous characteristics and ensure its stable quality, frequent control of physical, chemical, and mineralogical properties within power plants would be needed along with the grinding of FA, if necessary. In this way, more energy would be spent which would increase the cost of FA. Having this in mind, it is important to understand the variety of FA material properties before using it in concrete.

2.2.1. Physical properties of fly ash

Scanning electron microscopy shows that FA is a heterogeneous material containing particles of different dimensions and shapes. Generally, FA particles can

¹ Sections 2.2 - 2.5 and 2.7 - 2.9 of this thesis are based on the chapter 11: *Fly ash (Marinković and Dragaš)* of the book: *Waste and Supplementary Cementitious Materials in Concrete: Characterisation, Properties and Applications (Siddique and Cachim 2018)*

2. Literature review

be rounded, irregular, or angular but they are mostly spherical (Figure 2.1). Some of the particles are solid but most of them are hollow and may contain smaller particles. The irregularly shaped particles consist mainly of quartz, agglomerates, and unburned particles of coal, while the regularly shaped particles are mostly spheres (cenospheres, plerospheres, and ferrospheres) (Komljenović et al. 2010). The particle surface is usually smooth but it varies between different types of FA. The shape and quality of FA particles' surface affect the amount of water needed for a desired workability of FA concrete.

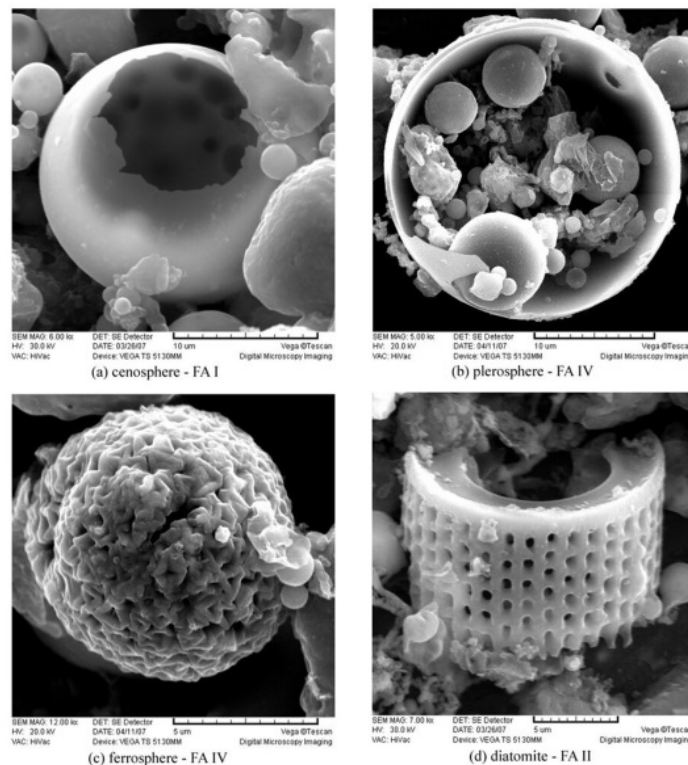


Figure 2.1 Different shapes of FA particle (Komljenović et al. 2010)

Besides shape and texture, size is one of the most important physical properties influencing particle motion in concrete mixture as well as FA pozzolanic activity. FA spherical particles range in diameter from 0.5 to 200 μm (Wesche 2004) and irregular and angular ones can be larger.

The particle size distribution is usually presented as FA fineness which can be determined in different ways and expressed through various parameters. The most used methods are wet and dry sieving of a FA sample. In this way, the residue on a 45 μm sieve is measured and the upper limit regarding this value is defined in

2. Literature review

some standards. Sieve analysis is a simple method for assessing the fineness of FA because it does not require special equipment, but the obtained information is limited and refers only to one sieve size. Particles larger than 45 μm are considered to be mostly inert, but the particle size distribution below this value is important for understanding FA efficiency (Bapat 2013). Another test often used for measuring the specific surface of powder materials as an indication of their activity is the air permeability test (Blaine test). It is based on the resistance offered by pulverized materials to an air flow and it is widely used for cement-specific surface determination defined in ASTM C204 (ASTM C204 2016) and EN 196-6 (CEN 2008) standards. This test is a simple and rapid method suitable for comparative analyses. However, some researchers argue that this is an inadequate method for FA fineness determination because of the unknown effect of unburned carbon in FA on the measuring process (Kiattikomol et al. 2001). Particle size distribution of FA influences the packing density of concrete and in this way, its workability and mechanical properties. In order to improve FA fineness, mechanical activation is often used. Grinding of FA increases its fineness and reduces its porosity.

Moisture of FA is an important physical property mostly because high moisture content in FA will cause its hardening, especially if a high calcium amount is present in FA. It is usually influenced by the storage conditions; this is the reason why ASTM C618 (ASTM C618 2015) limits the moisture content to 3%.

2.2.2. Chemical and mineralogical properties of fly ash

The chemical composition of FA is usually determined by X-ray fluorescence (XRF) and spectrometry techniques and defined in terms of oxides. Major constituents of most FAs are silica (SiO_2), alumina (Al_2O_3), calcium (CaO), and iron (Fe_2O_3) oxides. Besides them, FA also contains magnesium (MgO), sodium (Na_2O), titanium (TiO_2), sulfur (SO_3) and potassium (K_2O) oxides. Unburned carbon usually presented through the LOI is also an important constituent influencing high water and admixture requirement in concretes containing FA, because of the great porosity of unburned carbon. The range of oxides in FA presented in literature is shown in

2. Literature review

Table 2.1 (Bapat 2013; Hemalatha and Ramaswamy 2017; Siddique 2008; Wesche 2004).

Chemical analysis of various FAs shows a wide range of compositions, reflecting large variations in coal used in different power plants. Anthracite and bituminous coal usually produce FA with high SiO_2 and Al_2O_3 and low CaO content, while lignite and sub-bituminous coal produce FA with lower SiO_2 and Al_2O_3 and higher CaO content. The amount and mutual ratio of these oxides is important for the use of FA in concrete because it influences binding reactions that happen in concrete: hydration and the pozzolanic reaction.

Table 2.1 Chemical composition of various FAs (Bapat 2013; Hemalatha and Ramaswamy 2017; Siddique 2008; Wesche 2004)

Oxides	Range (%)
SiO_2	11.8–62.8
Al_2O_3	2.6–35.6
Fe_2O_3	1.4–24.4
CaO	0.5–54.8
MgO	0.1–6.7
Na_2O	0.1–3.6
K_2O	0.1–9.3
SO_3	0.0–12.9
LOI	0.0–32.8

Besides FA fineness and chemical composition, reactivity of FA in concrete and its efficiency are strongly influenced by its mineralogical characteristics. Chemical composition alone is not enough because not all oxides in FA are reactive. Owing to the rapid cooling of FA in the process, it is mostly (60–90%) composed of non-crystalline particles or glass, i.e., an amorphous phase (Malhotra and Mehta 2005). A small amount of FA occurs in the form of crystalline minerals and unburned carbon particles. X-ray diffraction (XRD) and infrared spectroscopy techniques are commonly used for mineralogical determination of FA. Minerals mostly occurring in FA are magnetite, hematite, quartz, and mullite (Paya et al. 1995). Mineralogical

2. Literature review

characterization of FA helps in understanding the pozzolanic reaction with cement hydration products in FA concrete.

The American Concrete Institute defines pozzolanic material as “siliceous and aluminous material, which in itself possesses little or no cementitious value but will, in finely divided form and in the presence of moisture, chemically react with Ca(OH)_2 at ordinary temperatures to form compounds possessing cementitious properties” (ACI 2000). Thus, pozzolanic activity of FA depends on the reactive amount of CaO, SiO_2 , and Al_2O_3 in FA. Some FAs have greater quantities of CaO and can exhibit a self-cementitious (hydraulic) activity, but pozzolanic activity is best expressed if FA is used in combination with Portland cement in concrete (Papadakis and Tsimas 2002). In this way, FA reacts with Ca(OH)_2 formed by cement hydration. Most of the crystalline phase is inert and the reactivity of FA and pozzolanic capacity are related to the amorphous phase. The main product of the pozzolanic reaction of FA in concrete is a hydrated gel, same as in the case of cement hydration: calcium silicate hydrate (CSH) and alumina hydrates (Papadakis 1999, 2000a). After the dissolution of FA’s amorphous SiO_2 and Al_2O_3 framework by hydroxide ions (OH^-) and generated heat during the early hydration of cement, free silicate and aluminate anions react with Ca(OH)_2 to form an amorphous calcium silicate aluminate phase. The reaction continues as long as there is available Ca(OH)_2 present in the concrete pore solution and until the hydrated gel fills in the capillary pores in concrete (Cao et al. 2000). The pozzolanic reaction needs time and takes place after the beginning of hydration, approximately at the age of 7–14 days or later (Lam et al. 2000; Wesche 2004). It is difficult to define the pozzolanic reaction looking only at FA characteristics. Many factors influencing this reaction, beside previously mentioned physical, chemical and mineralogical FA properties, are: physical and chemical characteristics of cement, alkali-hydroxide concentration of the reaction system and development of heat during the early phases of the hydration process (ACI 2002).

2. Literature review

2.2.3. Classification of fly ash

Having in mind the great spread of physical and chemical properties of FA it is clear that the possible use of this by-product in construction materials, especially in concrete, is rather large. In order to use FA as a raw material in cement and concrete production it is important to determine a classification and quality control based on important properties of FA. In studies regarding FA, it is mostly classified according to the American standard ASTM C618 (ASTM C618 2015). This standard classifies pozzolanic materials as natural pozzolans and by-products in three classes:

- Class N: natural pozzolans such as volcanic ashes, diatomaceous earth, calcined clay, metakaolin clay, and rice husk ash;
- Class F: FA produced by burning anthracite or bituminous coal with pozzolanic properties;
- Class C: FA produced by burning lignite or sub-bituminous coal with pozzolanic and cementitious properties.

ASTM C618 (ASTM C618 2015) categorizes FA primarily based on its chemical composition, according to the sum of SiO_2 , Al_2O_3 , and Fe_2O_3 . The sum of total oxides $\text{SiO}_2 + \text{Al}_2\text{O}_3 + \text{Fe}_2\text{O}_3$ must be greater than or equal to 70% and 50% for class F and C, respectively. Class C ashes usually contain more than 15% of CaO and can pose cementitious properties, unlike class F with usually less than 10% of CaO. In general, class C and class F ashes show different performance characteristics in concrete. Besides the chemical composition of FA, ASTM C618 also defines some of the physical and mechanical properties of FA.

European standards also define properties of FA for the use in cement in EN 197-1 (CEN 2011a) and concrete in EN 450-1 (CEN 2012). For the use of FA in cement two types of FA are defined in EN 197-1 as (CEN 2011a):

- Siliceous FA - V: amount of reactive CaO is less than 10%;
- Calcareous FA - W: amount of reactive CaO is more than 10%.

2. Literature review

The European standard EN 450-1 (CEN 2012) defines chemical, physical, and mechanical properties of FA for the use in concrete and classifies FA based on two parameters: LOI and fineness. Based on LOI, three categories are defined:

- A: maximum LOI less than 5%;
- B: maximum LOI less than 7%;
- C: maximum LOI less than 9%.

Based on fineness, two types of FA are defined:

- Type N: less than 40% of FA retrieved on sieve 45 μm ;
- Type S: less than 12% of FA retrieved on sieve 45 μm .

Table 2.2 sums up the most important requirements for FA according to ASTM C618 (ASTM C618 2015) and EN 450-1 (CEN 2012) standards for use in concrete.

Table 2.2 Chemical and physical properties of FA for use in concrete defined in ASTM C618 (ASTM C618 2015) and EN 450-1 (CEN 2012)

	ASTM C618		EN 450-1
	Class C	Class F	A / B / C
$\text{SiO}_2 + \text{Al}_2\text{O}_3 + \text{Fe}_2\text{O}_3$, (% , min)	50	70	70
SO_3 , (% , max)	5	5	3
Moisture content, (% , max)	3	3	-
Loss on ignition, (% , max)	6	6 (12)	5 / 7 / 9
Reactive CaO, (% , max)	-	-	10
Total content of alkalis, (% , max)	-	-	5
MgO, (% , max)	-	-	4
P_2O_5 , (% , max)	-	-	5
Amount retained on 45 μm sieve, (% , max)	34	34	40 / 12*
Strength activity index at 7 / 28 / 90 days, (% of control, min)	75 / 75 /-	75 / 75 /-	- / 75 / 85
Water requirement, (% of control, max)	105	105	95**
Autoclave expansion/contraction (% , max)	0.8	0.8	-

* Type N / S

**only for FA type S

2. Literature review

In order to use FA in concrete production, it has to satisfy the requirements in Table 2.2, but this does not automatically guarantee good performance of the concrete. For FA performance in concrete, the ratio of reactive SiO_2 and Al_2O_3 in FA to reactive CaO in FA and cement is more important than the sum of total oxides (Kuder et al. 2012; Papadakis et al. 2002). The amount of retrieved mass on a 45 μm sieve defines FA fineness but the particle size distribution provides better understanding of early and later age FA and cement reactions. For complete insight into FA's influence on workability, strength characteristics and durability of FA concrete, investigation through trial concrete mixtures must be carried out.

2.3. FLY ASH IN CONCRETE

The high variety of FA's physical and chemical properties enables different applications in concrete. FA has been used in concrete since the 1930s, firstly in the construction of mass gravity dams to reduce the heat of hydration. Since then, class F and class C FA types are used in concrete in amounts from only a few percent and up to 70–80% of the total cementitious materials (CM) mass.

As a mineral admixture, FA is often used as a filler in self-compacting concrete (SCC) (Bingöl and Tohumcu 2013; Kuder et al. 2012; Şahmaran et al. 2009; Da Silva and De Brito 2015). As a CM, FA can be used as a cement replacement having in mind its hydraulic (class C) and pozzolanic (class F) properties. FA also constitutes a part of some types of blended cements. In general, the effects of using blended FA cement and replacing cement with FA in concrete are similar. However, grinding of FA in blended cement's production improves FA's performance: its variability decreases, its fineness increases, and the addition of gypsum enables a desired setting time. There are commercially available blended cements with up to 55% of FA (CEN 2011a). Simultaneous use of two pozzolanic materials as a cement replacement—FA and granulated blast furnace slag—have shown positive effects on concrete properties (Hannesson et al. 2012; Kuder et al. 2012). In recent years, a lot of research was dedicated to alkali activated FA concrete where FA totally replaced cement (Duxson et al. 2006; Hardjito 2005; Pacheco-Torgal et al. 2008; Provis and van Deventer 2014).

2. Literature review

Concrete made with FA conforming to EN 450-1 (CEN 2012), with a maximum cement replacement of 33% of cement mass, is widely used and supported by extensive research (Dinakar et al. 2008, 2013; Duran-Herrera et al. 2011; Golewski and Sadowski 2014; Huang et al. 2013; Kayali and Sharfuddin Ahmed 2013; Kou and Poon 2013; Lam et al. 1998; Lima et al. 2013; Mathur et al. 2005; McCarthy and Dhir 2005; Mittal et al. 2006; Poon et al. 2000; Quan and Kasami 2013; Tokyay 1999). Research has shown that this type of concrete exhibits better workability, less bleeding and segregation, lower heat of hydration, a longer setting time of concrete, and similar or slightly lower compressive strength at all ages compared with concrete without FA with the same CM amount (Golewski and Sadowski 2014; McCarthy and Dhir 2005).

Depending on the type and amount of FA, its influence on concrete properties can be different and achieved through different mechanisms. The addition of FA fine particles in concrete improves concrete properties first through the filler effect, by filling the voids between cement particles, making it denser (Moosberg-Bustnes et al. 2004; Scrivener et al. 2015). Furthermore, FA improves the performance of concrete through the acceleration of cement hydration by acting as nucleation sites, becoming an integrated part of the cement paste (Moosberg-Bustnes et al. 2004). Finally, FA will improve concrete density and mechanical properties by forming more CSH gel during the pozzolanic reaction with cement hydration products. At early ages, the pozzolanic reaction of FA is not dominant and mechanical properties of concrete are improved mostly by the FA's filler effect and accelerated hydration (Hwang et al. 2004; Ogawa et al. 1980). The efficiency of FA at this age can be defined by analyzing the particle packing rather than the pozzolanic reaction. The pozzolanic reaction of FA is slower compared with cement hydration but continues for years after reacting with the concrete pore solution, contributing to strength gain longer than in cement concrete (Lam et al. 2000; Papadakis 1999).

Depending on the FA's fineness, it can also be used as a fine aggregate (sand) replacement in concrete. The influence of FA on physical and mechanical properties of concrete can be determined if referent and FA concrete have the

2. Literature review

same water-to-CM (W/CM) ratio. Part of the added FA will act as a filler and the rest will act like a pozzolanic material. The influence of partial replacement of sand with FA was analyzed based on the available research from literature (Deo and Pofale 2015; Rajamane et al. 2007; Rajamane and Ambily 2013; Siddique 2003). Available experimental results consisted of concretes made with 10-60% fine aggregate replacement with class F FA. All analyzed researchers concluded that FA has a positive effect on the compressive strength when a partial sand replacement was done (e.g. in Figure 2.2).

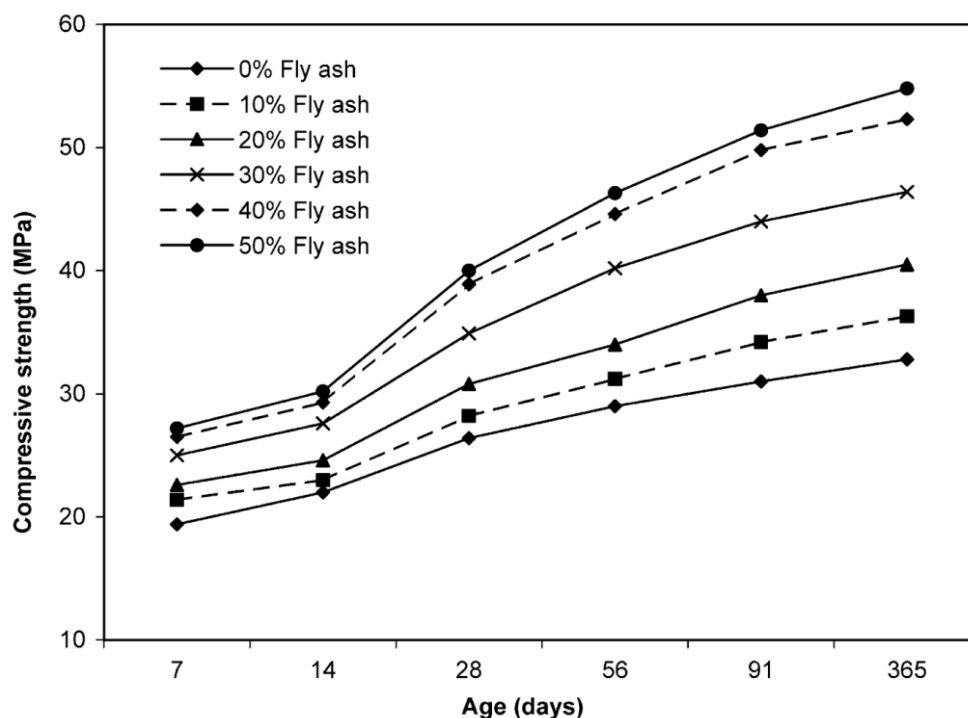


Figure 2.2 Compressive strength of FA concrete versus age (Siddique 2003)

In all selected studies the analysis was based on the comparison between referent cement concrete (RCC) and concrete with a partial sand replacement. In order to do so properly, FA concrete and RCC should have the same component materials, and W/CM ratio. However, different water amount in cement concrete and FA concrete was used. Having this in mind, the conclusions regarding FA influence on the compressive strength cannot be easily made. In order to evaluate all important parameters following analysis of available data was done.

The ratio of FA concrete (f_c^{FA}) and RCC (f_c^{RCC}) compressive strength compared with the sand replacement (FA/Sand) is shown in Figure 2.3 (Deo and Pofale 2015;

2. Literature review

Rajamane et al. 2007; Rajamane and Ambily 2013; Siddique 2003). It can be seen that no clear correlation between the presented compressive strength ratio and FA/Sand ratio is visible. The main reason lies in the different RCC and FA concrete W/CM ratios. In order to eliminate this effect, the ratio of FA concrete and RCC compressive strength are compared with the relation of W/CM ratios of tested FA concretes (W/CM^{FA}) and RCC (W/CM^{RCC}) and shown in Figure 2.4.

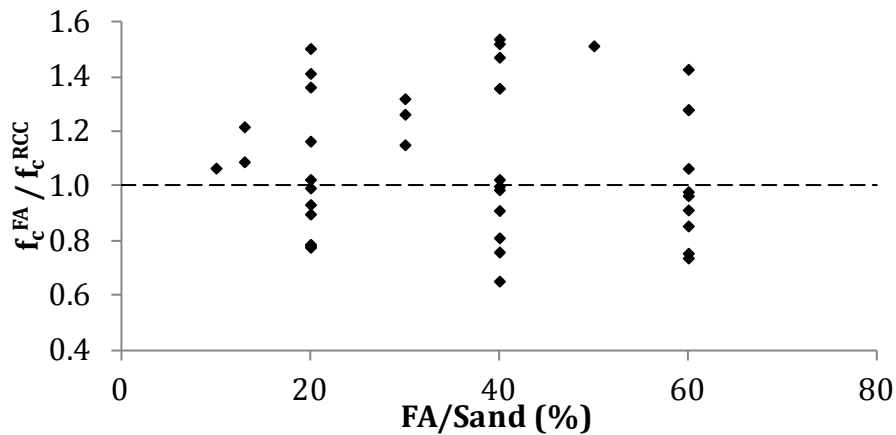


Figure 2.3 The ratio of FA concrete and RCC compressive strength versus sand replacement (Deo and Pofale 2015; Rajamane et al. 2007; Rajamane and Ambily 2013; Siddique 2003)

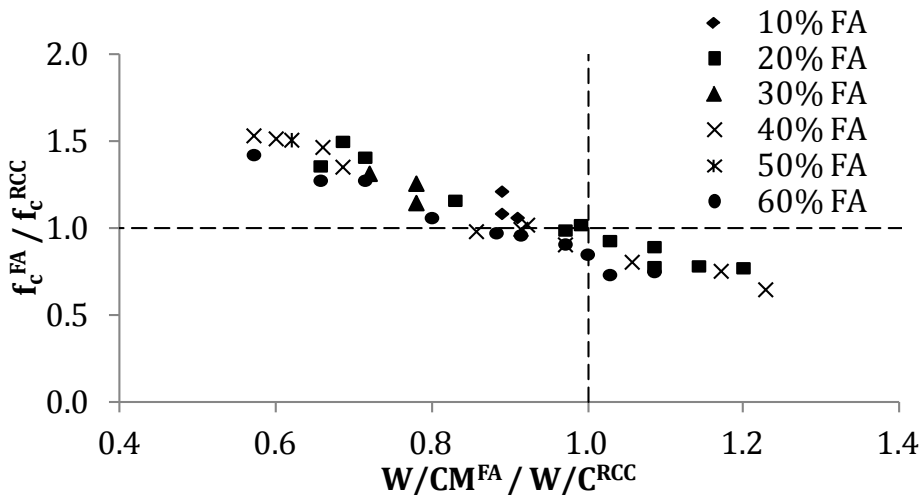


Figure 2.4 Compressive strength ratio of FA concrete and RCC versus FA concrete and RCC W/CM ratio (Deo and Pofale 2015; Rajamane et al. 2007; Rajamane and Ambily 2013; Siddique 2003)

2. Literature review

First, it can be seen that the compressive strength is highly correlated with W/CM ratio, as expected. Second, it is clear that the positive effect of FA on the compressive strength is mostly related to the lower W/CM ratio in FA concretes.

It is clear that the addition of FA as the replacement of sand can be beneficial to the compressive strength due to better particles packaging, pozzolanic activity and lower W/CM ratio, but this effect cannot be quantified based on the available results from the literature.

2.4. HIGH VOLUME FLY ASH CONCRETE – HVFAC

After years of experience with the use of FA in concrete governed by environmental, technical, and cost motives, the amount of FA in CM has increased. In 1985, the Advanced Concrete Technology Group at CANMENT, Canada, started a project to develop structural high-volume FA concrete (HVFAC) (Bouzoubaâ et al. 2001; Bouzoubaa and Malhotra 2001; Malhotra and Mehta 2005). Within the CANMENT project, typical mixture proportions for HVFAC of low, moderate, and high strength (20, 30, and 40 MPa, respectively) were provided, following these recommendations (Malhotra and Mehta 2005):

- Minimum 50% of class F FA in total CM mass (CM usually less than 400 kg/m³);
- Low water content (usually less than 130 kg/m³);
- Portland cement content usually smaller than 200 kg/m³;
- Superplasticizer is usually necessary for adequate workability of moderate and high-strength HVFAC.

When designing HVFAC concrete mixtures, the same component materials are used like in cement concrete. FA should meet the requirements defined in adequate standards (CEN 2012), as well as cement and aggregate. Both class C and F FA are used in HVFAC, however a large percentage of research conducted so far included class F. Main difference between these two types of FA refers to the strength increase governed by different binding reactions and their kinematics. The use of class C FA improves early age strength providing relatively good long-term strengths. On the other hand, class F FA provides slower strength increase and lower early age strengths but better long-term performance compared with a

2. Literature review

RCC. Further analysis of HVFAC done in this work refers to class F FA if not stated differently.

In designing concrete mixtures, the volumetric equation is usually used to determine component materials' mass. On the other hand, the FA amount in HVFAC is usually defined as a mass percent of total CM or cement replacement. Regardless of the FA class, its specific gravity (usually in the range 1900–2700 kg/m³) is significantly lower compared with cement (about 3150 kg/m³) and hence, the paste volume in HVFAC is higher compared with cement concrete. In order to satisfy the volumetric equation, the aggregate volume is usually lower in HVFAC compared with cement concrete. The decrease of the aggregate volume can be done in two ways: (1) by reducing the volume of all aggregates or (2) only the fine fraction (Figure 2.5).

Having in mind the fineness of FA, the reduction of fine aggregate is reasonable and can provide positive effects on compressive strength (Dragaš et al. 2016; Kou and Poon 2013). It is important that the aggregate particle size distribution remains in the limits prescribed by adequate standards ensuring good aggregate packing density and thus, good workability and strength.

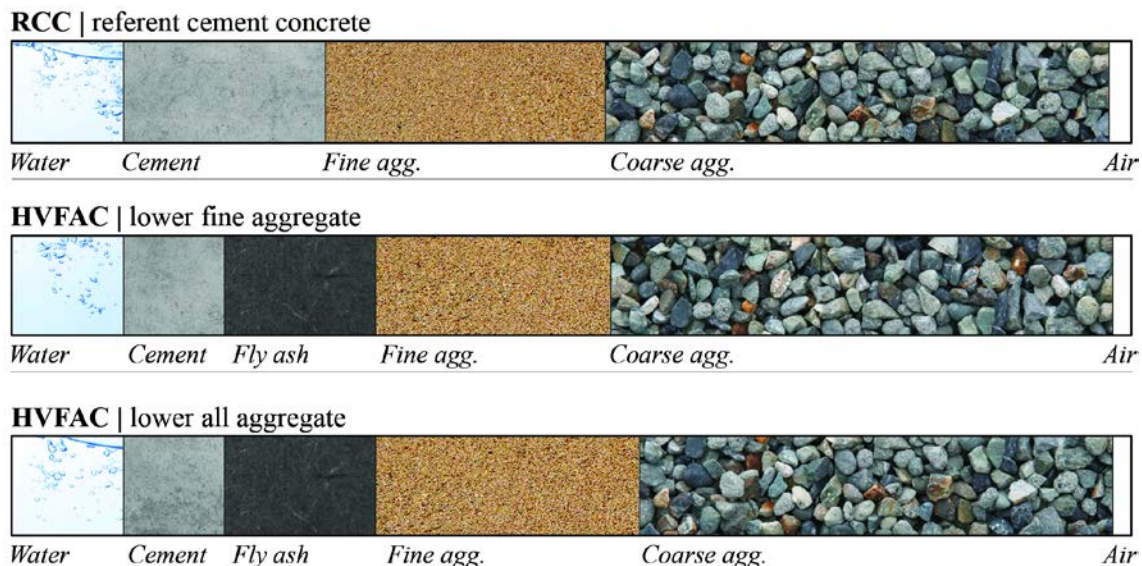


Figure 2.5 Volumetric proportion of component materials in RCC and HVFAC

2. Literature review

When designing HVFAC mixtures, it is important to take into account the influence of all component materials and their amount on the fresh and hardened properties of concrete. Different FA types and amounts were used in HVFAC in different studies over the past three decades, but some general conclusions about basic physical and mechanical properties of HVFAC can be drawn.

2.4.1. Physical properties of HVFAC

The most important physical properties of concrete that should be assessed are workability, bleeding and segregation, setting time, air content, and heat of hydration.

It is often stated that, in general, the use of FA in concrete reduces water demand for a given workability (Jiang and Malhotra 2000; Kim et al. 2012). It is practically impossible to define the relationship between FA characteristics and workability of concrete due to a wide range of factors influencing HVFAC workability: aggregate type and packing density, paste volume, W/CM ratio, FA fineness and amount of unburned carbon, FA particle shape, size and surface state, etc. (Bentz et al. 2012; Jiménez-Quero et al. 2013; Lee et al. 2003).

The influence of FA on water demand and workability is achieved through the following mechanisms. Mostly spherical and smooth FA particles reduce friction in a concrete mixture via a ball-bearing effect (Jiménez-Quero et al. 2013). Consequently, the water demand decreases as the particles are more spherically shaped and smooth (Cabrera et al. 1986). Due to the dilution effect, fine FA particles prevent cement flocculation, i.e. FA prevents cement particles from forming into blocks (Lee et al. 2003). The density of FA is lower than that of cement, as mentioned before. Accordingly, the paste volume of the mixture increases forming a positive effect on concrete workability (Lee et al. 2003). If FA particles are similar or smaller in size, compared with cement particles, its use increases the packing density of concrete by acting like a filler (Moosberg-Bustnes et al. 2004; Scrivener et al. 2015; Wang et al. 2004). In general, FA fine particles fill the voids between solid particles and thus, demand less water to lubricate the mixture (Kwan and Chen 2013; Lee et al. 2003). The packing density of particles in HVFAC depends on the aggregate and FA particle size distribution. With increasing

2. Literature review

FA fineness, the packing density of concrete also increases. On the other hand, higher fineness means a higher specific surface and could cause more water demand to lubricate FA particles. The dual effect of FA fineness indicates that its particle size distribution should be carefully assessed. In theory, good packing can be achieved with FA particles finer than cement but the optimum (minimum) size is a matter of analysis. Kwan and Chen (Kwan and Chen 2013) concluded that best effect on workability have particles smaller than cement, but larger than silica fume particles.

Based on the previously stated, it can be concluded that, depending on its properties, FA has a plasticizing effect on workability. On the other hand, it is observed that HVFAC with coarser FA exhibits lower workability due to large proportion of particles larger than 45 μm (Owens 1979). The adverse effect on workability is also observed in the presence of porous particles of unburned carbon (LOI) in FA which absorb part of water in the mixture (Alaka and Oyedele 2016). The plasticizing effect of FA is also influenced by the W/CM ratio and FA amount used in concrete. The optimum amount of FA for this effect is influenced by FA and cement properties and differs from case to case (Wesche 2004). It is also observed that by increasing the FA amount in concrete it becomes 'stickier' with pronounced thixotropic properties: during mixing it behaves in a very flowable manner and when the mixing stops, surface stiffness makes it difficult to remove the concrete from the mixing pan (Dragaš et al. 2016; Neundorf and Haebler 2000).

Having in mind a large amount of CM and usually low W/CM ratio used in HVFAC, the use of superplasticizers is very common. The usual dose used in cement concrete ranges between 0.5% and 2.5% (The Concrete Institute 2013). However, numerous studies used higher amounts of superplasticizer in HVFAC (Chen et al. 2013; Dinakar et al. 2008; Poon et al. 2000). With increasing superplasticizer amounts in concrete, its action decreases but the amount doesn't affect HVFAC mechanical properties (Alaka and Oyedele 2016). A wide range of superplasticizers were used in HVFAC and polycarboxylate-based ones seem to have the best effect on workability and longer slump retention (ACI 2014).

2. Literature review

Considering the positive effect of FA on workability of concrete, it is being used as a mineral admixture acting like a filler in SCC: a type of concrete that flows under the influence of gravity and does not need consolidation by vibration. This type of concrete usually requires an increased amount of cement so the use of FA helps decrease the cost and heat of hydration and improves workability (Bouzoubaa and Lachemi 2001; Ferraris et al. 2001; Nehdi et al. 2004).

Besides workability, the addition of FA also influences mixture stability, i.e., bleeding and segregation. Bleeding is a form of water segregation on the surface of fresh concrete due to inability of solid particles to hold all of the mixing water when settling (Neville 1981). Segregation is defined as a separation of concrete constituents so that their distribution is no longer uniform (Neville 1981). A high amount of segregated water affects the W/CM ratio on the surface, reducing strength and durability of concrete. Bleeding can be observed in concrete with a high water content, low cement mass, and poorly graded aggregates (Poon et al. 2007). Having in mind the low W/CM ratio, increased paste volume and better packing density of HVFAC, it is generally more cohesive and has decreased bleeding and segregation (Ferraris et al. 2001). Alongside with FA smooth spherical particles and their lubricating effect, HVFAC generally exhibits better pumpability.

After the concrete mixing and placing is done, hydration of CM starts and concrete workability changes to a more rigid state. Concrete (cement paste) stiffening is called the setting time and it is defined with an initial and a final setting time. The initial setting time defines the time at which fresh concrete can no longer be properly mixed and placed, i.e., the beginning of concrete solidification. The final setting time defines the beginning of the development of mechanical properties. Both initial and final setting times are generally delayed in HVFAC mixtures compared with RCC. In the first place, setting is delayed due to the reduction of hydration products because of the lower amount of cement in HVFAC. It is difficult to give an estimation of a prolonged setting time because of the many parameters influencing it; mainly, fineness and chemical composition of cement and FA, water content, and ambient temperature.

2. Literature review

Ravina and Mehta (Ravina and Mehta 1986) concluded that for the same cement replacement level, different FA types and amounts induced different retardation of setting, proving that FA affects the setting time on both physical and chemical levels during its interaction with cement and water. It is stated that alkalis and sulfate level in FA influence setting time. FA with a higher amount of alkalis tends to have rapid setting, sometimes even a 'flash set'. On the contrary, a higher sulfate level causes retardation of setting (Ravina and Mehta 1986). Class C FA setting time is usually more difficult to predict because of the positive effect of its hydraulic characteristics and usually more sulfate content stimulating retardation (Naik and Singh 1997; Ravina and Mehta 1986).

In general, as the cement replacement level and W/CM ratio increase, so does the setting time without retarding the hydration process (Duran-Herrera et al. 2011; Huang et al. 2013). This concrete property is important for construction industry work dynamics (especially influencing floor slabs finishing) so it should be determined for each FA and cement combination. HVFAC setting time can be accelerated by using finer cement (rapid set cement), finer FA with low amounts of sulfate, and adequate curing temperatures.

Another important fresh concrete property is its air content. In general, HVFAC has less entrained air compared with RCC (usually 1–3%). FA concrete has an entrapped air amount reduced by approximately 0.5–1% (Lane 1983) because of the influence of the FA amount, type, fineness, and LOI. The lower air content in HVFAC can be a consequence of higher FA fineness compared with cement and thus, better particle packing (Bouzoubaâ et al. 2001) with a decreasing tendency with increasing FA amounts (Duran-Herrera et al. 2011). The air content is an important factor, especially influencing concrete resistance to freezing/thawing, so the use of air-entraining agents (AEA) in HVFAC is needed in some cases. The European standard EN 206-1 (CEN 2011b) defines the minimum air content for concrete subjected to freezing/thawing for more severe exposure classes to be 4%. In order to achieve this, in general, HVFAC requires more AEA compared with cement concrete (Van Den Heede et al. 2013). This is mainly influenced by the increased absorption of the AEA by porous unburned carbon particles. FA with

2. Literature review

higher LOI and fineness usually requires a higher amount of AEA (Bouzoubaâ et al. 2000).

Hydration of cement is an exothermic process. When FA is used to replace cement in Portland cement concrete, the rate of heat development and overall heat of hydration are altered. Research showed that the temperature rise caused by the hydration of HVFAC may be significantly reduced (Atis 2002; Duran-Herrera et al. 2011; Poon et al. 2000), which is very beneficial in mass concrete construction.

2.4.2. Mechanical properties of HVFAC

The use of FA in concrete alters the concrete matrix influencing its mechanical characteristics along with its physical properties. The behavior of hardened HVFAC depends upon many factors, but mostly upon FA fineness, chemical and mineralogical properties, cement type, W/CM ratio, amount and mutual ratio of FA and cement, and curing conditions. It is difficult to draw general conclusions regarding mechanical properties of HVFAC – it is important to take into account the influence of all parameters in each particular case. Hardened concrete properties that define its behavior are mainly compressive strength, splitting tensile strength, modulus of elasticity, creep, and shrinkage.

The most common way to evaluate mechanical properties of HVFAC is by comparing it with RCC. In order to do so properly, HVFAC and RCC should have the same component materials, amount of CM and W/CM ratio. In further analysis, the term "RCC" is used for cement concrete made and tested in the selected study with a comment regarding the W/CM ratio and amount of CM.

HVFAC designed in the proper way, as previously defined, usually has lower 28-day compressive strength and slower development of compressive strength over time compared with RCC. Figure 2.6 shows the 28-day compressive strength ratios of HVFAC and RCC taken from literature, for HVFAC with class F FA amount ranging from 40% to 70% of total CM mass. Selected results are divided into two groups according to W/CM ratio of HVFAC and RCC mixtures. The first group contains concretes with the same W/CM ratio (Balakrishnan and Awal 2014; Berndt 2009; Bortz 2008; Dinakar et al. 2013; Hannesson G. 2010; Kayali and

2. Literature review

Sharfuddin Ahmed 2013; Kou and Poon 2013; Lam et al. 1998; Mittal et al. 2006; Papadakis 2000a; Poon et al. 2000; Siddique 2004; Tokyay 1999; Yoon et al. 2014; Zhao et al. 2016) while the second group contains HVFAC with a lower W/CM ratio compared with RCC (Bouzoubaâ et al. 2001; Jiang et al. 2000; Mathur et al. 2005). It can be seen that HVFAC compressive strength is lower for all mixtures with the same W/CM ratio as in RCC, and that it generally decreases with increasing FA amount. If the HVFAC W/CM ratio is lower, compressive strength can be similar or even higher than RCC compressive strength, which can also be seen in Figure 2.6. However, it seems that for very high FA amounts (70% of CM mass), it is not possible to obtain compressive strength similar to that of RCC, even with a lower W/CM ratio.

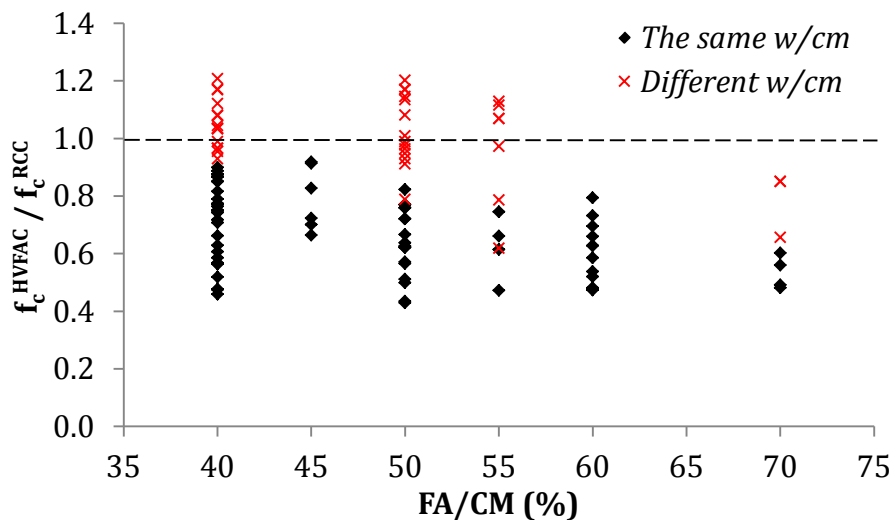


Figure 2.6 HVFAC and RCC compressive strength ratio for different FA amounts (Balakrishnan and Awal 2014; Berndt 2009; Bortz 2008; Bouzoubaâ et al. 2001; Dinakar et al. 2013; Hannesson G. 2010; Jiang et al. 2000; Kayali and Sharfuddin Ahmed 2013; Kou and Poon 2013; Lam et al. 1998; Mathur et al. 2005; Mittal et al. 2006; Papadakis 2000a; Poon et al. 2000; Siddique 2004; Tokyay 1999; Yoon et al. 2014; Zhao et al. 2016)

A great scatter of the results shown in Figure 2.6 is mostly a consequence of different characteristics of FA used in different studies. As already mentioned, FA has a dual effect on mechanical properties of concrete, through the filler effect and chemical activity. The filler effect improves the concrete density and

2. Literature review

microstructure and depends on FA fineness. The chemical effect is based on FA hydraulic and pozzolanic activity and depends on the amount of reactive CaO, SiO₂, Al₂O₃, and FA fineness.

Compressive strength development over time of HVFAC depends mostly on the type of FA, whether it is class C or class F. In HVFAC made with class C FA, the hydraulic reaction of FA takes place almost at the same time as the hydration of cement, contributing to both early and 28-day compressive strengths. This is a consequence of a substantial amount of reactive CaO in class C FA. Depending on the reactive SiO₂ and Al₂O₃ amount, class C FA will also improve concrete strength at later ages. On the other hand, class F FA has high SiO₂ and Al₂O₃ amounts and a relatively low CaO amount and thus, very little hydraulic potential and, dominantly, pozzolanic behavior. The pozzolanic reaction takes place after cement hydration and its products improve the concrete microstructure as long as there is enough water, Ca(OH)₂, SiO₂, and Al₂O₃ in the mixture. Having in mind that the pozzolanic reaction takes time to develop, HVFAC made with class F FA exhibits lower early age compressive strength but significant later strength increase. So, at early ages, class F FA contributes to compressive strength increase by acting like fine aggregate, and after 7–14 days the pozzolanic property becomes effective (Naik and Singh 1994; Zhang 1995).

Another important parameter influencing compressive strength development over time is the curing regime and its duration. As already mentioned, use of smaller amounts of FA in concrete can reduce the water needed for a required slump compared with RCC. On the other hand, the consumption of water during hydration and the pozzolanic reaction in HVFAC could be higher, so the lack of it can interrupt the reactions (Narmluk and Nawa 2011). At normal temperatures, the pozzolanic reaction is slower than the hydration of cement, so longer curing is needed for the full potential of FA to be reached (Gebler and Klieger 1986). It is generally recommended that HVFAC is moist cured for at least 7 days (Thomas 2007). Adequate duration of moist curing helps the successful development of hydration and pozzolanic reaction, and increased curing temperatures can improve early age strengths (Mehta and Gjrv 1982). However, results from the

2. Literature review

literature show that increased curing temperatures or steam curing, although helping the early age strength, can have adverse effect on the 28-day compressive strengths (Liu et al. 2005; Payá et al. 2000). In order to resolve the discrepancy of current results from literature, further studies are needed to determine the optimum curing temperature.

Figure 2.7 shows the compressive strength increase over time for HVFAC and RCC based on results taken from literature (Berndt 2009; Dinakar et al. 2013; Hannesson G. 2010; Lam et al. 1998; Mittal et al. 2006; Poon et al. 2000; Siddique 2004; Tokyay 1999; Yoon et al. 2014). HVFAC made with class F FA and cured under moist curing conditions is selected for this analysis. The amount of FA in CM mass varied from 40% to 70%. RCC had the same W/CM as corresponding HVFAC in all selected studies. Strength development is presented as a ratio of compressive strength at the age t and 28 days in order to evaluate a general trend.

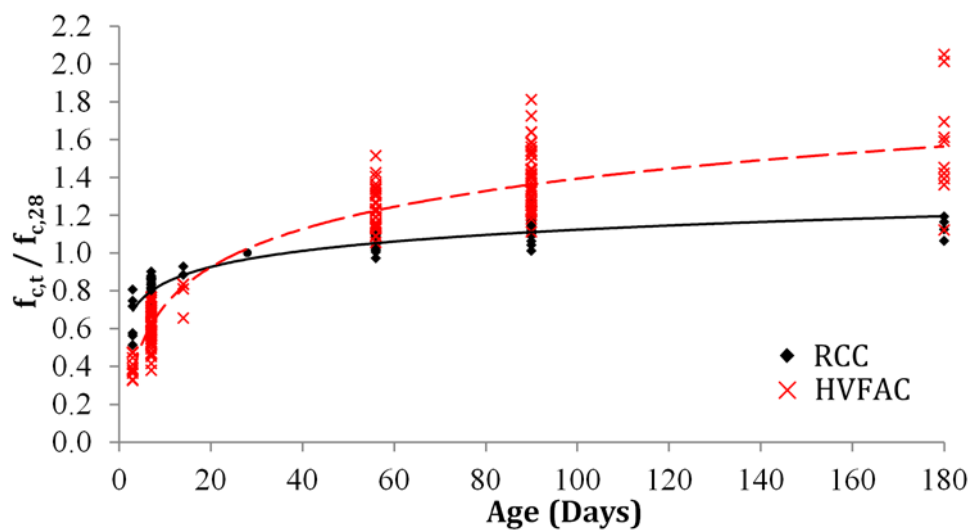


Figure 2.7 HVFAC and RCC compressive strength development over time (Berndt 2009; Dinakar et al. 2013; Hannesson G. 2010; Lam et al. 1998; Mittal et al. 2006; Poon et al. 2000; Siddique 2004; Tokyay 1999; Yoon et al. 2014)

Figure 2.7 clearly shows the difference between HVFAC and RCC compressive strength development: HVFAC has lower early age and higher later age compressive strengths compared with RCC. The age at which HVFAC strength overcomes RCC strength depends on the curing, FA type, amount, and W/CM ratio of concrete. At higher levels of FA, that age is usually later than 28 days. If low

2. Literature review

quality FA with coarser particles is used, HVFAC strength can be lower than RCC at all ages (Duran-Herrera et al. 2011). Since HVFAC compressive strength significantly increases even after 90 days, the question is raised whether to take the 28-day or 90-day compressive strength as the reference. The answer to that question may lie in the fact that, in most cases, the total construction load is not applied before 90 days. Regardless of that, it is possible to design a HVFAC mixture in a way that it has the required early and later (28-day or 90-day) compressive strength. Higher strengths will usually require a low W/CM ratio, the use of a superplasticizer, and sometimes, the use of accelerating admixtures.

The modulus of elasticity is an important property influencing concrete's short and long-term deformation behavior. Factors influencing the concrete modulus of elasticity are mainly the type, quality and volume of aggregates, the quality of cement (or cement and FA) paste and concrete porosity (Neville 1981). There is a relatively small number of results on HVFAC modulus of elasticity available in literature. Some research shows that the modulus of elasticity of HVFAC is similar or higher compared with RCC (ACI 2014; Kuder et al. 2012; McCarthy and Dhir 2005), but other proves that the modulus decreases with the use of high volumes of FA in concrete (Siddique 2004). Research done by Bouzoubaâ et al. (Bouzoubaâ et al. 2001) and Huang et al. (Huang et al. 2013) showed that HVFAC moduli are higher compared with RCC for the same 28-day compressive strength and that there is a significant increase after 28 days. The development of the modulus of elasticity over time is similar to the development of compressive strength: the HVFAC modulus is lower than the RCC modulus at early ages but continues to increase over time at greater extent (Dragaš et al. 2016; Langley et al. 1989).

Figure 2.8 (Bouzoubaâ et al. 2001; Dinakar et al. 2013; Huang et al. 2013; Kou and Poon 2013; Langley et al. 1989; Mittal et al. 2006; Yoo et al. 2015; Yoon et al. 2014) shows the modulus of elasticity ratio of HVFAC and RCC based on results from literature. In the selected studies not all RCC had the same W/CM ratio like in HVFAC. It can be seen that the HVFAC modulus of elasticity is generally lower than the RCC modulus, ranging from 0.59 to 1.14 of the RCC modulus with an average value of 0.9 (coefficient of variation is 15.7%). Higher moduli are mostly attributed

2. Literature review

Bouzoubaâ et al. 2001; Dinakar et al. 2013; Kou and Poon 2013; Lam et al. 1998; Nath 2010; Şahmaran et al. 2009; Siddique 2004).

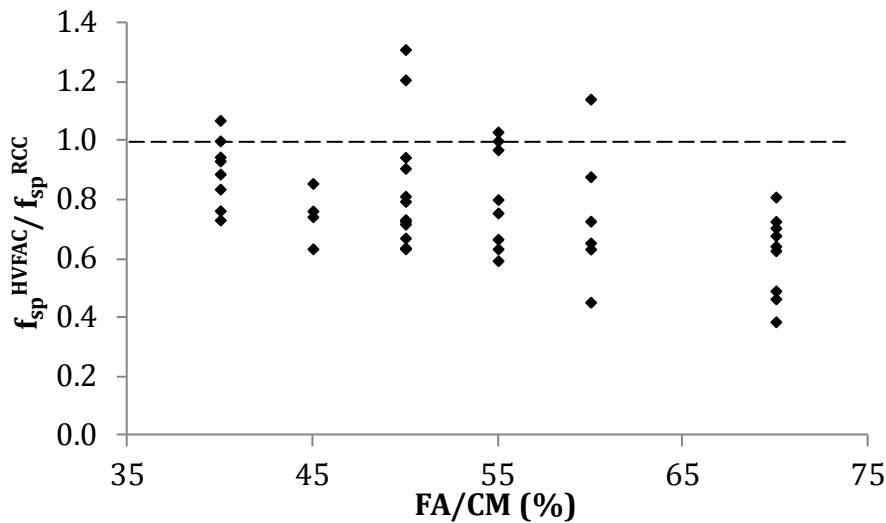


Figure 2.9 HVFAC and RCC splitting tensile strength ratio versus FA amount (Atis 2003a, 2005; Bouzoubaâ et al. 2001; Dinakar et al. 2013; Kou and Poon 2013; Lam et al. 1998; Nath 2010; Şahmaran et al. 2009; Siddique 2004)

Time-dependent behavior of concrete is significantly influenced by creep and shrinkage. Available results regarding shrinkage of HVFAC are very limited, leading to opposite conclusions drawn by different researchers. As it is already mentioned, depending on the FA amount and type, HVFAC needs less water for a certain workability compared with RCC, less cement and higher paste density which results in lower HVFAC shrinkage (Atis 2003a; Dragaš et al. 2016; Malhotra and Mehta 2005; Quan and Kasami 2013; Zhao et al. 2015a). Atis (Atis 2003b) also concluded that HVFAC shrinkage is decreasing with FA increase in the mixture. Bouzoubaa and Lachemi (Bouzoubaa and Lachemi 2001), on the other hand, concluded that HVFAC made with 40% and 50% of FA in CM has similar shrinkage as RCC. And finally, there are also results showing that HVFAC shrinkage can be higher compared with RCC (Huang et al. 2013).

Available results regarding creep of HVFAC are very limited. Concrete creep is a complex property depending on many parameters. One of them is the time of loading. Compressive strength development of HVFAC is slower than that of RCC at early ages resulting in higher creep of HVFAC if loaded at the same time as RCC. On

2. Literature review

the other hand, if HVFAC and RCC are loaded at the same compressive strength, HVFAC will exhibit lower creep because of the higher compressive strength increase after 28 days. Lower creep of HVFAC is mostly a consequence of the lower cement amount (Dragaš et al. 2016; Huang et al. 2013; Wendner et al. 2015; Zhao et al. 2015b).

2.4.3. Durability of HVFAC

During the past few decades, durability of concrete has become one of the main issues in the concrete research area; however, durability of HVFAC remains questionable. Systematization of the existing experimental results followed by more research regarding HVFAC durability is necessary for its greater application in concrete construction. The most important durability properties of concrete are carbonation, freezing/thawing resistance, and resistance to chloride ingress.

One of the main reasons of concrete deterioration is the corrosion of reinforcement that can be caused by concrete carbonation. Namely, CO_2 from the atmosphere penetrates the concrete matrix and, in the presence of moisture, firstly reacts with available $\text{Ca}(\text{OH})_2$ in hydrated Portland cement and, after $\text{Ca}(\text{OH})_2$ has been depleted, with CSH (Peter et al. 2008). As a result, calcium carbonate (CaCO_3) is formed and deposited in concrete pores decreasing its porosity and reducing the alkalinity of concrete to a pH value below 9 (Borges et al. 2010; Pacheco Torgal et al. 2012). With such a low pH value reinforcement is not protected anymore and is likely to corrode (Villain et al. 2007). Carbonation resistance is usually determined by measuring the depth of the carbonation layer in concrete.

In HVFAC, the amount of available $\text{Ca}(\text{OH})_2$ is reduced because of the lower cement amount and its consumption in the pozzolanic reaction. Furthermore, CSH gel as a result of the pozzolanic reaction is more prone to carbonation compared with CSH gel from cement hydration (Thomas et al. 2004). In this way, the CSH gel in HVFAC will be easily carbonated. However, contradicting results regarding the carbonation resistance of HVFAC compared with RCC can be found in literature (Wesche 2004). Some research shows that HVFAC made with 50% of FA can have a 2–3 times greater carbonation coefficient compared with cement concrete (Khunthongkeaw et al. 2006). Other authors also concluded that there is a

2. Literature review

significant increase of HVFAC carbonation (Sulapha et al. 2003) compared with RCC, and that it increases with the increase of FA amount (Jiang et al. 2000; Papadakis 2000b; Sisomphon and Franke 2007). On the other hand, Atis (Atis 2003b) concluded that HVFAC made with 50% and 70% of class F FA has similar or even lower carbonation compared with cement concrete.

The amount of entrained air along with the aggregate frost resistance and compressive strength are parameters having the greatest influence on concrete freezing/thawing resistance. Lower air content and slower strength development of HVFAC cause this concrete to have lower resistance to freezing/thawing compared with RCC. However, the entrained air amount can be sufficiently increased by using air-entraining agents. Improving the air-void system along with adequate curing and strength gain of HVFAC before concrete exposure to freezing/thawing can improve its resistance. In this way, HVFAC can achieve similar resistance to freezing/thawing as RCC (Malhotra 1990).

Lower permeability and porosity of HVFAC increases the chloride binding capacity and level of critical chloride content (Choi et al. 2006; Liang et al. 2010; Thomas and Bamforth 1999; Vasco et al. 2015). Because of that, HVFAC resistance to chloride ingress is increased compared with RCC. Furthermore, the FA amount increase results in the further increase in the resistance to chloride ingress (Dhir et al. 1997). One of the reasons influencing better chloride binding capacity of HVFAC is the high alumina amount in FA (Dhir and Jones 1999) resulting in an increased formation of Friedel's salt (Dhir et al. 1997). Besides, increased CSH gel formation caused by the pozzolanic reaction makes the structure denser enabling better physical absorption of chlorides (Kayyali and Haque 1988).

2.5. EXISTING REGULATIONS ON THE USE OF FLY ASH IN CONCRETE

CMs, especially FA, have been used in concrete for the past few decades. As a result, most countries have already adopted standards defining FA properties for use in concrete. The most commonly used standards are the already mentioned American ASTM C618 (ASTM C618 2015) and European standards EN 450-1 (CEN 2012) and EN 450-2 (CEN 2005). The most important parameters defined in these

2. Literature review

standards were shown previously in Table 2.2. The North American standards for concrete do not prohibit the use of HVFAC, except when the concrete is exposed to deicing salts, in which case the amount of FA is limited to 25% by mass of total CM (ACI 2014). In the most recent European codes for structural concrete, Model Code 2010, “concrete with a high content of FA” is mentioned along with a few recommendations for its behavior without any quantitative evaluation. According to those recommendations, concrete with high content of FA shows reduced compressive strength and modulus of elasticity in the early age but a considerable further gain at higher ages, lower creep and shrinkage due to lower cement amount and higher density of the matrix.

The European standard for concrete specification and performance EN 206-1 (CEN 2011b) includes the use of type II additions, such as FA, as a part of CM and defines three methods for the use of FA in concrete in order to insure its durability:

- k-value concept;
- principles of the equivalent performance concepts;
- equivalent performance of combinations concept.

The k-value concept is a prescriptive concept used to assess the influence of additions (FA) on the compressive strength of concrete. The EN 206-1 standard (CEN 2011b) defines requirements with regard to the W/CM ratio, the minimum cement content, and strength classes for different environmental conditions. The use of the W/CM ratio in predicting the compressive strength and durability properties in FA concrete is not straightforward. Therefore, the W/CM ratio is replaced with the effective ratio as $W/(C+k \cdot FA)$. The k-value concept is based on the compressive strength as a proxy-criterion for durability assessment. The value of the k factor is defined as 0.4 for cement types CEM I and CEM II/A conforming to the EN 197-1 (CEN 2011a) and the maximum amount of FA that can be taken into account as CM is limited to (CEN 2011b):

- $FA/cement \leq 0.33$ by mass, for the use with CEM I cement;
- $FA/cement \leq 0.25$ by mass, for the use with CEM II/A cement.

2. Literature review

The type of cement, the maximum FA amount and the value for k factor vary widely in the national regulations of different countries, from the use of only CEM I to the use of all cement types and with the k factor varying from 0.2 to 0.8 (CEN 2014).

It is important to emphasize that the k factor prescribed by EN 206-1 (CEN 2011b) does not provide any information about the effective performance of FA, as it is often mentioned in literature. The results from the literature indicate that the value for the k factor given in EN 206-1 (CEN 2011b), equal to 0.4, underestimates the contribution of FA to the mechanical properties of concrete (Dragaš et al. 2016; Kuder et al. 2012). This value is in fact a conservative prediction, derived by taking into account a certain safety margin and based on the results of concrete mixtures with different cements and more than 30 different FA types (all mixtures contained 20% of FA in total CM), (CEN 2014). However, some researchers attempted to determine the k factor for FA with regard to different degradation mechanisms (Aponte et al. 2012; Papadakis and Tsimas 2005).

Having in mind the variety of different FA properties and all parameters influencing FA efficiency regarding the compressive strength and durability properties, the question is whether a k-value concept could be universally applicable. The equivalent performance concept and the equivalent performance of combinations concept seem to be more suitable for FA concrete, especially for HVFAC design. The application of the equivalent performance concept requires experimental testing and confirmation that the concrete made with FA has the same performance as RCC regarding its durability properties for the relevant exposure class (CEN 2011b). The equivalent performance of combinations concept evaluates FA concrete by comparing the performance of the combination of cement and additions with the performance of standard cement of the same nominal composition (CEN 2011b). However, both of these concepts require experimental work and extensive testing in designing the concrete mixture, and are time and cost-consuming for practical applications.

2. Literature review

Relationships between various properties of concrete, their development over time as well as creep and shrinkage defined in the European standard EN 1992-1-1 (CEN 2004) for cement concrete need modification for application in HVFAC.

2.6. STRUCTURAL APPLICATIONS OF HVFAC

A large amount of research has been done regarding the physical and mechanical properties of HVFAC and in addition, work was also done on the evaluation of its material properties through the standards for cement concrete. The next step towards greater practical use of HVFAC is an extensive experimental evaluation of HVFAC's structural behavior. Available research carried out so far was focused on the bond strength, the flexural and the shear strength of HVFAC beams made with class F and class C FA.

2.6.1. Bond strength of reinforcing steel in HVFAC

Good bond action between concrete and steel reinforcement is a fundamental prerequisite for RC structures. There are only a few studies on the HVFAC bond strength evaluation, mostly via pull-out tests and beam splice tests with or without confinement. The concrete bond strength is mainly influenced by its compressive and tensile strength, leading to a conclusion that the bond can be lower at early ages in HVFAC compared with RCC, having in mind the previously mentioned slower compressive strength development. On the other hand, FA usually increases the paste volume in HVFAC which can improve its bond strength.

One of the first studies on the bond strength of HVFAC made with 70% of class C FA done by a pull-out test and a beam splice test was performed by Wolfe (2011). The results of these research were presented in one master thesis done by Wolfe (2011) and one journal paper (Arezoumandi et al. 2015). In the first part, this research consisted of extensive material testing developing a HVFAC mixture with satisfactory structural properties. As a result, the author developed the HVFAC mixture using 70% of FA with the addition of 4% gypsum and 10% calcium hydroxide to enable proper hydration. In the next stage, 12 pull-out samples and 12 full-scale beams were tested. The pull-out samples tested in this study were

2. Literature review

cylinder samples with a 300 mm diameter and a 200 mm height. The bars were embedded 5 times the bar diameter into the concrete. The beams had a rectangular section of 305·457 mm and the length of 4267 mm. The results of the pull-out test showed that both RCC and HVFAC samples failed by localized concrete crushing at similar normalized loads. Some differences in the RCC and HVFAC compressive strength were noticed and the author eliminated this effect by normalizing the applied load with the square root of the compressive strength. As reported, the initial slip occurred for both concrete mixtures at the similar load but once the concrete began to crush around the reinforcing bar, a slip occurred at a higher rate for the HVFAC specimens. The results of the beam splice test showed higher resistance of the HVFAC samples, before the splice failed, compared with the RCC. The analysis done by Wolfe (2011) was significant from the point of new experimental results addressing bond strength of HVFAC with 70% of FA. The conclusions obtained in this research were mostly based on the comparison between the RCC and HVFAC samples. The results showed similar or even superior behavior of the HVFAC samples compared with the RCC in terms of bond strength. These findings were valuable as one of the first ones indicating a good bond in HVFAC and encouraging its use in the RC structures. Perhaps an even more valuable conclusion was the one addressing the HVFAC behavior after failure and stressing that it was different compared with the RCC. A faster slip that occurred after the first surrounding concrete cracking can indicate lower tension softening in the HVFAC compared with the RCC. This issue needs to be addressed further.

Arezoumandi et al. (2015a) investigated the influence of the FA amount in CM on the HVFAC bond strength. In order to study the bond strength of reinforcing steel in HVFAC, nine pull-out samples and nine full-scale beams were tested. The pull-out samples tested in this study were cylinder samples with a 300 mm diameter. The bars were embedded 5 times the bar diameter into the concrete. To ensure a bond failure, the splice length was chosen as 70% of the development length. The beams had a rectangular section of 300·460 mm and the length of 3000 mm with a splice in the longitudinal steel centered at mid-span. The HVFAC samples with 50% and 70% of class C FA were designed with the addition of around 4% of gypsum

2. Literature review

and 10% of calcium hydroxide. The obtained compressive strengths of the RCC and HVFAC mixtures were not equal so the test results were normalized with both the square root and the fourth root of the compressive strength. The authors concluded that in terms of the load-slip behavior, both types of HVFAC samples showed similar load-slip behavior to the RCC samples. No clear correlation between the FA amount and bond behavior was obtained. It appeared that the bond strength obtained in the pull-out test was higher in HVFAC made with 50% of FA. The results of the splice beam tests showed that the load-deflection behavior of the HVFAC was similar to the RCC beams with similar crack patterns and failure types observed for the HVFAC and RCC beams. The authors also concluded that the HVFAC beams had higher average longitudinal reinforcement steel stress, up to 30%, compared with the RCC beams. It should also be noted that the pull-out samples experience bond shear failure, while all of the splice beam specimens failed in bond experiencing a splitting failure.

One of the most recent research analyzing the HVFAC bond strength was conducted by Zhao et al. (2016). In their research, 189 pull-out RCC and HVFAC samples were tested. The main experimental variables included the W/CM ratio, the FA amount and the type and the diameter of the reinforcing bar. All samples in this study were designed as cubic samples with the dimensions of 150·150·150 mm. Concrete mixtures were made with 0, 10, 20, 30, 40, 50, 60 and 70% of FA; 0.8-1.5% of lime and three different W/CM ratios of 0.3, 0.34 and 0.41. Based on the obtained results, the authors concluded that the concrete compressive strength had a significant influence on the bond strength especially for HVFAC with more than 50% of FA in CM. They also concluded that the increase of the compressive strength and the decrease of the W/CM ratio for the concrete with the same FA amount had a positive effect on the bond strength. When compared with the RCC samples, the bond strength in FA concrete decreased with the increase of FA.

A clear conclusion regarding the HVFAC bond strength cannot be made based on the available research found in the literature. Special attention should be paid to the bond strength when full-scale beams are tested because of the possibility of different behavior of HVFAC after the slip. Therefore, the HVFAC bond strength

2. Literature review

research ought to be continued in order to obtain further understanding of this problem. Additional research regarding bond strength tests on beam samples is necessary for future safe use of HVFAC as structural concrete.

2.6.2. Flexural behavior of HVFAC beams

Flexural behavior of RCC and HVFAC beams was investigated in a small number of studies found in the literature (Arezoumandi et al. 2015b; Putte Gowda B. et al. 2013; Srinivas and Rao 2015; Thangaraj and Thenmozhi 2016; Yoo et al. 2015). The researchers investigated the flexural strength of HVFAC beams made with 35% to 70% of class C or class F FA in CM mass. In all studies, the simply supported beams were tested in a four point bending test except one research with a three point bending test (Yoo et al. 2015). All studies had RCC beams made with the same W/CM ratio or the same designed compressive strength. HVFAC mixtures were made with 96.0 to 516 kg/m³ of CM, W/CM ratio from 0.30 to 0.48 and maximal aggregate size from 12.5 mm to 25 mm. The compressive strength measured on a cylinder sample was in the range of 8.1–58.4 MPa. The width of the beams cross section was in the range from 100 mm to 300 mm and the beams height in the range from 150 mm to 460 mm. The beams length was in the range from 1300 mm to 3600 mm and the longitudinal reinforcement ratio in the range from 0.79% to 3.18%.

One of the first available research regarding the flexural behavior of FA concrete beams was done by Gowda et al. (Putte Gowda B. et al. 2013). The aim of their research was to analyze the flexural behavior of the FA concrete beams made with the target compressive strength of 40 MPa. Their study consisted of three RCC beams and six FA concrete beams made with 20% and 35% of class F FA in CM. All beams had a rectangular cross section with the width of 125 mm, height of 250 mm and length of 1700 mm. All nine beams were divided in three groups according to the longitudinal reinforcement ratio: 0.988%, 1.772% and 2.512%. As reported, all beams were cured for 28 days and tested at that age. During the beams testing, the load-deflection behavior, ultimate load, short term deflections and crack width at the service load were measured and analyzed. The results

2. Literature review

showed no significant difference between different concrete types and the obtained concrete compressive strengths and ultimate flexural strength. On the other hand, it was noticed that the first flexural cracks appeared at the lower load level in FA concrete beams compared with the RCC beams. Also, higher ultimate deflection was reported in FA concrete beams compared with the RCC beams. The ductility of the beams was also evaluated and it was concluded that the beams made with the FA concrete expressed higher ductility compared with the RCC beams in most cases. The development of cracks was also monitored in this study and the results showed generally higher crack widths both at the service load level and the ultimate load level in FA concrete beams compared with the RCC beams. The comparison of the obtained flexural strength and the predictions defined in different standards like ACI 318 and EN 1992-1-1 (ACI Committee 318 2014; CEN 2004) was also done. The authors concluded that there were no significant differences between the application of previously mentioned standards on the RCC and the FA concrete flexural strengths determination.

Thangaraj and Thenmozhi (Thangaraj and Thenmozhi 2016) conducted the research analyzing the flexural behavior of RCC and HVFAC beams made with 50%, 55% and 60% of class F FA. All beams had a rectangular cross section and the width of 100 mm, height of 150 mm, length of 1300 mm and the longitudinal reinforcement ratio of 0.84%. All beams were cured for 28 days and tested at approximately that age. Two types of beams were tested. In the first group of beams no confinement of the compressed zone in the middle part of the beams was used. In the second group of beams, two types of compressed zone confinement of stirrups hoops were used. The authors concluded that the additional confinement increased the beams ductility as expected. The comparison of the HVFAC beams flexural strength and the RCC beams could not be done properly due to the fact that the corresponding beams did not have the same or similar compressive strength. The reason for that lies in the fact that the authors designed their research to compare the influence of the compressive zone confinement and not the different FA amount in concrete. It can generally be concluded that the HVFAC

2. Literature review

beams with 50% of FA in CM had higher flexural strength and ultimate deflection compared with the RCC beams with similar compressive strength.

Arezoumandi et al. (2015b) conducted the experimental research to analyze the flexural strength of full-scale RCC and HVFAC beams made with 70% of class C FA, 3% of gypsum and 6% of calcium hydroxide in CM mass. The experimental cracking, yielding, flexural strength and deflection at the ultimate loading were analyzed and compared with both the ACI 318 and EN 1992-1-1 code provisions (ACI Committee 318 2014; CEN 2004). The authors also evaluated the possibility of the modified compression field theory application of the HVFAC beams. All six beams had a rectangular cross section with a width of 300 mm; height of 460 mm; length of 4270 mm and longitudinal reinforcement ratio of 1.4%. The beams were cured for 7 days and tested at the age of 28 days. The authors reported that the ductile failure in all beams occurred after the longitudinal reinforcement yielding and compressed concrete crushing. The presented results indicated that there were no significant differences between the load-deflection curves, crack patterns and propagation, yielding moment, ultimate beam's deflection and the ultimate flexural strengths in the RCC and the HVFAC beams. It should be noted that there was a significant difference between the obtained compressive strengths in RCC and HVFAC beams, with the HVFAC beam having up to 30% lower compressive strength at the time of testing. On the other hand, the obtained splitting tensile strengths and modulus of elasticity were, on average, 10% and 3% higher compared with the RCC values respectively. The authors also concluded that there were no significant differences between the previously mentioned code provisions when applied to the RCC and HVFAC beams flexural strength determination.

The flexural behavior of the RCC and HVFAC beams designed with 35% and 50% of class F FA was tested by Yoo et al. (Yoo et al. 2015). The authors presented the results of a series of tests conducted on RC beams with various longitudinal reinforcement ratios and concrete compressive strengths to evaluate their flexural behavior. The evaluation was done in a three point bending test on 3300 mm long beams (cross section of 200·300 mm), on three different strength classes (20 MPa, 40 MPa and 60 MPa) and the longitudinal reinforcement ratio ranging from 0.79%

2. Literature review

to 3.18%. The authors concluded that the structural behavior of HVFAC beams was similar to that of RCC beams in terms of the deflection, first crack load, yield load, ultimate load, and load-deflection relationships of the beams. An average value of HVFAC and RCC ultimate strength ratio was 1.04. It should be noted that in the place of maximum bending moment shear stresses also exist, having in mind the three point bending test that was conducted in this study.

In all available studies, the testing of all beams was done at the age of 28 days. This is common for OPCC practice having in mind the development of the OPCC strength. On the other hand, in HVFAC beams the increase of strength over time is different with lower early age strength but a significant increase even after 28 days, as already mentioned. Providing the same compressive strength at the age of testing is the most important, but for the HVFAC beams, testing at the age of 90 days would be more appropriate. In this way, the biggest part of the ultimate compressive strength would be achieved in both OPCC and HVFAC beams. This modification would be in accordance with the current construction practice. Considering the dynamics of the current building construction, the total load is not being applied on the structure before the age of 90 days.

The selection of all available studies regarding FA concrete beams yielded only 12 HVFAC beams ($FA/CM \geq 0.5$) that were tested for flexural behavior. This small number is insufficient for any general conclusions, especially having in mind the variety of FA properties. More research on HVFAC flexural behavior is needed to get the full understanding of this phenomenon. Nevertheless, the previously presented results indicate that the ultimate flexural strength of RCC and HVFAC beams is not significantly different. On the other hand, the presented results did not provide enough conclusions regarding the HVFAC beams flexural crack propagation and the maximum width and length compared with the RCC beams. No clear conclusions regarding moment of the first flexural crack appearance and the beams' short-term deflection could be made based on the available results found in the literature.

2. Literature review

2.6.3. Shear behavior of HVFAC beams

Only a few research investigating the shear strength of HVFAC beams was found in the literature (Alghazali and Myers 2017; Arezoumandi et al. 2013c, 2015c; Arezoumandi and Volz 2013; Lisantono et al. 2017; Ortega 2012; Rao et al. 2011; Sadati et al. 2016). These researches investigated the shear strength of the HVFAC beams made with 50% to 70% of class C or class F FA in CM mass. In all studies, the simply supported beams were tested in a four point bending test. The HVFAC mixtures were made with 284.6 to 502 kg/m³ of CM, W/CM ratio from 0.32 to 0.62 and maximal aggregate size from 16 mm to 20 mm. The compressive strength measured on a cylinder sample was in the range of 11.7–54.8 MPa. The shear span-to-depth ratio of beams was ranging from 2.57 to 4.16 and the longitudinal reinforcement ratio from 0.58% to 4.50%. Collected results included both beams without shear reinforcement and beams with shear reinforcement ranging from 0.141% to 0.368%.

One of the first available research analyzing the shear behavior of FA concrete beams was done by Rao et al. (Rao et al. 2011). The aim of their research was to analyze the shear behavior of RCC and HVFAC beams without shear reinforcement made with different reinforcement ratios: 0.5%, 1.0%, 2.0% and 2.94%. Their study consisted of four RCC beams and four HVFAC beams made with 50% of class F FA in CM. All beams had a rectangular cross section with the width of 100 mm, height of 200 mm and the length of 1300 mm. No data regarding the beams' curing type and duration was reported. All beams were tested at the age of approximately 28 days. During the beams testing, the ultimate shear strength, the longitudinal reinforcement strains and the crack propagation were measured. The obtained compressive strengths of the HVFAC samples were around 30% lower compared with the RCC samples. The authors did not present any analyses regarding the RCC and HVFAC beams shear behavior that could provide valid conclusions. Nevertheless, these results showed up to 15% lower ultimate shear strengths of the HVFAC beams compared with the RCC when normalization of the compressive strength was done.

2. Literature review

The most extensive experimental research investigating the HVFAC shear strength was conducted by Ortega (Ortega 2012). The experimental program consisted of 36 full-scale RCC and HVFAC beams. During this research, the author investigated the influence of the concrete type, the amount of shear reinforcement and the amount of longitudinal reinforcement on the shear strength of beams. The beams were analyzed using the standard truss model, modified compression field theory and fracture mechanics formulations. For shear behavior testing, seven groups of beams with different amounts of longitudinal reinforcement were tested, four groups consisted of beams without stirrups, two groups consisted of beams with stirrups spaced at 178 mm (transverse reinforcement ratio of 0.262%) and beams with stirrups spaced at 127 mm (transverse reinforcement ratio of 0.368%). All beams had a rectangular cross section with the width of 305 mm; height of 457 mm; length of 3600 mm and shear span-to-depth ratios of three or greater. The beams were divided in four groups regarding the longitudinal reinforcement ratio: 1.59%, 2.03%, 2.71% and 4.50%. The HVFAC mixtures were made with 70% of class C FA, 3% of gypsum and 7% of calcium hydroxide in CM. All beams were moist cured for three days and after that air cured until testing at the age of approximately 28 days. During this research, the following measurements were conducted: strains in longitudinal reinforcement and stirrups, concrete strains in the beams' web and vertical deflection of the beams. Besides the full-scale tastings, a big number of small scale testing was performed to determine the hardened properties of the RCC and HVFAC mixtures used in this study. These tests included the compressive strength, splitting tensile strength, flexural strength, modulus of elasticity and thirty two tests performed on small scale beams to determine the fracture energy and other fracture parameters of both RCC and HVFAC mixtures. The fracture energy properties were tested on prismatic samples (150·150·600 mm) in three point bending tests with different notch sizes. The fracture behavior was characterized by the phenomenon of damage localization. The author explained in detail how all the groups of beams behaved under the shear loading stressing the beams' failure mode. Three beams out of all tested beams expressed flexure failure.

2. Literature review

Based on the concrete properties testing results, the author concluded that the HVFAC compressive strength values were lower than those of the RCC, but all other mechanical properties that were being tested were comparable to the results observed on the RCC samples. Independently of the concrete type, the author concluded that the HVFAC had fracture energy comparable to that of the RCC.

It was also concluded that there was a greater degree of concrete compression softening for HVFAC as a result of differences in the cementitious matrix. The author gave two possible explanations for this phenomenon: the HVFAC may exhibit a higher degree of micro cracking compared with the RCC; the dynamic modulus of elasticity for HVFAC is lower than predicted for the RCC of the same compressive strength.

The obtained results regarding the RCC and HVFAC beams testing showed no significant difference in the behavior and normalized shear strengths between these two types of concrete. During the full-scale testing, a difference in the sound produced by the failure of the RCC and HVFAC specimens was noticed. At failure, the RCC beams produced a very loud noise, while the HVFAC beams made a very soft, almost inaudible noise, as explained by the author. The author explained this effect as the result of the concrete compression softening. Based on the various code provision evaluation analyses, it was concluded that the HVFAC and RCC beams exhibited the same trend during the evaluation.

Previously presented experimental research done by Ortega (Ortega 2012) was very valuable as one of the first addressing the HVFAC shear behavior, especially to this extent. The most important conclusion that motivates further research is the possibility of concrete compression softening in HVFAC that needs to be addressed further. It should be noted that this research was done using class C FA with the addition of gypsum and calcium hydroxide leaving the question if these conclusions can be applied for class F HVFAC beams as well.

The research conducted by Ortega (Ortega 2012) was, obviously, the beginning of the HVFAC shear strength research conducted by the group of researchers employed at the Missouri University of Science and Technology. More research of the class C HVFAC beams shear strength was done by this group (Arezoumandi et

2. Literature review

al. 2013a, 2015c, Arezoumandi and Volz 2013, 2014). Arezoumandi and Volz (2014) conducted an experimental investigation to study the shear strength of full-scale SCC beams made with OPCC and FA concrete with 25% of class C FA in CM. This experimental program consisted of 12 beams without stirrups with three different longitudinal reinforcement ratios: 1.27%, 2.03% and 2.71%. The beams geometry, dimensions and the curing procedure were the same as described before in Ortega (Ortega 2012). The authors concluded that, in terms of crack morphology, crack progression, and load-deflection response, the behavior of the SCC and RCC beams was virtually identical. They also concluded that the obtained results were in good correlation with the existing code provision defining SCC and beams' shear behavior.

In another study, Arezoumandi et al. (2013b) investigated the influence of different class C FA amount in HVFAC mixtures on the shear behavior of beams tested in the four point bending test. Eighteen beams were constructed for the study, six RCC beams, six HVFAC beams made with 50% of FA and six HVFAC beams with 70% of FA in CM. The beams' geometry, dimensions, curing procedure and longitudinal reinforcement ratio were the same as described before in Ortega (Ortega 2012). All of the beams failed in shear. Similar compressive strengths were obtained in RCC and HVFAC made with 50% of FA. Approximately 50% lower compressive strength was obtained in HVFAC mixtures made with 70% of FA. Based on the presented results, the author concluded that, in terms of crack morphology and crack progression, the behavior of the RCC and both types of HVFAC beams was virtually identical. It was also noticed that in terms of load-deflection behavior the general behavior of the three concrete types was very similar. However, the HVFAC beams made with 70% of FA indicated earlier flexural cracking and lower peak load and deflection at failure. It should be noted that the load-deflection curves were plotted with the actual load and not the normalized value of shear stress. This was probably the reason for different load-deflection behavior expressed in the HVFAC beams made with 70% of FA.

One of the most recent studies investigating the HVFAC beams shear behavior was done by Lisantono et al. (Lisantono et al. 2017). In their research, Lisantono et al.

2. Literature review

(Lisantonio et al. 2017) investigated the shear behavior of eight RCC and HVFAC beams made with 50%, 60% and 70% of FA in CM. The tested beams had the rectangular cross section of 150·260 mm, the effective length of 2300 mm and longitudinal reinforcement ratio of 1.0%. The curing regime of beams was not specified and all the beams were tested at the age of 28 days. The obtained compressive strength was significantly lower in HVFAC mixtures compared with the RCC: 25%, 28% and 45% for HVFAC with 50%, 60% and 70% of FA respectively. The normalization of the shear stresses was not done and the comparison of the obtained results regarding HVFAC and RCC beams could not be done properly.

An experimental study was carried out by Alghazali and Myers (Alghazali and Myers 2017) to investigate the shear behavior of full-scale beams constructed with SCC made with 50% , 60% and 70% of class C FA in CM. There were no RCC beams made in this study. Twelve full-scale RC beams were casted and tested in order to analyze the influence of the FA amount, longitudinal reinforcement ratio and shear reinforcement ratio on the beams' shear behavior. All beams were 4000 mm in length, 457 mm in height and 305 mm in width. All beams were cured for three days and tested at approximately 28 days. The beams were divided in four groups regarding the FA amount and the each group consisted of three beams without shear reinforcement and one beam with 2.71% of longitudinal reinforcement and 0.262% of shear reinforcement. The beams without shear reinforcement had the longitudinal reinforcement of 1.59%, 2.03% and 2.71%. The obtained compressive strengths were similar in the HVFAC mixtures made with 50% and 60% of FA but 15% lower in the HVFAC mixture made with 60% of FA. In order to compare the behavior of the OPCC and the HVFAC beams, the authors used the results obtained by Ortega (Ortega 2012) and selected the four beams made with OPCC to use for comparison in this study. The average concrete compressive strength of these beams was approximately 35% higher compared with the compressive strengths obtained on HVFAC mixtures made in this study. This difference was in some way eliminated by the normalization of the shear stress that was done during the analysis. However, concretes made and tested by Ortega (Ortega 2012) were not

2. Literature review

SCC so the question of this influence on the conclusion obtained by Alghazali and Myers (Alghazali and Myers 2017) remained unanswered. Based on the obtained results regarding the tested HVFAC mixtures, the authors concluded that no significant difference between the normalized shear stress at the first cracking and at failure was noticed between different HVFAC beams with the same longitudinal reinforcement ratio. For the beams with shear reinforcement, the ductility increased with the increase of the FA amount by 35% for the increase from 50% to 70% of FA. It was also noticed that the HVFAC beams with 70% of FA experienced higher deflection and more cracks compared with the beams with 50% and 60% of FA. No clear conclusion regarding the HVFAC compared with the RCC behavior of beams could be made based on the results presented in study done by Alghazali and Myers (Alghazali and Myers 2017).

The selection of all available studies regarding the HVFAC beams yielded 21 beams without and 16 beams made with shear reinforcement that were tested for shear behavior. Having in mind a complex shear transfer mechanism in beams, many more beams needs to be tested in order get the full understanding of this phenomena. Nevertheless, the results presented in the obtained studies indicate that the ultimate shear strength of the RCC and HVFAC beams is not significantly different. On the other hand, more research is needed in order to evaluate the concrete compression softening for HVFAC beams. After reviewing the existing literature, it was clear that there was a lack of full-scale structural elements testing of HVFAC, especially made with class F FA. Without this background, there is no quantitative basis for implementing safe implementation of HVFAC in structural design.

2.7. ENGINEERING APPLICATIONS OF HVFAC

One of the first uses of HVFAC was in the construction of the Hungry Horse Dam in Montana finished in 1952 (ACI 2014), motivated by HVFAC's low heat of hydration temperature rise. Besides that, good workability of HVFAC was used as an advantage in roller-compacted concrete and in production of dams in the United States since the 1970s (Dunstan 1983). Since then, HVFAC was used in the

2. Literature review

construction of dams, foundation and retaining walls, marine slipways, sewage treatment works, concrete viaducts, and in buildings. Concrete mixtures and guidelines for HVFAC developed by the team of researchers at CANMENT (Malhotra and Mehta 2005) helped the promotion of HVFAC and its use in construction practice, especially in North America. Despite the fact that HVFAC is not yet defined in standards for concrete design, it has been used in concrete construction in many projects since 1985. One of the pioneers was the project Park Lane Hotel/Office Complex, Halifax, Canada built in 1988. During the construction of this building 55% of FA in total mass of CM was used in the construction of columns, beams, and floor slabs (Bouzoubâa and Fournier 2003). HVFAC was also used in the following projects:

- Lac Robertson Dam was made with 50% of FA in CM mass (Bouzoubâa and Fournier 2003);
- York University Computer Science Building in Toronto was made with 50% of FA in CM in concrete used for columns, walls, and suspended slabs and it had a specified strength of 25 MPa and 30 MPa (Hopkins et al. 2001);
- The Bayview (Vancouver, Canada) was built in 2002 with up to 55% of FA replacement achieved in all the footings;
- The Liu Centre for the Study of Global Issues, University of British Columbia (Vancouver, Canada) was built using concrete with 50% of FA in CM in all structural elements except exterior and precast slabs which were made with 33% of FA. The selected concrete mixture had early age strength after one day of 10 MPa reaching a 28-day compressive strength of 32 MPa and over 50 MPa after 90 days;
- The Nicola Valley Institute of Technology, University of the Cariboo (Merrit, British Columbia) built in 2001 using EcoSmart concrete design (Michel et al. 2001) and HVFAC made with 50% of FA in CM (Paterse 2008) for foundations and slabs;
- De Young Museum (San Francisco, California, United States) was made with HVFAC designed with 170 kg/m³ of cement and 170 kg/m³ of class F FA for the use in foundations, slabs, and beams (Malhotra and Mehta 2005);

2. Literature review

- Wurster Hall, University of California, Berkeley (United States) built in 2001 was made with 50% of FA concrete used in Wurster construction of piers and foundations (Malhotra and Mehta 2005).

Listed projects are only a part of all HVFAC possible applications. Reviewing the existing literature and available sources showed that HVFAC found its way into the construction sites but mostly as a part of foundations. After analyzing all advantages and disadvantages of HVFAC, the following reasons appear as the main obstacles for greater use of HVFAC:

- Inconsistency of FA characteristics;
- Lower early age strengths;
- Contradictions in results found in existing literature regarding physical, mechanical, and durability properties of HVFAC;
- Lack of results regarding full-scale structural elements made with HVFAC;
- Lack of adequate standards or amendments to the existing standard for concrete design;
- Poor durability of HVFAC exposed to carbonation.

In order to overcome these obstacles, a systematic analysis of available data is needed along with more experimental work to resolve contradicting results. The construction industry has always been conservative, so more experimental work regarding full-scale HVFAC structural elements and more in situ analyses are necessary.

2.8. THE ROLE OF FLY ASH IN SUSTAINABLE CONSTRUCTION

Over the past few decades, the development of energy and resource efficient technologies and products became a primary goal in a generally accepted principle around the world – sustainable development. The construction industry is no exception to this rule. It is responsible for 50% of the consumption of natural raw materials, 40% of the total energy consumption, and almost half of the total industrial waste generation (Oikonomou 2005). Concrete is the most widely used construction material today. It is estimated that roughly 25 billion tons of concrete are produced globally each year, or over 3.8 tons per person per year (WBCSD

2. Literature review

2009). Approximately one ton of the greenhouse gas CO₂ is released for each ton of Portland cement clinker produced (Bilodeau and Malhotra 2000), originating from the combustion of carbon-based fuels and the calcination of limestone. Because of that, the concrete industry is responsible for 7–8% of man-made CO₂ emissions, according to IPCC (IPCC 2005).

So far, a lot of effort has been put into finding sustainable solutions for concrete as a structural material. All of these efforts aim at the same environmental improvements: preservation of natural resources, lowering of CO₂ emissions, and decreasing the amount of generated waste. With FA as a partial replacement of cement in HVFAC or complete replacement of cement in alkali activated concrete, all these aims are accomplished: using waste instead of natural resources for concrete production, lowering CO₂ emissions from Portland cement production and decreasing the amount of deposited FA in landfills.

However, replacing virgin materials and cement with by-products or waste does not necessarily and directly lead to better environmental performance in the course of the concrete's life cycle. Any environmental assessment should be performed using a comprehensive, scientific-based approach. For that purpose, the well-recognized and standardized methodology of Life cycle assessment (LCA) is usually applied. It allows for evaluating the environmental impacts of processes and products during their life cycle. LCA is used according to the ISO 14040 standard (ISO 2006), which provides a framework, terminology and methodological phases of the assessment.

LCA studies performed on the environmental evaluation of HVFAC generally show that replacement of cement with FA reduces the environmental impacts of concrete (Celik et al. 2015; Van Den Heede and De Belie 2014; Teixeira et al. 2016). However, the LCA results depend on the system boundaries, whether an attributional or consequential approach is applied, on the chosen functional unit (FU), and whether lower carbonation resistance of HVFAC is taken into account or not.

In consequential modeling (Turk et al. 2015), allocation of FA is avoided by system expansion so it does not carry any upstream burdens into the model of concrete

2. Literature review

production. Besides, credits from the avoided waste landfilling are assigned to HVFAC. In the attributional approach, FA carries the allocated burdens from the electricity production and no avoided burdens are taken into account (Van Den Heede & De Belie 2014; Marinković et al. 2017; Teixeira et al. 2016; Celik et al. 2015). So the consequential approach is always beneficial for HVFAC in comparison to control cement concrete (concrete with the same compressive strength). In existing studies (Van Den Heede & De Belie 2014; Marinković et al. 2017), the FU reflected different carbonation resistance of HVFAC and control cement concrete.

If looking only at the global warming potential (GWP), all studies reported the reduction of this impact category in the case of HVFAC. No matter what modeling approach was applied, HVFAC had, on average, 25% lower GWP than control cement concrete. In studies where the FU include not only strength but also durability requirements, a slightly smaller GWP reduction was obtained, depending on the selected exposure class and duration of service life: 17% in Marinković et al. (Marinković et al. 2017) and 18–27% in Van Den Heede & De Belie (Van Den Heede and De Belie 2014). Therefore a significant GWP decrease is gained with HVFAC utilization.

2.9. CONCLUSIONS

Global tendencies for sustainable development had their influence on the construction industry as well. Regardless of sustainability, FA has been used in concrete for decades, because of its positive effects on some durability aspects and lower price. On its way from power plant landfills to concrete, FA overcame many obstacles, but there is still a long way until safe daily use in the construction industry is possible.

Despite the several decades-long use of FA in concrete, it is still a subject of much research. In the past years, a lot of studies have been dealing with the characterization of FA properties important for its use in concrete. A great variety of these properties made it difficult to draw general and unambiguous conclusions about its influence on concrete properties. Nevertheless, extensive results

2. Literature review

regarding different FA properties and its influence on physical and mechanical properties of concrete are available in literature and can be used as guidelines for further research. At this point, the heterogeneity of FA is still the main obstacle in the systematic analysis of FA's influence on concrete.

Promising results regarding the use of smaller amounts of FA in concrete encouraged the researchers to push the limits further by developing HVFAC. The tendency of using high amounts of FA in concrete is also motivated by sustainability and a need to use as much waste materials as possible. Studies on HVFAC have been focused on understanding and improving physical and mechanical properties of HVFAC through an extensive research mostly based on trial and error. Until now, depending on the type and amount of FA, HVFAC that possesses the following properties can be produced: good workability, low bleeding and segregation, lower air content, low heat of hydration, acceptable early age strength, good 28-day and high late compressive strengths, tensile strength and modulus of elasticity comparable with RCC, and lower creep and shrinkage. Durability of HVFAC is still a question that needs more research to be fully answered.

The analysis of available results regarding bond, flexural and shear strength of HVFAC beams was also done. Based on the collected results from the literature it was concluded that no significant difference between bond strength and flexural and shear behavior of HVFAC and RCC beams exists. These conclusions were obtained mostly on the HVFAC beams made with class C FA. More research regarding HVFAC made with class F FA is needed for general conclusions to be made. Based on the results from the literature no clear conclusions regarding flexural crack propagation and beams' deflection could be obtained. Furthermore, the HVFAC compression softening is also a parameter that needs more research to be fully defined.

Analysis done in this chapter imposes the conclusion that more research regarding HVFAC structural elements is necessary for its safe application in practice. Finally, the most important condition for an extensive use of HVFAC in the construction industry is the development of standards and guidelines for engineers that are still lacking.

3. FLEXURAL AND SHEAR STRENGTH OF REINFORCED CONCRETE BEAMS

3. Flexural and shear strength of reinforced concrete beams

3.1. INTRODUCTION

This section provides an overview of basic flexural and shear transfer mechanisms in RC beams. General assumptions and detailed design code provisions are also presented. During the design code evaluation the following standards were applied: Serbian standard for concrete and RC – Serbian Standard BAB '87 (Faculty of Civil Engineering 1995), European Standard EN 1992-1-1 (CEN 2004), *fib* Model Code 2010 (fib 2010a; b) and American Standard ACI 318 (ACI 2008).

3.2. FLEXURAL STRENGTH OF REINFORCED CONCRETE BEAMS

Classical beam theory provides a simple and accurate model for designing members to resist bending in combination with axial forces. The basic assumptions in the flexural design of RC beams and slabs are:

- Sections perpendicular to the axis of bending that are plane before bending remain plane after bending, i.e., strains in concrete and reinforcement are directly proportional to the distance from the neutral axis;
- The strain in reinforcement is equal to the strain in concrete – perfect bond between reinforcement and concrete exists;
- Concrete is assumed to not carry any tensile stresses;
- Stresses in concrete and reinforcement are defined using stress–strain curves for concrete and steel.

All these assumptions were applied and evaluated for HVFAC beams tested in this research. Own experimental testing of reinforcement and concrete bond was not conducted. However, based on results from literature (Arezoumandi et al. 2015; Wolfe 2011; Zhao et al. 2016), it was assumed that the bond between reinforcement and HVFAC is good and that the second assumption is valid. All tension reinforcement bars in tested beams were well anchored and the previous assumption was confirmed during beam testing. Ratio of tensile and compressive stress in HVFAC was the same as in OPCC and it was therefore reasonable to neglect the concrete tensile stresses. The same stress–strain curves were used for HVFAC as defined in different standards for OPCC.

3. Flexural and shear strength of reinforced concrete beams

3.3. CODE PROVISIONS – FLEXURAL BEHAVIOR OF REINFORCED CONCRETE BEAMS

This chapter describes the design provisions for evaluation of the flexural behavior of OPCC beams defined in the most widely used codes in practice, together with other significant design approaches. None of these provisions provide any recommendations for the flexural behavior of HVFAC members.

Standards that were analyzed in this section are: Serbian standard for concrete and RC – BAB '87 (Faculty of Civil Engineering 1995), European Standard EN 1992-1-1 (CEN 2004) and American Standard ACI 318 (ACI 2008). The flexural strength of RC beams was calculated using the equilibrium conditions differing only in the stress–strain relationship for concrete that was being used. For calculations based on the BAB '87 and EN 1992-1-1 standards, a parabola–rectangle diagram was chosen for the concrete stress–strain relation whereas for the reinforcement steel, transformed bi-linear stress–strain relation with a horizontal top branch was selected. Maximum concrete strain was 3.5‰, as defined in the standards. A constant stress distribution along the compressed concrete zone with a maximum concrete strain of 3‰ was used in ACI 318. Parameters defining the flexural behavior of RC beams analyzed in this study are the beams' flexural strength and cracking moment. The ultimate flexural strength of RC beams was also calculated using the modified compression field theory approach using the Response–2000 program.

3.3.1. Cracking moment

Cracking moment is the flexural moment under which first flexural cracks form. It is defined in a similar way in all analyzed standards as a product of flexural tensile strength and section modulus of a beam's cross-section. The differences between standards are expressed in different flexural strength or section modulus calculations.

Serbian standard for concrete and reinforced concrete – BAB '87 (Faculty of Civil Engineering 1995) defines the cracking moment as a product of flexural tensile strength and section modulus of transformed cross-section:

3. Flexural and shear strength of reinforced concrete beams

$$M_{cr} = f_{ct,fl} \cdot W_i \quad \text{Eq. 3.1}$$

where:

$f_{ct,fl}$ flexural tensile strength;

W_i section modulus of transformed cross-section.

Flexural tensile strength can be determined in different ways. Measured values of flexural tensile strength can be obtained in three-point bending tests according to standards. Flexural tensile strength is also defined as a function of the concrete compressive strength or concrete splitting tensile strength according to the following expressions:

$$f_{ct,fl} = f_{ct} \cdot \left(0.6 + \frac{0.4}{\sqrt[3]{d}} \right) \quad \text{Eq. 3.2}$$

$$f_{ct} = 0.25 \cdot f_c^{2/3} \quad \text{Eq. 3.3}$$

$$f_{ct} = 0.9 \cdot f_{ct,sp} \quad \text{Eq. 3.4}$$

where:

f_c concrete compressive strength determined on a cubic sample (200 · 200 · 200 mm);

f_{ct} concrete axial tensile strength;

$f_{ct,sp}$ concrete splitting tensile strength;

$f_{ct,fl}$ concrete flexural tensile strength.

The section modulus used in this standard takes into account the cross-section of concrete and longitudinal tensile reinforcement, i.e., the transformed cross-section.

Cracking bending moment can be calculated based on EN 1992-1-1 (CEN 2004) for RC elements without axial tensile stresses by using the following equation:

$$M_{cr} = f_{ct,fl} \cdot W_{c,1} \quad \text{Eq. 3.5}$$

where:

$W_{c,1}$ gross section modulus of a concrete cross-section.

3. Flexural and shear strength of reinforced concrete beams

The mean flexural tensile strength of RC members depends on the mean axial tensile strength and the cross-section depth:

$$f_{ctm,fl} = \max\{(1.6 - h/1000) \cdot f_{ctm}, f_{ctm}\} \quad \text{Eq. 3.6}$$

$$f_{ctm} = 0.30 \cdot f_c^{2/3} \quad \text{Eq. 3.7}$$

$$f_{ctm} = 0.9 \cdot f_{ct,sp} \quad \text{Eq. 3.8}$$

where:

f_c concrete compressive strength determined on a standard cylinder sample (150 · 300 mm);

f_{ctm} mean value of concrete axial tensile strength.

The section modulus used in this standard takes into account only the cross-section of concrete.

American standard ACI 318 (ACI 2008) defines the cracking moment as

$$M_{cr} = f_r \cdot W_c \quad \text{Eq. 3.9}$$

where:

f_r modulus of rupture (concrete flexural tensile strength);

W_c gross section modulus of a concrete cross-section.

The modulus of rupture is defined by the following expression:

$$f_r = 0.62 \cdot \sqrt{f_c'} \quad \text{Eq. 3.10}$$

where:

f_c' concrete compressive strength determined on a cylindrical sample (100 · 200 mm).

Splitting tensile strength of normal weight aggregate concrete can be calculated using the following equation:

$$f_{ct} = 0.56 \cdot \sqrt{f_c'} \quad \text{Eq. 3.11}$$

3. Flexural and shear strength of reinforced concrete beams

3.3.2. Modified compression field theory program Response–2000

The program Response–2000 is a sectional analysis program that calculates the strength and ductility of an RC cross-section subjected to shear, bending, and axial load using a layered section analysis approach. All three loads are considered simultaneously to find the full load-deformation response using the modified compression field theory. The program was developed at the University of Toronto by Evan Bentz as a part of his PhD thesis (Bentz 2000) in a project supervised by Professor Michael P. Collins.

The following assumptions are made in Response–2000:

- Plane sections remain plane;
- There is no significant transverse clamping stress acting through the depth of the beam;
- The modified compression field theory can be used for biaxial stress–strain behavior throughout the depth of the beam.

Using these three assumptions, a fiber model sectional analysis is extended to include the effects of shear (Bentz 2000). During calculations using Response–2000 concrete the *Popovics, Thorenfeldt and Collins* stress–strain curve was selected (Collins and Mitchell 1991).

3.4. SHEAR STRENGTH OF REINFORCED CONCRETE BEAMS

3.4.1. Basic shear transfer mechanisms

Extensive research on RC structures' flexural behavior followed with fundamental theoretical background led to a full understanding of flexural failure mechanisms. Structural RC elements that are exposed to transverse loading are subjected to both flexural and shear stresses. Unlike flexural behavior, RC structures' shear behavior is still being extensively analyzed in order to fully quantitatively explain it. Shear failure is still difficult to explain accurately in spite of more than 100 years of research. Even though a consensus on the exact definition of shear failure does not exist yet, a commonly accepted explanation is that shear failure is a brittle

3. Flexural and shear strength of reinforced concrete beams

failure occurring when diagonal cracks develop in the shear span (Sarkhosh 2014). For RC beams, shear failure stands for more different types of failure.

In beams with flexural reinforcement and without shear reinforcement, diagonal tension stresses are created close to supports causing diagonal cracks to appear in those zones. Failure occurs suddenly and shortly after the formation of diagonal cracks. Diagonal cracks are typically divided into two types (Figure 3.1) web-shear cracks and flexure-shear cracks (Nilson et al. 2010).

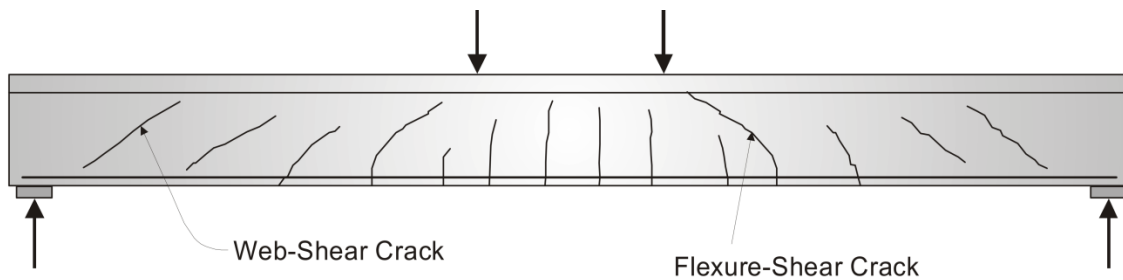


Figure 3.1 a) Web -shear cracking and flexure-shear cracking (Hawkins et al. 2005)

Shear transfer in un-cracked RC structures is mostly influenced by concrete properties—its tensile and compressive strength—and it is usually not ductile. Different shear failures in beams without shear reinforcement are related to different shear span-to-effective depth ratios (a/d) as proposed by Kani (Kani 1964). Kani conducted a large experimental study on the shear behavior of RC beams and classified them into four types depending on their a/d ratio: very short, short, slender, and very slender beams, as can be seen in Figure 3.2.

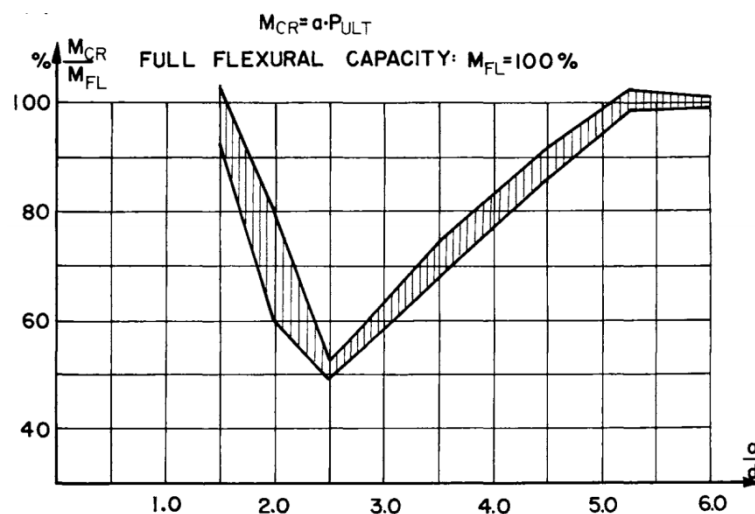


Figure 3.2 Beam capacities versus a/d ratios – Kani's Valley of Shear Failures

3. Flexural and shear strength of reinforced concrete beams

In very slender beams with $a/d > 6.0$, flexural failure usually appears before shear crack formation. In slender beams with $2.5 < a/d < 6.0$, some flexural cracks may incline after a certain point and become flexural-shear cracks along with diagonal crack formation. Shear cracks can propagate to the support and loading point and split the beam into two parts. Yielding of longitudinal reinforcement usually occurs and this type of failure is called diagonal tension failure (Figure 3.3).

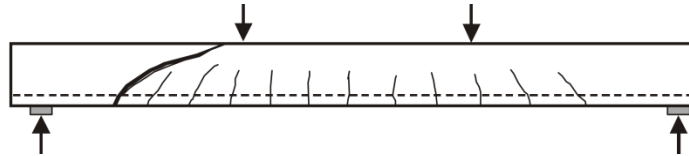


Figure 3.3 Diagonal tension failure (ASCE-ACI 426 1973)

In short beams ($1 < a/d < 2.5$) failure usually occurs in one of the two following ways (Figure 3.4): a shear crack can propagate toward the top of the beam causing the crushing of the compression concrete zone (shear compression failure), or a shear crack can propagate along the longitudinal reinforcement causing splitting between concrete and reinforcement (shear tension failure).

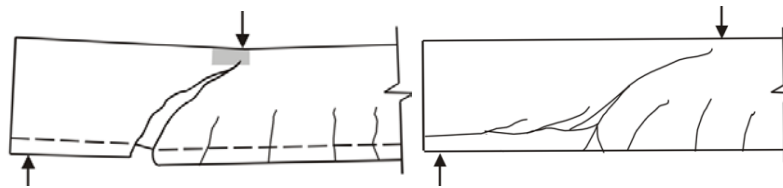


Figure 3.4 Failure types for $1 < a/d < 2.5$: a) shear compression failure, b) shear tension failure (ASCE-ACI 426 1973)

In very short beams with $a/d < 1$ most of the shear force is transferred by an arch action (Figure 3.5a) with different possible failure types which can occur: anchorage failure, bearing failure, flexural failure, tension failure, and compression strut failure (Figure 3.5b).

In order to insure the ductility and prevent brittle shear failure, shear strength of concrete must exceed flexural capacity to ensure flexural failure. Shear reinforcement (stirrups) is usually used to increase the shear capacity and ensure a ductile failure. After the appearance of the first shear crack, the behavior of beams reinforced with stirrups changes compared with beams with no shear

3. Flexural and shear strength of reinforced concrete beams

reinforcement. The main parameter affecting the beam's behavior and failure mode is the amount of shear reinforcement.

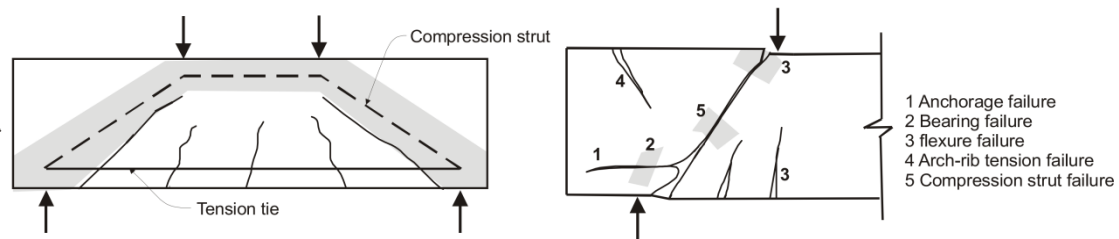


Figure 3.5 a) Arch action and b) different failure modes in short beams with $a/d < 1.0$
(ASCE-ACI 426 1973)

Shear reinforcement has very little effect prior to the formation of diagonal cracks. After cracking, stirrups influence the shear resistance in following ways: they resist shear forces, reduce crack penetration into the compressive concrete zone, restrict crack width growth, and help longitudinal reinforcement confinement (Nilson et al. 2010).

The main mechanisms for shear transfer differ significantly depending on crack formation, structural system and loading geometry, and the use of shear reinforcement. The understanding of shear transfer is usually based on the following mechanisms (ASCE-ACI 426 1973):

- Shear stress in the un-cracked concrete compressive zone (V_{cc});
- Shear transfer across the cracks – aggregate interlock effect (V_a);
- Dowel action of the longitudinal reinforcement (V_d);
- Arch action.

ASCE-ACI 445 Report (ACI-ASCE 445 1998) introduced a new mechanism, residual tensile stresses, which are transmitted directly across cracks. Small pieces of concrete bridge the crack and continue to transmit tensile forces as long as cracks do not exceed a certain width (Hawkins et al. 2005). ASCE-ACI 445 Report (ACI-ASCE 445 1998) gives five important shear transfer actions for beams with shear reinforcement (Figure 3.6a): shear in the un-cracked concrete zone, aggregate interlock effect, dowel action of the longitudinal reinforcement, residual tensile stresses across inclined cracks, and shear transfer of the shear reinforcement (ΣV_{si}).

3. Flexural and shear strength of reinforced concrete beams

Shear forces at a diagonal crack in beams without shear reinforcement and with shear reinforcement are shown in Figure 3.6b. In the un-cracked part of a RC cross-section, the stress distribution follows the theory of elasticity with a parabolic shear stress distribution above the neutral axis as assumed by Mörsh (Mörsh E. 1909). In a slender member, the shear force in the compression zone does not contribute significantly to the shear capacity because the depth of the compression zone is relatively small (Reineck 1991a), but it can range from 25% to 40% of the total shear force (Fenwick and T. 1968; Kokovic 2016).

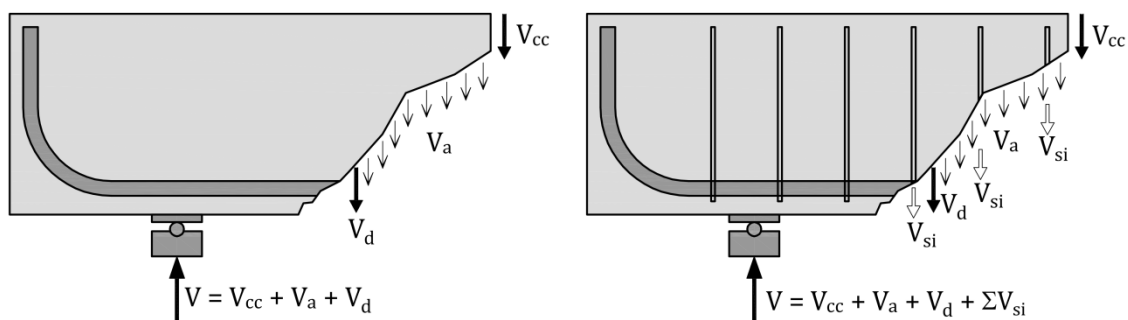


Figure 3.6 Forces at a diagonal crack in beams a) without shear reinforcement and b) with shear reinforcement

The aggregate interlock effect was clearly described in ASTM-ACI 426 (ASCE-ACI 426 1973): “Aggregates protruding from the crack surface provide resistance against slip.” This effect is caused by the relative tangential displacement of two cracked surfaces and residual tensile stress that can occur at a limited opening of the cracks. Aggregate interlock has been investigated since the 1960s with the most comprehensive experimental research done by Walraven (Walraven 1980). The main variables affecting aggregate interlock are concrete compressive strength, crack width, and aggregate size. Hence, the effect decreases with the increase of crack width and decrease of aggregate size and concrete compressive strength. The role of the aggregate interlock effect in the redistribution of diagonal compression fields in beams with stirrups is also important (ACI-ASCE 445 1998).

A dowel action of the longitudinal reinforcement is a shear transfer mechanism generated across cracks as a result of the interaction between the reinforcing bars and the surrounding concrete. Loss of dowel action due to the splitting cracks along the longitudinal reinforcement can cause the failure of RC beams. Dowel

3. Flexural and shear strength of reinforced concrete beams

action is mostly influenced by the number and arrangement of longitudinal bars, spacing of flexural cracks, concrete cover, flexural stiffness of the longitudinal bars, and the strength of the surrounding concrete (Ortega 2012; Taylor 1974). It can be significant in members with large amounts of longitudinal reinforcement, especially if longitudinal reinforcement is placed in more than one layer (ASCE-ACI 426 1973). The shear force contribution of longitudinal bars is typically about 15–25% compared with the overall shear capacity according to Regan (Regan 1993).

Shear transfers by arch action in short members subjected to concentrated loads close to supports ($a/d < 2.5$). Arch action occurs where shear forces cannot be transmitted so the portion of shear is transmitted directly to the support by an inclined strut. Direct strut action depends on the strength of the concrete, the inclination of the strut and the width of the support area (MacGregor 1997; Muttoni et al. 1997).

Residual tensile stresses exist in cracks if its width is sufficiently small. When concrete cracks, small pieces of concrete are still connecting the crack surfaces and continue to transmit tensile forces up to crack widths in the range of 0.05 to 0.15 mm (ACI-ASCE 445 1998). The cracked concrete can therefore also carry a part of shear stresses on the tips of inclined and flexural cracks. This phenomenon is significant in shallow members where the width of flexural and diagonal cracks is small (Reineck 1991b).

In members with shear reinforcement, a large portion of the shear is carried by the shear reinforcement after diagonal cracking occurs. The approximation of the distribution of internal shear force components is given in Figure 3.7. As can be seen, after diagonal cracking the portion of shear carried by stirrups (V_s) increases while the sum of the remaining components (V_{cc} , V_a , and V_d) remains nearly constant. When the stirrups yield, their contribution remains constant. With load increase, the diagonal cracks widen causing a decrease in aggregate interlock along with a decrease of the dowel effect caused by longitudinal splitting along the reinforcement.

3. Flexural and shear strength of reinforced concrete beams

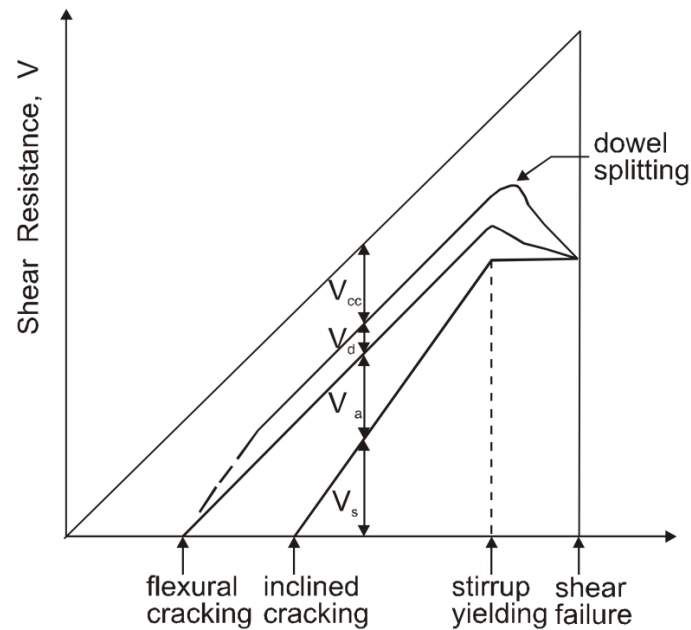


Figure 3.7 Distribution of internal shear forces (ASCE-ACI 426 1973)

Other parameters affecting shear resistance that should be mentioned are concrete compressive strength, members' depth (shear size effect), longitudinal reinforcement ratio, axial forces, and bond of reinforcing steel. Concrete compressive strength is an important parameter influencing shear resistance in two ways: first, through a shear component caused by un-cracked compressed concrete and second, by influencing the transfer of forces across cracks. As concrete strength increases, shear resistance also increases. Some researchers believe that concrete tensile strength has a greater influence on shear resistance than previously suggested. Tensile strength is usually defined using available experimental data of compressive strength and shear resistance is therefore taken as directly proportional to $2\sqrt{f_c}$, $3\sqrt{f_c}$, or $2\sqrt{f_c}^3$.

The size effect in shear can be explained in the following manner: nominal shear strength of RC beams without shear reinforcement decreases as the member depth increases. An extensive research on the size effect demonstrating the previously-stated was done by Kani and Shioya et al. (Kani 1967; Shioya et al. 1989) (Figure 3.8). There is general agreement that the main reason for this size effect is the larger width of diagonal cracks in larger beams (ACI-ASCE 445 1998; Kuchma and Collins 1998). Some researchers, on the other hand, give a different explanation of this phenomenon. Namely, the size effect can be a consequence of a large amount

3. Flexural and shear strength of reinforced concrete beams

of energy that is released in the cracking of large members leading to the faster propagation of inclined cracks and lower shear failure stresses (Bažant et al. 1986). The size effect plays only a minor role for members with shear reinforcement because the crack widths are mainly controlled by stirrups (Hawkins et al. 2005).

In RC structures, as the longitudinal reinforcement ratio decreases, crack widths increase and shear strength is lowered. Furthermore, the dowel action also decreases along with the longitudinal reinforcement ratio. Axial compression leads to the increase in the depth of the un-cracked compression zone and decrease of shear cracks' width, leading to increased shear resistance. Contrary to axial compression, concrete beams with axial tension have a lower shear resistance, since axial tension leads to wider cracks and reduces the height of the un-cracked compression zone.

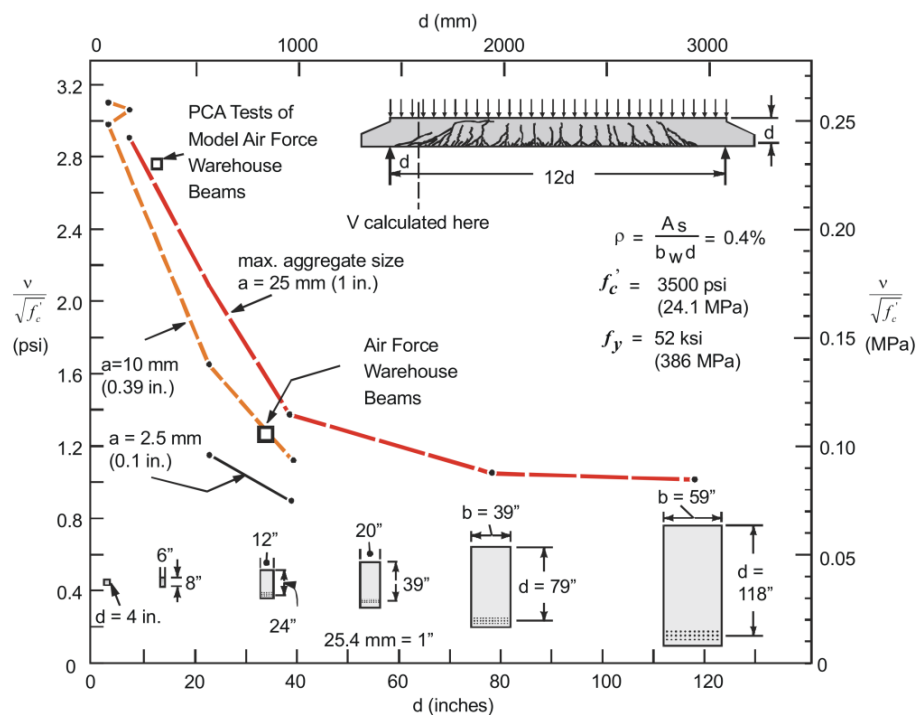


Figure 3.8 Shear size effect (ACI-ASCE 445 1998; Kani 1967; Kuchma and Collins 1998; Shioya et al. 1989)

3. Flexural and shear strength of reinforced concrete beams

3.4.2. Shear design models

In 1964, Kani proposed a model to explain the flexural shear failure mode in his well-known paper "The Riddle of Shear Failure and Its Solution" (Kani 1964) introducing the effect of the bending of the "teeth of the concrete" between the flexural cracks (Figure 3.9).

The concrete between two flexural cracks was considered to be analogous to a tooth in a comb. The concrete teeth were assumed to be cantilevers fixed in the compression zone of the beams and loaded by a horizontal force from the bonded reinforcement (Yang 2014). Although this theory did not cover most of the shear transfer mechanisms, it was the start of more rational approaches. The studies on the shear transfer mechanism based on comb models eventually evolved towards shear failure criteria based on aggregate interlock or crack width of a critical section.

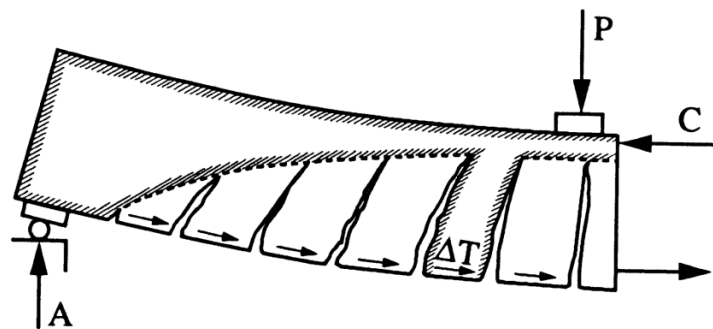


Figure 3.9 Kani's comb model for a cracked beam subjected to shear

For beams without shear reinforcement most of the models describing behavior of a member under shear and its failure are empirical. The American standard ACI 318 proposes an empirical equation as a function of the square root of compressive strength without taking into account the longitudinal reinforcement, beam height, loading conditions, etc. This relation, and many more, are taken from the assumption made by Mörsh relating the shear capacity of concrete beams without shear reinforcement to the tensile strength of concrete. European standard EN 1992-1-1 also defines shear strength of beams without shear reinforcement using empirical equations but takes into account the size effect and longitudinal reinforcement ratio. More recent empirical methods include fracture

3. Flexural and shear strength of reinforced concrete beams

mechanics into developing equations defining shear strength of beams without shear reinforcement. Gastebled & May (Gastebled and May 2001) presented a model based on the energy release due to the opening of a diagonal shear crack. They assumed that the ultimate shear load is reached when a splitting crack at the level of the longitudinal reinforcement starts to propagate. They proposed the following equation for shear strength:

$$V_c = \frac{1.109}{\sqrt{d}} \cdot \left(\frac{d}{a_s}\right)^{1/3} \cdot \rho^{1/6} \cdot (1 - \sqrt{\rho})^{2/3} \cdot f_c^{0.35} \cdot \sqrt{E_s} \cdot b_w \cdot d \quad \text{Eq. 3.12}$$

where:

ρ longitudinal reinforcement ratio;

a_s shear span;

E_s modulus of elasticity of longitudinal reinforcement steel.

Bažant and Yu (Bažant and Yu 2005) proposed an empirical, semi-fracture mechanics approach equation, with special attention to the size effect:

$$V_c = 10\rho^{3/8} \cdot \left(1 + \frac{d}{a_s}\right) \cdot \sqrt{\frac{f_c'}{d}} \cdot b_w \cdot d \quad \text{Eq. 3.13}$$

$$\sqrt{1 + \frac{d}{f_c'^{-2/3} \cdot 3800 \cdot \sqrt{d_a}}}$$

where:

d_a maximum aggregate size.

More recently, Xu et al. (Xu et al. 2012) proposed an equation based on the fracture energy required to release interface bond resistance between steel and concrete (Mode II fracture energy):

$$V_c = 1.018 \cdot \rho^{1/6} \cdot \left(\frac{d}{a_s}\right)^{1/3} \cdot (1 - \sqrt{\rho_s})^{2/3} \cdot (0.0255 \cdot f_c + 1.024) \cdot b_w \quad \text{Eq. 3.14}$$

Models defining shear transfer mechanisms in beams with shear reinforcement were first based on the truss model. The truss model has been widely used to understand shear behavior of cracked RC beams in the 1900's. The Swiss engineer Ritter (1989) developed a 45° truss model for explaining the flow of forces in cracked RC. In the truss model, after an RC beam cracks due to diagonal tensions

3. Flexural and shear strength of reinforced concrete beams

stresses, it can generally be seen as a parallel chord truss with compression diagonals inclined at 45° with respect to the longitudinal axis of the beam. In Ritter's model, the longitudinal reinforcement acts as a tension chord of the truss while the un-cracked compressive zone of the beam acts as the compression chord. Diagonal concrete struts were considered to be the diagonal members and the stirrups vertical members of the truss. The shear stresses are assumed to be uniformly distributed over an effective shear area. Morsch (1902) pointed out that the stirrups represent a continuous field of stresses rather than discrete diagonal compressive struts assuming that the diagonal struts extended across more than one stirrup. The tensile stresses in cracked concrete were neglected in this model and diagonal compression stresses were assumed to remain at 45° after the concrete cracked. The truss model is derived using the equilibrium condition between the external and internal forces. The 45° truss model gives overly conservative results for predictions of the shear strength of members with shear reinforcement because it lowers the effectiveness of stirrups. This is the reason why more attention was focused on determining a more realistic strut angle that can be flatter than 45° . The variable-angle truss model was therefore developed. In this model equilibrium equations can be derived in the same way as for the 45° truss model with four unknown parameters.

The strut and tie model (STM) was developed in the late 1980s and popularized by Schlaich et al. in his paper "*Toward a Consistent Design of Structural Concrete*" (Schlaich et al. 1987). It represents the flow of forces with concrete struts and steel tensile ties estimating the bearing capacities of beams exhibiting a shear compression failure with sufficient accuracy. This theory assumes regions near a discontinuity (concentrated loads, openings, or changes in the cross-section) that do not satisfy the Bernoulli hypothesis and are called D-regions (disturbed regions). Regions in between these areas are subjected to typical beam behavior and are called B-regions. STM was developed based on the truss model to account for these D-regions. They consist of struts, ties, and nodal zones. Struts are internal concrete compression members; ties are tension members within the model and consist of steel reinforcement, plus the portion of concrete surrounding the steel;

3. Flexural and shear strength of reinforced concrete beams

nodal zones are regions where struts, ties, and concentrated loads meet. There are a few problems in developing STMs like: uncertainties in obtaining dimensions, stiffness, and effective strength of strut, ties, and nodes for the truss models; the need to select the optimal STM and iteratively adjust and refine the truss geometry; the need to combine different load cases; and multiple potential solutions for statically indeterminate models (Ortega 2012).

The modified compression field theory (MCFT) was developed by Vecchio and Collins in 1986 (Vecchio and Collins 1986) as a further development of the compression field theory (CFT) derived by Collins and Mitchell in 1980. The theory was derived to determine the principal direction of the compressive stress in shear RC members as an alternative to the truss model. In the CFT it is assumed that a diagonal compression field carries shear after cracking and that the principal tensile stress is zero after the concrete has cracked. On the other hand, in the MCFT the effect of the residual stress in the concrete between the cracks is taken into account. The MCFT model consists of strain compatibility and equilibrium equations which can be used to predict the complete shear deformation response. All the compatibility equations are expressed in terms of average strains measured over base lengths long enough to include several cracks. The compatibility equations for both the CFT and the MCFT are obtained from a Mohr's circle (Figure 3.10) and given as following:

$$\tan^2 \theta = \frac{\varepsilon_x + \varepsilon_2}{\varepsilon_z + \varepsilon_2} \quad \text{Eq. 3.15}$$

$$\varepsilon_1 = \varepsilon_x + \varepsilon_z + \varepsilon_2 \quad \text{Eq. 3.16}$$

$$\gamma_{xz} = (\varepsilon_x + \varepsilon_2) \cot \theta \quad \text{Eq. 3.17}$$

where:

γ_{xz} shear strain;

ε_x strain in the x-direction;

ε_z strain in the z-direction;

$\varepsilon_1, \varepsilon_2$ principal strains in concrete.

3. Flexural and shear strength of reinforced concrete beams

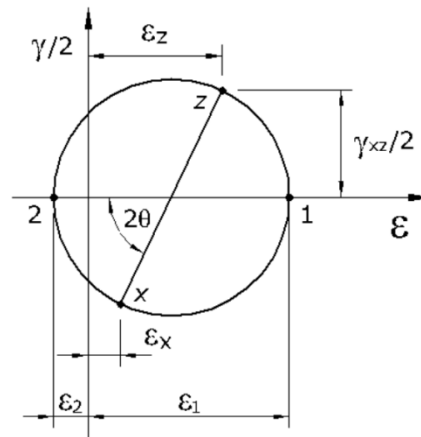


Figure 3.10 Mohr's circle for average concrete stresses (Kokovic 2016)

MCFT can provide accurate predictions of shear strength and deformation. The most important assumption made in MCFT is that of a rotating crack model in which previous cracks are assumed to be inactive. MCFT also assumes that the angles of the axes for the principal strains and principal stresses coincide. The crack in which all the checks are performed is assumed to be oriented at the same angle as the compressive stress field (Ortega 2012). The disadvantage of MCFT is that it usually requires the use of a computer in order to solve the system of equations.

3.5.CODE PROVISIONS - SHEAR BEHAVIOR OF REINFORCED CONCRETE BEAMS

A great number of parameters influencing shear strength of RC beams made it difficult to define one completely accurate and generally accepted model for practical use. Different countries defined their standards for shear design using different philosophies. Some of them are based on empirical formulas for estimating shear strength, while others rely on different concrete models previously explained. Most analytical models, such as MCFT (Bentz et al. 2006; Vecchio and Collins 1986) and STM (Brown 2005) also include some empirical expressions.

This chapter presents the shear design provisions for OPCC defined in the most widely used codes in practice, together with other significant design approaches.

3. Flexural and shear strength of reinforced concrete beams

None of these provisions provide any recommendations for HVFAC members' shear strength.

Standards that are analyzed here are the Serbian standard for concrete and RC – BAB '87 (Faculty of Civil Engineering 1995), European Standard EN 1992-1-1 (CEN 2004), American Standard ACI 318 (ACI 2008), and the *fib* Model Code 2010 (fib 2010a; b)

3.5.1. Serbian standard for concrete and reinforced concrete - BAB '87

This standard defines shear strength based on the variable-angle truss model. The standard defines shear strength for different shear stress levels τ_n :

$$\tau_n = \frac{T}{b \cdot z} \quad \text{Eq. 3.18}$$

If the shear stress is lower than concrete shear strength defined in the standard (τ_r) a member's shear strength can be calculated as:

$$T_c = \tau_r \cdot b \cdot z \quad \text{Eq. 3.19}$$

If the stress level is higher than τ_r , shear reinforcement is needed and shear strength carried by the reinforcement can be calculated as:

$$T_u = b \cdot h \cdot \frac{m \cdot a_u^{(1)}}{b \cdot e_u} \cdot (\cos \alpha + \sin \alpha \cdot \text{ctg} \theta) \cdot \sigma_v \quad \text{Eq. 3.20}$$

where:

- b width of the cross-section in the tensile area;
- h effective depth of a cross-section;
- z inner lever arm;
- m number of stirrups legs;
- $a_u^{(1)}$ cross-section of one stirrup leg;
- e_u longitudinal spacing between stirrups;
- α angle between shear reinforcement and the beam axis perpendicular to the shear force;

3. Flexural and shear strength of reinforced concrete beams

θ angle between the concrete compression strut and the beam axis;

σ_v stirrup yield strength.

Concrete contribution to the shear strength is taken into account if the shear stress is lower than $3\tau_r$ and can be calculated as:

$$T_{u,u} = \frac{2}{3} \cdot T_u + T_c \quad \text{Eq. 3.21}$$

In the case of shear stresses higher than $3\tau_r$, the concrete contribution is neglected and the member's shear strength can be calculated as:

$$T_{u,u} = T_u \quad \text{Eq. 3.22}$$

3.5.2. European Standard EN 1992-1-1: Design of concrete structures - Part 1-1: General rules and rules for buildings

The European Standard EN 1992-1-1 (CEN 2004) defines different shear strength provisions for RC members with and without shear reinforcement. For members that do not require shear reinforcement, shear strength is predicted using an empirical equation based on the evaluation of 176 carefully selected shear tests (König and Fischer 1995). The design value for the shear resistance, $V_{Rd,c}$, of a member not requiring shear reinforcement is given by:

$$V_{Rd,c} = \left[C_{Rd,c} \cdot k \cdot (100 \cdot \rho_l \cdot f_{ck})^{1/3} + k_1 \cdot \sigma_{cp} \right] \cdot b_w \cdot d \quad \text{Eq. 3.23}$$

with a minimum value of:

$$V_{Rd,c} = (v_{\min} + k_1 \cdot \sigma_{cp}) \cdot b_w \cdot d \quad \text{Eq. 3.24}$$

where:

$C_{Rd,c} = 0.18$;

$k_1 = 0.15$;

f_{ck} characteristic concrete compressive strength after 28 days on a standard cylinder (MPa);

3. Flexural and shear strength of reinforced concrete beams

$$k = 1 + \sqrt{\frac{200}{d}} \leq 2.0 \quad (d \text{ in mm});$$

$$\rho_l = \frac{A_{s1}}{b_w \cdot d} \leq 0.02;$$

A_{s1} area of tension reinforcement, which extends at least $(l_{bd} + d)$ beyond the section considered, l_{bd} is the bond development length;

b_w smallest width of the cross-section in the tensile area (mm);

d effective depth of a cross-section;

$$\sigma_{cp} = N_{Ed}/A_c < 0.2f_{cd} \text{ (MPa)};$$

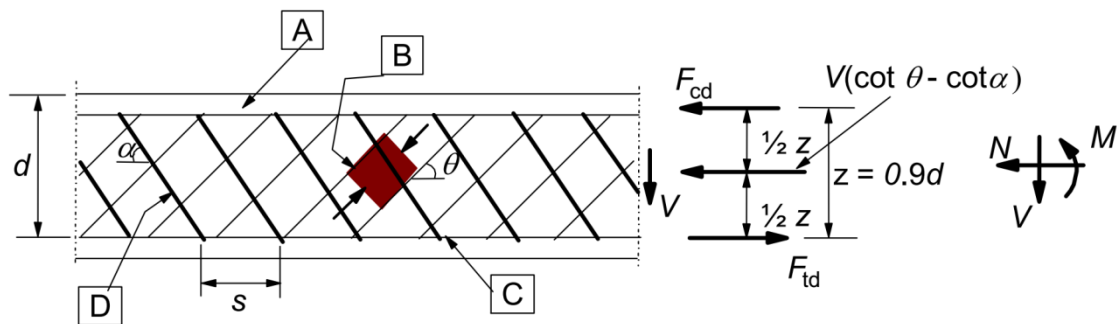
N_{Ed} axial force in the cross-section due to loading or prestressing (N),

$N_{Ed} > 0$ for compression;

A_c area of the concrete cross-section (mm²);

$$v_{min} = 0.035 \cdot k^{2/3} \cdot \sqrt{f_{ck}}$$

The design of members with shear reinforcement is based on a truss model with a variable angle between the concrete compression strut and the beam axis perpendicular to the shear force (θ) varying between 21.8° and 45° (Figure 3.11).



A - compression chord, **B** - struts, **C** - tensile chord, **D** - shear reinforcement

Figure 3.11 Truss model and notation for shear reinforced members (CEN 2004)

The following symbols are presented in Figure 3.11:

3. Flexural and shear strength of reinforced concrete beams

- α angle between shear reinforcement and the beam axis perpendicular to the shear force (measured positive as shown in Figure 3.11);
- θ angle between the concrete compression strut and the beam axis perpendicular to the shear force;
- F_{td} design value of the tensile force in the longitudinal reinforcement;
- F_{cd} design value of the concrete compression force in the direction of the longitudinal member axis;
- b_w minimum width;
- z inner lever arm, for a member with constant depth, corresponding to the bending moment in the element under consideration ($z \approx 0.9d$ without axial forces).

For members with vertical shear reinforcement, the shear resistance, V_{Rd} , is the smaller value of:

$$V_{Rd,s} = \frac{A_{sw}}{s} \cdot z \cdot f_{ywd} \cdot \cot \theta \quad \text{Eq. 3.25}$$

and

$$V_{Rd,max} = \frac{\alpha_{cw} \cdot v_1 \cdot f_{cd} \cdot b_w \cdot z}{\cot \theta + \tan \theta} = \alpha_{cw} \cdot v_1 \cdot f_{cd} \cdot b_w \cdot z \frac{\cot \theta}{1 + \cot^2 \theta} \quad \text{Eq. 3.26}$$

where:

- A_{sw} cross-sectional area of the shear reinforcement;
- s spacing of stirrups;
- f_{ywd} design yield strength of the shear reinforcement;
- v_1 = v , a strength reduction factor for concrete cracked in shear;
- α_{cw} coefficient taking account the state of stress in the compression chord:

$$\alpha_{cw} = 1 + \sigma_{cp}/f_{cd} \quad \text{for} \quad 0 < \sigma_{cp} \leq 0.25f_{cd};$$

$$\alpha_{cw} = 1.25 \quad \text{for} \quad 0.25f_{cd} < \sigma_{cp} \leq 0.5f_{cd};$$

$$\alpha_{cw} = 2.5(1 - \sigma_{cp}/f_{cd}) \quad \text{for} \quad 0.5f_{cd} < \sigma_{cp} < 1.0f_{cd}.$$

3. Flexural and shear strength of reinforced concrete beams

σ_{cp} mean compressive stress, measured positive, in the concrete due to the design axial force.

3.5.3. *fib* Model Code 2010

The European Standard EN 1992-1-1 is mostly based on *fib* Model Code 1990 recommendations, while *fib* Model Code 2010 (*fib* 2010a; b) has a different approach to shear design. Shear design given in *fib* Model Code 2010 was developed based on physical-mechanical models for beams with and without shear reinforcement. This approach is an improvement compared with EN 1992-1-1 shear design and its empirical estimation of shear strength for beams without shear reinforcement. Calculation of shear strength is done using “levels of approximation” (LoA) (Muttoni and Fernandez 2012; Sigrist et al. 2013) with higher levels giving more accurate results but requiring more time and calculations. The highest level was based on a precise mechanical model, and lower levels were derived from it introducing some approximations.

fib Model Code 2010 offers two LoAs for the shear resistance of members without shear reinforcement derived from the *Simplified Modified Compression Field Theory* (Bentz et al. 2006). Shear strength can be calculated as (Sigrist et al. 2013):

$$V_{Rd,c} = k_v \cdot \sqrt{f_{ck}} \cdot b_w \cdot z \quad \text{Eq. 3.27}$$

where:

k_v parameter accounting for shear resistance of cracked concrete;

f_{ck} characteristic concrete compressive strength after 28 days on a standard cylinder (MPa), $\sqrt{f_c} \leq 8$ MPa;

b_w minimum width;

z inner lever arm, for a member with constant depth (mm).

For LoAs II and I, the approximation for k_v is defined as:

LoA II:

3. Flexural and shear strength of reinforced concrete beams

$$k_v = \frac{0.4}{1 + 1500 \cdot \varepsilon_x} \cdot \frac{1300}{1000 + k_{dg} \cdot z} \quad \text{Eq. 3.28}$$

$$k_{dg} = \frac{32}{16 + d_g} \geq 0.75 \quad \text{Eq. 3.29}$$

LoA I:

$$k_v = \frac{180}{1000 + 1.25 \cdot z} \quad \text{Eq. 3.30}$$

where:

z inner lever arm, for a member with constant depth (mm);

ε_x longitudinal strain at mid-depth;

k_{dg} size effect;

d_g maximum aggregate size ≥ 16 mm (mm).

The equation for LoA I is deduced by assuming a maximum aggregate size larger than $d_g=9.6$ mm and $\varepsilon_x=1.25\%$ (half the yield strain of the longitudinal reinforcing bars with $f_{yk}=500$ MPa). The term $k_{dg} \cdot z$ represents the spacing between cracks, and for a maximum aggregate size of 16 mm, gives the spacing equal to the inner lever arm z .

Shear resistance calculation for members with shear reinforcement in *fib* Model Code 2010 was derived from the *Simplified Modified Compression Field Theory* (Bentz et al. 2006; Sigrist et al. 2013) and *Generalized Stress Field Approach* (Sigrist 2011). For members with at least a minimum shear reinforcement ratio of

$$\rho_w \geq 0.08 \cdot \frac{\sqrt{f_{ck}}}{f_{yk}} \quad \text{Eq. 3.31}$$

the shear resistance is the sum of the resistance provided by the concrete ($V_{Rd,c}$) and stirrups ($V_{Rd,s}$):

3. Flexural and shear strength of reinforced concrete beams

$$V_{Rd} = V_{Rd,c} + V_{Rd,s} \quad \text{Eq. 3.32}$$

$$V_{Rd,s} = \frac{A_{sw}}{s_w} \cdot z \cdot f_{ywd} \cdot \cot \theta \quad \text{Eq. 3.33}$$

where:

A_{sw} shear reinforcement cross-section area;

s_w spacing between shear reinforcement;

f_{ywd} yield strength of shear reinforcement steel;

θ inclination of the compressive stress field.

Resistance of concrete $V_{Rd,c}$ is calculated using the Eq. 3. 27. Three LoAs are defined in which the concrete contribution is accounted for differently. For LoAs I and II, $V_{Rd,c}$ is neglected, and only in LoA III, and in conjunction with the strut inclination $\theta = \theta_{\min}$, the concrete contribution is added. Strut inclination relative to the longitudinal axis of the member is calculated based on different LoAs, and is limited to:

$$\theta_{\min} \leq \theta \leq 45^\circ \quad \text{Eq. 3.34}$$

For LoA I, values for θ_{\min} are given in *fib* Model Code 2010 as:

- 30° for RC structures;
- 25° for prestressed concrete structures;
- 40° for members with significant axial force.

For LoAs II and III, strut inclination is calculated using the following equation:

$$\theta_{\min} = 20^\circ + 10000 \cdot \varepsilon_x \quad \text{Eq. 3.35}$$

where:

ε_x longitudinal strain at the mid-depth of the effective shear depth (Figure 3. 12)

For a preliminary analysis, ε_x can be taken as 0.001.

3. Flexural and shear strength of reinforced concrete beams

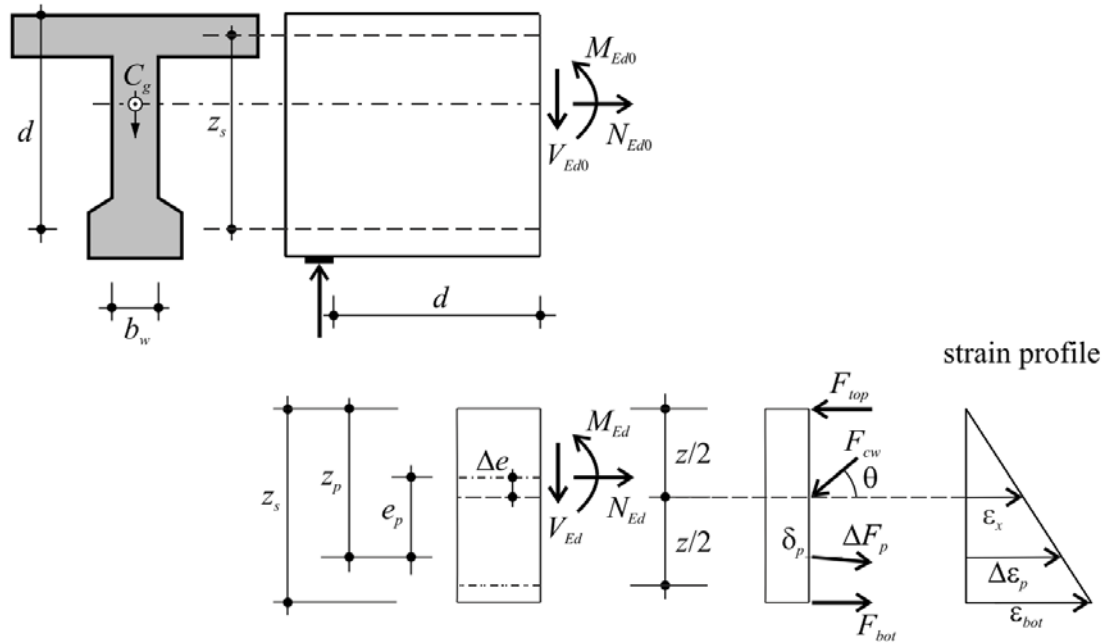


Figure 3.12 Longitudinal strain definition (fib 2010b)

Longitudinal strain at mid-depth can be approximately taken as one half of the longitudinal reinforcement strain:

$$0 \leq \varepsilon_x = \frac{\varepsilon_s}{2} \leq 0.003 \quad \text{Eq. 3.36}$$

Longitudinal reinforcement strain can be calculated using truss model with stirrups at the angle of 90° as:

$$\varepsilon_s = \frac{\frac{M}{Z} + V}{E_s \cdot A_s} \quad \text{Eq. 3.37}$$

where:

M bending moment in the control cross-section (at a location d from the face of the support) – a positive value;

V shear force in the control cross-section – a positive value;

E_s longitudinal reinforcement modulus of elasticity;

A_s longitudinal reinforcement area.

The k_v value, accounting for the concrete contribution in LoA III, is defined as:

3. Flexural and shear strength of reinforced concrete beams

$$k_v = \frac{0.4}{1 + 1500 \cdot \varepsilon_x} \cdot \left(1 - \frac{V_{Ed}}{V_{Rd,max}(\theta_{min})} \right) \quad \text{Eq. 3.38}$$

where:

$V_{Rd,max}(\theta_{min})$ crushing of the struts at a stress field inclination angle of θ_{min} .

Crushing of the concrete strut that can be calculated as:

$$V_{Rd,max} = k_c \cdot f_{ck} \cdot b_w \cdot z \cdot \sin \theta \cdot \cos \theta \quad \text{Eq. 3.39}$$

where:

k_c strength reduction factor calculated as $k_c = k_\varepsilon \cdot \eta_{fc}$

k_ε strain effect factor taken differently depending on the LoA.

η_{fc} brittleness factor η_{fc} can be calculated as

$$\eta_{fc} = \left(\frac{30}{f_{ck}} \right)^{1/3} \leq 1.0 \quad (f_{ck} \text{ in MPa}) \quad \text{Eq. 3.40}$$

In LoA I, the strain effect factor is taken as $k_\varepsilon = 0.55$. For LoAs II and III, the strain effect factor must be calculated using the following equation:

$$k_\varepsilon = \frac{1}{1.2 + 55 \cdot \varepsilon_1} \leq 0.65 \quad \text{Eq. 3.41}$$

where:

ε_1 principal strain calculated as:

$$\varepsilon_1 = \varepsilon_x + (\varepsilon_x + 0.002) \cdot \cot^2 \theta \quad \text{Eq. 3.42}$$

where:

ε_x strain in the x-direction;

θ compressive stress field inclination angle.

Inclination of the compressive stress field can be calculated using the following equation:

3. Flexural and shear strength of reinforced concrete beams

$$\theta = 29^\circ + 7000 \cdot \varepsilon_x \quad \text{Eq. 3.43}$$

3.5.4. American standard ACI 318

The ACI 318 (ACI 2008) shear design is based on a 45° truss model. Shear strength (V_n) is based on an average shear stress distribution across the entire cross-section, and is composed of a concrete component (V_c) and a shear reinforcement component (V_s):

$$V_n = V_c + V_s \quad \text{Eq. 3.44}$$

Concrete contribution for normal-weight, non-prestressed RC can be calculated using one of the two following equations:

$$V_c = \frac{\sqrt{f_c'}}{6} \cdot b_w \cdot d \quad (N) \quad \text{Eq. 3.45}$$

$$V_c = \left(\sqrt{f_c'} + 120 \cdot \rho_w \cdot \frac{V_u \cdot d}{M_u} \right) \cdot \frac{b_w \cdot d}{7} \leq 0.3 \cdot \sqrt{f_c'} \cdot b_w \cdot d \quad (\text{mm, MPa}) \quad \text{Eq. 3.46}$$

where:

f_c' concrete compressive strength measured on a cylinder (100 · 200 mm) (MPa);

d distance from the extreme compression fiber to the center of gravity of the longitudinal reinforcement (mm).

$$\rho_w = \frac{A_s}{b_w d};$$

A_s longitudinal reinforcement cross-section area;

V_u shear force acting on the section;

M_u factored bending moment acting on the section.

$$\left(\frac{V_u \cdot d}{M_u} \right) \leq 1.0 \quad \text{Eq. 3.47}$$

The shear reinforcement contribution V_s is calculated based on the 45° truss model as:

3. Flexural and shear strength of reinforced concrete beams

$$V_s = \frac{A_v \cdot f_v \cdot d}{s} \quad (mm, MPa) \quad \text{Eq. 3.48}$$

where:

A_v area of shear reinforcement;

f_v yield strength of the shear reinforcement;

s spacing of the transverse reinforcement.

4. EXPERIMENTAL PROGRAM AND TEST RESULTS

4. Experimental program and test results

4.1. INTRODUCTION

Program of own experimental research was divided in three phases:

- 1) Testing of HVFAC physical and mechanical properties;
- 2) Flexural behavior testing of RC beams;
- 3) Shear behavior testing of RC beams.

Having in mind the heterogeneity of FA physical and chemical properties and the lack of reliable predictions for HVFAC mechanical properties, an extensive experimental research regarding physical and mechanical HVFAC properties was conducted. The main objectives of this phase were to produce structural grade HVFAC with the maximum amount of FA and to analyze the influence of different FA amounts and design procedures on physical and mechanical properties of HVFAC. Two different HVFAC mixtures were selected for testing of RC beams.

The flexural behavior of RC beams was tested on OPCC and HVFAC beams with equally designed compressive strengths and different longitudinal reinforcement ratios. The shear behavior of RC beams was tested on OPCC and HVFAC beams with equally designed compressive strength and longitudinal reinforcement ratios differing in shear reinforcement ratios. The analysis of all relevant parameters influencing the flexural and shear behavior was done along with the comparison of the HVFAC and OPCC beams behavior. This section describes the fabrication process, test set-up and the instrumentation for the full-scale beams. The test results obtained during testing are also presented. The overall behavior of the specimens is described, with a focus on deflection, concrete and steel strains, principal concrete strains, crack patterns, failure modes, and flexural and shear strength.

4. Experimental program and test results

4.2. TESTING OF HVFAC PHYSICAL AND MECHANICAL PROPERTIES

4.2.1. Introduction

This chapter describes the process that was carried out to develop the HVFAC mix design using a class F FA from one power plant in Serbia. The main objective of this process was to produce a HVFAC mix design with the maximum possible FA amount that could yield a structural grade concrete. The first part of own experimental research consisted of testing component materials and HVFAC physical and mechanical properties. The standard chemical and physical properties of cement and FA, and physical properties of coarse and fine aggregate were tested. Concrete mix design optimization was also done in the first part. The testing of HVFAC physical and mechanical properties consisted of two phases. The first phase was a trial phase for the assessment of the possible application of the FA collected from one power plant in Serbia in HVFAC for structural use. The target strengths of 30 MPa after 28 days and 20 MPa after three days were selected. In the second phase, ten concrete mixtures were made to get a better understanding of the effect of cement, and FA amount on the physical and mechanical properties of HVFAC.

4.2.2. Component materials

Testing of the chemical composition and morphology of FA and cement, physical properties of coarse and fine aggregate, and the development of mix design are shown in this section.

4.2.2.1. Fly ash

During the initial preparation, samples of all available FA types from Serbia were obtained and tested. FA was obtained from five coal burning power plants, namely, "Kolubara" (FA-1), "Nikola Tesla B" (FA-2), "Kostolac" (FA-3), "Morava" (FA-4), and "Nikola Tesla A" (FA-5). Chemical composition of the tested FA is shown in Table 4.1 and their particle size distribution in Table 4.2. No significant difference in chemical composition between different FA chemical was noticed, while the sample FA-2 had the highest amount of particles passing through a 45 μm sieve.

4. Experimental program and test results

The selection of FA was done according to mean particle size and some preliminary tests on high volume FA pastes. The best results regarding FA concrete workability and compressive strength were obtained using the FA-2 so it was chosen for further testing in HVFAC. Total amount of 1500 kg of FA was obtained from power plant "Nikola Tesla B." The lowest amount of particles larger than 45 μm in this type of FA was a consequence of pneumatic transport mechanisms available in the "Nikola Tesla B" power plant. In the 2009/2010 repair of the "Nikola Tesla B" power plant, a new system for dry FA collection, transport, and disposal was installed. During its pneumatic transport, FA was separated into four fractions according to the particle size and weight, and the separate collection of each fraction was possible.

Sampling of FA was done for the finest available fraction (Figure 4.1a). The color of the obtained sample was similar to the color of sand, as can be seen in Figure 4.1b, c. The chemical composition of the FA samples, given in Table 4.2, was determined by X-ray fluorescence (XRF) analysis.

Table 4.1 Chemical composition and physical properties of FA from Serbia

	FA-1	FA-2	FA-3	FA-4	FA-5
<i>SiO₂, %</i>	50.21	58.24	56.38	56.78	53.59
<i>Al₂O₃, %</i>	23.83	20.23	17.57	20.26	21.18
<i>Fe₂O₃, %</i>	9.89	5.33	10.39	6.44	6.20
<i>TiO₂, %</i>	0.54	0.45	0.52	0.5	0.56
<i>CaO, %</i>	4.79	7.62	7.46	8.19	7.61
<i>MgO, %</i>	3.12	2.01	2.13	2.69	2.74
<i>P₂O₅, %</i>	0.05	0.00	0.025	0.09	0.03
<i>SO₃, %</i>	5.24	2.21	0.95	0.82	0.78
<i>Na₂O, %</i>	0.35	0.52	0.38	0.63	0.44
<i>K₂O, %</i>	0.44	1.51	0.57	1.37	1.22
<i>MnO, %</i>	0.03	0.03	0.03	0.05	0.03
<i>LOI, %</i>	1.84	1.64	2.94	2.19	4.91
<i>Specific gravity, kg/m³</i>	2125	2075	2220	2280	2200

4. Experimental program and test results

Table 4.2 Percent of FA passing by mass (%)

Sieve size [mm]	FA-1	FA-2	FA-3	FA-4	FA-5
0.000	0.0	0.0	0.0	0.0	0.0
0.003	9.6	19.2	6.7	6.2	8.6
0.005	11.8	34.6	7.1	8.2	8.6
0.009	15.3	56.0	7.6	9.3	11.0
0.015	27.1	70.1	14.3	16.2	16.7
0.026	39.5	81.9	23.8	25.4	22.9
0.045	51.3	89.6	32.9	36.0	29.9
0.056	58.0	91.6	38.0	49.2	33.0
0.063	60.7	94.8	43.7	55.4	38.8
0.090	69.1	96.1	55.3	74.8	48.6
0.200	92.2	98.9	90.2	89.3	82.3
0.315	96.4	100.0	96.6	95.4	91.1
0.500	98.6	100.0	99.4	97.8	95.6
0.710	99.0	100.0	99.6	99.2	98.0
1.000	99.6	100.0	100.0	100.0	98.9
2.000	100.0	100.0	100.0	100.0	100.0



Figure 4.1 a) Sampling location in "Nikola Tesla B" power plant, b, c) FA sample

The selected FA sample satisfied the requirements defined in the ASTM C 618 (ASTM 2010) standard for class F FA: $\text{SiO}_2 + \text{Al}_2\text{O}_3 + \text{Fe}_2\text{O}_3 > 70\%$ and $\text{LOI} < 6\%$. Particle size distribution was tested using the Malvern Instruments *Mastersizer 2000*. The average mean particle size for the selected FA type was $8.533 \mu\text{m}$. Specific gravity was determined according to EN 450-1 (CEN 2012) as 2075 kg/m^3 .

4. Experimental program and test results

4.2.2.2. Cement and chemical admixtures

The commercially available blended Portland cement CEM II/A-M (S-L) 42.5R was used. This type of cement has additions (ground slag and limestone) up to 20% of the total mass but it does not contain FA. Chemical properties and specific gravity of cement are presented in Table 4.3 along with selected FA properties.

Table 4.3 Chemical and physical properties of cement and FA

Property	CEM II 42.5R	FA-2	EN 450-1
SiO_2 (%)	21.04	58.24	-
Al_2O_3 (%)	5.33	20.23	-
Fe_2O_3 (%)	2.37	5.33	-
$SiO_2 + Al_2O_3 + Fe_2O_3$	-	83.80	min 70 (%)
TiO_2 (%)	-	0.45	-
CaO (%)	60.43	7.62	-
MgO (%)	2.43	2.01	max 4 (%)
P_2O_5 (%)	-	0.00	max 5 (%)
SO_3 (%)	3.55	2.21	max 3 (%)
Na_2O (%)	0.22	0.52	max 5 (%)
K_2O (%)	0.70	1.51	-
MnO (%)	-	0.03	-
LOI (%)	3.53	2.19	max 5 (%)
Fineness (>45 μm , %)	9.14	10.4	max 12 (%)
Activity index, 28 days (%)	-	87.4	min 75 (%)
Activity index, 90 days (%)	-	101.8	min 85 (%)
Specific gravity (kg/m^3)	3040	2075	-

It can be seen that the selected FA had a particle size distribution similar to cement. In this way, high pozzolanic reactivity of FA-2 with the selected cement was enabled. In order to improve the workability of concrete, a polycarboxylate ether polymer-based superplasticizer (Glenium ACE, BASF d.o.o.) was used in some mixtures. The density of the superplasticizer was 1070 kg/m^3 .

4. Experimental program and test results

4.2.2.3. Coarse and fine aggregate

Two types of commonly used coarse aggregate were used in this research, crushed stone and river aggregate. In the first phase, river sand and coarse crushed stone aggregate with a 16 mm nominal maximum size were used. In the second phase, river sand and coarse river aggregate with a 16 mm nominal maximum size were used. Density and absorption of aggregates are presented in Table 4.4. Particle size distributions of river and crushed stone aggregate used in the first and second phase are shown in Figures 4.2 and 4.3, respectively.

Table 4.4 Dry density and absorption of aggregate

		Dry density (kg/m ³)	Absorption (%)
The first phase	0-4 mm river sand	2788	2.00
	4-8 mm crushed stone	2709	0.72
	8-16 mm crushed stone	2658	0.77
The second phase	0-4 mm river sand	2573	1.20
	4-8 mm river gravel	2548	1.24
	8-16 mm river gravel	2591	1.04

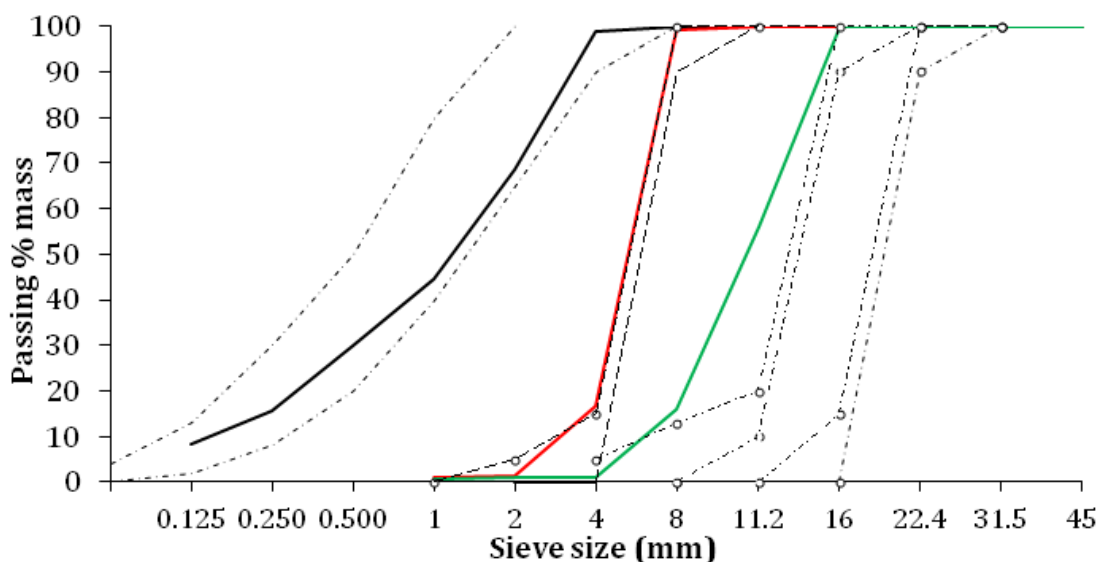


Figure 4.2 Particle size distribution of aggregate used in the first phase

4. Experimental program and test results

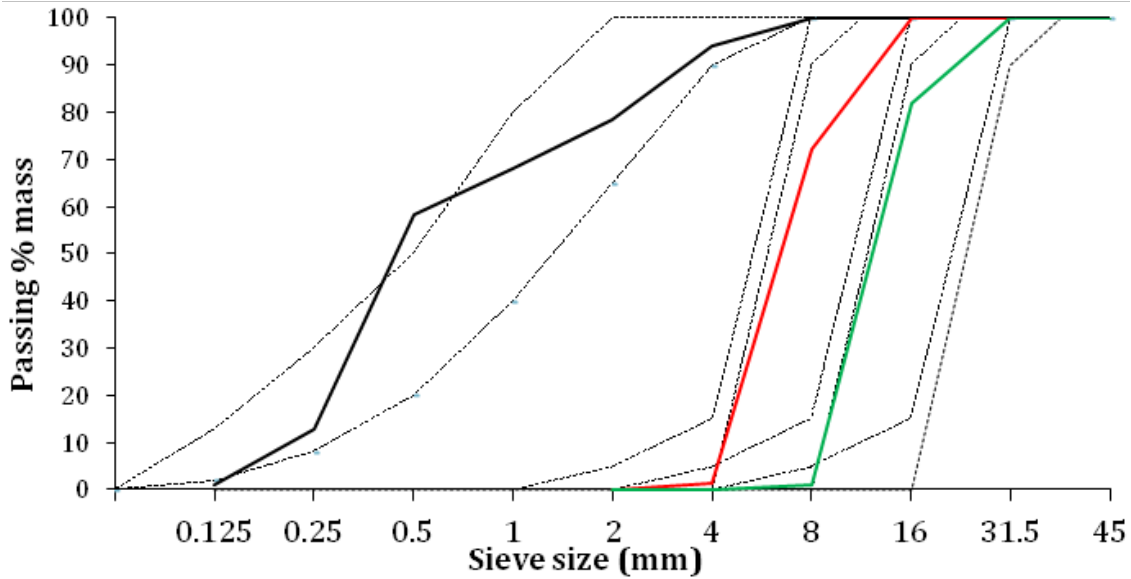


Figure 4.3 Particle size distribution of aggregate used in the second phase

4.2.3. Casting, curing and testing of specimens

Proportioning of concrete mixtures was based on the absolute volume method and was done using the following equation:

$$\frac{m_c}{3040} + \frac{m_v}{1000} + \frac{m_{lp}}{2075} + \frac{m_{0/4}}{2573} + \frac{m_{4/8}}{2548} + \frac{m_{8/16}}{2591} + \frac{m_{pl}}{1070} + 0.015 = 1 \quad \text{Eq. 4.1}$$

The mixing procedure began with mixing sand and coarse aggregate in a mixing pan for 1 min, adding cement and FA and mixing for another minute. Water and superplasticizer (when necessary) were added during the next 30 s. After that, the mixing continued for approximately 2.5 min; hence, the complete mixing lasted for approximately 5 min. Concrete cubes (100 mm) were cast for compressive strength testing, 150·150 mm cylinders for splitting tensile strength testing, and 150·300 mm cylinders for testing the modulus of elasticity. All specimens were cast in steel moulds and concrete was compacted using a vibrating table. After finishing, the specimens were covered with wet fabric and stored in a casting room at $20 \pm 2^\circ\text{C}$. They were unmolded after 24 h and kept in a water tank until testing. Reported values of various properties represent the mean value of three measurements, i.e., three samples were made for testing each property.

4. Experimental program and test results

Fresh concrete properties—workability (slump or flow) and density—were measured for all concrete mixtures. In the first phase, only compressive strength was tested, at the age of 3 and 28 days. In the second phase, the compressive and tensile strength as well as the modulus of elasticity were tested, at various ages. All tests on mechanical properties were performed in accordance with the appropriate European Standards (CEN 2009a; b; c).

4.2.4. The first phase of the HVFAC research

4.2.4.1. Concrete mixtures

The first phase was a trial phase carried out in order to assess the possibility of using FA from "Nikola Tesla B" power plant in HVFAC for structural use. Three goals for the first step were set up regarding the basic physical and mechanical requirements:

- 1) producing HVFAC with 28-day compressive strength similar to that of a RCC without FA;
- 2) obtaining suitable early (3-day) compressive strength (higher than 20 MPa) in order to meet construction practice demands;
- 3) ensuring proper workability and easy casting.

The RCC mixture was designed to reach a 28-day compressive strength of 45 MPa on a 100 mm cube specimen. The parameters that were varied in this phase were: percentage of cement in the RCC replaced by FA (FA/C), FA-to-total CM mass ratio (FA/CM), and water-to-CM ratio (W/CM). FA was used as a partial replacement of cement and sand. The concrete mixture proportions in the first phase are presented in Table 4.5. The designation of a particular mixture includes the cement (C) amount, the FA (F) amount, and the W/CM ratio. The first phase was divided into two stages. In the first stage, in the C192F192_055 mixture, 50% of cement was replaced with FA while in the C192F346_039 mixture, 30% of sand was additionally replaced with FA. The mass of sand that was replaced with FA was the maximum possible amount satisfying the required aggregate mixture particle size distribution according to standard EN 12620 (CEN 2010), Figure 4.4.

4. Experimental program and test results

Compressive strength of the RCC in the first stage did not reach the target 28-day compressive strength of 45 MPa; hence, in the second stage, a new RCC (C384F0_052) was made with a lower W/C ratio and the same cement mass. In this stage of the first phase, different cement replacement levels and W/CM ratios of mixtures with 30% sand replacement were investigated, Table 4.5.

Table 4.5 Mixture proportions of HVFAC in the first phase

Concrete mix	FA/	W/	W	C	FA	Sand	Coarse	SP*
	CM	CM						
	%	-	kg/m ³					
C384F0_055	0	0.55	212	384	0	683	985	0
C192F192_055	50	0.55	212	192	192	650	937	0
C192F346_039	64	0.39	212	192	346	452	937	1.9
C384F0_052	0	0.52	201	384	0	758	1015	0
C192F346_037	64	0.37	201	192	346	524	969	1.9
C230F307_037	57	0.37	201	230	307	524	985	1.5
C250F288_037	54	0.37	201	250	288	524	993	1.5
C192F346_034	64	0.34	180	192	346	524	1026	2.6
C192F346_030	64	0.30	161	192	346	524	1076	3.7

*Superplasticizer

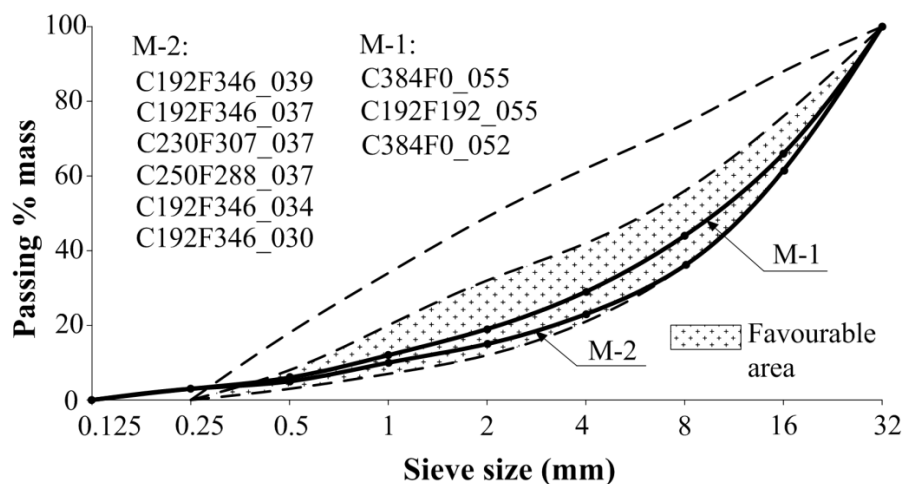


Figure 4.4 Particle size distribution of the aggregate mixtures in HVFAC in the first phase

4. Experimental program and test results

4.2.4.2. Results and discussion

Fresh and hardened concrete properties are shown in Table 4.6. Superplasticizer was added to some mixtures in the amount of 0.60% to 1.93% of cement mass. The slump values presented in Table 4.6 show that concretes with a higher mass of FA required a higher amount of superplasticizer to get a workable mixture. As expected, for mixtures with the same mass of FA, the amount of superplasticizer increases as the W/CM ratio decreases.

Table 4.6 Fresh and hardened concrete properties of HVFAC in the first phase

Concrete mix	Fresh concrete density (kg/m ³)	Slump (cm)	Hardened concrete density (kg/m ³)	Compressive strength (MPa)	
				3 Days	28 Days
C384F0_055	2370	5.7	2388	22.6	41.2
C192F192_055	2298	6.0	2307	9.9	31.0
C192F346_039	2270	16.8	2273	11.6	36.1
C384F0_052	2395	4.2	2401	31.3	50.7
C192F346_037	2300	14.8	2310	15.0	45.7
C230F307_037	2266	4.5	2270	18.5	47.8
C250F288_037	2300	7.5	2323	21.3	48.2
C192F346_034	2311	1.5	2315	19.0	54.0
C192F346_030	2349	18.0	2365	25.5	63.3

In Figure 4.5 compressive strength of mixtures is expressed as the relative percentage of the compressive strength of the RCC C384F0_055. HVFAC made with 50% cement replacement and the same W/CM ratio as the RCC had significantly lower compressive strength after both 3 and 28 days, Figure 4.5. By additionally replacing 30% of sand, the compressive strength increased from 44% to 51% at the age of 3 days and from 75% to 88% at the age of 28 days compared with the RCC, Figure 4.5. The first stage showed that HVFAC mixtures did not reach the 28-day compressive strength of the RCC and that the 3-day compressive strength was significantly lower than the target strength of 20 MPa, Table 4.6.

4. Experimental program and test results

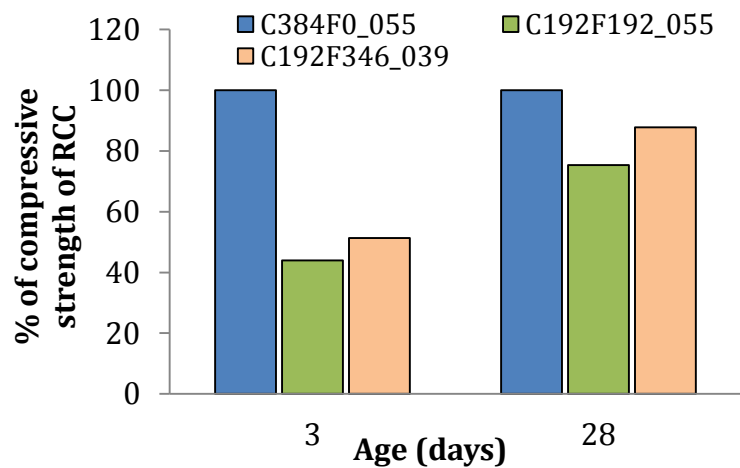


Figure 4.5 Compressive strength of HVFAC with different FA content at the age of 3 and 28 days-the first stage

Having this in mind, in the second stage a new RCC (C384F0_052) and new mixtures with 50%, 40%, and 35% of cement replacement and 30% of sand replacement (C192F346_037, C230F307_037 and C250F288_037, respectively) were designed. In Figure 4.6, compressive strength of the mixtures is expressed as the relative percentage of the compressive strength of the new RCC.

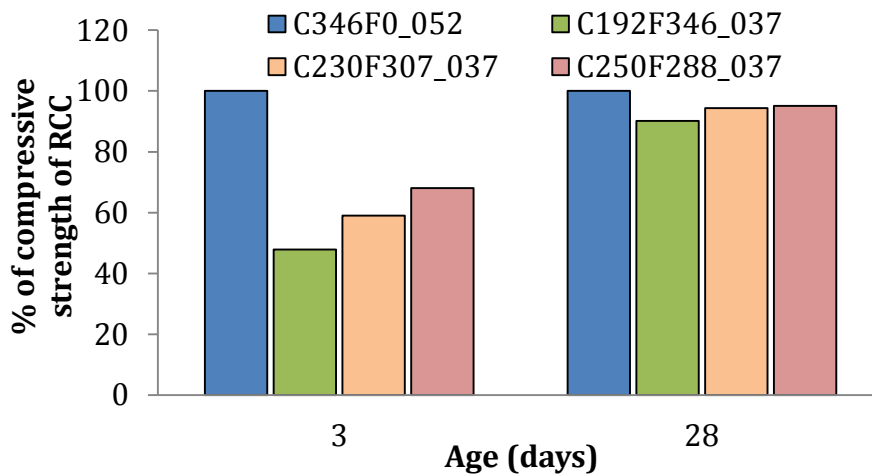


Figure 4.6 Compressive strength of HVFAC with different cement and FA content at the age of 3 and 28 days-the second stage

At the age of 28 days, compressive strength of all HVFAC mixtures was lower than the RCC by not more than 10%, and all four concretes had a compressive strength higher than the targeted 45 MPa. The 3-day compressive strength of HVFAC

4. Experimental program and test results

mixtures was 33% to 44% of their 28-day compressive strength but still lower than the targeted 20 MPa.

The last two HVFAC mixtures in the second stage (C192F346_034 and C192F346_030, Table 4.6) were designed to investigate the influence of the W/CM ratio on compressive strength of HVFAC, together with mixtures C192F346_039 and C192F346_037. Results of compressive strength comparison are presented in Figure 4.7 and it can be seen that HVFAC compressive strength increases with a decreasing W/CM ratio at both ages, as expected.

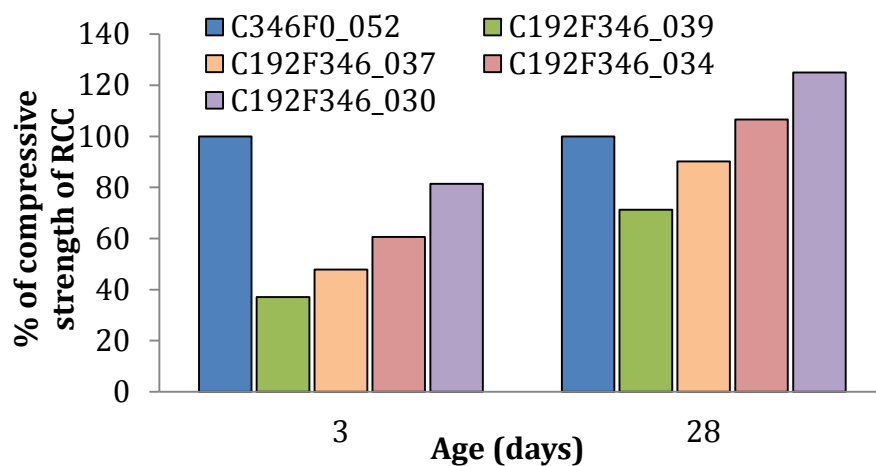


Figure 4.7 Compressive strength of HVFAC with various W/CM ratios at the age of 3 and 28 days-the second stage

At low W/CM ratios of 0.34 and 0.30, the compressive strength of HVFAC after 28 days is greater than the RCC compressive strength, by 7% and 25%, respectively. The 3-day compressive strength of these two HVFAC mixtures was 19.0 MPa and 25.5 MPa, respectively, which is similar to or higher than the targeted 20 MPa, and sufficient for structural use of concrete.

The presented results show that all three objectives which were set at the beginning of the first phase can be fulfilled (C192F346_034, C192F346_030). HVFAC suitable for structural use (satisfactory compressive strength at the age of 3 and 28 days and adequate workability) with FA from "Nikola Tesla B" power plant and with only 192 kg/m³ of cement was successfully produced. Higher compressive strength was obtained with additional FA replacement of sand. The

4. Experimental program and test results

W/CM ratio is also an important factor influencing the compressive strength of HVFAC, similar to cement concrete.

4.2.5. The second phase of the HVFAC research

4.2.5.1. Concrete mixtures

In the second phase, ten concrete mixtures were produced in order to get a better understanding of the favorable effect of sand replacement with additional FA on the compressive strength, observed in the first phase. The mixture proportions of concrete in the second phase are presented in Table 4.7.

Table 4.7 Mixture proportions of HVFAC in the second phase

Concrete mix	FA/ CM	W/ CM	W	C	FA	Sand	Coarse	SP
	%	-						
<i>C200F200_049</i>	50	0.49	195	200	200	811	810	0.0
<i>C200F250_043</i>	55	0.43	195	200	250	749	810	1.0
<i>C200F300_039</i>	60	0.39	195	200	300	687	810	1.2
<i>C200F350_036</i>	64	0.36	195	200	350	625	810	2.2
<i>C200F400_033</i>	67	0.33	195	200	400	563	810	2.4
<i>C150F150_061</i>	50	0.61	183	150	150	879	878	0.0
<i>C150F200_052</i>	57	0.52	183	150	200	817	878	0.0
<i>C150F250_046</i>	63	0.46	183	150	250	755	878	0.0
<i>C150F300_041</i>	67	0.41	183	150	300	693	878	0.3
<i>C150F350_037</i>	70	0.37	183	150	350	631	878	1.1

Two groups of HVFAC were made. The cement content of 200 kg/m³ in the first group of mixtures was chosen similar to the cement content in the first phase and the cement content of 150 kg/m³ in the second group was chosen so as to be different enough to enable an analysis of the influence of cement content on HVFAC properties. The mass of FA was varied from 200 to 400 kg/m³ in the first group and from 150 to 350 kg/m³ in the second group. The mass of FA in all mixtures was chosen to be at least 50% but it went up to 70% of the CM mass. The

4. Experimental program and test results

maximum sand content that could be replaced was determined on the basis of the required aggregate mixture particle size distribution according to standard (CEN 2010) as in the first phase. Within one group, the mass of water and the mass of coarse aggregate were kept constant and the mass of sand was determined using the absolute volume method for each mass of cement and FA.

4.2.5.2. Results and discussion

Fresh concrete properties of HVFAC mixtures are presented in Table 4.8. Workability was determined using the slump test (Abrams cone), and for concrete mixtures that had higher slump values than 220 mm, flow table tests were performed. With increasing the FA content, concrete mixtures became stiffer and those with more than 400 kg/m³ of CM required the addition of a superplasticizer in order to obtain a workable mix. Again, it was noticed that the content of superplasticizer should be increased with the increase of FA, which is in accordance with the results from literature (Wang et al. 2003).

However, the behavior of mixtures with the highest content of FA and the lowest W/CM ratio (C200F400_0.33 and C150F350_037) was rather different compared with the behavior of fresh cement concrete. Before adding the superplasticizer, the mixtures were very dry and disjointed. Only after adding the superplasticizer they became uniform, but stickier and their slump turned into flow. These mixtures showed pronounced thixotropy: during mixing they behaved in a very flowable manner but when the mixing stopped it was very hard to take concrete out of the mixing pan because of the surface stiffness. The observed behavior is similar to the behavior of geopolymer concrete with dense, sticky but workable mixtures (Mandal et al. 2011; Wang et al. 2003). It was also noticed that small changes of the superplasticizer content resulted in a significant change of workability. The slump/flow values and superplasticizer content in mixtures C200F350_036 and C200F400_033 and in mixtures C150F300_041 and C150F350_037 are shown in Tables 4.8 and 4.7, respectively. No segregation and bleeding were noticed in any of the mixtures.

4. Experimental program and test results

Table 4.8 Fresh concrete properties of HVFAC in the second phase

Concrete mix	Slump/Flow (cm)	Fresh concrete density (kg/m ³)
C200F200_049	12.7	2285
C200F250_043	14.8	2278
C200F300_039	2.8	2230
C200F350_036	3.3	2245
C200F400_033	70.0*	2237
C150F150_061	8.2	2355
C150F200_052	5.8	2309
C150F250_046	8.3	2311
C150F300_041	4.0	2281
C150F350_037	58.5*	2268

*Flow values

The density and compressive strength of concrete mixtures are shown in Table 4.8. It is evident that the group of HVFAC mixtures made with 200 kg/m³ of cement had higher compressive strength compared with the group made with 150 kg/m³ of cement, for all FA contents and all ages. With the increase of FA content, compressive strength generally increased at all ages for both concrete groups, although the increase is rather low, maximally 20%. It is probably the consequence of a 'filler' effect of FA, resulting in a more compact structure of the concrete matrix.

Splitting tensile strength results shown in Table 4.9 indicate a large scatter and no reliable correlation with the FA content was found.

The modulus of elasticity of HVFAC increased over time, with the exception of the concrete mixture C150F300_041 for which the modulus of elasticity remained nearly constant, Table 4.9. Comparing HVFAC mixtures with the same FA content, in most cases higher moduli of elasticity were observed in concrete mixtures with greater cement content. However, at the age of 180 days, the modulus of elasticity generally decreased with increasing FA content for both HVFAC with 200 kg/m³ and 150 kg/m³ of cement.

4. Experimental program and test results

Table 4.9 Density and compressive strength of HVFAC in the second phase

Concrete mix	Hardened density (kg/m ³)	Compressive strength (MPa)					
		3 days	7 days	14 days	28 days	90 days	180 days
C200F200_049	2303	11.1	22.7	30.4	34.2	44.2	53.1
C200F250_043	2295	16.3	22.9	32.0	38.2	42.3	49.7
C200F300_039	2244	15.5	22.2	32.2	36.7	42.8	42.9
C200F350_036	2268	17.6	27.1	36.2	42.0	47.9	59.5
C200F400_033	2255	14.8	23.3	37.2	40.2	54.2	60.6
C150F150_061	2352	8.2	12.9	19.3	24.3	28.5	40.6
C150F200_052	2313	8.5	15.6	20.2	25.7	32.8	41.6
C150F250_046	2316	11.8	14.2	22.0	24.5	33.8	43.5
C150F300_041	2291	10.0	16.1	25.3	26.8	38.0	41.4
C150F350_037	2283	9.9	16.0	25.0	29.8	39.3	46.7

Table 4.10 Splitting tensile strength and modulus of elasticity of HVFAC in the second phase

Concrete mix	Splitt. tens. strength (MPa) 28 days	Modulus of elasticity (GPa)					
		3 days	7 days	14 days	28 days	90 days	180 days
C200F200_049	2.9	26.7	30.5	32.1	31.3	34.8	37.1
C200F250_043	2.7	-	-	-	32.1	33.7	37.4
C200F300_039	2.9	-	-	-	31.8	32.5	36.8
C200F350_036	3.7	29.6	31.1	33.7	33.2	35.1	34.7
C200F400_033	2.0	-	-	-	32.7	33.3	34.9
C150F150_061	2.5	-	-	-	29.0	35.5	38.1
C150F200_052	2.3	-	-	-	31.9	34.6	38.0
C150F250_046	3.1	-	-	-	30.0	32.6	36.2
C150F300_041	2.9	-	-	-	30.1	30.2	29.6
C150F350_037	3.2	-	-	-	30.2	33.1	32.5

4. Experimental program and test results

4.2.6. Conclusions

The presented results show that HVFAC suitable for structural use (satisfactory compressive strength at the age of three and 28 days and adequate workability) can be made with class F FA from "Nikola Tesla B" power plant. Based on the analysis presented in this chapter, following conclusions valid for this FA type can be drawn:

- with replacement of 50% of cement with class F FA, the compressive strength decreased to 44% and 75% at the age of three days and 28 days compared with the RCC, respectively;
- by additionally replacing 30% of sand (together with 50% of cement replacement), the HVFAC compressive strength increased from 44% to 51% at the age of three days and from 75% to 88% at the age of 28 days compared with the RCC;
- HVFAC with 50% of cement replacement with FA, 30% of sand replacement with FA, low W/CM ratio (lower than 0.35) and up to 2% of superplasticizer can be made to have equal or higher compressive strength compared with the RCC;
- with replacement of 50% of cement and additional 30% of sand with FA, a HVFAC made with only 192 kg/m³ of cement with the 3-day compressive strength higher than 20 MPa, the 28-day strength higher than 40 MPa and adequate workability for structural use can be obtained;
- by increasing the FA content in amounts greater than the mass of cement (FA/CM ratio 50–70%), the HVFAC compressive strength increased by 22% on average at all tested ages, but the viscosity and effect of thixotropy of the fresh concrete also increased.

All HVFAC mixtures made in the second phase were suitable for structural application. Having in mind the objectives of this study and the available equipment, two different HVFAC mixtures were selected for experimental research on beam elements. Flexural strength was tested on beams made with the C200F350_036 HVFAC mixture (hereinafter C200F350) and shear strength on beams made with the C200F200_049 (hereinafter C200F350) HVFAC mixture.

4. Experimental program and test results

4.3. TESTING OF REINFORCED CONCRETE BEAMS' FLEXURAL BEHAVIOR

4.3.1. Introduction

A considerable amount of research has been performed regarding the physical and mechanical properties of HVFAC and some work was also done on the evaluation of its material properties through standards for cement concrete. The next step closer to the greater practical use of HVFAC is an extensive experimental evaluation of HVFAC structural behavior. Available research completed so far was focused on bond strength (Wolfe, 2011; Arezoumandi, Wolfe and Volz, 2013; Arezoumandi, Looney and Volz, 2015; Zhao, Cai and Yang, 2016), flexural (Arezoumandi, Ortega and Volz, 2015; Yoo, Ryu and Choo, 2015) and shear (Rao, Mohan and Sekar, 2011; Ortega, 2012; Arezoumandi and Volz, 2013; Arezoumandi *et al.*, 2013; Sadati *et al.*, 2016; Lisantono, Wigroho and Purba, 2017) strength of HVFAC beams made with class F and class C FA.

Extensive research of the OPCC RC structures' flexural behavior followed with fundamental theoretical background led to the full understanding of flexural failure mechanisms. This is probably the reason why there are only a few available studies in the literature investigating the flexural behavior of HVFAC beams. It is assumed that it is possible to predict flexural behavior of beams based on available material properties. Having in mind a new binding material and a great variety of parameters influencing the flexural behavior of RC members, the effect of the new binder type has to be assessed experimentally. There are limited results from the literature analyzing the flexural behavior of HVFAC; therefore, this part of own experimental research is carried out in order to gain more information regarding the behavior of HVFAC beams under bending.

An experimental program was designed to give comparative results of HVFAC and OPCC beams' flexural behavior. Two HVFAC and two referent OPCC beams with a targeted equal 90-day compressive strength were made and tested. The geometry and properties of corresponding HVFAC and OPCC beams along with the experimental set-up were designed to be identical, differing only in the concrete type. All other factors influencing flexural behavior were the same in the tested

4. Experimental program and test results

HVFAC and OPCC beams: cross-section dimensions, shear reinforcement ratio, cement, FA, and aggregate type.

4.3.2. Material properties

4.3.2.1. Concrete

The RC beams for flexural testing were made with HVFAC with 200 kg/m³ of cement and 350 kg/m³ of FA (concrete mixture C200_F350). The referent cement concrete (OPC_F) was designed to have 90-day compressive strength and workability the same as HVFAC mixture C200_F350. The component materials (aggregate, cement and FA) for both HVFAC and OPCC were the same as those in the material testing phase of this research (Section 4.2). The concrete mixture design used for this set of beams is shown in Table 4.11.

Table 4.11 Concrete mix design for flexural test beams

Component materials	Type	C200_F350	OPC_F	
Aggregate (kg/m ³)	River	0/4	624	821
	River	4/8	486	547
	River	8/16	324	456
Cement (kg/m ³)	CEM II 42.5 R	200	300	
FA (kg/m ³)	Class F	350	0	
Water (kg/m ³)	Tap water	195	175	
Admixtures (kg/m ³)	Superplasticizer	2.2	0	
W/CM	Water-to-CM ratio	0.355	0.583	
FA/CM	FA-to-CM ratio (%)	63.6	0	

The mixing procedure lasted for 4 min and consisted of (1) mixing total aggregate for 30 s, (2) adding cement and FA and mixing for another 30 s, and (3) adding water and superplasticizer and mixing for another 3 min all together. Concrete was made in the Laboratory for Materials at the University of Belgrade's Faculty of Civil Engineering and then transported to the Laboratory for Structures at the same Faculty. Beams were cast over a period of two days, two HVFAC beams on the first

4. Experimental program and test results

day and two OPCC beams on the second day. The average temperature in the laboratory during the HVFAC preparation was $22.2\pm 2^{\circ}\text{C}$, the humidity was $46.6\pm 5\%$ with an average concrete temperature of 21.4°C after mixing. The average temperature during OPCC preparation was $21.8\pm 2^{\circ}\text{C}$, the humidity was $31.2\pm 5\%$ with the average concrete temperature of 20.4°C after mixing. Figure 4.8 shows the C200_F350 and OPC_F concrete mixtures prepared for casting.



Figure 4.8 a) HVFAC mixture C200_F350 b) OPCC mixture OPC_F

After mixing, the concrete was placed in formwork for the beams and in molds for concrete specimen casting. Different concrete specimens were made for testing different properties of both HVFAC and OPCC. The sample types, number, dimensions, testing property, and curing conditions are shown in Table 4.12.

Table 4.12 Specimens for testing concrete properties

Sample size	No.	Testing property	Curing
Cube $100 \cdot 100 \cdot 100 \text{ mm}$	15	Compressive strength	In water
Cube $100 \cdot 100 \cdot 100 \text{ mm}$	9	Compressive strength	The same as beams
Cylinder $\varnothing 150 \cdot 150 \text{ mm}$	3	Splitting tensile strength	In water
Cylinder $\varnothing 150 \cdot 150 \text{ mm}$	3	Splitting tensile strength	The same as beams
Cylinder $\varnothing 150 \cdot 300 \text{ mm}$	3	Modulus of elasticity	In water
Cylinder $\varnothing 150 \cdot 300 \text{ mm}$	3	Modulus of elasticity	The same as beams
Prism $120 \cdot 120 \cdot 360 \text{ mm}$	3	Flexural strength	In water
Prism $120 \cdot 120 \cdot 360 \text{ mm}$	3	Flexural strength	The same as beams

4. Experimental program and test results

Standard curing implies curing in the laboratory conditions under the wet burlap for 24 hours after casting and then in a water tank until testing. The samples cured in the laboratory conditions in the same way as the beams for 14 days were used to measure the properties of concrete placed in the beams.

4.3.2.2. Steel reinforcement

The longitudinal reinforcement in beams consisted of B500B $\varnothing 8$ and $\varnothing 18$ ribbed bars as tension reinforcement and $\varnothing 8$ ribbed bars as compression reinforcement. As shear reinforcement, $\varnothing 8$ and $\varnothing 10$ reinforcing bars were used as vertical stirrups. The characteristics of the reinforcing bars were tested and shown in section 4.6.3.2 of this chapter. The characteristics of the reinforcing bars provided by the supplier are presented in Table 4.13.

Table 4.13 Reinforcing bar characteristics

Size	Type	Tensile strength R_m (MPa)	Elongation A_{10} (%)	Yield strength R_e (MPa)
$\varnothing 8$	B500B	669	9.9*	559
$\varnothing 18$	B500B	626	11.6*	535

* Elongation at maximum force

4.3.3. Preparation of beam elements

For the purpose of this research two HVFAC beams (C200_F350) and two OPCC beams (OPC_F) were made. The total length of each beam was 3.5 m. All beams were simply supported with a span length of 3.0 m. The beam cross-section was rectangular with a height of 300 mm and a width of 200 mm.

The design of the beams was chosen in order to analyze the behavior of RC beams with different longitudinal reinforcement ratios. Two sets of beams were made.

In the first group both HVFAC and OPC beams were made with a minimum longitudinal reinforcement ratio of 0.28% achieved with 3 $\varnothing 8$ tension reinforcement bars and 2 $\varnothing 8$ compression reinforcement bars. The same shear reinforcement was used over the entire beam length: stirrups $\varnothing 8/150$ mm. In this

4. Experimental program and test results

way, flexural failure was assured. In the second group, both HVFAC and OPCC beams were made with a longitudinal reinforcement ratio of 1.46% achieved with $3\varnothing 18$ tension reinforcement bars and $2\varnothing 8$ compression reinforcement bars. The same shear reinforcement was used over the entire length of the beam: stirrups $\varnothing 10/75$ mm. The beam notation, concrete type, longitudinal and shear reinforcement are presented in Table 4.14. The reinforcement in the wooden formwork is shown in Figure 4.9 and the reinforcement layout of the beams in Figure 4.10.

Table 4. 14 Notation of beams tested in flexural failure

Notation	Concrete	Longitudinal tensile reinforcement	Shear reinforcement
OPC-1	OPC_F	$3\varnothing 8$ mm	$\varnothing 8/150$ mm
OPC-2		$3\varnothing 18$ mm	$\varnothing 10/75$ mm
HVFAC-1	C200_F350	$3\varnothing 8$ mm	$\varnothing 8/150$ mm
HVFAC-2		$3\varnothing 18$ mm	$\varnothing 10/75$ mm

The total beam length was 250 mm longer than its clear span on both ends, in order to provide sufficient anchorage of the longitudinal reinforcement. More shear reinforcement was used ($\varnothing 8/50$ mm) to ensure a higher degree of confinement at these parts. In this way, failure by reinforcement slip was prevented. All beams were made in the Laboratory for Materials at the University of Belgrade's Faculty of Civil Engineering. Casting of concrete was done carefully with buckets and trowels.



Figure 4.9 Reinforcement of beams tested in flexure in formwork

4. Experimental program and test results

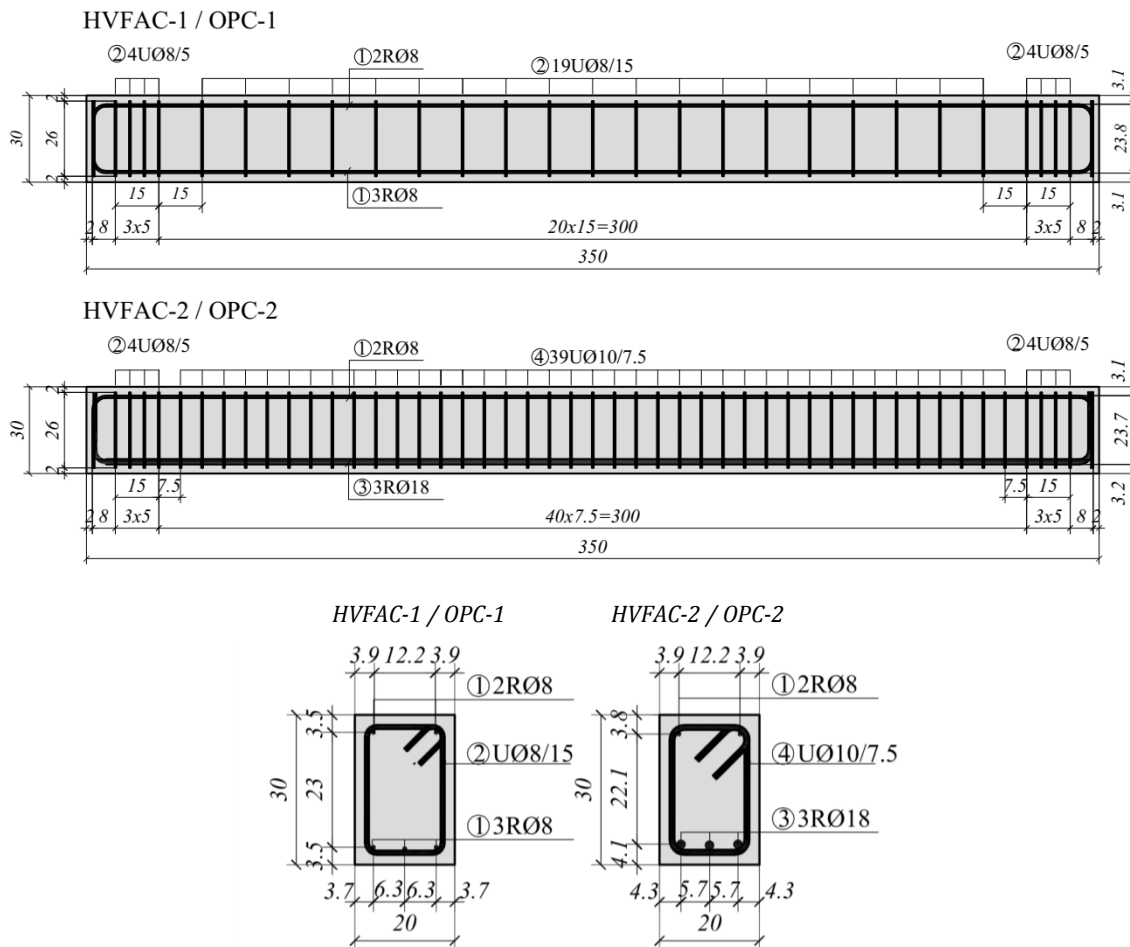


Figure 4.10 Layout of beams reinforcement

After casting of concrete into the wooden formwork, the consolidation of concrete was improved using a concrete vibrator (Figure 4.11). In this way the amount of air pockets inside the concrete mass was reduced. After proper casting, the concrete beams were covered with wet burlap and plastic foil (Figure 4.12). Three days after casting, the beams were sprayed with water three times a day to keep the burlap wet. After three days, one side of the formwork was removed and the beams were again covered and sprayed with water two times a day for another four days. After seven days, the formwork was removed and the beams were covered with plastic foil for another seven days. The beams were sprayed with water once a day during that period. After the age of 14 days no special curing of beams was done until testing. The beams were kept in the Laboratory at an average temperature of $24.3 \pm 2^\circ\text{C}$ and an average humidity of $50.7 \pm 5\%$. All beams were simply supported with the supports shown in Figure 4.13a, b. In order to

4. Experimental program and test results

easily manipulate with the beams two steel hooks were placed on the top side of the beams close to the supports (Figure 4.13c).



Figure 4. 11 Concrete casting and vibration



Figure 4. 12 Curing of the beams



Figure 4. 13 The beams: a) free support b) fixed support, and c) steel hook

4. Experimental program and test results

4.3.4. Test set-up

The analysis of the behavior under transverse loading was done in a four point bending test. Thus, stresses in the testing region (middle part of the beam) were a consequence of solely bending action (Figure 4.14).

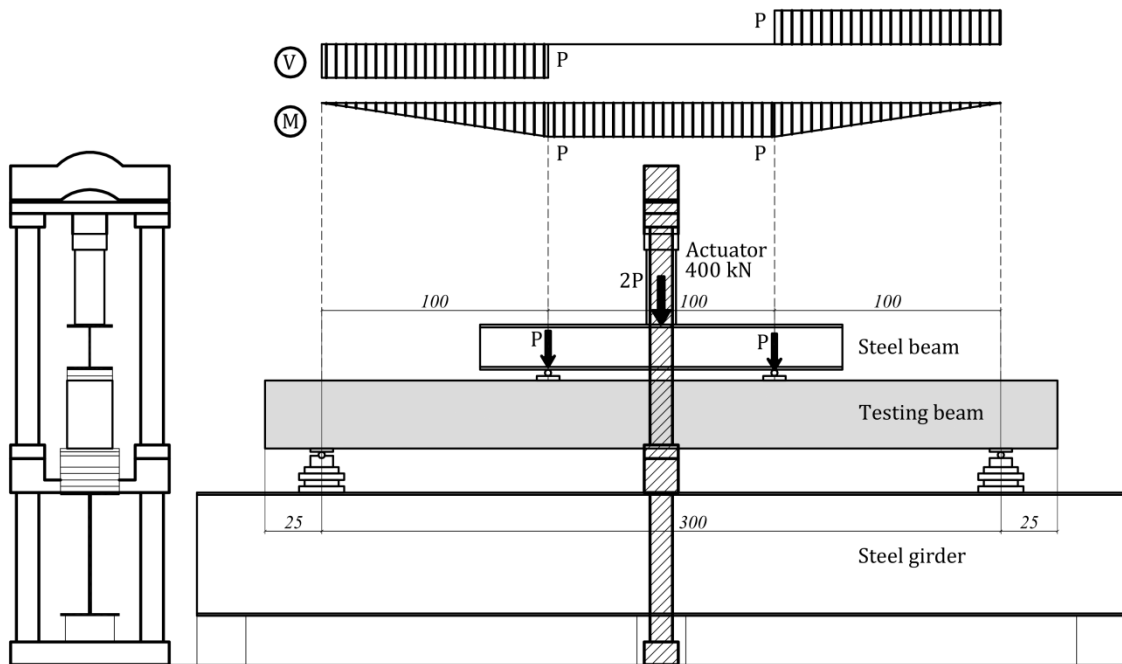


Figure 4.14 Four point bending test set up

The maximum capacity of the hydraulic press available in the Laboratory for Structures at the University of Belgrade's Faculty of Civil Engineering was 400 kN and the beams were designed accordingly. The hydraulic press applied load by pushing the steel beam downward to distribute the load onto two points in thirds of the beam span. The load was applied under force control in increments of 5, 10, and 20 kN until failure with the hydraulic press shown in Figure 4.15.



Figure 4.15 Hydraulic press

4. Experimental program and test results

All beams were tested until failure with the following parameters measured during testing: vertical displacement of the beams, concrete strains and longitudinal reinforcement strains.

4.3.5. Instrumentation

The beams were equipped with different instruments for testing. Test data were collected with an MGCplus (Hottinger Baldwin Messtechnik GmbH) data acquisition system shown in Figure 4.16.

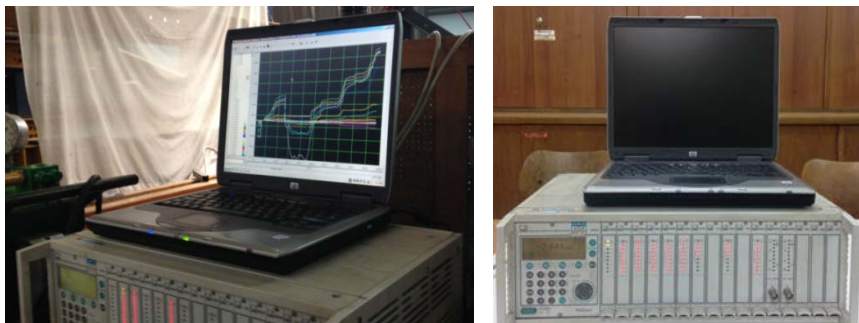


Figure 4.16 MGCplus data acquisition system

4.3.5.1. Deflection measurements

The vertical deflection of tested beams was measured using the Linear Variable Displacement Transducers (LVDT) and Mechanical Deflection Gauges (MDGs), shown in Figure 4.17a. Two MDGs (D1 and D7) were positioned above the supports to measure the displacement of supports during testing (Figure 4.17b). The vertical displacement of beams was measured in five sections with eight LVDTs (D2-D7, D9, D10, and D11) and two MDGs (D8 and D12) as shown in Figure 4.18.



Figure 4.17 a) LVDT and b) MDG

4. Experimental program and test results

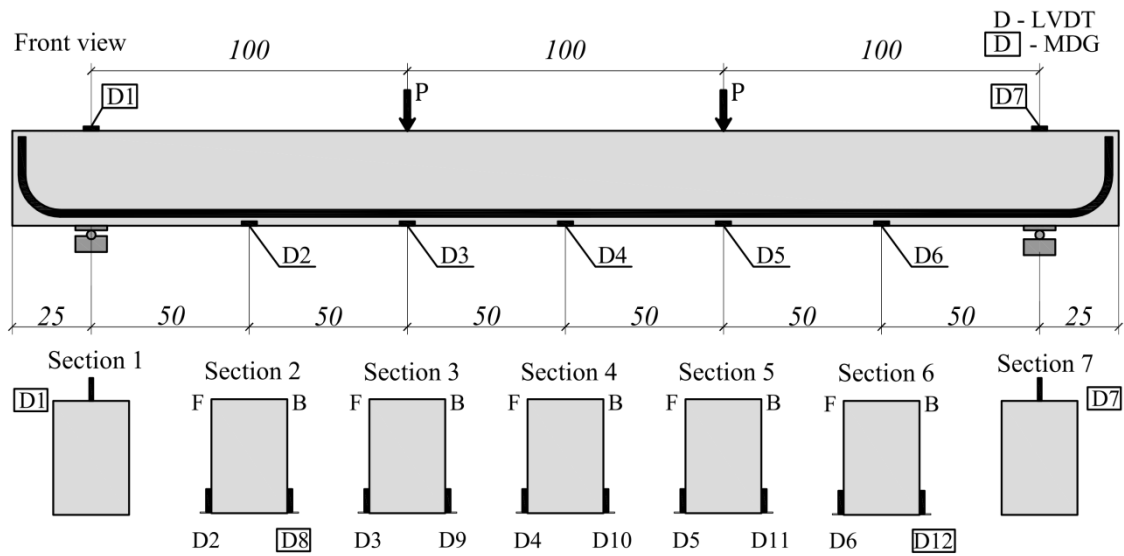


Figure 4.18 Deflection gauge setup

The LVDTs were placed to measure the deflection of beams' midpoint (Section 4), point under force application (Sections 3 and 5), and in the middle of the beams' shear span (Sections 2 and 6). Magnetic bases were used for connecting the LVDTs to the beam and holding them in the right position (Figure 4.17a). The measuring was done on both sides of the beam (front and back) and an average value of these two measurements was used in the results analysis. The vertical displacement was measured continuously until failure and data was collected using the MGCplus acquisition system. One MDG was used to control the vertical displacement of the steel girder.

4.3.5.2. Strain measurements

In order to understand the behavior of beams under transverse loading, measuring of concrete and reinforcement strains was done continuously. The measuring of concrete strains was done using Vibrating Wire Strain Gauges (VWSGs). Each VWSG sensor consisted of two end blocks with a tensioned steel wire between them so that it was free to vibrate at its natural frequency. As the concrete surface deforms, the end blocks will move relative to each other altering the tension of the wire and its vibrating frequency. The resulting frequency readings are used to calculate the strains. The end blocks were carefully glued to the specially treated concrete surface at the designed positions on the beam.

4. Experimental program and test results

In the experiment, the concrete surface was cleaned and prepared in the way that helped the adhesion and the *Sika Dur 31* adhesive was used for gluing the sensors. They were held in the right position with metal clamps for 24 hours before testing. The wire vibrations were induced using the magnetic assembly/coil at the center of the sensor between the end blocks as shown in Figure 4. 19.

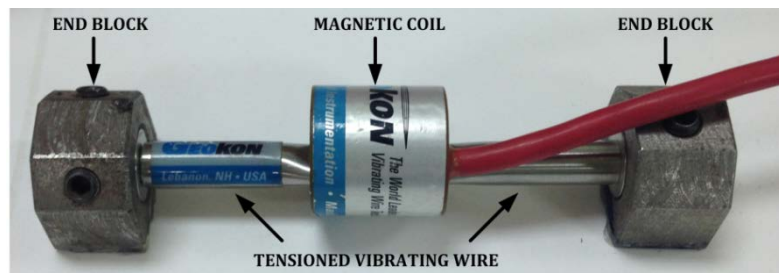


Figure 4.19 VWSG sensor

In the experiment, sensors were connected to a data taker (*Geo data logger - DT85G*) shown in Figure 4.20. Sensor arrangement and the position in the beams' midpoint and under the applied force are shown in Figure 4.21. The position of all sensors on testing beams is shown in Figure 4.22.



Figure 4.20 Data taker DT85G

Electric resistance strain gauges (SG) were used to monitor strains in the longitudinal reinforcement. The strain gauges were type PL-60-11, purchased from *Tokyo Sokki Kenkyujo Co., Ltd.* with test data shown in Figure 4.23a. Reinforcing bars were cleaned and prepared for the strain gauge gluing using a two-component HBM glue (Figure 4.23b). The strain gauges were used to measure strains in the longitudinal reinforcement in cross-sections 2, 3, 4, 5, and 6 and they were placed on each tension bar as shown in Figure 4.22. Fifteen strain gauges were used in each beam.

4. Experimental program and test results

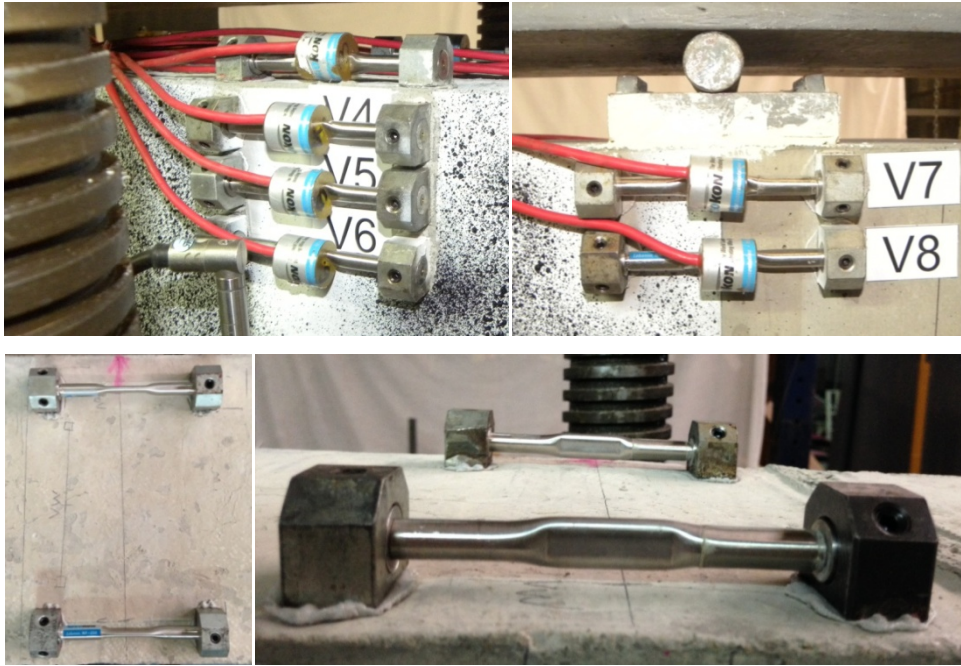


Figure 4.21 VWSG sensors measuring strains a) in the beam midpoint and b) under the applied force

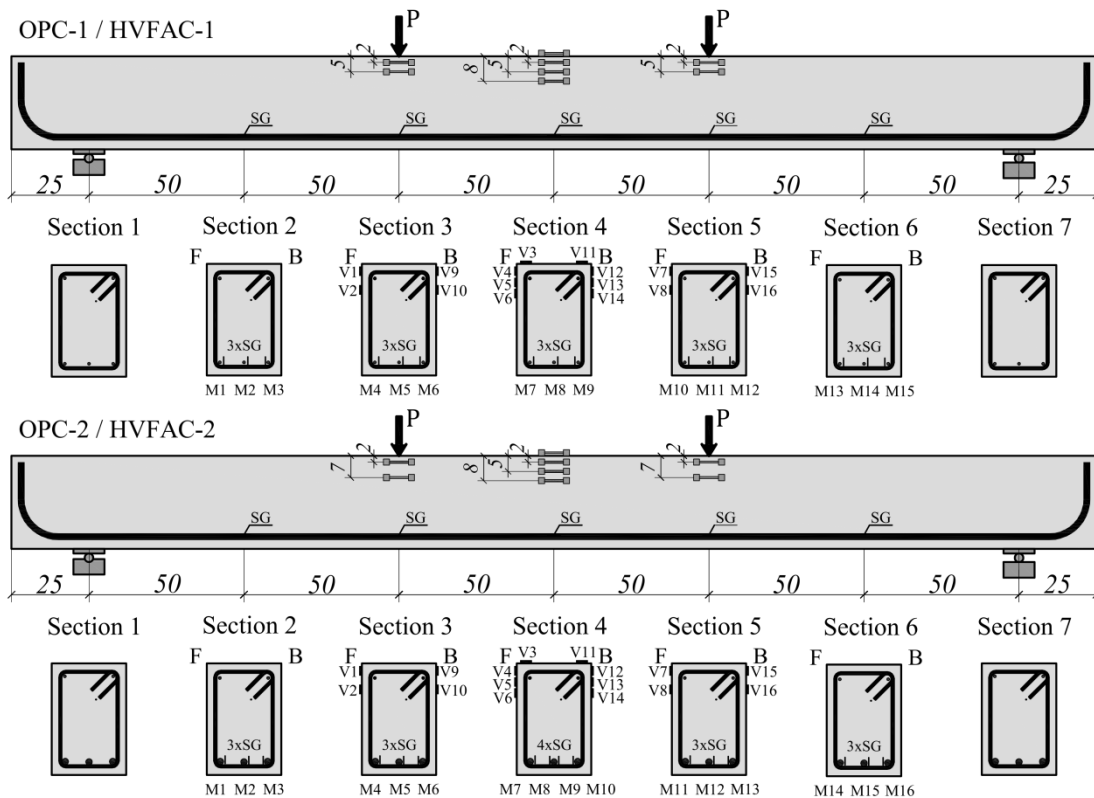


Figure 4.22 VWSG and SG arrangement on beams

4. Experimental program and test results



Figure 4.23 a) Strain gauge test data and b) HBM glue for strain gauges

4.3.5.3. Crack measurements

Hand measurements of crack width and pattern formations were taken at the end of each load step while load was held constant. For this purpose, a plastic crack comparator that measures a crack width of at least 0.03 mm, was used (Figure 4.24a). A magnifying glass was also used to improve the visibility of cracks (Figure 4.24b.).



Figure 4.24 a) Crack width comparator, b) magnifying glass (10x)

In order to analyze the crack patterns during loading cycles, a permanent marker was used to draw lines following the crack pattern next to it (Figure 4.25a.). The value of the loading force and measured crack width in each loading step were written on the current top of the crack (Figure 4.25b.).

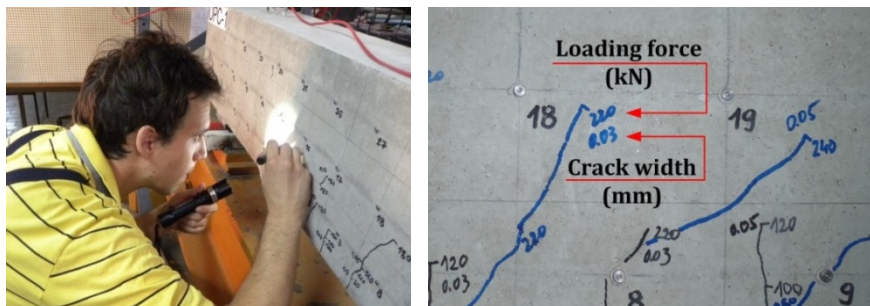


Figure 4.25 a) Marking of crack patterns b) crack width at each load step notation

4. Experimental program and test results

In order to get a better understanding of the development and geometry of cracks, a Digital Image Correlation (DIC) system was used to map the flexural cracks in the middle part of one side of the tested beams. DIC is a measurement technique used for measuring the displacement of areas of interest within a series of digital images providing full-field surface displacement measurements. In the structural engineering field, DIC has been primarily used to measure beams' deflections in comparison to traditional measuring methods (Küntz *et al.*, 2006) and to measure the increase of flexural crack widths in RC beams (Lecompte, Vantomme and Sol, 2006; Barazzetti and Scaioni, 2010; Destrebecq, Toussaint and Ferrier, 2011).

In the DIC method, digital images of a region of interest (ROI) are captured at different deformation states and post-processed by matching the same points (or pixels) between the two images recorded before and after deformation (M. Dutton, 2012). In general, the implementation of the DIC method requires preparation of the specimen, recording images of the planar specimen surface before and after the loading, and processing the obtained images using adequate software to obtain the desired displacements. The camera recording photographs must be placed with its optical axis perpendicular to the specimen surface at a specific distance from the specimen. Out-of-plane motion of the specimen during measuring should be small enough to be neglected. The displacements at points in the ROI are determined by correlating small sets of pixels (subsets) characterized usually by a grey level and relative location in the image before and after deformation. The ROI on the specimen surface must have a random texture (i.e., a random speckle pattern) at the pixel scale for matching between images. The speckle pattern can be the natural texture of the specimen surface or artificially made by spraying black and/or white paints, or other techniques (Pan *et al.*, 2009; Michael Dutton, 2012). After recording the digital images of the specimen surface, the DIC computes the motion of each image point by comparing the digital images of the test object surface in different states using shape functions and appropriate interpolation functions assuming continuous deformation. One of the most important parameters influencing the results obtained using this type of 2D DIC is the quality of acquired images and the number of information that they can provide. Special

4. Experimental program and test results

care should be taken in the specimen preparation phase regarding white and gray/black areas, contrast, size of the dots, and their distribution.

In this experiment setup, the middle part of the beam was chosen as an ROI in order to map the flexural cracks formed in that zone. The chosen ROI was a rectangle between the two loading points 1000·300 mm in size as shown in Figure 4.26.

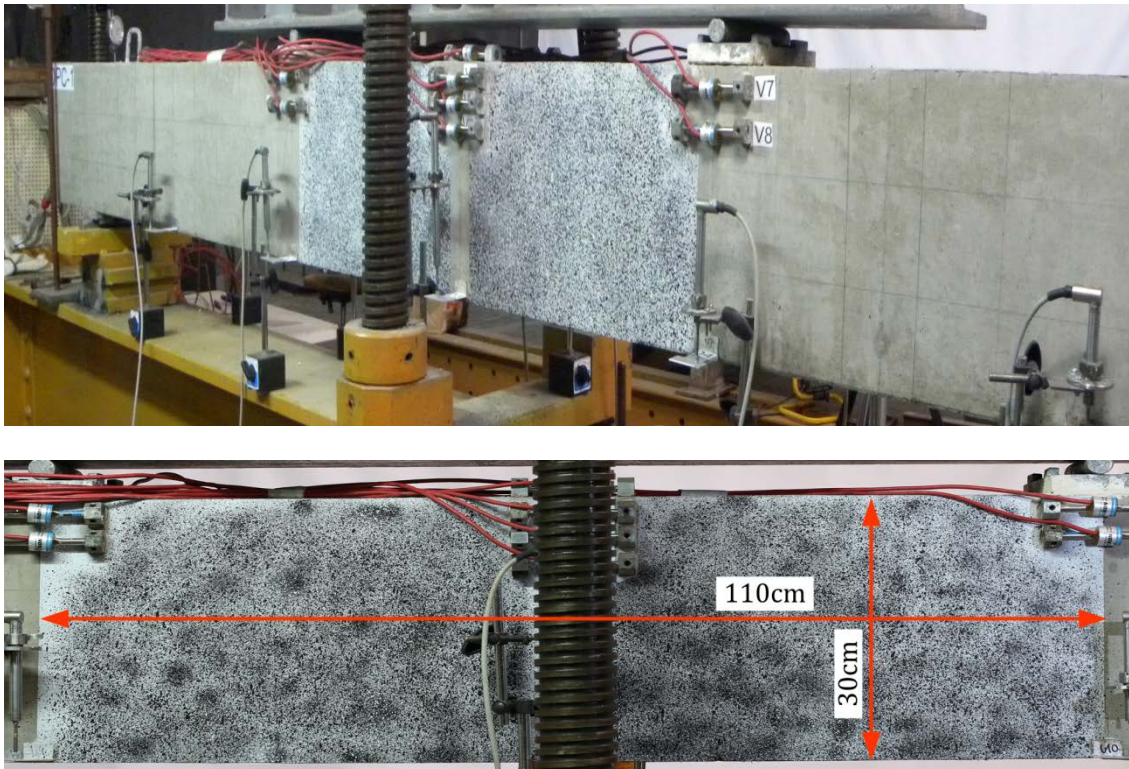


Figure 4.26 ROI on the front side of the beam

The acquisition of the digital images during the experiment was done with a DSLR (digital single-lens reflex) Canon 6D (sensor 32·24 mm, resolution 5472·3648 pixels) and a Canon EF 100mm 2/2.8L telephoto lens. The camera was placed on a tripod and triggered remotely. The tripod was located 3.1 m from the beam's surface, corresponding to a field of view of the entire ROI of the beam as shown in Figure 4.27a. This distance resulted in an average spatial resolution of 0.181 mm/pixel. LED lamps and matte paint were used in order to decrease reflection. During the experiment, the beams were photographed after each loading step immediately after stopping the actuator and before the next loading step.

4. Experimental program and test results

The most care was taken during the beams ROI preparation. Matte white paint was used first and sprayed on the entire region as a background that provides more contrast than the gray concrete color. Black paint packed in a spraying can was used to produce the needed patterns on the beams' surface. Application was done carefully by hand using the small pipe on the spraying can lid to produce a desired pattern (Figure 4.27b). DIC analysis was done using an open source 2D MATLAB program – Ncorr (Blaber, Adair and Antoniou, 2015).

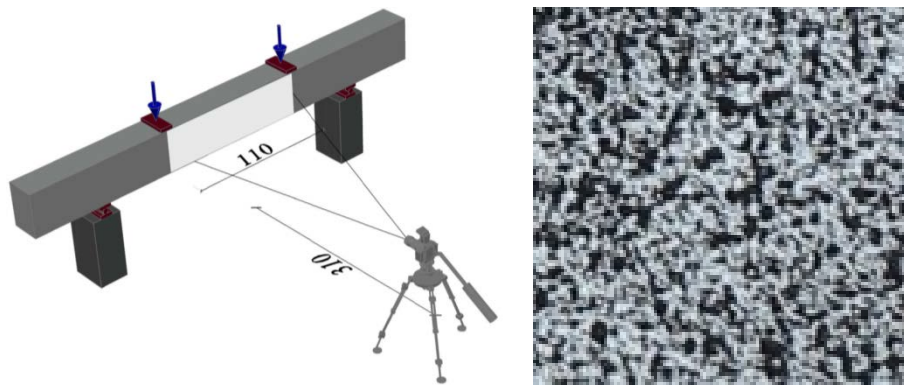


Figure 4.27 a) Camera position during the experiment and b) random speckle pattern on the ROI

4.3.6. Testing results of concrete and steel reinforcement properties

4.3.6.1. Fresh and hardened concrete properties

Testing of the fresh and hardened concrete properties was performed in the Laboratory for Materials at the University of Belgrade's Faculty of Civil Engineering. Beside the concrete temperature during mixing, the density and workability of fresh concrete mixtures was also measured. The density of compacted fresh HVFAC and OPCC was done according to the European Standard EN 12350-6 (CEN, 2009b). The workability of concrete was determined using the slump test according to the European Standard EN 12350-2 (CEN, 2009a). Testing and evaluation of the hardened concrete properties were performed in accordance with applicable European Standards. The conducted tests included the measurement of the hardened concrete density (CEN, 2009g), compressive strength (CEN, 2009d), splitting tensile strength (CEN, 2009f), flexural strength (CEN, 2009e), and the modulus of elasticity (CEN, 2009c) at various ages.

4. Experimental program and test results

The average measured values and CoV of the fresh and hardened concrete density together with the slump/flow test values are given in Table 4.15. The slump/flow test measurements of HVFAC C200_F350 and OPCC OPC_F are shown in Figure 4.28. Similar to the previous concrete testing phase, HVFAC mixture C200_F350 had a very plastic consistency described with a flow value. No segregation was observed in any of the HVFAC batches.

The workability of the OPC_F mixture corresponds to slump class S3 (slump between 100 and 150 mm) and workability of the HVFAC mixture C200_F350 to flow class F5 (flow between 560 and 620 mm) according to the EN 206 (CEN, 2011). The density of both fresh and hardened concrete was up to 7.5% higher in the OPCC mixture compared with the HVFAC mixture. The results of compressive strength, splitting tensile strength, and modulus of elasticity tests on concrete samples cured in standard laboratory conditions (water curing) are shown in Table 4.16.

Table 4.15 Density of fresh and hardened concrete and slump values for C200_F350 and OPC_F concrete mixtures

Concrete type	Density of fresh concrete (kg/m ³)		Density of hardened concrete (kg/m ³)		Slump/flow value (mm)	
	Average	CoV	Average	CoV	Average	CoV
<i>C200_F350</i>	2236.6	3.4	2240.0	1.2	568	14.8
<i>OPC_F</i>	2410.3	1.7	2372.0	2.4	113	14.9



Figure 4.28 Slump/flow measurements of mixtures a) C200_F350 and b) OPC_F

4. Experimental program and test results

Table 4.16 Compressive strength, splitting tensile strength, and modulus of elasticity of water-cured samples

Age (days)	Compressive strength (MPa)					Split. tensile str. (MPa)	Modulus of elasticity (GPa)	
	3	7	14	28	90	28	28	90
C200_F350	17.8	32.4	41.6	49.6	53.0	3.34	31.5	34.7
	19.0	32.6	37.8	34.4	50.2	3.74	34.5	29.5
	19.5	30.6	37.6	42.0	57.4	3.57	27.9	36.5
Average	18.8	31.9	39.0	42.0	53.5	3.6	31.3	33.6
CoV(%)	3.80	2.82	4.72	14.77	5.54	4.62	8.67	8.88
OPC_F	28.0	34.8	37.8	49.6	53.2	3.1	40.4	38.9
	28.5	37.2	42.2	44.0	49.0	3.1	34.5	43.3
	32.1	39.8	48.0	40.4	55.0	4.1	30.4	36.0
Average	29.5	37.3	42.7	44.7	52.4	3.4	35.1	39.4
CoV(%)	6.18	5.48	9.79	8.47	4.80	13.73	11.68	7.60
HVFAC/OPCC	0.64	0.86	0.91	0.94	1.02	1.06	0.89	0.85

The difference between HVFAC and OPCC 90-day compressive strength was less than 3%. Besides the water-cured samples, the concrete samples cast from the same batch of concrete used for the beam construction were made and cured in the same way as the beams. The hardened concrete properties of these samples are shown in Table 4.17. Three samples for compressive strength testing were made for each beam and they were tested on the same day as the corresponding beam. Other mechanical properties were tested at the age of 90 days.

The compressive strength development of the water-cured concrete mixtures and the values of the compressive strength of samples cured the same as beams are shown in Figure 4.29. It can be seen that the compressive strength of OPC_F exceeds the compressive strength of C200_F350 at earlier ages, but that they are very similar after 90 days with C200_F350 having only 2% higher compressive strength. After 90 days of curing the samples in the same way as beams, the OPC_F compressive strength was around 20% higher compared with that of C200_F350.

4. Experimental program and test results

Table 4.17 Compressive strength, splitting tensile strength, flexural strength, and modulus of elasticity of samples cured like beams

Age (days)	Compressive strength (MPa)		Split. tensile str. (MPa)	Flex. str. (MPa)	Modulus of elasticity (GPa)
	92	87	90	90	90
C200_F350	48.4	54.2	2.63	4.77	27.81
	52.8	52.6	2.77	4.97	28.96
	41.6	52.4	2.89	4.90	26.04
Average	47.6	53.1	2.8	4.90	27.6
CoV (%)	9.68	1.52	3.84	1.70	4.35
Age (days)	79	83	90	90	90
OPC_F	62.6	61.4	2.08	6.25	32.9
	55.0	63.2	2.72	6.93	32.2
	58.0	62.6	3.51	5.99	33.9
Average	58.5	62.4	2.8	6.4	33.0
CoV (%)	5.34	1.20	21.11	6.18	2.15
HVFAC/OPCC	0.81	0.85	1.00	0.77	0.84

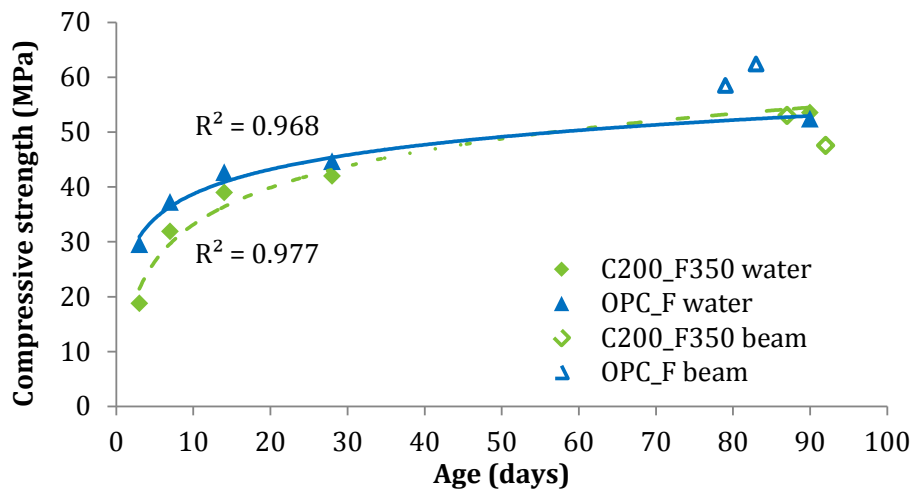


Figure 4.29 Compressive strength development of the C200_F350 and OPC_F concrete mixtures

4. Experimental program and test results

HVFAC and OPCC samples cured the same like beams had, on average, 7% lower and 14% higher compressive strengths compared with the samples cured in water, respectively.

The splitting tensile strength showed similar results for both types of concrete under both types of curing. On the other hand, flexural strength of OPC_F was 24% higher compared with C200_F350. HVFAC and OPCC samples cured the same like beams had, on average, 22% and 18% lower splitting tensile strengths compared with the samples cured in water, respectively.

The modulus of elasticity was higher in the OPC_F concrete mixture compared with C200_F350 after both 28 and 90 days, especially for the samples cured the same as the beams where the difference was 16%. The difference in the modulus of elasticity between two types of curing was more pronounced in the HVFAC mixture compared with the OPCC (Figure 4.30). Samples cured in the same way as the beams had a lower modulus of elasticity compared with the water-cured samples for both C200_F350 and OPC_F mixtures by 22% and 19% respectively.

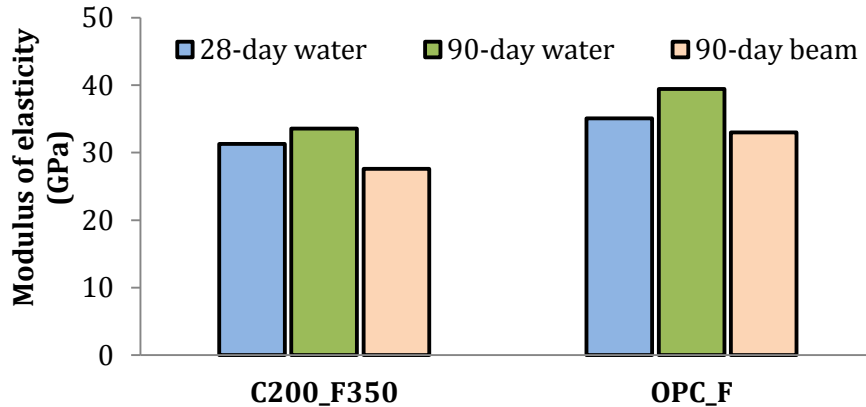


Figure 4.30 Modulus of elasticity of the C200_F350 and OPC_F concrete mixtures at different ages

4.3.6.2. Steel reinforcement properties

In order to fully understand the steel reinforcement behavior testing of all used bars was done. Testing was done at the University of Belgrade's Faculty of Technology and Metallurgy, using a 250 kN capacity testing machine shown in

4. Experimental program and test results

Figure 4.31. The obtained results are shown in Table 4.18 and the stress–strain relationship diagrams for tested bars in Figure 4.32.

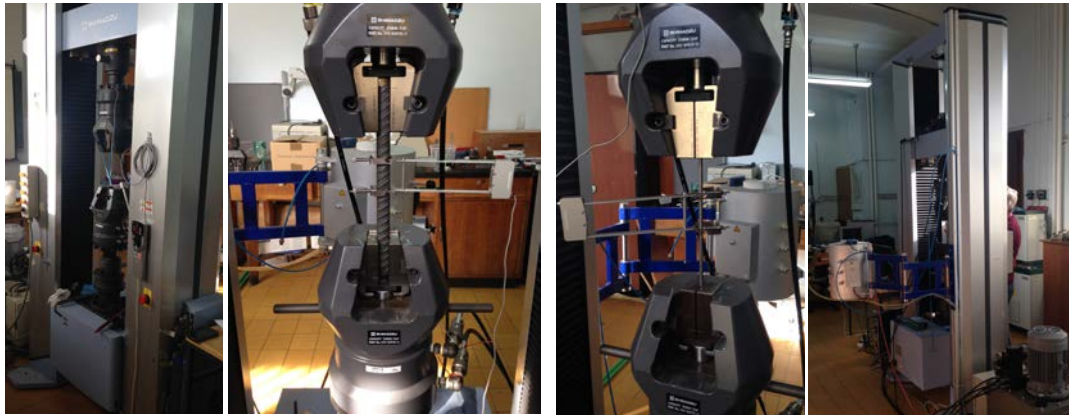


Figure 4.31 Testing of the reinforcement and stress–strain relationship determination

Table 4. 18 Test results on reinforcement bars

d (mm)	Type	$\sigma_{0.2\%}$ (MPa)	σ_m (MPa)	E (GPa)	ϵ_{break} (%)
8	Ribbed	623.7	732.9	202.0	21.3
10	Ribbed	626.8	749.4	210.0	24.7
18	Ribbed	560.4	645.6	200.0	33.6

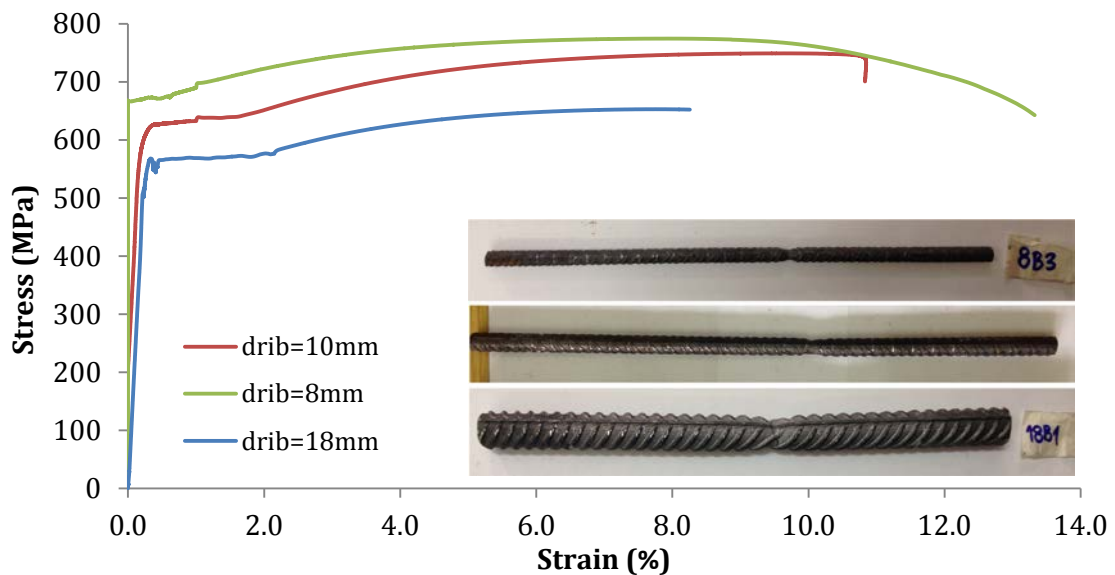


Figure 4.32 Stress–strain relationship for reinforcing bars used in beams tested for flexural behavior

4. Experimental program and test results

As can be seen, $\varnothing 18$ mm reinforcement showed lower yielding and ultimate strength, and modulus of elasticity compared with the other two tested reinforcing bar diameters. This type of the reinforcing bar was more ductile with a higher elongation at failure compared with other tested bar diameters. The yielding of reinforcement was pronounced in all three bar specimens.

4.3.7. Reinforced concrete beams' flexural behavior

The purpose of this part of the study was to investigate the HVFAC full-scale RC beams' flexural behavior and to compare it with the behavior of OPCC beams. The overall behavior of beams was analyzed first, with a focus on the levels of force inducing cracking and failure. Next, the beam deflection, and concrete and longitudinal reinforcement strains were analyzed. Finally, the appearance and distribution of flexural cracks was analyzed using crack patterns carefully drawn on the beam surface in each loading step (after 5, 10 or 20 kN) together with DIC crack mapping. Two groups of beams were made and tested in order to analyze the flexural behavior of beams with a minimum and higher than minimum longitudinal reinforcement ratio. Each group consisted of one HVFAC and one OPCC beam with the same longitudinal and shear reinforcement.

4.3.7.1. Overall behavior of beams tested for flexural behavior

Table 4.19 summarizes all the important parameters for the evaluation of overall flexural behavior. The table includes beam notation and longitudinal reinforcement, load at first flexural crack formation ($2P_{fl,cr}$), load at the beams' yielding point ($2P_y$), maximum load at failure – ultimate load ($2P_u$), midpoint beam deflection under service load level (a_{ser}), midpoint beam deflection at the point of beam yielding (a_y), midpoint beam deflection under the ultimate loading (a_u), the ultimate deflection-to-deflection at yielding ratio (a_u/a_y), flexural crack width at the service load level ($w_{ser,max}$), maximum vertical crack length at the service load level ($l_{ser,max}$), maximum concrete and reinforcing steel strains in the middle section of the beam (ϵ_c and ϵ_s).

The a_u/a_y ratio was calculated as an indicator of beam ductility, i.e., beams' bearing capacity after yielding. The global behavior of RC beams was also described with

4. Experimental program and test results

the beams deflection in the service load level (taken as 40% of the ultimate loading) and at the maximum loading level.

In further analyses, beams' self-weight, weight of the steel girder and the hydraulic press were neglected when presenting load values (2P) because they were significantly lower compared with the load induced by the press. The weight of these elements was taken into account only when the results were compared with the standards for the design of RC structures.

Table 4.19 Experimental results of the flexural testing of beams

Beam notation	Long. reinf.	2P _n (kN)	2P _y (kN)	2P _u (kN)	a _{ser} (mm)	a _y (mm)	a _u (mm)	a _u /a _y (-)	w _{ser,max} (mm)	l _{ser,max} (mm)	ε _c (‰)	ε _s (‰)
OPC-1	3Ø8	20	40	51.3	2.2	11.5	127.5	11.1	0.08	90	4.3	51.6
HVFAC-1		15	35	55.1	4.3	17.8	122.0	6.9	0.03	210	4.7	66
OPC-2	3Ø18	30	210	224.1	7.1	22.7	45.2	2.0	0.05	154	4.6	5.7
HVFAC-2		20	210	225.3	7.4	23.6	57.6	2.4	0.08	228	4.9	21.0

As expected, all beams failed in flexure with a higher ultimate load in beams with a higher reinforcement ratio, for both types of concrete. The crack propagation in beams began with the appearance of flexural cracks in the flexural span of the beam. As additional load was applied, more flexural cracks formed in that region and in the shear spans. The flexural cracks developed vertically and inclined flexure-shear cracks began to appear close to the beams' supports at a load level of approximately 50% of the ultimate load. It is usually difficult to determine the formation of the first crack by the naked-eye, so the beam load-deflection curves were analyzed. A closer look at the beams load-deflection curves for the moment when the cracking was visually spotted is plotted in Figure 4.33.

A point when the stiffness of beams started to decrease was marked as the moment when the first cracks appeared. Values obtained in this way coincide with

4. Experimental program and test results

the values obtained by the naked-eye. As it can be seen from Table 4.19, the first flexural cracks appeared at lower loading levels for the HVFAC beams compared with the OPCC ones: 39% and 27% of the ultimate load for beams OPC-1 and HVFAC-1 and 13% and 10% of the ultimate load for beams OPC-2 and HVFAC-2. Flexural cracks patterns for all beams are shown in Figure 4.34 for the service load.

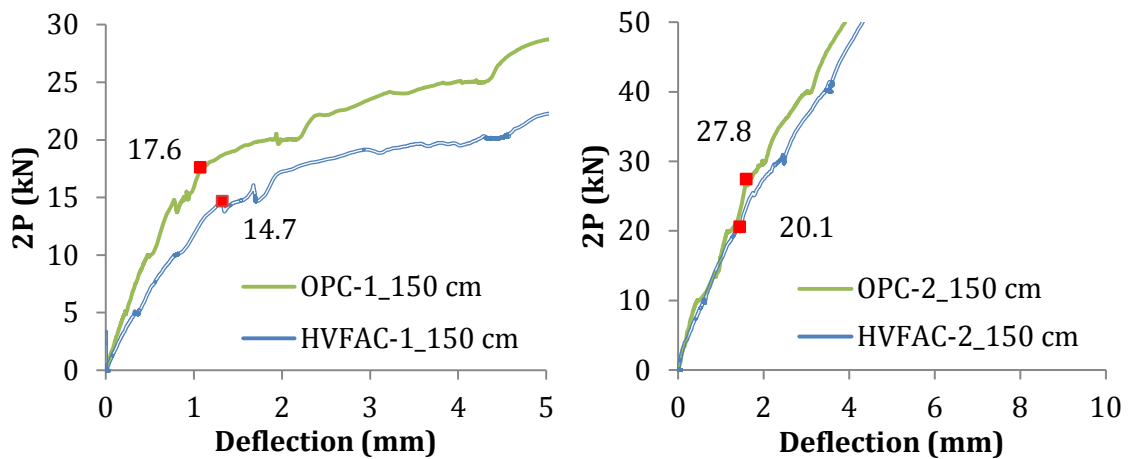


Figure 4.33 Load-deflection curves for a) beams from the first group and b) beams from the second group

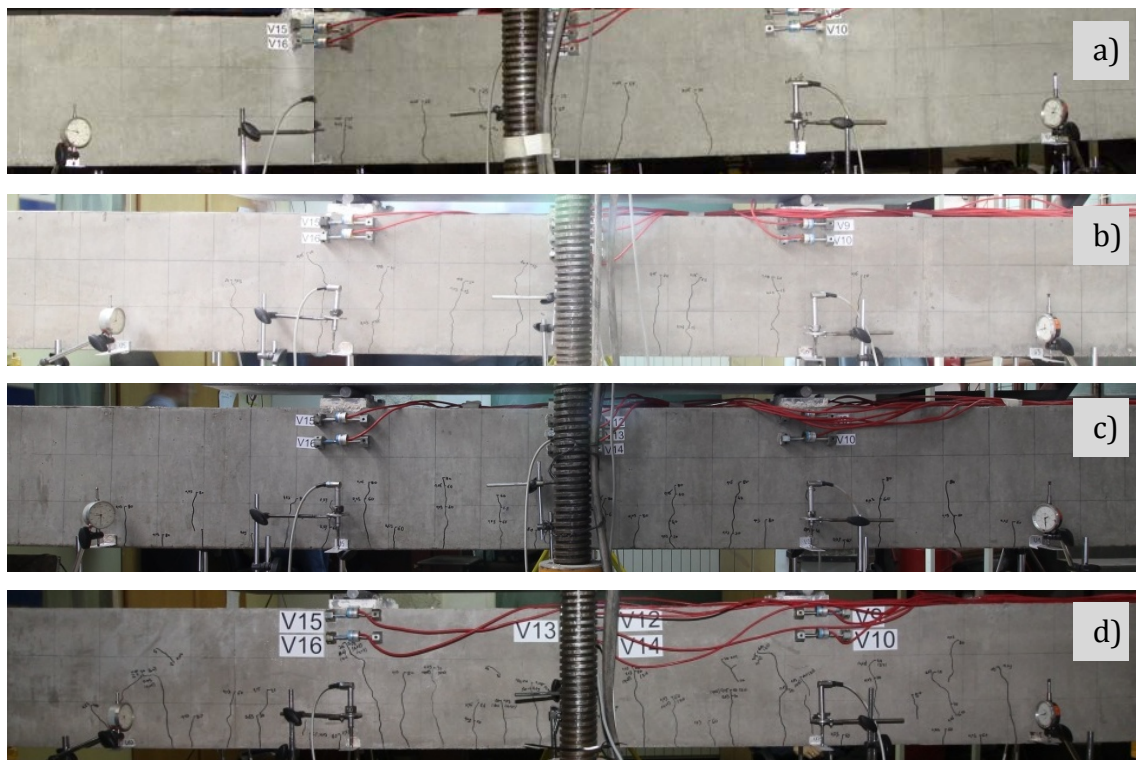


Figure 4.34 Crack formation at service load level for a) OPC-1, b) HVFAC-1, c) OPC-2, and d) HVFAC-2 beams

4. Experimental program and test results

It can be seen that more cracks developed in the HVFAC beams compared with the OPCC beams for both service and ultimate load level. Crack patterns at failure load for beams with a minimum reinforcement ratio are shown in Figures 4.35 and 4.36.

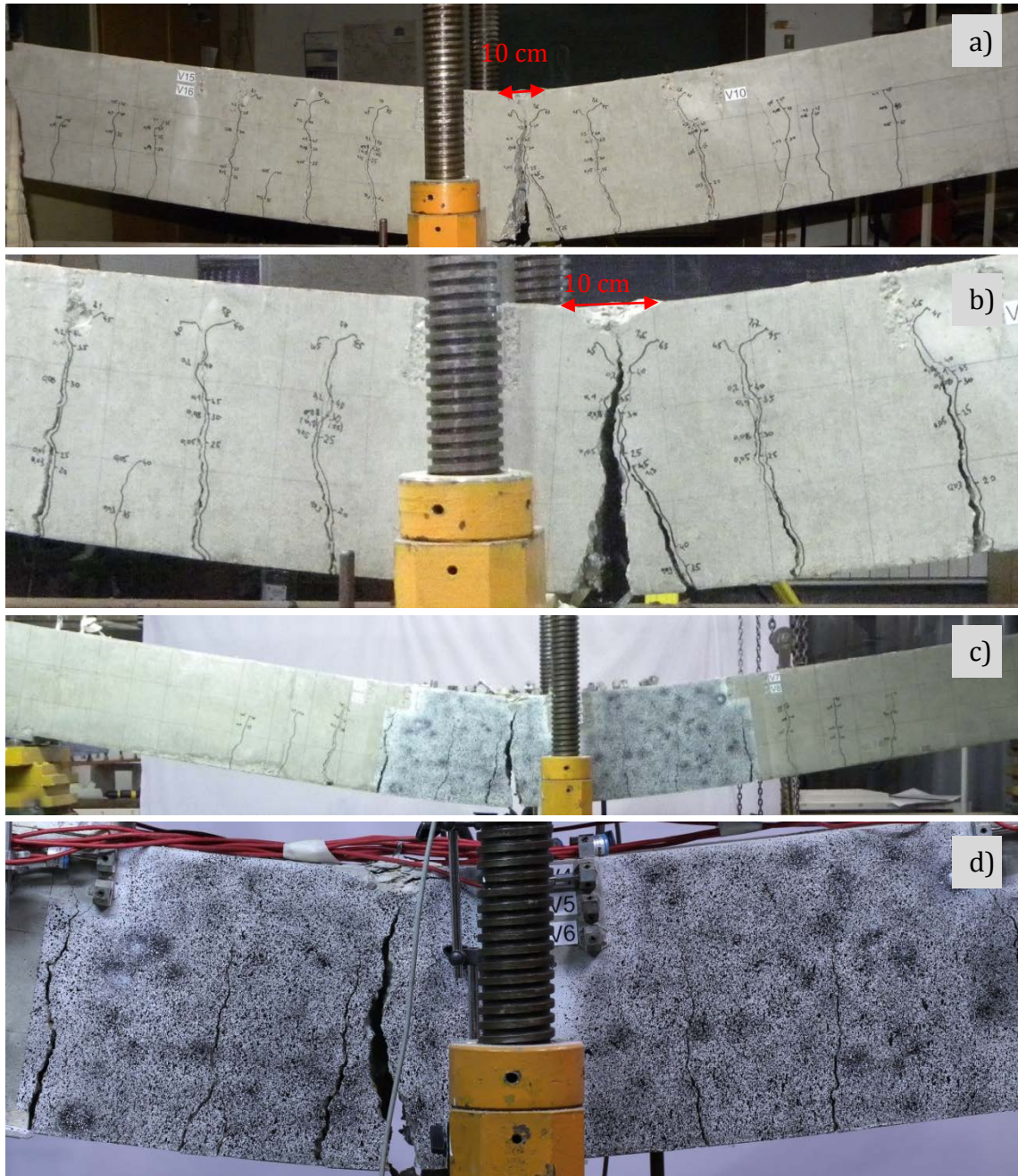


Figure 4.35 Crack patterns at failure load for the OPC-1 beam: a) back side of beams' clear span, b) backside of beams' flexural span, c) front side of beams' clear span and d) front side of beams' flexural span

4. Experimental program and test results

Both beams showed a ductile behavior and after yielding of the longitudinal reinforcement large mid-span deflections were recorded – up to 150 mm. Crack distribution was visibly similar in both beams with uniform and symmetrical distribution along the beam length.

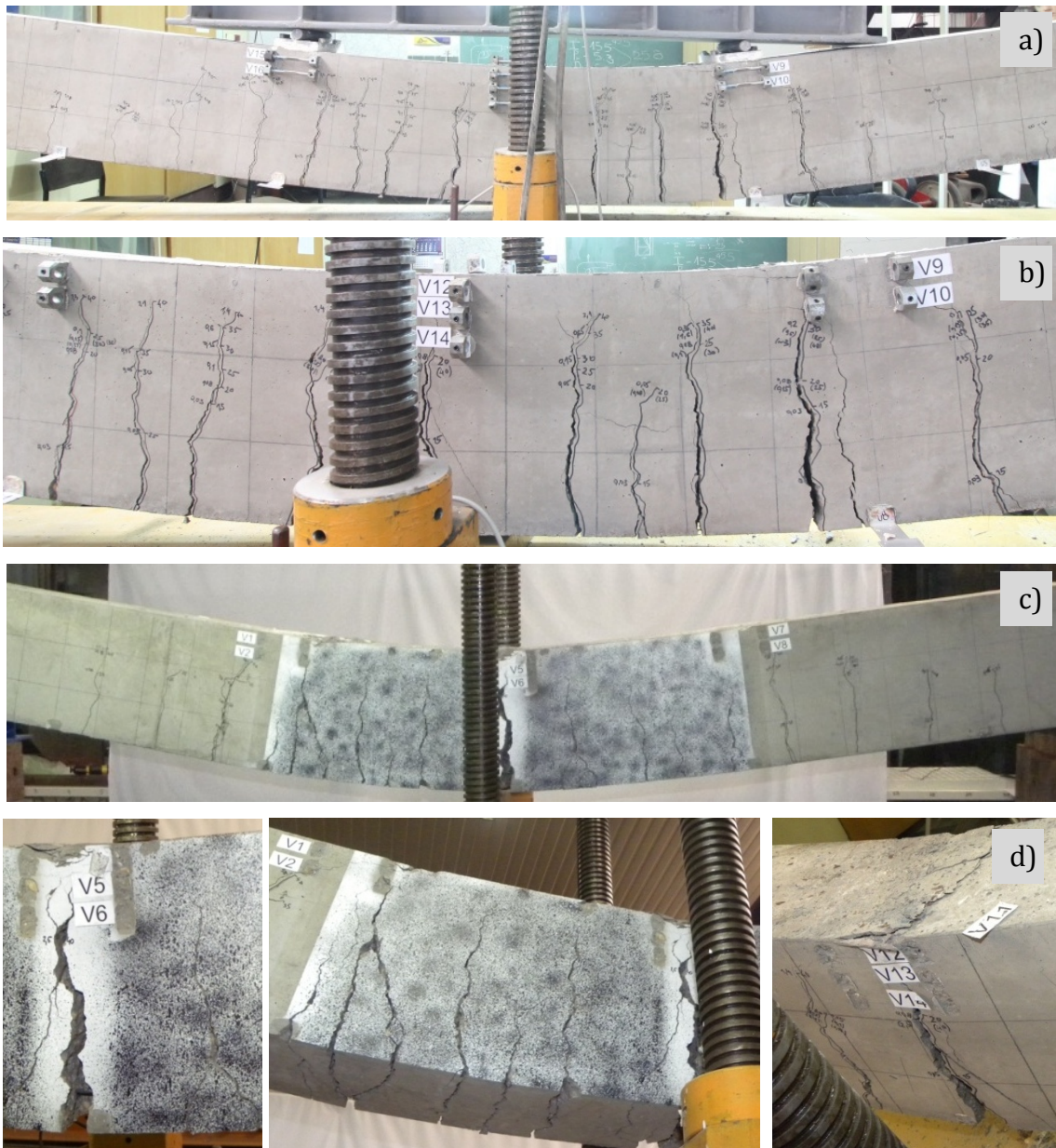


Figure 4.36 Crack patterns at failure load for HVFAC-1 beam: a) back side of beams' clear span, b) backside of beams' flexural span, c) front side of beams' clear span and d) front side of beams' flexural span

Flexural cracks formed similar patterns on the front and the back side of the beams. Flexural cracks in the middle part of the beam practically reached the

4. Experimental program and test results

compression reinforcement with one critical crack in the middle point of the beam. In the OPC-1 beam all cracks formed as flexural without the formation of shear cracks. In the HVFAC-1 beam one flexural-shear crack formed close to the beams support at 50% of the ultimate loading but did not progress further. Failure occurred with concrete crushing followed by the longitudinal reinforcement breaking. The crushed concrete zone was relatively small – around 100 mm in both beams. Both OPC-1 and HVFAC-1 beams exhibited the same failure type with a very similar volume of crushed concrete and similar crack patterns. In both OPC-1 and HVFAC-1 beams similar crack branching was noticed on the top of some flexural cracks. Crack branching may occur when some micro-cracks close to the crack tip are present, thus more energy is required for crack propagation leading to crack branching (Fayyad and Lees, 2017). Flexural cracks started to bifurcate at approximately 70% of the ultimate loading in both beams.

Crack patterns at the failure load for beams with a reinforcement ratio higher than minimum are shown in Figures 4.37 and 4.38. The flexural cracks are uniformly and symmetrically distributed along the beams' length with more cracks developed at failure in the HVFAC-2 beam. In the OPC-2 beam, flexural cracks in the middle part of the beam were oriented in the vertical direction, as expected. In the HVFAC-2 beam, beside vertical cracks, some short cracks in different directions also formed in the middle part of the beam. The first flexural cracks close to the beams supports developed at 70% and 60% of the ultimate loading for the OPC-1 and the HVFAC-1 beams, respectively. More flexural–shear cracks developed in the shear span after that point. Flexural cracks formed similar patterns on the front and back side of the beams. In general, a denser crack pattern was noticed in the HVFAC-2 beam compared with the OPC-2 beam. The longitudinal reinforcement yielded in both beams inducing a ductile behavior of the beams. Failure occurred after concrete crushing in the midpoint section of the beams. Fracture of the longitudinal reinforcement was not noticed and the compression reinforcement buckled in the failure section in the OPC-2 beam. The crushed concrete zone was larger than in the case of beams with minimum longitudinal reinforcement. In the

4. Experimental program and test results

OPC-2 beam, the crushed concrete zone affected a relatively large concrete area (850·280 mm) as can be seen in Figure 4.37.

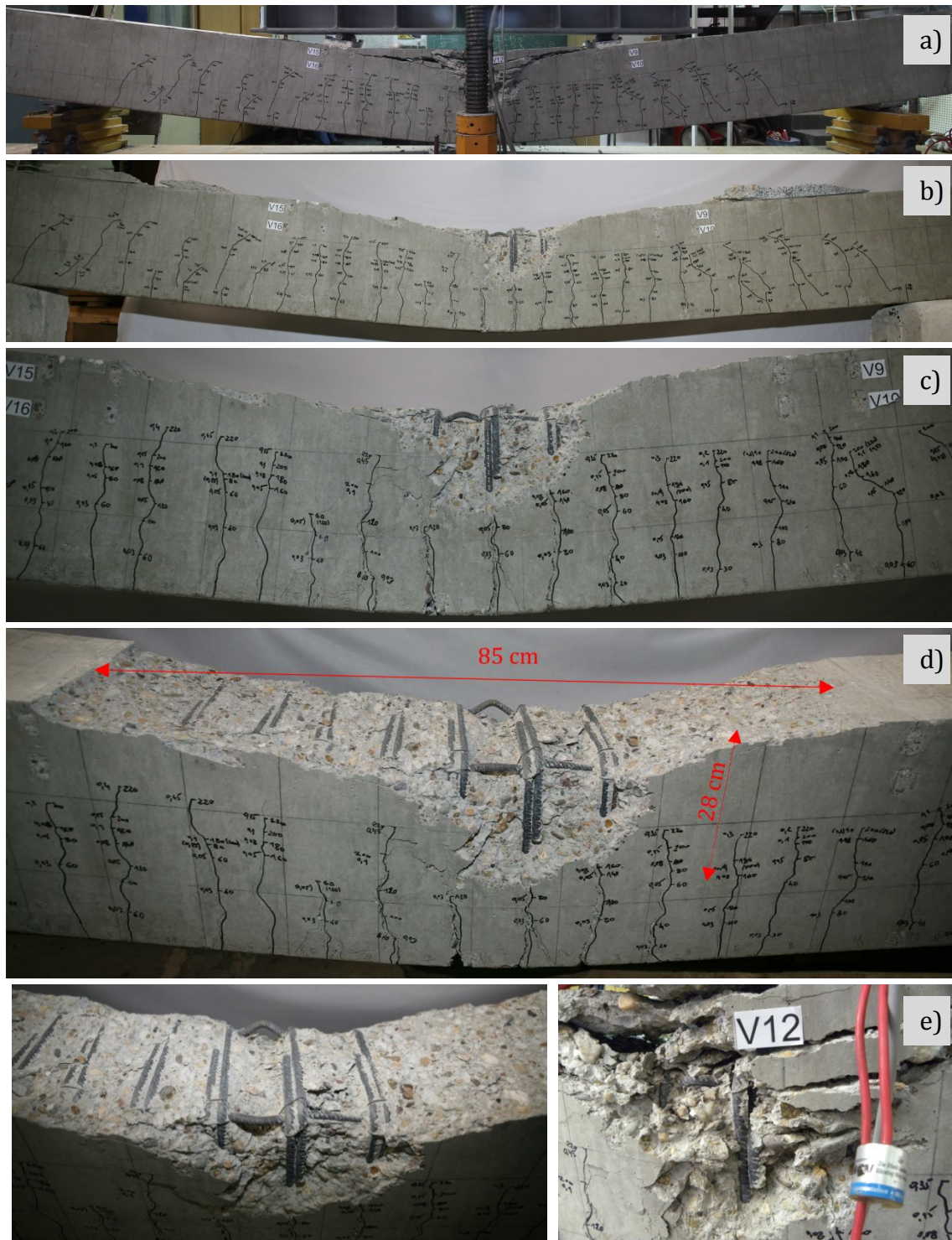


Figure 4.37 Crack patterns at the failure load for the OPC-2 beam: a-b) back side of beams' clear span, c-d) back side of beams' flexural span, e) buckling of the compressed reinforcement

4. Experimental program and test results

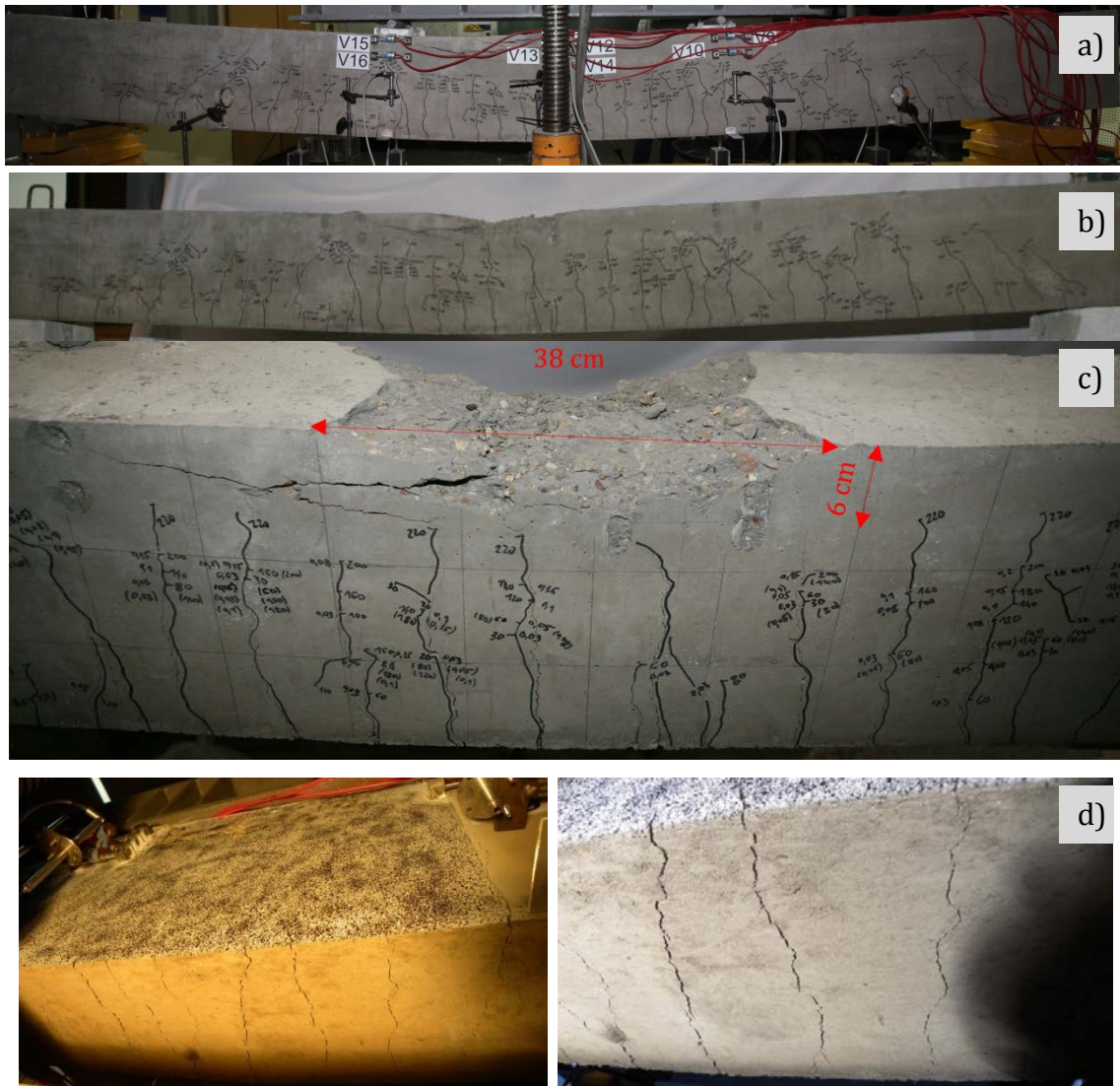


Figure 4.38 Crack patterns at the failure load for the HVFAC-2 beam: a-b) back side of beams' clear span, c) back side of beams' flexural span, d) cracks development along the beams' width

In the HVFAC-2 beam, the crushed concrete area was smaller (380·60 mm) as shown in Figure 4.38. In the HVFAC beam specimens, a small number of narrow longitudinal cracks were noticed on the beam surface before loading. These cracks were marked in order to track their development during loading (Figure 4.39). These cracks were barely noticeable with a naked eye but they were marked as precisely as possible. None of these cracks developed further during loading, so they were not marked in the crack patterns shown in the following analyses. The possible explanation may lie in the casting procedure of the HVFAC beams. All beams were cast in a few layers (usually three) due to the available technology in

4. Experimental program and test results

the Laboratory. During the casting of HVFAC beams, the concrete mixture C200_F350 stiffened quickly after mixing and in some cases more work during compacting of concrete in formwork was needed. Having in mind that the cracks presented in Figure 4.39 are oriented and positioned between these layers, the casting technology can be a cause of their development. These cracks were not noticed in the OPCC beams.



Figure 4.39 Longitudinal cracks in HVFAC beams prior to loading

In order to understand the behavior of beams and evaluate their stiffness, load-deflection curves of all tested beams (the deflection was measured at the beams midpoint) are shown in Figure 4.40. Before the first flexural crack formation, all of the beams showed similar linear-elastic behavior. After additional load was applied, the longitudinal steel yielded. With further load increase, compressed concrete was crushed and the beams failed.

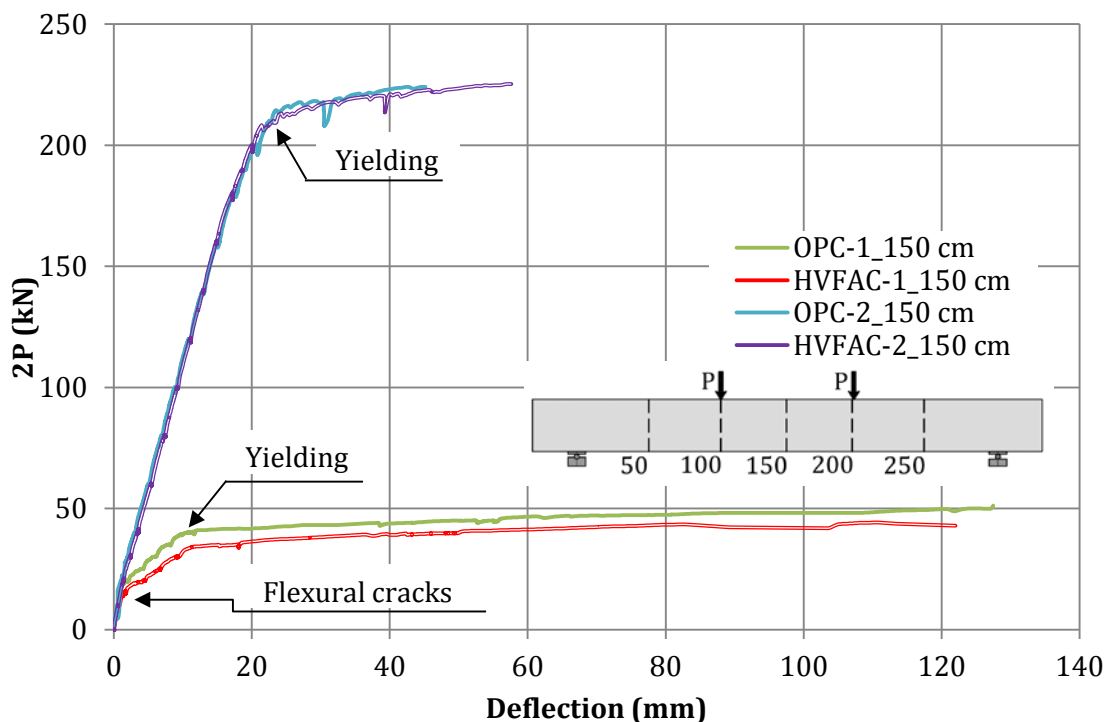


Figure 4.40 Load-deflection curves for all beams tested in flexure

4. Experimental program and test results

As expected, the ductility of beams decreased as the reinforcement ratio increased. Both beams with a minimum reinforcement ratio exhibited linear-elastic behavior approximately until the formation of the first flexural cracks. The stiffness of both tested beams upon this point was similar with the load-deflection curve having the same slope until the beams' yielding point. Approximately after that point, the OPC-1 beam showed higher stiffness until failure. In the beams with a higher than minimum longitudinal reinforcement ratio, a shift in the load-deflection curves first occurred after the flexural crack formation by decreasing the stiffness and keeping the linear-elastic behavior until the beams yielding point. The stiffness of both tested beams upon this point was similar with the load-deflection curves having the same slope. In the beams with a minimum longitudinal reinforcement ratio, the failure occurred after the crushing of concrete and braking of the longitudinal reinforcement (tension failure). The beams with a higher than minimum reinforcement ratio failed by crushing of the compressed concrete and yielding of the longitudinal reinforcement. The crushed concrete zone at failure was only a few centimeters high.

All beams tested for flexural behavior exhibited ductile failure caused by the concrete crushing after yielding of the reinforcement. The difference between the OPCC and HVFAC ultimate loading falls within a 10% margin and can be considered as negligible.

The ductility of beams was evaluated using the ductility ratio (a_u/a_y) that showed the following (Figure 4.41a):

- The HVFAC-1 beam had around 40% lower ductility compared with the OPC-1 beam;
- The HVFAC-2 beam exhibited 20% higher ductility compared with the OPC-2 beam.

The ductility ratio and the ultimate-to-yielding load ratio for all tested beams are shown in Figure 4.41b. Yielding of the beams with a higher than a minimum reinforcement ratio occurred at approximately 94% of the ultimate loading (determined based on the load-deflection curve). For the beams with a minimum reinforcement ratio, the yielding of the beams occurred at 78% and 64% of the

4. Experimental program and test results

ultimate loading for the OPC-1 and HVFAC-1 beams, respectively. For beams with a minimum reinforcement ratio, around 20% higher increase in bearing capacity after yielding was noticed in the HVFAC-1 beam compared with the OPC-1 beam. The same ultimate-to-yielding load ratio for the beams with a higher than minimum reinforcement ratio indicates the same bearing capacity after yielding for both OPC-2 and HVFAC-2 beams.

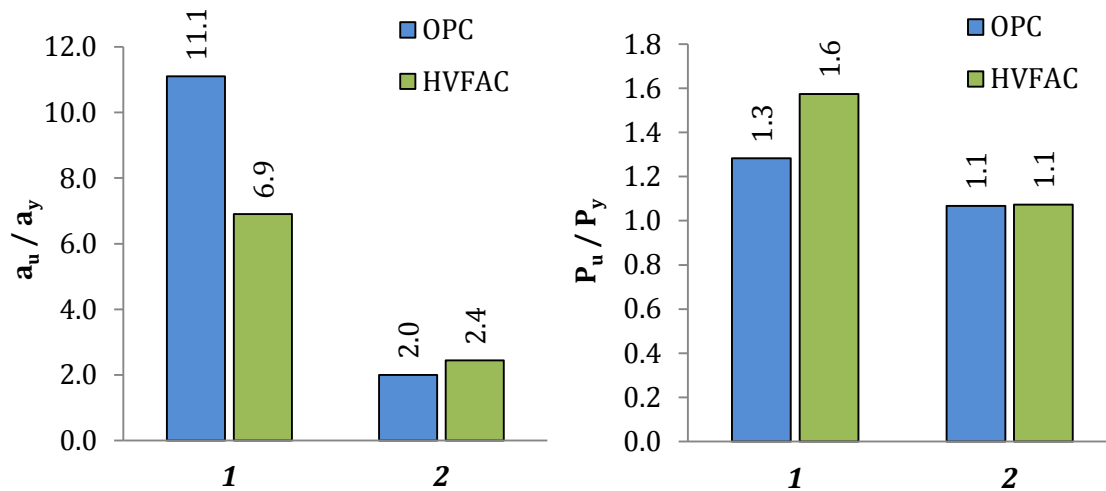


Figure 4.41 a) The ductility ratio and b) the ultimate to yielding load ratio for all tested beams

4.3.8. Deflection of beams

The monitoring of the beams' deflection was done by measuring the vertical displacement in five sections along the beams' span and above supports. The diagrams of deflection along the beams' length at selected load levels (20%, 40% and 60% of the ultimate load level) are shown in Figure 4.42 and 4.43. The deflection lines during the loading were symmetrical until failure in all beams with maximum deflection at the midpoint, as expected.

In beams with a minimum longitudinal reinforcement ratio, deflection at the service load level (40%) was around 50% higher for the HVFAC-1 beam compared with the OPC-1 beam (Figure 4.42). The deflection lines at approximately 20% of the ultimate loading showed a similar trend with approximately 30% higher deflection of the HVFAC-1 beam compared with the OPC-1 while no flexural cracks appeared in neither of the beams up to that point.

4. Experimental program and test results

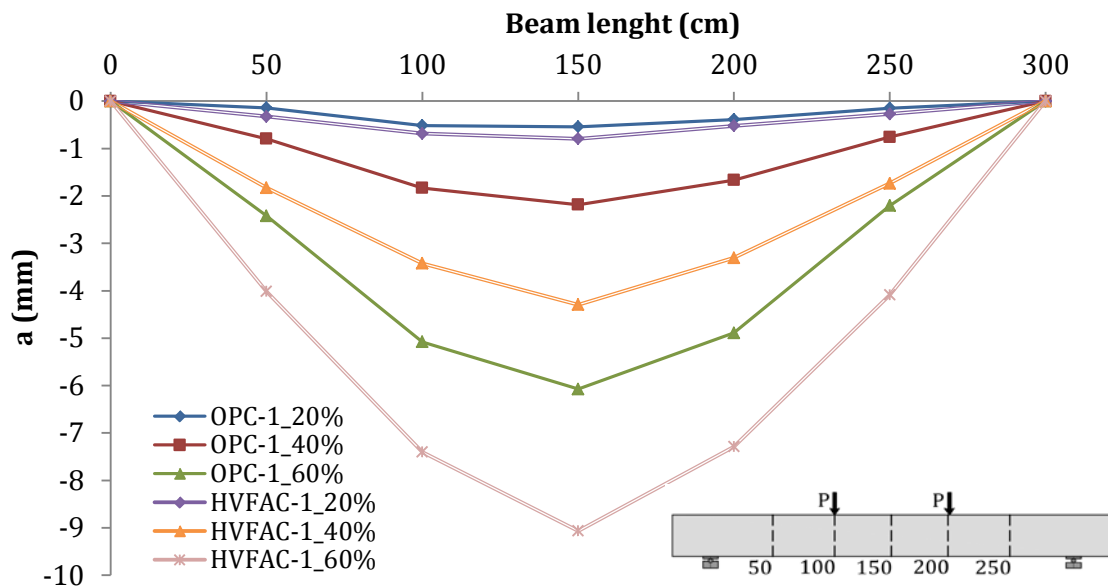


Figure 4.42 Deflection of the OPC-1 and HVFAC-1 beams at selected loading steps

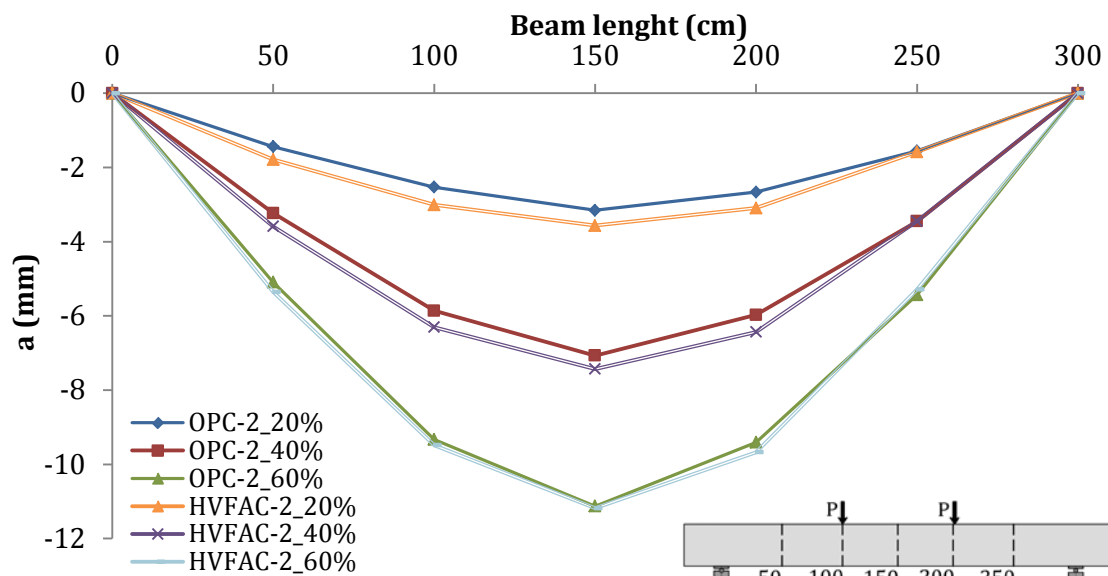


Figure 4.43 Deflection of OPC-2 and HVFAC-2 beams at selected loading steps

The most probable reason for these differences is the difference in the crack patterns and modulus of elasticity of the OPCC and HVFAC beams. At the service load level, the HVFAC-1 beam had significantly more flexural cracks compared with beam OPC-1, thus lowering its stiffness. Furthermore, the modulus of elasticity was 15% lower for the HVFAC beam compared with the modulus of elasticity of the OPCC beam.

The deflection lines at 20%, 40% and 60% of the ultimate loading level were practically the same for beams with a higher than minimum longitudinal

4. Experimental program and test results

reinforcement (Figure 4.43). The maximum deflection of the HVFAC-2 beam was up to 12% higher compared with the OPC-2 beam at all presented loading stages.

The maximum deflections at service load level, beams' yielding point and the ultimate loading stage are shown in Figure 4.44. At the beams' yielding point, the maximum deflection difference was approximately 36% for the HVFAC-1 beam compared with beam OPC-1. This difference was only 4% for beams with a higher than minimum reinforcement ratio. The ultimate deflections were similar for beams with a minimum reinforcement ratio, but significantly higher in HVFAC-2 beam compared with beam OPC-2. The reason behind a higher ultimate deflection of the HVFAC-2 beam was a significantly denser crack pattern and lower modulus of elasticity.

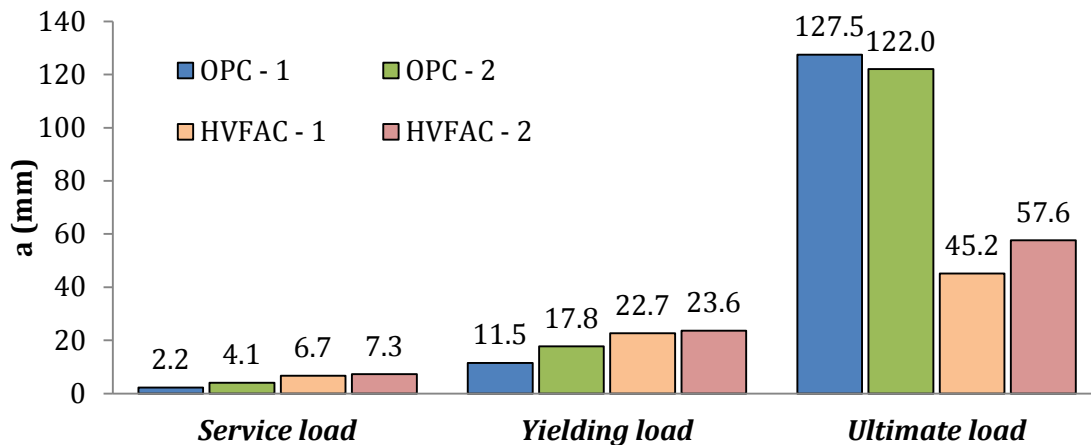


Figure 4.44 Maximum deflections at service, yielding, and ultimate load level

In order to further evaluate the stiffness of beams, the load-deflection curves for all beams and cross-sections other than midpoint are shown in Figures 4.45 – 4.48. The inclination of the linear-elastic part of the load-deflection curve was similar for OPC-1 and HVFAC-1 beams in all sections until flexural crack formation—the difference was up to 3%. After that point, the stiffness of the OPC-1 beam exceeded the stiffness of the HVFAC-1 beam until failure, by up to 11%. The difference in the ultimate deflection in the OPC-1 and HVFAC-1 beams in measured sections was negligible.

4. Experimental program and test results

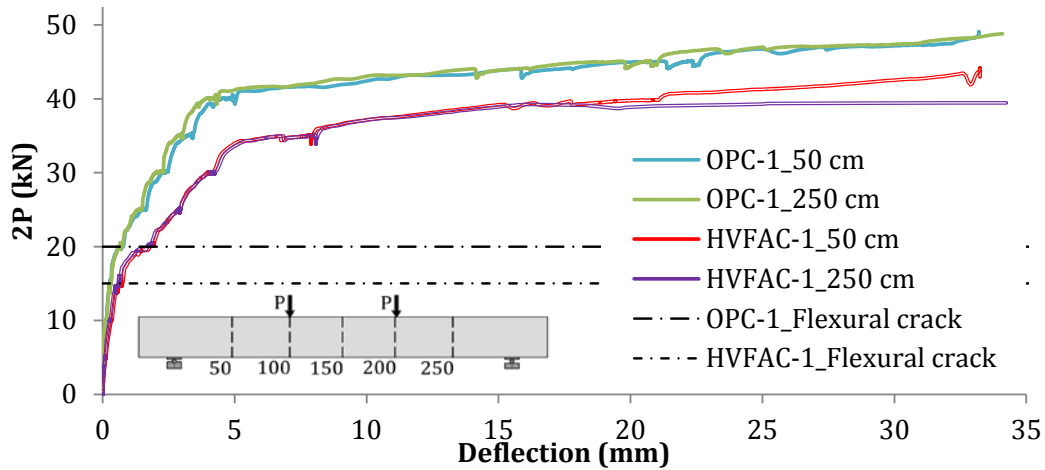


Figure 4.45 OPC-1 and HVFAC-1 load-deflection curves for sections 2 (50 cm) and 6 (250 cm)

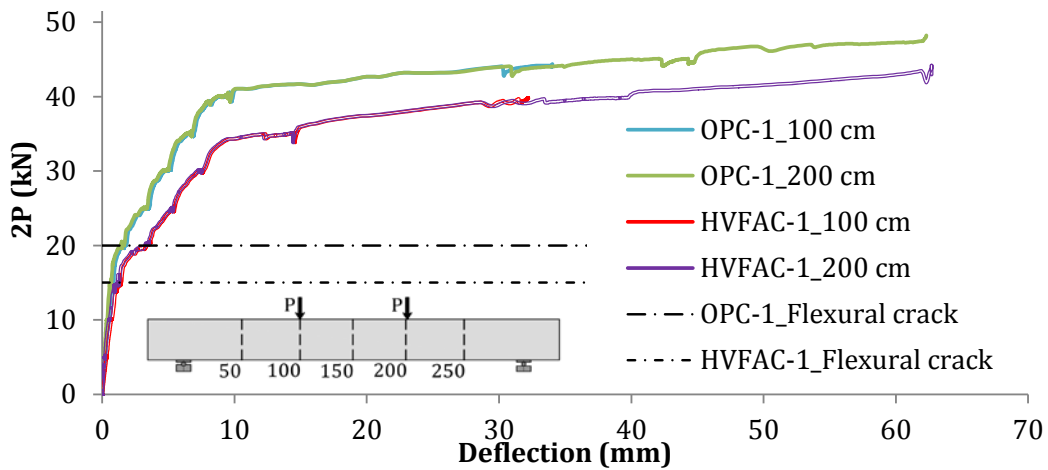


Figure 4.46 OPC-1 and HVFAC-1 load-deflection curves for sections 3 (100 cm) and 5 (200 cm)

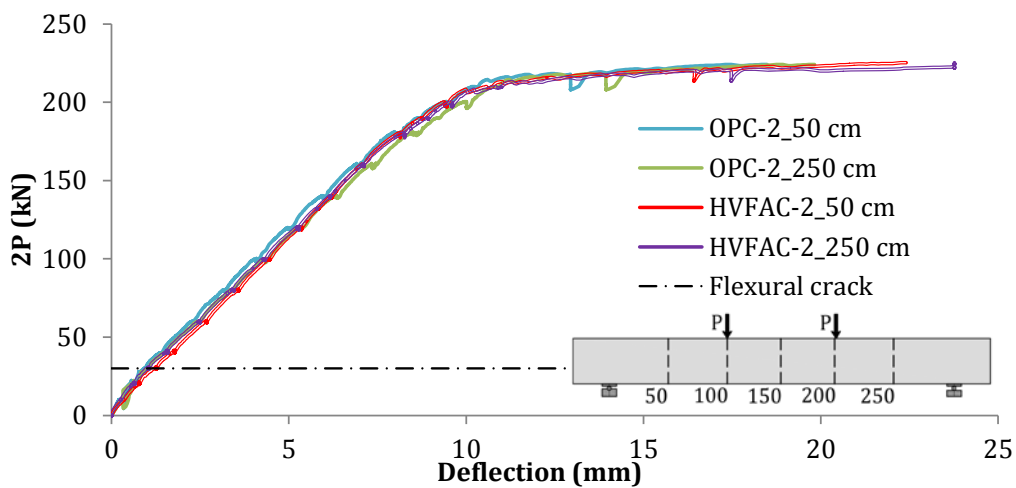


Figure 4.47 OPC-2 and HVFAC-2 load-deflection curves for sections 2 (50 cm) and 6 (250 cm)

4. Experimental program and test results

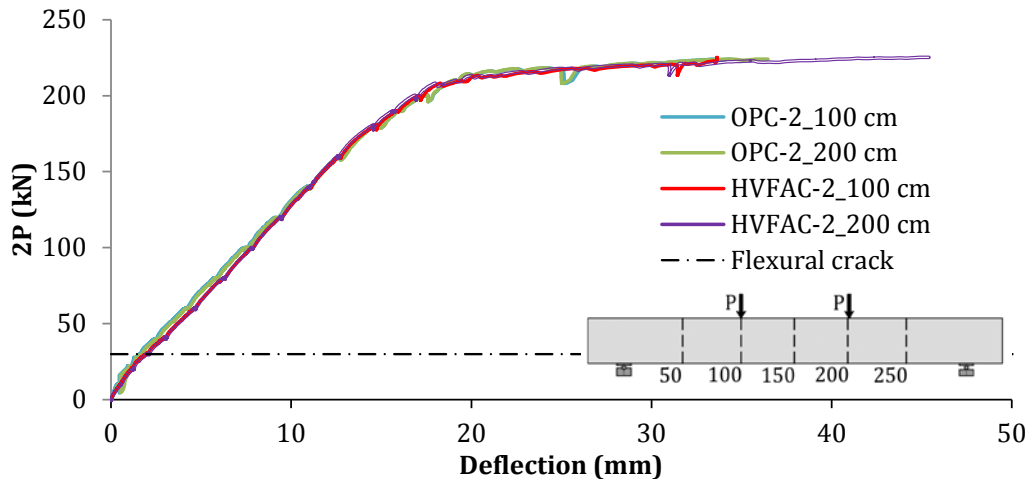


Figure 4.48 OPC-2 and HVFAC-2 load–deflection curves for sections 3 (100 cm) and 5 (200 cm)

The load–deflection curves for the OPC-2 and HVFAC-2 beams almost fully coincide even after flexural crack formation. The only difference is higher deflection at the ultimate loading stage similar as in the midpoint section described before.

It can be concluded that the stiffness of tested HVFAC beam with a minimum reinforcement ratio was lower than the stiffness of OPCC beam due to the fact that more flexural cracks developed in the HVFAC beams and that they had a lower modulus of elasticity compared with the OPCC beams.

4.3.9. Longitudinal reinforcement strains

The longitudinal reinforcement strains were measured in the same five sections as in the case of deflection measurements. The measuring SGs were positioned on each tension reinforcement bar in order to prevent complete data loss in case one or more SGs malfunction. Sixty two SGs were used during this testing and malfunctioning was noticed in four gauges in the HVFAC-1 beam (M1, M3, M7, and M12) and eight gauges in the HVFAC-2 beam (M1, M2, M5, M6, M7, M9, M10, and M12). The malfunctioning of installed SGs in the HVFAC beams was most probably caused by the long concrete compacting period with a vibrating needle. As it was mentioned before, HVFAC mixture C200F350 started to harden not long after mixing was completed so special effort was needed for casting the HVFAC beams properly. Nevertheless, at least one SG in each section was working properly. The strain measurements in each SG in all sections are shown in Figures 4.49 – 4.68.

4. Experimental program and test results

The yielding of reinforcement was achieved approximately after the measured reinforcing bar yielding strain of 3.1‰ for OPC-1 and HVFAC-1 beams and 2.8‰ for OPC-2 and HVFAC-2 beams. In sections close to the supports (sections 2 and 6) reinforcement did not reach a yielding point in any of the tested beams except section 6 in beam OPC-1. The yielding of the reinforcement was noticed in the sections positioned in the middle part of the beams. Tension reinforcement strains developed in the same way for all measuring points in one section, so an average value of strains in one section was chosen for further evaluation Figures 4.69 – 4.78.

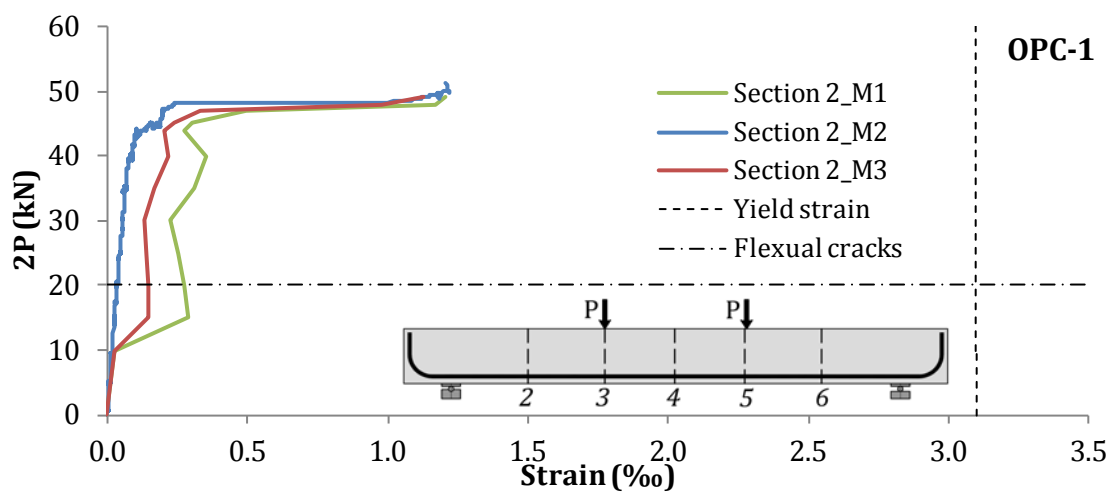


Figure 4.49 Longitudinal reinforcement strains in the OPC-1 beam in section 2

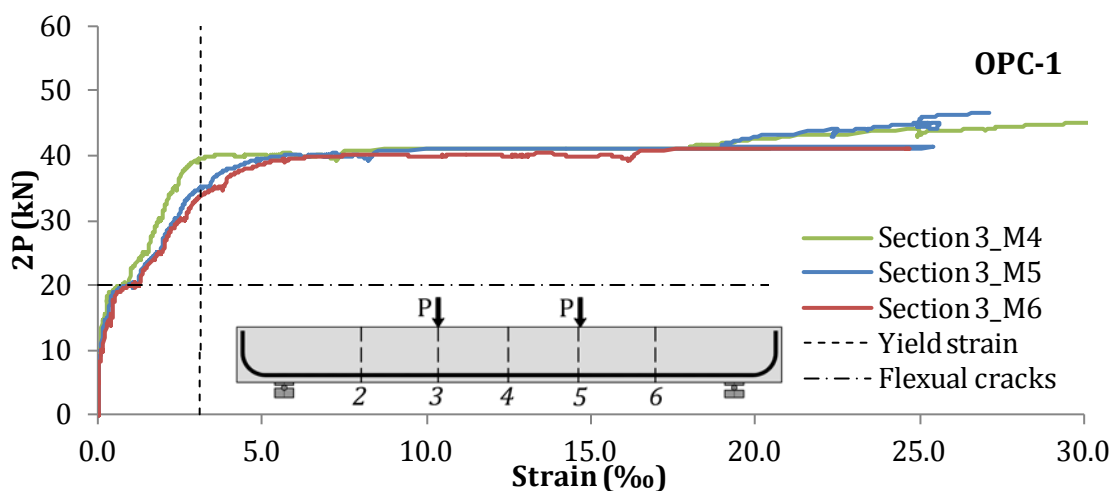


Figure 4.50 Longitudinal reinforcement strains in the OPC-1 beam in section 3

4. Experimental program and test results

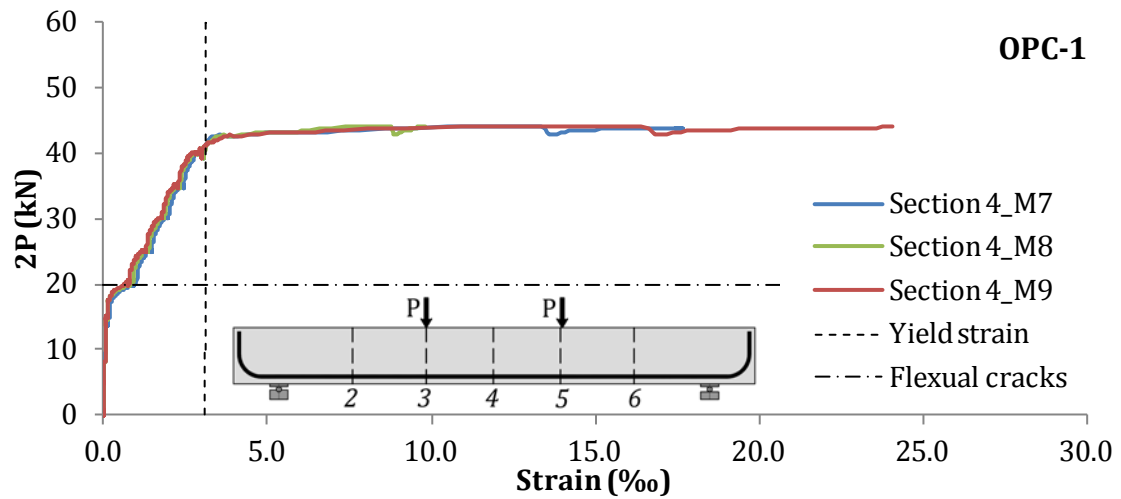


Figure 4.51 Longitudinal reinforcement strains in the OPC-1 beam in section 4

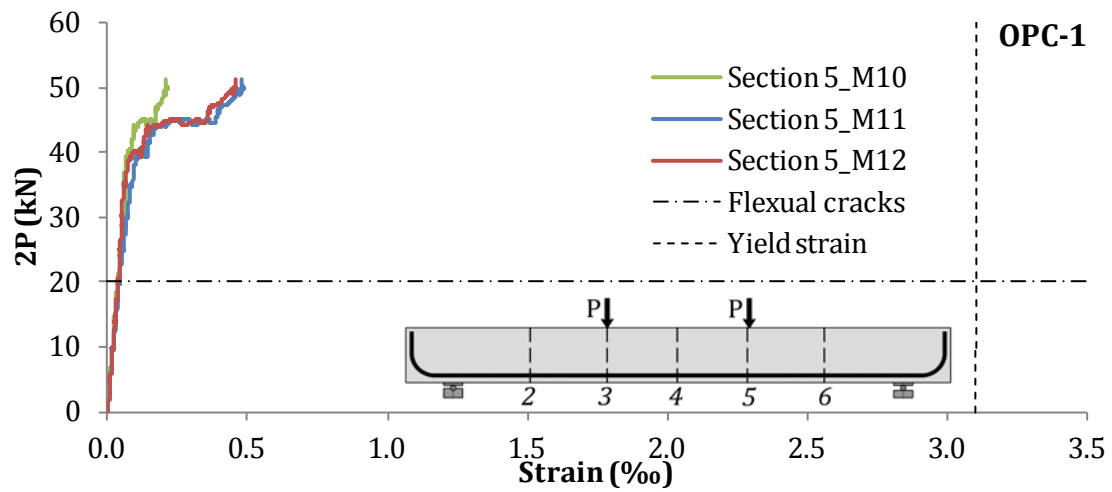


Figure 4.52 Longitudinal reinforcement strains in the OPC-1 beam in section 5

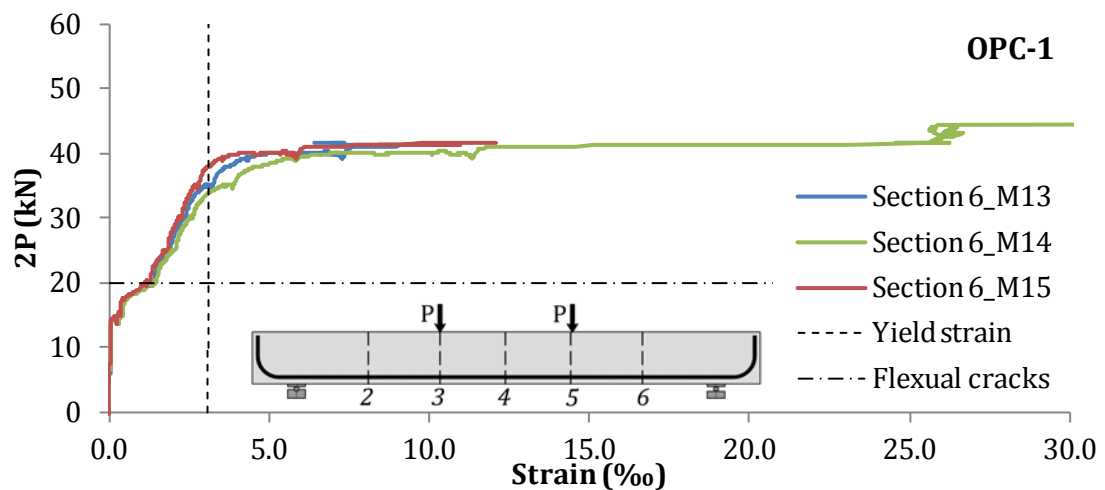


Figure 4.53 Longitudinal reinforcement strains in the OPC-1 beam in section 6

4. Experimental program and test results

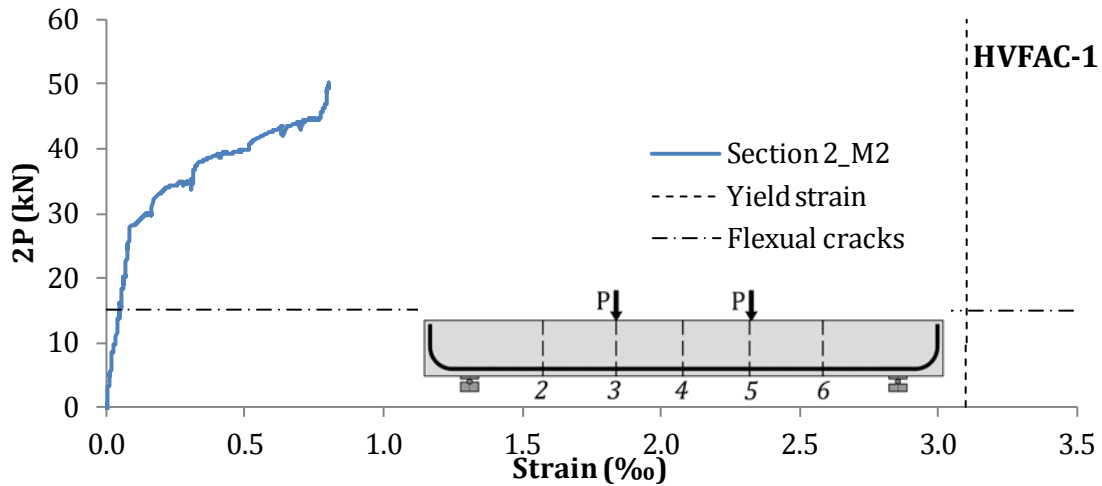


Figure 4.54 Longitudinal reinforcement strains in the HVFAC-1 beam in section 2

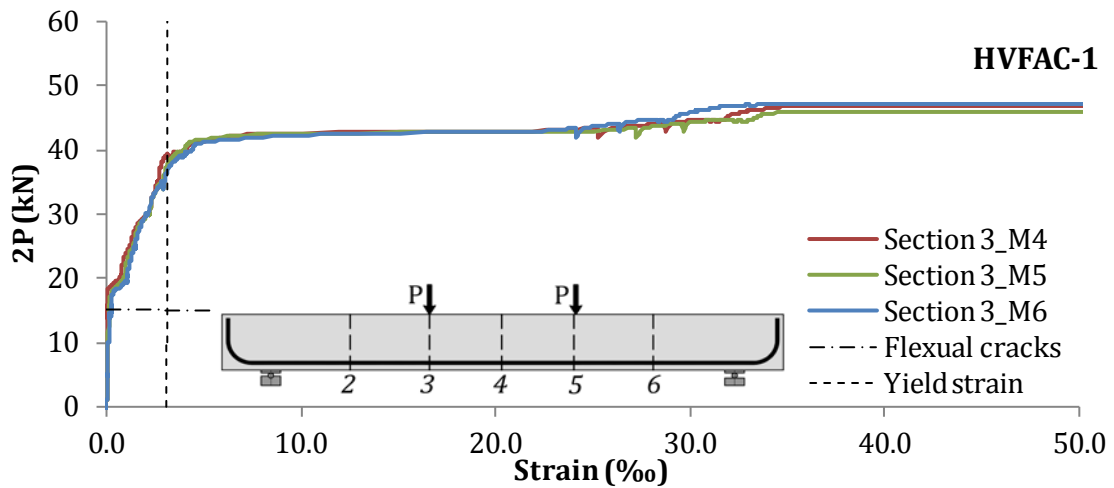


Figure 4.55 Longitudinal reinforcement strains in the HVFAC-1 beam in section 3

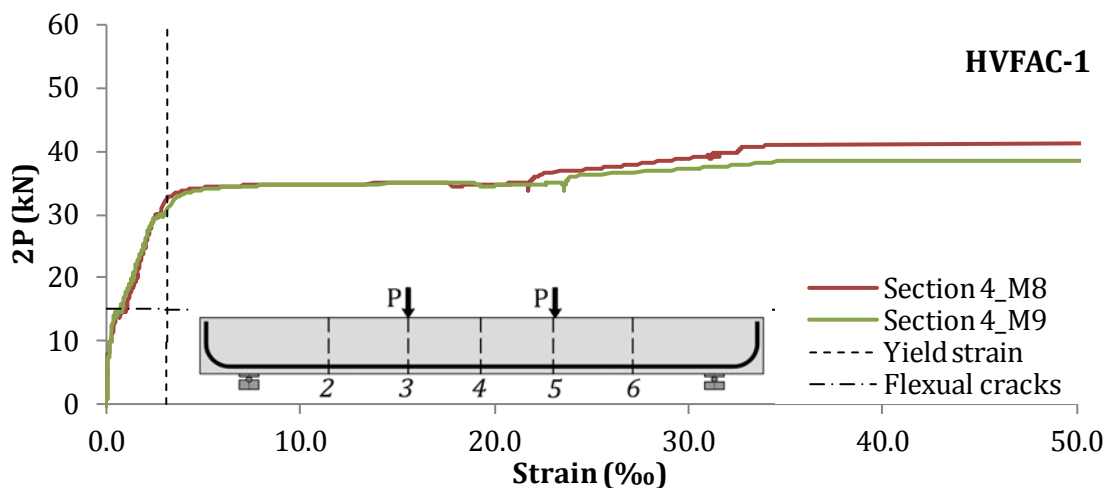


Figure 4.56 Longitudinal reinforcement strains in the HVFAC-1 beam in section 4

4. Experimental program and test results

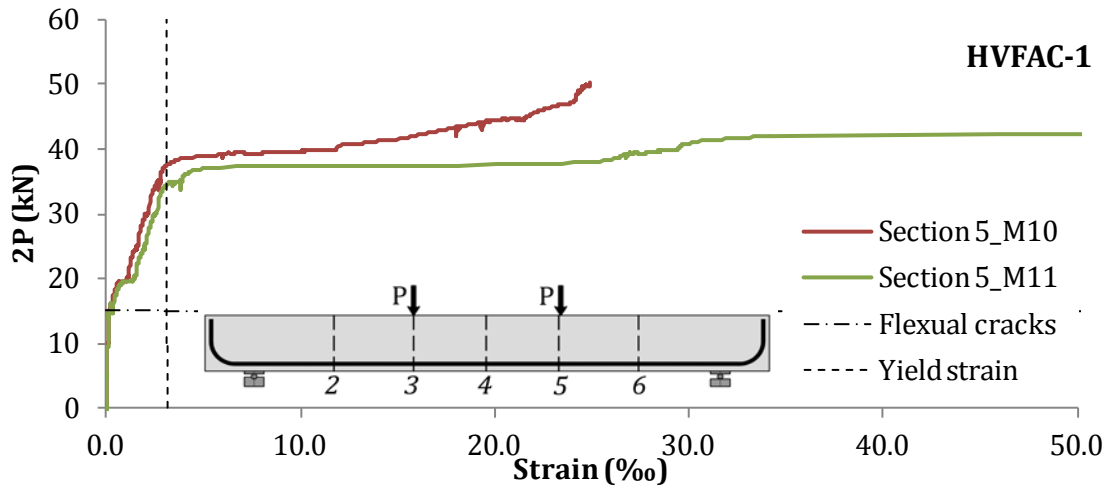


Figure 4.57 Longitudinal reinforcement strains in the HVFAC-1 beam in section 5

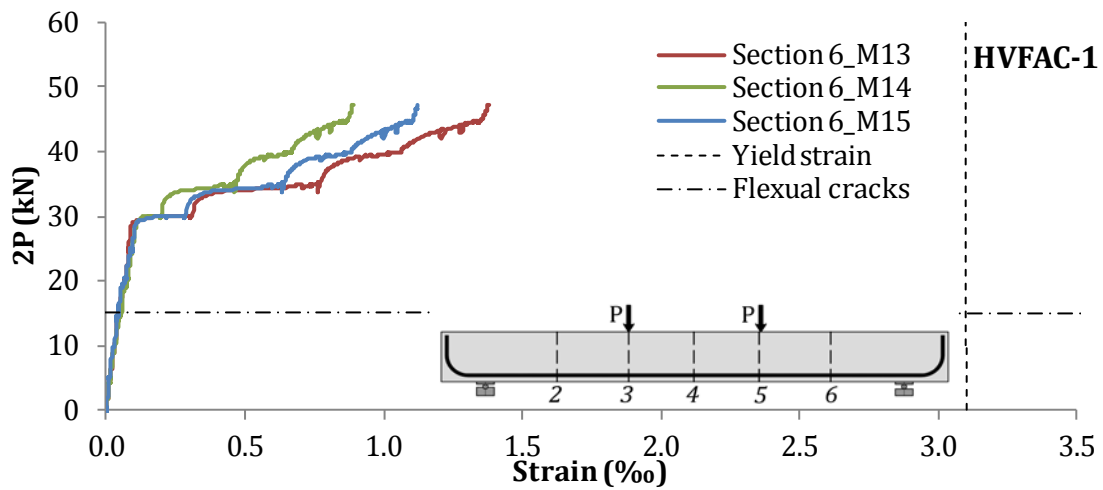


Figure 4.58 Longitudinal reinforcement strains in the HVFAC-1 beam in section 6

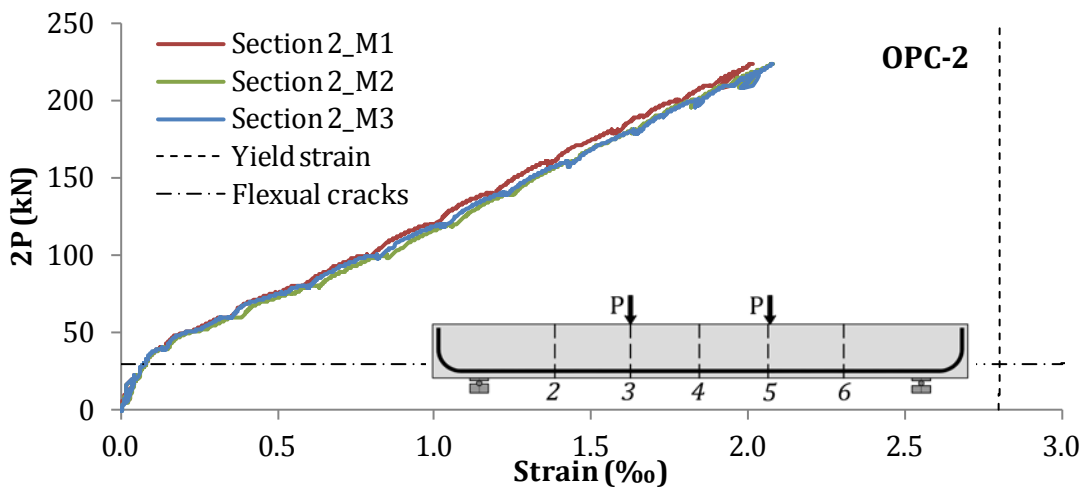


Figure 4.59 Longitudinal reinforcement strains in the OPC-2 beam in section 2

4. Experimental program and test results

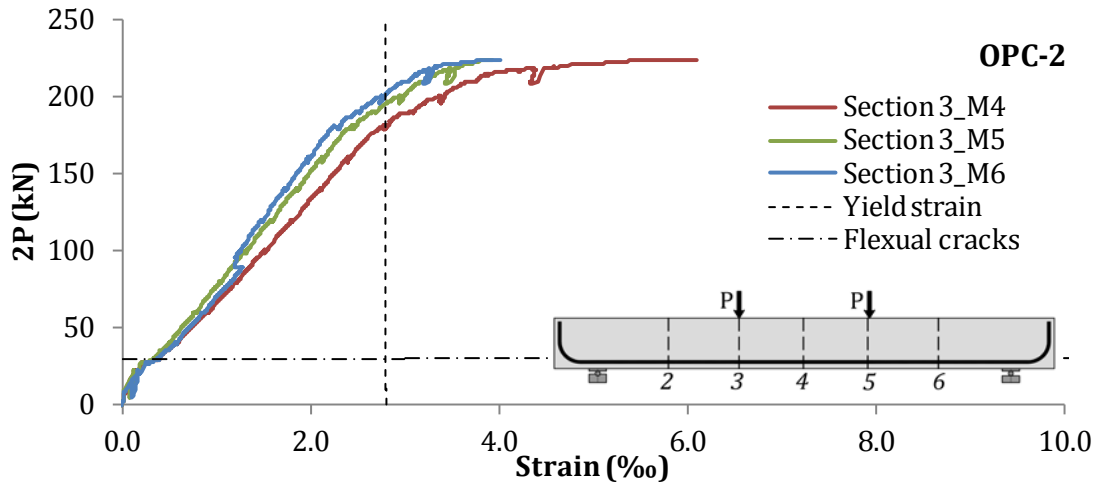


Figure 4.60 Longitudinal reinforcement strains in the OPC-2 beam in section 3

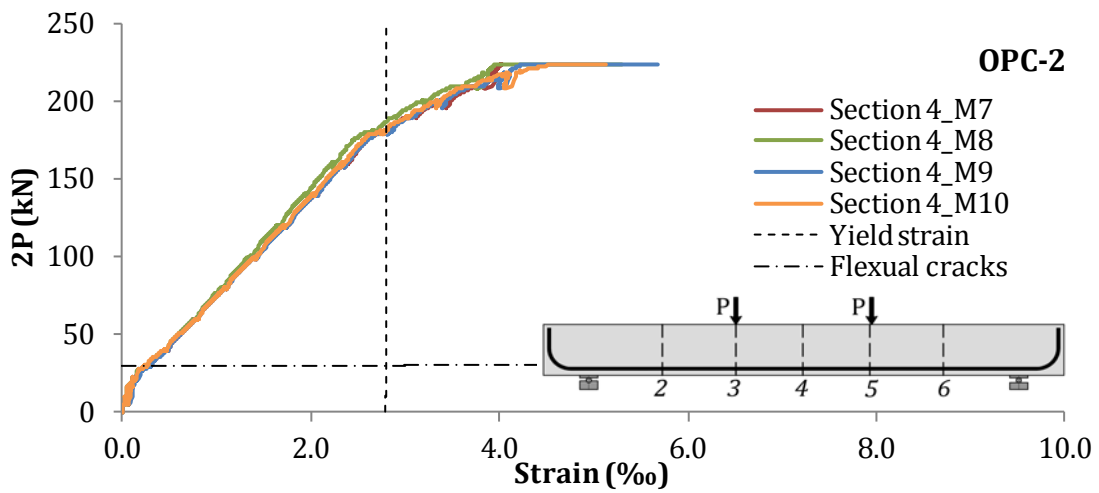


Figure 4.61 Longitudinal reinforcement strains in the OPC-2 beam in section 4

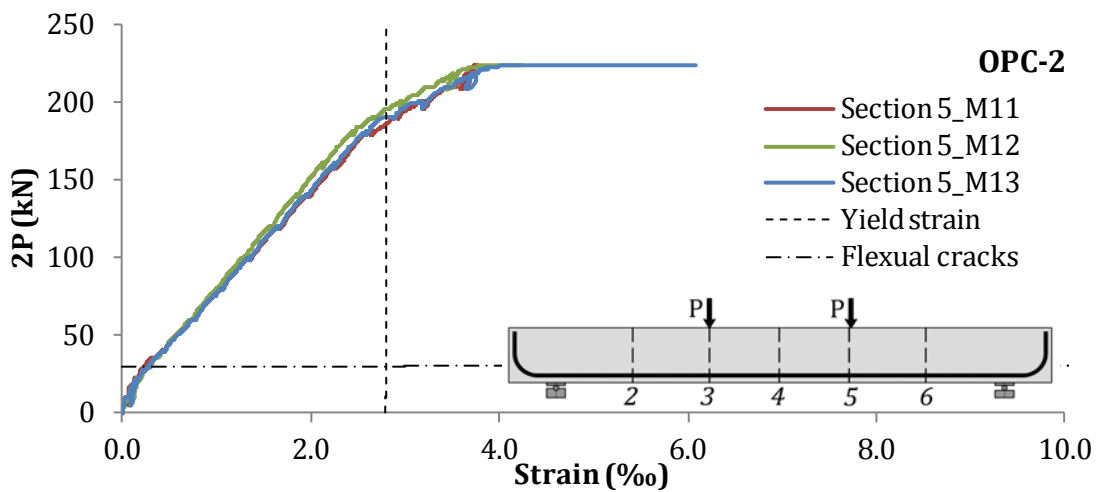


Figure 4.62 Longitudinal reinforcement strains in the OPC-2 beam in section 5

4. Experimental program and test results

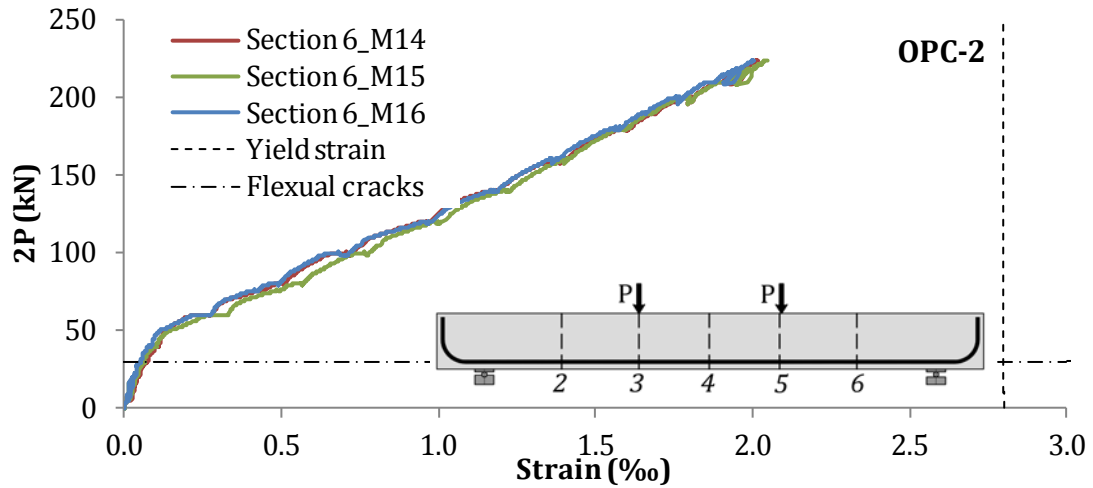


Figure 4.63 Longitudinal reinforcement strains in the OPC-2 beam in section 6

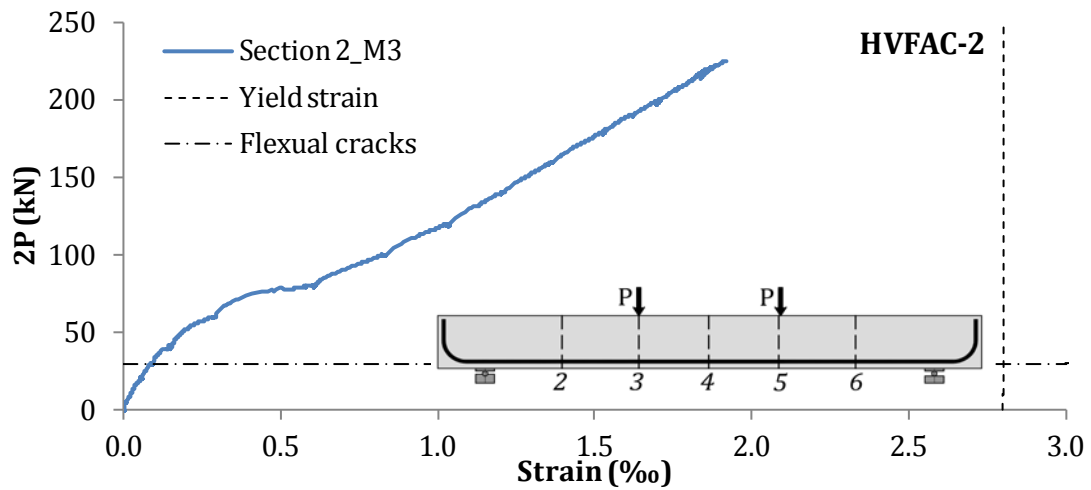


Figure 4.64 Longitudinal reinforcement strains in the HVFAC-2 beam in section 2

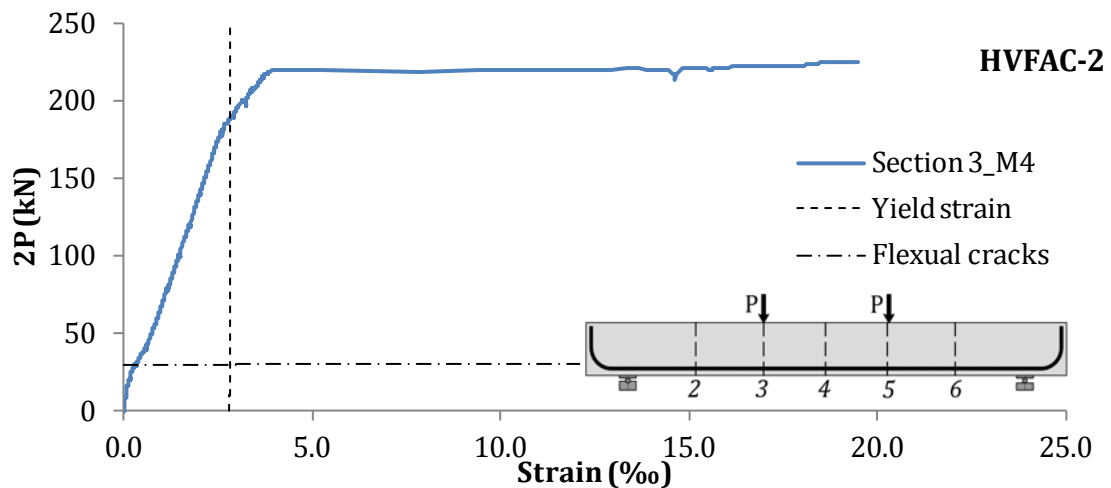


Figure 4.65 Longitudinal reinforcement strains in the HVFAC-2 beam in section 3

4. Experimental program and test results

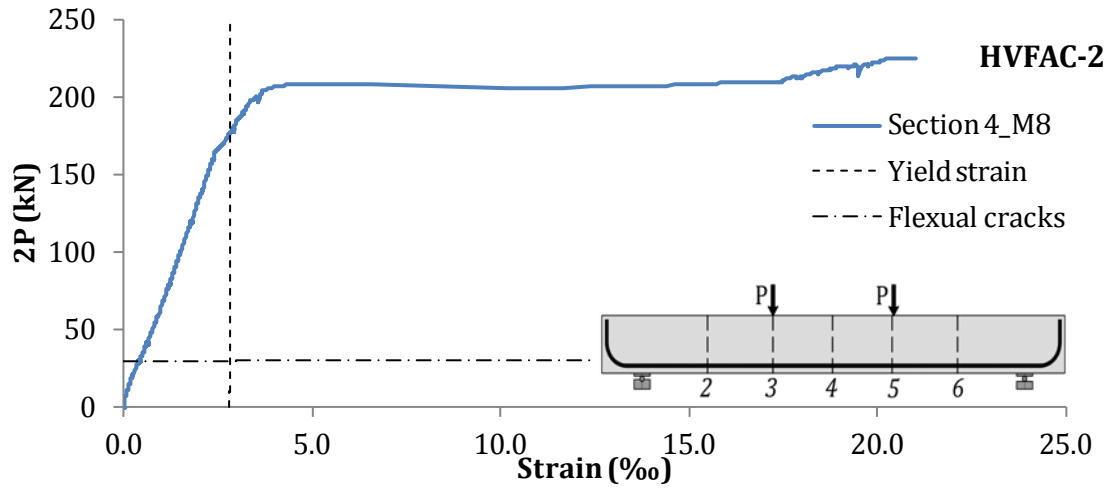


Figure 4.66 Longitudinal reinforcement strains in the HVFAC-2 beam in section 4

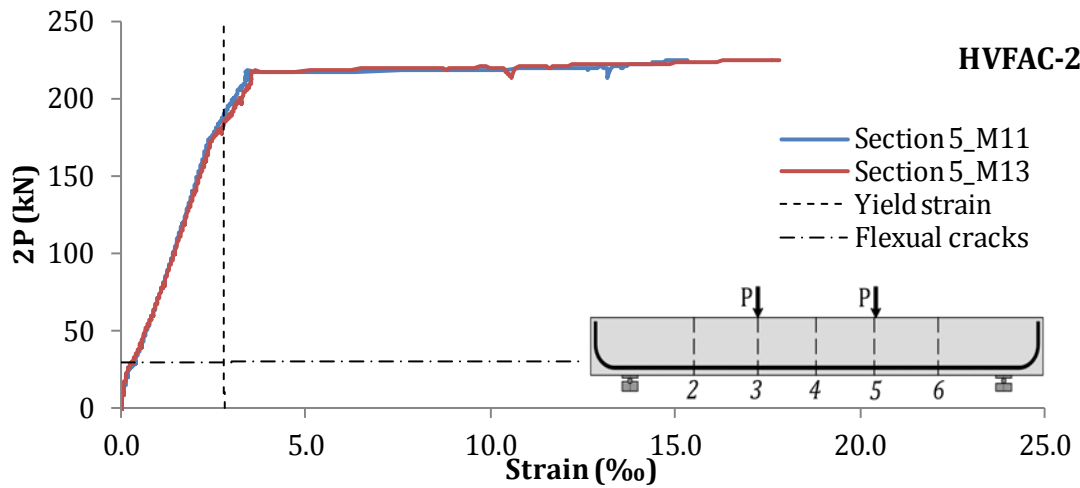


Figure 4.67 Longitudinal reinforcement strains in the HVFAC-2 beam in section 5

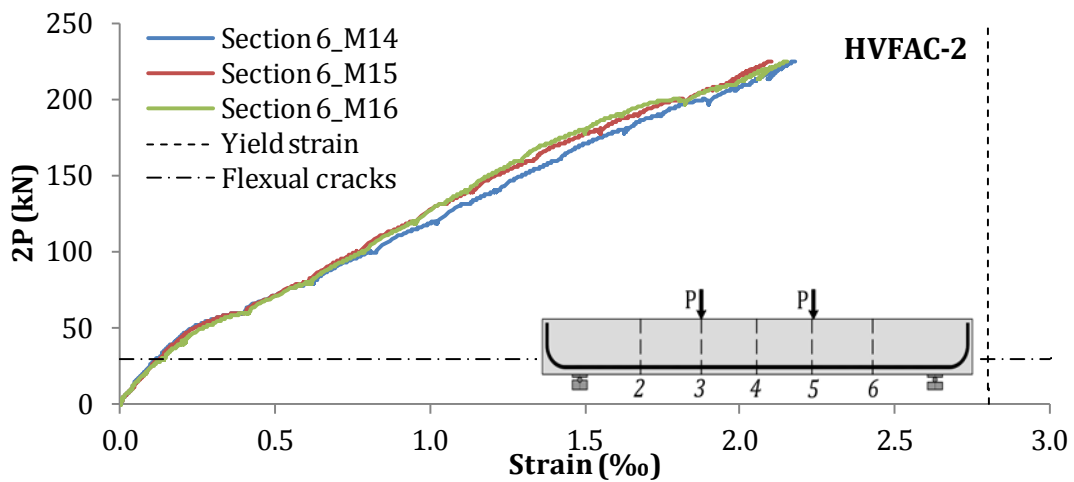


Figure 4.68 Longitudinal reinforcement strains in the HVFAC-2 beam in section 6

4. Experimental program and test results

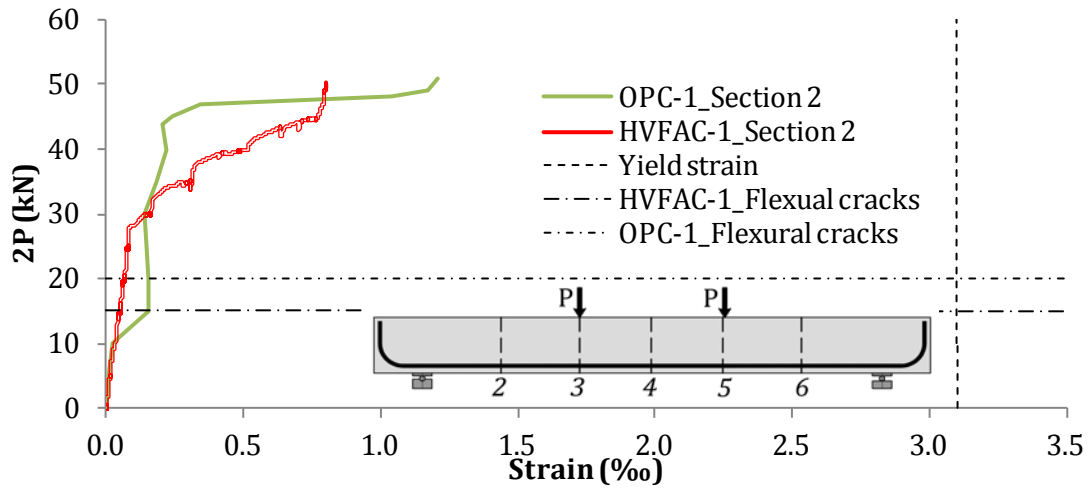


Figure 4.69 Longitudinal reinforcement strains in OPC-1/HVFAC-1 beams in section 2

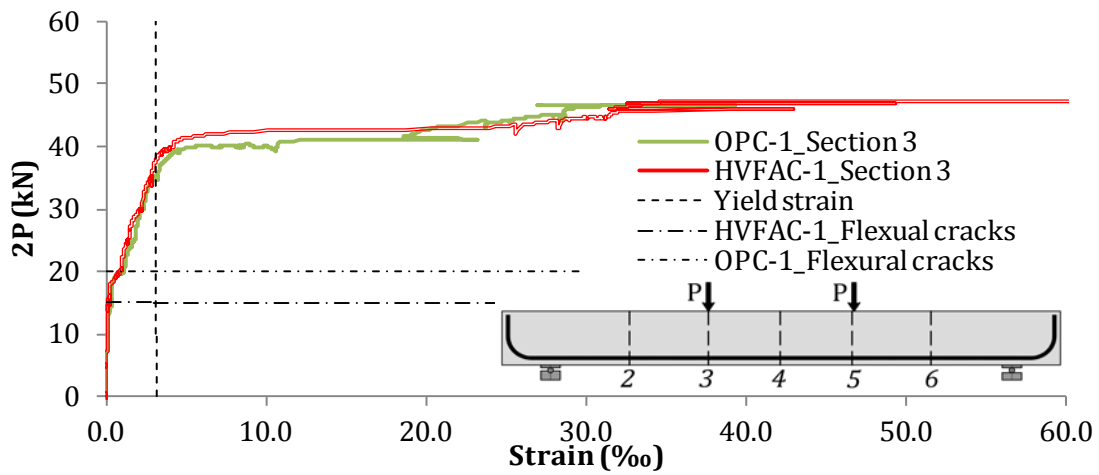


Figure 4.70 Longitudinal reinforcement strains in OPC-1/HVFAC-1 beams in section 3

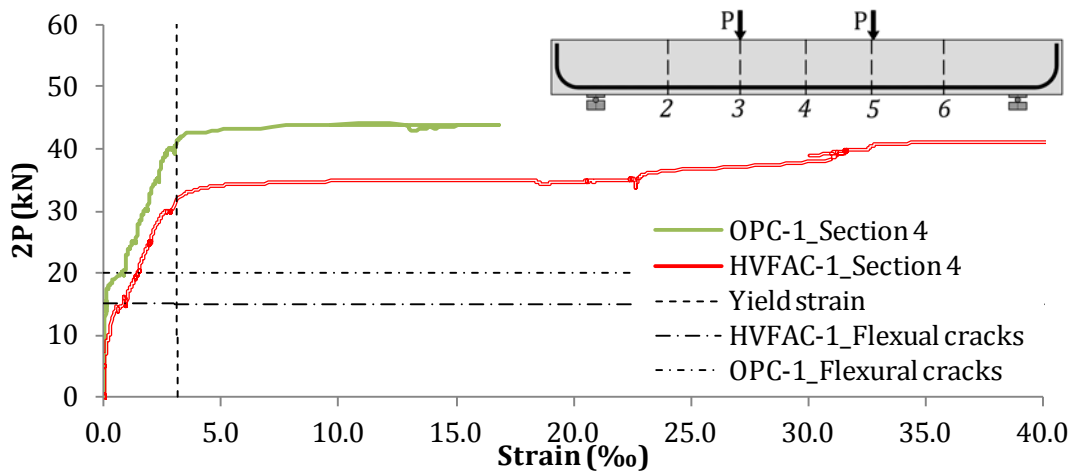


Figure 4.71 Longitudinal reinforcement strains in OPC-1/HVFAC-1 beams in section 4

4. Experimental program and test results

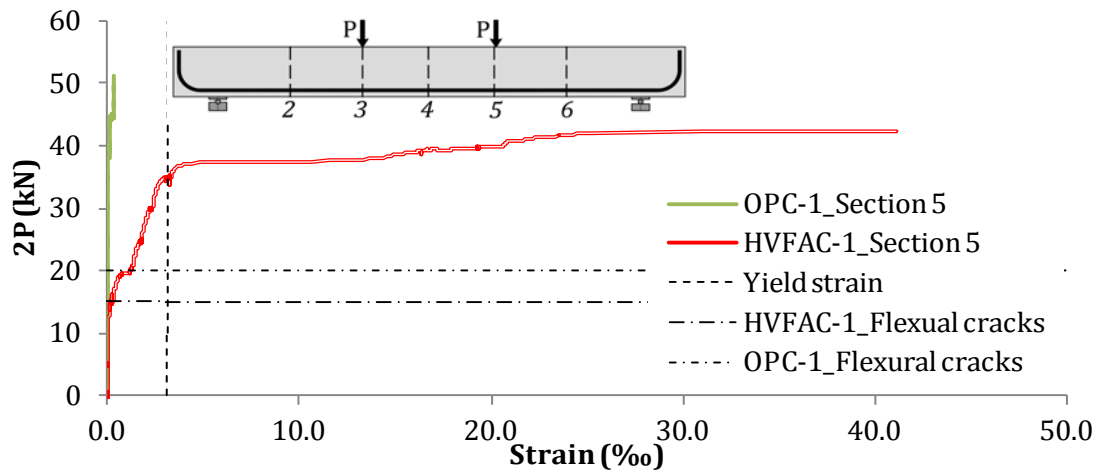


Figure 4.72 Longitudinal reinforcement strains in OPC-1/HVFAC-1 beams in section 5

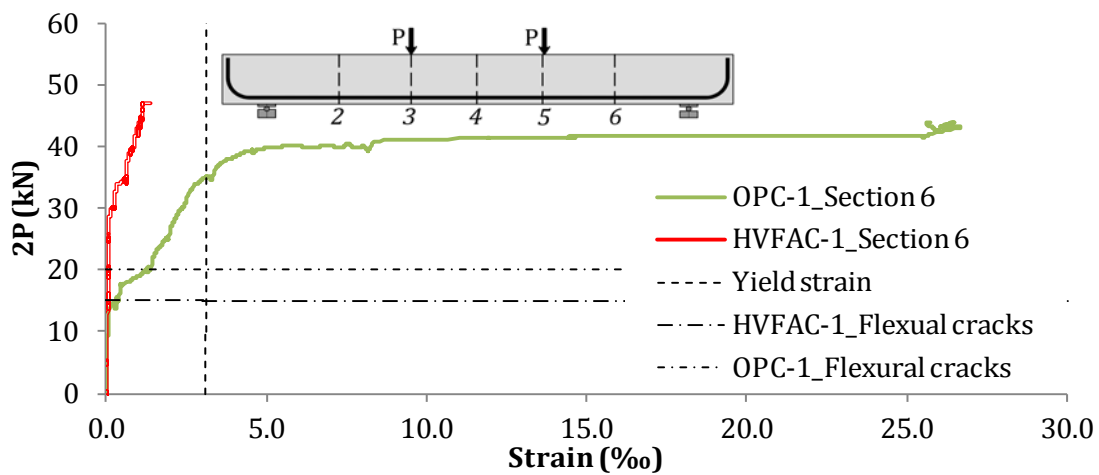


Figure 4.73 Longitudinal reinforcement strains in the OPC-1/HVFAC-1 beams in section 6

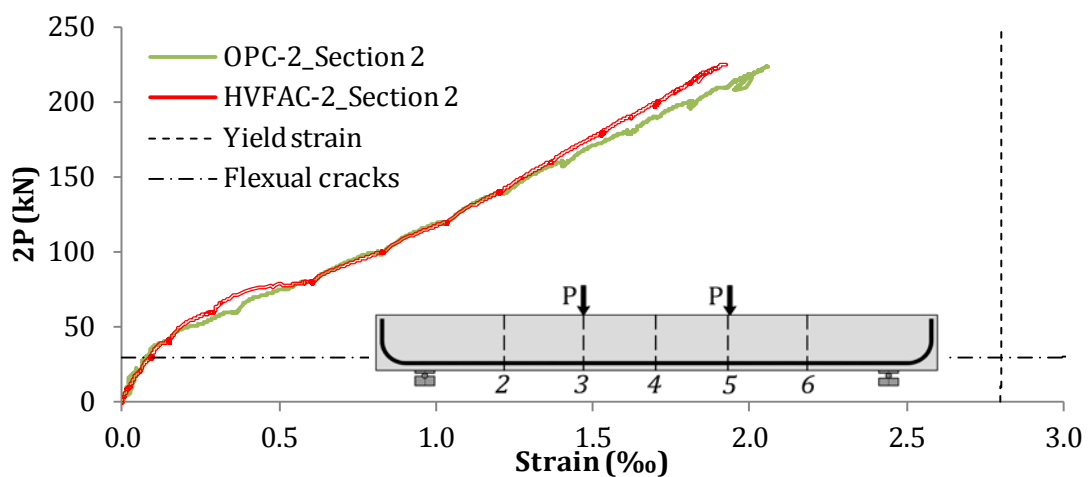


Figure 4.74 Longitudinal reinforcement strains in OPC-2/HVFAC-2 beams in section 2

4. Experimental program and test results

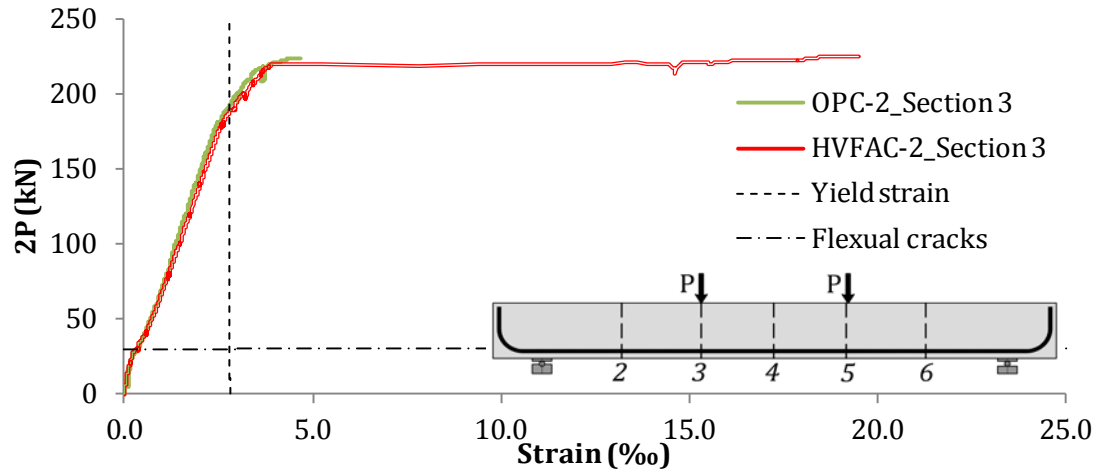


Figure 4.75 Longitudinal reinforcement strains in OPC-2/HVFAC-2 beams in section 3

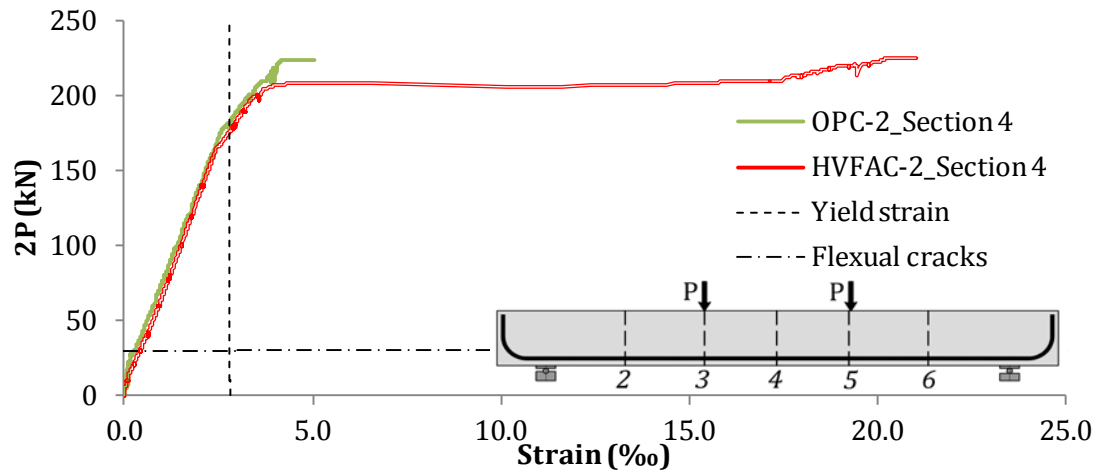


Figure 4.76 Longitudinal reinforcement strains in OPC-2/HVFAC-2 beams in section 4

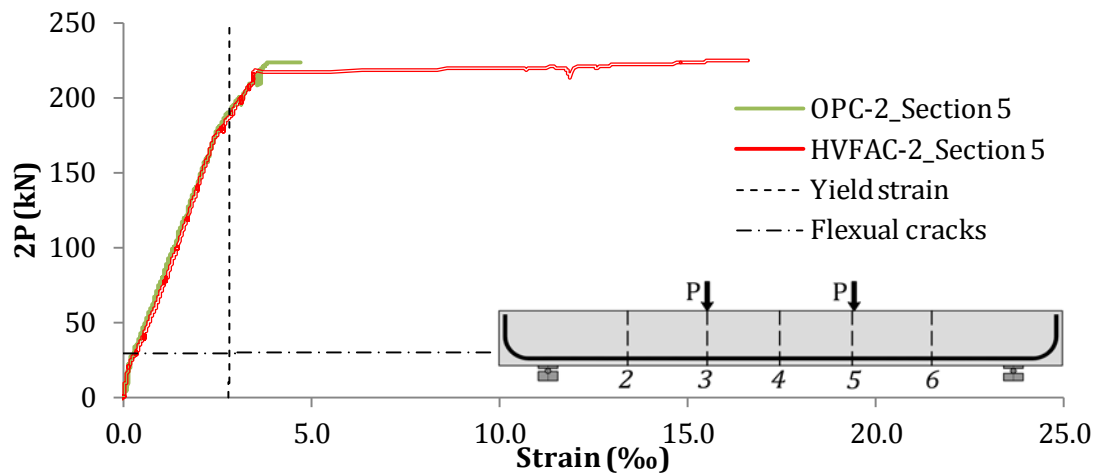


Figure 4.77 Longitudinal reinforcement strains in OPC-2/HVFAC-2 beams in section 5

4. Experimental program and test results

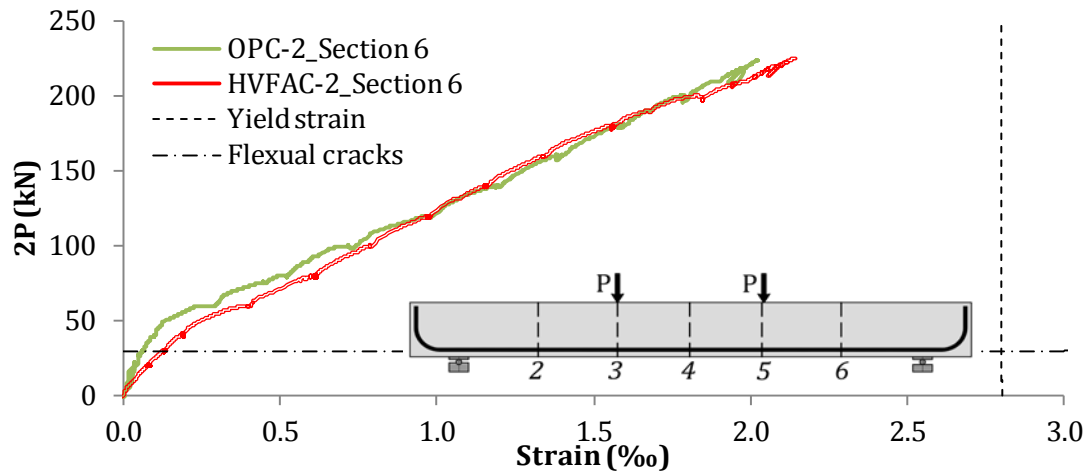


Figure 4.78 Longitudinal reinforcement strains in OPC-2/HVFAC-2 beams in section 6

The beams with a minimum reinforcement ratio displayed three distinct parts in their respective load-strain curves in both OPCC and HVFAC beams. The behavior of longitudinal reinforcement was linear-elastic until the formation of the first flexural cracks. After that point the relationship was still linear but with a different angle of the curve until the yielding point was reached, namely beams' stiffness was reduced. After the yielding point, strains continued to increase with no load increase until failure occurred. A comparative analysis of reinforcement strains in beams OPC-1 and HVFAC-1 showed that there were no significant differences between the load-strain curves of the different beams prior to flexural cracking. In sections 2 and 3, the load-strain curves of the OPC-1 and HVFAC-1 beams coincide to a large degree, unlike in sections 4, 5, and 6 in the part after flexural cracking. In sections 4 and 5, the yielding of the HVFAC beam was pronounced, resulting in higher strains in beam HVFAC-1 compared with beam OPC-1. However, in section 6, strains were higher in the OPC-1 beam than in the HVFAC-1 beam after flexural cracking. This was mostly a consequence of the crack pattern due to a large influence of crack vicinity on the reinforcement strain measurement.

In the beams with a higher than minimum reinforcement ratio, three parts of the load-strain curves can also be defined in a similar way as in the case of beams with a minimum reinforcement ratio. The linear-elastic behavior was also expressed up to the reinforcement yielding point. The decrease in stiffness was noticed after flexural crack formation but to a smaller extent compared with beams with a minimum reinforcement ratio. The load-strain curves in the sections close to the

4. Experimental program and test results

supports showed negligible differences between OPCC and HVFAC beams. In the beams' mid-point section, the behavior of OPCC and HVFAC beams was the same up to the yielding of reinforcement. After that point, in the HVFAC-2 beam yielding of the reinforcement was more pronounced compared with the OPC-2 beam. The maximum strain values in all sections are given in Figures 4.79 and 4.80.

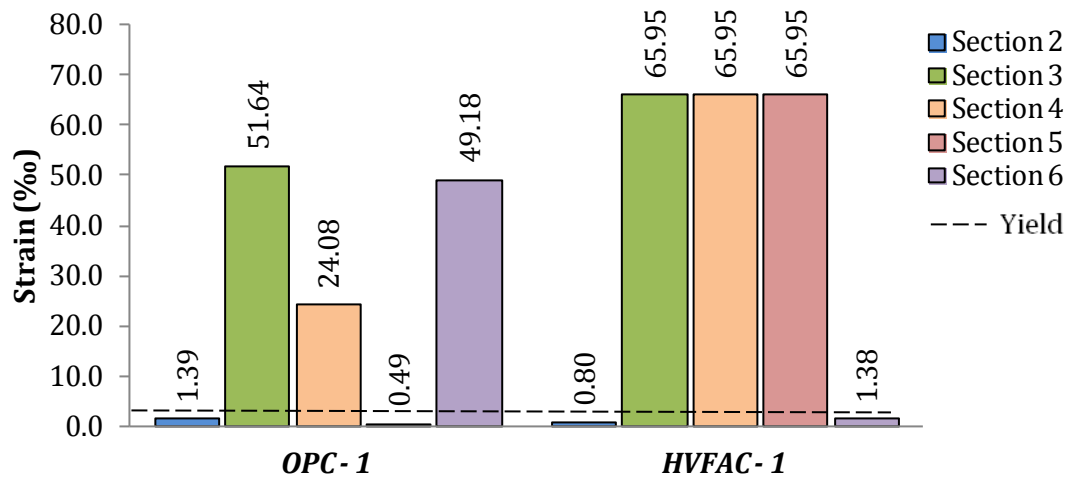


Figure 4.79 Maximum longitudinal reinforcement strains in beams with a minimum reinforcement ratio

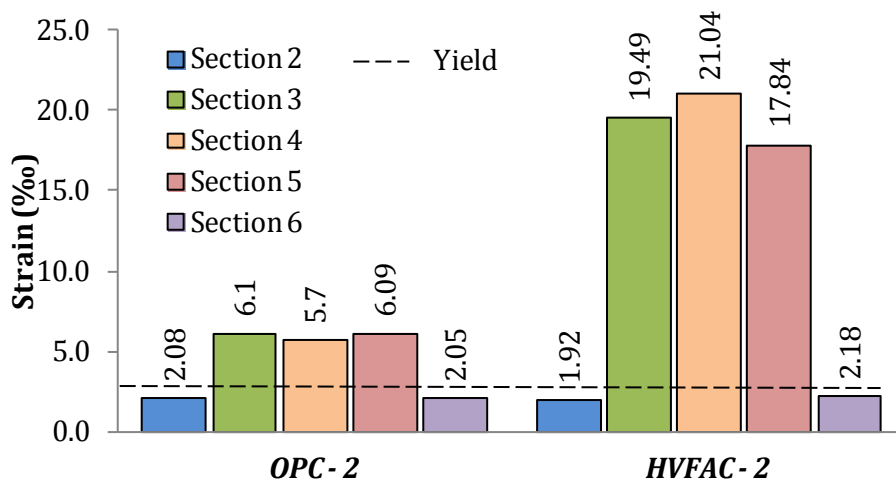


Figure 4.80 Maximum longitudinal reinforcement strains in beams with a higher than minimum reinforcement ratio

The reinforcement strains in the HVFAC beams were generally higher compared with the strains in the OPCC beams. The longitudinal reinforcement strains in the HVFAC beam with a minimum reinforcement ratio in sections 3, 4, and 5 reached

4. Experimental program and test results

the maximum measuring value of SGs of 65.95‰. In the OPC-1 beam, in sections 3 and 4, pronounced yielding was noticed while in section 5 strain values did not reach the yielding point. The bending moment was constant in the region between sections 3 and 5 so the difference in the reinforcement strains in the OPC-1 beam can be explained by the crack patterns in that region. In the beams with a higher than minimum reinforcement ratio, strain distribution along the beam length was uniform. The difference in reinforcement strains in sections 3, 4, and 5 was within a 10% margin. The strain values were higher in the HVFAC-2 beam compared with beam OPC-1 in sections 3, 4, and 5 by 69%, 73%, and 66%, respectively. In sections close to the supports (sections 2 and 6) the difference between strains in beams OPC-2 and HVFAC-2 was up to 10%.

4.3.10. Concrete strains

Concrete compressive strains were measured in three sections along the beams length (section 3, 4, and 5). The measured concrete strains by all VWSGs in each section are shown in Figures 4.81 – 4.92 for all tested beams. Measured concrete strains on the front and back side are in good agreement so their average values were used for evaluation. In some VWSGs, tension strains were the consequence of the position of the neutral axis in that section or cracks passing through the measurement base of the sensors.

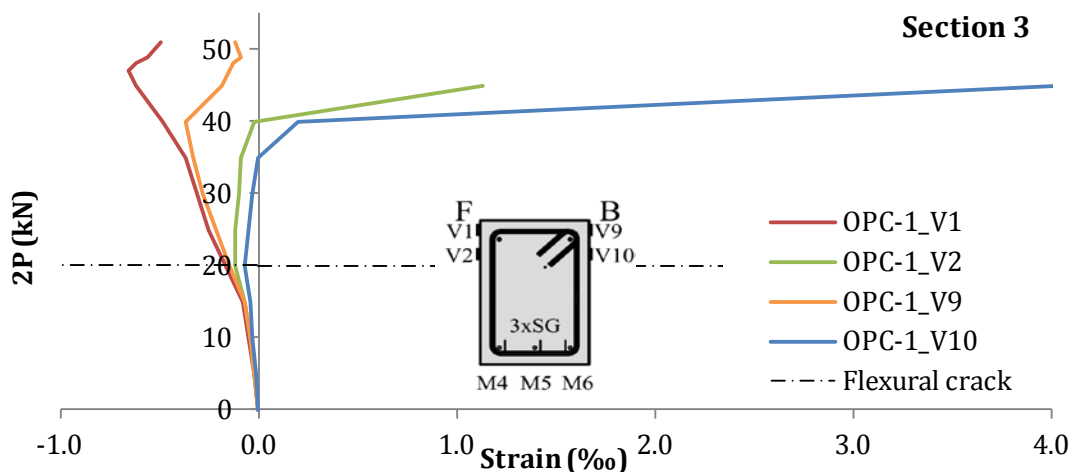


Figure 4.81 Concrete strains in section 3 - beam OPC-1

4. Experimental program and test results

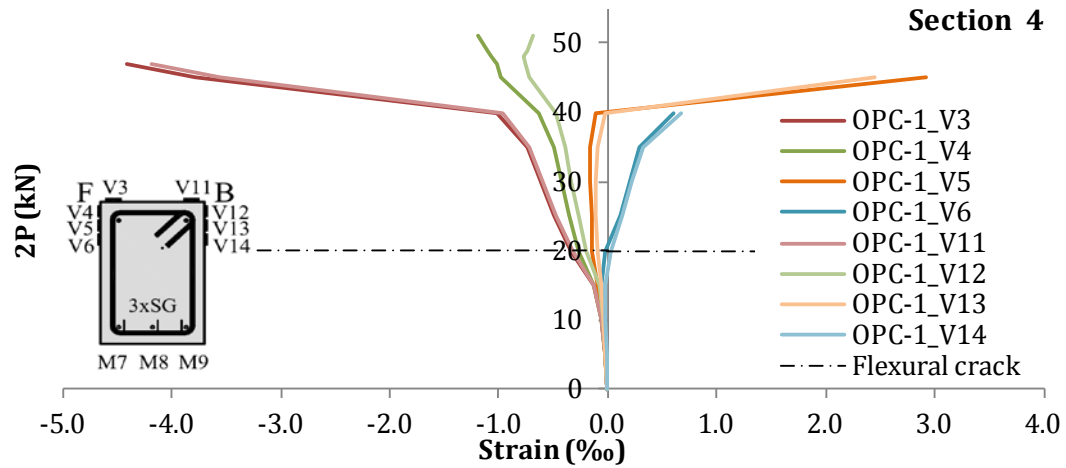


Figure 4.82 Concrete strains in section 4 - beam OPC-1

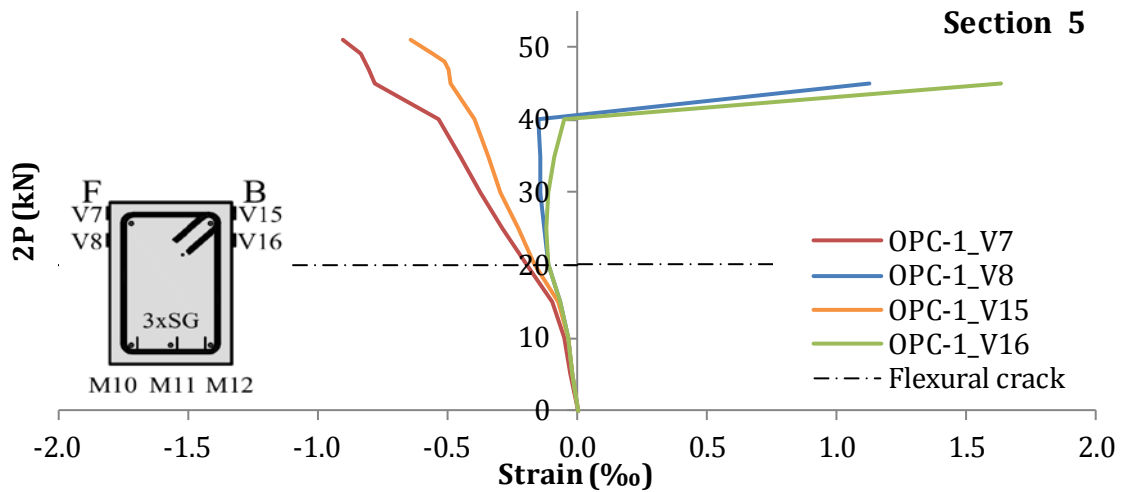


Figure 4.83 Concrete strains in section 5 - beam OPC-1

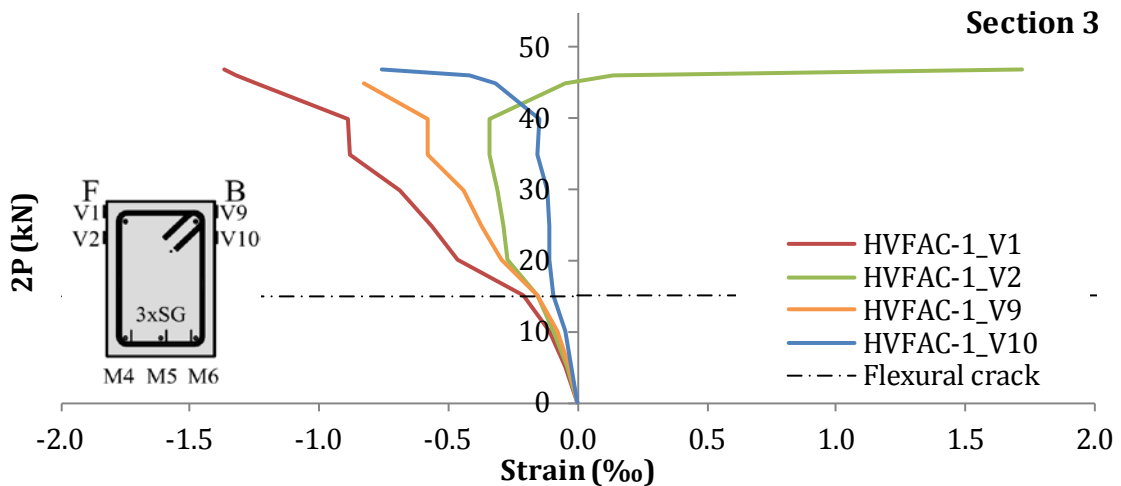


Figure 4.84 Concrete strains in section 3 - beam HVFAC-1

4. Experimental program and test results

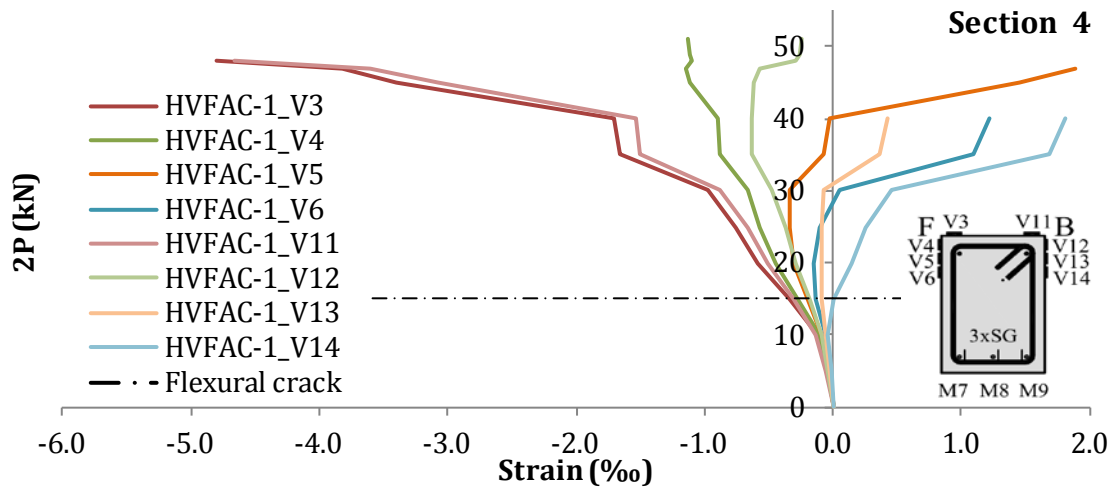


Figure 4.85 Concrete strains in section 4 - beam HVFAC-1

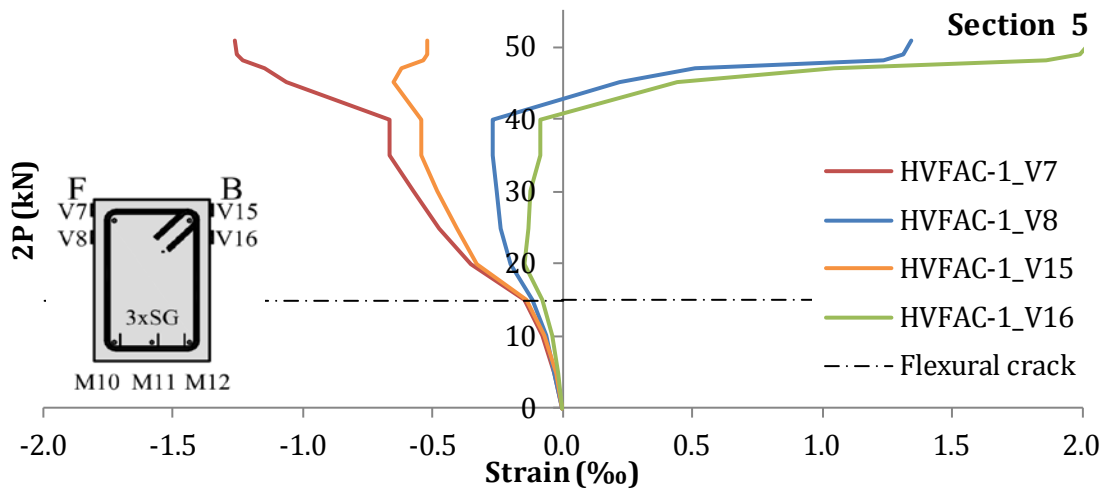


Figure 4.86 Concrete strains in section 5 - beam HVFAC-1

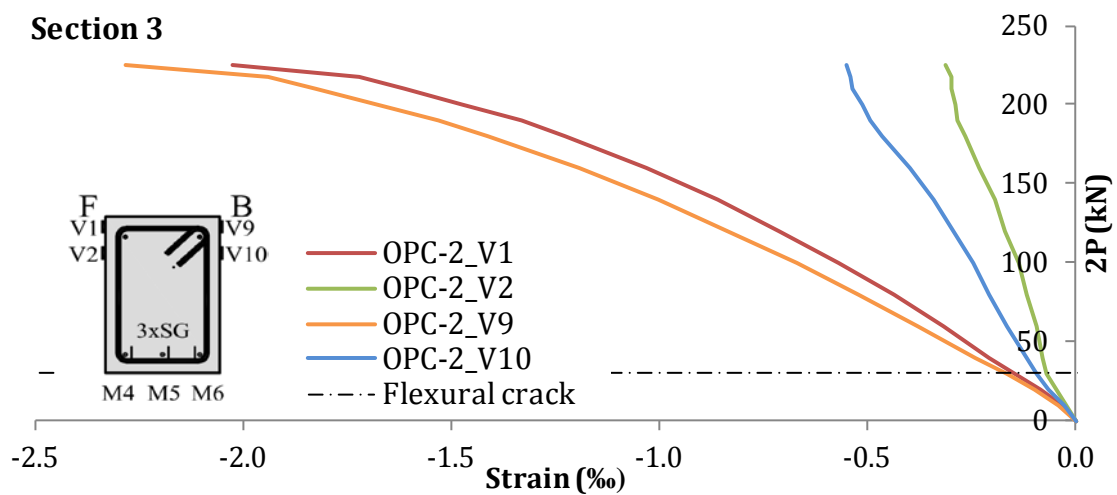
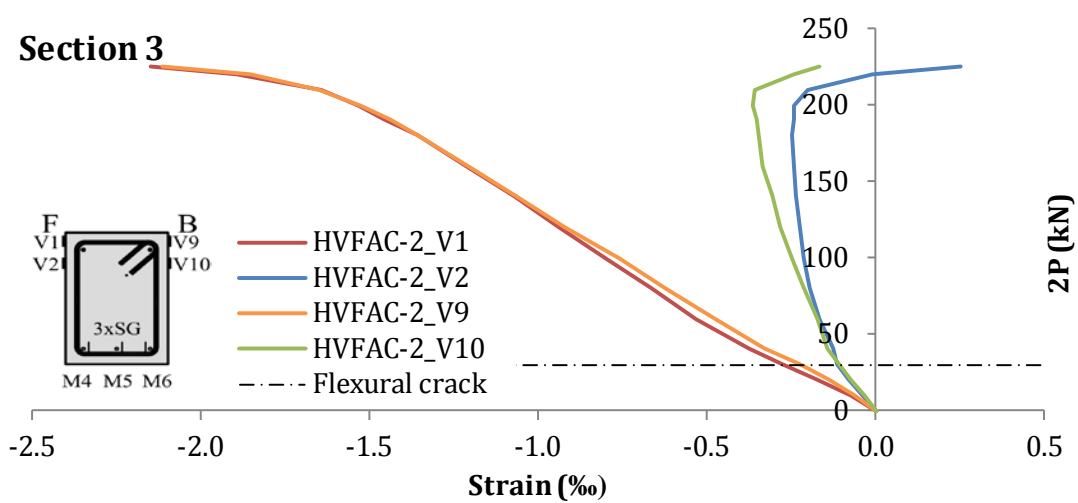
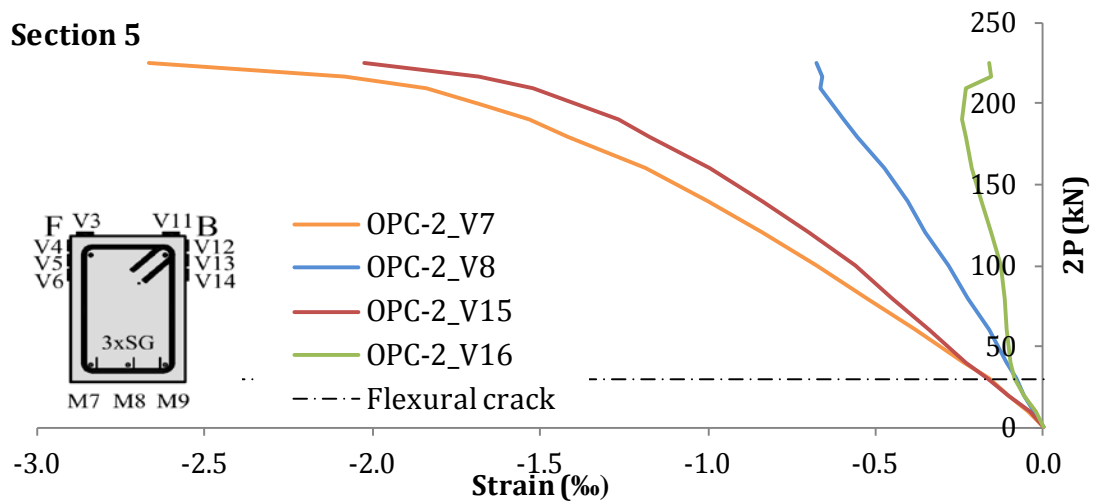
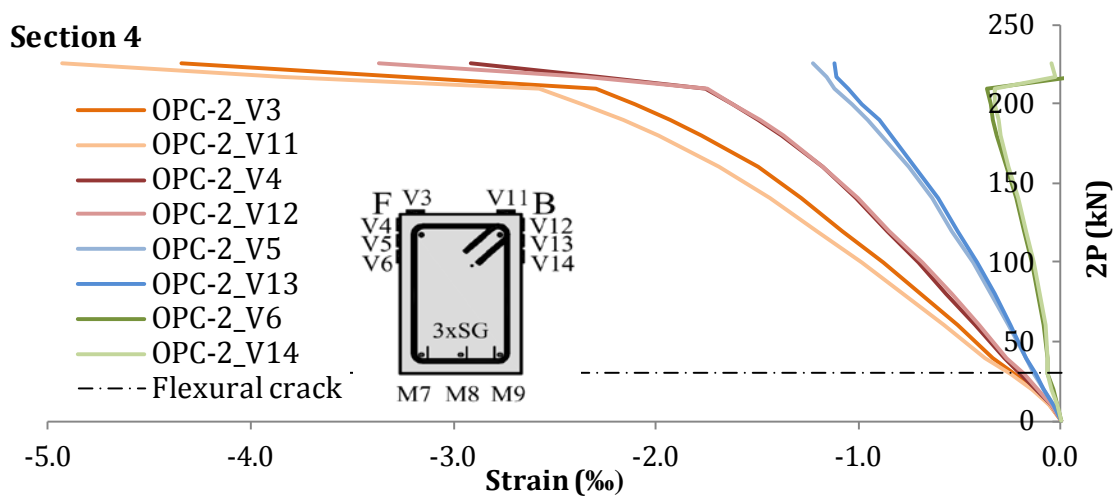


Figure 4.87 Concrete strains in section 3 - beam OPC-2

4. Experimental program and test results



4. Experimental program and test results

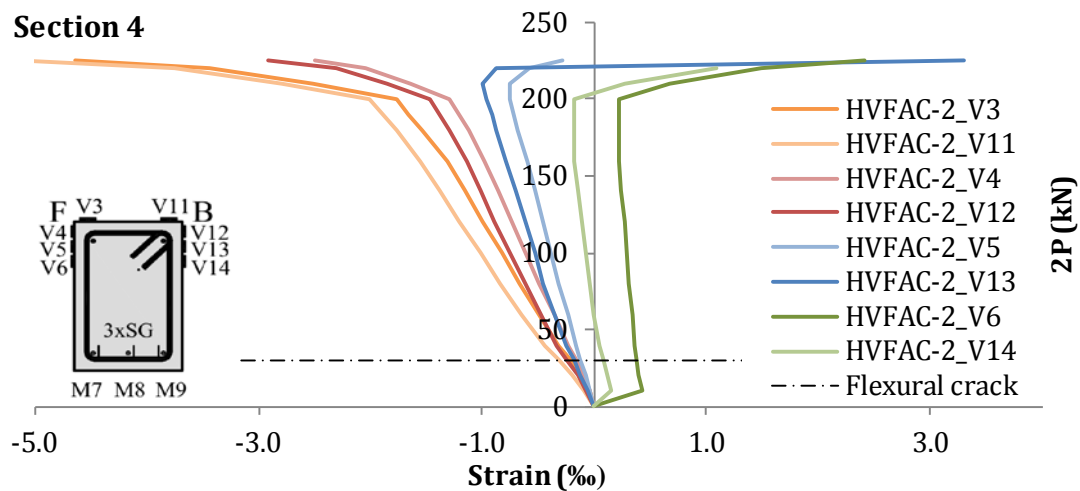


Figure 4.91 Concrete strains in section 4 - beam HVFAC-2

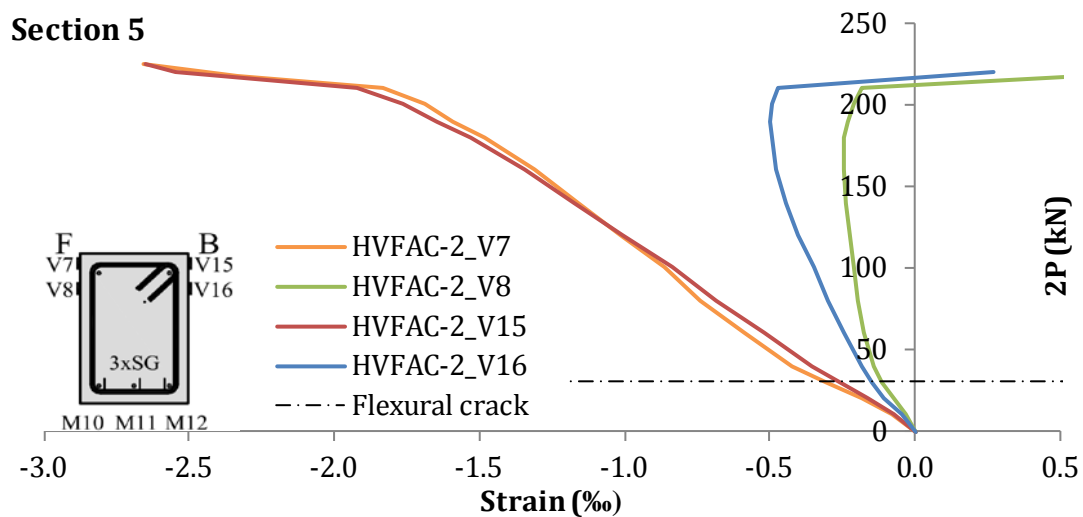


Figure 4.92 Concrete strains in section 5 - beam HVFAC-2

In order to compare the concrete strains in the OPCC and HVFAC beams, diagrams with the average values of measured strains in sections 3, 4, and 5 are shown in Figures 4.93 – 4.100. The highest concrete strains were noticed in section 4 for all beams, as expected. The concrete strains of both beams with a minimum reinforcement ratio were the same for all sections until the formation of flexural cracks. After that point, the load–strain relationships were similar for both beams but with higher strains in the HVFAC-2 beam in all sections. The significant strain increase was noticed at approximately 40 kN corresponding to the yielding force defined based on the load–deflection curves.

4. Experimental program and test results

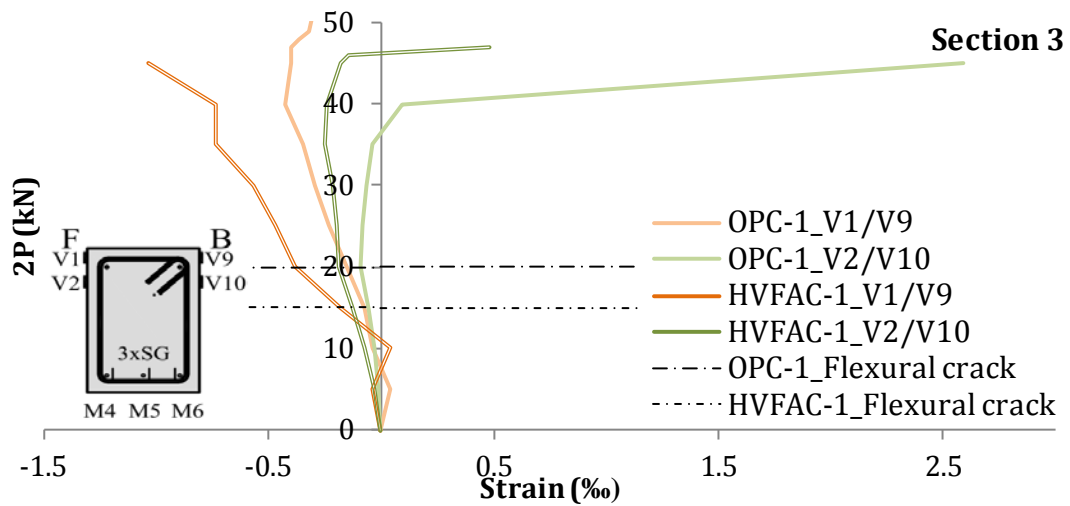


Figure 4.93 Concrete strains in section 3 of the OPC-1 and HVFAC-1 beams

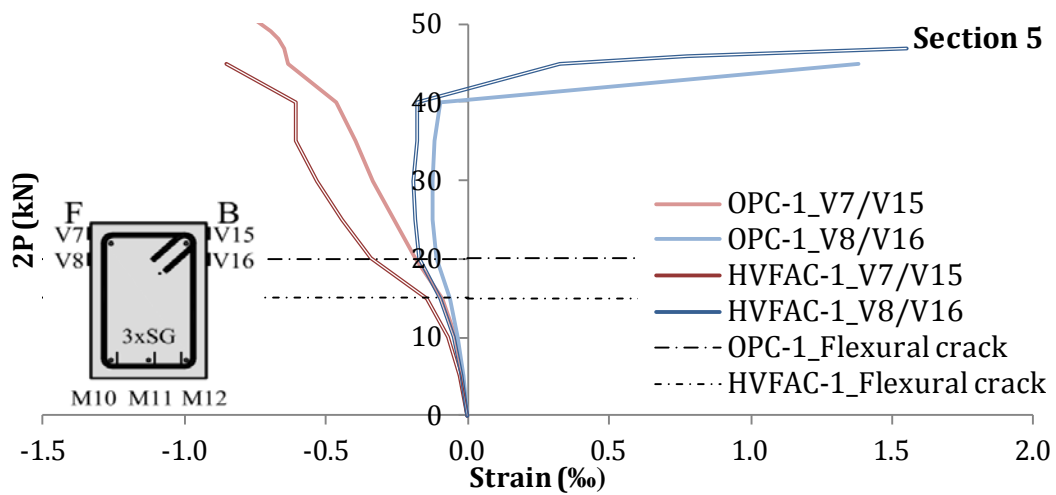


Figure 4.94 Concrete strains in section 5 of the OPC-1 and HVFAC-1 beams

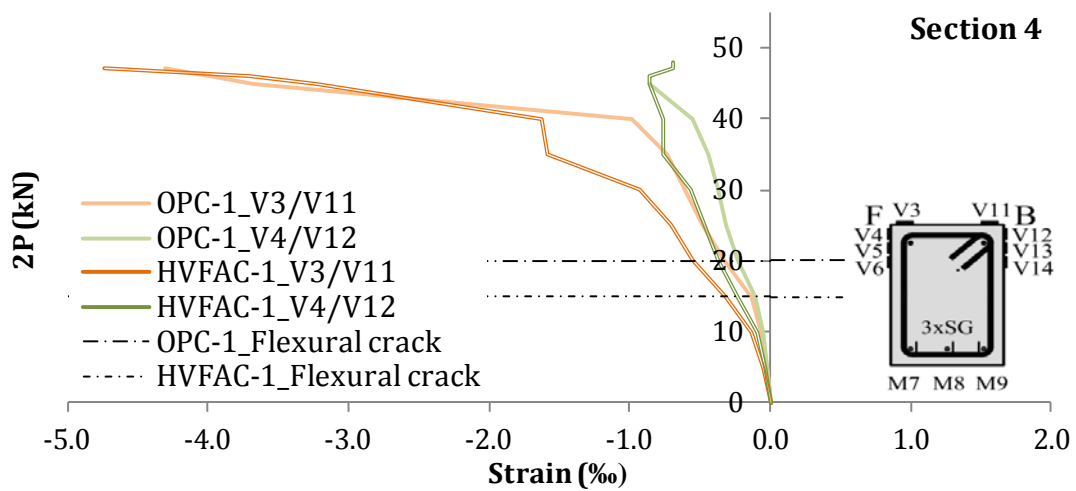


Figure 4.95 Concrete strains in section 4 of the OPC-1 and HVFAC-1 beams

4. Experimental program and test results

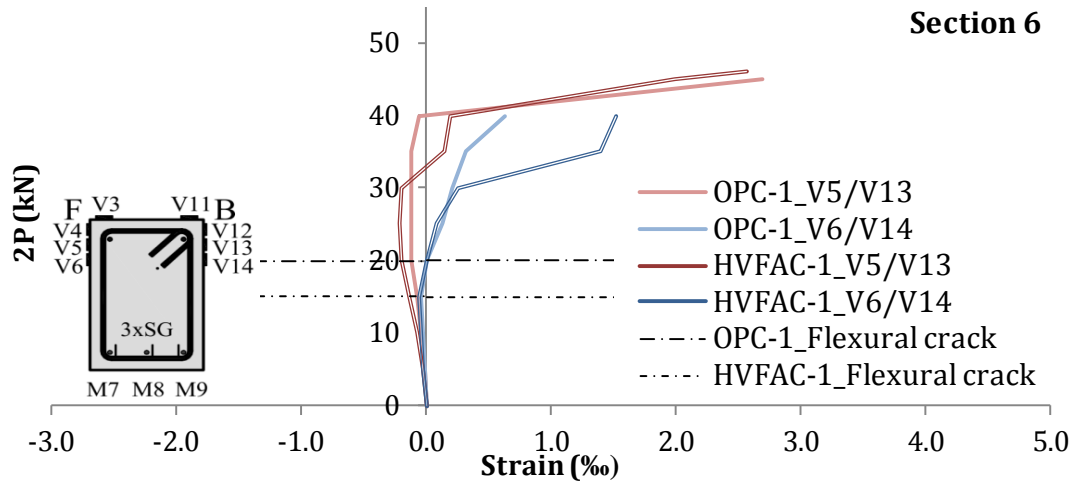


Figure 4.96 Concrete strains in section 6 of the OPC-1 and HVFAC-1 beams

The concrete strains for both beams with a higher than minimum reinforcement ratio had the same trend with beam HVFAC-2 exhibiting higher strains in sections 3 and 5. Formation of the first flexural cracks did not have a significant influence on the development of concrete strains. The load–strain curve was close to linear up to a force of 210 kN, corresponding to the yielding point defined in the load–deflection curves. After reaching 210 kN, a faster increase in concrete compressive strains was noticed in both beams in all sections. The ultimate concrete strain values for the OPCC and the HVFAC beams are shown in Figure 4.101. The concrete compressive strains at failure were higher in HVFAC beams but the difference was up to 7% for all sections.

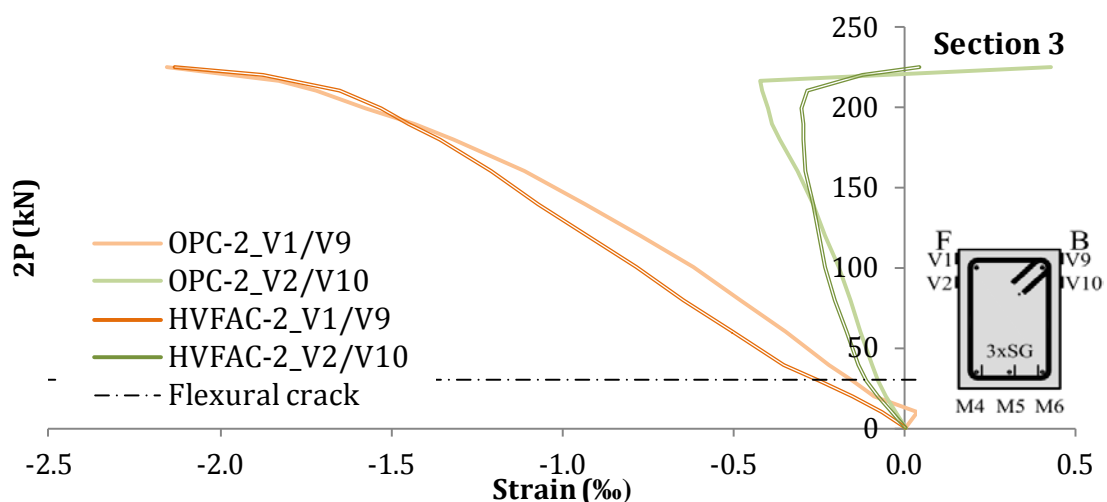


Figure 4.97 Concrete strains in section 3 of the OPC-2 and HVFAC-2 beams

4. Experimental program and test results

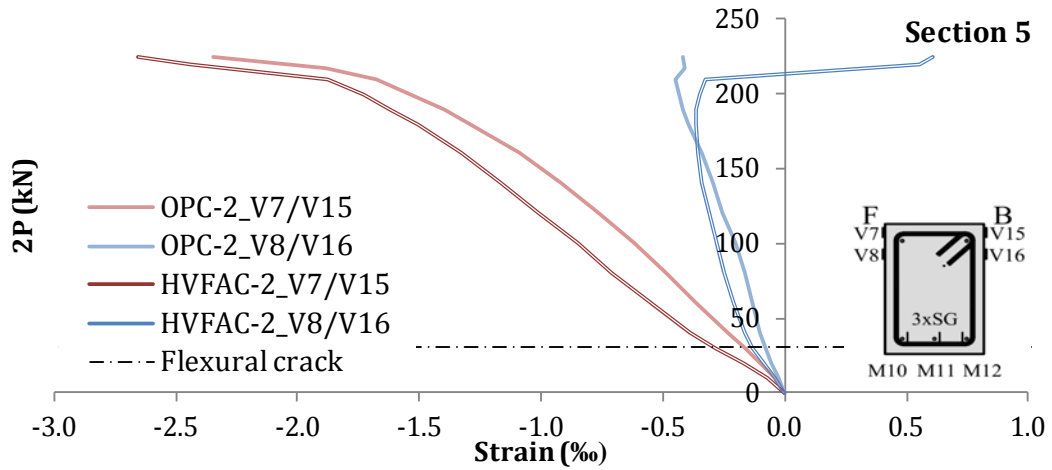


Figure 4.98 Concrete strains in section 5 of the OPC-2 and HVFAC-2 beams

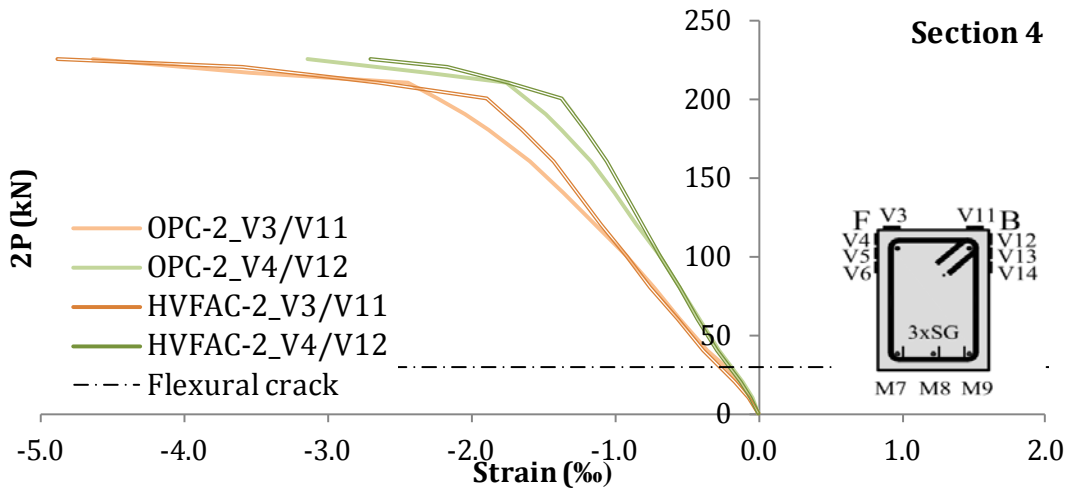


Figure 4.99 Concrete strains in section 4 of the OPC-2 and HVFAC-2 beams

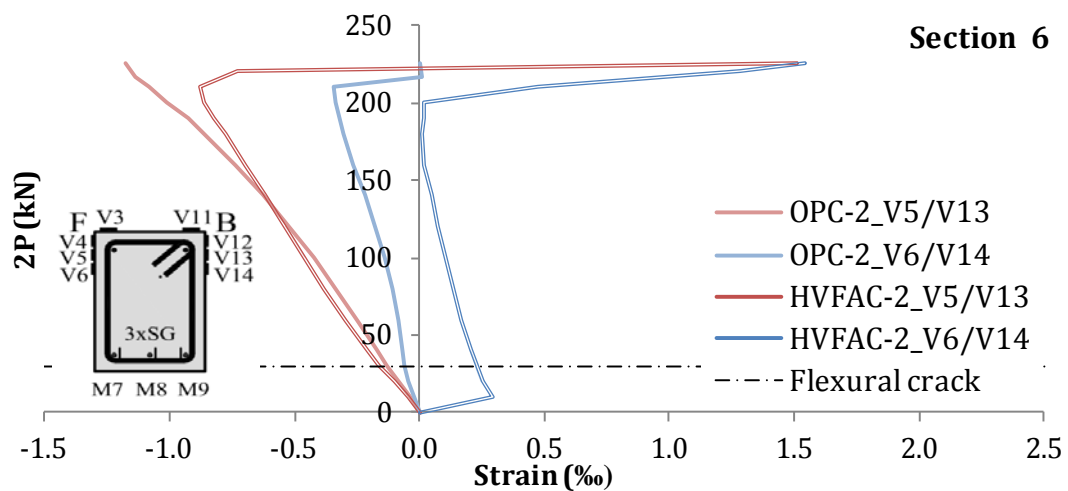


Figure 4.100 Concrete strains in section 6 of the OPC-2 and HVFAC-2 beams

4. Experimental program and test results

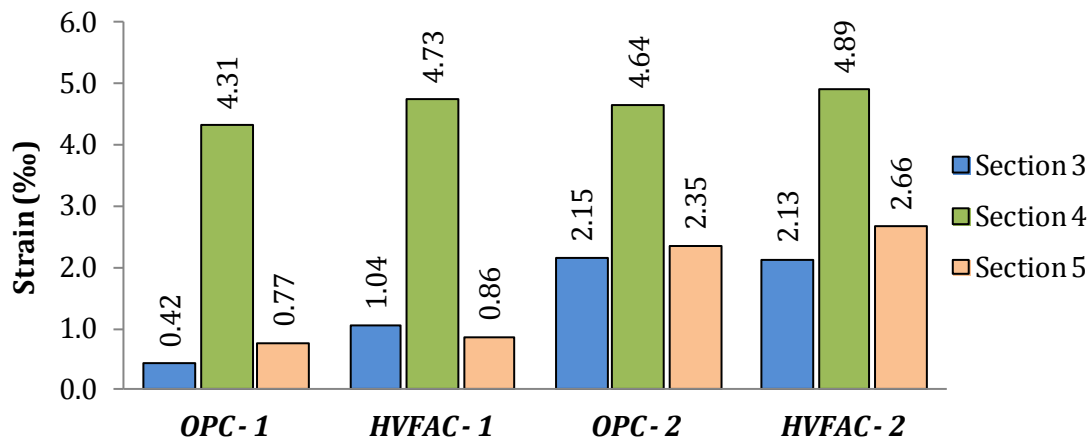


Figure 4.101 Ultimate concrete strains for the OPCC and HVFAC beams

4.3.10.1. Distribution of strains

The strain distribution in section 4 for beams from the first and the second group are plotted in Figures 4.102 and 4.103, respectively. The distribution of strains can be considered as linear for all of the beams. The difference between OPC-1 and HVFAC-1 beams' concrete strains in the top fiber, and strains in the reinforcement was 35% and 36%, respectively. For OPC-2 and HVFAC-2 beams the differences between maximum concrete strain and maximum reinforcement strain was 10% and 7%, respectively.

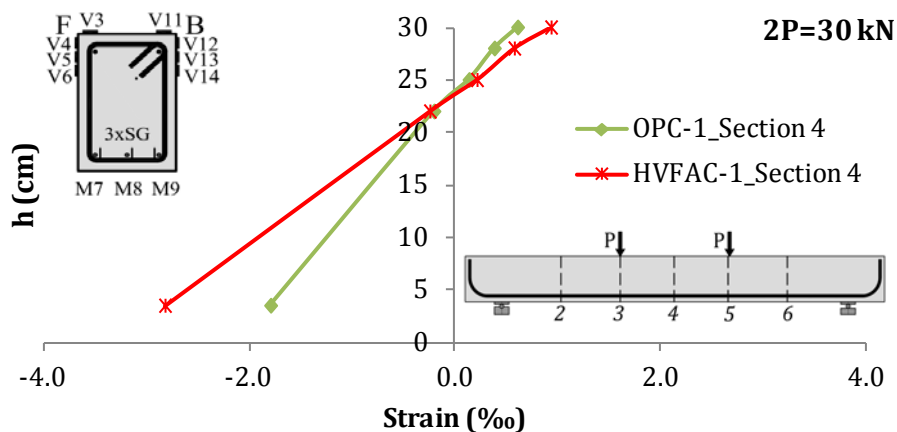


Figure 4.102 Strain distribution in section 4 of the OPC-1 and HVFAC-1 beams

When comparing the height of the compressed part of the cross-section, small differences between the OPCC and HVFAC beams were observed. For the beams with a minimum reinforcement ratio, the height of the compression zone was

4. Experimental program and test results

approximately 66 mm and 65 mm for the OPC-1 and HVFAC-1 beams, respectively. For beams with a higher than a minimum longitudinal reinforcement ratio, it was about 105 mm and 91 mm for the OPC-2 and HVFAC-2 beams, respectively.

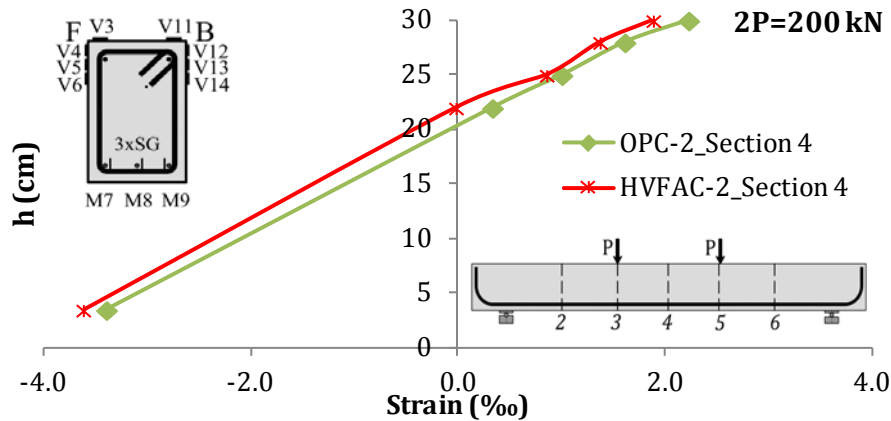


Figure 4.103 Strain distribution in section 4 of the OPC-2 and HVFAC-2 beams

4.3.11. Concrete cracks

Cracks represent a common phenomenon in RC structures under service load. It is important to analyze and evaluate the development of cracks especially because of concrete durability and the reduction of beams' rigidity. Two methods of evaluation were used in this study to determine the development of cracks, as already described. Visual inspection and tracking of cracks was done to get an insight into crack development over the entire length of the beams. This analysis was also done in more detail for the middle part of the beam where the most cracks were expected. A DIC system, previously presented, was used to get a more precise picture of the developed cracks in the middle part of the beams' front side. The crack patterns for each beam were marked at the front surface of the beams.

In order to give a quantitative comparison of flexural crack patterns and their development, the following parameters were chosen and presented in Table 4.20: maximum vertical crack length at service load ($l_{ser,max}$) and ultimate load ($l_{u,max}$), number of flexural cracks at service load (n_{ser}) and ultimate load (n_u), and average spacing between cracks at service load ($s_{ser,avg}$) and ultimate load ($s_{u,avg}$). All values presented in Table 4.20 are based on the visual inspection of cracks. Evaluation of

4. Experimental program and test results

the crack widths was done separately by comparing the sum of all crack width measured visually on the back side of the beams.

Table 4.20 Flexural and shear crack parameters for beams subjected to flexure

Beam notation	$l_{ser,max}$ (mm)	$l_{u,max}$ (mm)	n_{ser} (-)	n_u (-)	$S_{ser,avg}$ (mm)	$S_{u,avg}$ (mm)
OPC-1	90	290	4	16	178	134
HVFAC-1	210	269	10	18	151	128
OPC-2	154	216	20	29	95	89
HVFAC-2	228	252	31	40	72	74

The development of cracks on the back side of the beams, obtained using visual inspection, is graphically presented in Figures 4.104 – 4.107. Crack patterns in the middle part of the front side of the beams, obtained using DIC system, are shown in Figures 4.109 – 4.127.

As can be seen from the crack patterns, more flexural cracks developed in the HVFAC beams compared with the OPCC beams. The branching of cracks was noticed in both OPC-1 and HVFAC-1 beams as explained before. The crack patterns obtained using the DIC system corresponded well to the cracks identified by visual inspection. The results obtained using the DIC system showed that the first flexural cracks appeared at the same loading level as it was determined by previous analysis for all beams. The only significant difference that emerged was shown in the cracks' branching patterns. The crack branching that appeared close to the beams' failure load was not completely identified during the visual monitoring of cracks. More crack branching was identified using the DIC system in both OPCC and HVFAC beams. It is clear that the crack patterns in the OPCC and HVFAC beams were different. In the OPCC beams, flexural cracks developed mostly vertically within one branch. The crack branching was apparent only at the crack tips at the loading close to failure. However, the crack branching in the HVFAC beams developed throughout the entire crack length even at the service load level. More short flexural cracks on the tension side were connected, building a crack net different from the one in the OPCC beams' crack patterns.

4. Experimental program and test results

The first flexural cracks appeared at 20 kN and 15 kN for the OPC-1 and HVFAC-1 beams, respectively. No shear cracks developed during loading, except one flexural-shear crack in beam HVFAC-1. The crack patterns were evaluated in the service load and ultimate load level. At the service load level, flexural cracks in the HVFAC-1 beam had 57% higher maximum vertical length and 60% higher number of cracks developed in that state compared with the OPC-1 beam. This difference decreased in the ultimate loading state: maximum vertical length was 7% higher and the number of developed cracks was 10% higher in the HVFAC-1 beam compared with beam OPC-1.

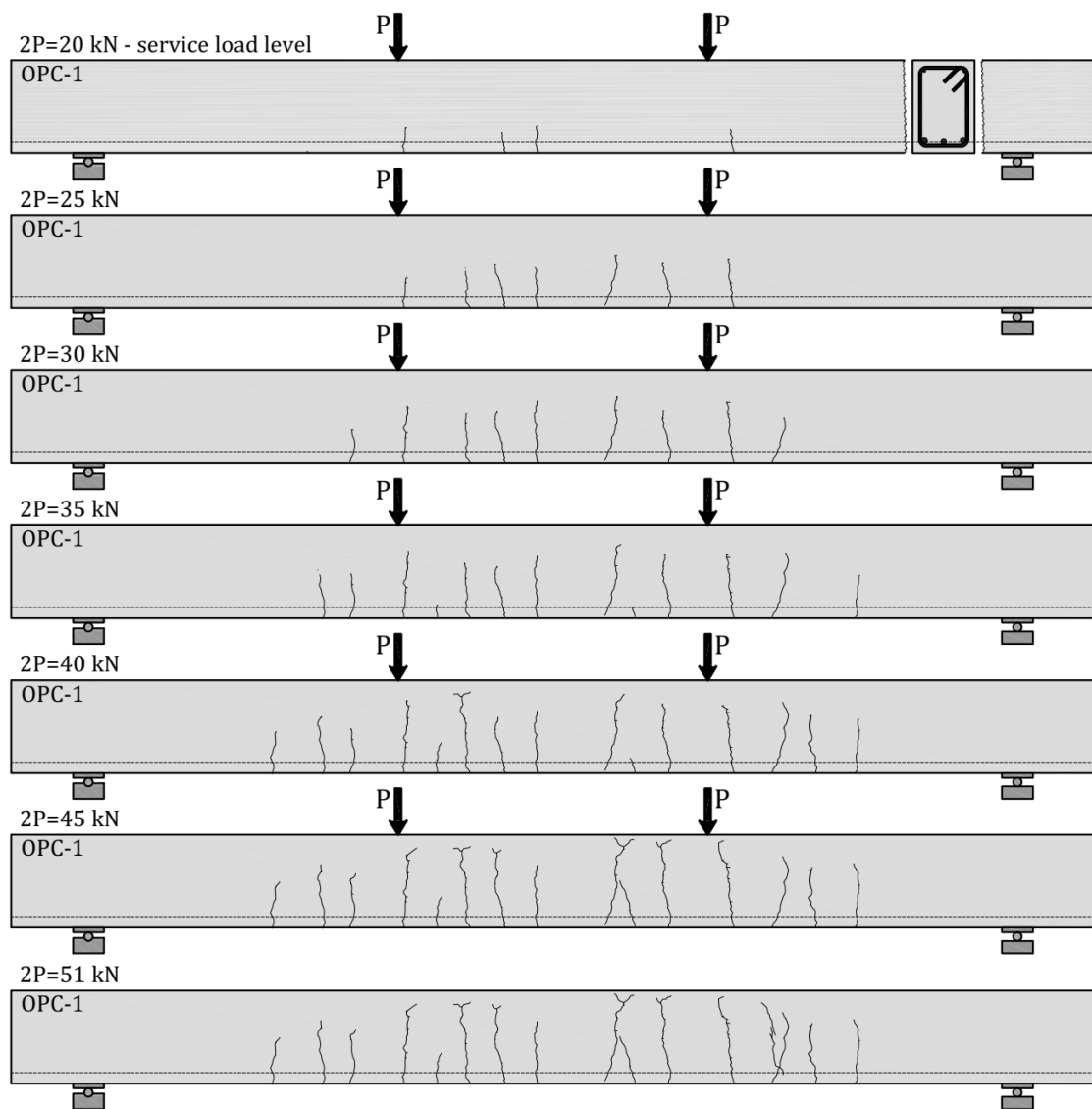


Figure 4.104 Crack patterns in beam OPC-1

4. Experimental program and test results

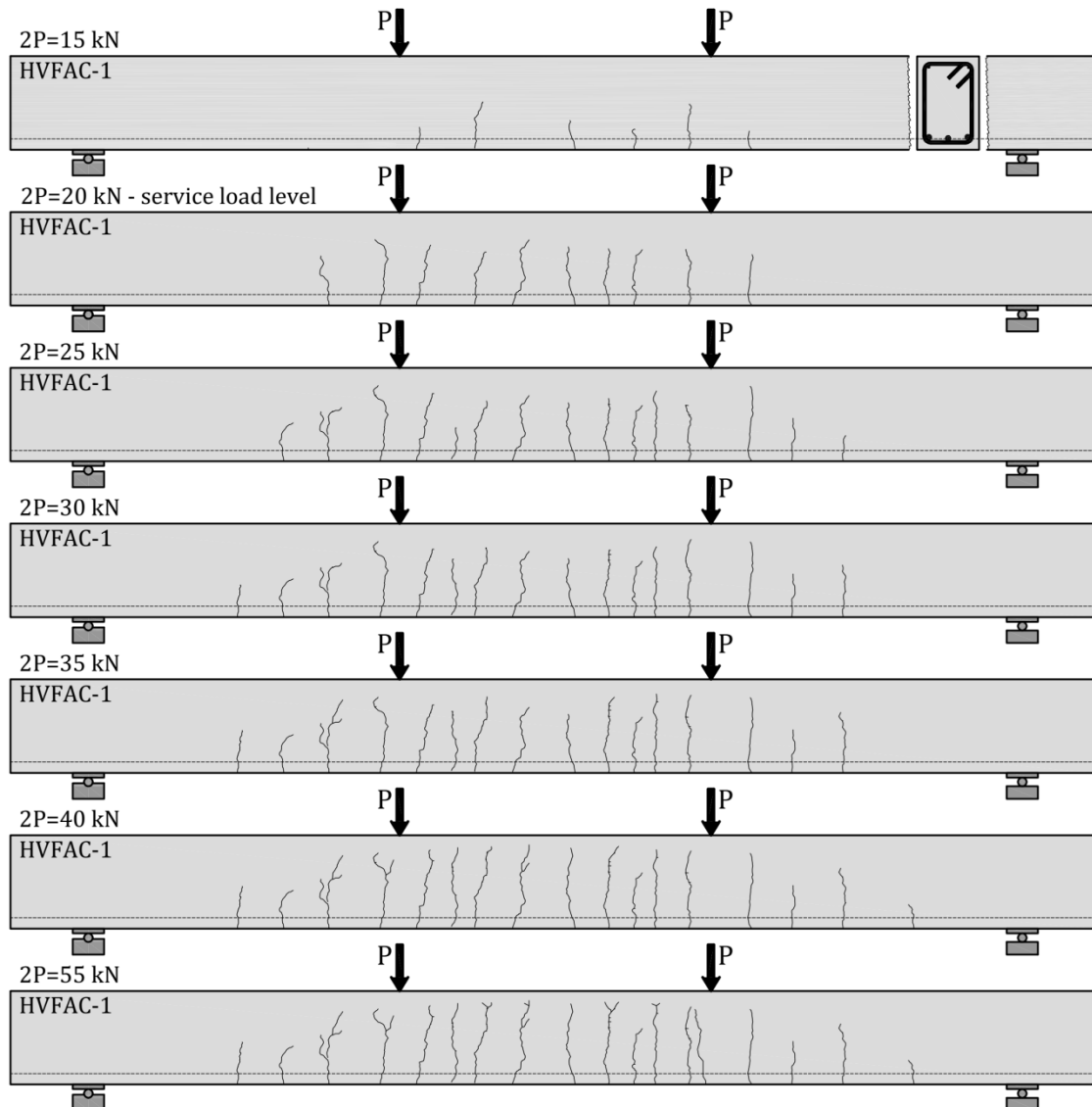


Figure 4.105 Crack patterns in beam HVFAC-1

The average spacing between cracks was smaller in the HVFAC-1 beam compared with beam OPC-1 by 15% and 5% at the service and ultimate load, respectively. The difference between crack patterns decreased as the loading increased with similar ultimate loading state crack patterns. The first flexural cracks developed at 30 kN and 20 kN for OPC-2 and HVFAC-2 beams, respectively. In the HVFAC-2 beam, most of the cracks were vertically oriented but there were some cracks in other directions formed along with the first flexural cracks. At the service load level, flexural cracks in the HVFAC-2 beam had 33% higher maximum vertical length and 55% higher number of cracks developed in that state compared with beam OPC-2.

4. Experimental program and test results

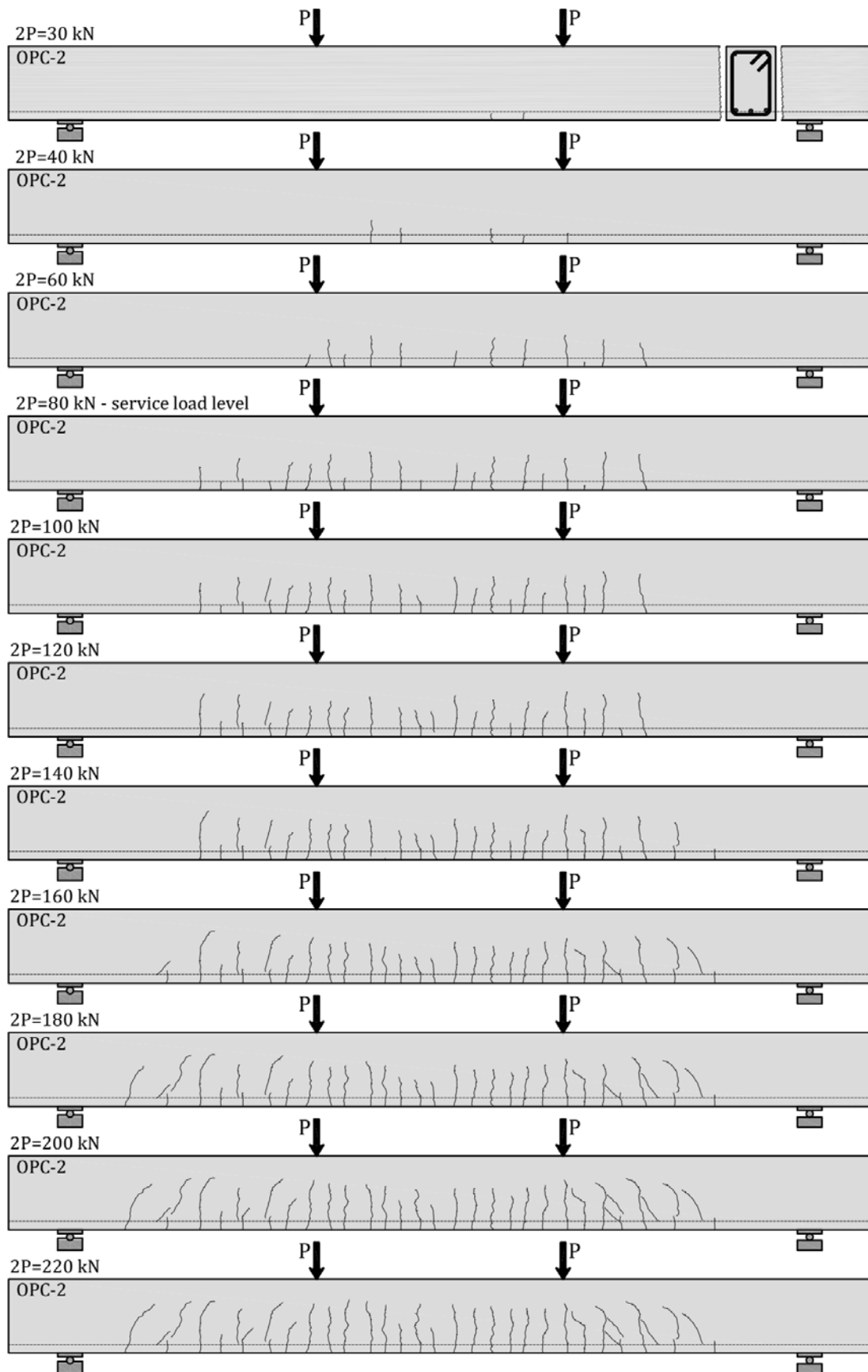


Figure 4.106 Crack patterns in beam OPC-2

4. Experimental program and test results

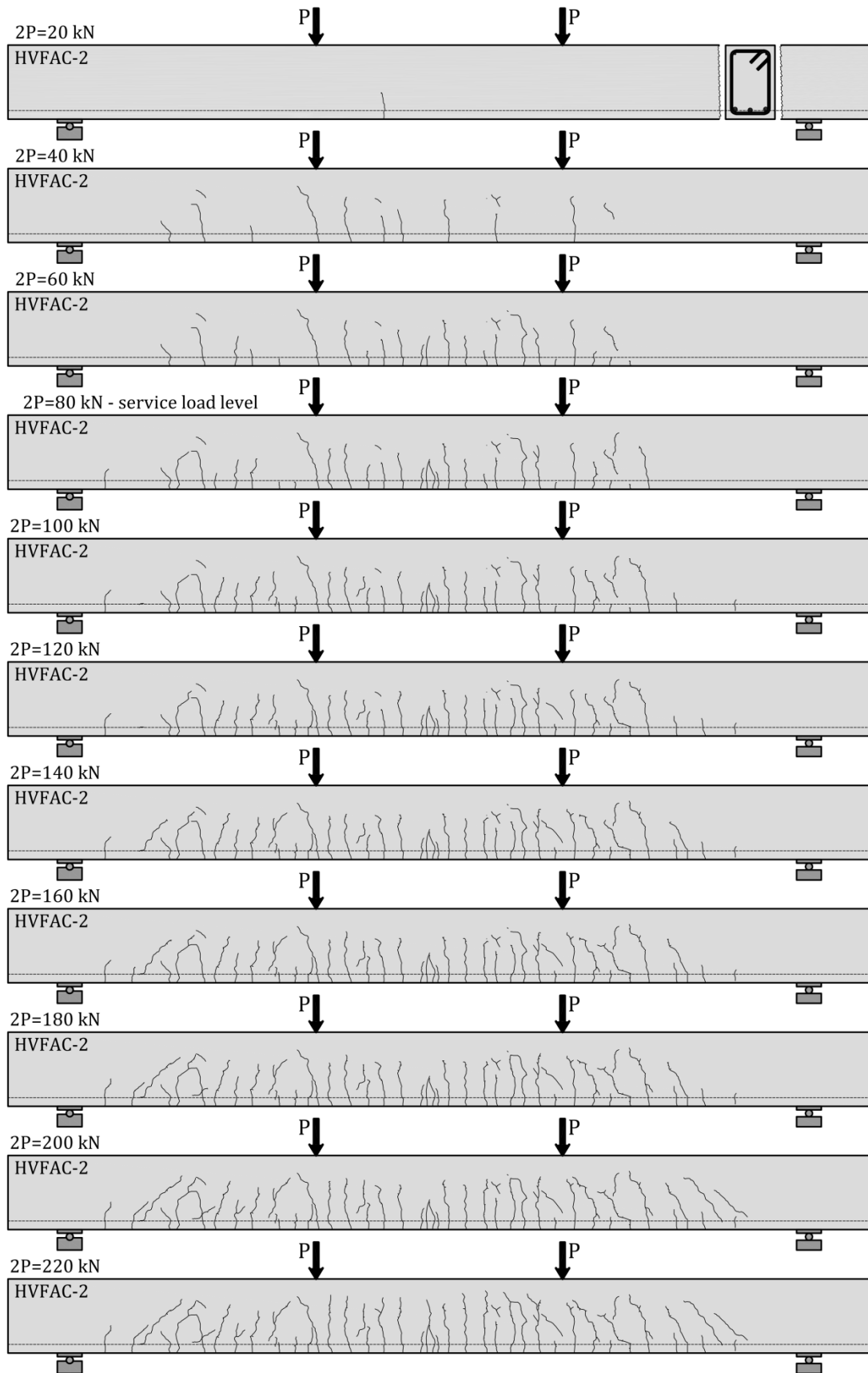


Figure 4.107 Crack patterns in beam HVFAC-2

4. Experimental program and test results

This difference decreased in the ultimate loading state: the maximum vertical length was 17% higher and the number of developed cracks was 38% higher in beam HVFAC-2 compared with beam OPC-2. The average spacing between cracks was smaller in the HVFAC-2 beam compared with beam OPC-2 by 24% and 17% at the service and ultimate load, respectively. The difference between crack patterns decreased as the loading increased with similar ultimate loading state patterns. In the HVFAC-2 beam a certain number of short cracks was present along the beam, unlike in the OPC-2 beam.

Previous analysis showed that more cracks developed in HVFAC beams compared with the OPCC beams. In order to quantify this difference, the sum of all crack widths along the beams' length was chosen as a parameter for comparison. The sum of visually measured crack widths for all cracks that developed along the length of the beams was calculated for 40%, 60% and 80% of the ultimate loading level and shown in Figure 4.108.

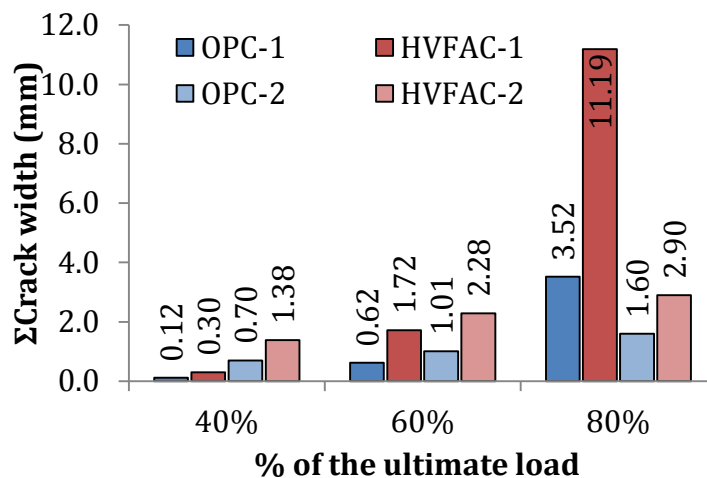


Figure 4.108 Crack width sum for different loading levels

It can be seen that beam OPC-1 had lower sum of crack widths compared with the HVFAC-1 beam for 60%, 64% and 69% at 40%, 60% and 80% of the ultimate loading level, respectively. Beam OPC-2 had 49%, 56% and 45% at 40%, 60% and 80% of the ultimate loading level, respectively. It can be concluded that beams HVFAC-1 and HVFAC-2 had, on average, 2.8 and 2.0 times higher sum of crack widths compared with the corresponding OPCC beams, respectively.

4. Experimental program and test results

One of the reasons for higher crack widths in HVFAC beams was the difference in flexural tensile strength of HVFAC and OPCC. The compressive strength of HVFAC and OPCC beams cured in water was different by not more than 3% but the difference was higher for specimens cured the same as beams—up to 19%. Flexural tensile strength of HVFAC beams was up to 24% lower compared with the OPCC beams. On the other hand, the splitting tensile strength of both HVFAC and OPCC beams was the same.

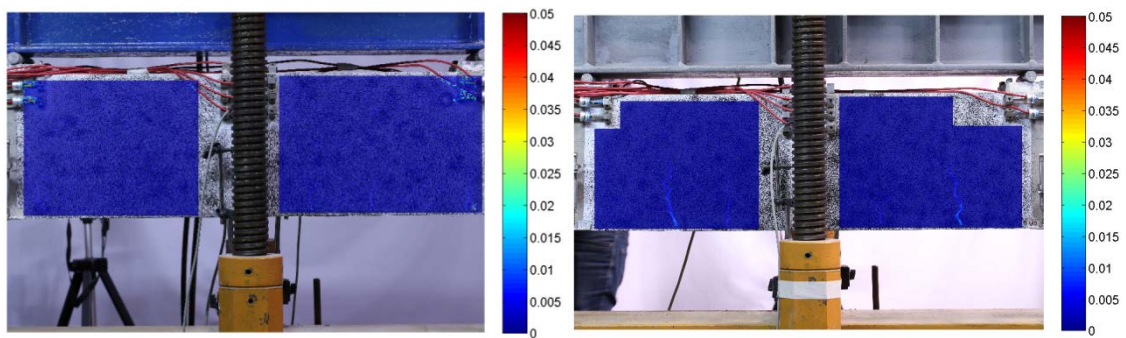


Figure 4.109 Crack patterns in beams OPC-1 and HVFAC-1 at $2P=15$ kN

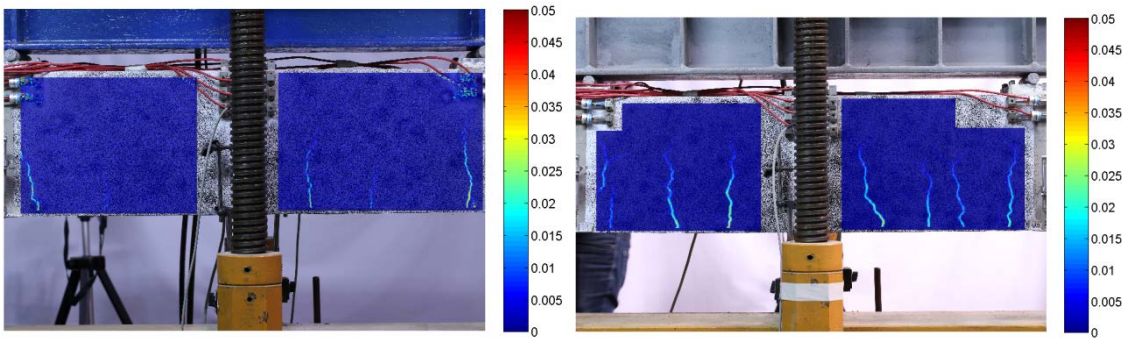


Figure 4.110 Crack patterns in beams OPC-1 and HVFAC-1 at $2P=20$ kN

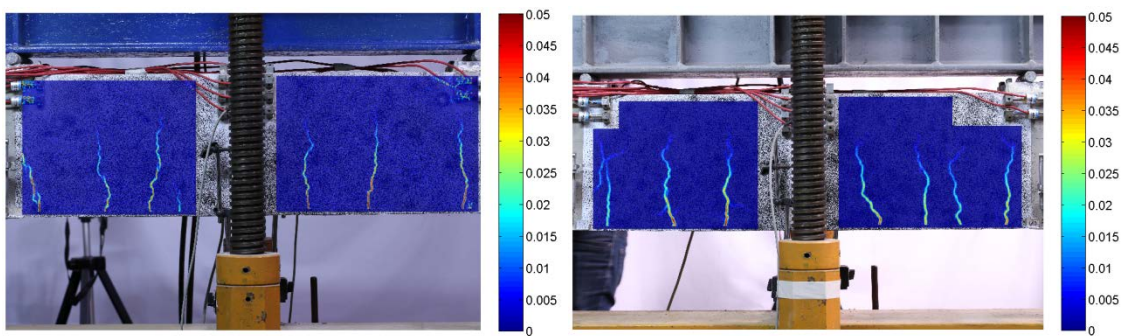


Figure 4.111 Crack patterns in beams OPC-1 and HVFAC-1 at $2P=25$ kN

4. Experimental program and test results

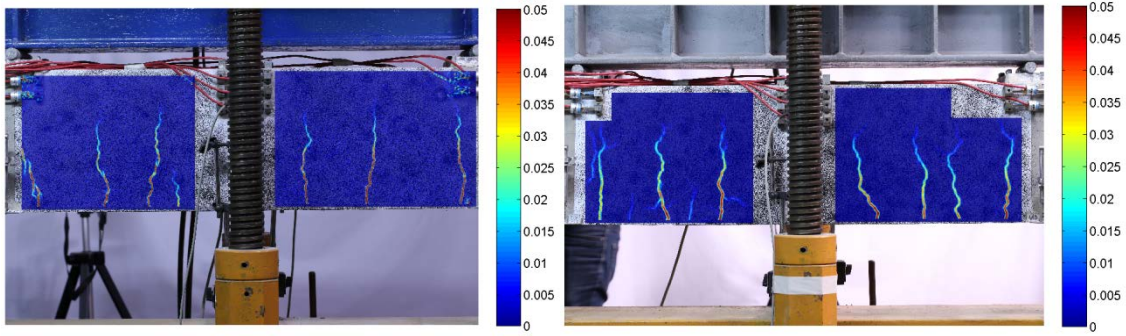


Figure 4.112 Crack patterns in beams OPC-1 and HVFAC-1 at $2P=30$ kN

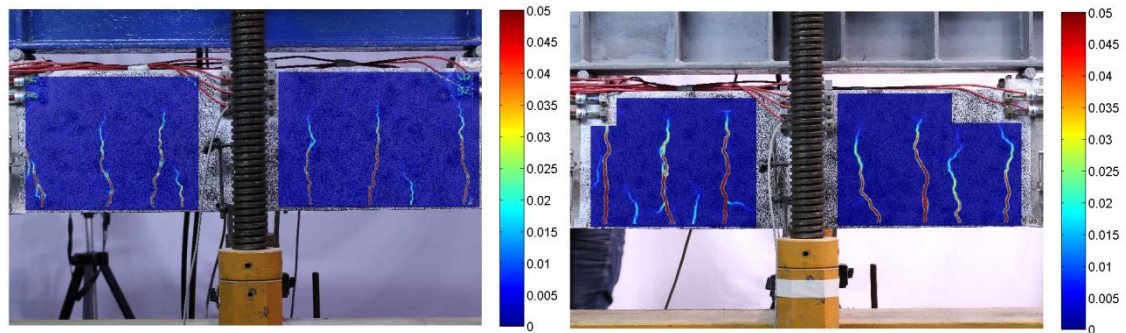


Figure 4.113 Crack patterns in beams OPC-1 and HVFAC-1 at $2P=35$ kN

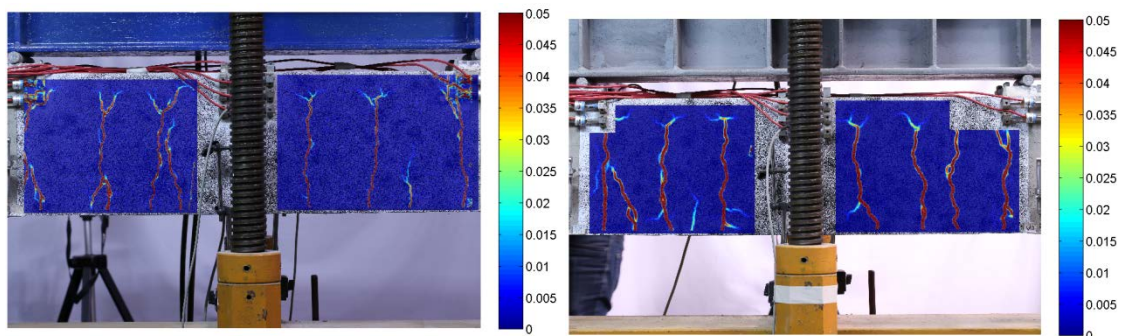


Figure 4.114 Crack patterns in beams OPC-1 and HVFAC-1 at $2P=40$ kN

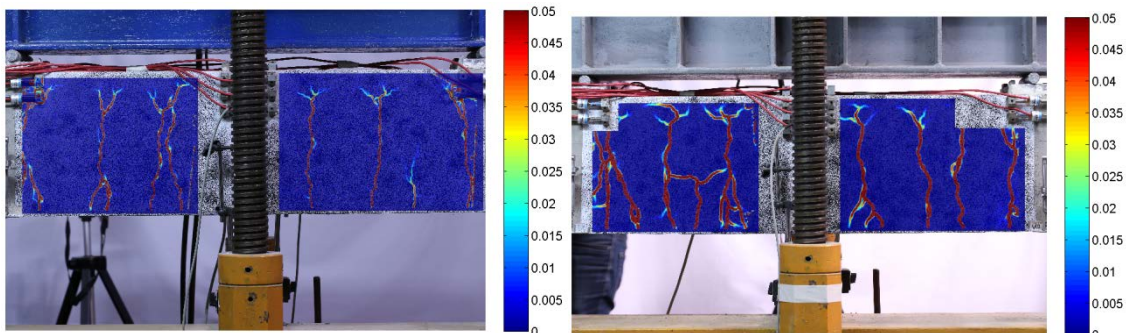


Figure 4.115 Crack patterns in beams OPC-1 and HVFAC-1 at 50 kN

4. Experimental program and test results

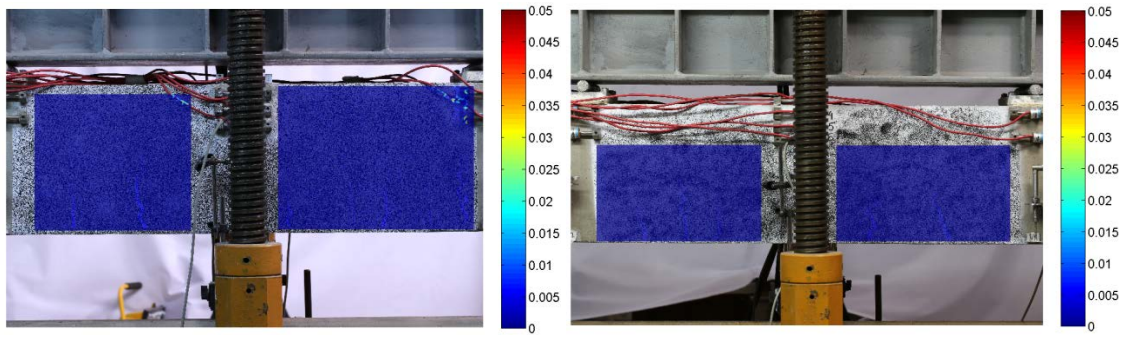


Figure 4.116 Crack patterns in beams OPC-2 and HVFAC-2 at $2P=20$ kN

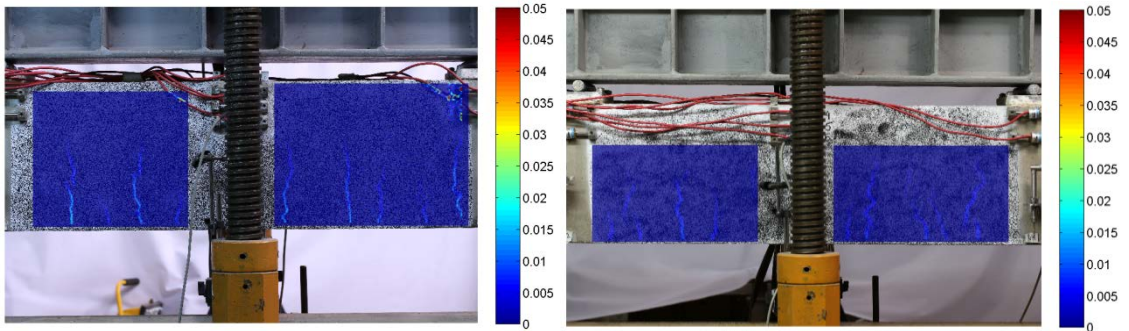


Figure 4.117 Crack patterns in beams OPC-2 and HVFAC-2 at $2P=40$ kN

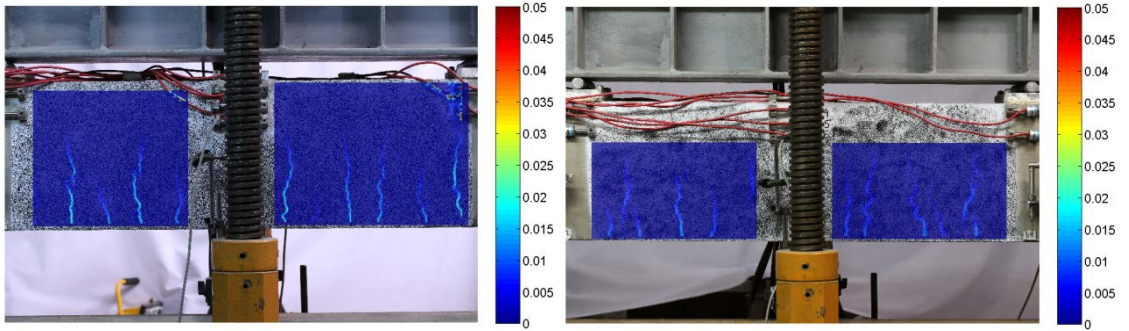


Figure 4.118 Crack patterns in beams OPC-2 and HVFAC-2 at $2P=60$ kN

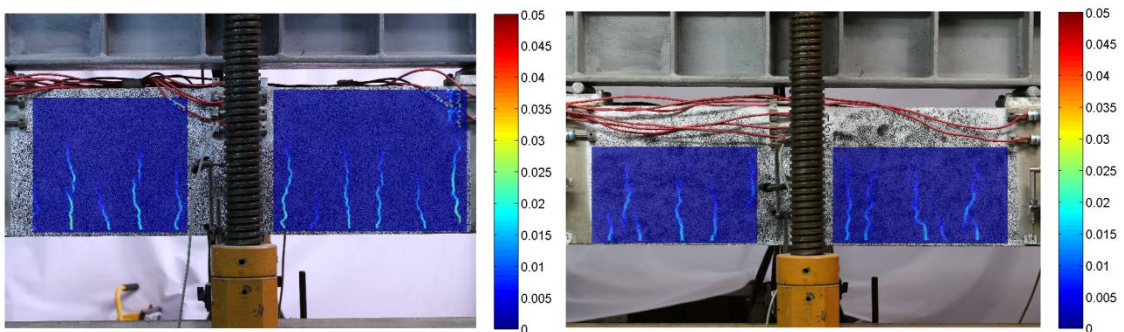


Figure 4.119 Crack patterns in beams OPC-2 and HVFAC-2 at $2P=80$ kN

4. Experimental program and test results

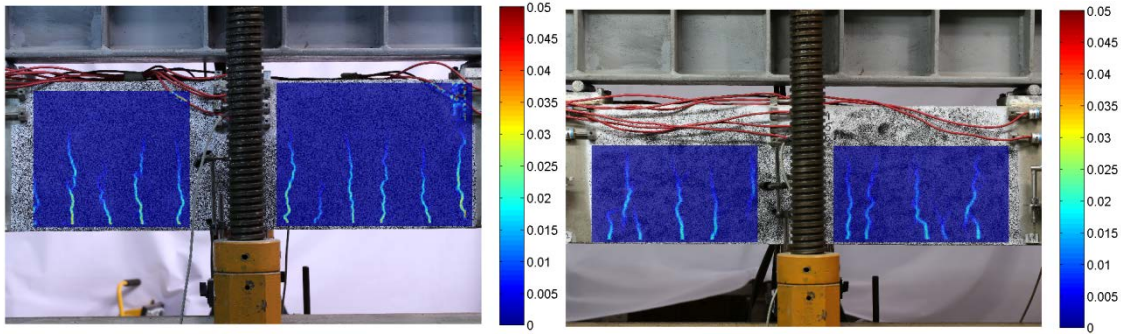


Figure 4.120 Crack patterns in beams OPC-2 and HVFAC-2 at $2P=100$ kN

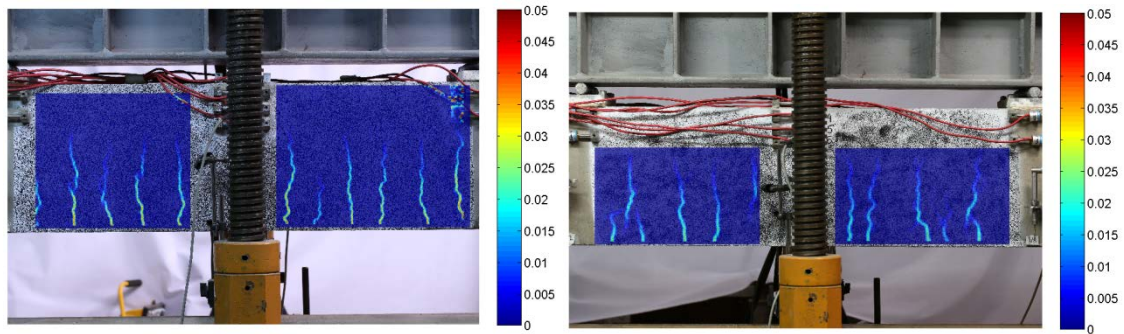


Figure 4.121 Crack patterns in beams OPC-2 and HVFAC-2 at $2P=120$ kN

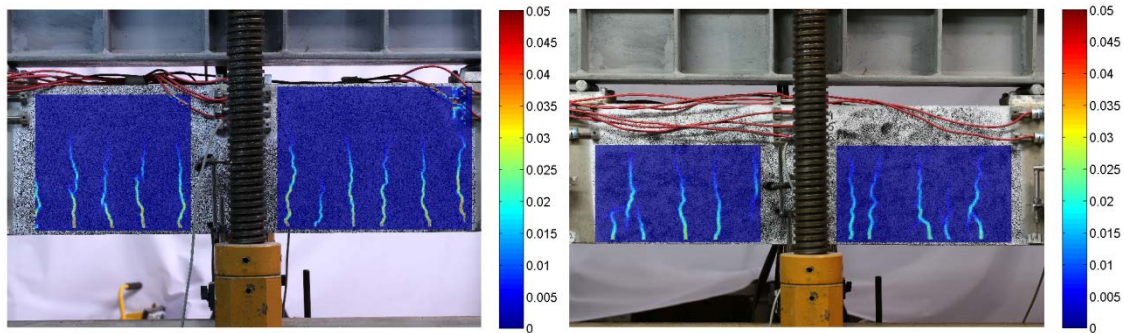


Figure 4.122 Crack patterns in beams OPC-2 and HVFAC-2 at $2P=140$ kN

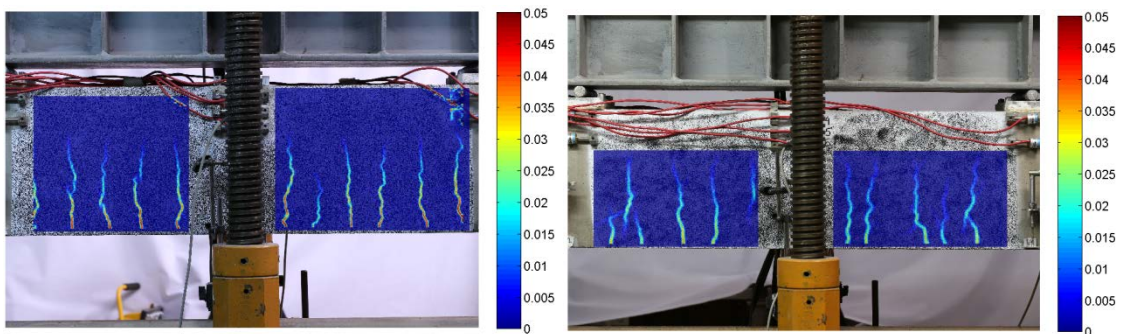


Figure 4.123 Crack patterns in beams OPC-2 and HVFAC-2 at $2P=160$ kN

4. Experimental program and test results

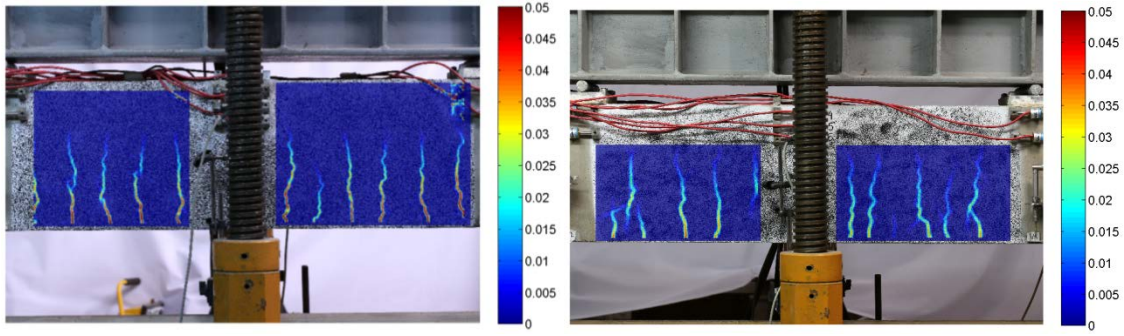


Figure 4.124 Crack patterns in beams OPC-2 and HVFAC-2 at $2P=180$ kN

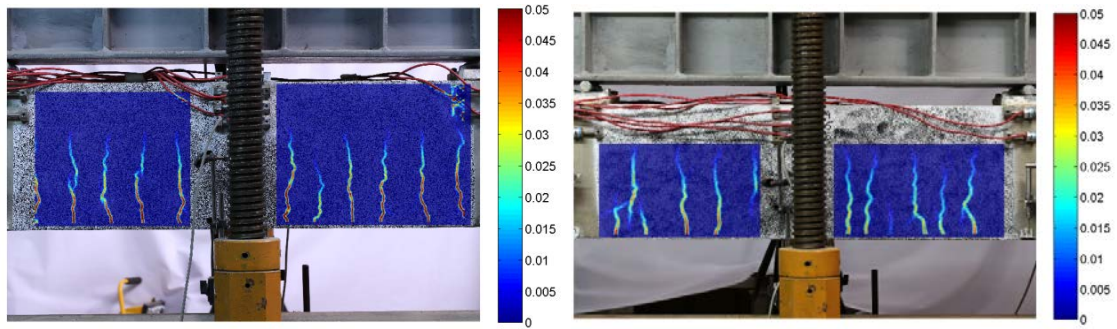


Figure 4.125 Crack patterns in beams OPC-2 and HVFAC-2 at $2P=200$ kN

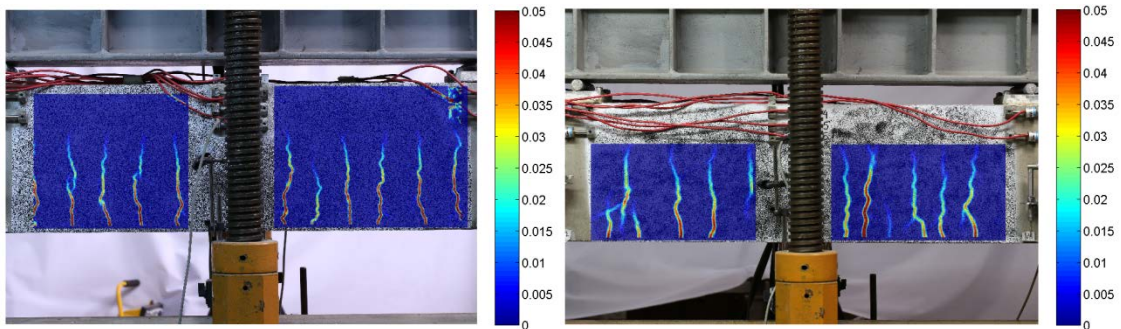


Figure 4.126 Crack patterns in beams OPC-2 and HVFAC-2 at $2P=210$ kN

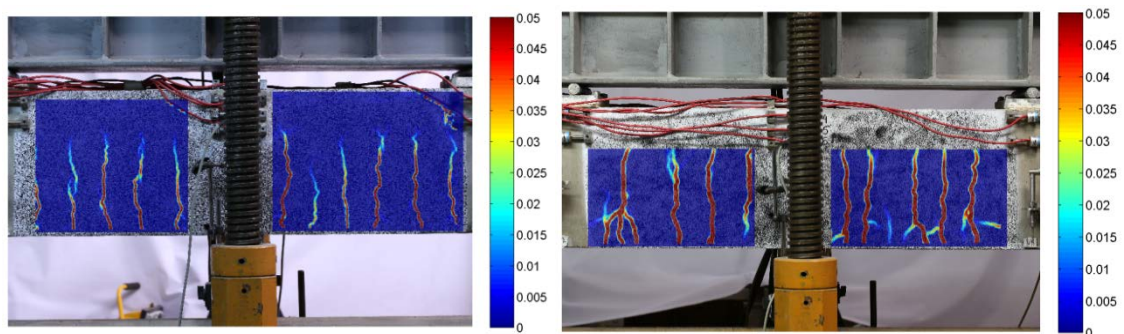


Figure 4.127 Crack patterns in beams OPC-2 and HVFAC-2 at $2P=215$ kN

A more detailed analysis of crack length and width development was performed for cracks forming in the middle part of the beams. The crack patterns and numbering for the evaluated region are shown in Figure 4.128. The change in crack

4. Experimental program and test results

lengths for OPC-1, HVFAC-1, OPC-2 and HVFAC-2 beams is shown in Figures 4.129 – 4.132. Monitoring of all cracks in the middle part of the beams was done but crack number 10 in the HVFAC-1 beam was not analyzed due to its appearance only in the final loading step.

It can be seen that most of the cracks developed in a similar way with a practically linear length increase until the final loading step in both OPC-1 and HVFAC-1 beams. The crack lengths in both OPC-2 and HVFAC-2 beams increased until the service load level and after that point remained practically constant. The increase of crack length was more pronounced in the HVFAC-2 beam in the loading range up to 30 kN.

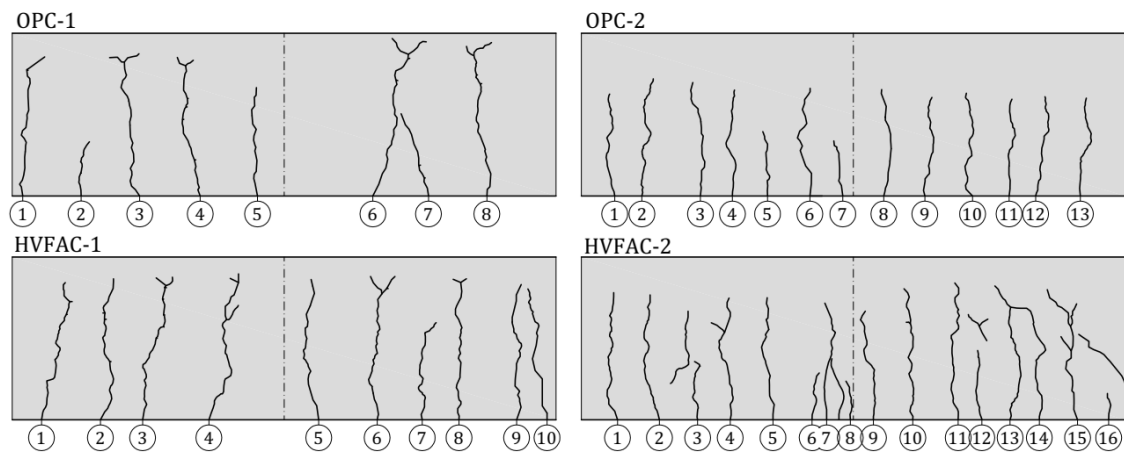


Figure 4.128 Crack patterns and numbering in the middle part of all tested beams

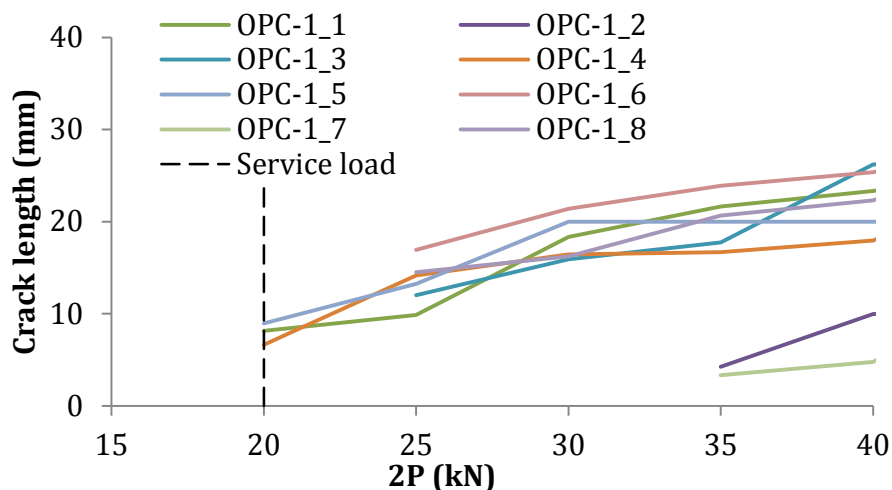


Figure 4.129 Crack length development against loading force for beam OPC-1

4. Experimental program and test results

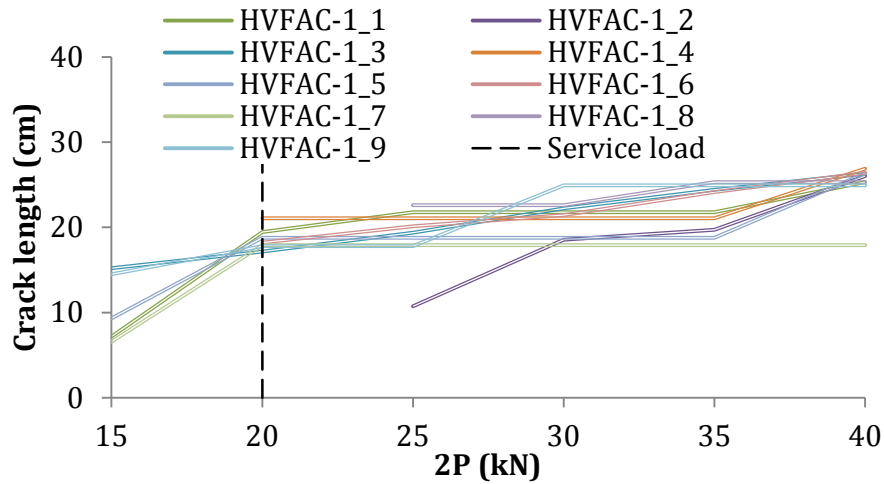


Figure 4.130 Crack length development against loading force for beam HVFAC-1

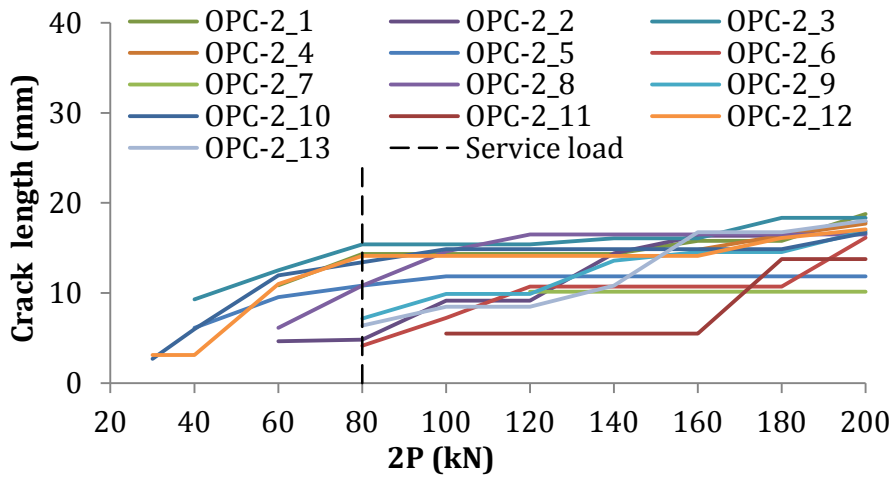


Figure 4.131 Crack length development against loading force for beam OPC-2

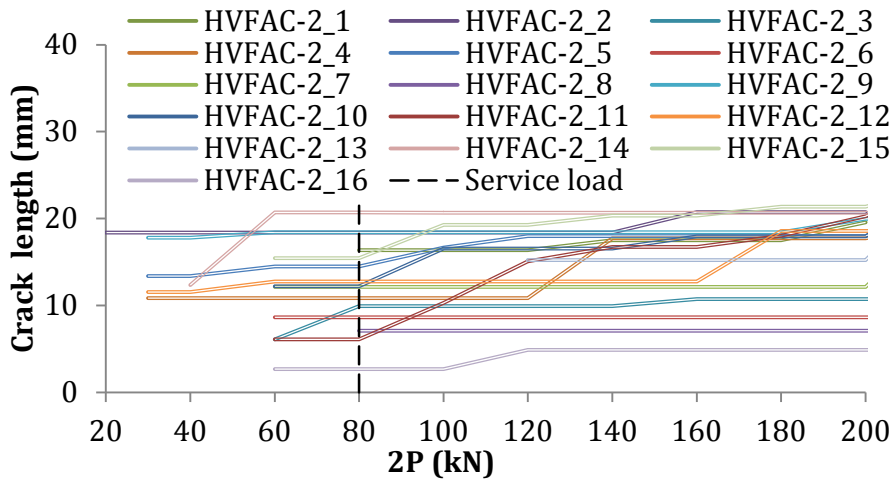


Figure 4.132 Crack length development against loading force for beam HVFAC-2

4. Experimental program and test results

In order to compare the crack lengths, diagrams for corresponding OPCC and HVFAC beams are plotted and shown in Figures 4.133 and 4.134. It can be seen that the crack lengths were higher in HVFAC beams compared with the OPCC beams, as previously concluded.

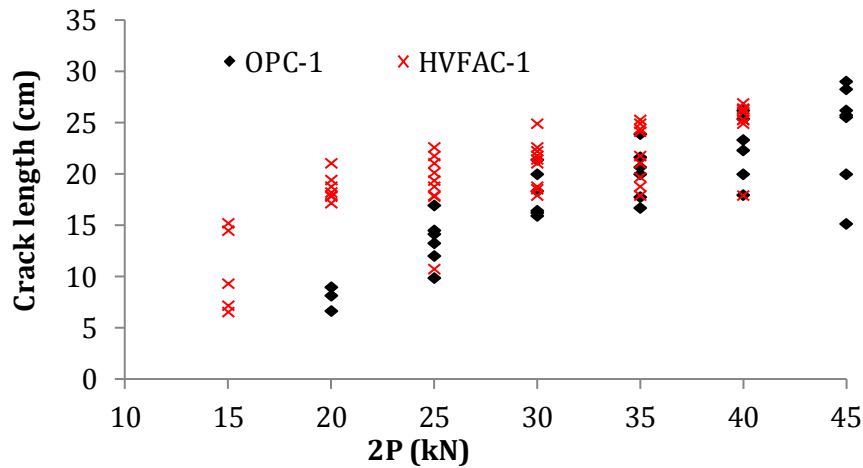


Figure 4.133 Crack length development for the OPC-1 and HVFAC-1 beams

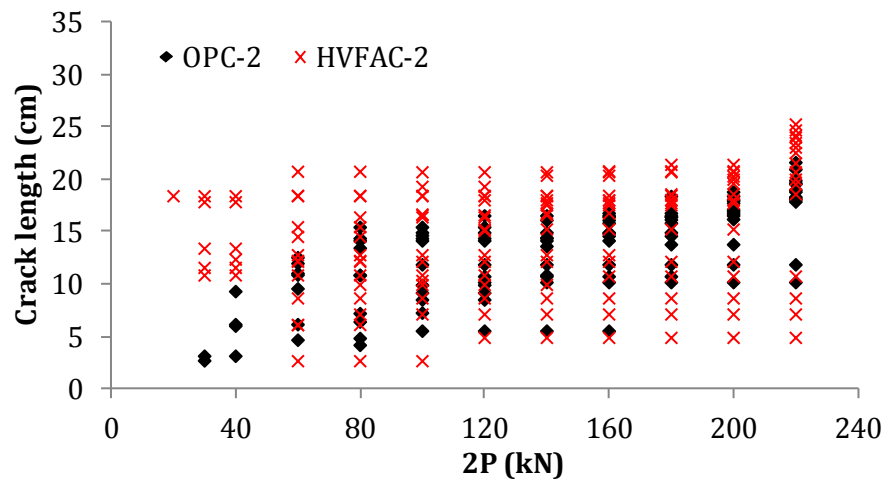


Figure 4.134 Crack length development for the OPC-2 and HVFAC-2 beams

In order to analyse the flexural crack width, development of crack width versus the applied load was plotted for all beams based on the results obtained using both visual inspection of cracks and DIC system in Figures 4.135 – 4.142. The crack width increased in a similar way in the OPC-1 and HVFAC-1 beams until approximately 60% of the ultimate loading. In the HVFAC-1 beam crack widths increased in a more pronounced way at 30 kN, and in the OPC-1 beam at 35 kN.

4. Experimental program and test results

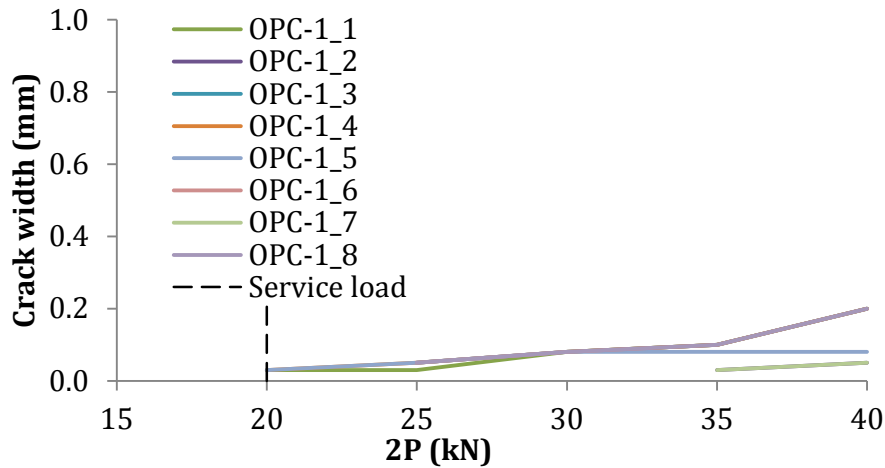


Figure 4.135 Crack width development versus loading force for beam OPC-1 – visual inspection

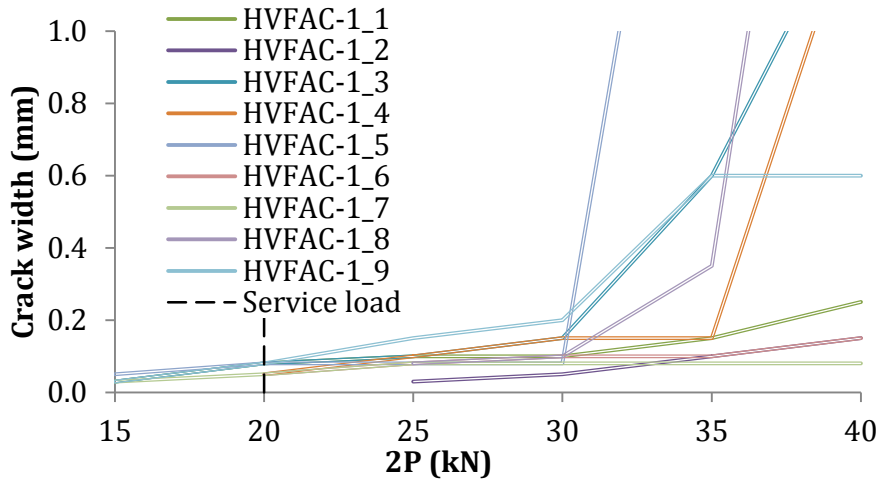


Figure 4.136 Crack width development against loading force for beam HVFAC-1 – visual inspection

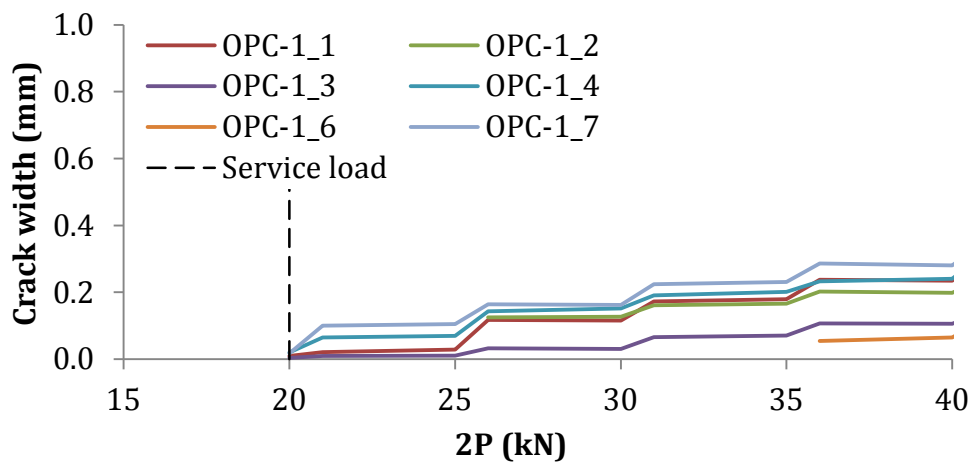


Figure 4.137 Crack width development versus loading force for beam OPC-1 – DIC

4. Experimental program and test results

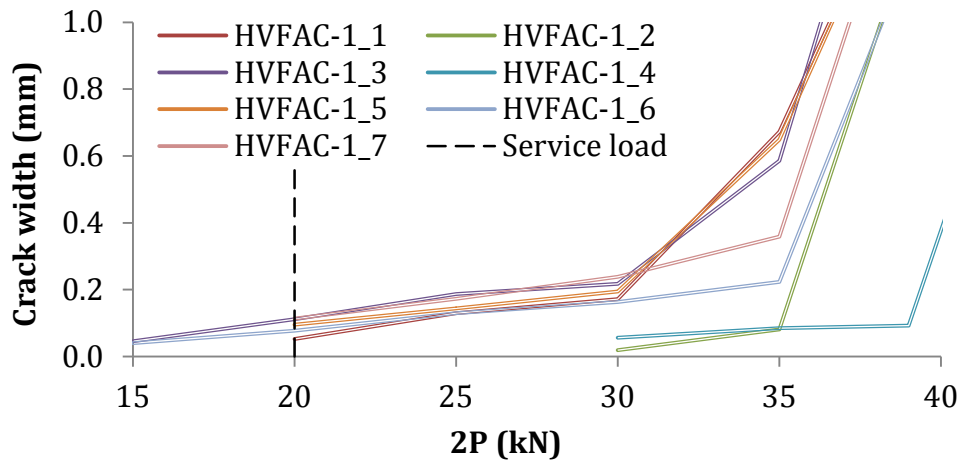


Figure 4.138 Crack width development versus loading force for beam HVFAC-1 – DIC

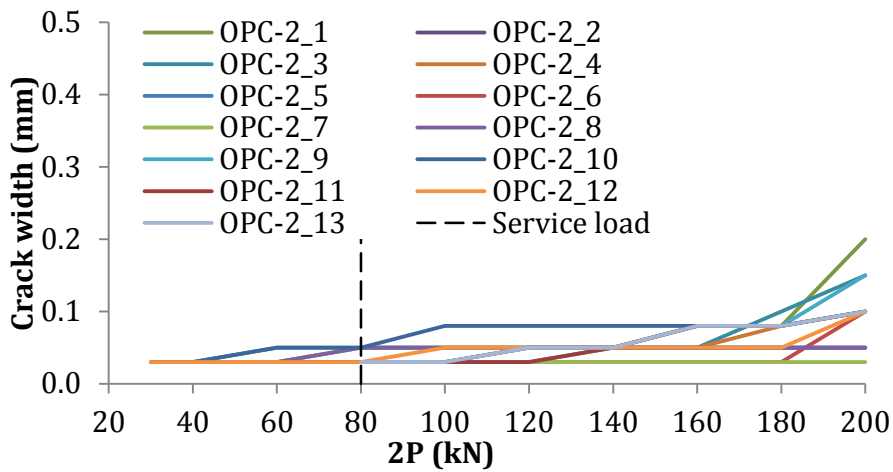


Figure 4.139 Crack width development against loading force for beam OPC-2 – visual inspection

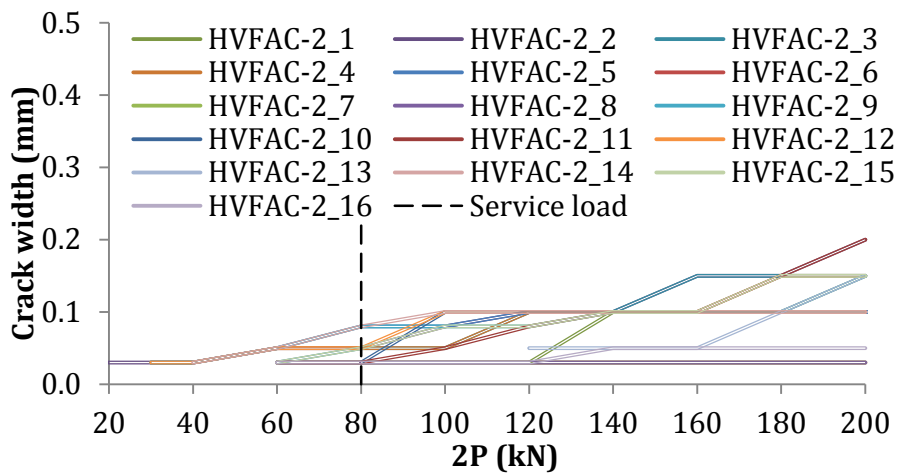


Figure 4.140 Crack width development against loading force for beam HVFAC-2 – visual inspection

4. Experimental program and test results

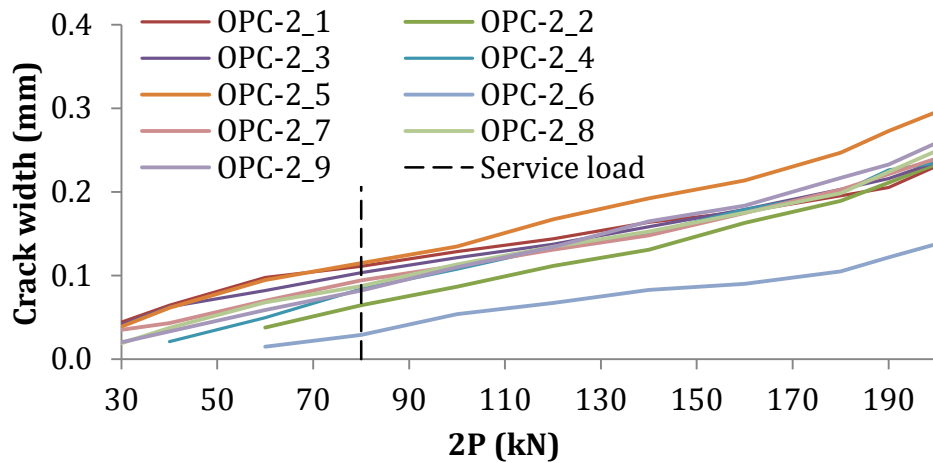


Figure 4.141 Crack width development versus loading force for beam OPC-2 – DIC

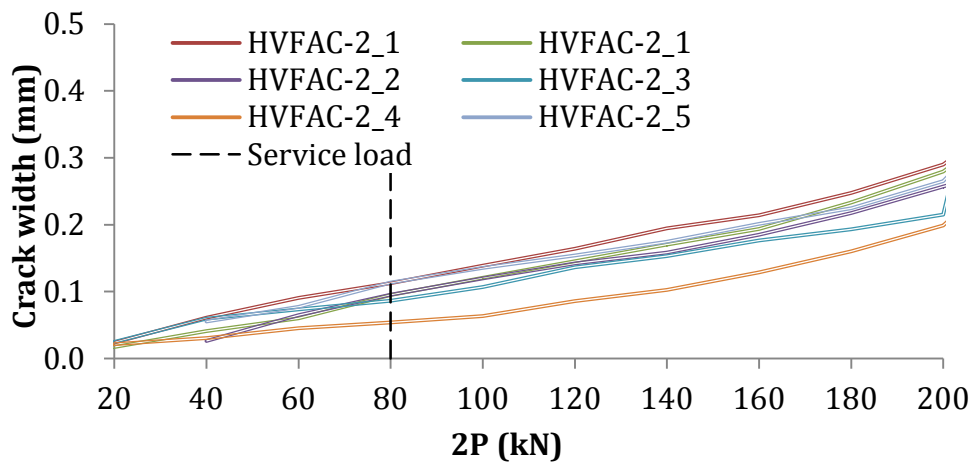


Figure 4.142 Crack width development versus loading force for beam HVFAC-2 – DIC

The increase of crack widths was similar in both OPC-2 and HVFAC-2 beams until a few steps before the ultimate loading. In order to compare the crack widths, diagrams for corresponding OPCC and HVFAC beams are plotted and shown in Figures 4.143 and 4.144.

It can be seen that the crack widths were higher in HVFAC beams compared with OPCC beams, as previously concluded. The difference between the OPCC and HVFAC beams was greater for the beams with a minimum longitudinal reinforcement ratio. For the OPC-2 and HVFAC-2 beams, the differences decreased as the beams approached failure.

4. Experimental program and test results

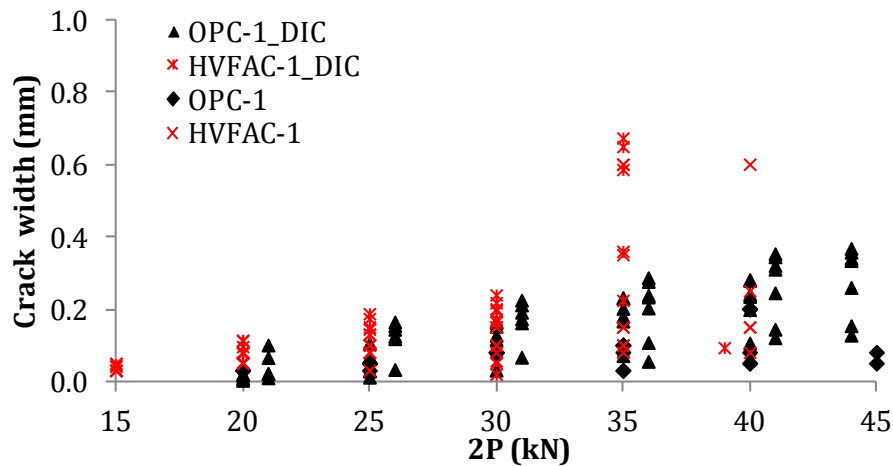


Figure 4.143 Maximum crack width development for the OPC-1 and HVFAC-1 beams

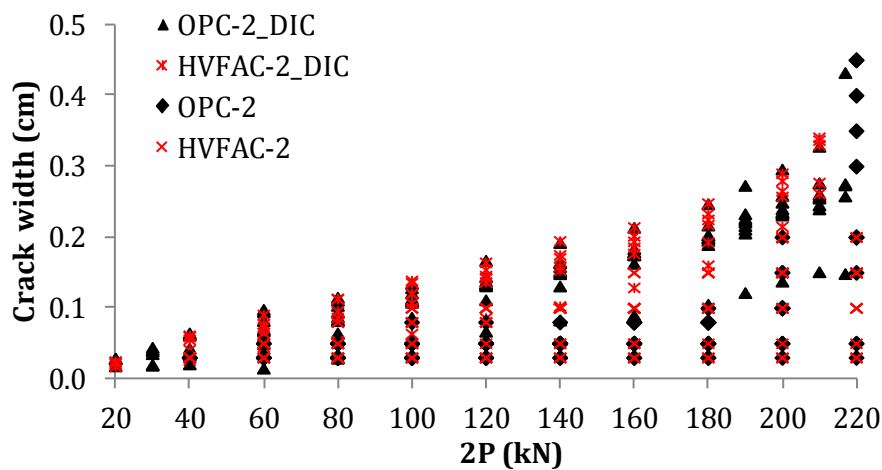


Figure 4.144 Crack width development for OPC-2 and HVFAC-2 beams

The previously presented figures showed similar trend of crack width increase for both measuring methods that were used in this analysis. However, the higher crack widths were obtained using the DIC methods, for 40-100% on average, compared with the visual crack inspection. Higher differences were noticed for cracks with lower crack width. Absolute values of crack widths at the service load level obtained using DIC were: 0.02 mm, 0.11 mm, 0.11 mm and 0.11 mm for beams OPC-1, HVFAC-1, OPC-2 and HVFAC-2, respectively. Maximum crack widths development for all beams obtained using both measuring methods are plotted in Figures 4.145 and 4.146. It can be seen that the maximum crack widths were higher in HVFAC-1 beam compared with the OPC-1 beam using both methods of measurement. However, development of maximum crack widths in beams with a

4. Experimental program and test results

higher longitudinal reinforcement ratio showed no significant difference or even the same trend by using DIC measurements. Having in mind more flexural cracks, higher crack lengths and widths, and more crack branching, it is safe to conclude that cracks developed in a more pronounced way in the HVFAC beams compared with the corresponding OPCC beams. In this way, the stiffness of HVFAC beams could be lower compared with the referent OPCC beams after cracking. This phenomenon was more pronounced in the beams with a minimum longitudinal reinforcement ratio compared with the beams with a higher than minimum reinforcement ratio.

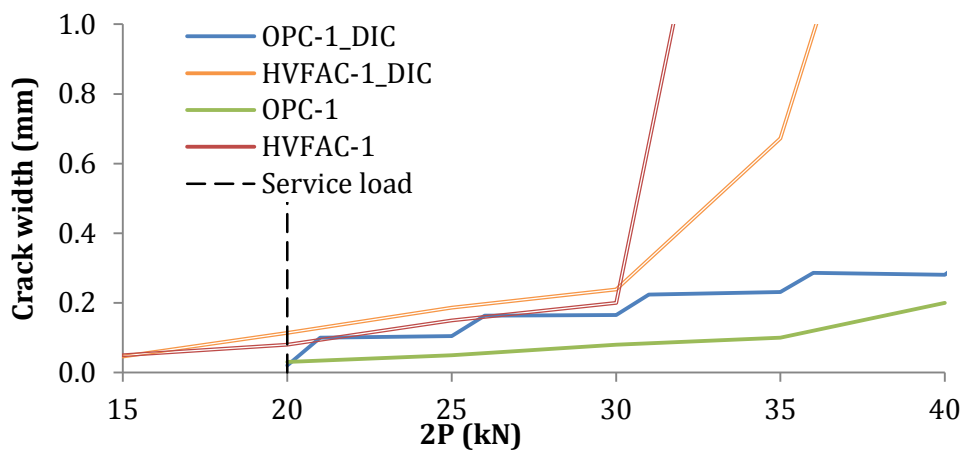


Figure 4.145 Maximum crack width development for OPC-1 and HVFAC-1 beams

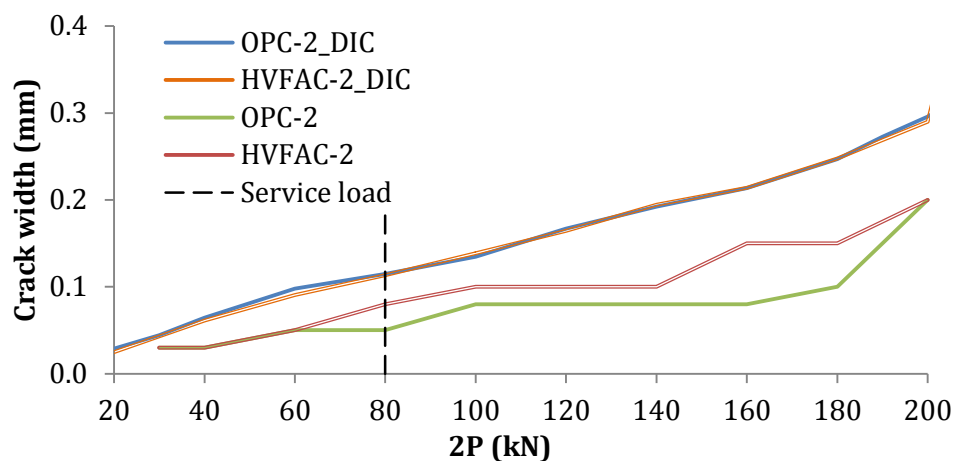


Figure 4.146 Maximum crack width development for OPC-2 and HVFAC-2 beams

4. Experimental program and test results

4.3.12. Conclusions

In the first part of the beams' flexural behavior testing, fresh and hardened concrete properties of selected HVFAC and OPCC were tested.

- The test results showed that HVFAC mixture C200F350 had up to 7% lower fresh and hardened concrete density compared with the OPC_F mixture. Workability of the mixtures was different with tested OPC_F mixture that corresponded to the slump class S3 according to the EN 206. HVFAC mixture C200F350 was more flowable, due to the use of the superplasticizer, and corresponded to the flow class F5 according to the EN 206.
- The 90-day compressive strength of HVFAC and OPCC samples cured in water was different by not more than 3% but the difference was higher for the specimens cured the same as beams—up to 19%.
- HVFAC and OPCC samples cured the same like beams had, on average, 7% lower and 14% higher compressive strengths compared with the samples cured in water, respectively.
- The splitting tensile strength showed similar results for both types of concrete under both types of curing. On the other hand, the flexural tensile strength of OPC_F was 24% higher compared with C200_F350.
- It can be concluded that the different curing regime had a higher influence on the tensile strength compared with the compressive strength.
- The modulus of elasticity was higher in the OPC_F concrete mixture compared with C200_F350 after both 28 and 90 days, especially for the samples cured the same as the beams where the difference was 16%.

The crack propagation in the beams began with the appearance of flexural cracks in the maximum moment region. The first flexural cracks appeared at lower loading levels for HVFAC beams compared with the OPCC ones: 25% lower for beams with a minimum reinforcement ratio and 16% lower for beams with a higher reinforcement ratio. Before the first flexural crack formation, all of the beams showed similar linear-elastic behavior. After the additional load was applied, the longitudinal steel yielded. With further load increase, compressed concrete crushed and the beams failed. In the beams with the minimum

4. Experimental program and test results

longitudinal reinforcement ratio, failure occurred after the crushing of concrete and braking of the longitudinal reinforcement. The difference between the OPCC and HVFAC ultimate loading falls within a 10% margin and can be considered as negligible.

The analysis of the ductility of beams showed that the HVFAC-1 beam had around 40% lower ductility compared with the OPC-1 beam and the HVFAC-2 beam 20% higher ductility compared with the OPC-2 beam.

The maximum deflections of HVFAC beams at the service load level were higher compared with the OPCC beams.

- In beams with the minimum longitudinal reinforcement ratio, deflection at the service load level (40%) was around 50% higher for the HVFAC-1 beam compared with the OPC-1 beam. The deflection lines at approximately 20% of the ultimate loading showed a similar trend with approximately 30% higher deflection of the HVFAC-1 beam compared with the OPC-1, while no flexural cracks appeared in either of the beams up to that point. The maximum deflection of the HVFAC-2 beam was up to 12% higher compared with the OPC-2 beam at all presented loading stages.
- The analysis of load-deflection curves showed that the stiffness of the tested HVFAC beam with the minimum reinforcement ratio was lower than the stiffness of the OPCC beam, differing by not more than 11%. This difference was relatively small in beams with a higher than minimum reinforcement ratio.

The comparative analysis of the longitudinal reinforcement strains in the HVFAC and OPCC beams showed no significant difference between the load-strain curves of different concrete beams prior to flexural cracking. The reinforcement strains in HVFAC beams were generally higher compared with the strains in the OPCC beams after cracking.

- In comparison with the OPCC beams, the reinforcement strains were higher in HVFAC beams for 35% in the first group and 70% in the second group. Having in mind the significant influence of crack vicinity to the measuring place on the reinforcement strains values, no specific conclusions can be made.

4. Experimental program and test results

- The concrete compressive strains at failure were higher in HVFAC beams compared with the OPCC, but the difference was only up to 7% for all measured sections.
- The distribution of strains along the beams' height was linear for all of the beams. For the beams with the minimum reinforcement ratio, the height of the compression zone was 2% and 13% higher for the OPC-1 and OPC-2 beams compared with the corresponding HVFAC beams, respectively.

The analysis of the flexural crack maximum length, number, width and the sum of all crack widths along the beam was done.

- The first flexural cracks appeared at a 25% and 33% lower loading levels for HVFAC-1 and HVFAC-2 beams compared with the corresponding OPCC beams. At the service load level, the flexural cracks in the HVFAC-1 beam had a 57% higher maximum vertical length and 60% higher number of cracks developed in that state compared with the OPC-1 beam. This difference decreased in the ultimate loading state: the maximum vertical length was 7% higher and the number of developed cracks was 10% higher in the HVFAC-1 beam compared with the OPC-1. The average spacing between cracks was smaller in the HVFAC-1 beam compared with the OPC-1 by 15% and 5% at the service and ultimate load, respectively.
- The first flexural cracks developed at 30 kN and 20 kN for OPC-2 and HVFAC-2 beams, respectively. In the HVFAC-2 beam, most of the cracks were vertically oriented but some cracks formed in other directions along with the first flexural cracks. At the service load level, flexural cracks in the HVFAC-2 beam had 33% higher maximum vertical length and 55% higher number of cracks developed in that state compared with beam OPC-2. This difference decreased in the ultimate loading state: the maximum vertical length was 17% higher and the number of developed cracks was 38% higher in beam HVFAC-2 compared with beam OPC-2. The average spacing between cracks was smaller in the HVFAC-2 beam compared with beam OPC-2 by 24% and 17% at the service and ultimate load, respectively.

4. Experimental program and test results

- The sum of crack widths in beam OPC-1 was lower compared with the HVFAC-1 beam for 60%, 64% and 69% at 40%, 60% and 80% of the ultimate loading level, respectively. Beam OPC-2 had 49%, 56% and 45% at 40%, 60% and 80% of the ultimate loading level, respectively. It can be concluded that beams HVFAC-1 and HVFAC-2 had, on average, 2.8 and 2.0 times higher sum of crack widths compared with the corresponding OPCC beams, respectively.
- The analysis showed a similar trend of crack width increase for both visual inspection and the DIC system. However, higher crack widths were obtained using the DIC methods, for 40-100% on average, compared with the visual crack inspection. Absolute values of crack widths at the service load level obtained using DIC were: 0.02 mm, 0.11 mm, 0.11 mm and 0.11 mm for beams OPC-1, HVFAC-1, OPC-2 and HVFAC-2, respectively.
- It can be concluded that the maximum crack widths were higher in HVFAC-1 beam compared with the OPC-1 beam using both methods of measurement. However, development of maximum crack widths in beams with a higher longitudinal reinforcement ratio showed no significant difference rather even the same trend by using DIC measurements.
- Having in mind more flexural cracks, higher crack lengths and widths, and more crack branching, it is safe to conclude that cracks developed in a more pronounced way in the HVFAC beams compared with the corresponding OPCC beams. In this way, the stiffness of HVFAC beams could be lower compared with the referent OPCC beams after cracking. This phenomenon was more pronounced in beams with the minimum longitudinal reinforcement ratio compared with the beams with a higher than minimum reinforcement ratio.

4. Experimental program and test results

4.4. TESTING OF REINFORCED CONCRETE BEAMS' SHEAR BEHAVIOR

4.4.1. Introduction

Extensive research of reinforced concrete structures flexural behavior followed with fundamental theoretical background led to a full understanding of flexural failure mechanisms. Unlike flexural behavior, RC structures shear behavior is still being extensively analyzed in order to fully quantitatively explain it. Having in mind a great variety of parameters influencing shear transfer and many models proposed in literature, the effect of a new binder type, like in HVFAC, has to be experimentally assessed. There are limited results from literature analyzing HVFAC structural behavior (Rao, Mohan and Sekar, 2011; Ortega, 2012; Arezoumandi and Volz, 2013; Arezoumandi *et al.*, 2013, 2014; Sadati *et al.*, 2016; Lisantono, Wigroho and Purba, 2017) and therefore, this part of own experimental research was done in order to gain more information regarding shear transfer mechanisms in HVFAC beams.

Experimental program was designed to provide comparative results of HVFAC and OPCC beams shear behavior. Three HVFAC and three OPCC beams with equally designed 90-day compressive strength were made and tested. The geometry and properties of beams along with experimental set-up were designed to be the same, differing only in concrete type. In order to analyze the contribution of concrete strength to shear behavior of RC, beams without stirrups were made with HVFAC and OPCC. The behavior of beams made with stirrups and the effect of different shear reinforcement ratios was tested on two HVFAC and two OPCC beams. All other factors influencing shear behavior were the same in beams being tested: beam cross section dimensions, shear span-to-depth ratio, longitudinal reinforcement ratio and aggregate type.

4. Experimental program and test results

4.4.2. Material properties

4.4.2.1. Concrete

The RC beams for shear testing were made with HVFAC with 200 kg/m³ of cement and 200 kg/m³ of FA (concrete mixture C200_F200). The RCC was designed to have the same 90-day compressive strength and workability (OPC_S) like HVFAC mixture C200_F200. The component materials (aggregate, cement and FA) for both HVFAC and OPCC were the same as those in the material testing phase of this research (Section 4.2). The concrete mixtures designed for the shear testing were different than the mixtures used in the phase of flexural behavior testing. The only reason for this was the lower compressive strength achieved with C200_F200 compared with already used C200_F350. In this way, the larger range of ultimate forces can be applied in line with the available experimental set up and force actuator capacity. The concrete mixtures design used for this set of beams is shown in Table 4.21.

Table 4.21 Shear test beams concrete mix design

Component materials	Type	C200_F200	OPC_S
Aggregate (kg/m ³)	River	0 / 4	804.5
	River	4 / 8	482.7
	River	8 / 16	321.8
Cement (kg/m ³)	CEM II 42.5 R	200.0	284.6
FA (kg/m ³)	Class F	200.0	0
Water (kg/m ³)	Tap water	195.0	175.0
Admixtures (kg/m ³)	-	0	0
W/CM	Water-to-CM ratio	0.488	0.615
FA/CM	FA-to-CM ratio (%)	50	0

The mixing procedure was the same as the one in the first phase of beam testing. The concrete was made in the Laboratory for Materials at the University of Belgrade's Faculty of Civil Engineering and then transported in the Laboratory for Structures at the same Faculty. Beams were casted in two days, three HVFAC

4. Experimental program and test results

beams in one day and three OPCC beams on the second day. The average temperature in the laboratory during the HVFAC preparation was $24.1\pm 2^{\circ}\text{C}$, the humidity was $48.8\pm 2\%$ with the average concrete temperature of 22.9°C after mixing. Average temperature during OPCC preparation was $18.5\pm 2^{\circ}\text{C}$, humidity was $53\pm 2\%$ with the average concrete temperature of 21.0°C after mixing. Figure 4.147 shows the C200_F200 and OPC_S concrete mixtures prepared for casting.



Figure 4.147 a) HVFAC mixture C200_F200 b) OPCC mixture OPC_S

There was no significant difference in the workability of these two mixtures. After mixing, the concrete was placed in beam formwork and in molds for sample casting. Different samples were made for different property testing for both HVFAC and OPCC. Sample types, number and dimensions, testing property and curing conditions are the same as those shown in Table 4.12.

Standard curing implies curing in the laboratory conditions under the wet burlap for 24 hours after casting and then in a water tank until testing. The samples cured in the laboratory conditions in the same way as the beams for 14 days were used to measure the properties of concrete placed in the beams. In order to confirm the compressive strength of concrete casted in beams cylindrical cores were taken out of each beam after testing. The dimension of the core samples was approximately $\text{Ø}99\cdot 100$ mm.

4.4.2.2. Steel reinforcement

The same type of steel reinforcement was used as in the first phase of beam testing. The longitudinal reinforcement for beams consisted of B500B ribbed $\text{Ø}22$

4. Experimental program and test results

(reinforcement in tension) and $\varnothing 8$ (reinforcement in compression) reinforcing bars. The shear reinforcement consisted of hot rolled SAE1008 $\varnothing 6$ and $\varnothing 8$ reinforcing bars. The characteristics of reinforcing bars provided by the supplier are presented in Table 4.22.

Table 4.22 Reinforcing bar characteristics

Size	Type	Tensile strength	Elongation	Yield strength
		R_m (MPa)	A_{10} (%)	R_e (MPa)
$\varnothing 8$	B500B	669	9.9*	559
$\varnothing 22$	B500B	681	12.6*	577
$\varnothing 6$	SAE1008	410	31.0	NA**
$\varnothing 8$	SAE1008	386	32.0	NA

* Elongation at maximum force

** Not available

4.4.3. Preparation of beam elements

For the purpose of this research three HVFAC beams (C200_F200) and three OPCC beams (OPC_S) were made. The total length of each beam was 3.5 m. All beams were simply supported with the span length of 3.0 m. The beam cross section was rectangular with the height of 300 mm and the width of 200 mm. The shear span-to-effective depth ratio was 4.2.

The design of beams was chosen in order to analyze the behavior of RC beams with different shear reinforcement ratios. All beams had the same longitudinal reinforcement, made of 5 $\varnothing 22$ reinforcing bars for tension and 2 $\varnothing 8$ for compression. The longitudinal reinforcement ratio was the same in all beams ensuring at least 1.2 times higher flexural resistance compared with the shear bearing capacity. The beams were designed according to the EN1992-1 (CEN, 2004). For specimens with shear reinforcement, stirrups were designed to ensure shear failure prior to flexural failure. Two beams (HVFAC-1 and OPC-1) were made with 0% of shear reinforcement, two beams (HVFAC-2 and OPC-2) with a minimum shear reinforcement according to EN 1992-1-1 (CEN, 2004) of 0.14%, and two beams with reinforcement ratio higher than minimum chosen as 0.28%.

4. Experimental program and test results

Beam notation, concrete type, longitudinal and shear reinforcement are presented in detail in Table 4.23.

Table 4.23 Notation of beams tested in shear failure

Notation	Concrete	Longitudinal tensile reinforcement	Shear reinforcement
<i>HVFAC-1</i>		5 Ø 22 mm	No stirrups
<i>HVFAC-2</i>	C200_F200	5 Ø 22 mm	Ø6/200 mm
<i>HVFAC-3</i>		5 Ø 22 mm	Ø6/100 mm
<i>OPC-1</i>		5 Ø 22 mm	No stirrups
<i>OPC-2</i>	OPC_S	5 Ø 22 mm	Ø6/200 mm
<i>OPC-3</i>		5 Ø 22 mm	Ø6/100 mm

In order to optimize the measuring equipment, only one test region was chosen for the analysis. In this way the reinforcement layout was not symmetrical due to a significantly higher transverse reinforcing ratio in the middle part of the beam and in the other shear span to prevent failure in these regions. Hence, it was possible to predict the failure location and localize the measuring equipment accordingly. The reinforcement layout of the beams is shown in Figure 4.148 and reinforcement of beams in Figure 4.149a.

The total beam length was 250 mm longer than its span on both ends in order to provide sufficient anchorage of the longitudinal reinforcement at both ends. Higher shear reinforcement was used (Ø8/50 mm) to ensure a higher degree of confinement by the shear reinforcement at these parts. In this way, failure by reinforcement slip was prevented. All beams were made in the Laboratory for Materials at the University of Belgrade's Faculty of Civil Engineering. The mixing procedure, casting, vibrating and the curing procedure were the same as described in Section 4.3. The wooden formwork and placed reinforcement for this series of beams are shown in Figure 4.149b.

4. Experimental program and test results

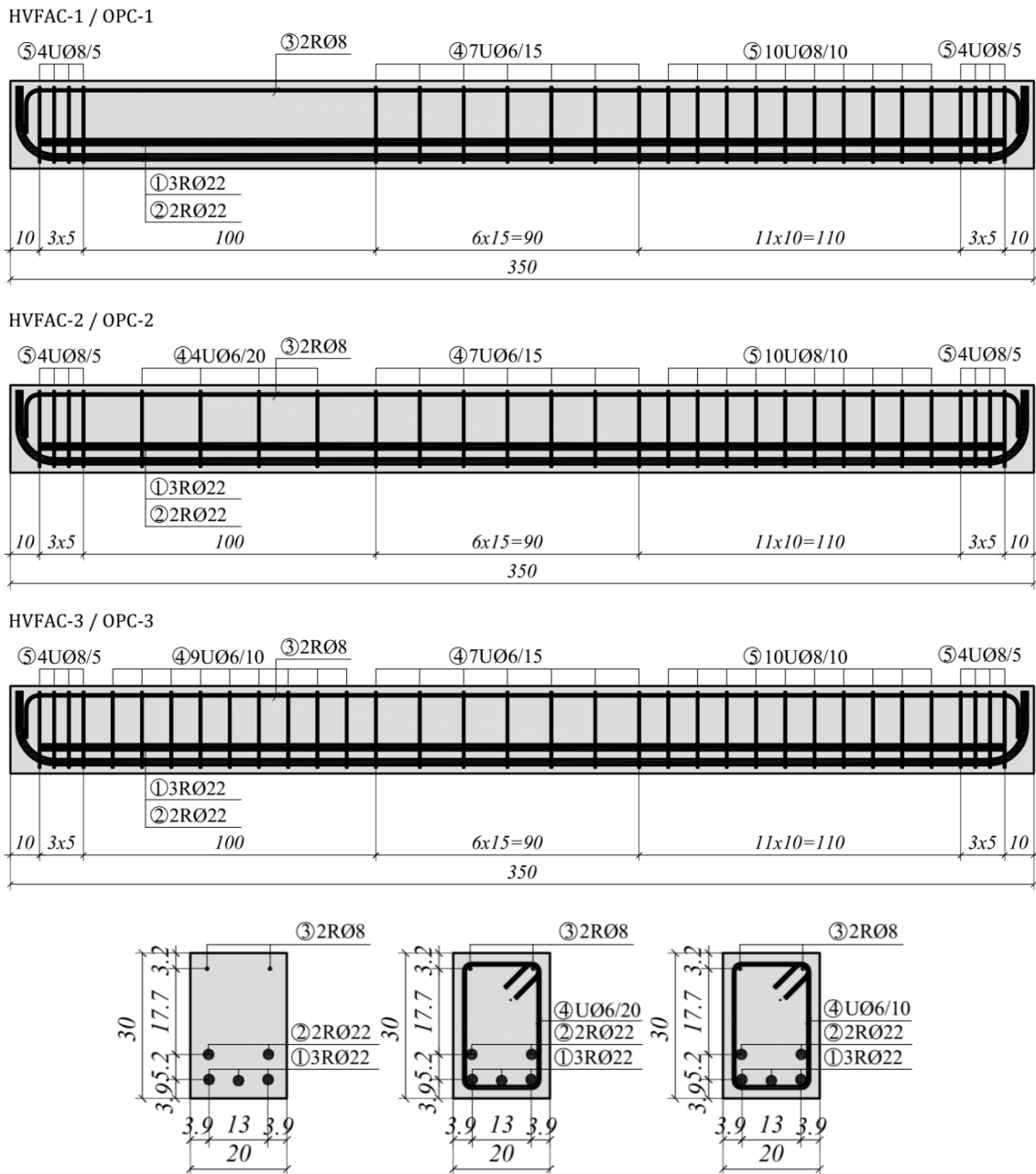


Figure 4.148 Reinforcement layout of beams tested in shear failure



Figure 4.149 a) Reinforcement of beams tested in shear and b) beams' formwork

4. Experimental program and test results

4.4.4. Test set-up

All beams were simply supported and the analysis of the behavior under transverse loading was done in a four point bending test, as in the case of the flexural beam testing. In this way stresses in the testing region are a consequence of combined shear and bending action which is a common situation in RC structures (Figure 4.150).

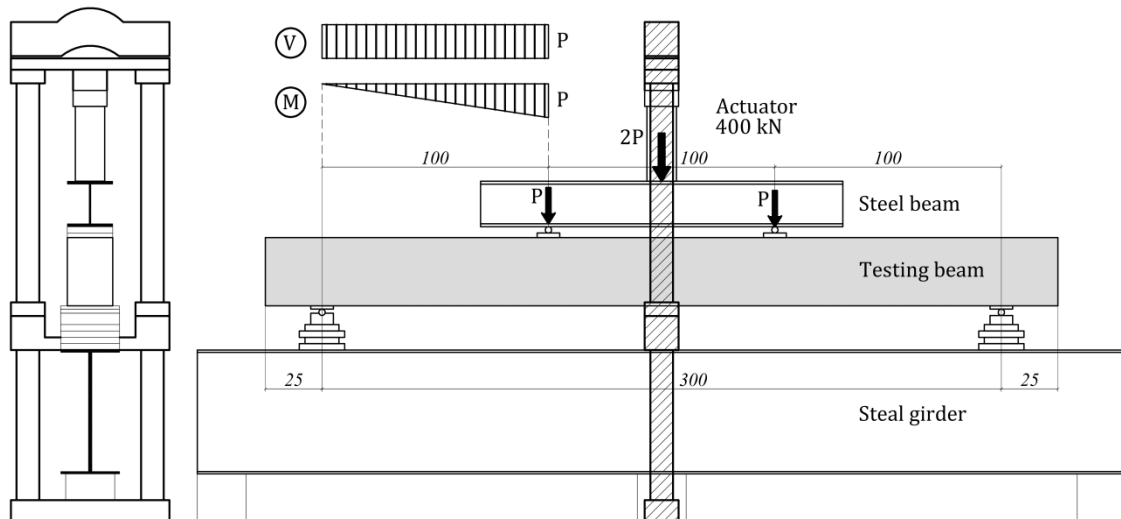


Figure 4.150 Four point bending test set up

The maximum capacity of hydraulic press available in the Laboratory for Structures at the University of Belgrade's Faculty of Civil Engineering was 400 kN and the beams were designed accordingly. The actuators applied load by pushing the steel beam downward to distribute the load onto two points in thirds of the beam span. The load was applied under force control in increments of 5 kN, 10 kN and 20 kN until failure with the hydraulic press.

All beams were tested until failure with following parameters measured during testing:

- Deformation of beams;
- Concrete strains;
- Longitudinal and shear reinforcement strains;
- Crack formation and development.

4. Experimental program and test results

4.4.5. Instrumentation

The beams were equipped with different instruments for testing global and local deformation along with the concrete and steel strains. The load was measured with data acquisition system MGCplus (Hottinger Baldwin Messtechnik GmbH) shown in Figure 4.16.

4.4.5.1. Deflection measurements

The vertical deflection of tested beams was measured using LVDTs. Two LVDT devices (D1 and D7) were positioned above two supports to measure the deflection of supports during the testing (Figure 4.151b,e).

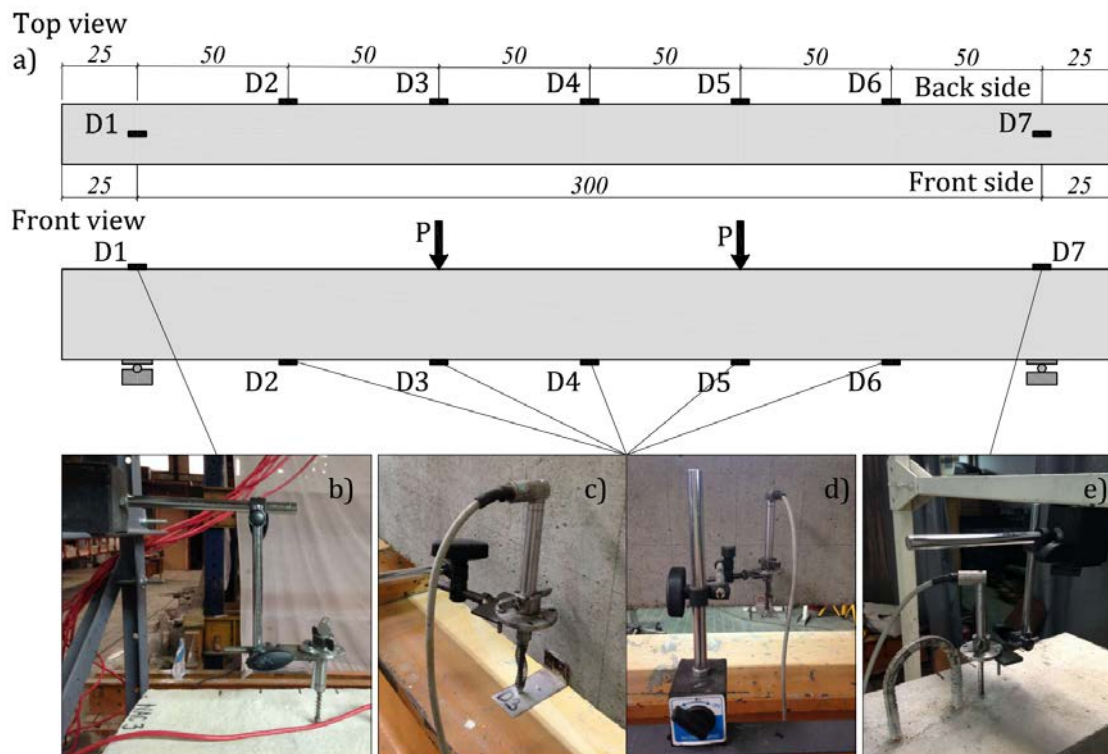


Figure 4.151 a) LVDT set up b) LVDT at the left support c) LVDT placement on the beam side d) LVDT at the right support

The vertical deflection of beams was measured with five LVDTs (D2-D6) positioned on the bottom edge of the back side of the beam (Figure 4.151a). They were placed in order to measure the deflection of beam midpoint (D4), point under the force application (D3 and D5) and in the middle of the shear span (D2 and D6). Magnetic bases were used for connecting the LVDTs to the beam and holding them in the right position (Figure 4.151c,d). The vertical deflection was measured

4. Experimental program and test results

continuously until failure and data was collected using the MGCplus acquisition system. One mechanical displacement measuring system was used to control the vertical movement of the steel girder.

4.4.5.2. Strain measurements

In order to get the insight of principal strains in the web, the displacement of discrete points was measured. Measuring was done using the *Insize* mechanical strain gauge with the gauge length of 100 mm (Figure 4.152). Steel pins were attached to the concrete with glue and used as bases for measuring the change in length. Measuring was done only on the front side of the testing shear span region (Figure 4.153). The notation and the geometry of steel pins are shown in Figure 4.154.



Figure 4.152 Insize mechanical strain gauge system

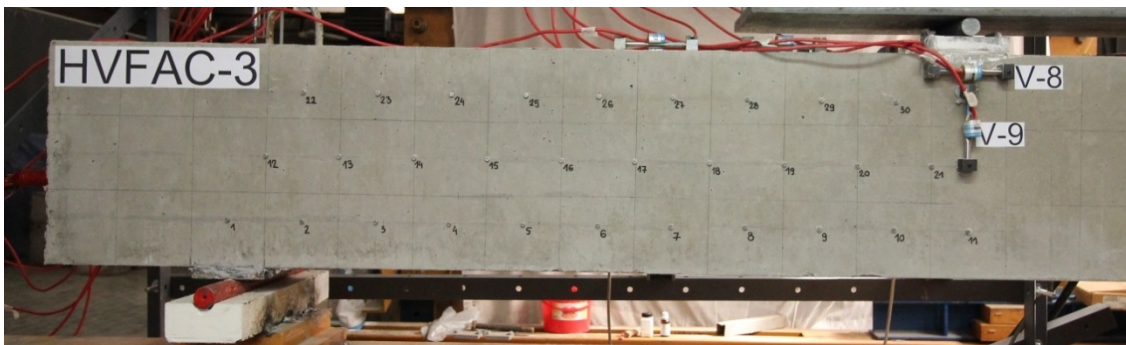


Figure 4.153 Insize steel pins on the front side of the shear span region

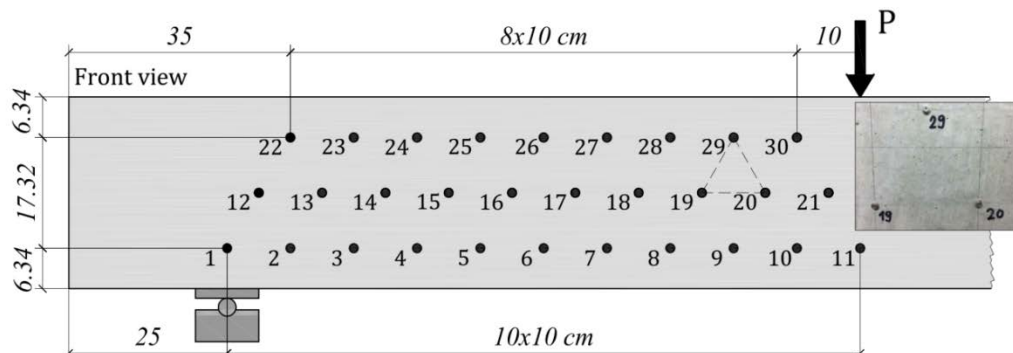


Figure 4.154 Insize point notations

4. Experimental program and test results

Steel pins were arranged in three lines at a distance of 100 mm so that they formed one-sided triangles among themselves. Measuring was done at every step of force application manually with the *Insize* mechanical strain gauge.

In order to understand the behavior of beams under shear loading, measuring of concrete and reinforcement strains was done continuously. Measuring of concrete strains was done using VWSG. Each VWSG sensor was of the same type as in the first phase of beam testing (Figure 4.19 and Figure 4.155). The position of all sensors on testing beams is shown in Figure 4.156. In the experiment, sensors were connected to data taker (*Geo data logger - DT85G*) shown in Figure 4.20.

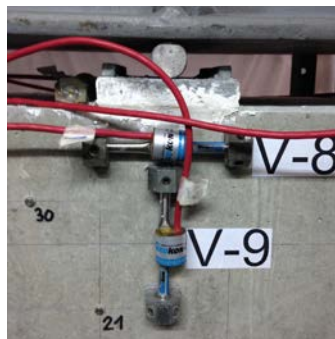


Figure 4.155 VWSG sensors measuring strains under acting force

Electric resistance SGs were used to monitor strains in the longitudinal tensile reinforcement and in stirrups. Strain gauges were the PL-60-11 type purchased from *Tokyo Sokki Kenkyujo Co., Ltd.* with test data shown in Figure 4.29a. Reinforcing bars were cleaned and prepared for strain gauge gluing using two-component HBM glue (Figure 4.23b). Strain gauges were used to measure strains in longitudinal reinforcement in cross sections where VWSG were placed to measure concrete strains in beams (sections 1, 2 and 3). Strain gauges were placed at corner bars, two in each cross section as shown in Figure 4.157.

Strains in the shear reinforcing bars were measured with strain gauges placed in different positions on the stirrup web. Preparation, gluing and protection of strain gauges are shown in Figure 4.158. Ten strain gauges were used in beams HVFAC-2 and OPC-2 and 16 in beams HVFAC-3 and OPC-3. Position of strain gauges in beams with stirrups is shown in Figure 4.159.

4. Experimental program and test results

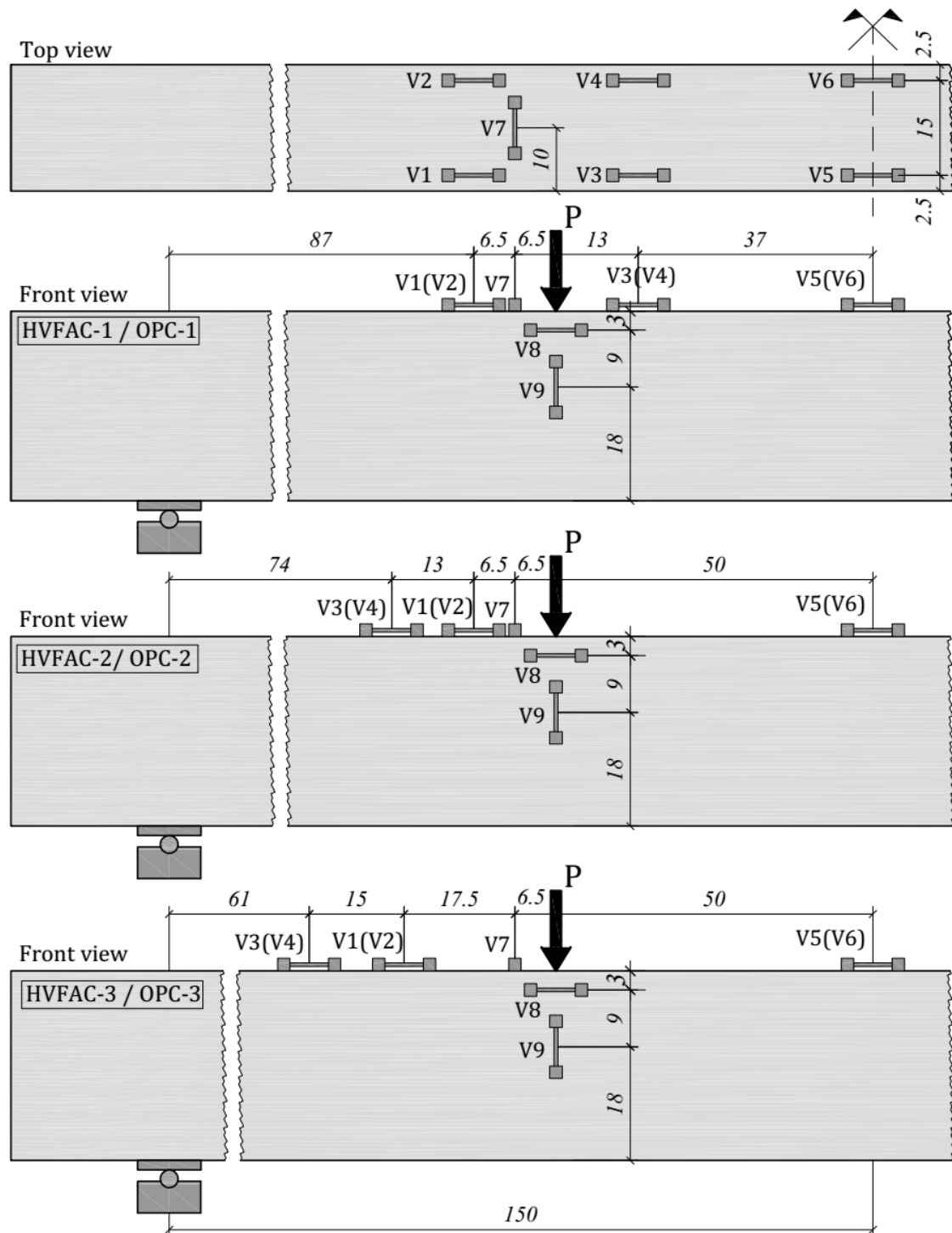


Figure 4.156 VWSG arrangements on beams

4. Experimental program and test results

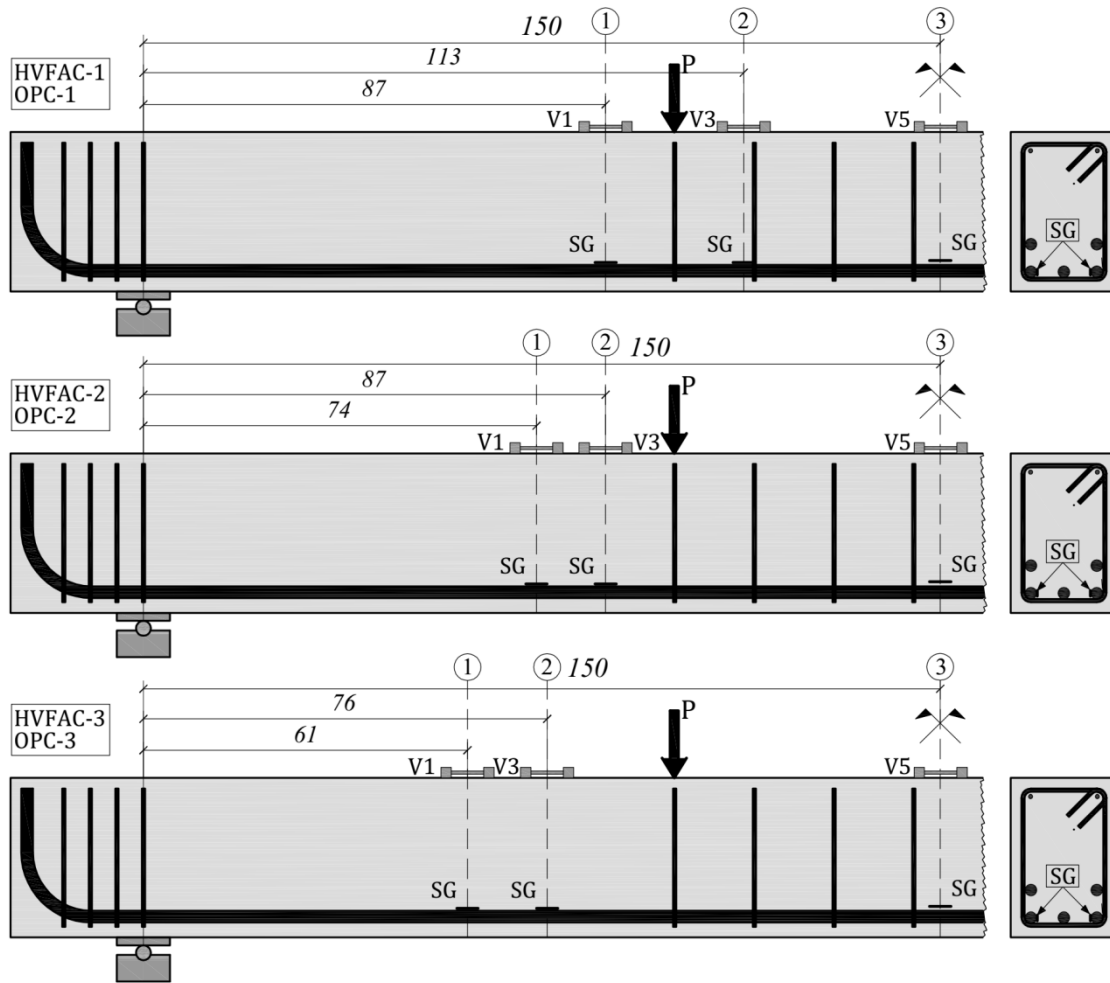


Figure 4.157 Strain gauges on longitudinal reinforcement

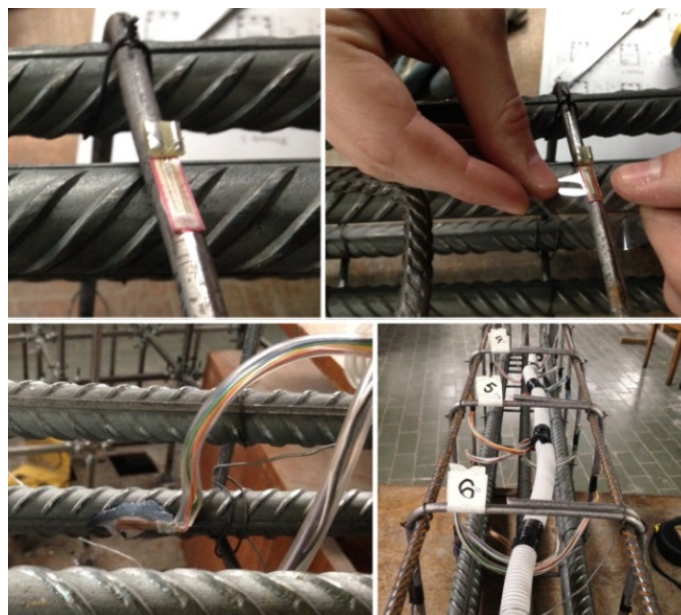


Figure 4.158 Strain gauges positioning

4. Experimental program and test results

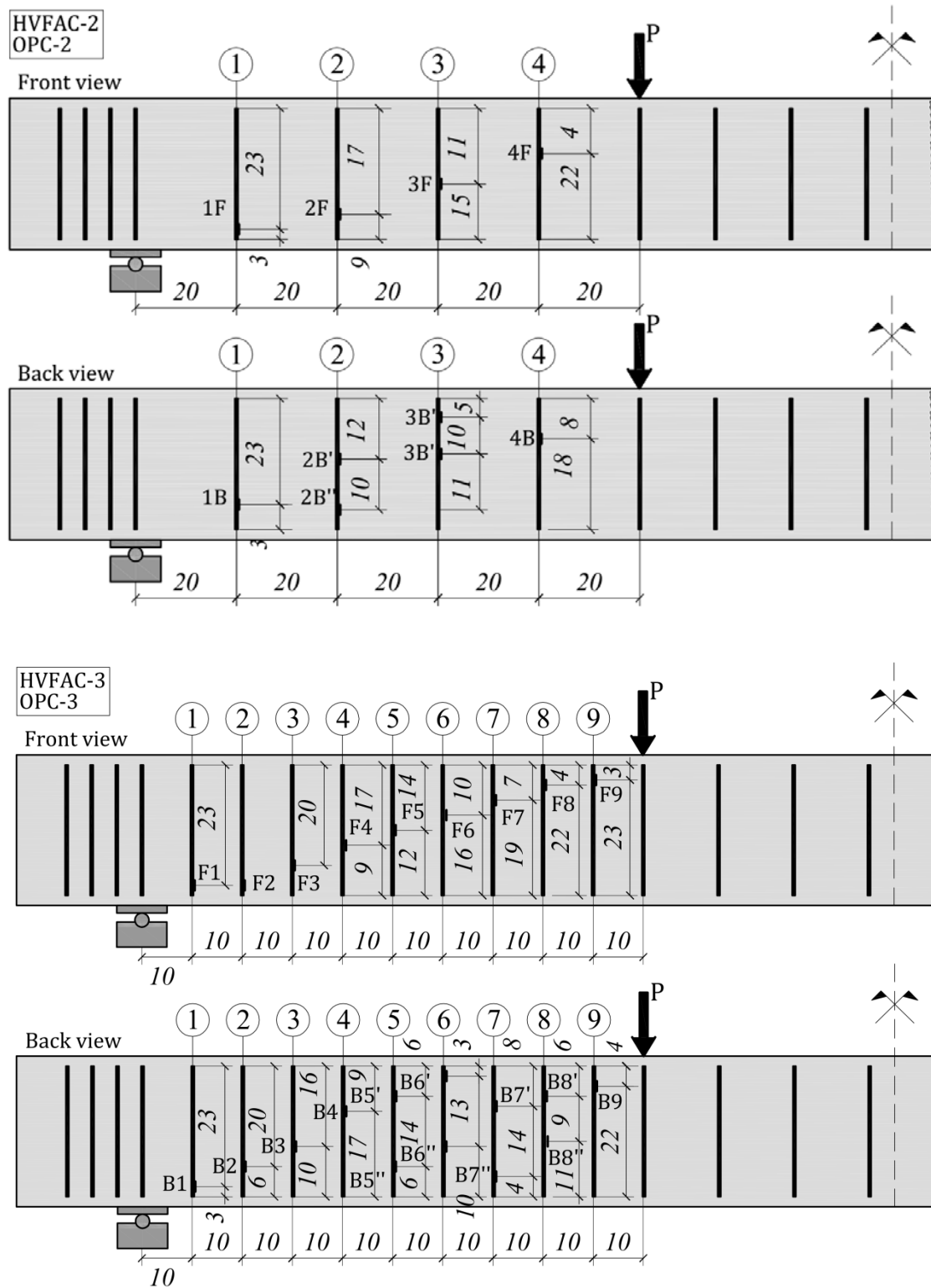


Figure 4.159 Strain gauges position on stirrups on beams a) HVFAC-2 and OPC-2 and b) HVFAC-3 and OPC-3

4. Experimental program and test results

4.4.5.3. Crack measurements

Hand measurements of crack width and pattern formations were taken at the end of each load step while the load was paused. For this purpose, a plastic crack comparator that measures a crack width of at least 0.03 mm, was used (Figure 4.24a). A magnifying glass was also used to improve the visibility of cracks (Figure 4.24b). In order to analyze the crack pattern during loading cycles, a permanent marker was used to draw lines following the crack pattern next to it (Figure 4.25a). The value of the loading force and measured crack width in each loading step was written on the current top of the crack (Figure 4.25b). The crack patterns drawn on beam specimens were used to measure crack inclination angles and the crack distribution.

4.4.6. Testing results of concrete and steel reinforcement properties

4.4.6.1. Fresh and hardened concrete properties

Testing of the fresh and hardened concrete properties was performed in the Laboratory for Materials at the University of Belgrade's Faculty of Civil Engineering according to the adequate standards. Beside the concrete temperature during mixing, the density and workability of fresh concrete mixture was also measured. Measuring density of compacted fresh HVFAC and OPCC was measured according to the European standard EN 12350-6 (CEN, 2009b). The workability of concrete was determined using the slump test according to the European standard EN 12350-2 (CEN, 2009a). Testing and evaluation of the hardened concrete properties were performed in accordance with the applicable European standards. The conducted tests included the measurement of the hardened concrete density (CEN, 2009g), compressive strength (CEN, 2009d), splitting tensile strength (CEN, 2009f), flexural strength (CEN, 2009e) and the modulus of elasticity (CEN, 2009c) at various ages. The method of mixing, casting, curing and testing of samples was previously described and it was the same as described in section 4.2 of this chapter. The average measured values and CoV of the fresh and hardened concrete density together with the slump test values are shown in Table 4.24. The slump test measurements of C200_F200 and OPC_S are shown in Figure 4.160. The

4. Experimental program and test results

density of both fresh and hardened concrete was 5% higher in OPCC compared with the HVFAC mixture.

Table 4.24 Density of fresh and hardened concrete and slump values for C200_F200 and OPC_S concrete mixtures

Concrete type	Density of fresh concrete (kg/m ³)		Density of hardened concrete (kg/m ³)		Average slump values (mm)	
	Average	CoV	Average	CoV	Average	CoV
C200_F200	2308.6	1.1	2273.3	1.9	103.0	25.3
OPC_S	2423.0	1.3	2396.8	0.9	112.0	39.3



Figure 4.160 Slump measurements of a) C200_F200 and b) OPC_S concrete mixtures

The workability of concretes tested at this stage correspond to the slump class S3 (slump between 100 and 150mm) according to the European standard EN 206 (CEN, 2011). The results of the compressive strength, splitting tensile strength and the modulus of elasticity of concrete samples cured in standard laboratory conditions (water curing) are shown in Table 4.25.

Besides the water cured samples, the concrete samples constructed from the same batch of concrete used for the beam construction are made and cured in the same way like the beams. The hardened concrete properties of the samples cured like beams are shown in Table 4.26. Three samples for the compressive strength testing were made for each beam and they were tested on the same day like corresponding beam. Other mechanical properties were tested at the age of 90 days.

4. Experimental program and test results

Table 4.25 Compressive strength, splitting tensile strength and the modulus of elasticity of water cured samples

Age (days)	Compressive strength (MPa)					Split. tensile str. (MPa)	Modulus of elasticity (GPa)	
	3	7	14	28	90	28	28	90
C200_F200	13.4	20.2	25.6	32.6	41.8	2.6	34.1	39.1
	12.9	18.4	26.8	32.2	40.9	2.7	30.8	35.6
	12.9	19.4	25.4	32.4	41.2	2.9	35.2	46.6
Average	13.1	19.3	25.9	32.4	41.3	2.7	33.4	40.4
CoV (%)	1.8	3.8	2.4	0.5	0.9	4.6	5.6	11.4
OPC_S	27.2	31.9	38.5	42.0	47.0	2.9	37.1	41.4
	26.8	24.0	40.5	42.0	46.0	2.3	37.0	47.4
	27.8	30.0	35.5	44.0	44.6	3.1	37.4	49.1
Average	27.3	31.0	38.2	42.7	45.9	2.8	37.2	46.0
CoV (%)	1.5	11.8	5.4	2.2	2.2	12.3	0.5	7.2
HVFAC/OPCC	0.48	0.62	0.68	0.76	0.90	0.96	0.90	0.88

The compressive strength development of the water-cured concrete samples and the values of the compressive strength of samples cured the same like beams are shown in Figure 4.161. It can be seen that the compressive strength of OPC_S exceeds the compressive strength of C200_F200 at all ages. The average difference in compressive strength at the age of 90 days was 10% and 16% for water curing and curing regime the same like beams, respectively. HVFAC and OPCC samples cured the same like beams had, on average, 2% and 8% higher compressive strengths compared with the samples cured in water, respectively.

The splitting tensile strength for water cured samples showed similar results for both types of concrete. On the other hand, the difference for the curing regime, the same like beams was significant, and OPC_S concrete had 46% higher splitting tensile strength compared with the C200_F200 concrete mixture. The difference for flexural strength was even more pronounced having in mind the 75% higher

4. Experimental program and test results

value for concrete OPC_S. It can be concluded that the different curing regime had a higher influence on the tensile strength compared with the compressive strength. HVFAC and OPCC samples cured the same like beams had, on average, the same and 30% higher splitting tensile strengths compared with the samples cured in water, respectively.

Table 4.26 The compressive strength, splitting tensile strength, flexural strength and the modulus of elasticity of samples cured like beams

Age (days)	Compressive strength (MPa)			Split. tensile str. (MPa)	Flex. str. (MPa)	Modulus of elasticity (GPa)
	90	92	97	90	90	90
<i>C200_F200</i>	38.8	43.0	43.8	2.4	3.9	31.5
	40.4	44.2	41.6	2.6	4.7	34.5
	41.2	-	40.4	3.1	4.2	27.9
Average	40.1	43.6	41.9	2.7	4.3	31.3
CoV (%)	2.5	20.6	3.4	10.9	7.7	8.6
<i>Age (days)</i>	85	90	92	90	90	90
<i>OPC_S</i>	50.5	52.5	52.0	3.3	8.1	40.5
	46.4	40.0	56.5	3.4	7.0	42.9
	50.6	47.5	52.8	5.1	7.3	41.5
Average	49.2	46.7	53.8	3.9	7.5	41.6
CoV (%)	4.0	11.0	3.6	21.0	6.2	2.4
<i>HVFAC/OPCC</i>	0.82	0.93	0.78	0.69	0.57	0.75

The modulus of elasticity was higher in the OPC_S concrete mixture compared with the C200_F200 for both 28 days and 90 days, especially for the curing regime the same as the beams where the difference was 25%. The difference in modulus of elasticity between two types of curing was more pronounced in the HVFAC mixture compared with the OPCC (Figure 4.162). Samples cured in the same way like beams had a lower modulus of elasticity compared with the water curing for both C200_F200 and OPC_S concrete mixtures for 30% and 10%, respectively.

4. Experimental program and test results

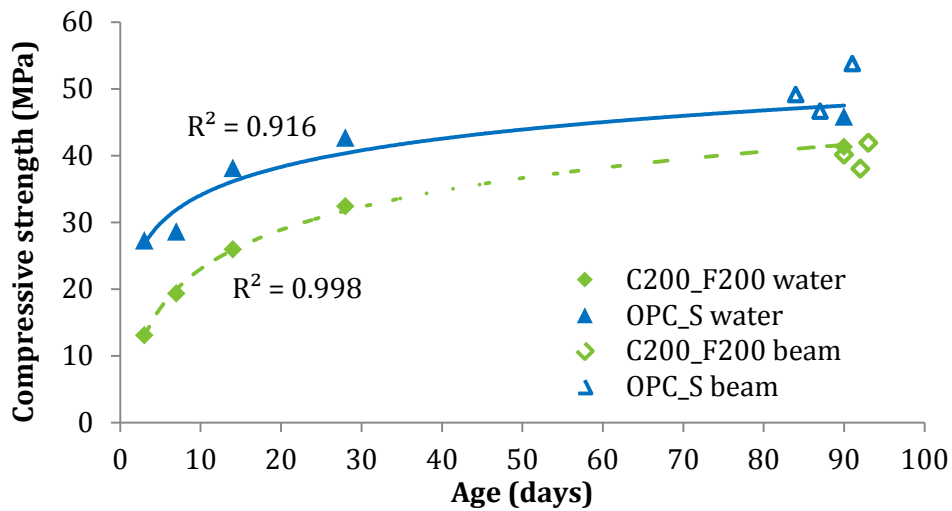


Figure 4.161 The compressive strength development of C200_F350 and OPC_S concrete mixtures

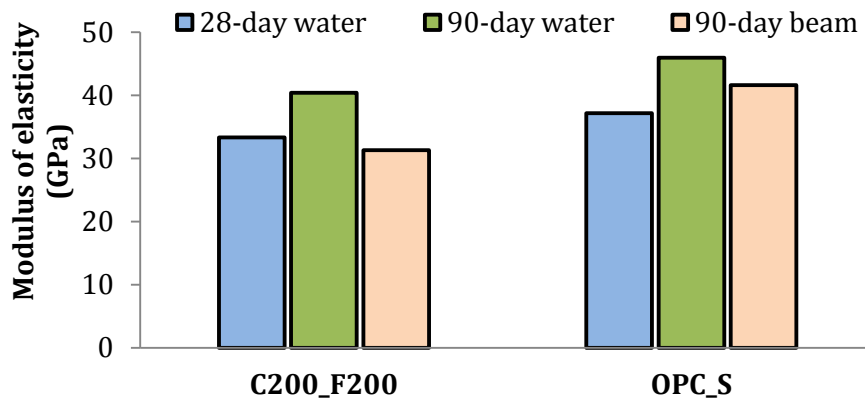


Figure 4.162 Modulus of elasticity of C200_F200 and OPC_S concrete mixtures at different ages

4.4.6.2. Steel reinforcement properties

Beams tested for bending and shear were made and tested at different times and a different batch of reinforcement was used. In order to fully understand the steel reinforcement behavior, all used bars were tested. The testing was done at the University of Belgrade's Faculty of Technology and Metallurgy, using 250 kN capacity testing equipment shown in Figure 4.31.

Obtained results are shown in Table 4.27 and stress-strain relationship diagrams for tested bars in Figures 4.163 and 4.164. As can be seen, shear reinforcement without ribs showed lower yielding and ultimate strength with higher modulus of

4. Experimental program and test results

elasticity. The yielding of reinforcement was pronounced in all four bar specimens. Measured values were similar like the values given by the producer varying from -13% up to +8.5% regarding ultimate strength.

Table 4.27 Reinforcing bars testing results

d (mm)	Type	$\sigma_{0.2\%}$ (MPa)	σ_m (MPa)	E (GPa)	ϵ_{break} (%)
6	No ribs	362.5	444.0	206.7	25.6
8	No ribs	335.7	421.4	221.6	26.8
8	Ribbed	532.4	605.2	180.2	17.9
22	Ribbed	531.3	601.8	203.9	38.0

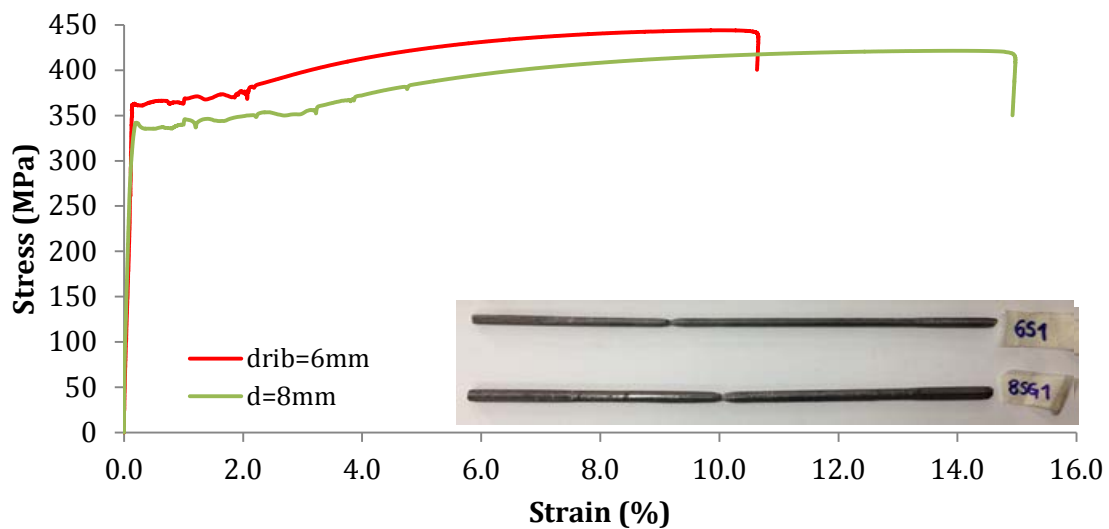


Figure 4.163 Stress-strain relationships for reinforcing bars used as stirrups

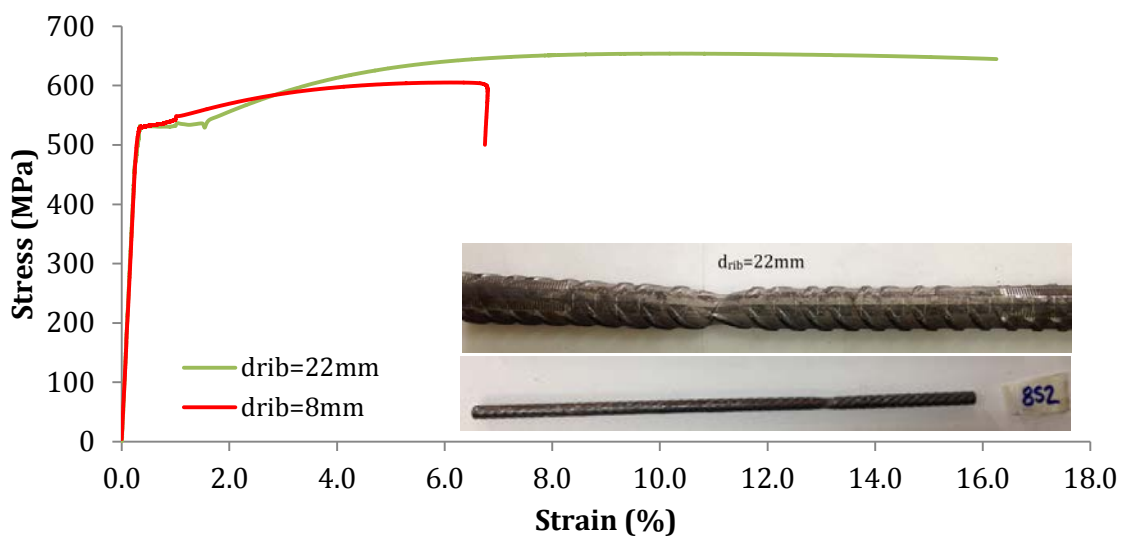


Figure 4.164 Stress-strain relationships for longitudinal reinforcement

4. Experimental program and test results

4.4.7. Overall behavior of beams tested for shear behavior

The purpose of this part of the study was to investigate the HVFAC full-scale RC beams' shear behavior and to compare it with the behavior of the OPCC beams. Motivation can be found in the fact that this matter has not been fully investigated in the literature and without this background there is no quantitative basis for the HVFAC structural application.

The overall behavior of beams was analyzed first, with a focus on the failure modes, levels of load inducing shear cracking and failure. Next, beam deflection and normalized shear stress–deflection curves were analyzed and compared. The appearance and distribution of flexural and shear cracks was monitored and recorded with crack patterns carefully drawn on the beam surface in each loading step. In order to further understand the shear transfer mechanism, concrete strain and longitudinal and shear reinforcement strains were presented and discussed. The principal concrete strains were calculated based on the *Insize* gauge measurements to discuss the principal strain evolution in different concrete types.

Table 4.28 summarizes all the important parameters for overall shear behavior evaluation. The table includes: shear load at the first flexural crack formation ($2P_{fl}$), shear load at the diagonal crack formation ($2P_{dc}$), maximum shear load at failure - ultimate shear load ($2P_u$), ultimate shear stress normalized with respect to the cube root of the compressive strength ($v_u/\sqrt[3]{f_c}$), ratio of the ultimate shear load to the load at the diagonal cracking (P_u/P_{dc}), midpoint beam deflection under the service load level (a_{ser}), midpoint beam deflection under ultimate loading level (a_u), main shear crack angle (θ) and failure mode (S – shear, F – flexural). In order to describe the behavior of beams subjected to shear loading, three values of loading force were chosen as significant and shown in Table 4.28 ($2P_{fl}$, $2P_{dc}$, $2P_u$). The P_u/P_{dc} ratio was used as an indicator of the beam ductility i.e., beams bearing capacity after diagonal crack formation and extent of stress redistribution. All six beams in this part of the study were designed to have the same 90-day compressive strength, but as can be seen in Table 4.26 the difference between C200_F200 and OPC_S concretes compressive strengths existed.

4. Experimental program and test results

Table 4.28 Experimental results of beams shear testing

Beam notation	Stirrups	2P _n (kN)	2P _{dc} (kN)	2P _u (kN)	$v_u / \sqrt[3]{f_c}$	P _u /P _{dc} (kN)	a _{ser} (mm)	a _u (mm)	θ (°)	Failure mode
OPC-1	No stirrups	40	160	221.1	0.150	1.4	4.4	12.7	27	S
HVFAC-1		20	160	210.7	0.153	1.3	4.3	11.4	27	S
OPC-2	Ø6/200	60	180	315.0	0.218	1.8	6.0	21.0	32	S
HVFAC-2		50	180	343.6	0.243	1.9	6.0	21.0	33	S
OPC-3	Ø6/100	50	180	380.2	0.251	2.1	7.9	34.0	34	F
HVFAC-3		20	180	370.2	0.265	2.1	6.8	23.3	36	S

In order to compensate for this difference, normalized shear stress was calculated and used instead of loading force in further analysis of different parameters. Normalization was done with the respect to the cube root of the compressive strength using the following equation:

$$v_u = \frac{P_u}{0.9 \cdot d \cdot b_w \cdot \sqrt[3]{f_c}} \quad \text{Eq. 4.3}$$

where:

- P_u ultimate shear load acting on the beam (one half of the ultimate loading force);
- b_w beam web width (b_w=200 mm);
- d effective beams' height (d=240 mm);
- f_c concrete compressive strength (value measured on the 100·100·100 mm cube sample).

The global behavior of reinforced concrete beams was also described with beam deflection in the service loading state (taken as 40% of the ultimate loading) and at the maximum loading. The shear crack angle was measured in each beam

4. Experimental program and test results

specimen. The inclination of the diagonal crack was measured based on the crack pattern in the middle height and length of the beams shear span. Based on the obtained results, the failure mode was defined as shear failure (S) or in the case of the OPC-3 beam, flexural failure (F).

Having in mind the influence of cracks on the serviceability of reinforced concrete structures, the analysis of crack distribution, its width, length and inclination was done in further text. The maximum crack width of flexural cracks was displayed for the service loading level. The diagonal cracks appeared only at the loading level exceeding 40% of maximum force, so their crack widths were displayed for the ultimate loading.

4.4.7.1. Overall behavior of beams without shear reinforcement

Both beam specimens without shear reinforcement (OPC-1 and HVFAC-1) failed as expected, both in shear and the brittle manner. The crack progression began with flexural cracks occurring in the beam maximum moment region close to the location of applied load points. The first cracks appeared at the applied load of 40 kN and 20 kN for OPC-1 and HVFAC-1, respectively (Figure 4.165).

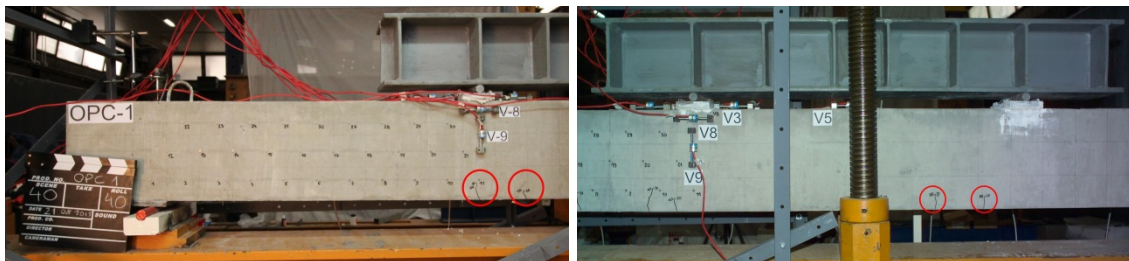


Figure 4.165 The first flexural crack in a) OPC-1 and b) HVFAC-1 beams

As the load increased, the number of flexural cracks increased in the middle part of the beam and in the shear span. Approximately until 50% of the ultimate load for both beams, flexural cracks developed vertically and symmetrically regarding midpoint of the beam. Further load increase led to the crack propagation toward the compression zone along with the crack width increase. Flexural cracks progressed vertically approximately up to the second row of the longitudinal reinforcement and after that started to develop as flexural-shear cracks close to the support. At a point of approximately 75% of ultimate load (160 kN for both

4. Experimental program and test results

tested beams), short diagonal shear crack began to appear in the middle part of the shear region (Figure 4.166).

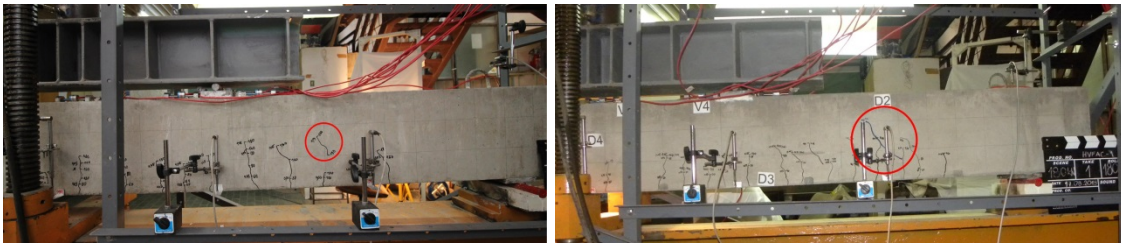


Figure 4.166 Diagonal crack appearances at the a) OPC-1 and b) HVFAC-1 beams

Diagonal cracks appeared both separately and as an extension of flexural cracks. As the additional load was applied, a critical shear crack progressed both toward the applied load plate and the beam support at the other end. The failure of both beams occurred abruptly when the diagonal crack reached the loading point. Failure modes and crack patterns on the back side of beams OPC-1 and HVFAC-1 at the ultimate load are shown in Figures 4.167 and 4.168. The back side of the beams showed one critical diagonal crack that led to failure spanning from the support plane to the loading plane. The front side of the beams showed that beside critical diagonal cracks additional shear cracks were also formed.

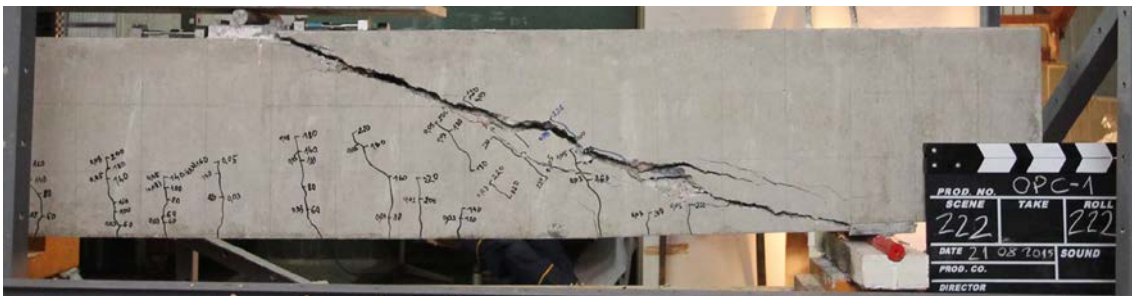


Figure 4.167 OPC-1 beam failure crack pattern



Figure 4.168 HVFAC-1 beam failure crack pattern

4. Experimental program and test results

The front side crack patterns in the step before the ultimate loading and in the failure mode for both OPC-1 and HVFAC-1 beams are shown in Figures 4.169 – 4.172. Additional shear cracks on the front side of the beam appeared as a consequence of the aggregate interlock effect present in the critical shear crack due to the low crack width before failure (0.05 mm). The crack patterns on the front and on the back side are different only in the failure mode in regard to the width of the additional diagonal cracks developed in a more pronounced manner on the front side of the beam. The slightly asymmetrical behavior was a consequence of beam supporting conditions and the geometry of the beam specimen that can never be absolutely symmetrical.

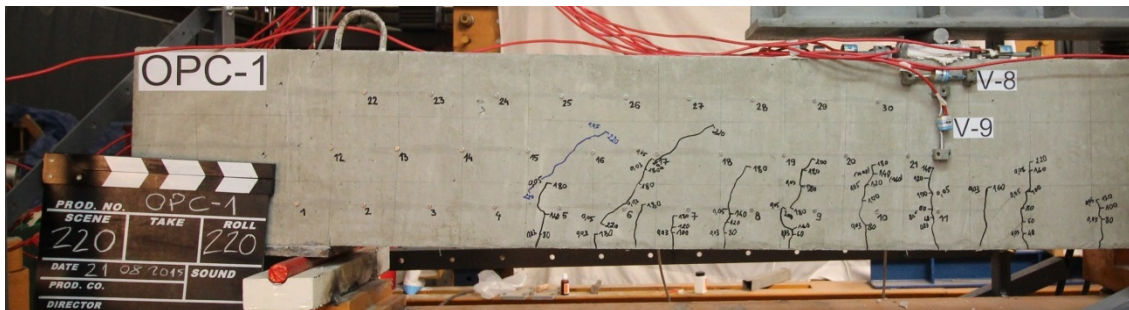


Figure 4.169 Crack pattern on the front side of OPC-1 beam just before failure

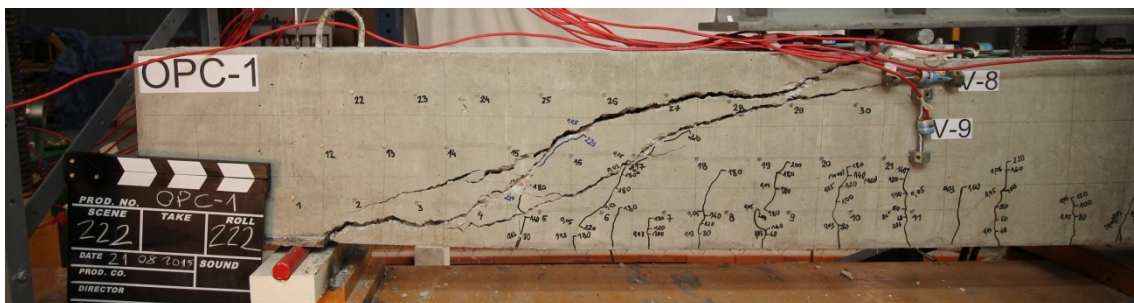


Figure 4.170 Crack pattern on the front side of OPC-1 after failure

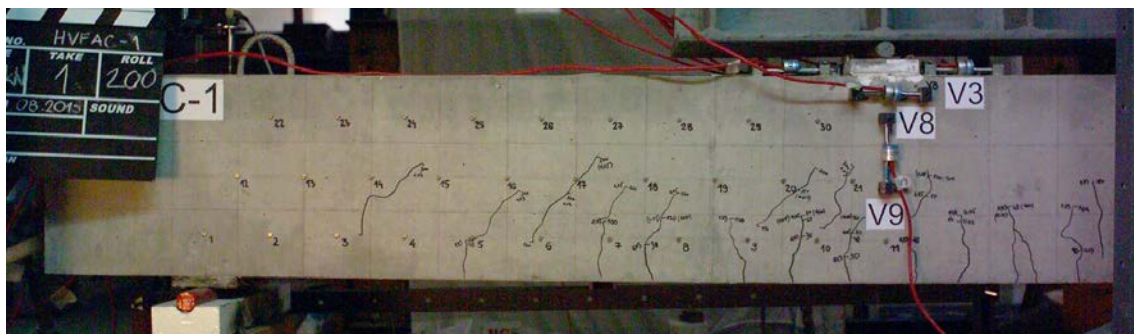


Figure 4.171 Crack pattern on the front side of HVFAC-1 beam just before failure

4. Experimental program and test results

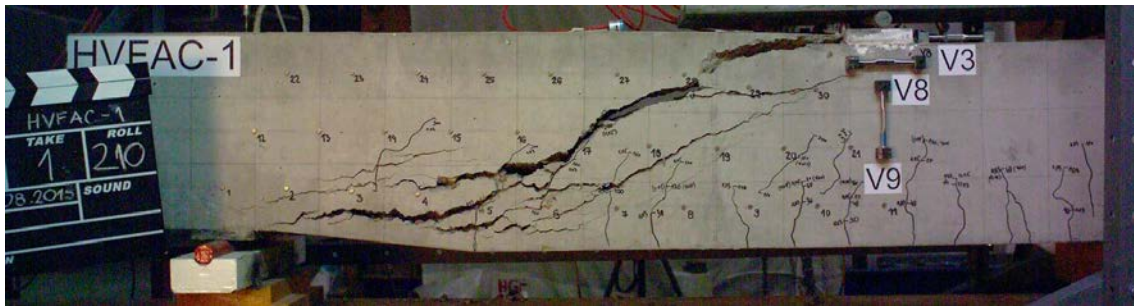


Figure 4.172 Crack pattern on the front side of HVFAC-1 after failure

The diagonal crack inclination was different in regions close to the support or the loading point and in the midpoint of the shear span. The diagonal crack angle in the midpoint of the shear span was in the range from 17° to 31° and from 18° to 46° in the OPC-1 and HVFAC-1 beams, respectively (Figure 4.173.). In both OPC-1 and HVFAC-1 beams the crack angle decreases close to the support and the loading point to approximately 10° .

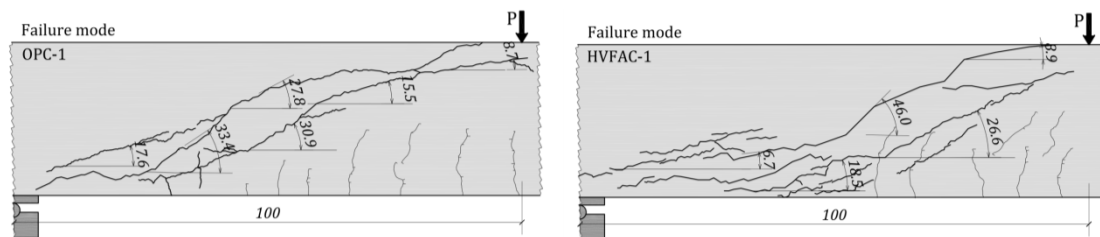


Figure 4.173 Diagonal shear crack inclination in a) OPC-1 and b) HVFAC-1

The maximum crack width ranged from 0.03 mm when first formatted at 160 kN to 0.05 mm at the point just before failure. After a sudden beam failure, the critical diagonal crack width increased to 22 mm and 24.4 mm for OPC-1 and HVFAC-1 beams, respectively (Figure 4.174). The average diagonal crack width in failure mode was 12.3 mm and 15.1 mm for OPC-1 and HVFAC-1, respectively. More diagonal cracks appeared in the zone close to the support in the HVFAC-1 than in the OPC-1 beam specimen.

The failure mode in OPC-1 and HVFAC-1 beams shown in Figures 4.169 – 4.172 indicates that diagonal tension failure occurred in both beams. On the other hand, a shear crack propagated horizontally of the place of longitudinal reinforcement in both beams during failure. This failure zone was more pronounced in the HVFAC-1 beam, as can be seen in Figure 4.175. No horizontal cracks were noticed in this zone prior to the failure, so the bond between the concrete and the reinforcement

4. Experimental program and test results

was not corrupted and the failure mode was similar to the shear tension failure in short beams. In order to understand the behavior of beams and evaluate their stiffness, diagrams of midpoint deflection versus normalized shear stress in the shear span are shown in Figure 4.176.

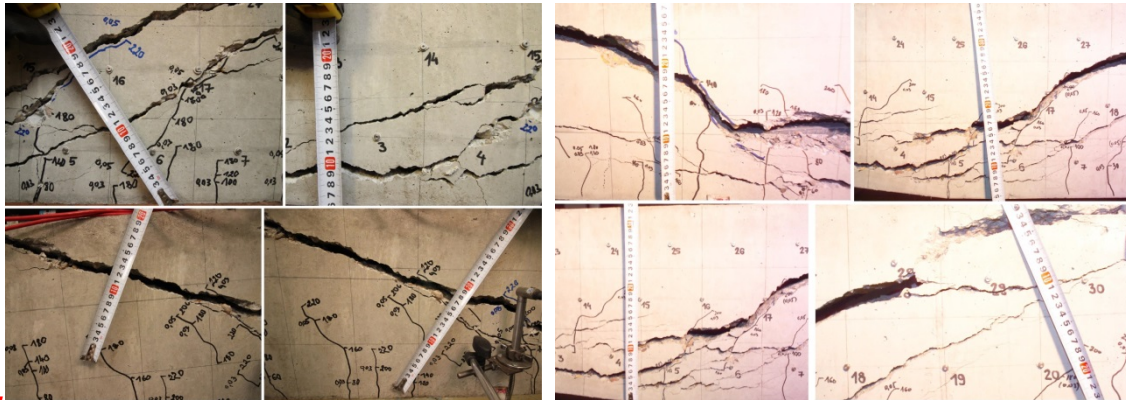


Figure 4.174 Diagonal shear cracks for a) OPC-1 and b) HVFAC-1 beams

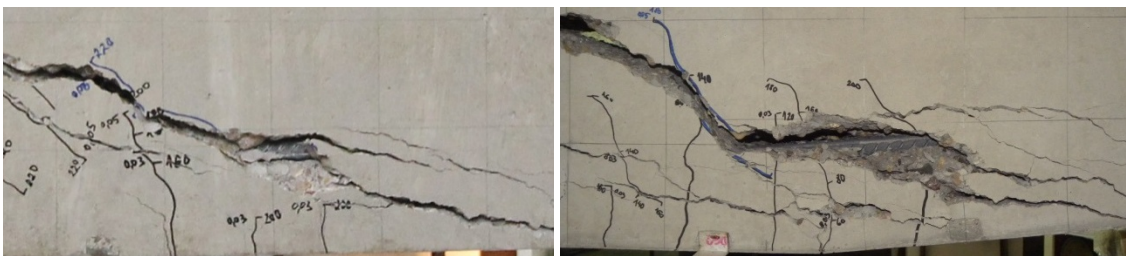


Figure 4.175 Failure cracks in OPC-1 and HVFAC-1 in the zone close to support

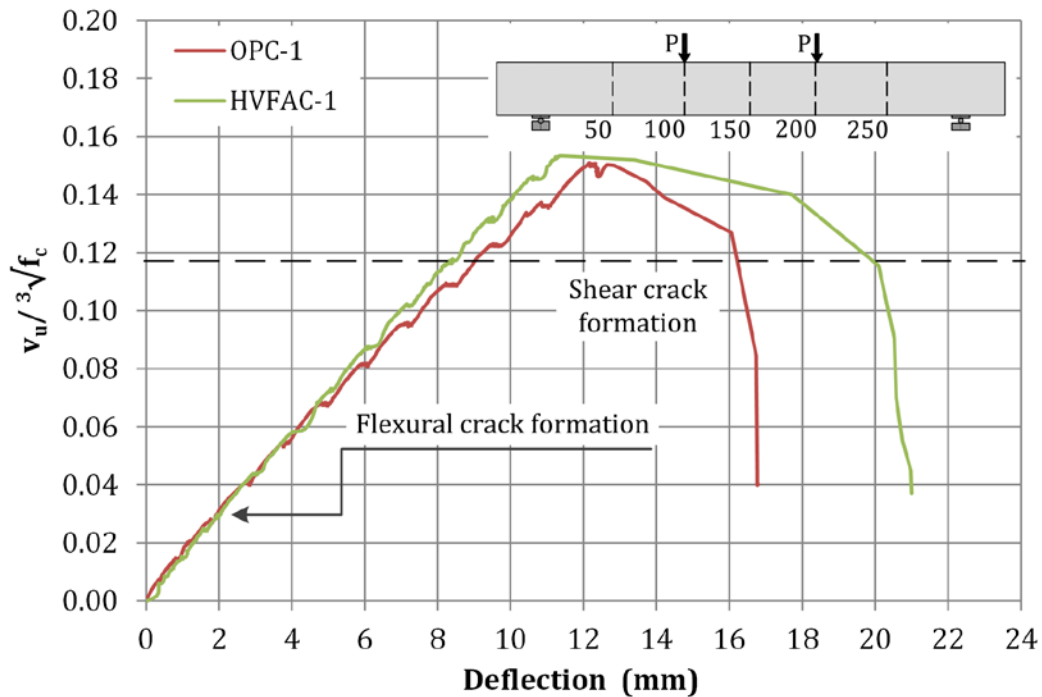


Figure 4.176 Deflection of OPC-1 and HVFAC-1 beams' midpoint versus shear stress

4. Experimental program and test results

As can be seen, Figure 4.176 shows that both the OPC-1 and HVFAC-1 beams exhibited linear-elastic behavior approximately up to the maximum shear load. An important point in the reinforced concrete beams' behavior under transverse loading is the formation of the first flexural cracks. A shift in the load-deflection curve first occurred after the flexural crack formation by decreasing the stiffness and keeping the linear-elastic behavior until the diagonal crack formation. The stiffness of both tested beams upon this point was similar to the load-deflection curve, having the same slope until the flexural crack formation. Approximately after that point, the HVFAC-1 beam showed higher stiffness until failure. After the formation of diagonal cracks, the deflection of both beams started to increase with constant loading followed by the effect of strengthening where deflection increased along with loading. This strengthening effect was a consequence of the aggregate interlock effect acting until certain crack width. However, it is not possible to evaluate the aggregate interlock effect based on this diagram. Both beams showed a significant bearing capacity after the diagonal crack formation until failure. The ductility of beams was evaluated using the P_u/P_{dc} ratio showing that the HVFAC-1 beam had around 5% lower ductility compared with the OPC-1 beam. After reaching the ultimate loading and critical shear crack propagation to supports, deflection increased along with decreasing loading.

4.4.7.2. Overall behavior of beams with shear reinforcement

The evaluation of shear transfer in beams with stirrups was performed on two sets of beams with different shear reinforcement ratios. The first set of beams (OPC-2 and HVFAC-2) were made with the minimum shear reinforcement ratio (CEN, 2004) of 0.14%, and the other set (OPC-3 and HVFAC-3) with two times higher reinforcement ratio of 0.28% .

All beam specimens with stirrups experienced a shear failure, except beam OPC-3 that failed in flexure. Flexural failure was located at the midpoint of the beam caused by the crushing of the concrete at the compression zone. A higher shear reinforcement ratio was chosen in order to increase the shear capacity, but designed to ensure shear failure prior to any flexural failure. However, the OPC-3 beam exhibited flexural failure due to the fact that the actual concrete strength was

4. Experimental program and test results

lower than the designed strength. This was only the case in this beam specimen, regardless of the fact that all three OPCC beams were casted on the same day. The reason for this can only be assumed as a consequence of the lower quality of the aggregate, cement, compacting or curing conditions. In order to confirm the assumption of the lower compressive strength of concrete, cylinder cores were drilled from the OPC-3 and HVFAC-3 beams at the age of 114 days. Compressive strengths obtained on these cores and recalculated to 100·100·100 mm cube samples were 41.0 MPa and 44.2 MPa for the OPC-3 and HVFAC-3 beams, respectively. Recalculation was done by multiplying the obtained compressive strength on cylinder core samples with the coefficient 1.12. Due to the fact that the recalculation of strengths on different samples, shapes and sizes is not reliable, these values of strength can only be used as the approximate ones and as a trend indicator. It was clear that the compressive strength of the OPC-3 beam is lower than the strength in the HVFAC-3 beam, opposite from results obtained on cube samples. In order to evaluate the trend of the compressive strength obtained on the cube samples, cylinder cores from all beam specimens were drilled at the age of 168 days. The results of the drilled cores compressive strength recalculated on 100 mm cube samples are shown in Figure 4.177 along with the already obtained results on the cube samples.

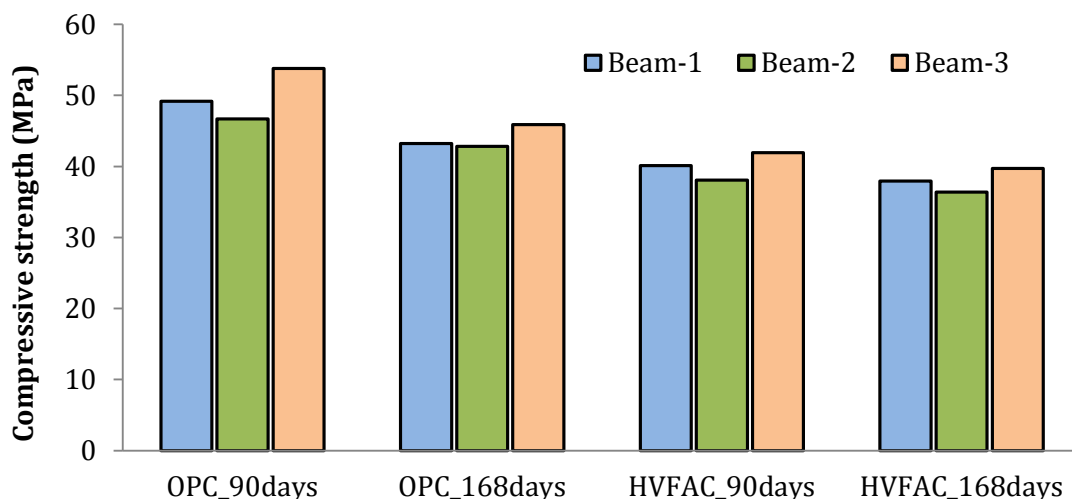


Figure 4.177 Compressive strength results of cube samples at the age of beam testing (90 days) and from drilled cores (168 days)

4. Experimental program and test results

As can be seen, the trend of the compressive strength distribution among beams was the same as what was already obtained on the samples tested at the age of 90 days. A smaller difference in the case of OPC beams was also noticeable at the age of 168 days, also indicating lower strength in the OPC-3 beam.

The crack propagation in all four beam samples began with the flexural cracks formation in the middle part of the beam. The first visible flexural crack appeared at 60 kN and 50 kN for beams OPC-2 and OPC-3, similar like in beam OPC-1. The first flexural cracks in the HVFAC-2 and HVFAC-3 beams were spotted at 50 kN and 20 kN, respectively. As the load increased, the number of flexural cracks increased in the middle part of the beam and in both shear spans. Flexural cracks progressed vertically approximately up to the second row of longitudinal reinforcement until the first shear crack formation.

The first visible shear crack appeared in all four beams at 180 kN (Figure 4.178 and 4.179). The behavior of beams with shear reinforcement was similar to the behavior of beams without stirrups up to this point. After that, flexural cracks started to incline along with more shear cracks appearing in the shear span. As the additional load was applied, all flexural cracks in the tested shear span progressed as flexural-shear cracks toward the loading point.

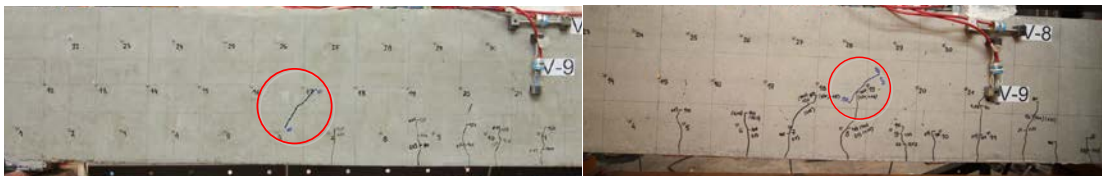


Figure 4.178 The first shear crack in a) OPC-2 and b) HVFAC-2 beams

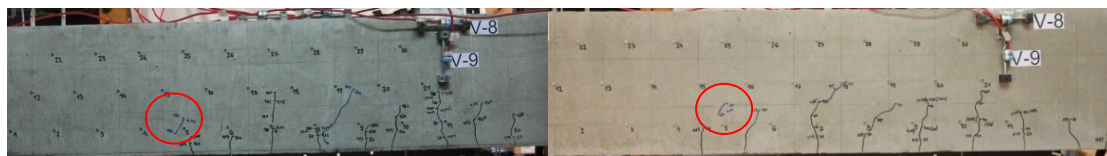


Figure 4.179 The first shear crack in a) OPC-3 and b) HVFAC-3 beams

Crack patterns on the front and on the back side of beams OPC-2, HVFAC-2, OPC-3 and HVFAC-3 are shown in Figures 4.180 – 4.189. It can be seen that the crack patterns on the front and the back side of the beam are very similar, with small differences regarding the secondary shear cracks that can be noticed.

4. Experimental program and test results

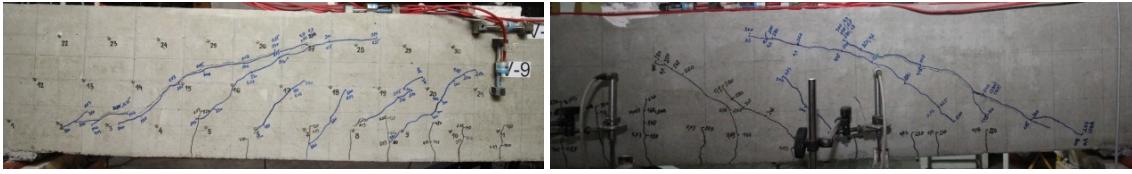


Figure 4.180 Crack pattern in a) the front side and b) the back side of the OPC-2 beam prior to failure

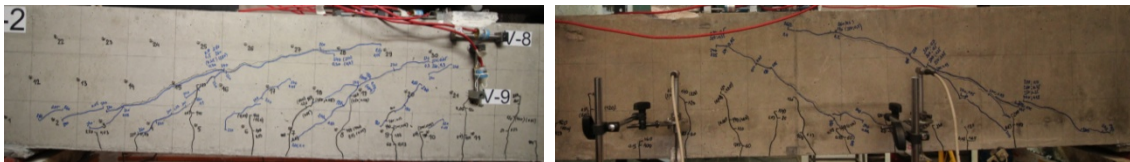


Figure 4.181 Crack pattern in a) the front side and b) the back side of the HVFAC-2 beam prior to failure

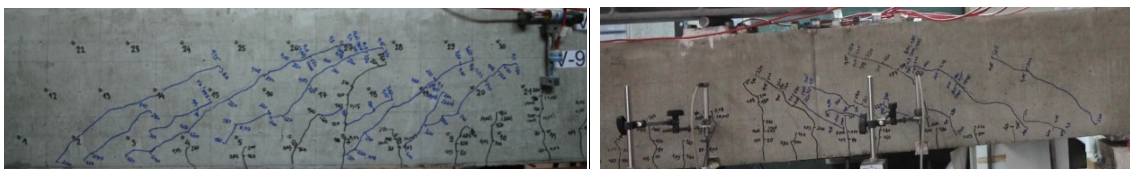


Figure 4.182 Crack pattern in a) the front side and b) the back side of the OPC-3 beam prior to failure

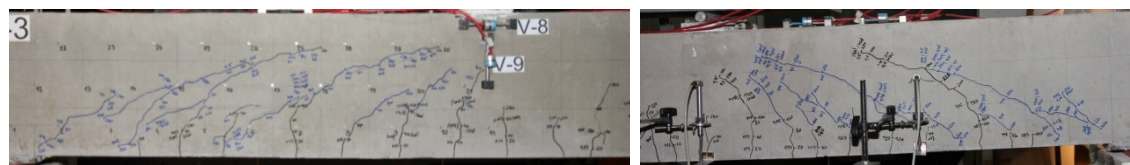


Figure 4.183 Crack pattern in a) the front side and b) the back side of the HVFAC-3 beam prior to failure

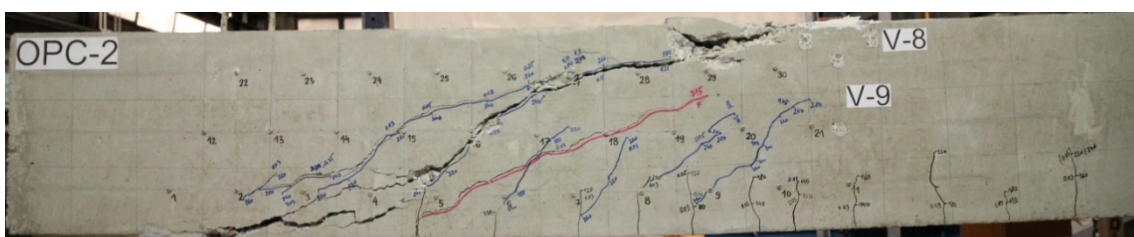


Figure 4.184 Crack pattern in the front side of the OPC-2 beam after failure

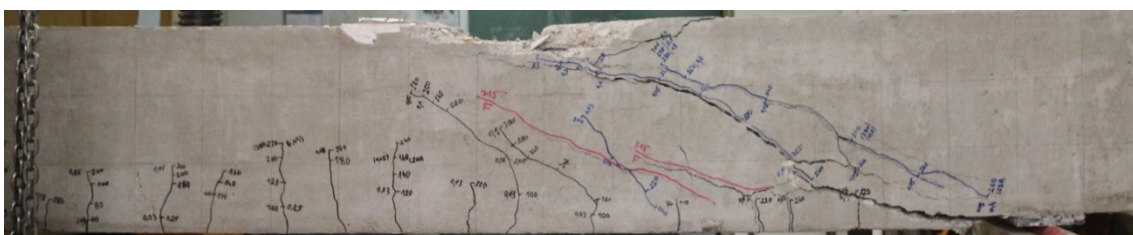


Figure 4.185 Crack pattern in the back side of the OPC-2 beam after failure

4. Experimental program and test results

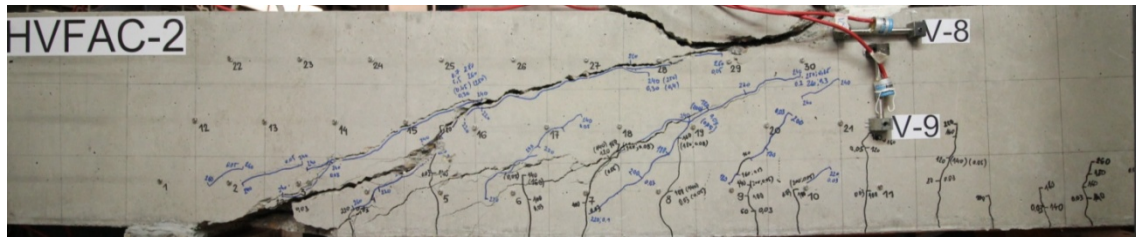


Figure 4.186 Crack pattern in the front side of the HVFAC-2 beam after failure

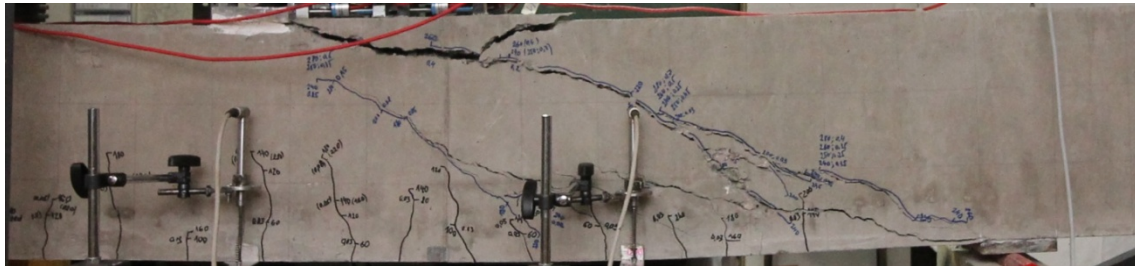


Figure 4.187 Crack pattern in the back side of the HVFAC-2 beam after failure

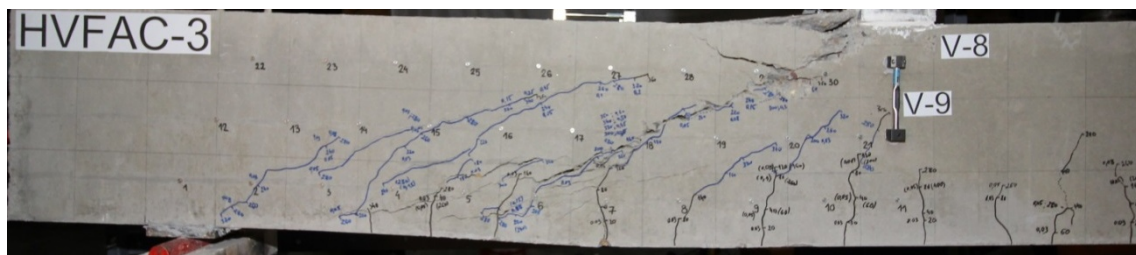


Figure 4.188 Crack pattern in the front side of the HVFAC-3 beam after failure

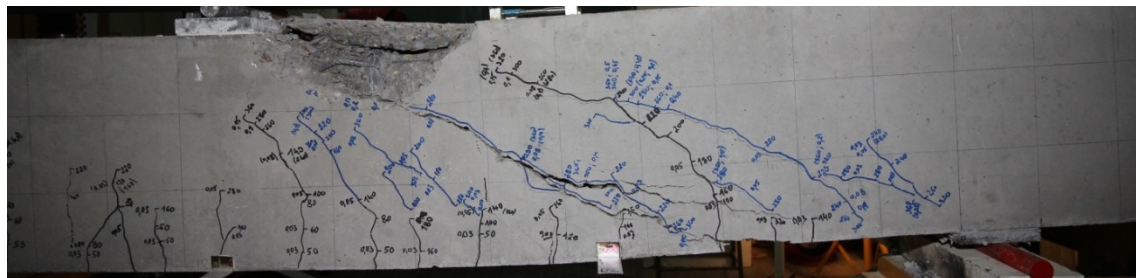


Figure 4.189 Crack pattern in the back side of the HVFAC-3 beam after failure

The dominant shear cracks formed in beams OPC-2, HVFAC-2 and HVFAC-3 with the inclination angle of 32° , 33° and 36° , respectively. This crack patterns indicated the formation of compression struts. In further loading steps, the dominant shear cracks propagation toward the loading point and widening was pronounced. More shear cracks were also formed in this region in OPC-2, HVFAC-2 and HVFAC-3 with the inclination angle between 20° - 60° , 16° - 48° , and 20° - 46° , respectively. In the OPC-3 beam, four shear cracks with angles between 26° and 37° developed in the

4. Experimental program and test results

shear span. Failure of beams OPC-2, HVFAC-2 and HVFAC-3 occurred when one of the dominant shear cracks progressed to loading point causing concrete crushing in the zone close to the loading point (Figures 4.180 – 4.189).

The failure of these three beams was brittle. A larger zone was crushed in the HVFAC-2 and HVFAC-3 beams (307·57 mm, 270·60 mm) compared with the zone formed in the OPC-2 beam (200·40 mm). The buckling of longitudinal reinforcement in compression was noticed after the failure in all three beams (Figure 4.190).



Figure 4.190 Buckling of the compressed reinforcement at failure in the OPC-2, HVFAC-2, and HVFAC-3 beams

The crack pattern of the front and back side of the OPC-3 beam is shown in Figures 4.191 and 4.192.



Figure 4.191 Crack pattern in the front side of the OPC-3 beam after failure



Figure 4.192 Crack pattern in the back side of the OPC-3 beam after failure

The failure was brittle and it was as a consequence of the compressed concrete crushing in the zone of maximum bending moment. The crushed zone was not located exactly in the midpoint of the beam, but closer to tested shear span. The crushed concrete zone included a significant part of the concrete cross section (483·137 mm) followed with the reinforcement buckling (Figure 4.193).

4. Experimental program and test results

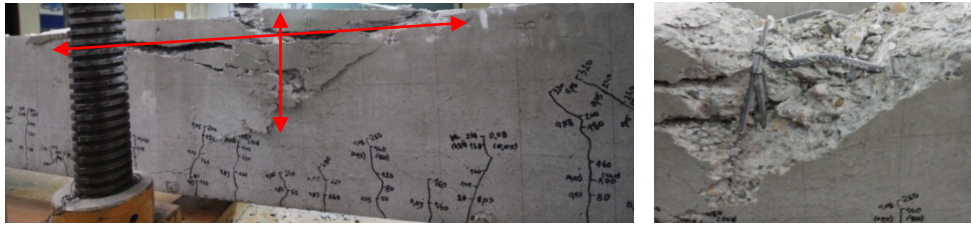


Figure 4.193 Failure zone and compression reinforcement buckling in the OPC-3 beam

The diagram of the midpoint deflection versus the normalized shear stress in the shear span for the OPC-2, HVFAC-2 and HVFAC-3 beams is shown in Figure 4.194.

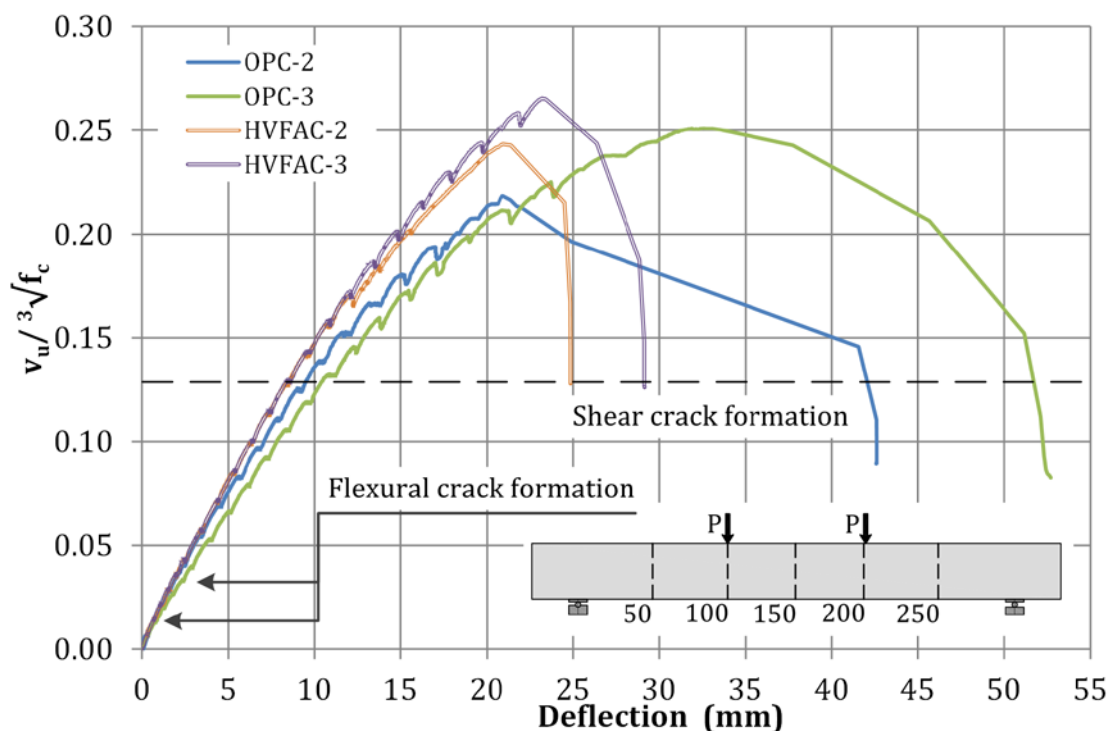


Figure 4.194 Deflection of OPC-2, HVFAC-2, OPC-3 and HVFAC-3 beams midpoint versus shear stress

The normalized shear stress level which refers to the first visible shear crack formation (180 kN) is presented with a dashed line in Figure 4.194. The normalized shear stress level in which the first flexural crack appeared is also marked in Figure 4.194 for the loading force of 20 kN and 60 kN. It can be seen that all four beams expressed the linear-elastic behavior approximately until the formation of a diagonal crack. The shift in the load-deflection curve first occurred after the flexural crack formation by decreasing the stiffness for all four beams. The stiffness of the OPC-2, HVFAC-2 and HVFAC-3 beams upon this point was

4. Experimental program and test results

similar to the load-deflection curve, having the same slope until the flexural crack formation. The load-deflection curves of the HVFAC-2 and HVFAC-3 beams had the same slope until the shear crack formation. After that point, beam HVFAC-3 showed higher stiffness. The load-deflection curve of the OPC-3 beam had lower stiffness than the OPC-2 beam, but the same trend up to the ultimate loading force. The ductility of the beams was evaluated using P_u/P_{dc} ratio showing that the HVFAC-2 beam had around 8% higher ductility compared with the OPC-2 beam as shown in Figure 4.195b. The ductility of the beams in group three was very similar, with only 3% higher value for the OPC-3 beam.

As described above, the beams without shear reinforcement presented flexural cracking prior to the initiation of shear cracking in the web. Shear failure was brittle and occurred when this diagonal crack reached the loading point. Brittle shear failure of the OPC-2, HVFAC-2 and HVFAC-3 beams can be explained with the compression zone crushing due to the combination of shear and compression forces, the yielding of the shear reinforcement but not of the longitudinal reinforcement. It was observed that the degree of cracking increased as the shear reinforcement ratio increased. Multiple shear and flexural-shear cracks developed in the shear span as opposed to the specimens without stirrups where only one diagonal crack developed and led to failure.

The ultimate normalized shear stress for all three groups of beams is shown in Figure 4.195a. Shear stress capacity in the beams without shear reinforcement represents concrete shear capacity, while in beams with stirrups refers to the sum of concrete and the stirrups shear capacity. As expected, the ultimate shear stress increases together with the stirrups ratio. The OPCC beams shear stress increased for 45% and 67% for the minimum and higher shear reinforcement ratio, respectively. In the HVFAC beam increase was even higher, 59% for the minimum and 73% for higher reinforcement ratio. The ultimate shear stress was higher for the HVFAC beams in groups 1, 2 and 3 for 2%, 11% and 6%, respectively. Having in mind different results of the compressive strength obtained on the cube samples and cores drilled from beams, this can be seen as a consequence of the lower compressive strength used for the normalization in the HVFAC beams. Therefore, it

4. Experimental program and test results

can be concluded that no significant differences between the OPCC and HVFAC ultimate shear stress existed.

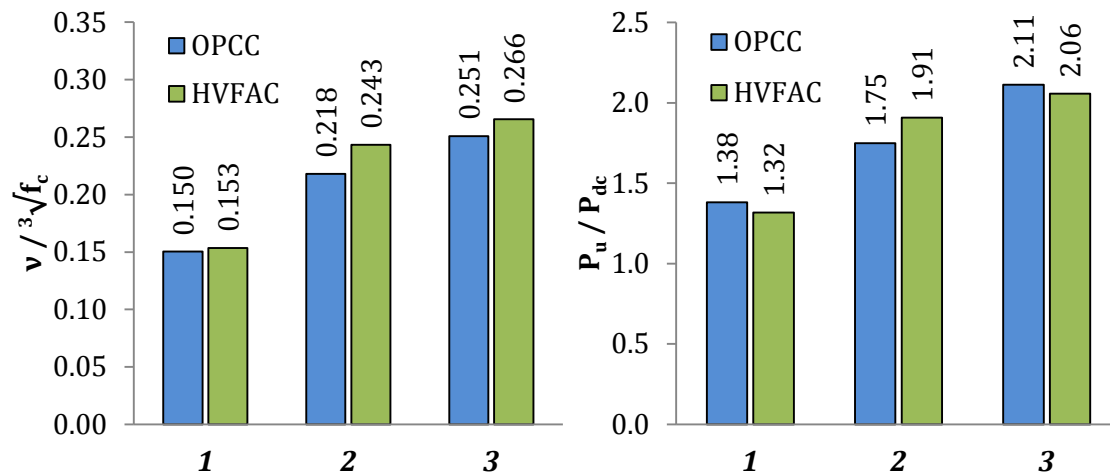


Figure 4.195 a) Ultimate normalized shear stress and b) ductility of all beams tested for shear

All four beams showed a significant bearing capacity after the diagonal crack formation until failure as can be seen in Figure 4.195b. The OPCC beams showed a more ductile behavior, except in the case of beams with minimum shear reinforcement ratio. The difference between OPCC and HVFAC falls within a 10% margin.

4.4.8. Deflection of beams

The monitoring of the beam deflection was done by measuring the deflection in five points along the beam span and above supports. The diagrams of deflection (a) along the beam length at selected normalized shear stress values are shown in Figures 4.196 – 4.198. As can be seen the deflection lines during the loading were symmetrical until failure in the shear span for all beams. The deflection lines at service load were practically the same for all groups of beams.

The maximum deflection under service loading was the same in the OPCC and HVFAC beams for the first and the second group of beams. In beams with higher shear reinforcement, this deflection was around 14% higher in the OPC-3 beam (Figure 4.199). This is mostly a consequence of the different failure modes of the OPC-3 and HVFCA-3 beams.

4. Experimental program and test results

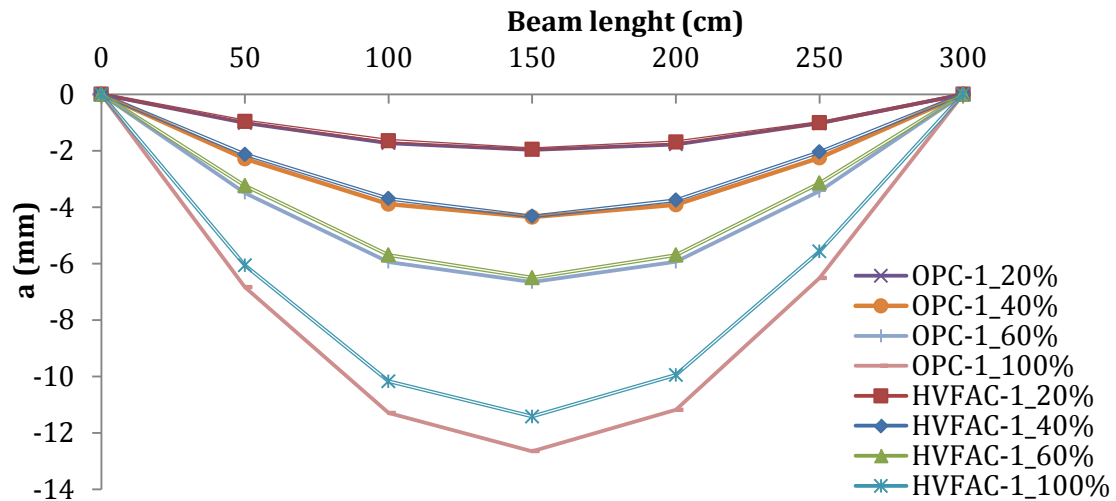


Figure 4.196 Deflection of the OPC-1 and HVFAC-1 beams at selected loading steps

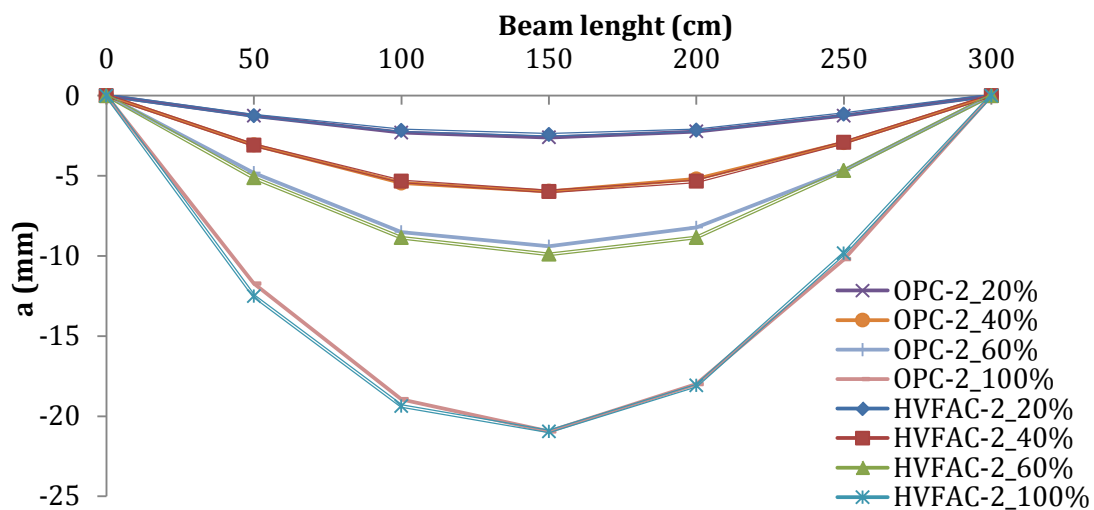


Figure 4.197 Deflection of the OPC-2 and HVFAC-2 beams at selected loading steps

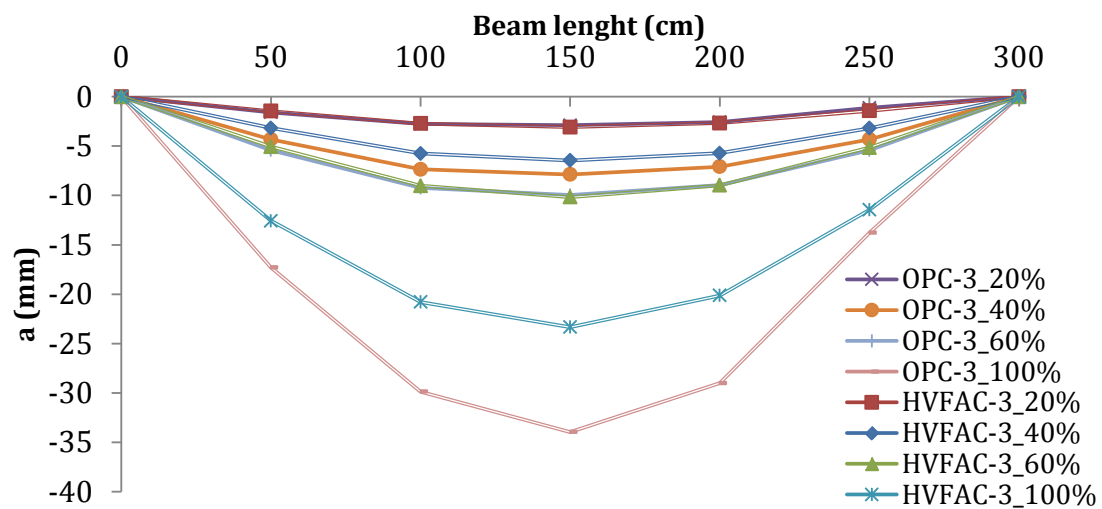


Figure 4.198 Deflection of the OPC-3 and HVFAC-3 beams at selected loading steps

4. Experimental program and test results

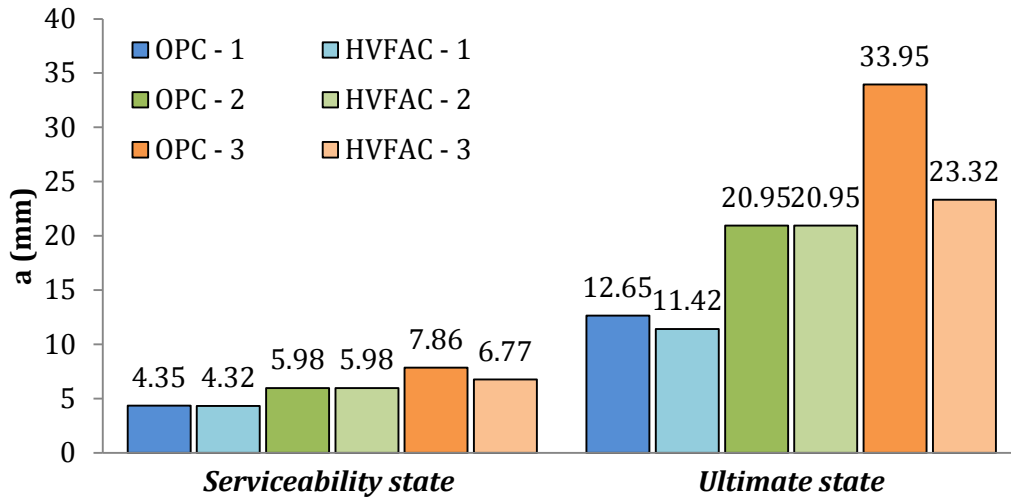


Figure 4.199 Service and ultimate loading state deflections

Normalized shear stresses versus the deflection curves in cross sections other than the beams' midpoint are shown in Figure 4.200 – 4.202. The inclination of the linear-elastic part of the deflection-stress relationship was up to 10 higher for all HVFAC beams compared with the OPCC ones. There was a greater deflection of the OPCC beams for the same value of normalized shear stress. The load-deflection curve of the OPC-3 beam shows more ductile failure compared with the brittle shear failure in other tested beams.

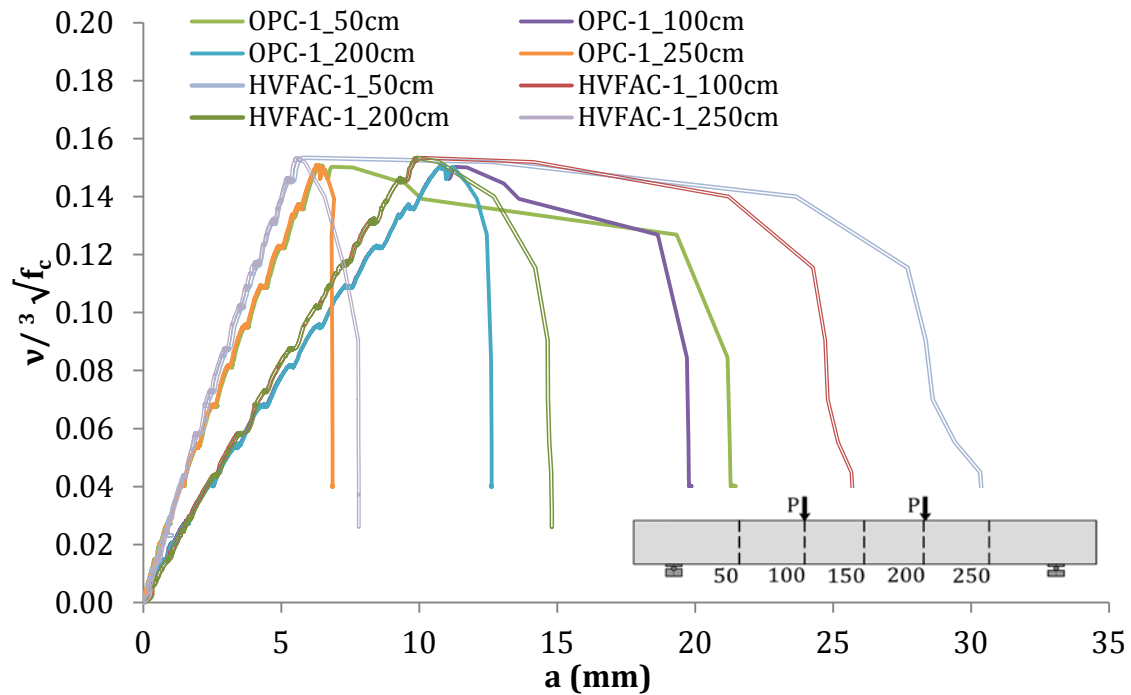


Figure 4.200 OPC-1 and HVFAC-1 deflection versus normalized stress curves

4. Experimental program and test results

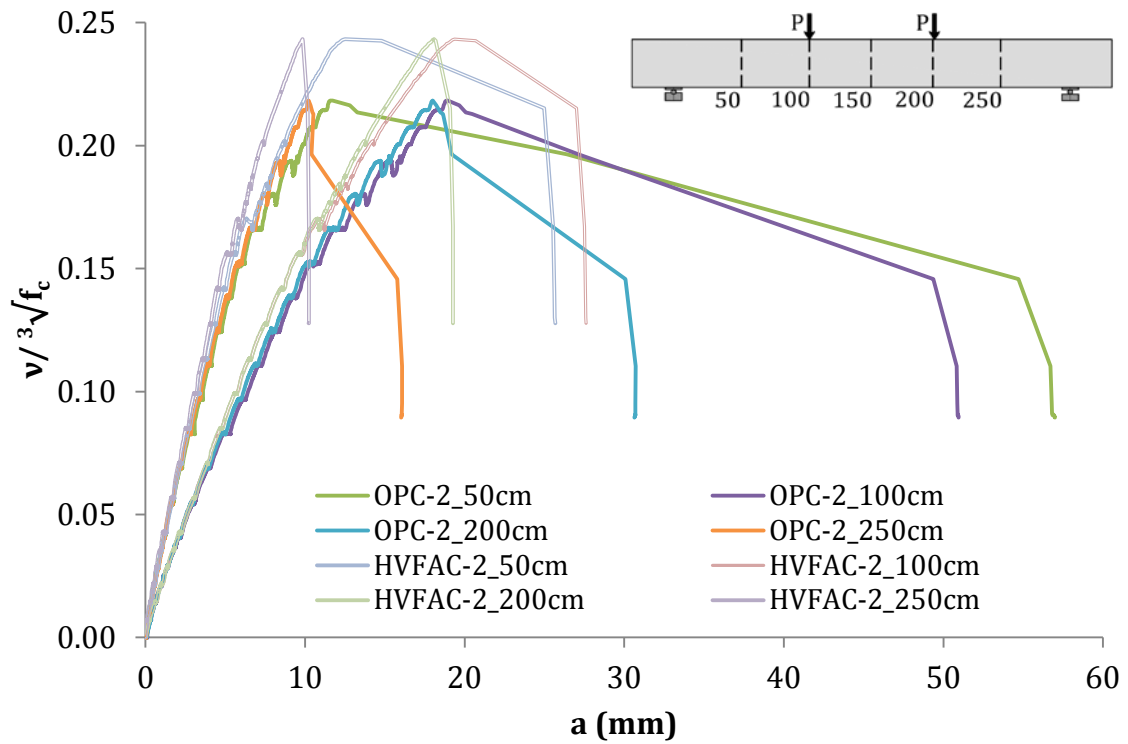


Figure 4.201 OPC-2 and HVFAC-2 deflection versus normalized stress curves

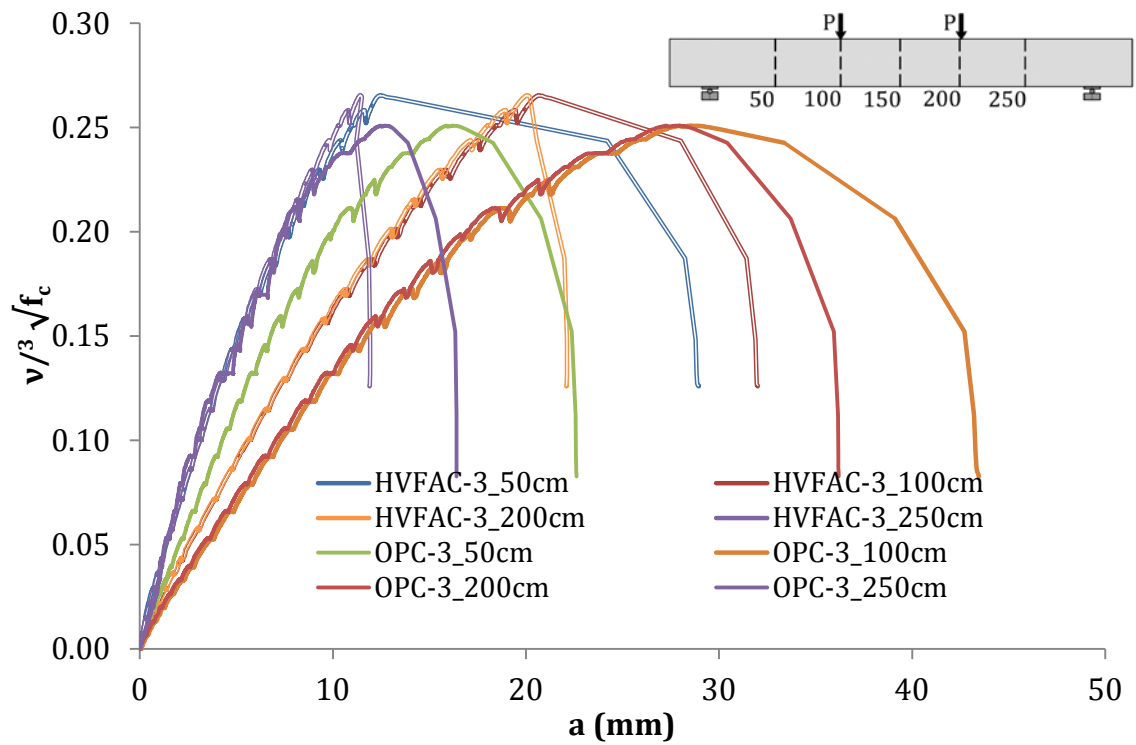


Figure 4.202 OPC-3 and HVFAC-3 deflection versus normalized stress curves

4. Experimental program and test results

4.4.9. Longitudinal reinforcement strains

The maximum strain values for all beams and for each section are shown in Figure 4.203. Longitudinal reinforcement strains versus normalized shear stress for all tested beams are shown in Figures 4.204 – 4.206.

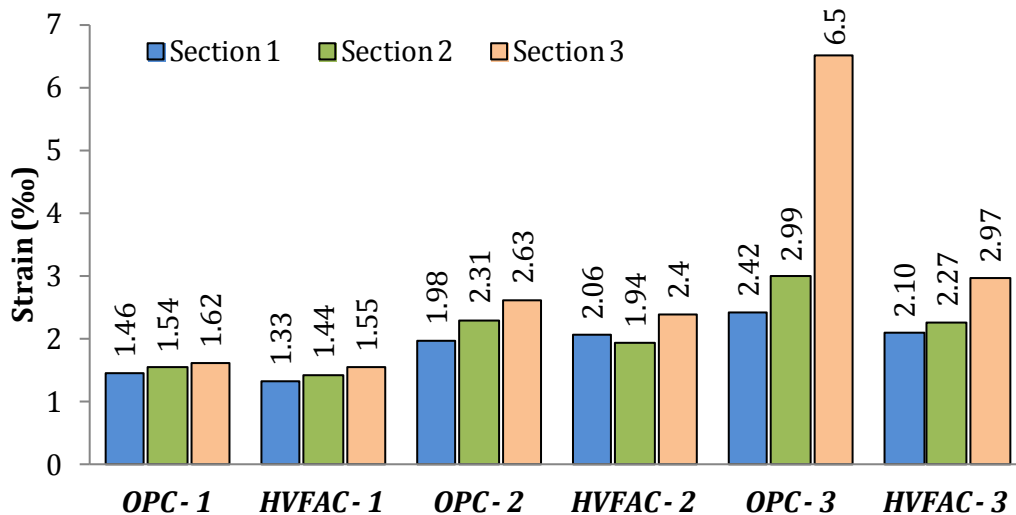


Figure 4.203 Maximum longitudinal reinforcement strains

Longitudinal reinforcement strains for beams without shear reinforcement are shown in section 1 (87 cm), section 2 (113 cm) and section 3 (150 cm, beams' midpoint). The relationship between normalized shear stress and longitudinal reinforcement strains was linear and no yielding up to failure was achieved. Reinforcement strains developed in the same way for both OPC-1 and HVFAC-1 beams until the first flexural cracks appeared. After that point in all three sections, the OPC-1 beam had higher strains for the same normalized shear stress. The formation of the shear crack did not have any significant influence on the development of longitudinal reinforcement strains.

The maximum strain values in each section given in Figure 4.203 show that the difference between the OPC-1 and HVFAC-1 beams was in the 10% margin. The OPC-1 beam had 10%, 7% and 5% higher strains compared with the HVFAC-1 beam for sections 1, 2 and 3 respectively.

4. Experimental program and test results

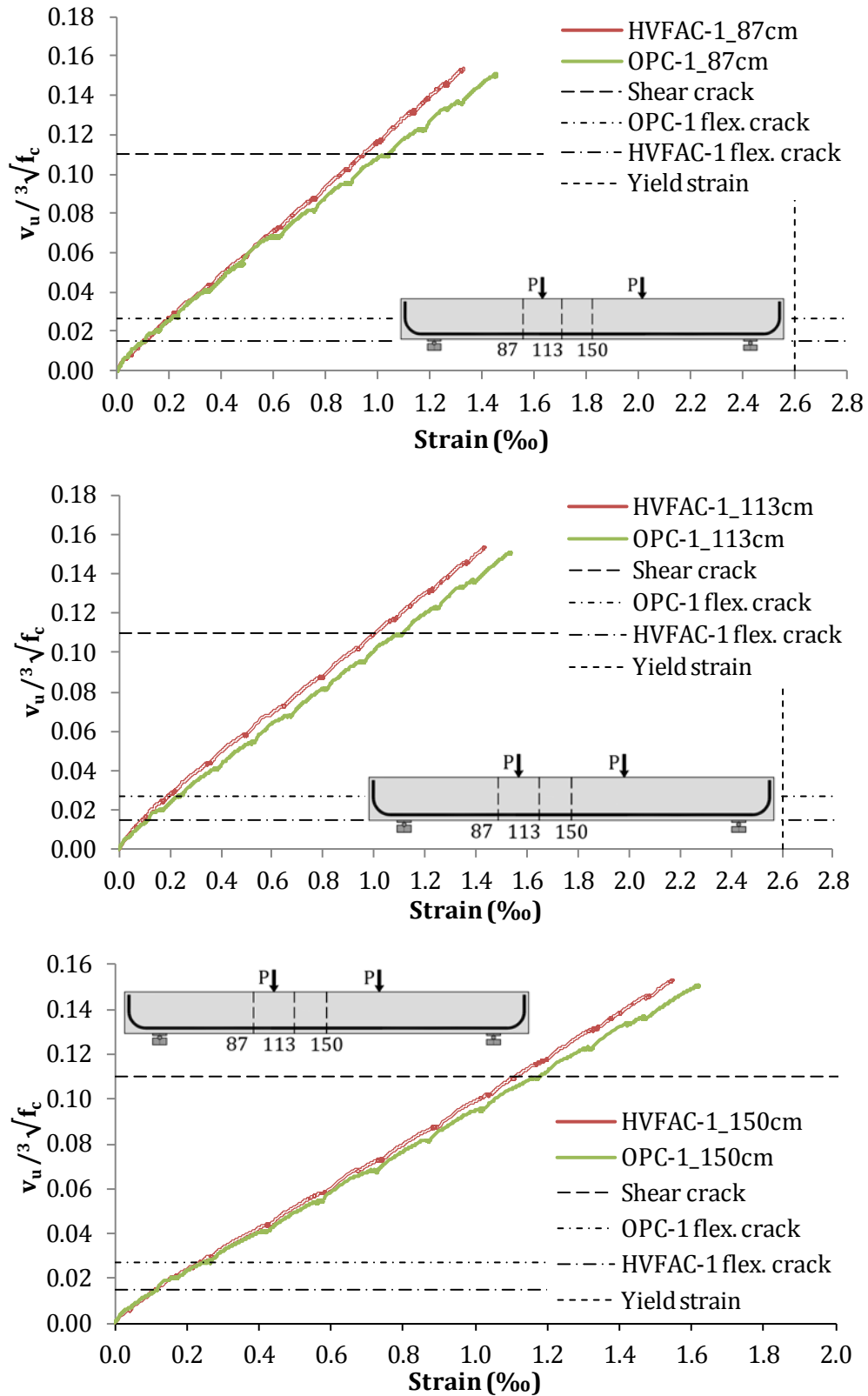


Figure 4.204 Longitudinal reinforcement strains for the OPC-1 and HVFAC-1 beams in sections at 87, 113 and 150 cm

4. Experimental program and test results

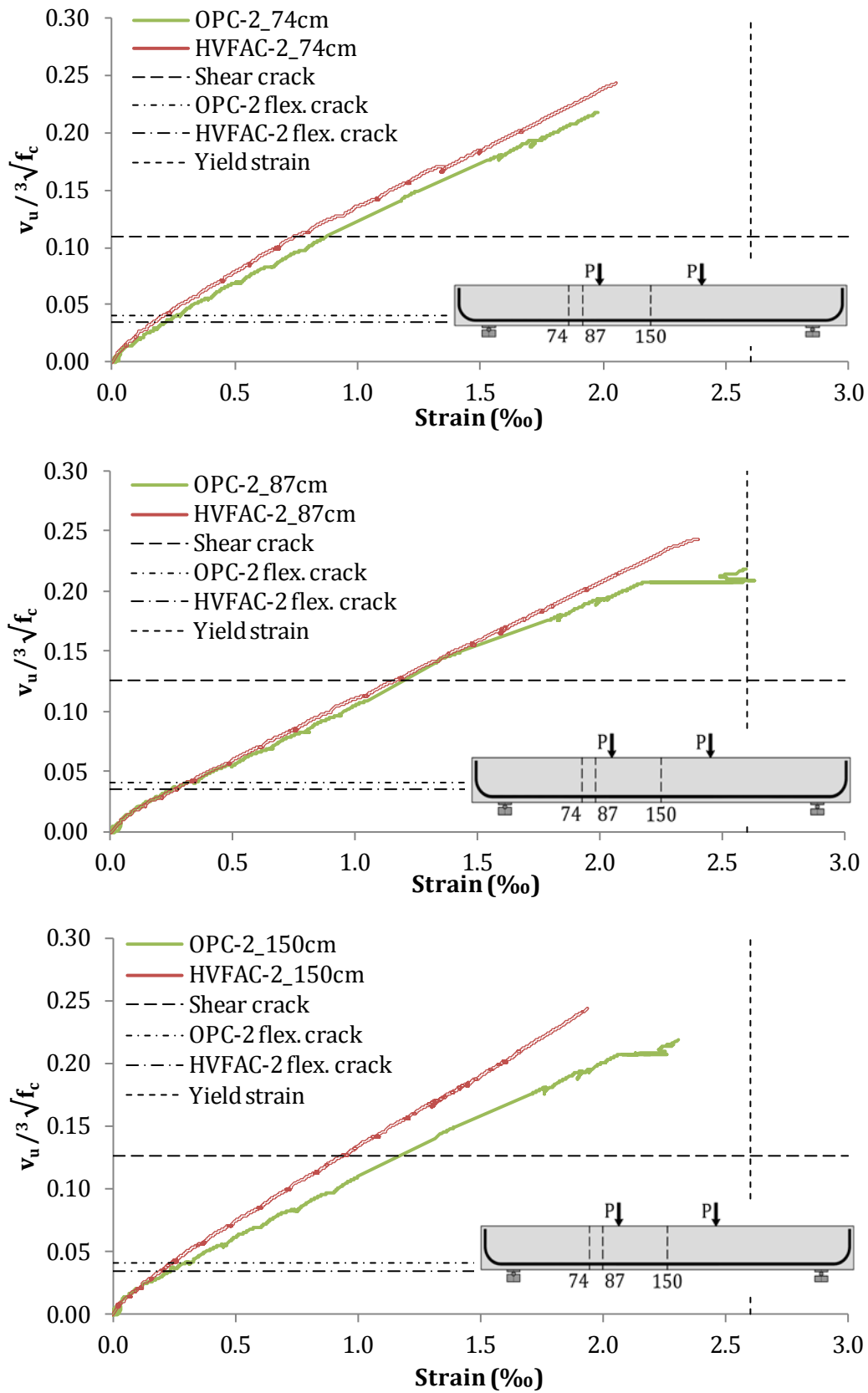


Figure 4.205 Longitudinal reinforcement strains for the OPC-2 and HVFAC-2 beams in sections at 74, 87 and 150 cm

4. Experimental program and test results

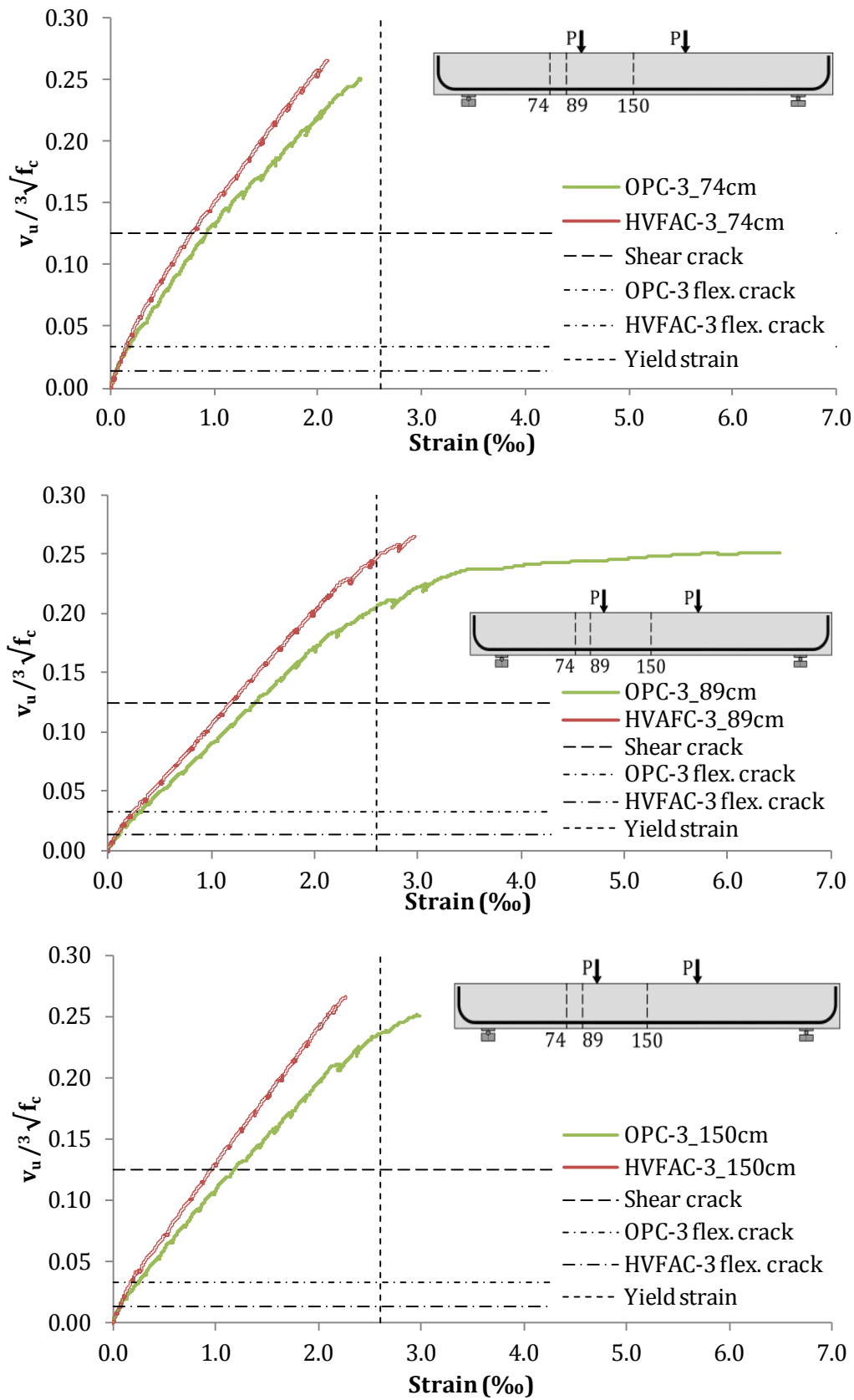


Figure 4.206 Longitudinal reinforcement strains for the OPC-3 and HVFAC-3 beams in sections at 74, 89 and 150 cm

4. Experimental program and test results

The longitudinal reinforcement strains versus normalized shear stress for beams with reinforcement are shown in Figures 4.205 and 4.206 for section 1 (74 cm), section 2 (87/89 cm) and section 3 (150 cm, beams' midpoint). The strains in the longitudinal reinforcement close to the yielding point ($\approx 2.6\%$ as shown in Table 4.27) at failure were achieved in section 2 (closest to loading point) in the OPC-2 and HVFAC-2 beams. In beams OPC-3 and HVFAC-3, the longitudinal reinforcement strain level in all sections was higher compared with the OPC-2 and HVFAC-2 beams. The strains close to the yield point were reached in sections 1 and 3 and the yielding of reinforcement was achieved in section 2 for both OPC-3 and HVFAC-3 beams. Higher strains were observed in the OPC-3 beam mostly due to the fact that it failed in bending between sections 2 and 3.

Reinforcement strains developed in the same way for all four beams until flexural cracks appeared. After that point, the OPCC beams had higher strains for the same normalized shear stress in all sections. The longitudinal reinforcement strains in the OPC-2 beam were higher than in the HVFAC-2, with the difference being within the 20% margin. The only exception was noticed in section 1, where the strains were 4% lower in the OPC-2 beam compared with the HVFAC-2 beam. The difference between the OPC-3 and HVFAC-3 beams was more pronounced and in favor of the OPC-3 beam. This information can only be qualitatively assessed having in mind a different failure mode. The longitudinal reinforcement strains were higher in all three OPCC beams in all sections except the OPC-2 section 1. The difference was the highest in section 3 - midpoint of the beam with maximum bending moment.

The influence of different shear reinforcement ratios on the longitudinal reinforcement strains is shown in Figures 4.207 and 4.208. The strains in section 87/89 cm and beams' midpoint are plotted for all OPCC and HVFAC beams. It can be seen that the longitudinal reinforcement strains increased with the increase of the shear reinforcement ratio, as expected. The same development of strains can be seen with some differences in the midpoint section among OPCC beams. This can be explained, like before, with the different failure mode of the OPC-3 beam effecting mostly longitudinal strains in beams' midpoint section.

4. Experimental program and test results

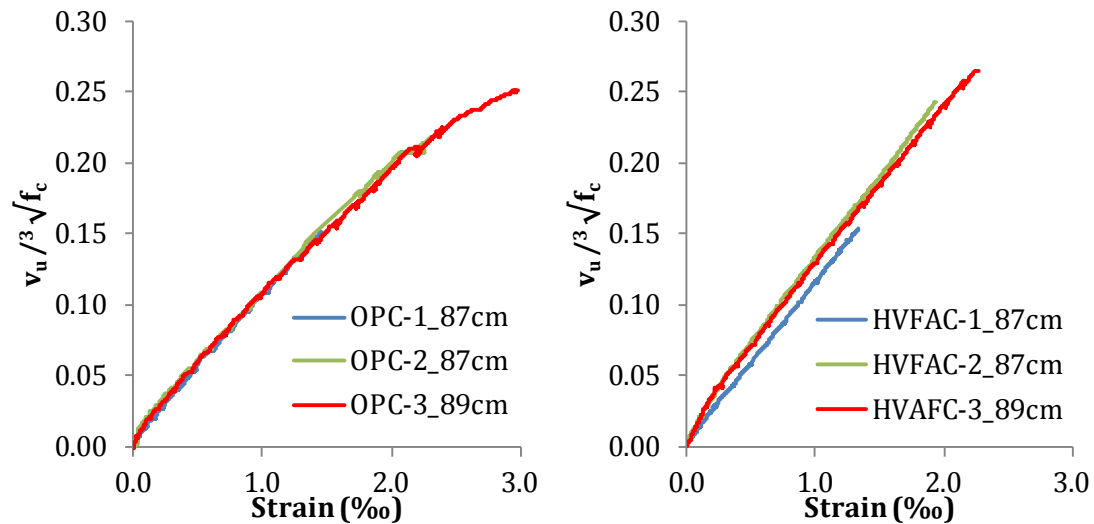


Figure 4.207 Effect of shear reinforcement ratio on longitudinal strains in section at 87(89)cm

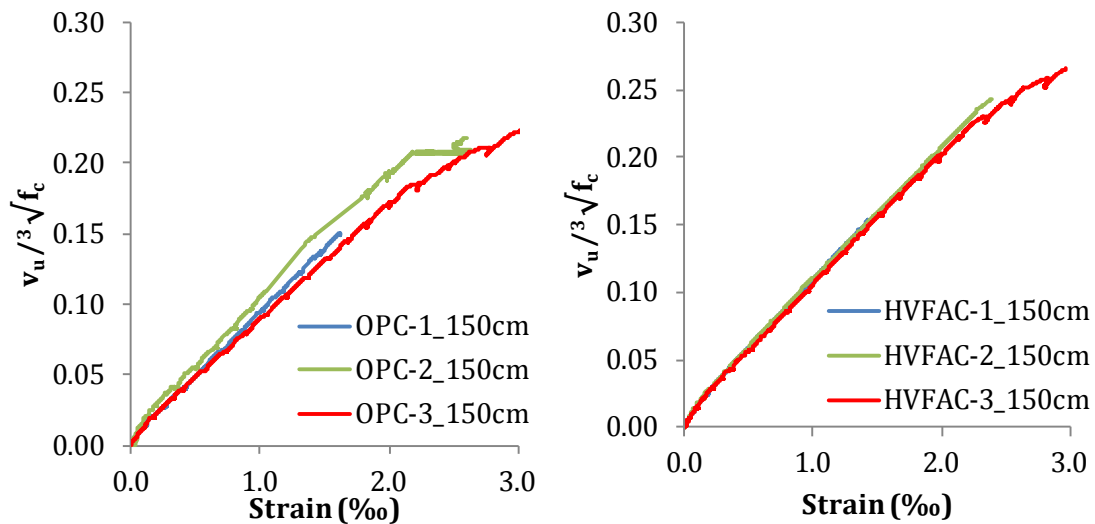


Figure 4.208 Effect of shear reinforcement ratio on longitudinal strains in section 150 cm

4.4.10. Shear reinforcement strains

The crack patterns and stirrups strain gauge layout on the front and back side of the beams with a minimum and higher reinforcement are presented in Figures 4.209 and 4.210, respectively. A different position of the strain gauges on stirrup legs was chosen in order to improve the possibility of the cracks propagating through the strain gauge, at least on one side of the beam. Crack patterns were drawn as precisely as possible based on the photographs taken during the testing, taking into account the beams' deformation. Since very short strain gauges in

4. Experimental program and test results

stirrups were used (10 mm), the crack patterns can help to approximately determine the distance of strain gauges from the cracks.

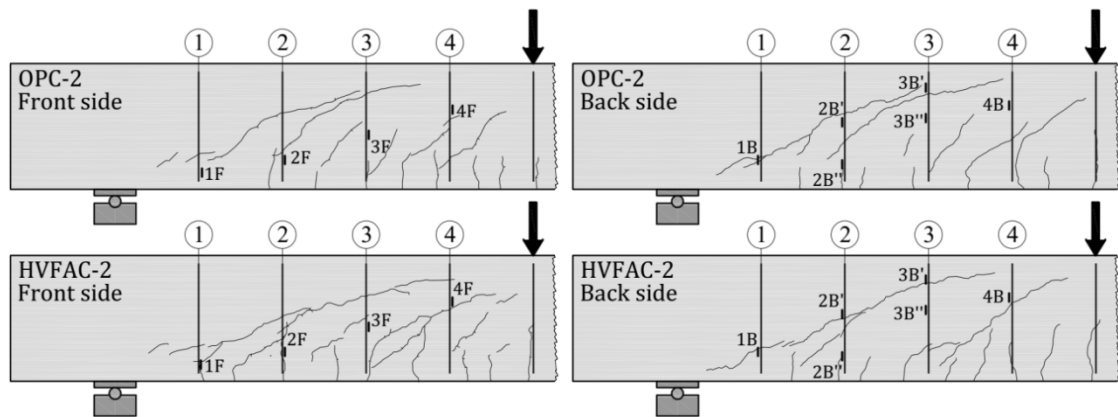


Figure 4.209 Crack patterns prior to failure in beams OPC-2 and HVFAC-2

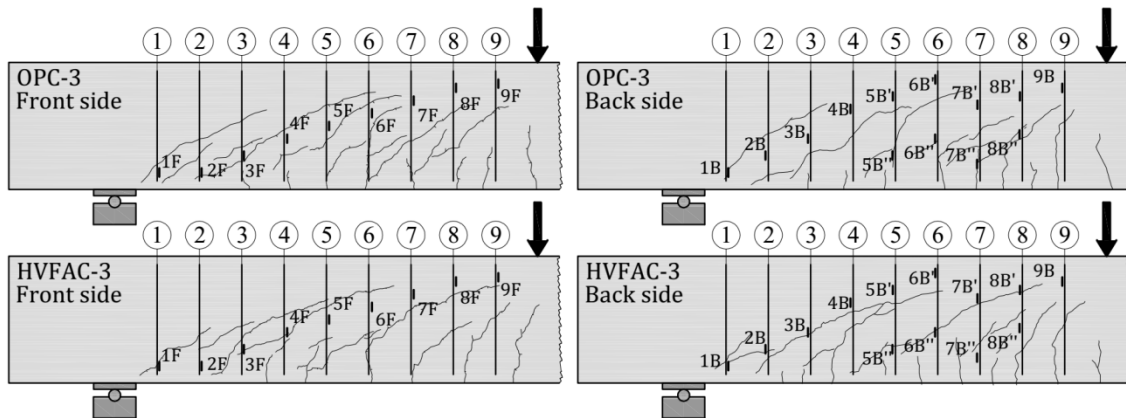


Figure 4.210 Crack patterns prior to failure in beams OPC-3 and HVFAC-3

The measured strains in all stirrups versus normalized shear stress are grouped based on cross sections and shown in Figures 4.211 and 4.212 for beams in group 2 and in Figures 4.213 - 4.216 for beams in group 3. The first shear crack formation and stirrups yield strain are marked in these figures. The yield strain of 1.75‰ was adopted based on the measured stress-strain diagram of the stirrups' steel shown in Table 4.27. The yielding strain of 1.75‰ is in agreement with the obtained measurements of the stirrups strains. The measured strains in stirrups are greatly affected by the distance between strain gauges and position of shear cracks. If the shear crack did not pass through strain gauge or close to it, its measurement could significantly differ from the one in the strain gauges directly intersected by the shear crack.

4. Experimental program and test results

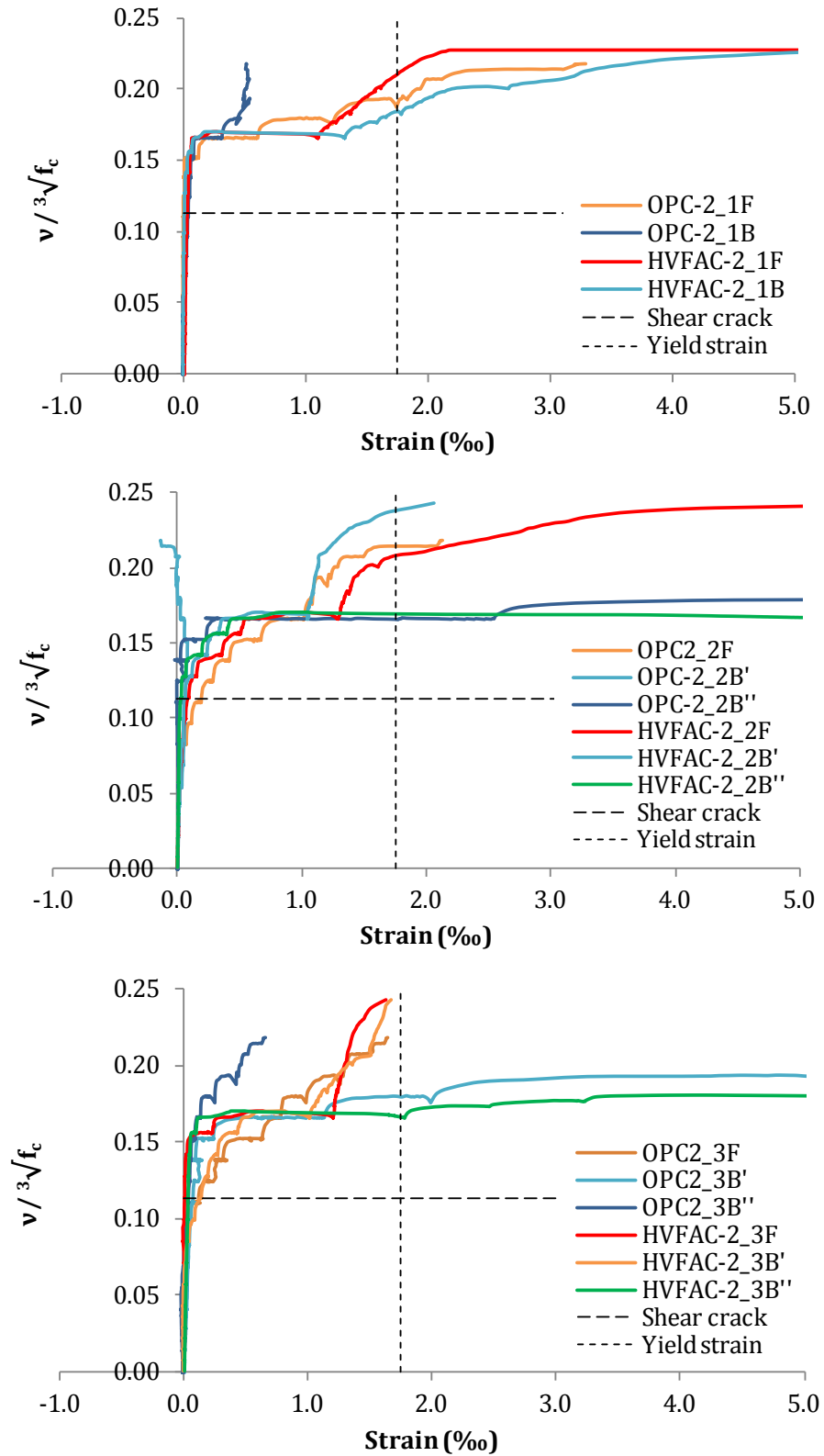


Figure 4.211 Strains in stirrups in beams OPC-2 and HVFAC-2 - sections 1, 2, and 3

4. Experimental program and test results

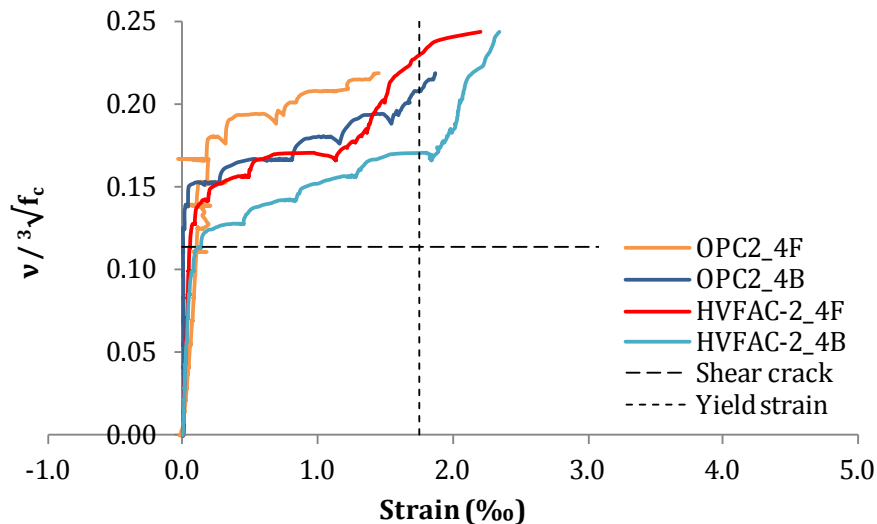


Figure 4.212 Strains in stirrups in beams OPC-2 and HVFAC-2 – section 4

It is important to compare the measured stirrups strains having in mind the shear crack propagation. Until the first shear crack formed no significant strains were noticed, stirrups were practically free of stresses before shear cracking, as expected. The same trend between the OPC2 and HVFAC beams and only small differences between strains in stirrups before yielding were noticed.

At failure load, most of the stirrups reached yielding point or a value close to it. In beams with a minimum longitudinal reinforcement ratio, the strain measurements that did not reach the yielding point were: OPC-2_1B, OPC-2_2B' and OPC-2_2B''. The strain measurements close to the yielding point were: OPC-2_3F, OPC-2_4F, HVFAC-2_3F and HVFAC-2_3B'. These measuring points were placed between the formed cracks or above them. For this strain gauge layout, more measuring strains reached yielding point in the HVFAC-2 beam compared with the OPC-2. For the same shear stress level, the HVFAC-2 beam stirrups reached higher strains compared with the OPC-2 beam.

The highest value of the strains was obtained in cross sections 2 and 3, with maximum strains higher in the HVFAC-2 beam compared with the OPC-2 beam. The stirrups reached the yielding point at approximately the same normalized shear stress level for both the OPC-2 and HVFAC-2 beams. In beams with a higher shear reinforcement ratio, even more measured strains did not reach a yielding point. All strains in the cross section 1 and 9 had maximum strains lower than

4. Experimental program and test results

1.75‰. This was mostly the consequence of the cross sections position: cross section 1 was only 100 mm distanced from the beam support and cross section 9 only 100 mm from loading point.

In beams with a higher reinforcement ratio, strain measurements that did not reach the yielding point were: OPC-3_8B', OPC-3_8B'' and HVFAC-3_6B'. Strain measurements close to the yielding point were: OPC-3_2F, OPC-3_2B, OPC-3_4F, OPC-3_5B', OPC-3_7F, OPC-3_7B', OPC-3_7B'', HVFAC-3_2F, HVFAC-3_5F and HVFAC-3_8B''. These measuring points were placed between the formed cracks or above them. Similar like in the beams with the minimum shear reinforcement, more measured strains reached the yielding point in the HVFAC-3 beam compared with the OPC-3 beam. For the same shear stress level, stirrups in HVFAC-3 beam reached higher strains compared with the OPC-3 beam.

The highest value of the strains was obtained in cross sections 3, 4, 5 and 6, with maximum strains higher in the HVFAC-3 beam compared with the OPC-3 beams. The stirrups reached the yielding point at approximately the same normalized shear stress level for both the OPC-3 and HVFAC-3 beams.

It is impossible to do an exact comparison of stirrup strains in the OPCC and HVFAC beams but some general conclusions can be made. The ultimate strains in stirrups for both groups of beams are given in Figures 4.217 and 4.218.

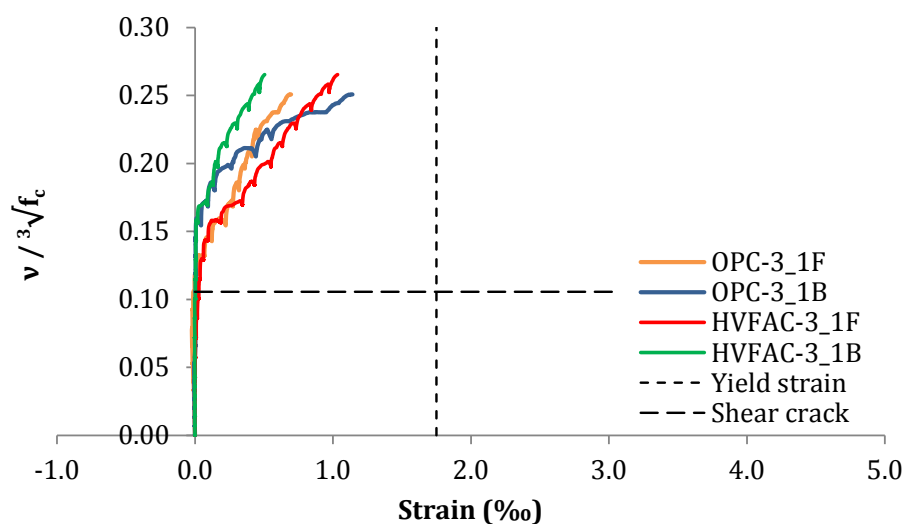


Figure 4.213 Strains in stirrups in beams OPC-3 and HVAF3-3 in section 1

4. Experimental program and test results

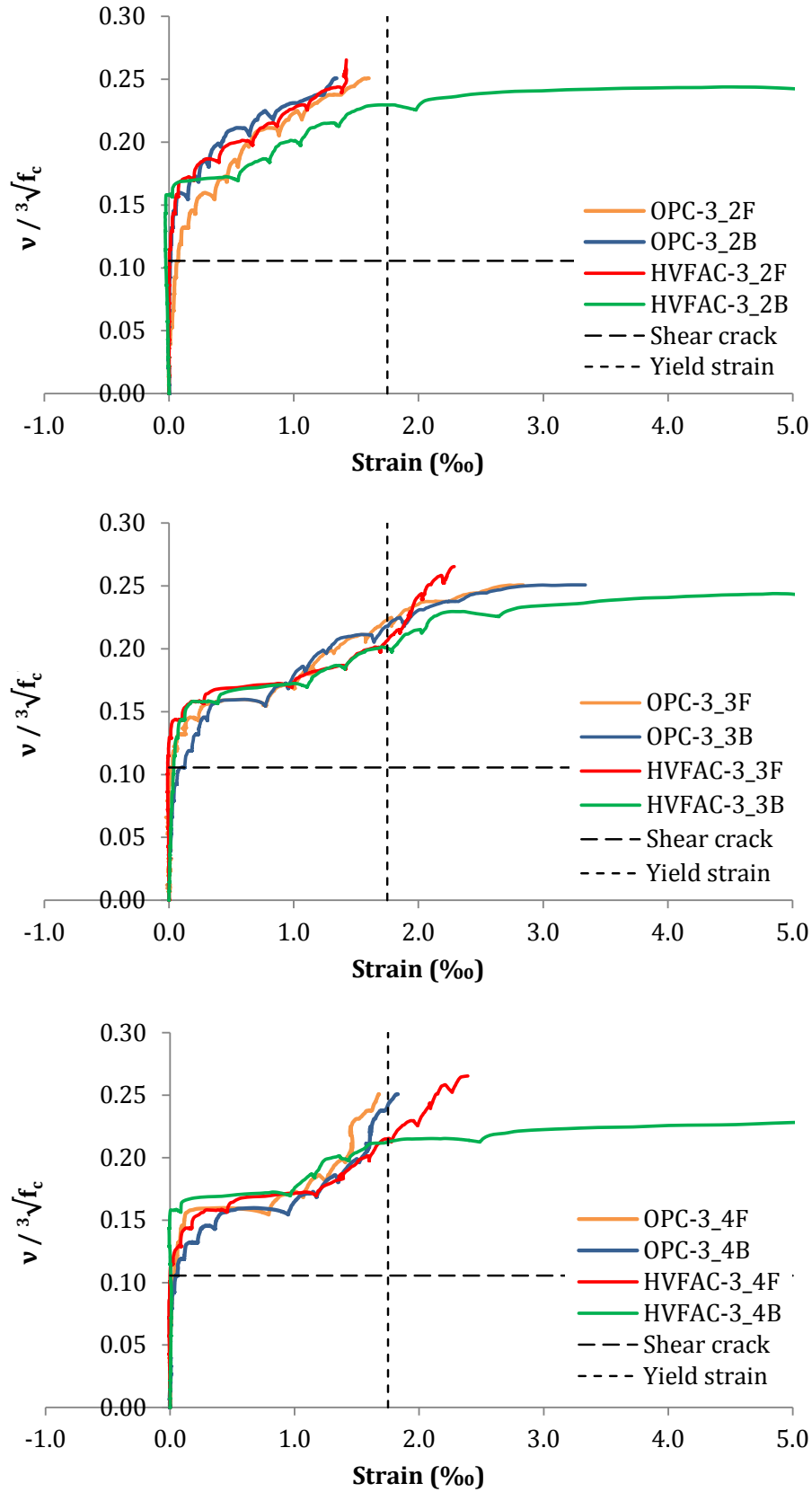


Figure 4.214 Strains in stirrups in beams OPC-3 and HVFAC-3 in sections 2, 3, and 4

4. Experimental program and test results

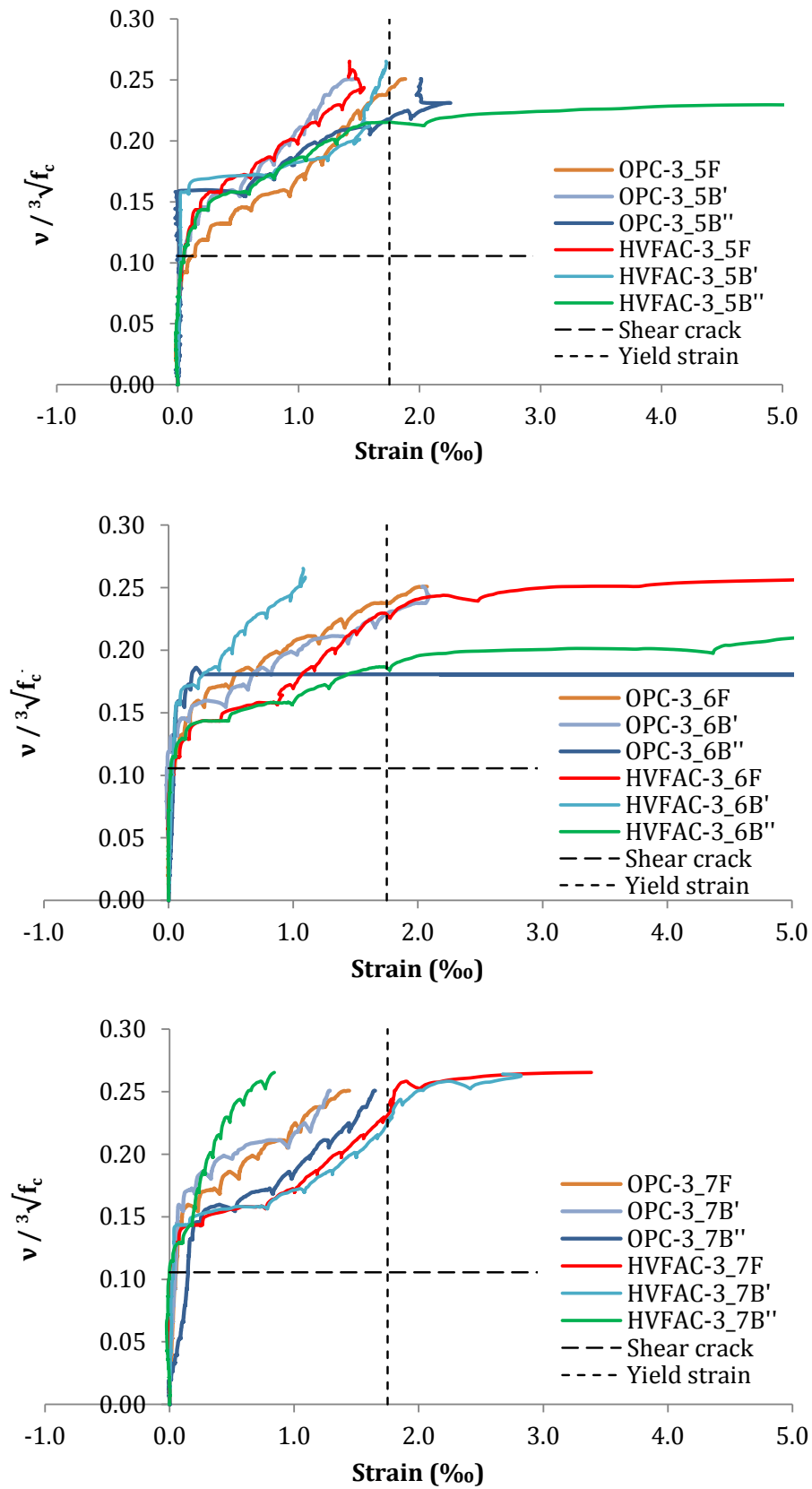


Figure 4.215 Strains in stirrups in beams OPC-3 and HVFAC-3 in sections 5, 6 and 7

4. Experimental program and test results

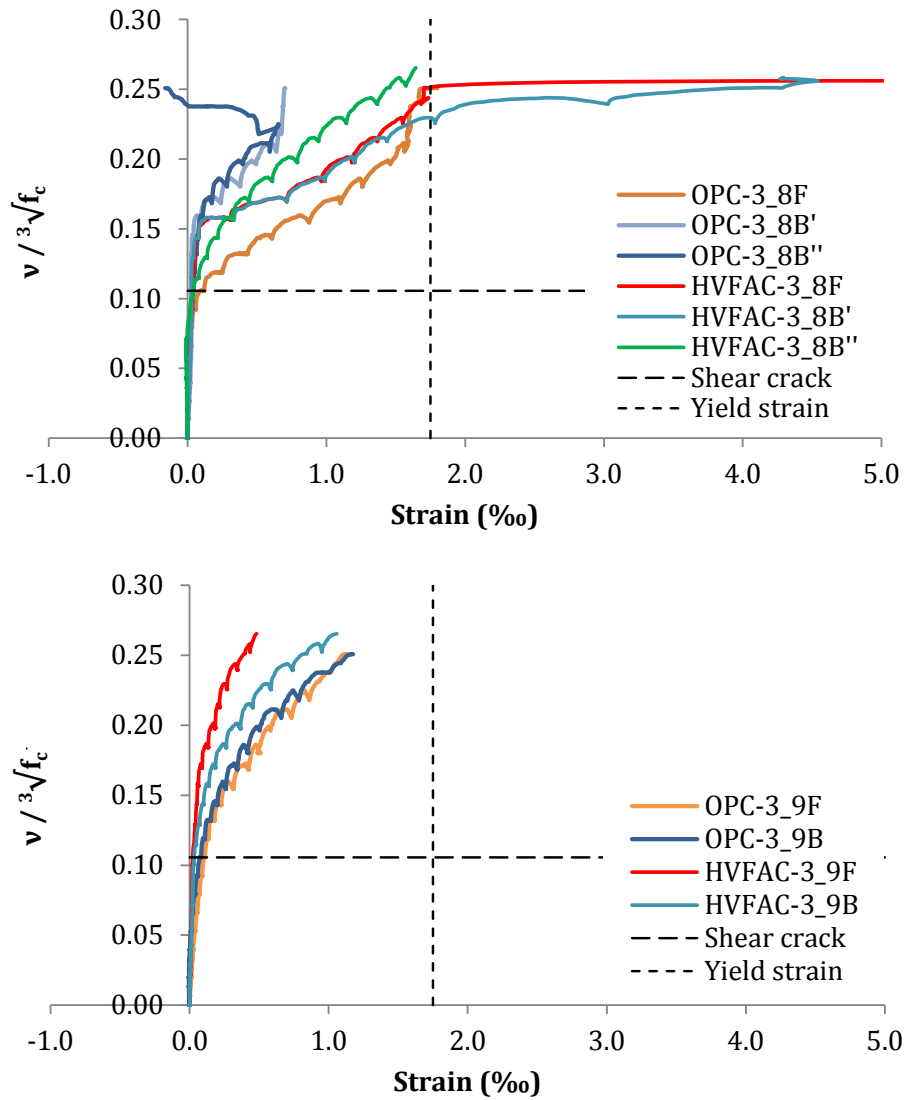


Figure 4.216 Strains in stirrups in beams OPC-3 and HVAF3-3 in sections 8 and 9

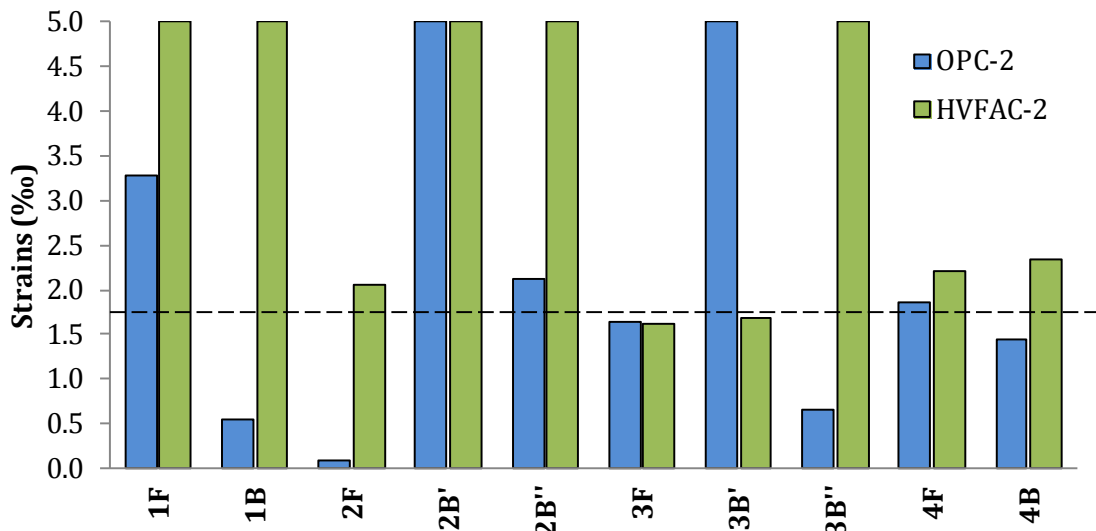


Figure 4.217 Maximum stirrups strains in beams from group 2

4. Experimental program and test results

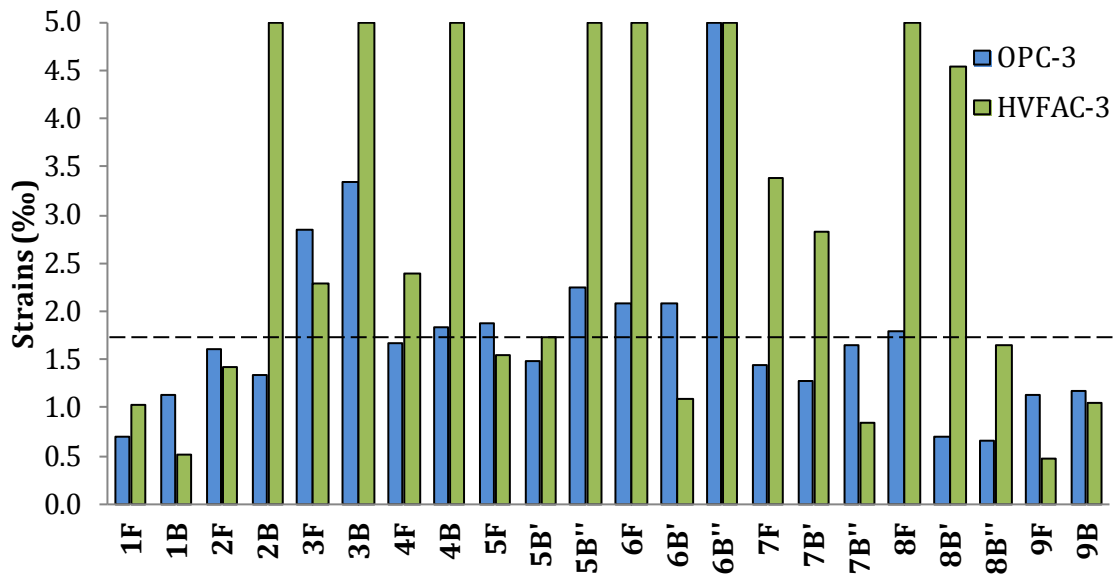


Figure 4.218 Maximum stirrups strains in beams from group 3

Only strain values up to 5‰ are displayed for clarity reasons. In both cases a general trend is showing higher stirrups strains in the HVFAC beams compared with the OPCC ones. This leads to a conclusion that some other components of shear transference mechanism may be lower in the HVFAC beams compared with the OPCC ones.

The shear transfer mechanism after cracking is based on the bearing capacity of stirrups, the uncracked concrete zone at the head of the shear crack, the aggregate interlock action and the dowel effect. The yielding of stirrups was achieved in all cross sections in beams with a minimum shear reinforcement. In beams with a higher reinforcement, the yielding of stirrups was not achieved in cross sections 1 and 9 in beams OPC-3 and HVFCA-3 due to the cross section position, but also in sections 2 and 7 in the HVFAC-3 beam. The lower strains in the OPC-3 beam can be seen as a consequence of different failure modes, caused by the dominant bending effect in the OPC-3 beam. Nevertheless, the strains in the stirrups were lower for the OPCC in both groups of beams.

The compressive strength of the OPCC was higher than the HVFAC for 7% and 22% for the beams in group 2 and group 3 respectively. The difference between the OPC-3 and HVFAC-3 beam compressive strength on drilled cores after 114 days was significantly lower (8%) and in the favor of the HVFAC beam. Diagrams

4. Experimental program and test results

showing strains in stirrups versus normalized shear stress calculated with the measured drilled cores compressive strength are shown in Figures 4.219 – 4.221. It can be seen that no significant difference exist except even higher strains in the HVFAC-3 beam compared with the OPC-3 beam. In beams OPC-2, HVAFC-2 and HVFAC-3 failure occurred in the direction of the main diagonal cracking along with crushing of concrete in the vicinity of the load. Having all this in mind, it can be concluded that the compressive strength of the OPCC and HVFAC beams was similar in both groups of tested beams; hence, the capacity of the uncracked concrete was not significantly different.

The uncracked concrete at the head of the shear crack contributes to shear bearing capacity after cracking along with stirrups. In beams with the minimum shear reinforcement the yielding of stirrups started at the normalized shear stress value of around 0.200, while failure corresponded to the stress level of approximately 0.218 and 0.243 for the OPC-2 and HVFAC-2 beams, respectively. In the OPC-3 and HVFAC-3 beams the yielding of stirrups started at the normalized shear stress value of around 0.240, while failure corresponded to the stress level of approximately 0.251 and 0.266 for the OPC-3 and HVFAC-3 beams, respectively. For beams with a minimum reinforcement, the load increase after the stirrups yielding was around 10% and 20% for the OPC-2 and HVFAC-2 beams respectively. For beams with higher shear reinforcement, load increase after stirrups yielding was around 5% and 10% for the OPC-3 and HVFAC-3 beams respectively.

It can be assumed that the dowel effect was similar in all beams owing to the same longitudinal and shear reinforcement ratio. Splitting cracks along the longitudinal reinforcement prior to failure were not noticed in any of the tested beams. Shear cracks propagated with the less inclined angle close to the support, but no longitudinal cracks in the anchorage zone were noticed. This is in agreement with the results from literature showing similar bond strength of HVFAC compared with OPCC (Arezoumandi, Looney and Volz, 2015).

The last shear transfer component that can be different in OPCC and HVFAC is the aggregate interlock effect. Based on everything previously stated, it can be concluded that the aggregate interlock was less effective in tested HVFAC beams.

4. Experimental program and test results

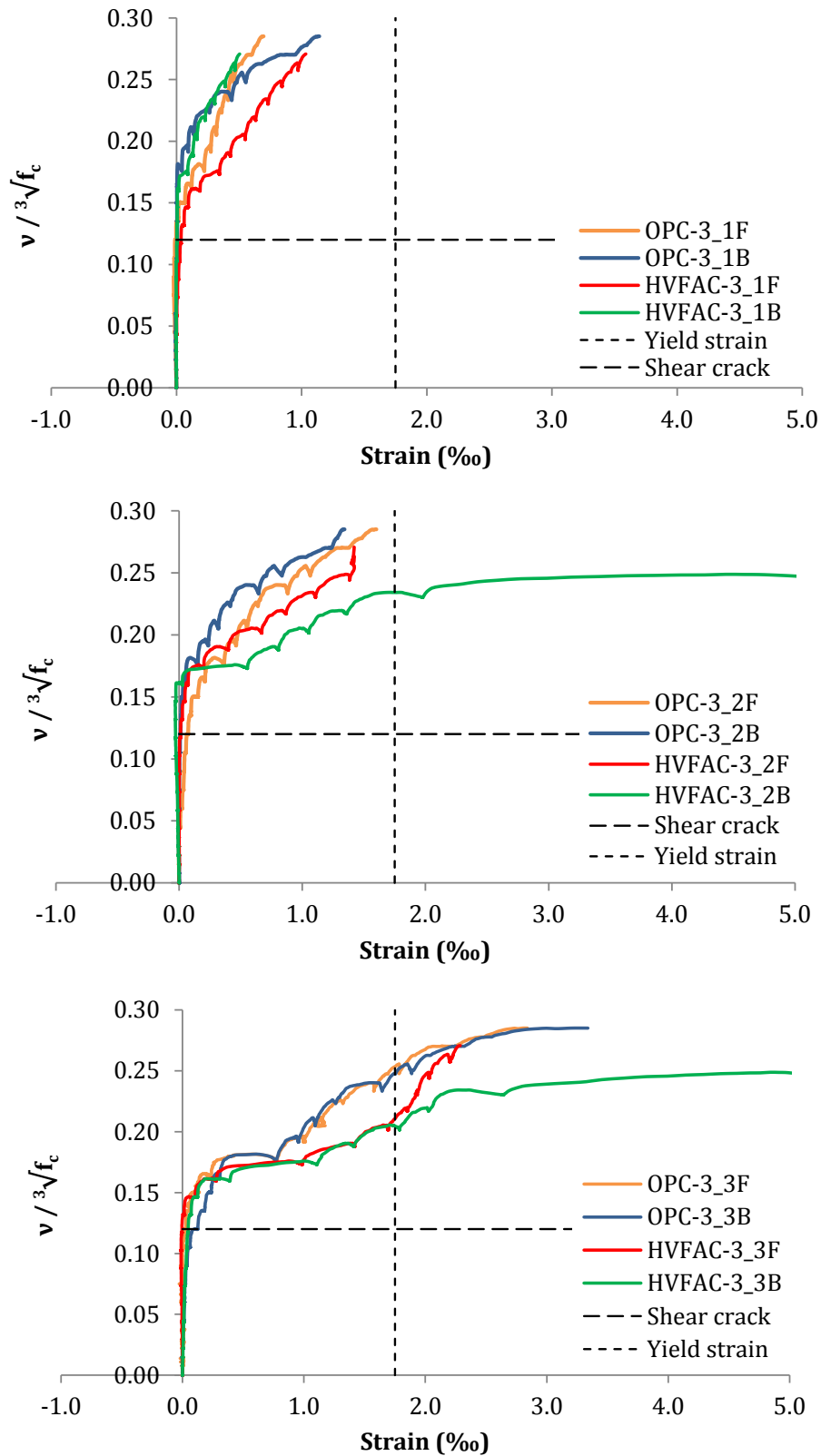


Figure 4.219 Stirrups strains in beams OPC-3 and HVFAC-3 in sections 1, 2 and 3 versus shear stress normalized with drilled core compressive strength

4. Experimental program and test results

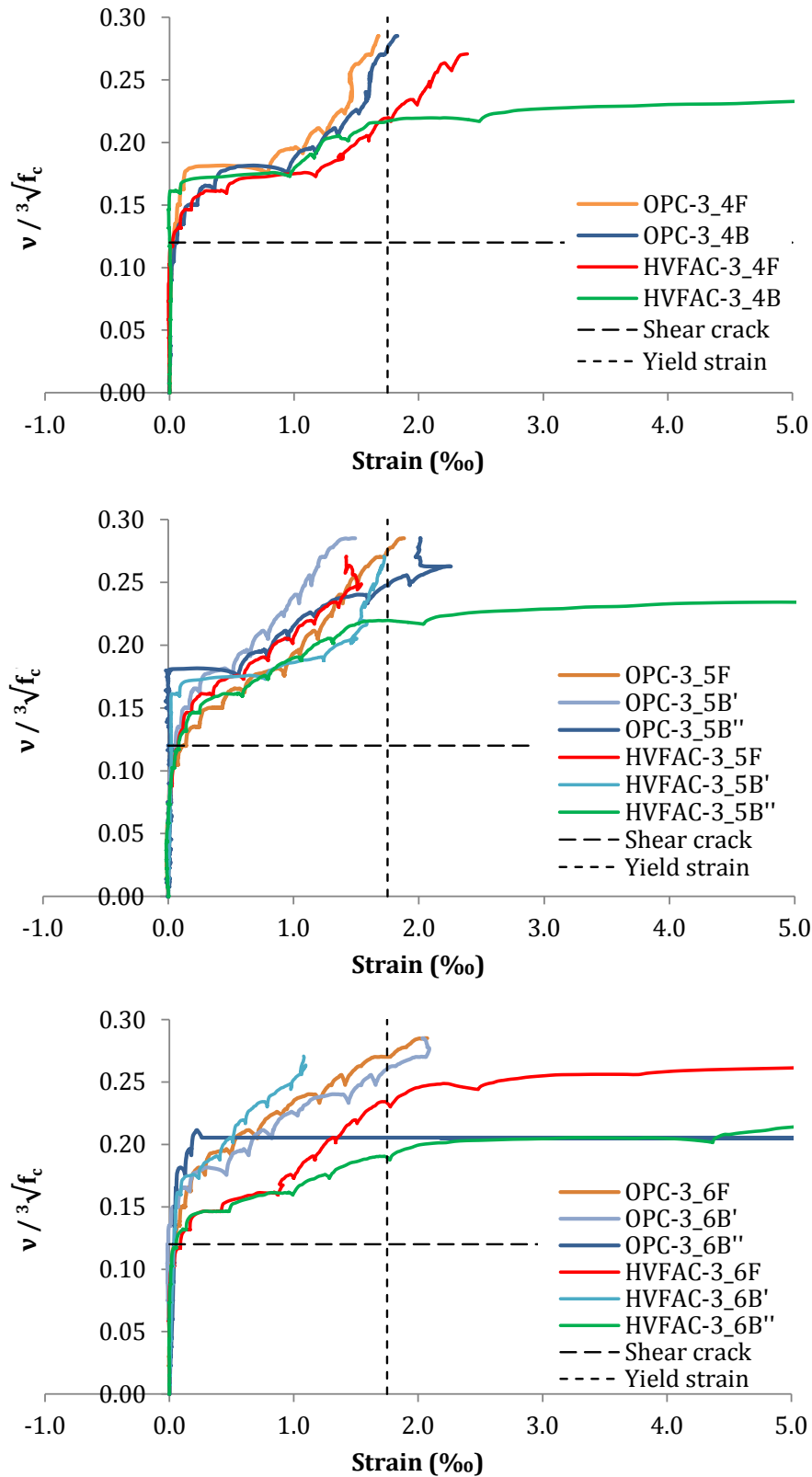


Figure 4.220 Stirrups strains in beams OPC-3 and HVFAC-3 in sections 4, 5 and 6 versus shear stress normalized with drilled core compressive strength

4. Experimental program and test results

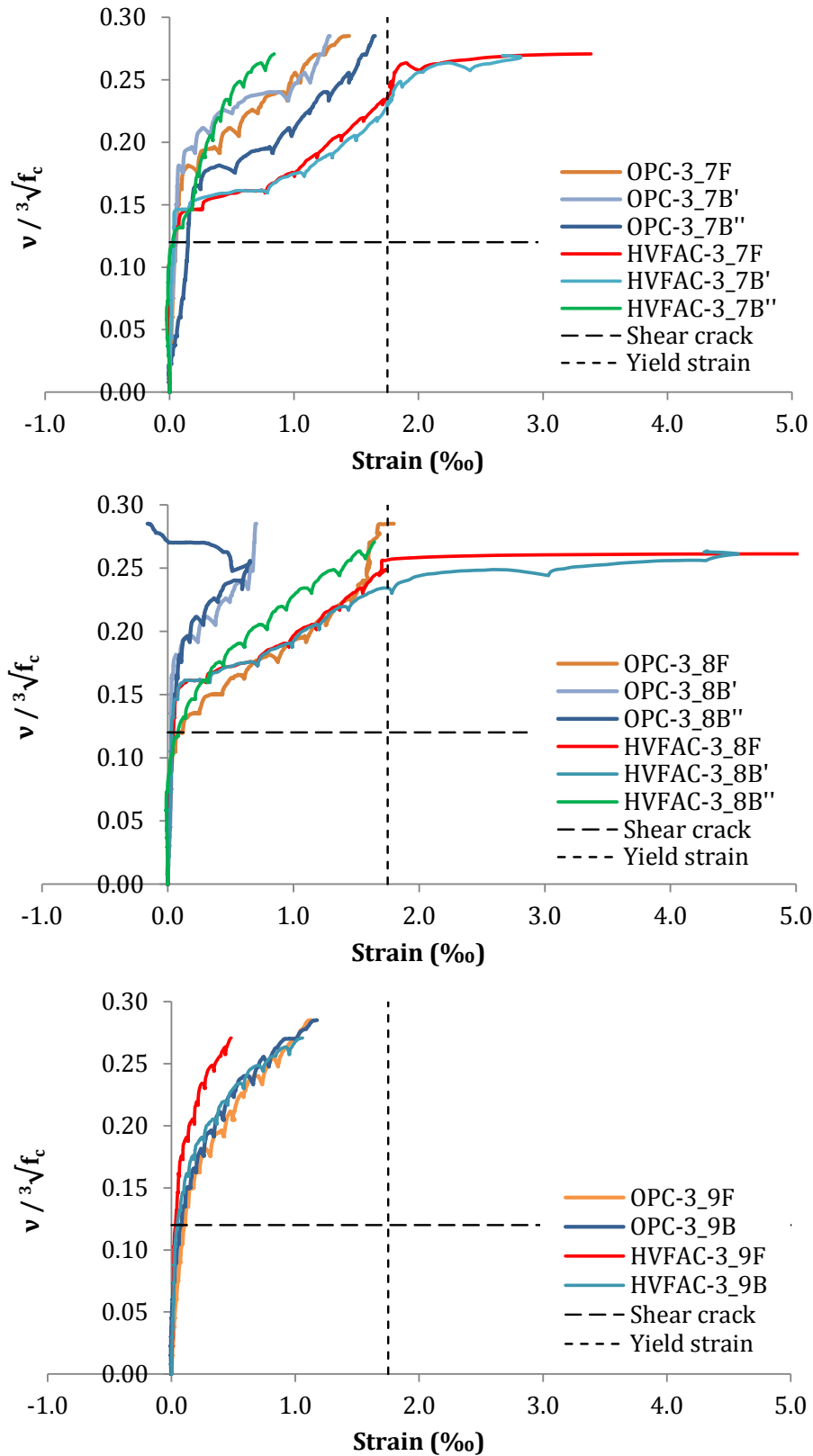


Figure 4.221 Stirrups strains in beams OPC-3 and HVFAC-3 in sections 7, 8 and 9 versus shear stress normalized with drilled core compressive strength

4. Experimental program and test results

The specific weight of FA used for HVFAC production was 46.5% lower compared with the specific weight of cement. This led to about 20% lower aggregate volume used for HVFAC production compared with OPCC. The volume of the fine aggregate was similar in both concrete mixtures, but 12.4% and 29.9% less volume of the coarse aggregate 4/8 mm and 8/16 mm was used in HVFAC compared with OPCC, respectively. The HVFAC mixtures prepared in this way had higher paste content and lower aggregate volume resulting in potentially reduced aggregate interlock effect.

Shear reinforcement has practically no effect before the shear crack formation. After the shear cracks develop, stirrups participate in the shear transfer directly with the bearing capacity of the bars crossing the shear crack. Indirectly, stirrups reduce the crack penetration into the concrete compression zone leaving more uncracked concrete at the head of the crack; shear reinforcement reduces crack widening and improves the aggregate interlock effect; stirrups help reduce the splitting of concrete along the longitudinal reinforcement improving the dowels effect. It can be assumed that the behavior of beams with stirrups is similar to the beams without shear reinforcement up to shear cracking. After this point, the part of the shear carried by the stirrups is increasing linearly, while the sum of other three shear components stays approximately constant (ASCE-ACI 426, 1973). The ultimate shear force (V_u) that can be carried is the sum of the force carried by stirrups (V_s) and the contribution of concrete (V_c). Force carried by stirrups is the vertical force calculated as:

$$V_s = n \cdot A_{sw} \cdot f_{ywd} \text{ (kN)} \quad \text{Eq. 4. 4}$$

where:

n number of stirrups intersected by the main shear crack;

A_{sw} cross section area of stirrups (cm^2);

f_{ywd} yield stress in stirrups (kN/cm^2).

The number of stirrups transferring the main shear crack was determined based on the crack patterns in beams OPC-2, HVFCA-2 and HVFAC-3 shown in Figure 4.222a. In beams with the minimum shear reinforcement, three out of four stirrups

4. Experimental program and test results

in shear span intersected the main shear crack. In the HVFAC-3 beam five out of nine stirrups intersected the main shear crack.

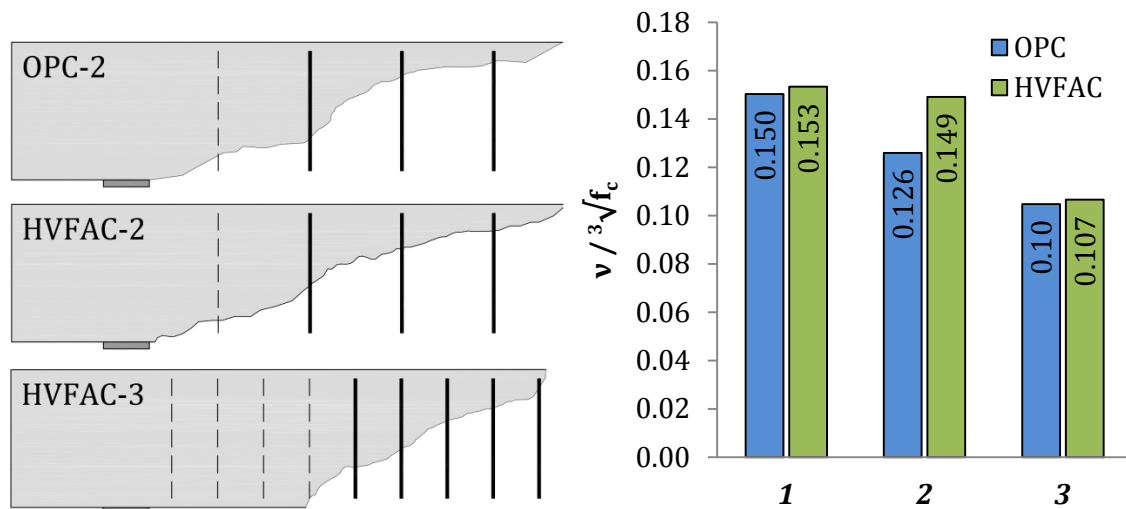


Figure 4.222 a) Stirrups intersecting the main shear crack, b) normalized shear stress carried by concrete

In all selected stirrups yielding point was achieved and stress of 36.25 kN/cm² was used in calculations. It was calculated that about 42% and 39% of the failure load was resisted by stirrups in the OPC-2 and HVFAC-2 beams. In the beams from group three, about 58% and 60% of the failure load was resisted by stirrups in the OPC-3 and HVFAC-3 beams. Beam OPC-3 exhibited a flexural failure and the part of the force resisted by stirrups is calculated with the assumption that the same number of stirrups as the number in the HVFAC-3 beam participated in the shear transfer. This assumption was based on the similar crack patterns in the OPC-3 and HVFAC-3 beams in the tested shear span. The contribution of concrete was calculated by subtracting the ultimate shear force and the force carried by stirrups with the results shown in Figure 4.222b. It can be seen that the concrete contribution was around 16% higher in the HVFAC-2 beam compared with the OPC-2, and only 2% in the case of the beams from group three. The concrete contribution to the shear resistance in beams with stirrups was lower than the shear resistance of beams without shear reinforcement for 16%, 3%, 30% and 32% for the OPC-2, HVFAC-2, OPC-3 and HVFAC-3 beams, respectively.

4. Experimental program and test results

4.4.11. Concrete strains

Concrete compressive strains versus normalized shear stress in six VWSG sensors (V1-V6) are shown in Figures 4.223 and 4.224 for the OPC-1 and HVFAC-1 beams respectively. Measured concrete strains on the front and on the back side were in agreement with the slightly higher concrete strains measured on the back side of the beam. The highest concrete strains were noticed in the section in the middle of the beam for the OPC-1 beam and for the section at 113 cm for the HVFAC-1 beam. In order to compare the concrete strains in the OPC-1 and HVFAC-1 beams, diagrams with the average value of measured strains in sections at 87 cm (V1 and V2), 113 cm (V3 and V4), 100 cm (V8) and 150 cm (V5 and V6) are shown for both beams in Figures 4.225 and 4.226. Concrete strains in the HVFAC-1 beam were the same or lower compared with the OPC-1 until the formation of shear crack for all sections except midpoint measurement. In the midpoint section (150 cm), concrete strains in the HVFAC-1 were the same like those in the OPC-1 beam approximately until the formation of the flexural crack. After that point, the OPC-1 concrete strains exceeded the HVFAC-1 ones for the same normalized shear stress values. The ultimate concrete strains were higher in the OPCC in measured cross sections.

The control of the concrete strains under the loading point in three orthogonal directions, perpendicular to the beam axis (V7), parallel to the beam axis (V8) and in the load direction (V9) was done and the results are plotted in Figure 4.227 for the OPC-1 and HVFAC-1 beams. In the V7 direction, tension strains up to 0.1‰ and 0.3‰ developed for the OPC-1 and HVFAC-1 beams respectively. In the OPC-1 beam, practically no strains in the direction of the load application developed. In the HVFAC-1 beam, in this direction, compressive strains up to 0.15‰ were reached. Given that strains V7 are in tension for both beams, maximum compressive strains are not significantly high and range between 1.2‰ and 1.4‰.

The concrete compressive strains versus the normalized shear stress for beams with stirrups are shown in Figures 4.228 - 4.231. It can be seen that concrete strains increase along with the loading for all measured sections until failure with the exception of the V1 and V2 measuring points in the first cross section (74 cm) for beams HVFAC-2 and HVFAC-3.

4. Experimental program and test results

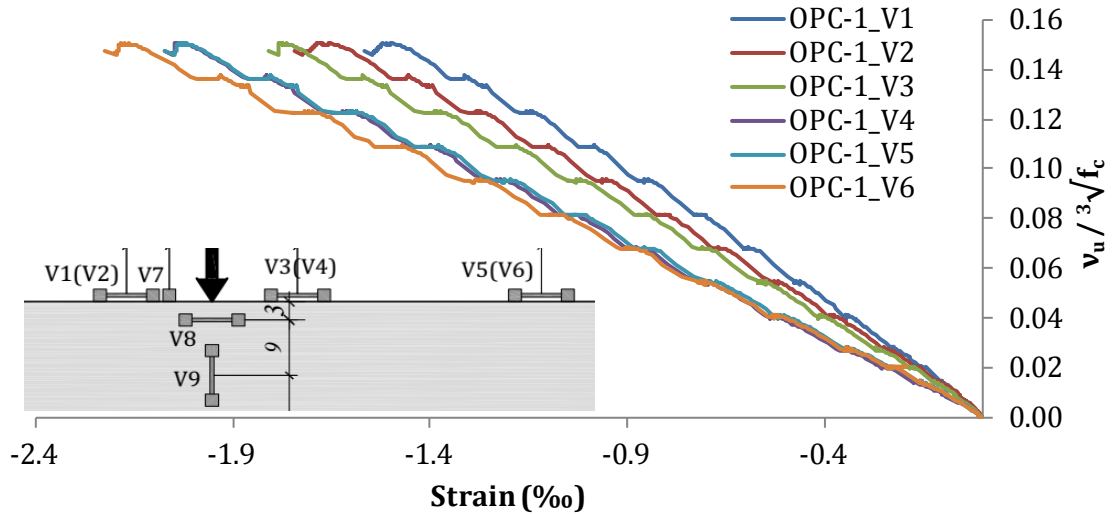


Figure 4.223 Concrete strains in VWSG sensors V1-V6 for the OPC-1 beam

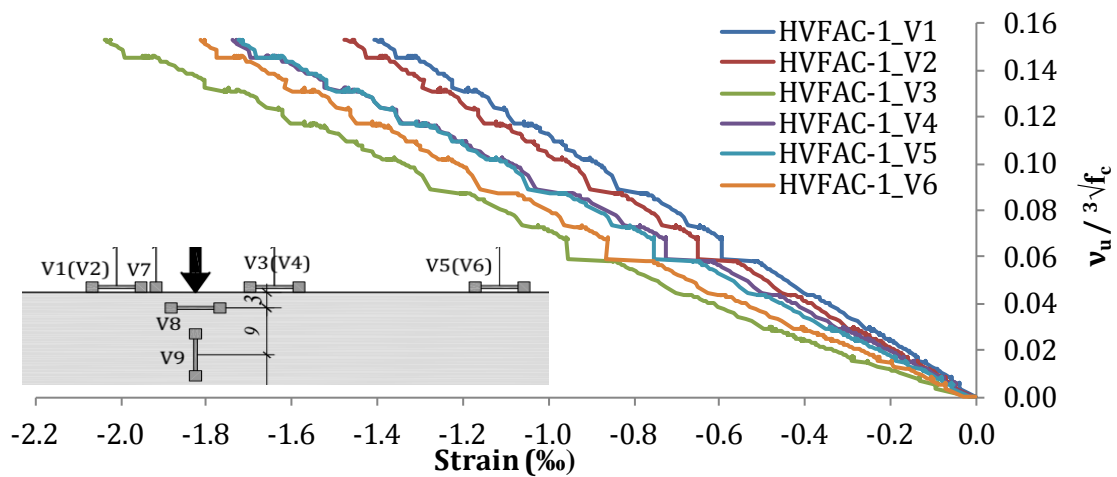


Figure 4.224 Concrete strains in VWSG sensors V1-V6 for the HVFAC-1 beam

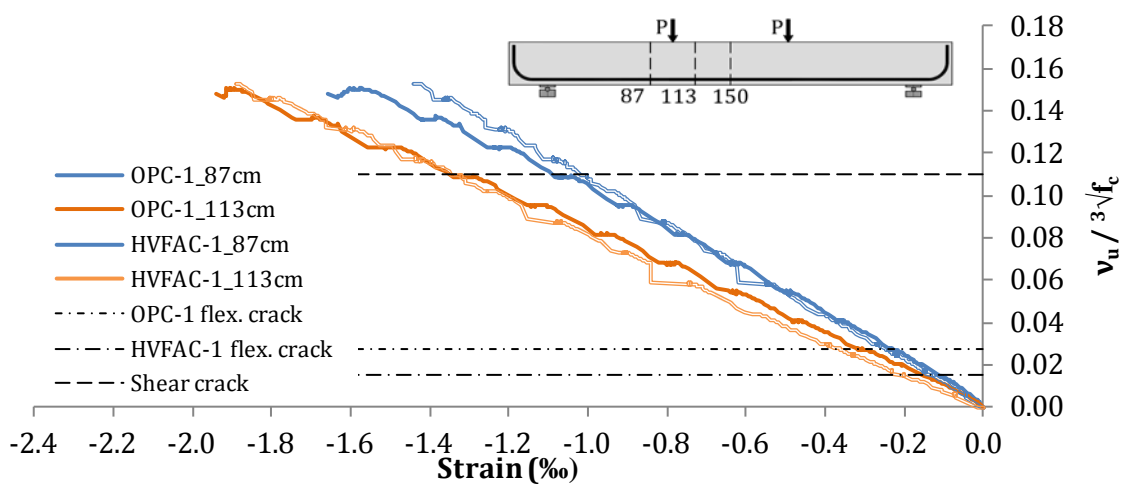


Figure 4.225 Concrete strains in sections at 87 and 113 cm for the OPC-1 and HVFAC-1 beams

4. Experimental program and test results

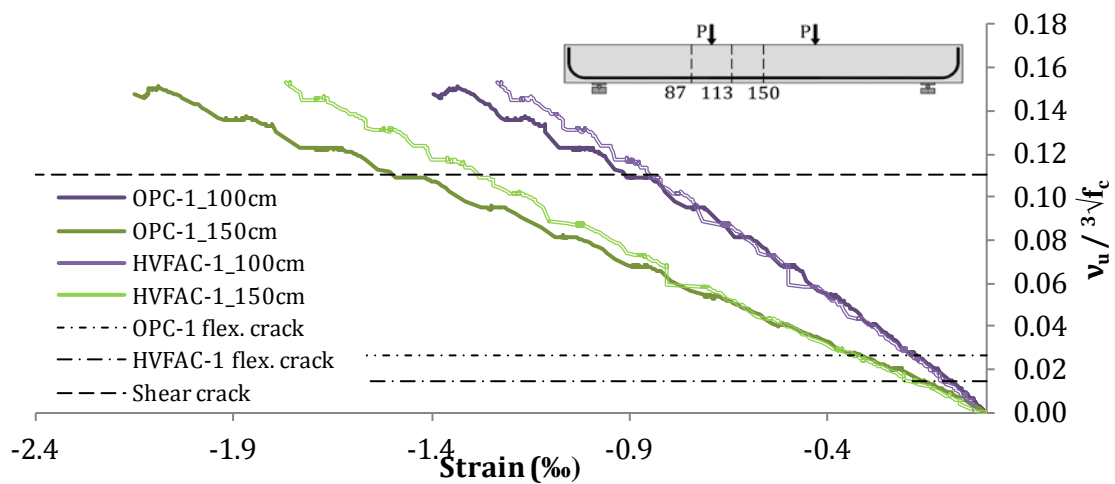


Figure 4.226 Concrete strains in sections at 100 and 150 cm for the OPC-1 and HVFAC-1 beams

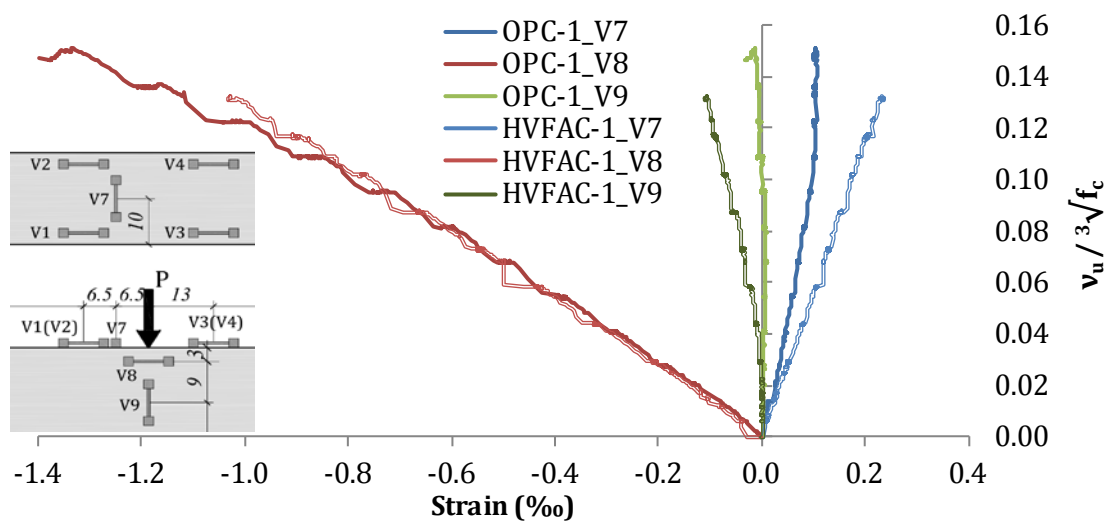


Figure 4.227 Concrete strains in V7, V8 and V9 for the OPC-1 and HVFAC-1 beams

Measured concrete strains on the front and on the back side are in agreement with the slightly higher concrete strains measured on the front side for the OPC-2, OPC-3 and HVFAC-3 beams. Concrete strains were similar or higher on the back side of the HVFAC-2 beam.

The maximum strains were the highest in the beams' midpoint for the OPC-2 and HVFAC-3 beams; the section on the right side of loading point for the HVFAC-2 beam; the measuring section under the loading point for the OPC-3 beam. Diagrams with the average value of measured strains for both groups of beams

4. Experimental program and test results

with stirrups are shown in Figures 4.232 – 4.235. Concrete strains in the HVFAC-2 beams were the same or lower compared with the OPC-2 until the formation of the shear crack. After that point, the OPCC beam strains exceeded concrete strains in HVFAC beam for the same normalized shear stress. In beams with a higher shear reinforcement ratio, concrete strains were similar for both OPCC and HVFAC only up to the first flexural cracking. After that point the OPC-3 concrete strains exceeded the HVFAC-3 ones for the same normalized shear stress values in all cross sections.

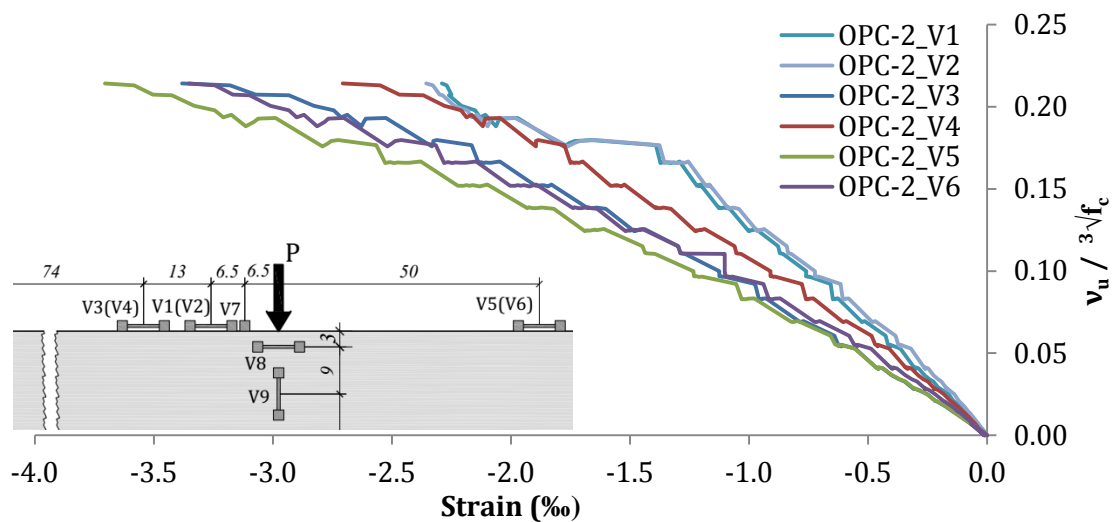


Figure 4.228 Concrete strains in VWSG sensors V1-V6 for the OPC-2 beam

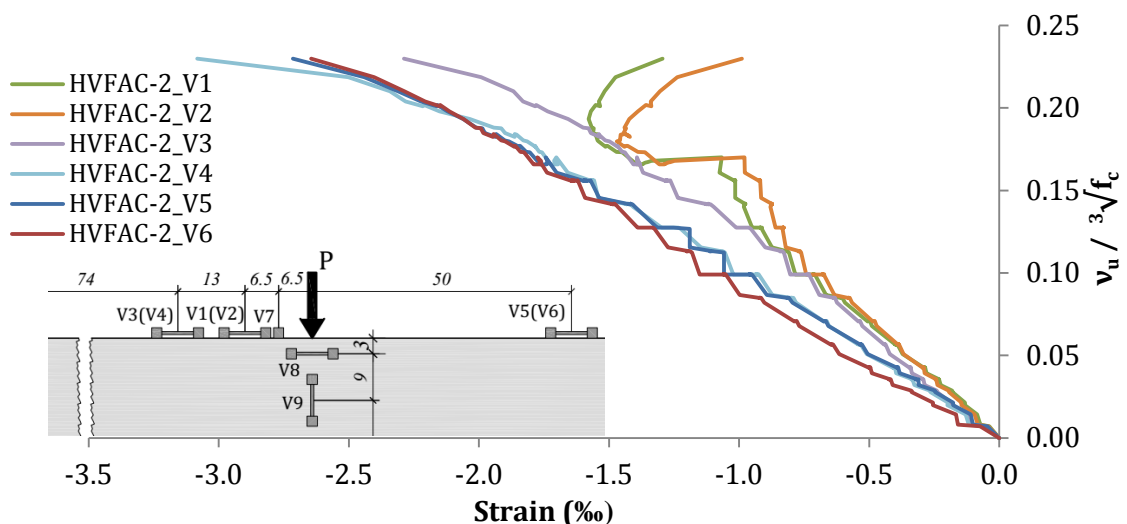


Figure 4.229 Concrete strains in VWSG sensors V1-V6 for the HVFAC-2 beam

4. Experimental program and test results

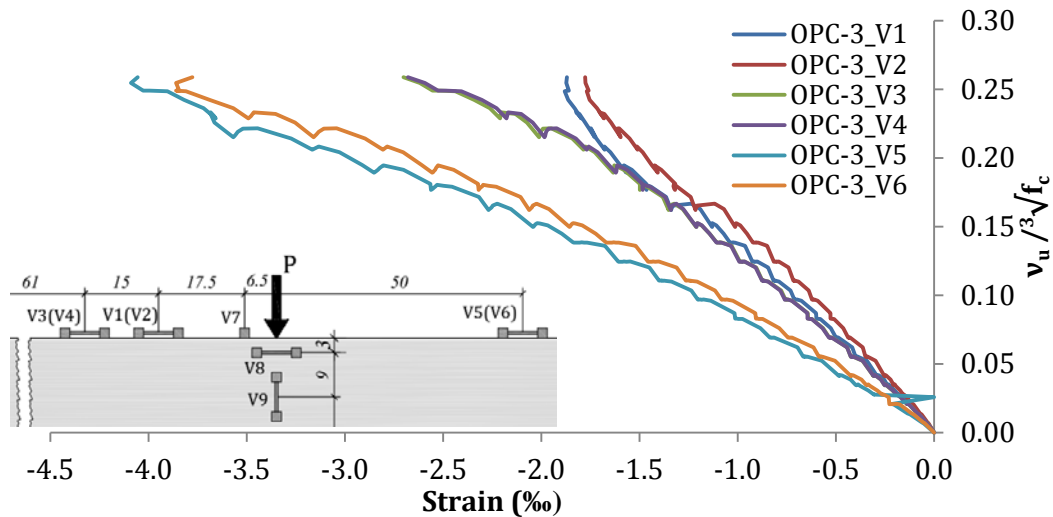


Figure 4.230 Concrete strains in VWSG sensors V1-V6 for the OPC-3 beam

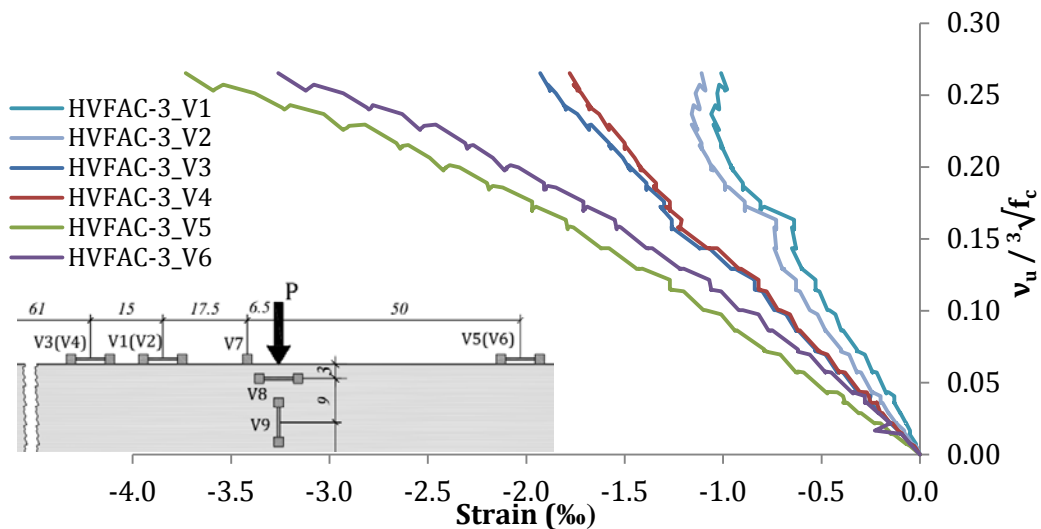


Figure 4.231 Concrete strains in VWSG sensors V1-V6 for HVFAC-3 beam

In the first cross section at 74 cm compressive strains started to decrease in both HVFAC-2 and HVFAC-3 beams at the load close to failure. This effect is noticed in similar beam testing found in literature (Ignjatović, Marinković and Tošić, 2017). Compressive strain decrease with load increase in sections close to the shear span midpoint suggests the existence of one type of an arching action by developing an elbow-shaped strut that deviates the compression strut to avoid the cracks (Muttoni and Fernández Ruiz, 2008) as shown in Figure 4.236.

The development of the elbow-shaped strut strongly depends on the actual crack pattern resulting in the formation of tension ties in the area of the first section of concrete strain measurements (Figure 4.236a). In beams without shear

4. Experimental program and test results

reinforcement the first measuring section was at 87 cm from the support and out of the mentioned zone. Therefore, it cannot be said with certainty that this phenomenon was not also present in beams without stirrups. In the HVFAC beams with stirrups, the compressive strength at that point started to decrease closely after the first shear crack appeared. In the OPCC beams this effect was not noticed indicating that a direct strut or a combination of the two formed (Figure 4.236a). A direct strut can be formed if the aggregate interlock is effective (Muttoni and Fernández Ruiz, 2008), leading to a conclusion that the OPCC beams may have a stronger aggregate interlock effect compared with the HVFAC beams.

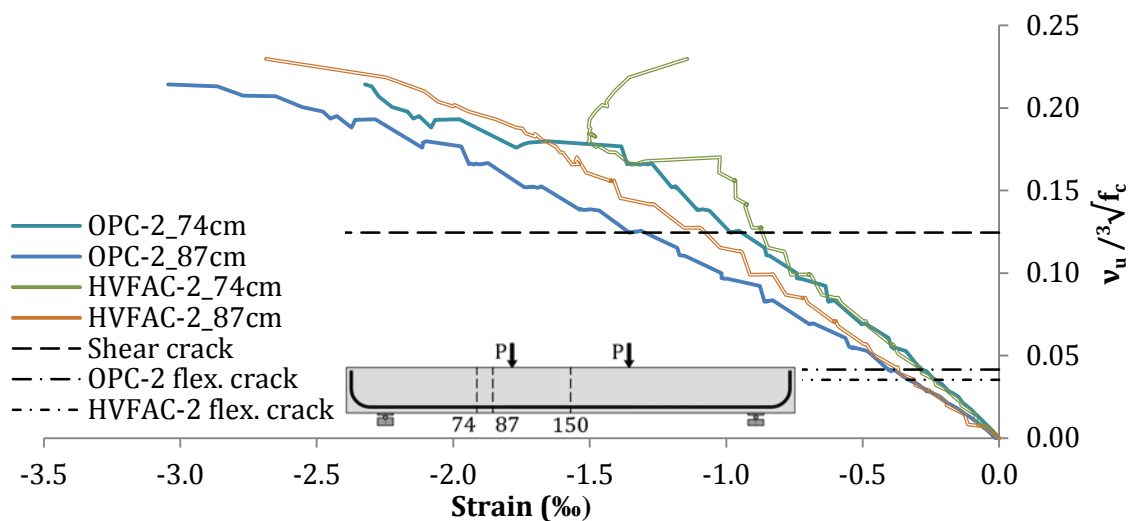


Figure 4.232 Concrete strains in sections 74 cm and 87 cm for beams in group 2

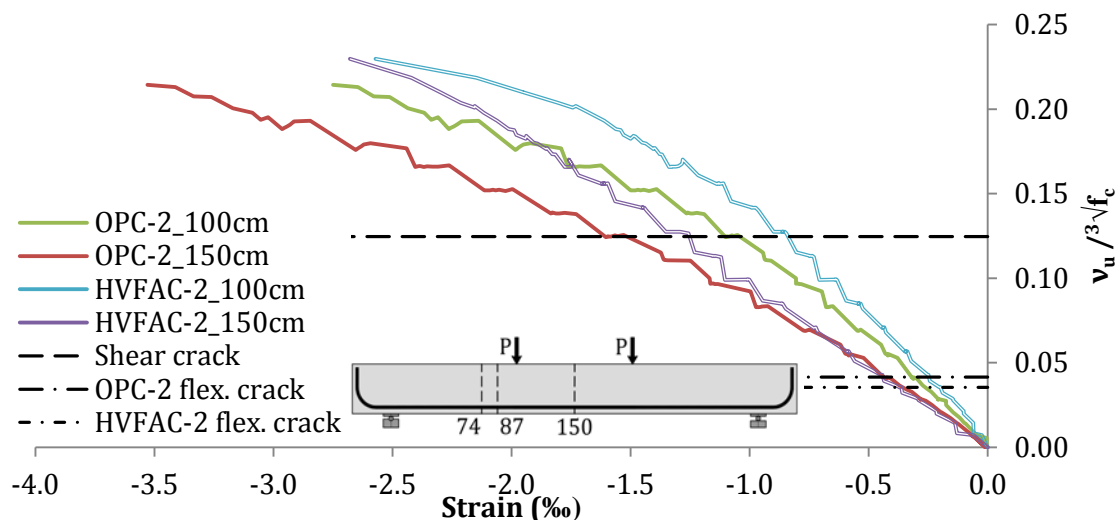


Figure 4.233 Concrete strains in sections 100 cm and 150 cm for beams in group 2

4. Experimental program and test results

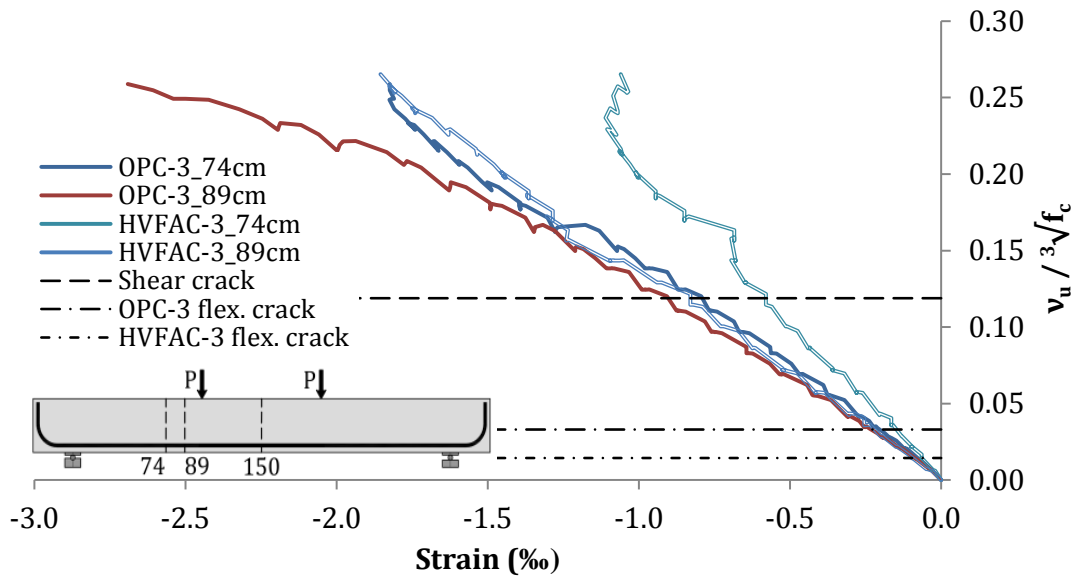


Figure 4.234 Concrete strains in sections 74cm and 89cm for beams in group 3

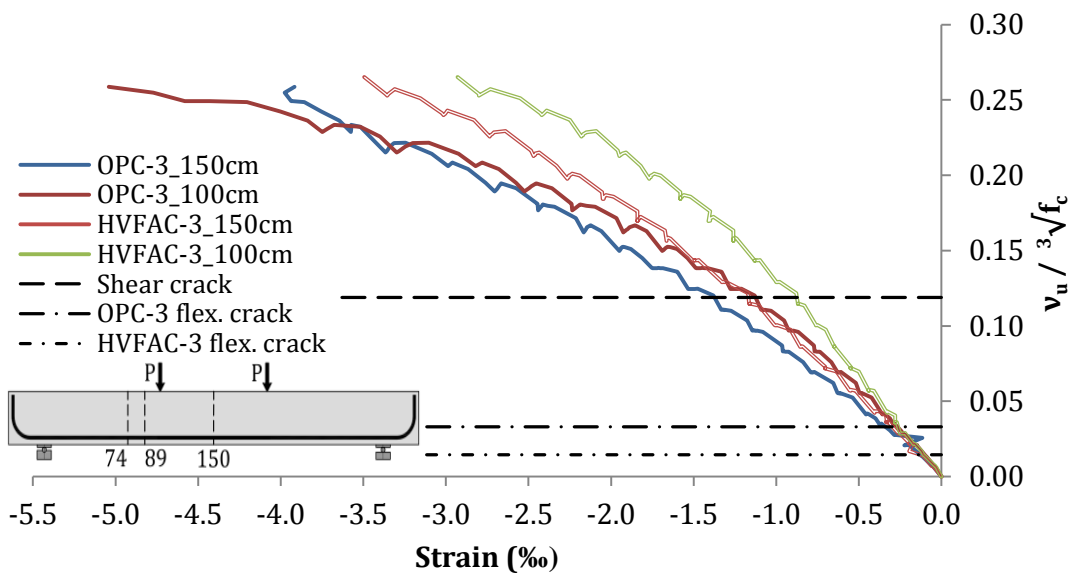


Figure 4.235 Concrete strains in sections 100 cm and 150 cm for beams in group 3

Concrete strains under the loading point are plotted in Figures 4.237 and 4.238 for beams from groups 2 and 3. In the V7 sensor direction tension strains from 0.5‰ to 1.0‰ developed for all beams in a similar manner. Strains in the direction of the load application were close to zero in all beams except in the HVFAC-2.

4. Experimental program and test results

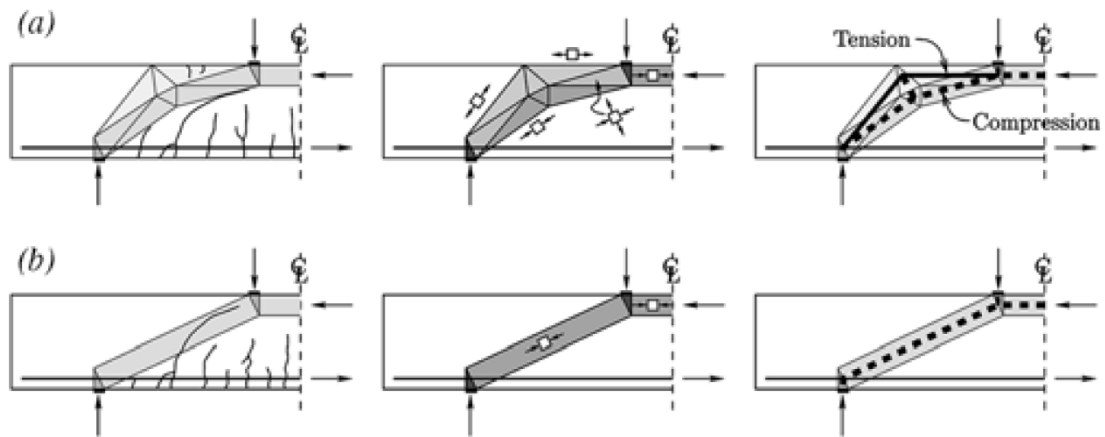


Figure 4.236 Load-carrying mechanisms after development of critical shear crack: (a) elbow-shaped strut (b) straight strut (Muttoni and Fernández Ruiz, 2008)

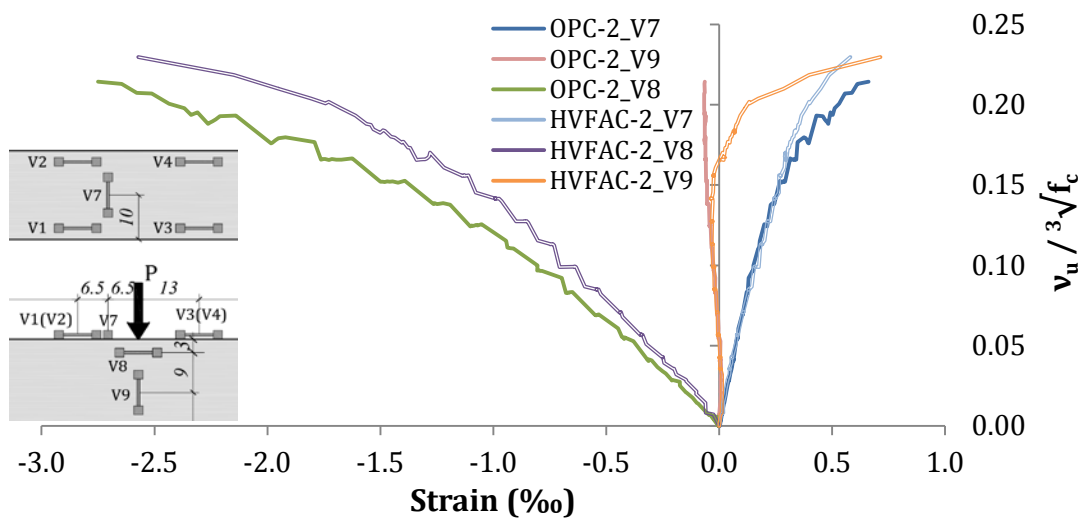


Figure 4.237 Concrete strains in V7, V8 and V9 for OPC-2 and HVFAC-2 beams

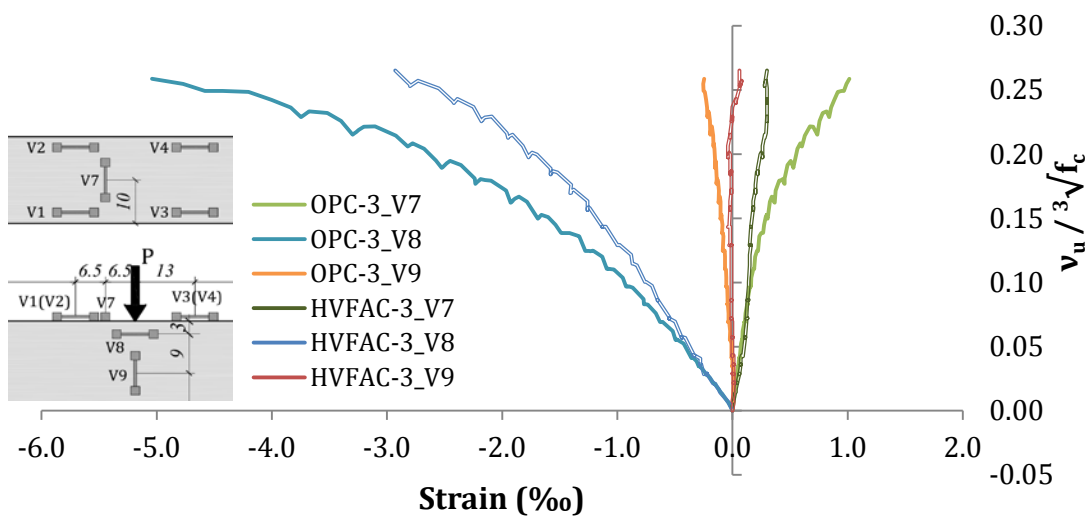


Figure 4.238 Concrete strains in V7, V8 and V9 for OPC-3 and HVFAC-3 beams

4. Experimental program and test results

This measurement showed tension strains up to 0.7‰ probably due to the crack propagation through the VWSG measuring base. The ultimate compressive strains in V8 sensors showed higher strains compared with beams without stirrups ranging between 2.5‰ in the OPC-2, HVFAC-2 and HVFAC-3 beam and 5.0‰ in the OPC-3 beam. The ultimate concrete strain values for OPCC and HVFAC beams are shown in Figure 4.239 and 4.240.

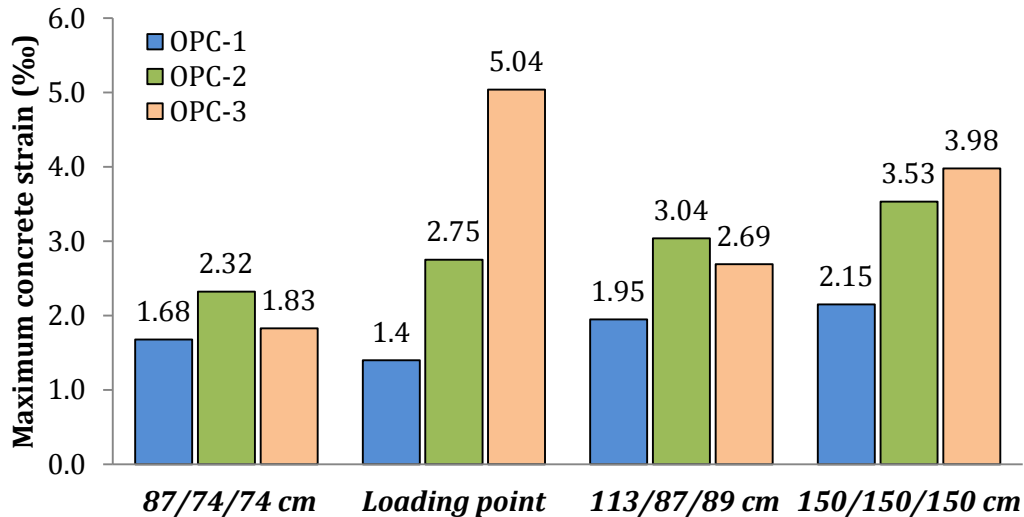


Figure 4.239 Maximum concrete strains for OPCC beams at failure

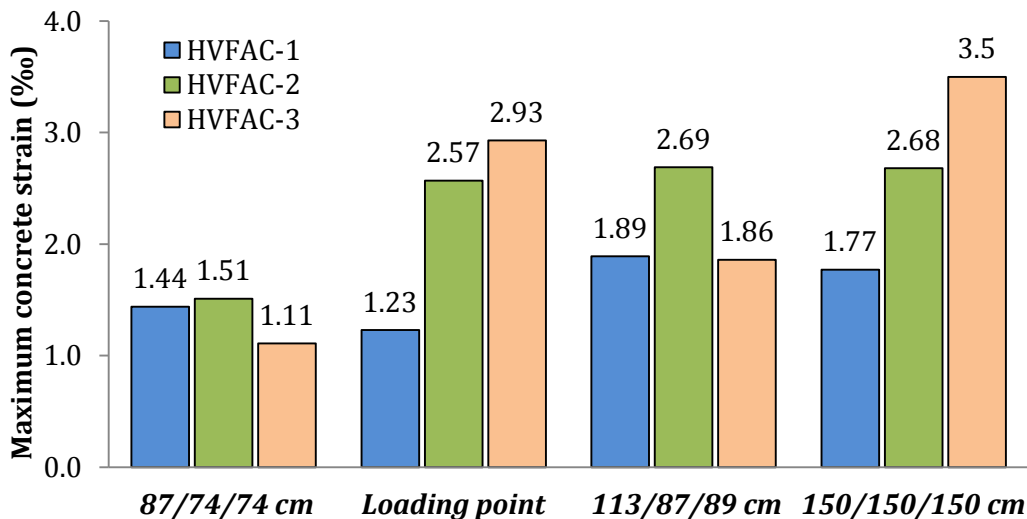


Figure 4.240 Maximum concrete strains for HVFAC beams at failure

Concrete strains in the first group of beams increased from section 1 to midpoint with the exception of the section under the loading point where VWSG sensors were not located on the top of the beam as in others but 3 cm lower. Concrete

4. Experimental program and test results

compressive strains at failure were higher in the OPC-1 beam for 14.3%, 12.1%, 3.1% and 17.7% for sections at 87 cm, 100 cm, 113 m and 150 cm respectively. The ultimate concrete strains ranged between 1.77‰ and 2.15‰ for beams without stirrups.

Concrete strains were generally higher in beams with shear reinforcement in all sections except in the section closest to the shear span midpoint. Concrete compressive strains at failure were higher in OPCC beams compared with the HVFAC ones: in the OPC-2 beam they were higher for 35%, 7%, 12% and 24% for sections at 74 cm, 87 cm, 100 cm and 150 cm respectively; in the OPC-3 beam they were higher for 39%, 42%, 31% and 12% for sections at 74 cm, 89 cm, 100 cm and 150 cm respectively. The ultimate concrete strains range from 2.68‰ to 3.98‰. The highest compressive strain was reached in the OPC-3 beam midpoint cross section which resulted in flexural failure caused by concrete crushing. The concrete compressive strains were, on average, 12%, 19% and 31% higher in OPC-1, OPC-2 and OPC-3 beams compared with the HVFAC-1, HVFAC-2 and HVFAC-3 beams, respectively.

4.4.11.1. Distribution of strains

In order to compare the area of uncracked concrete, strain distribution in cross sections 1, 2 and 3 for all beams is plotted in Figures 4.241 – 4.243. Having in mind that all other parameters influencing the concrete compression capacity are the same in all beams, their concrete capacity can be compared. It can be seen that compressive zone has the biggest height in beams without stirrups and that it decreased as the shear reinforcement ratio was increasing in all sections. This was expected due to a different mechanism of shear transfer in beams with stirrups and without them. Compressed concrete shear component was obviously higher in beams without stirrups because shear reinforcement was taking its part in shear transfer.

Neutral axis was moving downwards from the section 1 to the section 3 in the middle of the beam. The compressive zone height was similar in OPCC and HVFAC beams except in the OPC-3 beam in the middle of the beams span where it was

4. Experimental program and test results

significantly lower compared with the HVFAC-3 beam. This was also expected having in mind flexural failure that occurred in this beam. Regardless of the fact that all beams were designed to have the same 90-day compressive strength, some differences were noticed. The concrete compressive zone height was divided with the cube root of compressive strength in order to eliminate the influence of a different compressive strength. The results are shown for all beams and sections in Figure 4.244. The section 3 was in the same place in all beams, in the beams' midpoint, and it was clear that compressed concrete height was practically the same in all beams except in the OPC-3 as already mentioned.

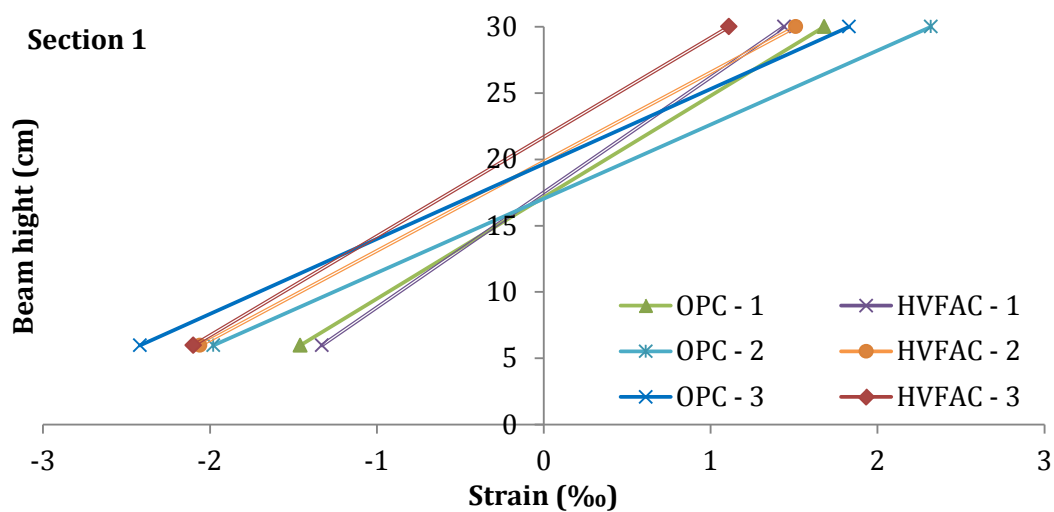


Figure 4.241 Strain distributions in cross section 1 for all beams

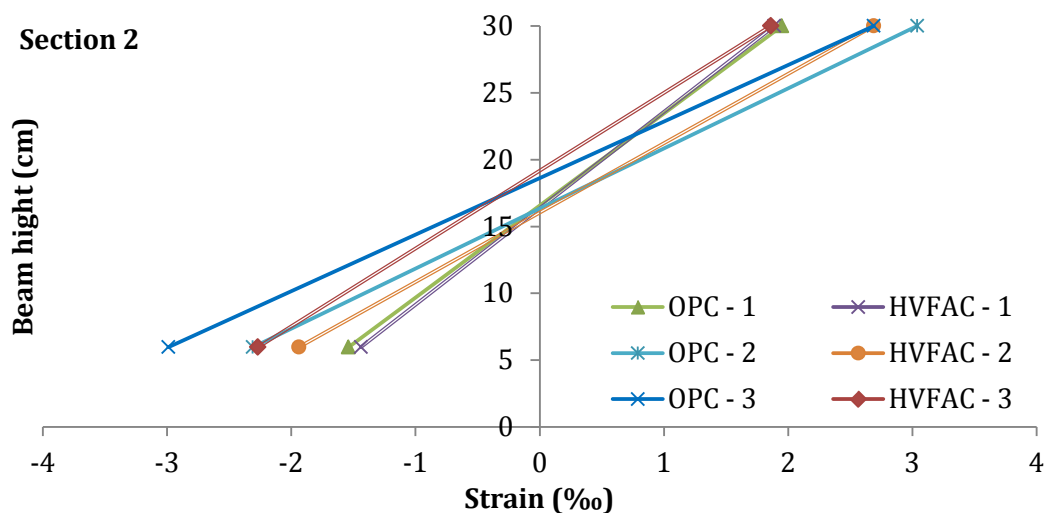


Figure 4.242 Strain distributions in cross section 2 for all beams

4. Experimental program and test results

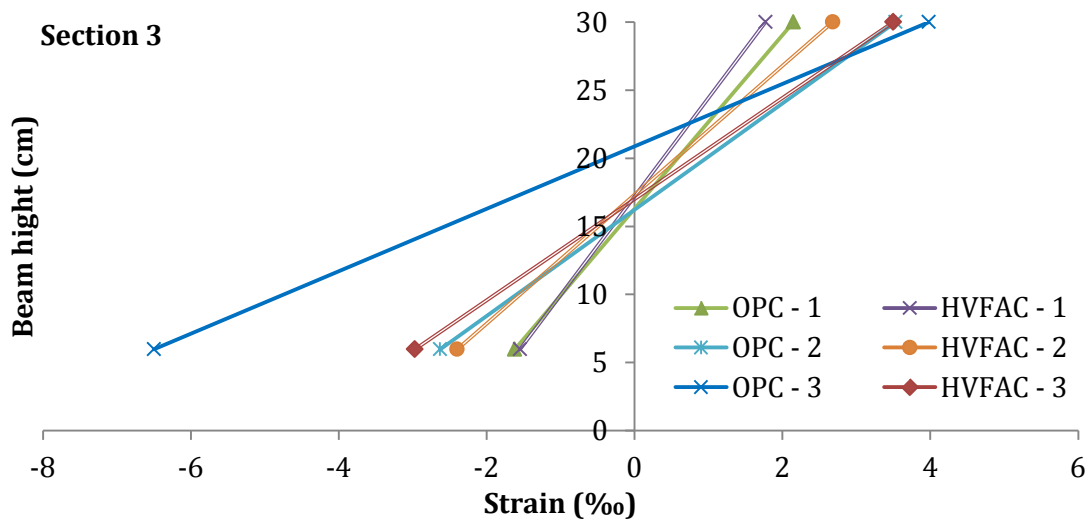


Figure 4.243 Strain distributions in cross section 3 for all beams

In sections 1 and 2, the compressive concrete height was similar in OPCC and HVFAC beams from the same group except the 20% lower height in the HVFAC-2 beam compared with the OPC-2 beam in section 1. It can be generally concluded that no significant difference between OPCC and HVFAC beams compressed concrete shear component existed.

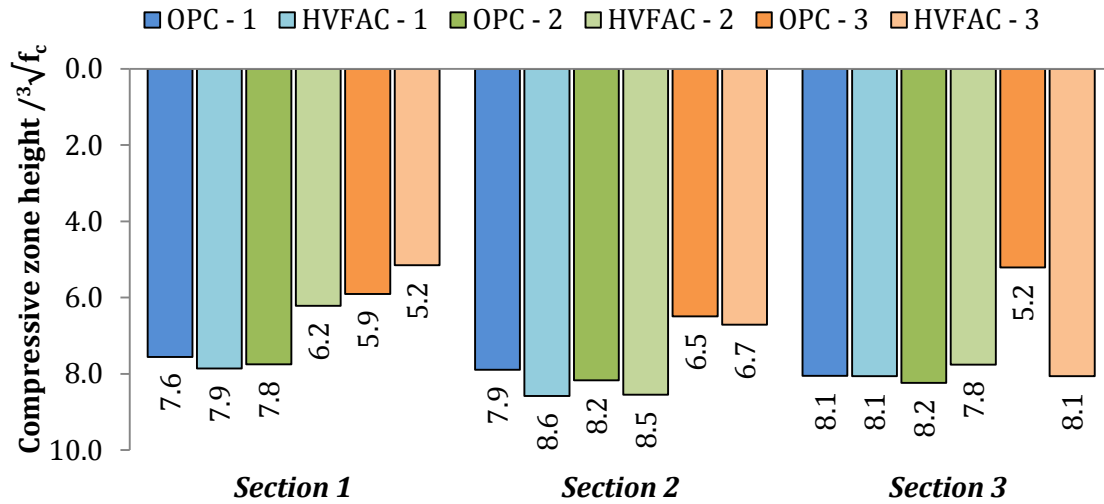


Figure 4.244 Height of the concrete compression zone normalized with the compressive strength cube root

4. Experimental program and test results

4.4.12. Concrete cracks

The crack pattern for each beam was marked at the front surface of the beam sample and subsequently drafted in AutoCAD. No cracks were noticed on the beams' surface before loading. In order to give a quantitative comparison of crack patterns and their development, the following parameters were chosen and presented in Table 4.29: maximum flexural crack width at service loading state ($w_{fl,ser}$), maximum flexural crack width at the ultimate state ($w_{fl,u}$), maximum vertical crack length at service ($l_{ser,max}$) and the ultimate state ($l_{u,max}$), number of flexural cracks at service state ($n_{fl,ser}$) and the ultimate state ($n_{fl,u}$), average spacing between cracks at service ($s_{ser,avg}$) and the ultimate state ($s_{u,avg}$), diagonal crack width at the ultimate loading level ($w_{sc,u}$). The development of flexural cracks width with loading is presented in Table 4.30. The same analysis was performed for shear crack evaluation and the results are shown in Table 4.31.

Beam samples without stirrups reached failure directly after the shear crack formation, disabling further shear crack propagation and width increase. For this reason, shear crack width analysis for the OPC-1 and HVFAC-1 beams could not be performed. The development of cracks is graphically presented in Figures 4.245 and 4.246 for the OPC-1 and HVFAC-1 beams, respectively.

Table 4.29 Flexural and shear crack parameters for beams subjected to shear

Beam notation	$w_{fl,ser}$ (mm)	$w_{fl,u}$ (mm)	$l_{fl,ser}$ (mm)	$l_{fl,u}$ (mm)	$n_{fl,ser}$ (-)	$n_{fl,u}$ (-)	$s_{ser,avg}$ (mm)	$s_{u,avg}$ (mm)	$w_{sc,u}$ (mm)
OPC-1	0.03	0.08	6.8	13.5	12	27	13.2	9.0	22.0
HVFAC-1	0.05	0.10	12.3	16.7	13	22	10.5	8.7	24.4
OPC-2	0.05	0.08	9.8	11.9	10	22	14.5	10.8	9.0
HVFAC-2	0.05	0.08	12.9	18.8	23	26	9.2	8.9	8.8
OPC-3	0.05	0.08	11.9	15.1	21	27	9.1	9.1	-
HVFAC-3	0.05	0.08	15.4	19.0	20	25	11.2	10.0	6.0

4. Experimental program and test results

Table 4.30 Maximum flexural crack width development

2P (kN)	Flexural crack width (mm)					
	OPC-1	HVFAC-1	OPC-2	HVFAC-2	OPC-3	HVFAC-3
20	-	0.03	-	-	-	0.03
40	0.03	0.03	-	-	-	0.03
50	0.03	0.03	-	0.03	0.03	0.03
60	0.03	0.03	0.03	0.03	0.03	0.05
80	0.03*	0.05*	0.03	0.03	0.03	0.05
100	0.05	0.05	0.03	0.03	0.03	0.05
120	0.05	0.05	0.05*	0.05*	0.03	0.05
140	0.05	0.05	0.05	0.05	0.05*	0.05*
160	0.08	0.08	0.05	0.05	0.05	0.05
180	0.08	0.08	0.05	0.08	0.05	0.08
200	0.08	0.08	0.05	0.08	0.08	0.08
240	0.08	0.08	0.08	0.08	0.08	0.08

*Flexural crack width at service loading state

Table 4.31 Shear crack width development

2P (kN)	Shear crack width (mm)					
	OPC-1	HVFAC-1	OPC-2	HVFAC-2	OPC-3	HVFAC-3
160	0.03	0.03	-	-	-	-
180	0.03	0.05	0.03	0.03	0.03	0.03
200	0.05	0.05	0.03	0.05	0.03	0.05
220	0.08	-	0.03	0.10	0.05	0.08
240	-	-	0.05	0.30	0.08	0.15
250	-	-	0.08	0.45	0.08	0.15
260	-	-	0.25	0.50	0.15	0.15
280	-	-	0.70	0.70	0.20	0.20
290	-	-	0.80	-	0.20	0.20
300	-	-	0.90	-	0.25	0.35
320	-	-	-	-	0.30	0.45
340	-	-	-	-	0.40	0.50
360	-	-	-	-	0.60	0.60

4. Experimental program and test results

As can be seen, the general crack patterns for both OPC-1 and HVFAC-1 beams were similar in all phases with vertical flexural cracks starting to incline after reaching the second row of longitudinal reinforcement. In the OPC-1 beam cracks started to incline at approximately 140 kN with the first separate shear crack noticed at 160 kN on the back side of the beam. In the HVFAC-1 beam sample the first flexural cracks were noticed in the first loading step at loading force of 20 kN, and at 60 kN they already reached the longitudinal reinforcement line and started to incline. The first inclined shear crack in the shear span appeared at the force of 160 kN, as it did in the OPC-1 beam.

4.4.12.1. Concrete cracks in the OPC-1 and HVFAC-1 beams

The maximum flexural crack widths at service and the ultimate state were slightly higher for the HVFAC-1 than the OPC-1 beam, as can be seen in Table 4.29. The vertical length of cracks was higher in the HVFAC-1 beam compared with the OPC-1. In service loading state, the length of the vertical cracks was 80% longer in HVFAC-1 beam, with the decreasing difference in the ultimate loading state (23%). The number of cracks is practically the same in service loading state, but higher in the OPC-1 beam at the ultimate loading state with more uniformly distributed cracks along the beam length. The crack distance corresponds to the stirrup distance at the ultimate loading state and it was higher in the OPC-1 beam at service load for 20%. The shear crack width was similar in both OPC-1 and HVFAC-1 beams, with slightly higher widths in the HVFAC-1 beam at the same loading step. Having in mind different compressive strengths, Figure 4.247 shows the flexural and shear crack widths development versus normalized shear stress to get a better understanding of this matter. As can be seen, when compressive strength was taken into account, the difference became smaller and even in favor of the HVFAC-1 at higher loading steps. Shear cracks had similar, relatively small width before failure and similar width at failure mode.

4. Experimental program and test results



Figure 4.245 Crack patterns on the OPC-1 beam

4. Experimental program and test results

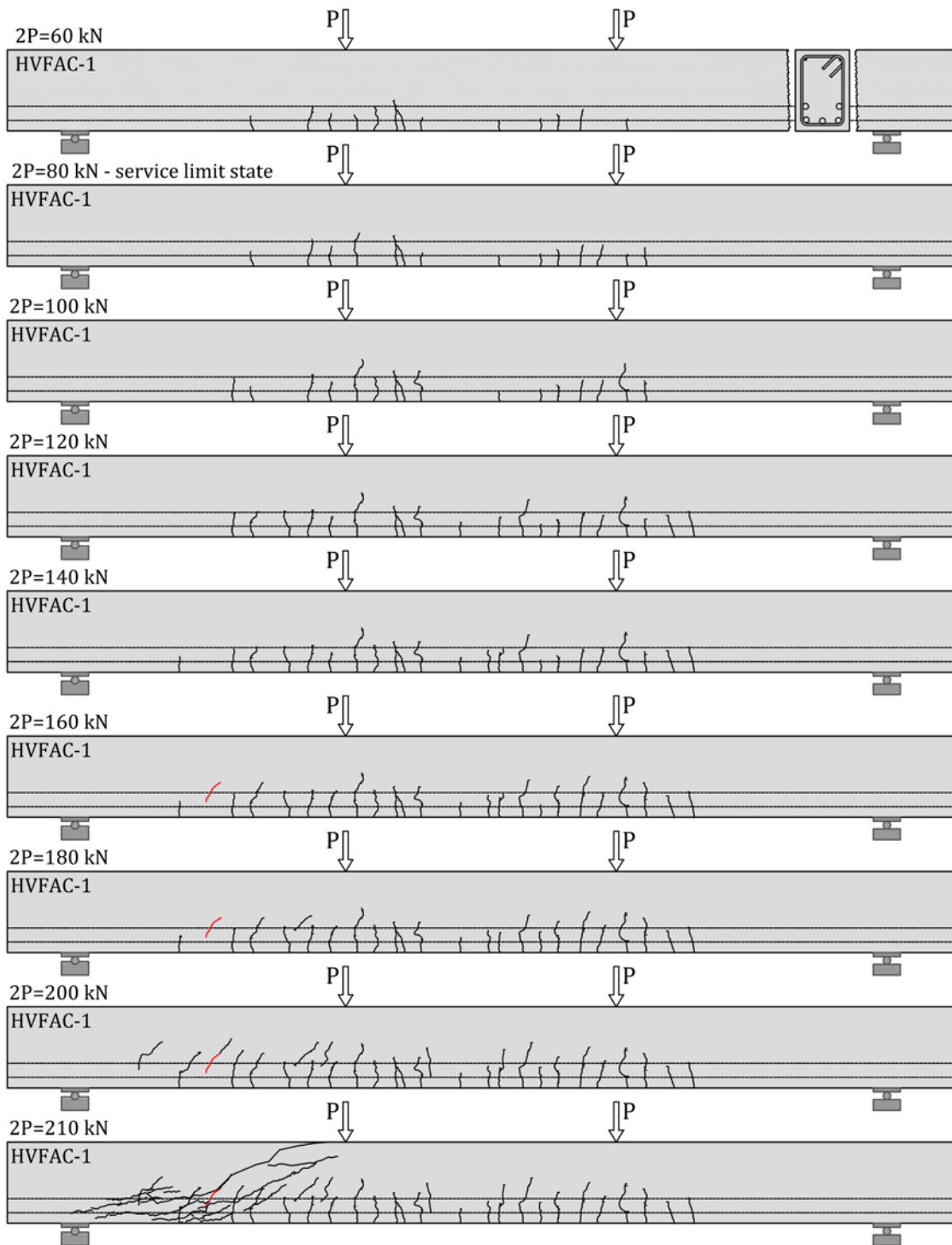


Figure 4.246 Crack patterns on the HVFAC-1 beam

After everything previously mentioned, the following conclusions can be made:

- Similar crack patterns developed in both beams with the vertical cracks inclination starting after the second row of the longitudinal reinforcement was reached;

4. Experimental program and test results

- No significant difference in flexural and shear crack width was noticed;
- The length of vertical flexural cracks in the HVFAC-1 beam was higher compared with the OPC-1 beam, both in service and the ultimate state;
- The number and spacing between cracks was similar in both beams.

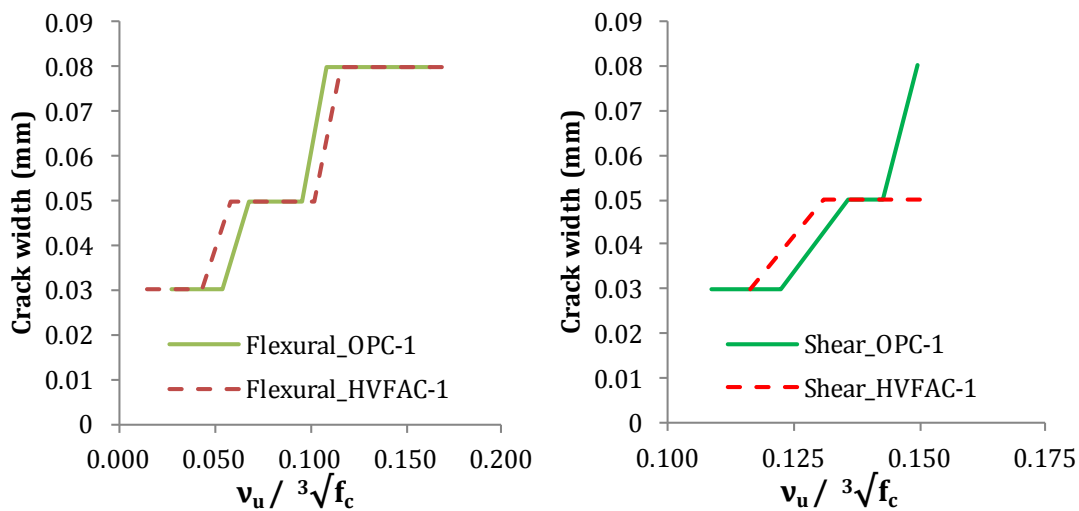


Figure 4.247 Flexural and shear crack width in the OPC-1 and HVFAC-1 beams versus normalized shear stress

4.4.12.2. Concrete cracks in the OPC-2 and HVFAC-2 beams

The development of cracks for OPC-2 and HVFAC-2 beams is graphically presented in Figures 4.248 and 4.249, respectively. As can be seen, the general crack patterns for both OPC-2 and HVFAC-2 beams were similar in all phases, with the vertical flexural cracks starting to incline after reaching the second row of the longitudinal reinforcement. In the OPC-2 beam, the first shear crack in the testing region appeared as separate at 180 kN, followed by the formation of more shear cracks. It was not absolutely clear if these shear cracks appeared as separate or as an extension to the existing flexural cracks that propagated at certain angle after reaching the longitudinal reinforcement point but were not seen by the naked eye during the experiment.

4. Experimental program and test results

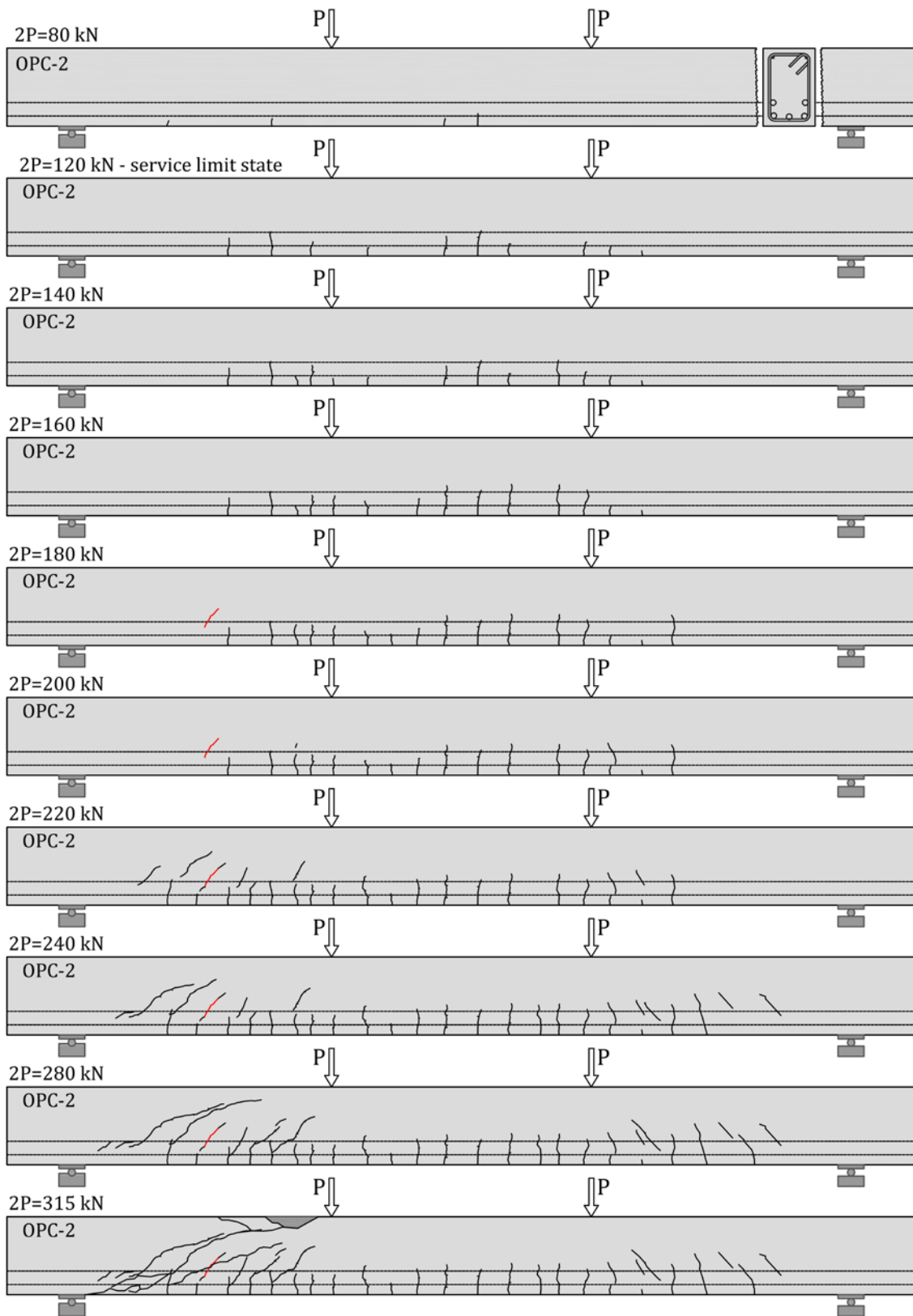


Figure 4.248 Crack patterns on the OPC-2 beam

4. Experimental program and test results

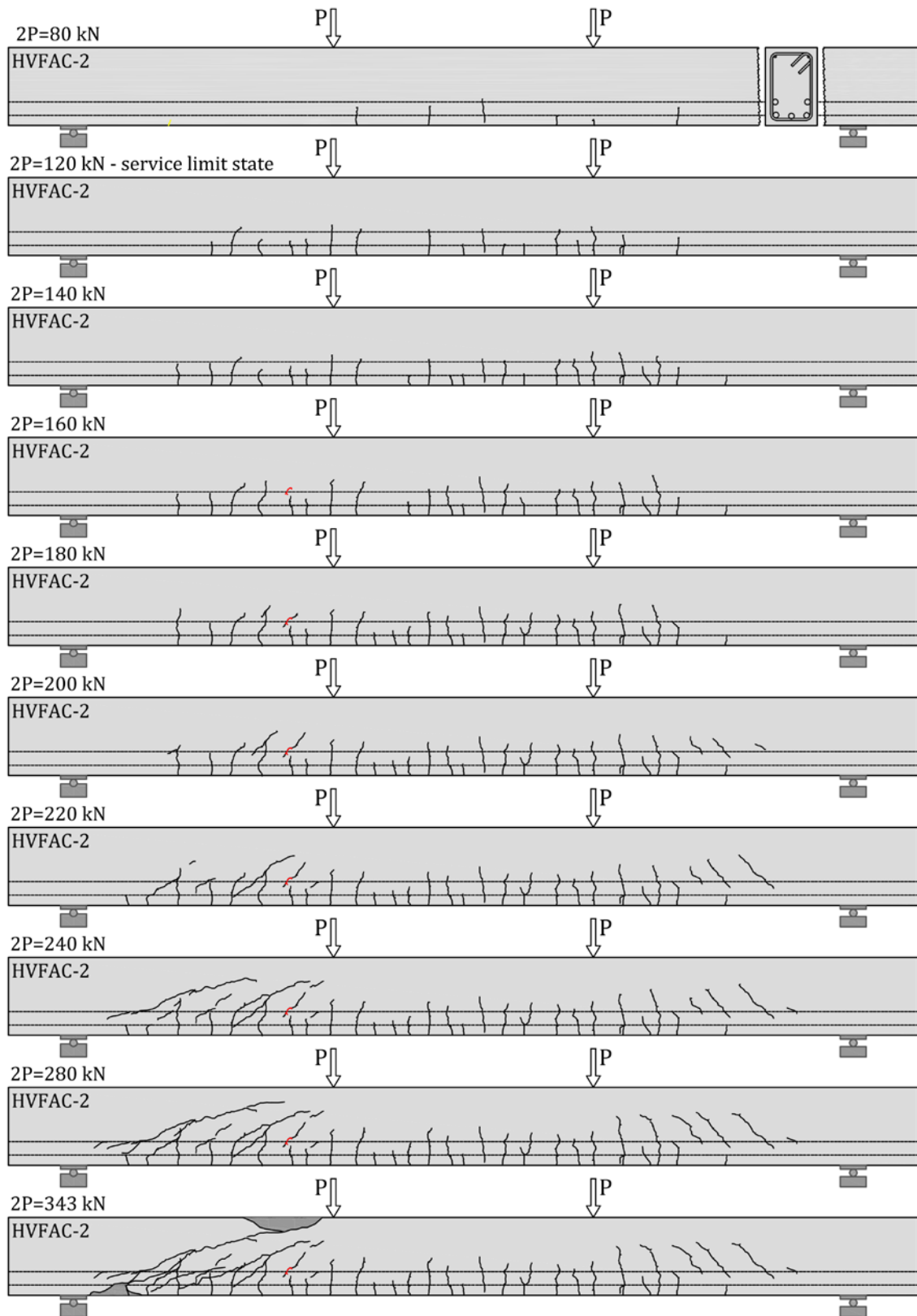


Figure 4.249 Crack patterns on the HVFAC-2 beam

4. Experimental program and test results

Similar shear crack development was noticed in the HVFAC-2 beam with two dominant shear cracks progressing towards supports, and causing failure in the same way as in the OPC-2 beam. Flexural cracks at service and the ultimate state had the same width for both beams, as can be seen in Table 4.30. The vertical length of cracks was higher in the HVFAC-2 beam compared with the OPC-2 beam. In service state, the length of vertical cracks was 30% longer in the HVFAC-2 beam, with increasing difference in the ultimate loading state (58%).

The number of cracks in the HVFAC-2 beam was significantly higher in service state (130%), but only 18% higher in the ultimate state. The crack distance corresponded to the stirrup distance at the ultimate loading state and it was higher in the OPC-2 beam at service state for 36%. The flexural and shear crack width development was similar in both OPC-2 and HVFAC-2 beams with slightly higher widths in the HVFAC-2 beam in higher loading steps. Figure 4.250 shows the flexural and shear crack width development versus normalized shear stress. As can be seen, even when compressive strength was taken into account, the HVFAC-2 beam exhibited a higher flexural crack width at higher loads. The shear crack width in the HVFAC-2 was higher than in the OPC-2 in all loading steps. However, the shear crack width at failure was similar in both OPC-2 and HVFAC-2 beams.

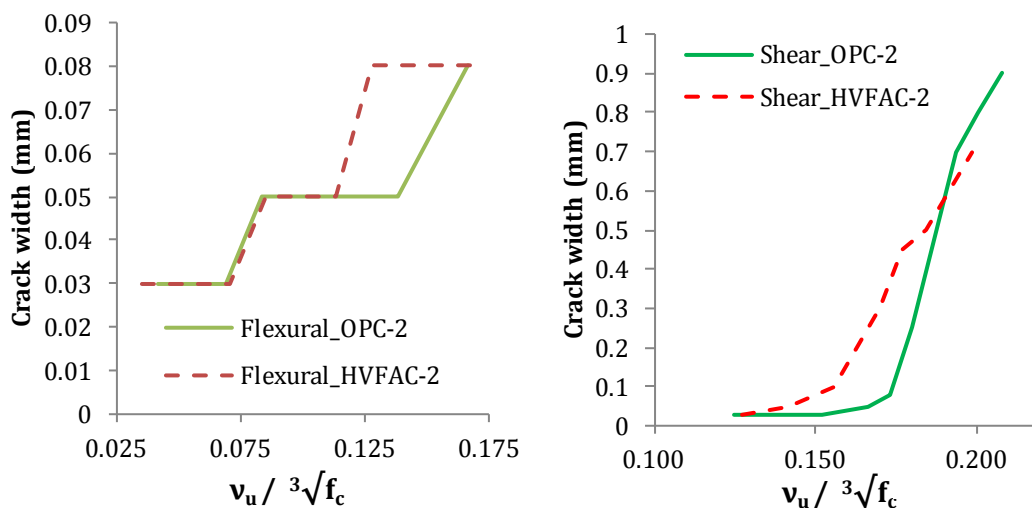


Figure 4.250 Flexural and shear crack width in OPC-2 and HVFAC-2 beams versus normalized shear stress

After everything previously mentioned, the following conclusions can be made:

4. Experimental program and test results

- Similar crack patterns developed in both beams with vertical cracks inclination starting after the longitudinal reinforcement was reached;
- Significantly higher flexural and shear crack width were noticed in the HVFAC-2 beam;
- The number and length of vertical flexural cracks in the HVFAC-2 beam were higher compared with the OPC-2 beam both in service and ultimate state;
- The spacing between cracks was similar in both beams.

4.4.12.3. Concrete cracks in the OPC-3 and HVFAC-3 beams

The development of cracks for the OPC-3 and HVFAC-3 beams was graphically presented in Figures 4.251 and 4.252, respectively. General crack patterns for both OPC-3 and HVFAC-3 beams were similar in the beginning phases but different close to failure due to different failure modes in the OPC-3 and HVFAC-3 beams. Shear cracks in the HVFAC-3 beam developed after 180 kN as short separate shear crack or an extension of vertical flexural cracks inclining after reaching the first row of the longitudinal reinforcement.

Shear cracks developed nearly symmetrically on both shear spans of the beam regardless of the different shear reinforcement. In the OPC-3 beam the first shear crack in the testing region appeared as separate at 180 kN followed the formation of more shear cracks. The shear cracks did not reach the loading point because of the concrete crushing in the middle part of the beam.

Flexural cracks at service and the ultimate state were of the same width for both beams, as can be seen in Table 4.30. The vertical length of cracks was higher in the HVFAC-3 beam compared with the OPC-3. In service state the length of the vertical cracks was 30% longer in the HVFAC-3 beam, with a decreasing difference in the ultimate loading state (26%). There was no significant difference in the number of cracks in the OPC-3 and HVFAC-3 beams. The crack distance corresponded to the stirrups distance at service and the ultimate loading state in both beams with no practical difference. The flexural crack width development was similar in both OPC-3 and HVFAC-3 beams with higher width in the HVFAC-3 beam in lower loading steps.

4. Experimental program and test results

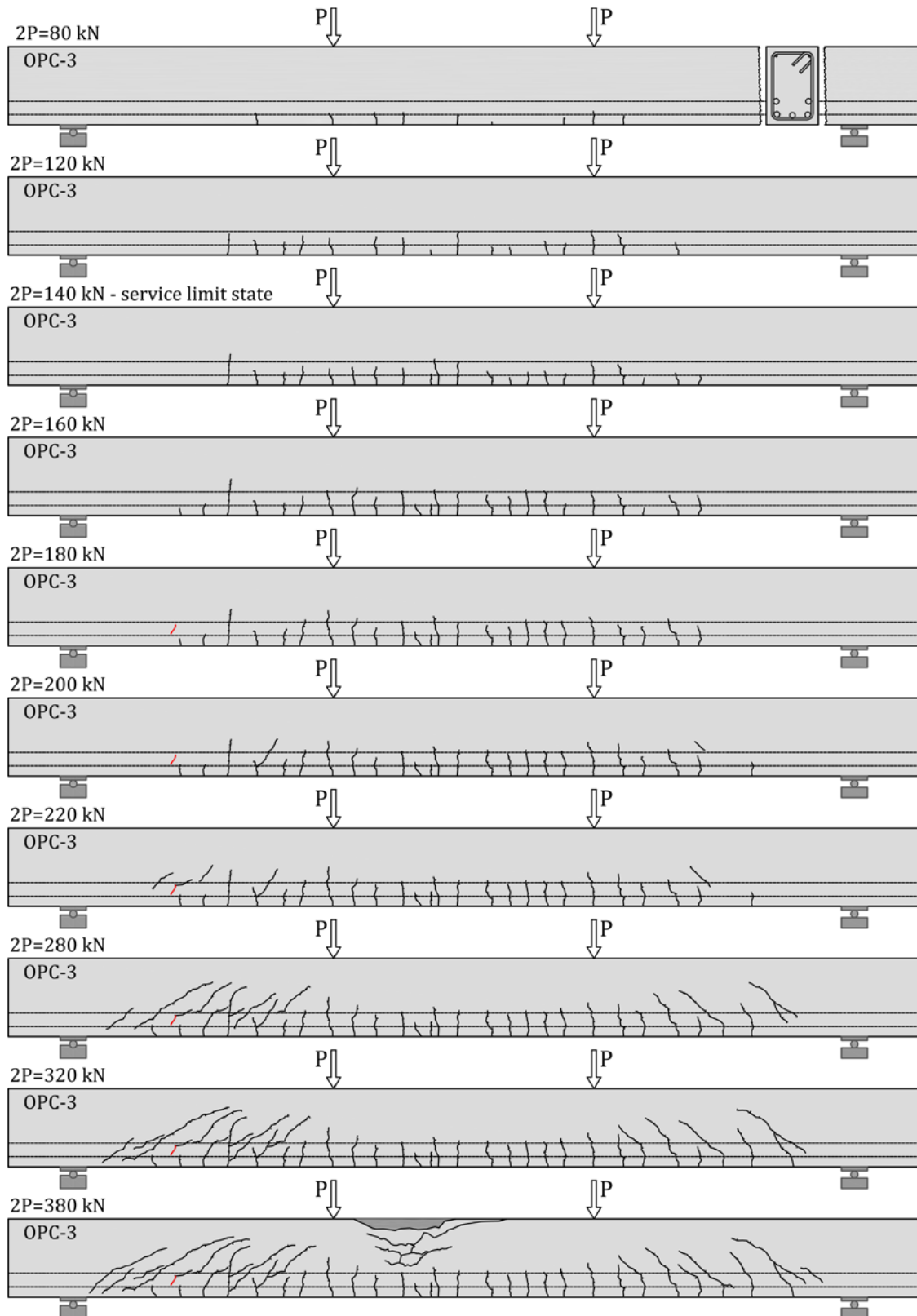


Figure 4.251 Crack patterns on the OPC-3 beam

4. Experimental program and test results

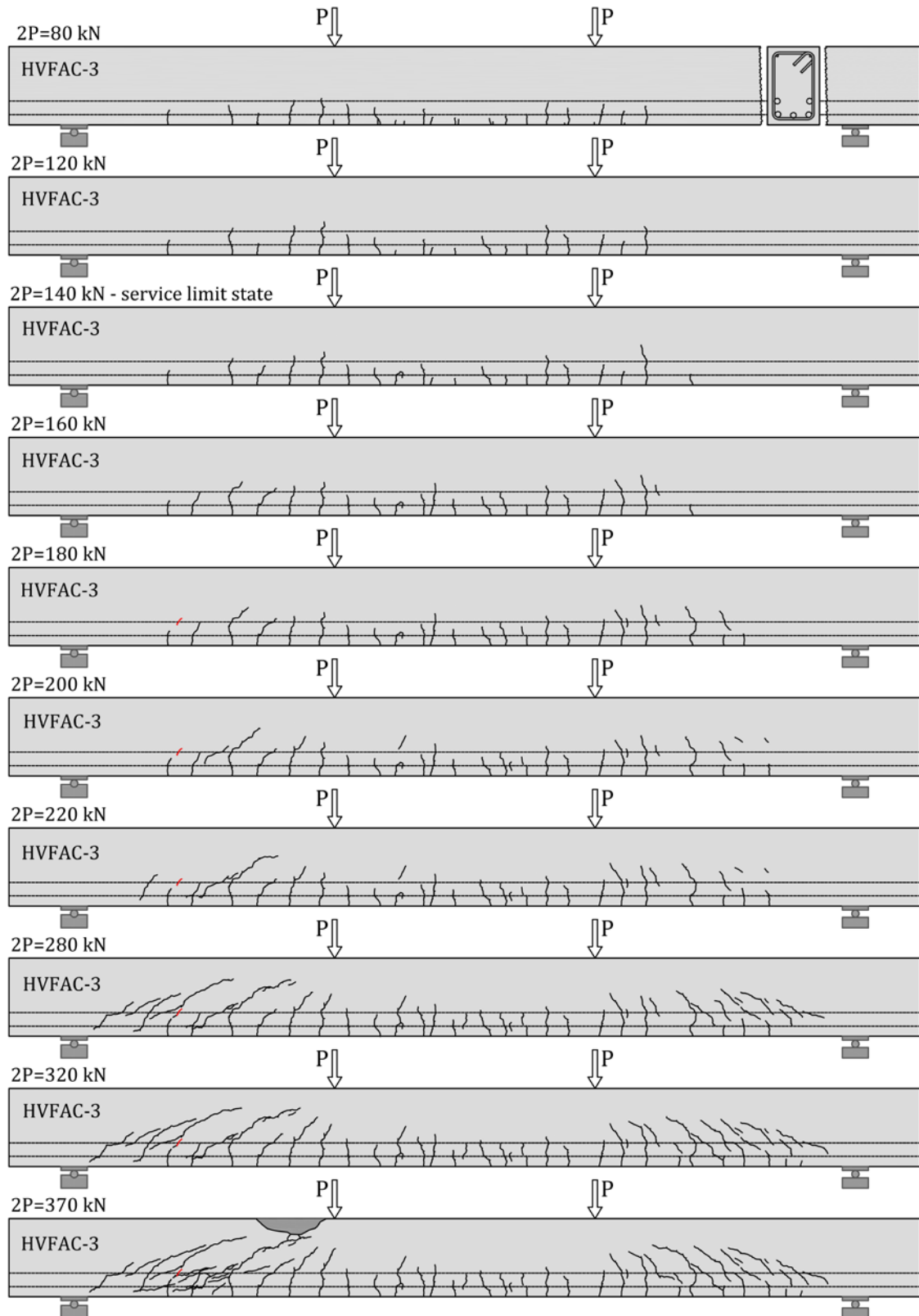


Figure 4.252 Crack patterns on the HVFAC-3 beam

4. Experimental program and test results

Figure 4.253 shows the flexural and shear crack width development versus normalized shear stress. As can be seen, even when the compressive strength was taken into account, the HVFAC-3 beam exhibited higher flexural crack width at lower loads. The shear crack width in the HVFAC-3 was similar or even lower than the OPC-3. It should be noted that shear cracks in the OPC-3 beam did not develop in the full matter because of the flexural failure mode.

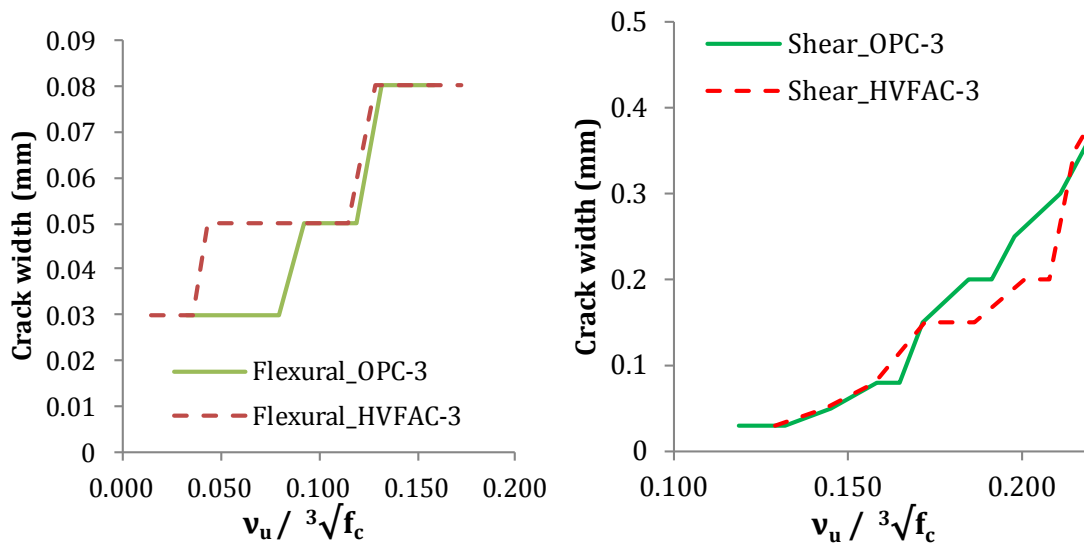


Figure 4.253 OPC-3 and HVFAC-3 beams crack width versus normalized shear stress

After everything previously mentioned, the following conclusions can be made:

- Similar crack patterns developed in both beams in the lower loading steps differing in the failure mode due to the flexural failure of the OPC-3 beam;
- Higher flexural crack widths were noticed in the HVFAC-3 beam practically in all loading steps;
- Shear crack width in the HVFAC-3 beam was the same or lower than the one in the OPC-3 beam but a quantitative conclusion cannot be made based on these results;
- The length of the vertical flexural cracks in the HVFAC-3 beam were higher compared with the OPC-3 beam both in service and the ultimate state;
- The number and spacing between cracks was similar in both beams.

Crack development is a very important issue from the point of sustainability but it also influences the behavior of beams subjected to shear in a great manner. The

4. Experimental program and test results

extent of the reinforced concrete damage caused by cracks leads to the deterioration of the compressive strength of cracked concrete. Consequently, several parameters were chosen to describe the state of cracks and enable the comparison between different concrete types. The previous analysis showed no significant difference between the crack number and spacing in OPCC and HVFAC samples. However, HVFAC beams showed higher flexural and shear crack width in all cases of the shear reinforcement ratios. In order to quantify this difference, the sum of all crack widths along the beams' length was chosen as a parameter for comparison. The sum of visually measured crack widths for all cracks that developed along the length of the beams was calculated for service load level and shown in Figure 4.254. It can be seen that OPCC beams had lower sum of crack widths compared with the HVFAC beams for 32%, 46% and 3% for beams from the first, the second and the third group, respectively. One of the reasons for higher crack widths in HVFAC beams was the difference in compressive and flexural tensile strength of HVFAC and OPCC. Flexural tensile strength of HVFAC beams was up to 75% lower compared with the OPCC beams.

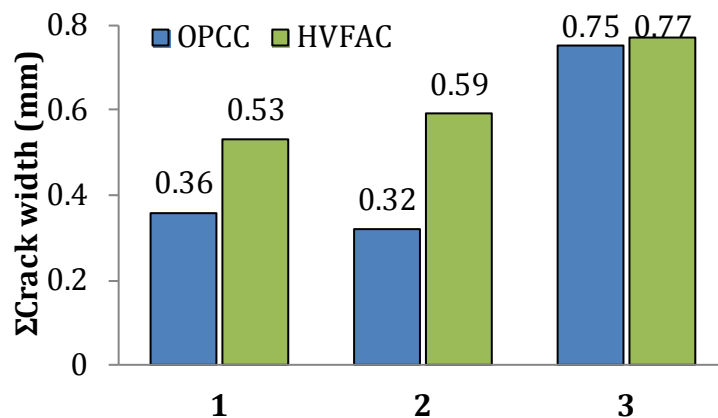


Figure 4.254 Sum of all crack widths at the service load level

The length of the flexural vertical cracks was also higher in HVFAC beams in all three sets of beams. At the service load level, maximum crack length in HVFAC beams was, on average, 30% higher compared with the OPCC beams. In the ultimate loading stage, this difference decreased to 25%. It can be concluded that cracks developed in more pronounced way in the HVFAC compared with the OPCC tested in this part of the study.

4. Experimental program and test results

4.4.13. Principal concrete strains

In order to evaluate principal concrete strains in OPCC and HVFAC under shear, the loading calculation was done based on the measured strains. Principal concrete strains were calculated for strain measurements in three directions $\varphi=0^\circ$, 60° and 120° , ε_0 , ε_{60} and ε_{120} respectively (Figure 4.255).

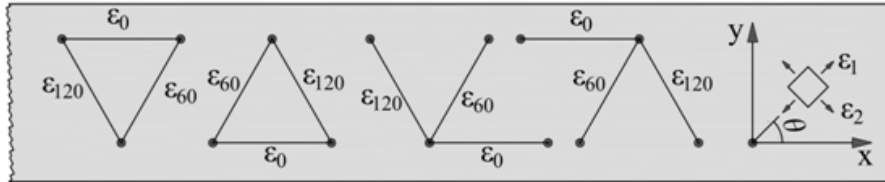


Figure 4.255 Principal strain measurements

Equations for the principal strain and stress calculation were derived based on the assumption that the principal strain and stress directions match. Principal strains (ε_1 and ε_2) and stresses (σ_1 and σ_2) values along with their axis angle (θ) were calculated based on the following equations:

$$\varepsilon_x = \varepsilon_0 \quad \text{Eq. 4.5}$$

$$\varepsilon_y = \frac{2}{3} \cdot \varepsilon_{60} + \frac{2}{3} \cdot \varepsilon_{120} - \frac{1}{3} \cdot \varepsilon_0 \quad \text{Eq. 4.6}$$

$$\gamma_{xy} = \frac{2}{\sqrt{3}} \cdot (\varepsilon_{60} - \varepsilon_{120}) \quad \text{Eq. 4.7}$$

$$\varepsilon_{1,2} = \frac{\varepsilon_x + \varepsilon_y}{2} \pm \sqrt{\left(\frac{\varepsilon_x - \varepsilon_y}{2}\right)^2 + \left(\frac{\gamma_{xy}}{2}\right)^2} \quad \text{Eq. 4.8}$$

$$\text{tg}2\theta_1 = \frac{\gamma_{xy}}{\varepsilon_x - \varepsilon_y}; \quad \theta_2 = \theta_1 + 90^\circ \quad \text{Eq. 4.9}$$

$$\sigma_1 = \frac{E}{1-\nu^2} \cdot (\varepsilon_1 + \nu \cdot \varepsilon_2); \quad \sigma_2 = \frac{E}{1-\nu^2} \cdot (\varepsilon_2 + \nu \cdot \varepsilon_1) \quad \text{Eq. 4.10}$$

The calculation of stresses based on the measured parameters requires the explanation of all the uncertainties adopted here. The modulus of elasticity was measured for both concrete types at the age of 90 days. This modulus was measured in compression in a standardized test with 30% of the ultimate force applied. Concrete is a heterogenic and anisotropic material with different damage mechanisms in compression and tension with applied loads higher than 30% of the

4. Experimental program and test results

ultimate strength. There is a limited amount of experimental tests of the stress-strain relationship of concrete in tension due to a complicated set up that can provide reliable results. These results are based on the uniaxial concrete tension and do not take into account the crack development in concrete due to shear and flexural cracking, like in the beams loaded with transverse forces.

Poisson's coefficient (ν_c) was not measured during this experiment and the value of 0.2 was chosen for stress calculation as it was proposed by *fib* Model Code 2010. Experimental results showed that Poisson's coefficient increases with the increase of the stress level. When the compressive stress is lower than 50% of concrete compressive strength, ν_c is approximately a constant of the value 0.17, which is the Poisson's ratio corresponding to concrete in the elastic stage. When the compressive stress is higher than 50% of the concrete compressive strength, ν_c increases due to the internal crack development. In the state close to failure, ν_c can reach the value as 0.5 or even higher (Gu, Jin and Zhou, 2015). Having all this in mind, principal stresses were calculated with the measured values of modulus of elasticity and $\nu_c=0.2$ but taken only for the descriptive evaluation of concrete stresses keeping in mind all above mentioned uncertainties.

The main purpose of these measurements was the determination of the principal tensile strains before shear crack formation. The tensile failure of concrete is always a discrete phenomenon. The *fib* Model Code 2010 proposes a bilinear stress-strain relationship to describe the tensile behavior of uncracked concrete, and a stress-crack opening diagram after crack formation. At tensile stresses of about 90% of the tensile strength micro-cracking starts to reduce the stiffness in a small failure zone. Micro cracks grow and form a discrete crack at stresses close to the tensile strength. In the fracture zone, the maximum tensile strain is estimated to a value of 0.15‰.

During this analysis the ultimate tensile strain is calculated based on the measured results for both concrete mixtures and for each beam in the two following ways:

- 1) Based on the measured 90-day modulus of elasticity and splitting tensile strength:

4. Experimental program and test results

$$\varepsilon_{max}^{exp} = E_{90}^{exp} \cdot 0.9 \cdot f_{ct,sp,90}^{exp} (\text{‰}) \quad Eq. 4.11$$

- 2) Based on the modulus of elasticity and tensile strength calculated using measured 28-day compressive strength using the equations from EN 1992-1-1:

$$\varepsilon_{max}^{EN1992} = E_{90}^{EN1992} \cdot 0.9 \cdot f_{ct,sp,90}^{EN1992} (\text{‰}) \quad Eq. 4.12$$

$$E_{90}^{EN1992} = (\beta_{cc})^{0.3} \cdot 22 \cdot \left(\frac{f_{c,28}^{exp}}{10} \right)^{0.3} (\text{GPa}) \quad Eq. 4.13$$

The ultimate tensile strain for both concrete mixtures was: $\varepsilon_{max}^{exp}=0.08\text{‰}$ and $\varepsilon_{max}^{EN1992}=0.09\text{‰}$. The calculated values were lower than the limit defined in the *fib* Model Code 2010 and the maximum tensile strain of 0.10‰ was adopted for the evaluation of the principal strains. This value was used during the following analysis to determine the moment of shear crack formation in the fracture zone.

The following steps were applied for each beam principal strain calculation:

- 1) In order to perform the control of the measured strains, diagrams of strains against normalized shear stresses were plotted. The expected sign (tension or compression) and value range of strains was controlled. No major errors were found, and all measured values were used as such. Figures of all measured strains are given in the Appendix A.
- 2) The calculation of principal strains was done according to Eq. 4.5 – 4.10. The calculation was done for all phases of loading, but only the values until the occurrence of cracks were used for the principal strain evaluation.
- 3) Principal strains are shown in the shear span in the points where they were calculated with two lines corresponding to the principal strain directions. The line length represents the strain intensity in the appropriate proportion. The strain intensity in all loading steps after the crack appearance was presented with dashed lines.
- 4) The part of the shear span where the first shear crack appeared was chosen to evaluate the maximum principal strains. The evolution of principal strains and stresses in that region is shown in tables in order to determine the moment of the shear crack appearance and the maximum concrete strains.

4. Experimental program and test results

- 5) In order to compare the stress and strain values for different concrete types the diagrams of the principal strain and stress against normalized shear stress for OPCC and HVFAC corresponding beams were plotted.

4.4.13.1. Principal strains in the OPC-1 and HVFAC-1 beams

In order to compare the measured strains in different concrete types, the values of all measured strains in the first and in the last loading step before failure are shown in Figures 4.256 and 4.257.

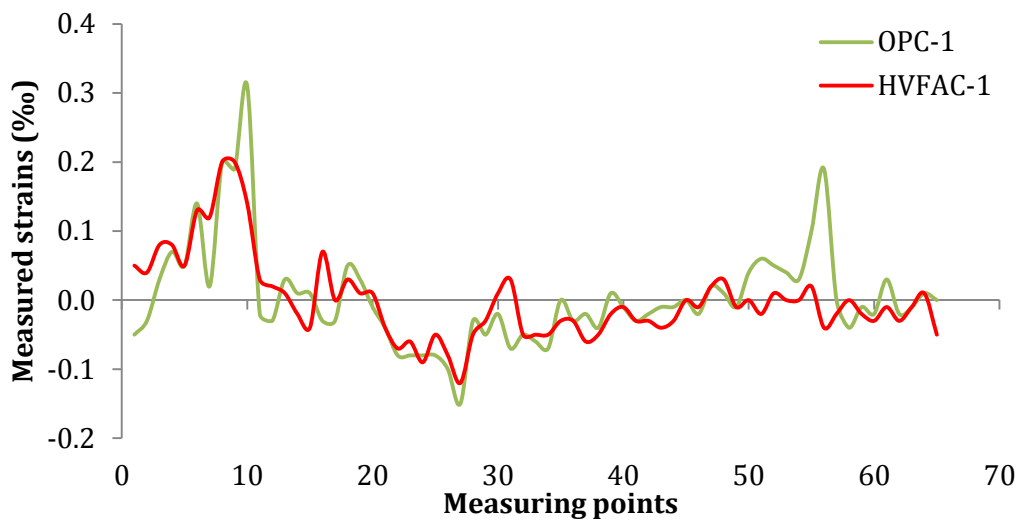


Figure 4.256 Measured values of strains in the first loading step for the OPC-1 and HVFAC-1 beams

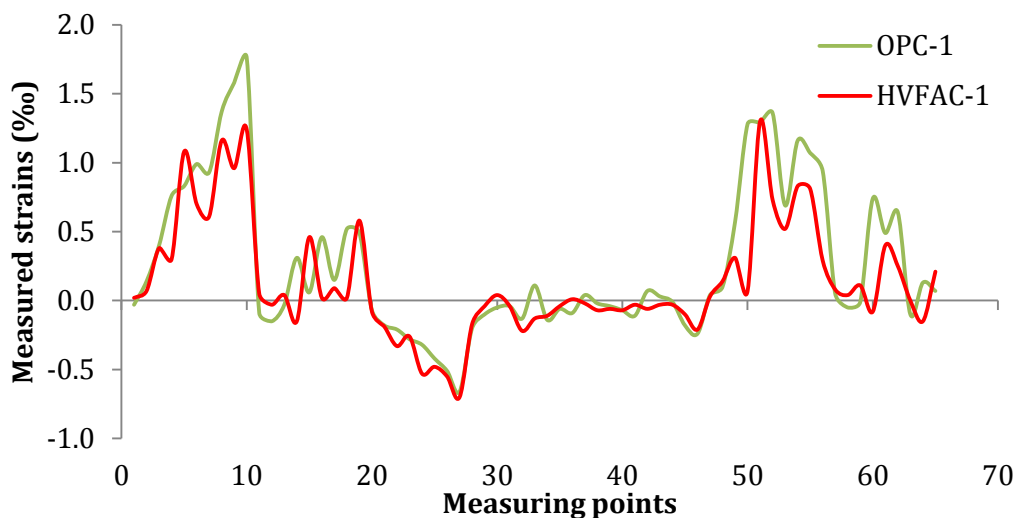


Figure 4.257 Measured values of strains in the last loading step for the OPC-1 and HVFAC-1 beams

4. Experimental program and test results

The notation of measuring point is given in Figure A.1 in the Appendix A. Strain values represent average concrete strains if the measuring was done before cracking and a sum of average concrete strain and crack width if measured after cracking. It can be seen that the development of measured strains was similar in both OPC-1 and HVFAC-1 beams. An exception from this conclusion can be noticed in some measuring zones where wider cracks appeared in the OPC-1 beam compared with the HVFAC-1. In order to compare the strains in different beams, the sum of all measured strains was calculated and presented versus the normalized shear stress in Figure 4.258.

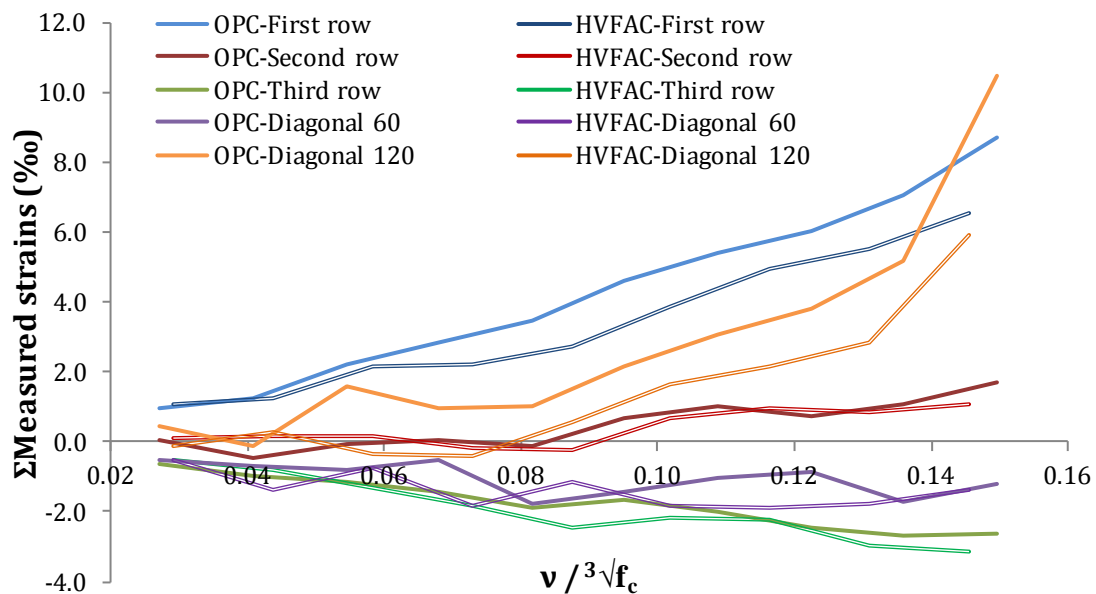


Figure 4.258. Sum of all measured strains in OPC-1 and HVFAC-1 beams versus normalized shear stress

It can be seen that the measured strains in OPC-1 beam in the first row and in the 120° direction were higher compared with the corresponding strains in the HVFAC-1 beam. The difference was approximately up to 30-45%. No specific conclusions regarding measured strains can be obtained due to different crack patterns that developed in different beams.

The directions and the intensity of the principal strains for beams OPC-1 and HVFAC-1 are shown in Figures 4.259–4.262. In the first loading step, the directions of the principal strains correspond to simply supported beam made from homogenous and elastic material. In that loading step, a small difference between

4. Experimental program and test results

the OPC-1 and HVFAC-1 beam principal strain direction can be noticed. The principal tension strains in the first two rows closer to the middle part of the beam were approximately horizontal in the HVFAC-1 beam.

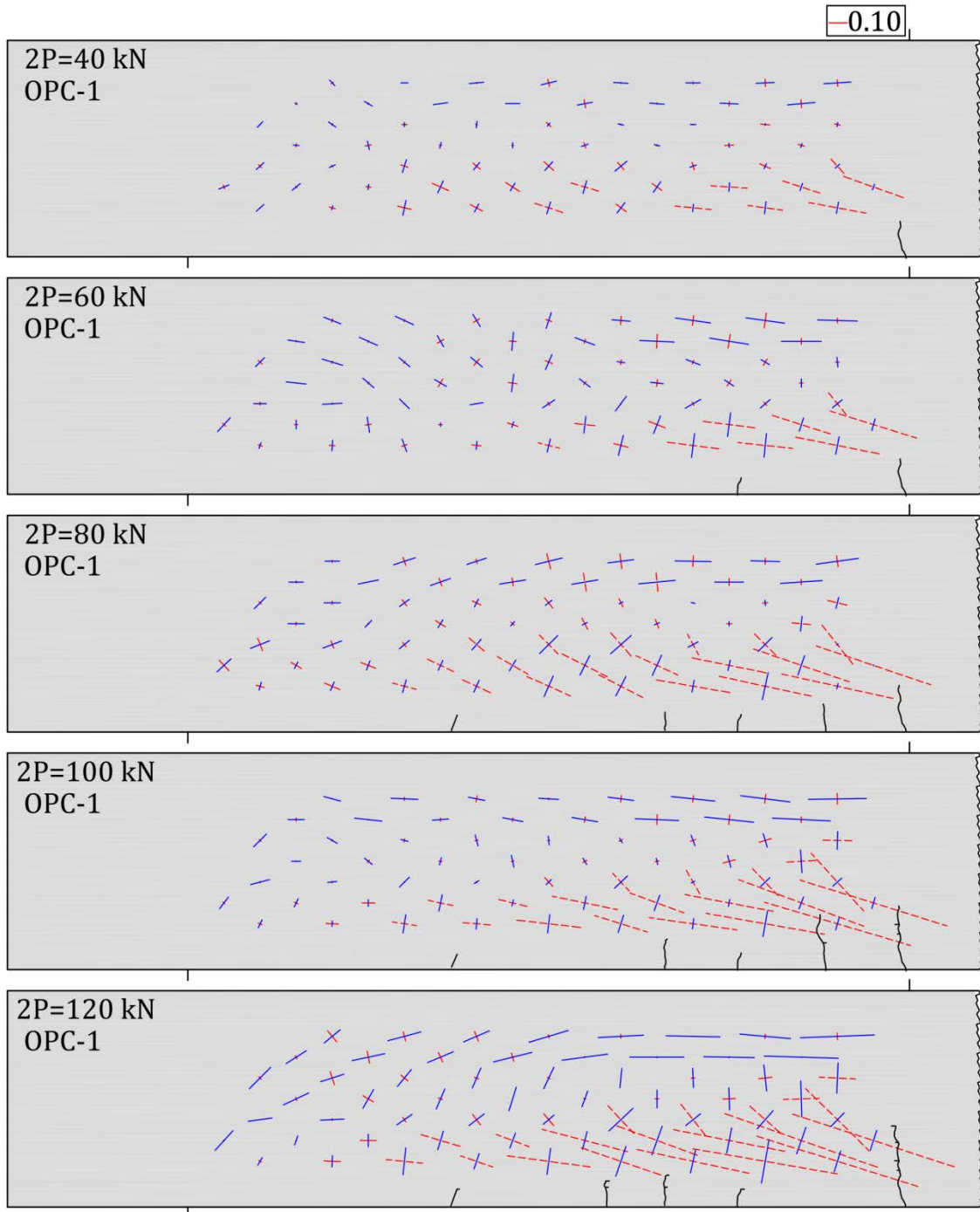


Figure 4.259 Principal strains and crack patterns in OPC-1 beam up to the loading level of 120 kN

4. Experimental program and test results

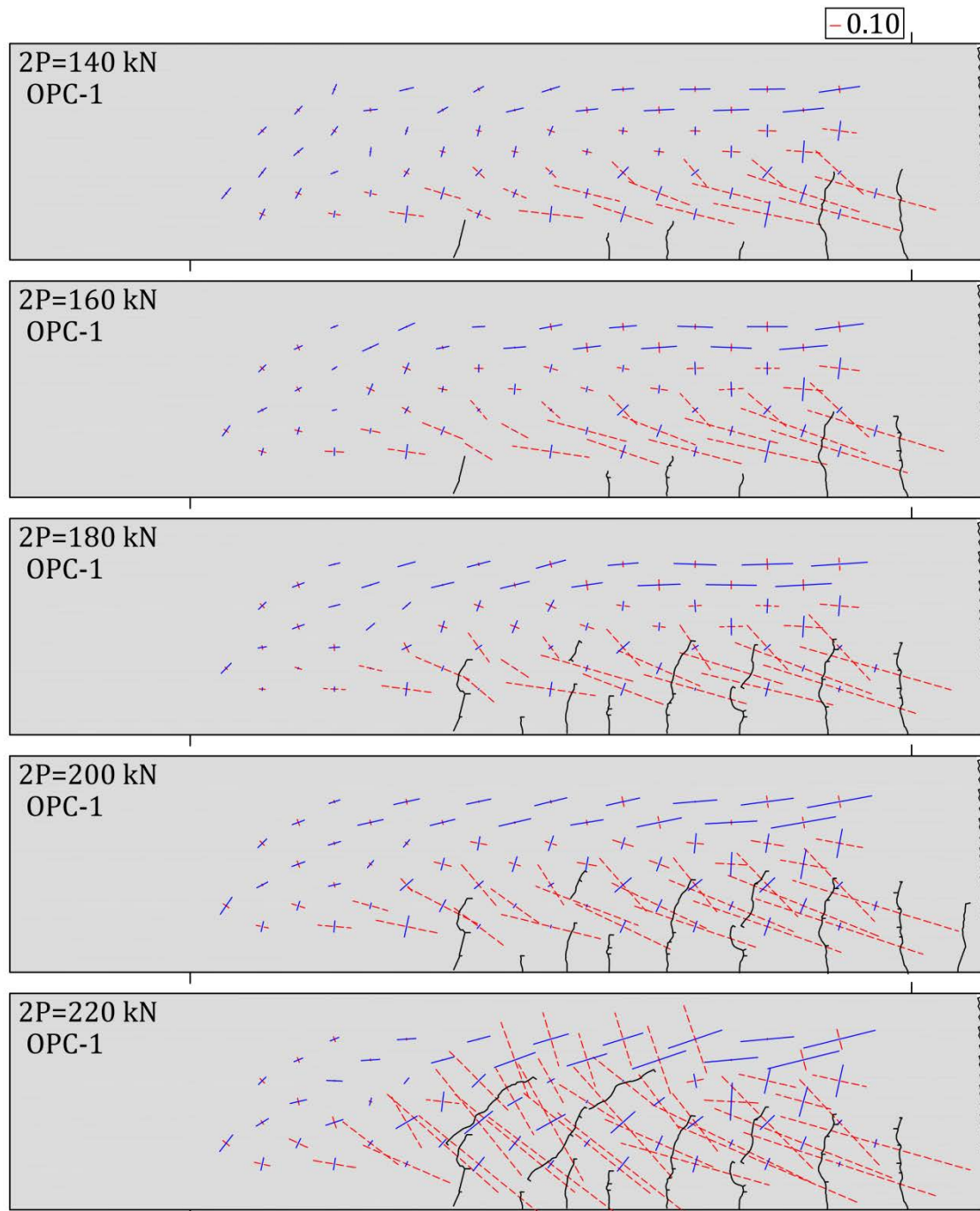


Figure 4.260 Principal strains and crack patterns in OPC-1 beam up to the loading level of 220 kN

4. Experimental program and test results

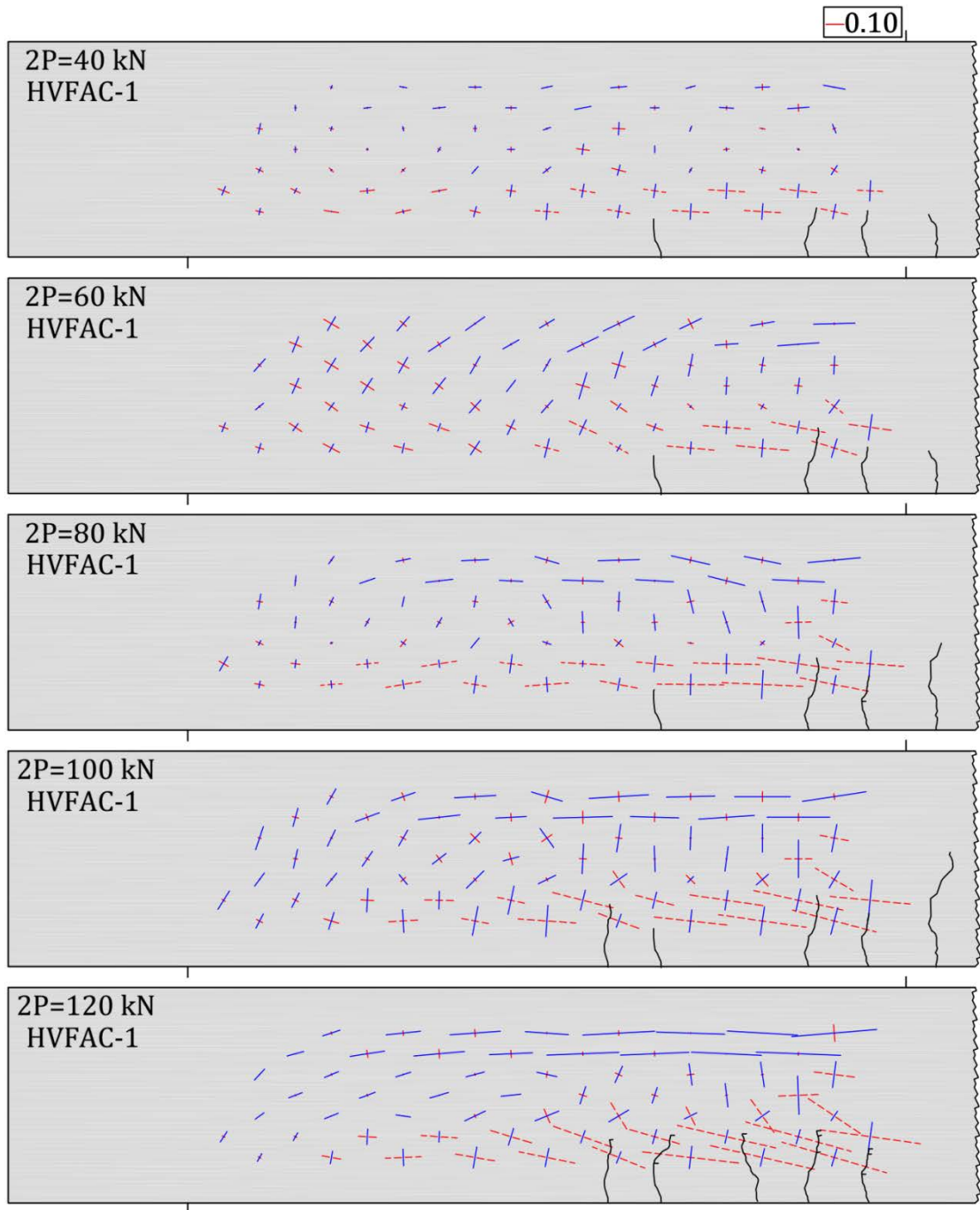


Figure 4.261 Principal strains and crack patterns in HVFAC-1 beam up to the loading level of 120 kN

4. Experimental program and test results

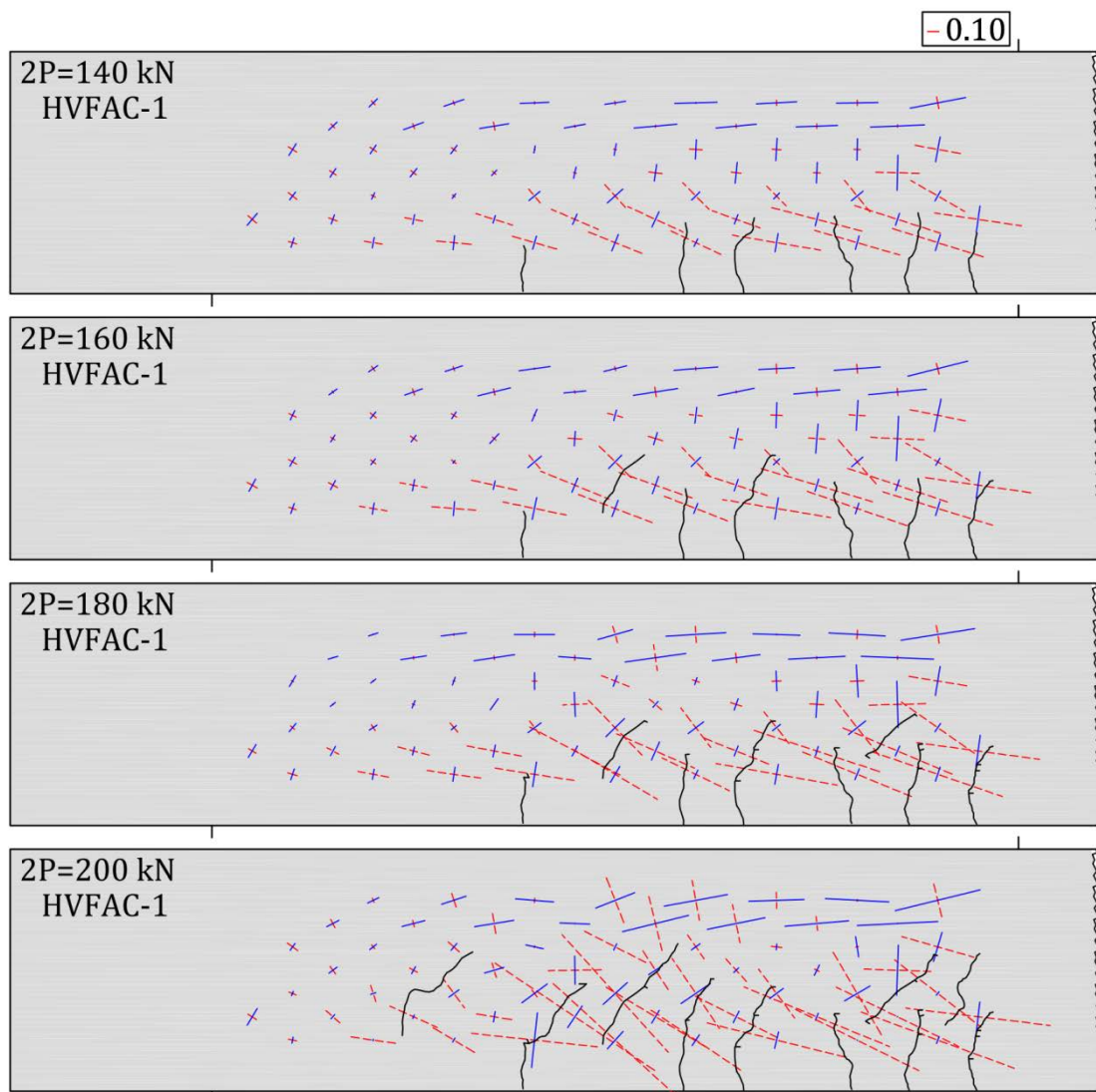


Figure 4.262 Principal strains and crack patterns in HVFAC-1 beam up to the loading level of 200 kN

This was a consequence of the longer flexural cracks dictating principal strains in this part. With further load increase and approaching the point of shear crack formation, the directions of principal strains increase inclination according to future shear crack angle. The direction of the principal tensile strains (red lines) were perpendicular to formed flexural and shear cracks in most cases.

The principal stress and strain directions and values were similar in both beams. During the beam testing, the first visible shear crack was marked and this zone of the beam was selected for maximum strain evaluation. Evolution of the principal

4. Experimental program and test results

strains and stresses in the first shear crack zone for the OPC-1 and HVFAC-1 beams are shown in Tables 4.32 and 4.33.

Loading steps with the principal tension strains higher than 0.10‰ were identified as the moments of concrete cracking. The loading step before cracking was chosen for the closest maximum strain evaluation. For both OPC-1 and HVFAC-1 beams the maximum strains appeared in the loading steps between 120 kN and 140 kN at similar normalized shear stress values. This was approximately 60 kN lower than the loading level marked as the first visible shear crack for both OPC-1 and HVFAC-1 beams. The principal strain and stress values versus normalized shear stress for OPC-1 and HVFAC-1 beams are plotted in Figures 4.263 and 4.264.

Table 4.32 Principal strains/stresses in the OPC-1 beam first shear cracking zone

2P (kN)	60	80	100	120	140	160	180	200	220
$v/\sqrt[3]{f_c}$	0.041	0.054	0.068	0.082	0.095	0.109	0.122	0.136	0.150
ϵ_1 (‰)	0.02	0.14	0.07	0.09	0.13	0.23	0.25	0.46	1.29
ϵ_2 (‰)	-0.08	-0.14	-0.04	-0.08	-0.04	-0.02	-0.05	-0.06	-0.32
σ_1 (MPa)	0.18	2.50	1.88	3.01	5.43	9.97	10.60	19.45	53.17
σ_2 (MPa)	-3.30	-1.11	-0.84	-2.67	-0.58	1.12	0.15	1.35	-2.56

Table 4.33 Principal strains/stresses in the HVFAC-1 beam first shear cracking zone

2P (kN)	40	60	80	100	120	140	160	180	200
$v/\sqrt[3]{f_c}$	0.029	0.044	0.058	0.073	0.087	0.102	0.116	0.131	0.146
ϵ_1 (‰)	-0.02	0.02	0.02	-0.02	0.08	0.27	0.39	0.66	1.37
ϵ_2 (‰)	-0.05	-0.09	-0.05	-0.11	-0.14	-0.18	-0.16	-0.22	-0.29
σ_1 (MPa)	-0.97	0.08	0.40	-1.34	1.79	7.60	11.66	20.21	42.90
σ_2 (MPa)	-1.89	-2.95	-1.44	-3.62	-4.14	-4.21	-2.80	-2.99	-0.39

4. Experimental program and test results

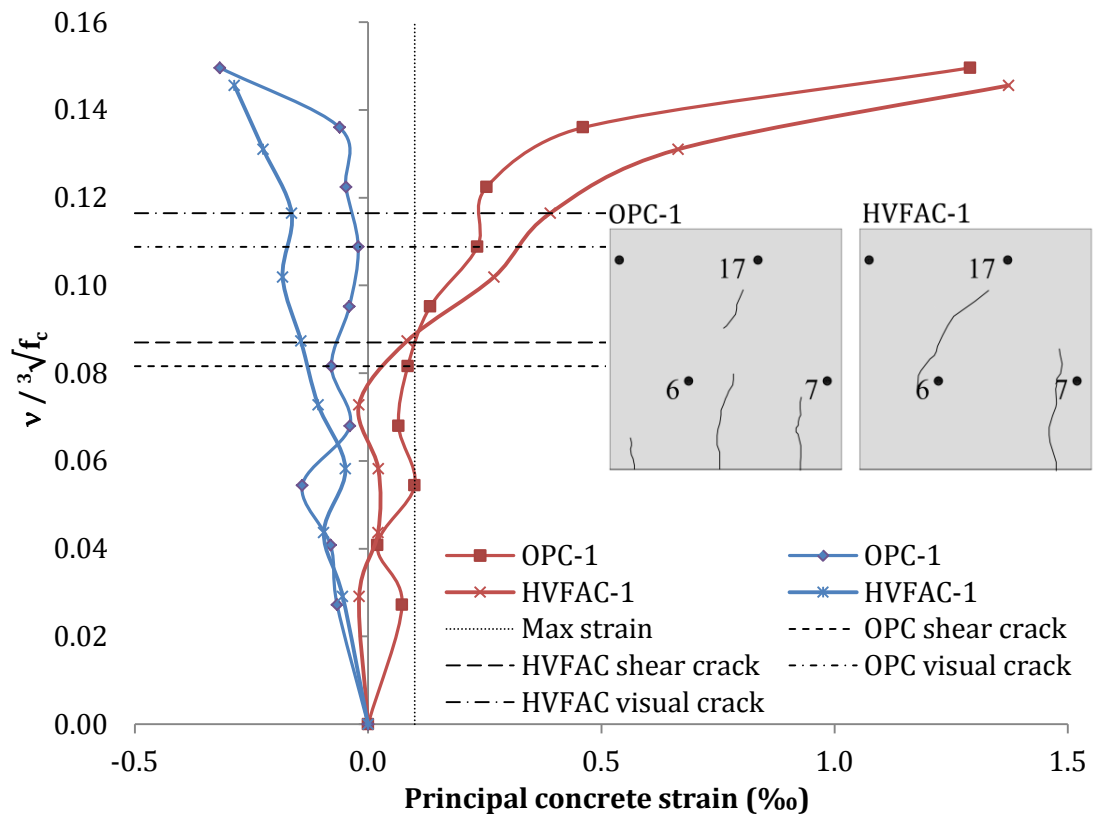


Figure 4.263 Principal concrete strain developments for beams OPC-1 and HVFAC-1

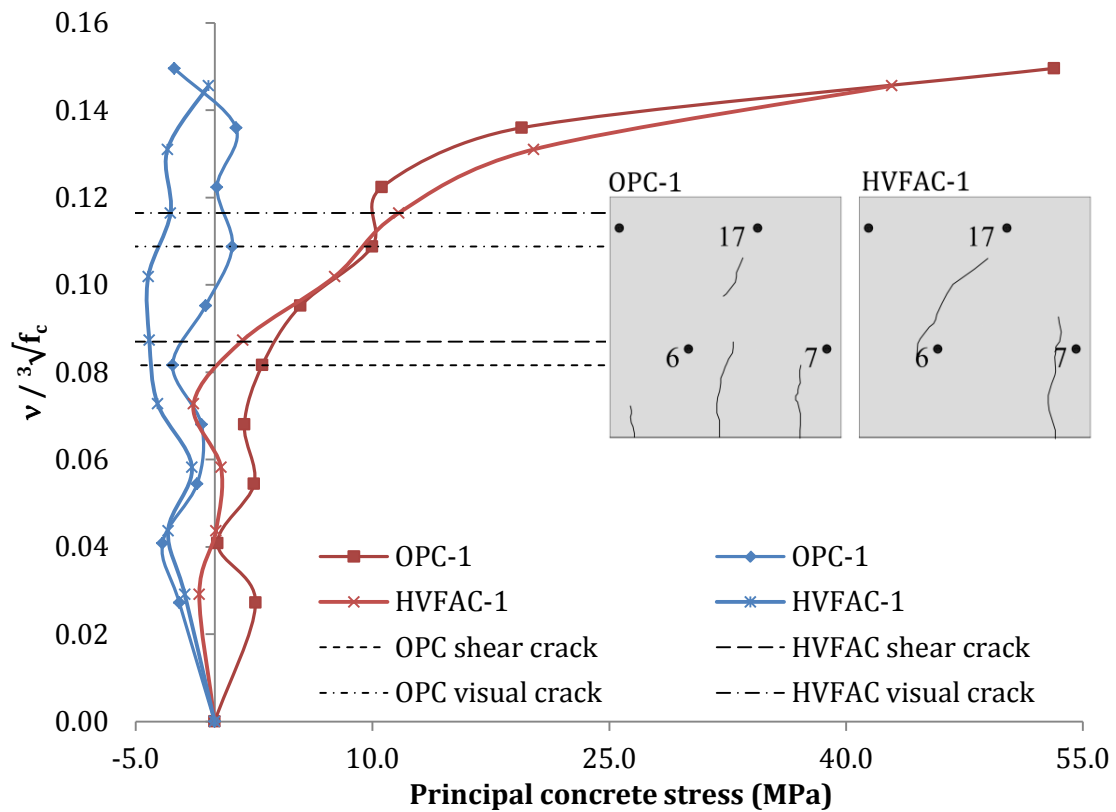


Figure 4.264 Principal concrete stress developments for beams OPC-1 and HVFAC-1

4. Experimental program and test results

Four loading levels are marked in these types of diagrams: normalized shear stress values at the first visible shear crack and at calculated shear crack formation in the OPC-1 and HVFAC-1 beams. The value of the maximum principal strain of 0.10‰ is also marked with a vertical line. It can be seen that the principal strains have similar trend in both beams, with higher values of strains in the OPC-1 beam after cracking. Compressive principal strains were lower than 0.5‰ in both beams. Stress development was similar in both OPCC and HVFAC beams with smaller difference compared with the principal strains due to 25% higher modulus of elasticity in OPCC. The first shear cracking occurred at the principal tensile stresses in the range from 3.0 MPa to 5.4 MPa in the OPC-1 beam and in the range from 1.8 MPa to 7.6 MPa in the HVFAC-1 beam.

4.4.13.2. Principal strains in the OPC-2 and HVFAC-2 beams

All measured strains in the first and in the last loading step before failure in the OPC-2 and HVFAC-2 beams are shown in Figures 4.265 and 4.266. The sum of all measured strains was calculated and presented versus the normalized shear stress in Figure 4.267.

It can be seen that the development of measured strains was similar in both OPC-2 and HVFAC-2 beams. The sum of all measured strains shown in Figure 4.269 indicates similar development of strains in both OPCC and HVFAC beams.

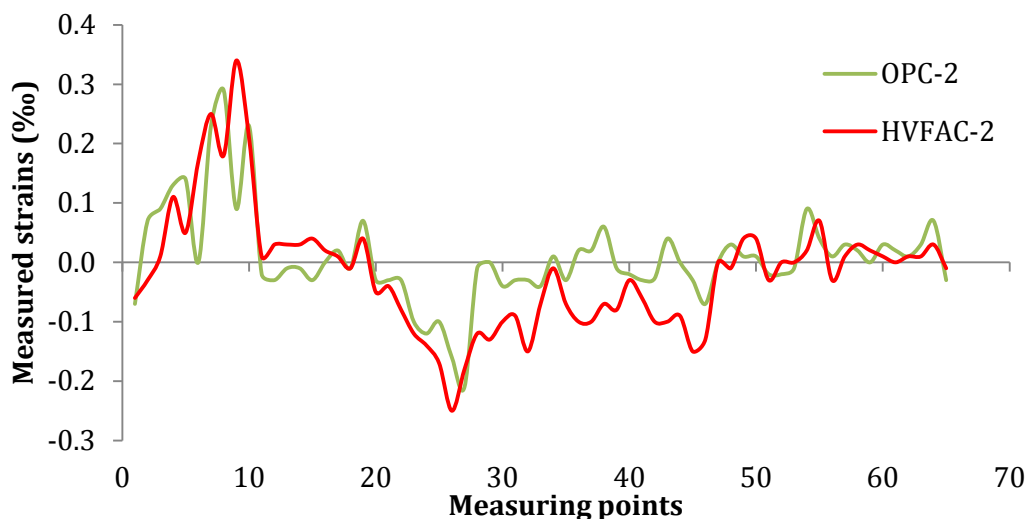


Figure 4.265 Measured values of strains in the first loading step for OPC-2 and HVFAC-2 beams

4. Experimental program and test results

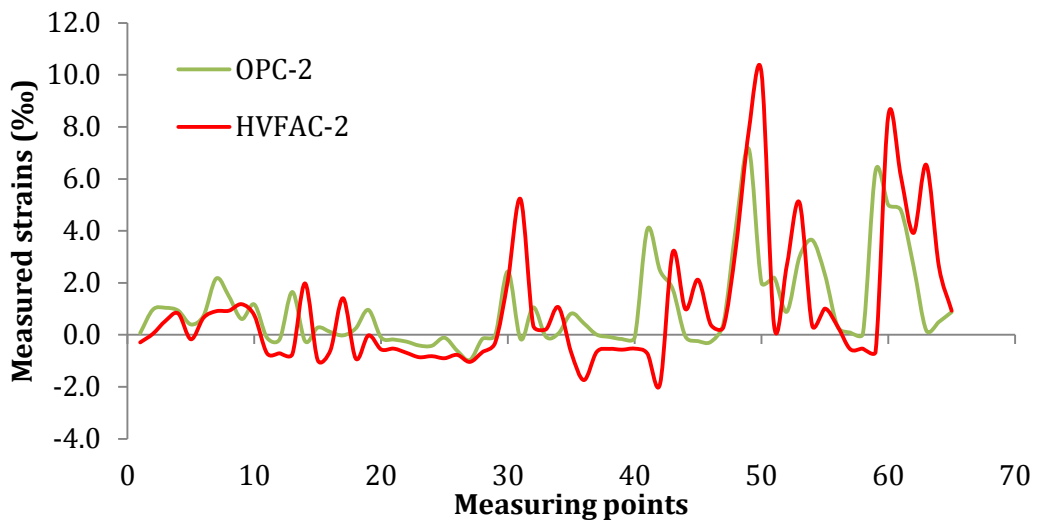


Figure 4.266 Measured values of strains in the last loading step for the OPC-2 and HVFAC-2 beams

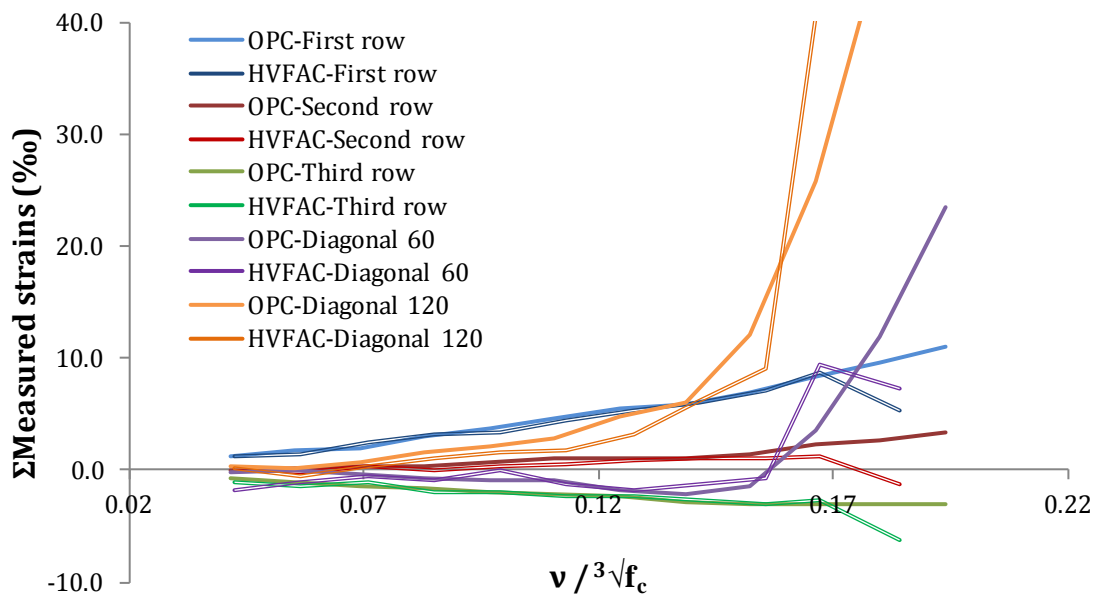


Figure 4.267. Sum of all measured strains in OPC-2 and HVFAC-2 beams versus normalized shear stress

The directions and intensity of the principal strains for beams OPC-2 and HVFAC-2 are shown in Figures 4.268 – 4.271. Due to the longer flexural cracks in the HVFAC-2 beam, the principal tension strains close to the beam midpoint were oriented approximately horizontally. The evolution of the principal strains and stresses in the shear crack zone for the OPC-2 and HVFAC-2 beams is shown in Tables 4.34 and 4.35.

4. Experimental program and test results

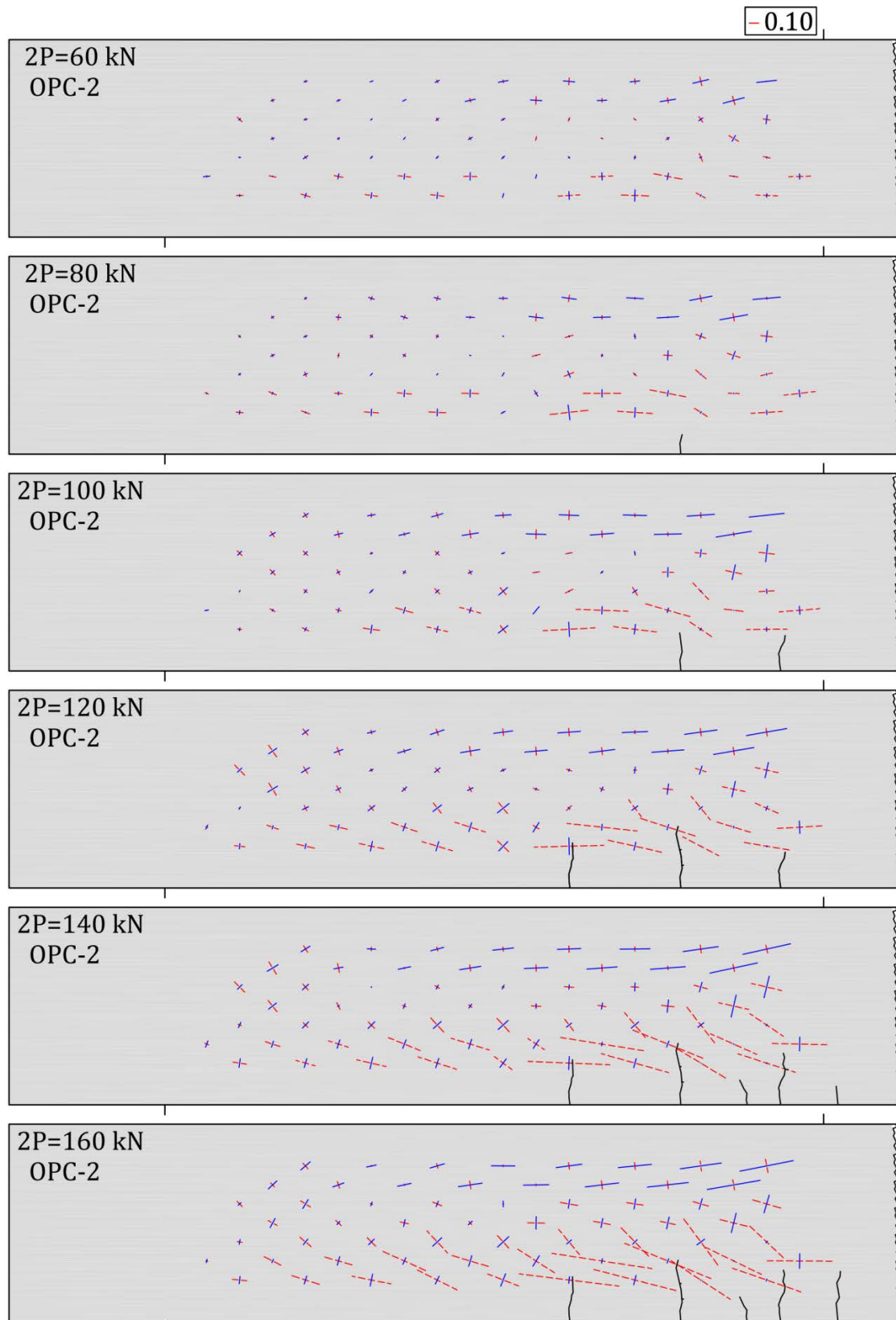


Figure 4.268 Principal strains and crack patterns in the OPC-2 beam up to the loading level of 160 kN

4. Experimental program and test results

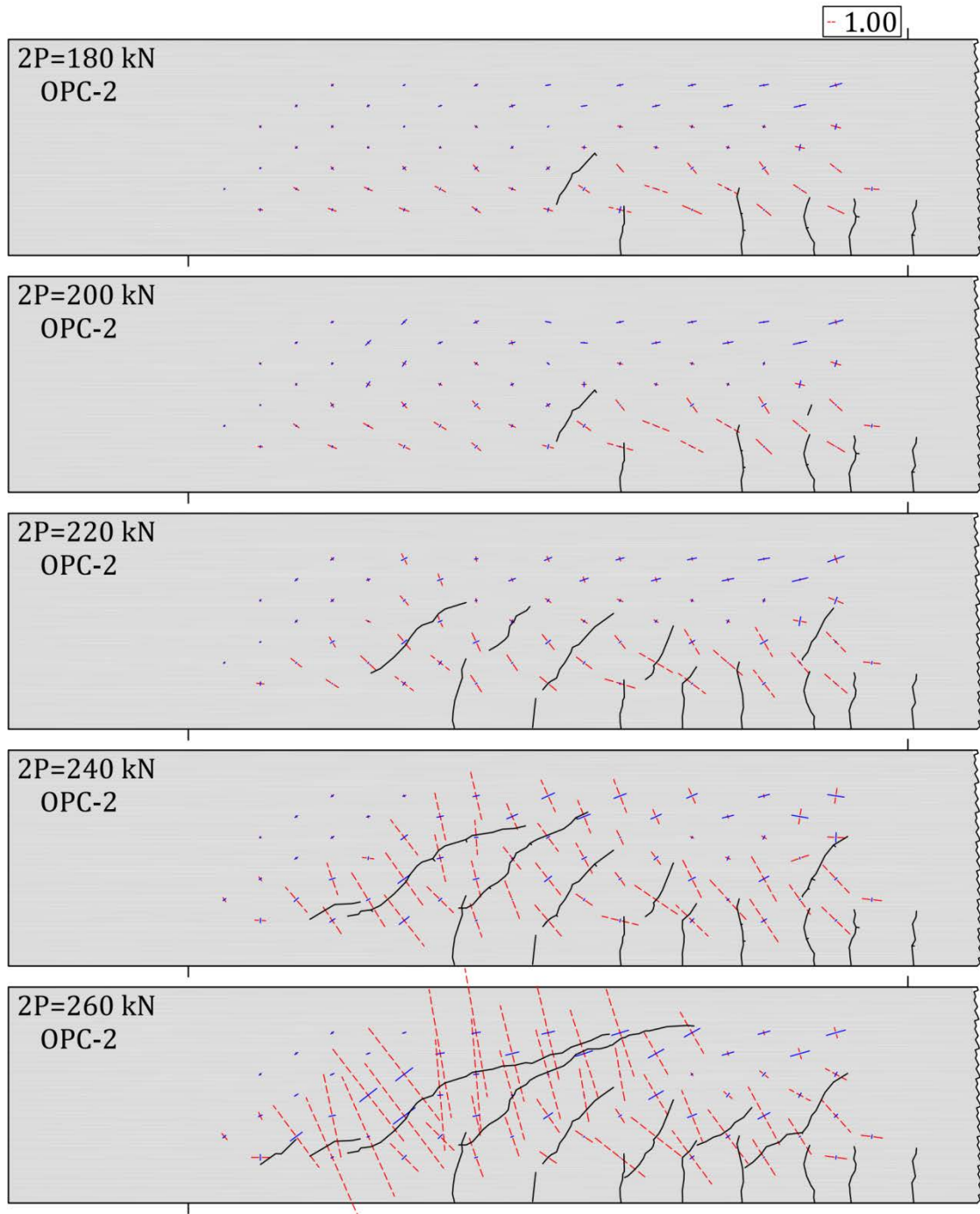


Figure 4.269 Principal strains and crack patterns in the OPC-2 beam up to the loading level of 260 kN

4. Experimental program and test results

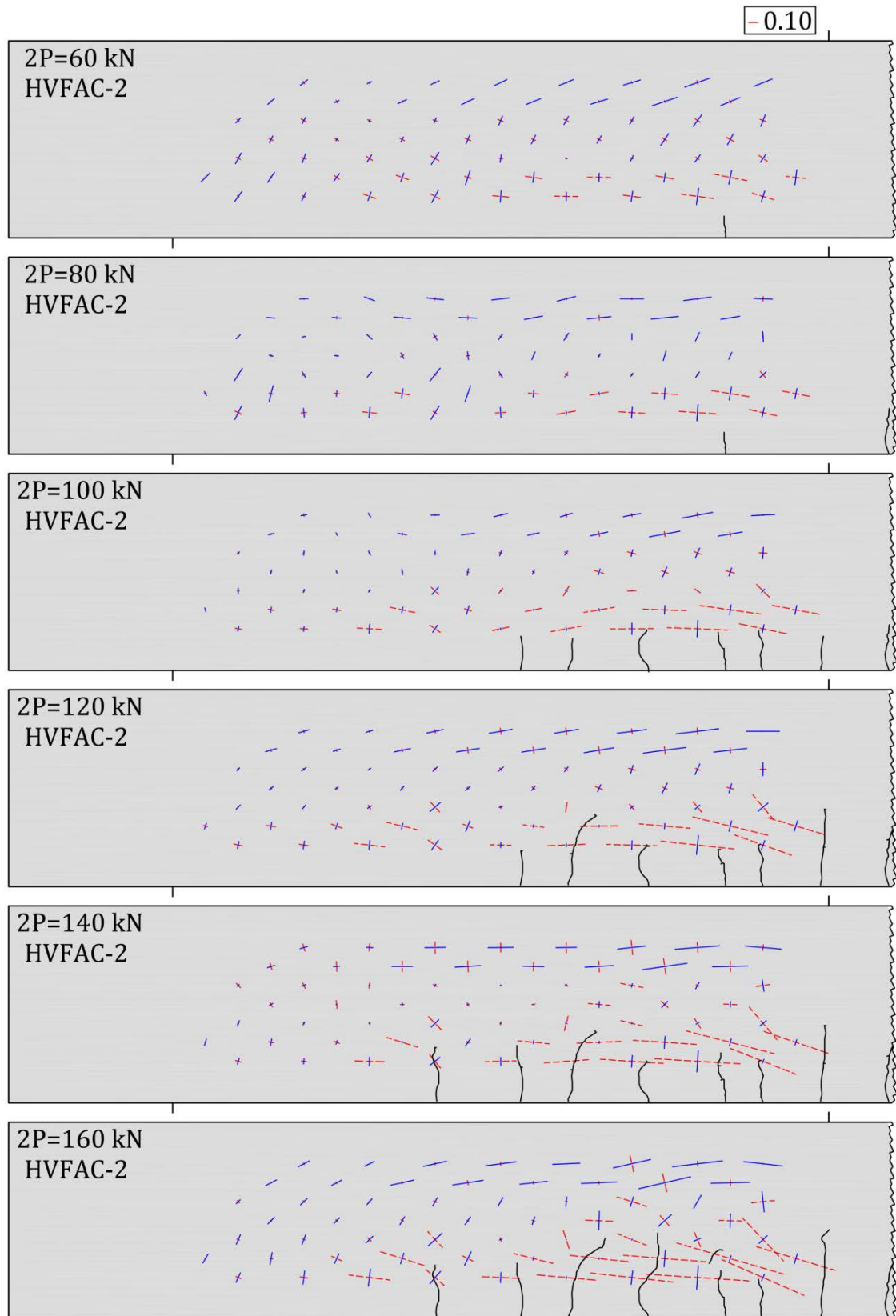


Figure 4.270 Principal strains and crack patterns in the HVFAC-2 beam up to the loading level of 160 kN

4. Experimental program and test results

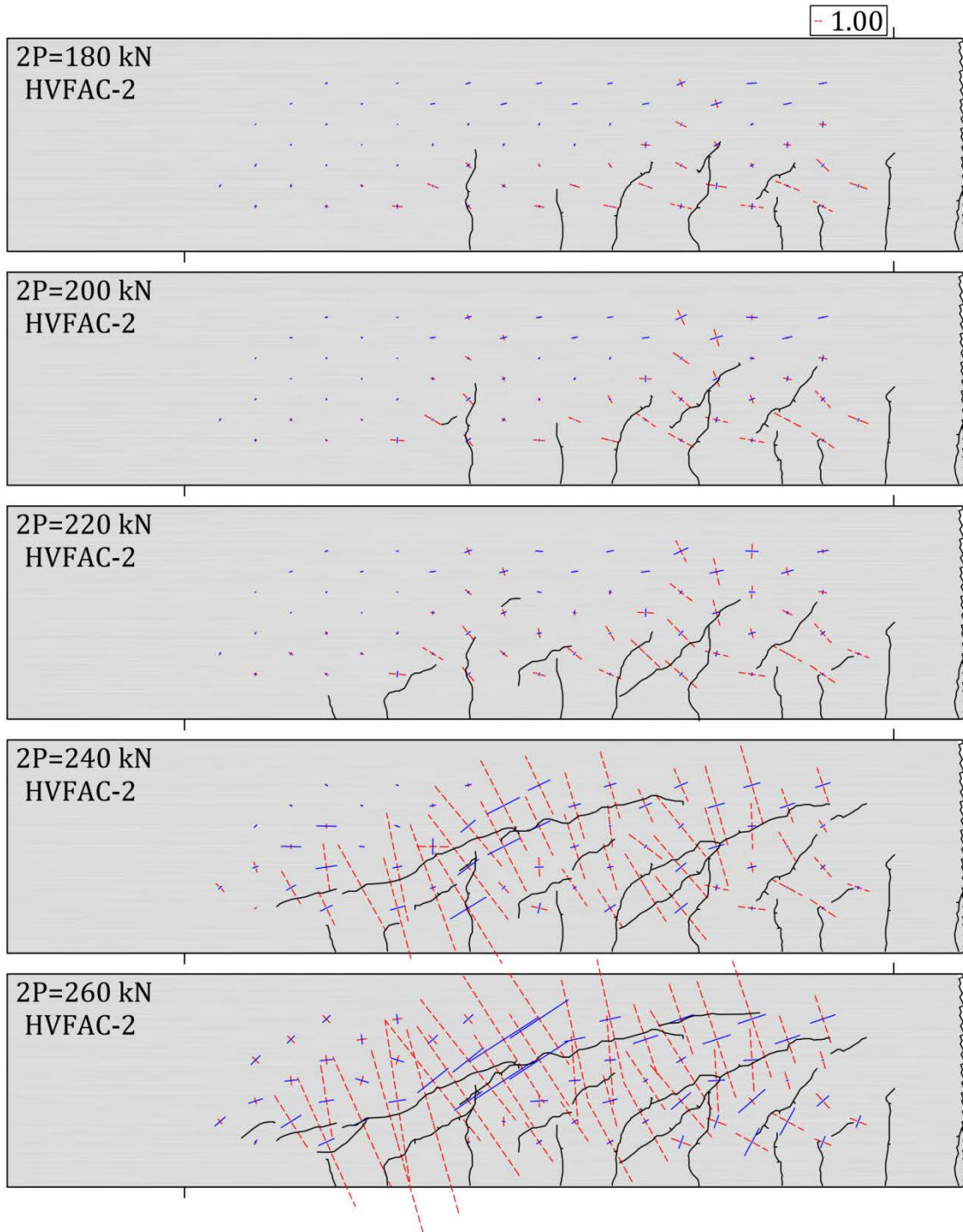


Figure 4.271 Principal strains and crack patterns in the HVFAC-2 beam up to the loading level of 260 kN

The principal tension strains indicated cracking at the loading between 120 kN and 140 kN for similar normalized shear stress values for both beams. In order to compare different types of concrete, the principal strain and stress versus

4. Experimental program and test results

normalized shear stress for the OPC-2 and HVFAC-2 beams are plotted in Figures 4.272 and 4.273.

The principal strains showed the same trend until approximately 180 kN when shear crack was first seen on the beam surface but after that point the HVFAC-2 beam exhibited higher strains in this zone. The principal stress distribution in the cracked zone was similar in both beams with higher stress values in the HVFAC-2 beam after 220 kN caused by the shear crack width increase in the HVFAC-2 beam. The first shear cracking occurred at the principal tensile stresses in the range from 2.1 MPa to 8.2 MPa in the OPC-2 beam and in the range from 1.9 MPa to 7.6 MPa in the HVFAC-2 beam.

Table 4.34 Principal strains and stresses in the first shear cracking zone in the OPC-2 beam

2P (kN)	80	100	120	140	160	180	200	260	280
$v/\sqrt[3]{f_c}$	0.055	0.069	0.083	0.097	0.111	0.125	0.138	0.180	0.194
ϵ_1 (‰)	-0.03	0.00	0.07	0.21	0.46	0.73	0.92	1.12	1.11
ϵ_2 (‰)	-0.07	-0.10	-0.12	-0.11	-0.13	-0.18	-0.20	-0.08	-0.08
σ_1 (MPa)	-1.91	-0.77	2.14	8.20	19.00	30.06	38.02	47.11	47.32
σ_2 (MPa)	-3.29	-4.43	-4.57	-3.00	-1.67	-1.63	-0.58	6.37	6.06

Table 4.35 Principal strains and stresses in the first shear cracking zone in the HVFAC-2 beam

2P (kN)	80	100	120	140	160	180	200	240	260
$v/\sqrt[3]{f_c}$	0.057	0.071	0.085	0.099	0.113	0.127	0.142	0.167	0.184
ϵ_1 (‰)	0.00	0.10	0.07	0.24	0.33	0.65	1.08	4.41	6.55
ϵ_2 (‰)	-0.07	-0.07	-0.09	-0.04	-0.11	-0.15	-0.15	-0.37	-0.59
σ_1 (MPa)	-0.43	2.78	1.85	7.56	10.05	20.09	34.18	141.24	209.66
σ_2 (MPa)	-2.17	-1.74	-2.38	0.26	-1.44	-0.78	2.08	16.82	23.52

4. Experimental program and test results

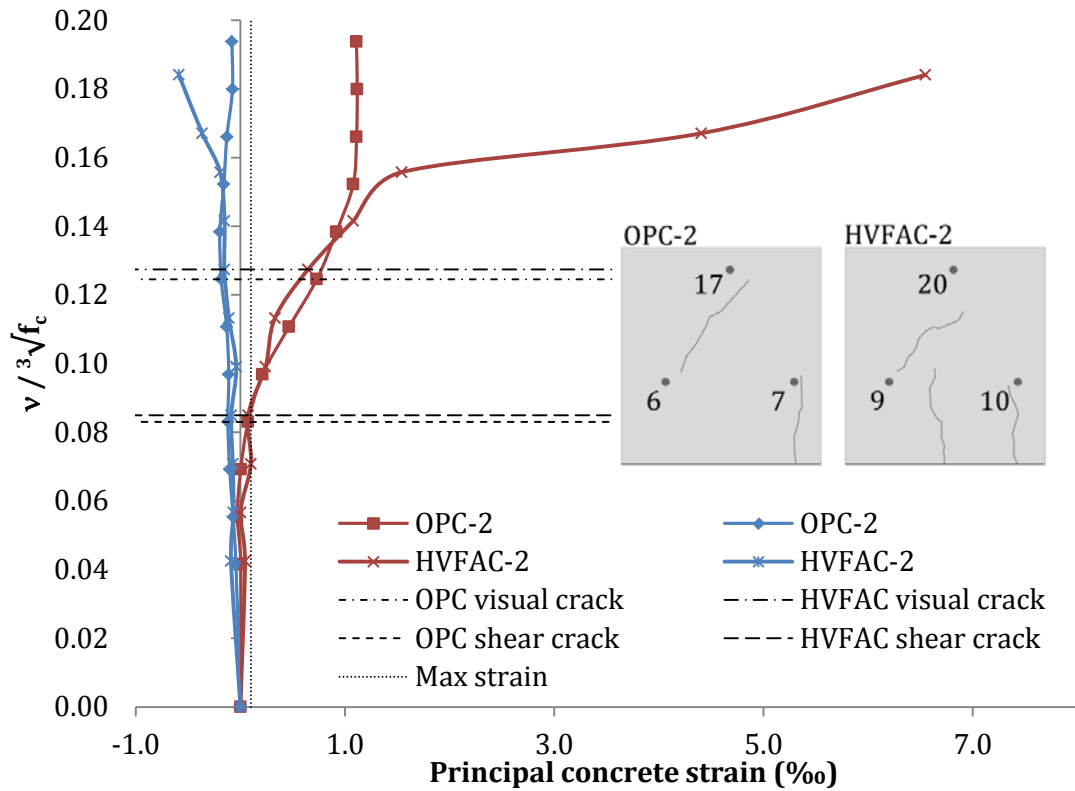


Figure 4.272 Principal concrete strain developments for beams OPC-2 and HVFAC-2

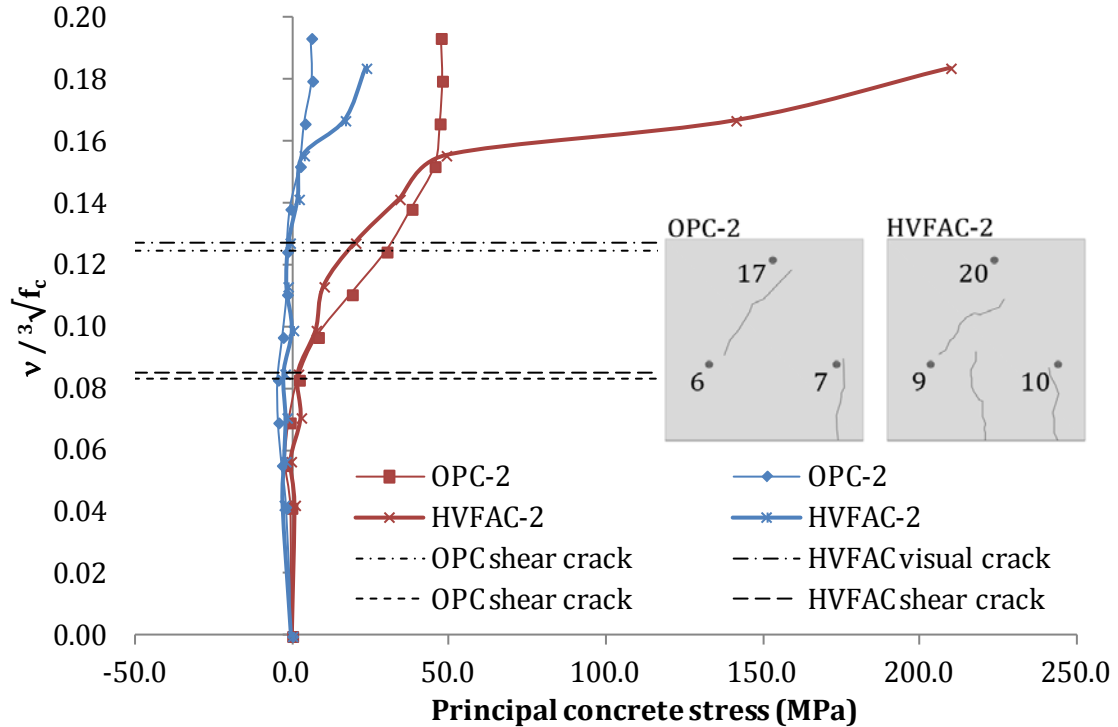


Figure 4.273 Principal concrete stress developments for beams OPC-2 and HVFAC-2

4. Experimental program and test results

4.4.13.3. Principal strains in the OPC-3 and HVFAC-3 beams

The following figures and tables are presented for OPC-3 and HVFAC-3 beams: measured strains in the first and in the last loading step before failure (Figures 4.274 and 4.275); the sum of all measured strains (Figure 4.276); directions and the intensity of the principal strains (Figures 4.277 - 4.280); evolution of the principal strains and stresses in the shear crack zone is shown in Tables 4.36 and 4.37; the concrete principal strain and stress versus normalized shear stress (Figures 4.281 and 4.282).

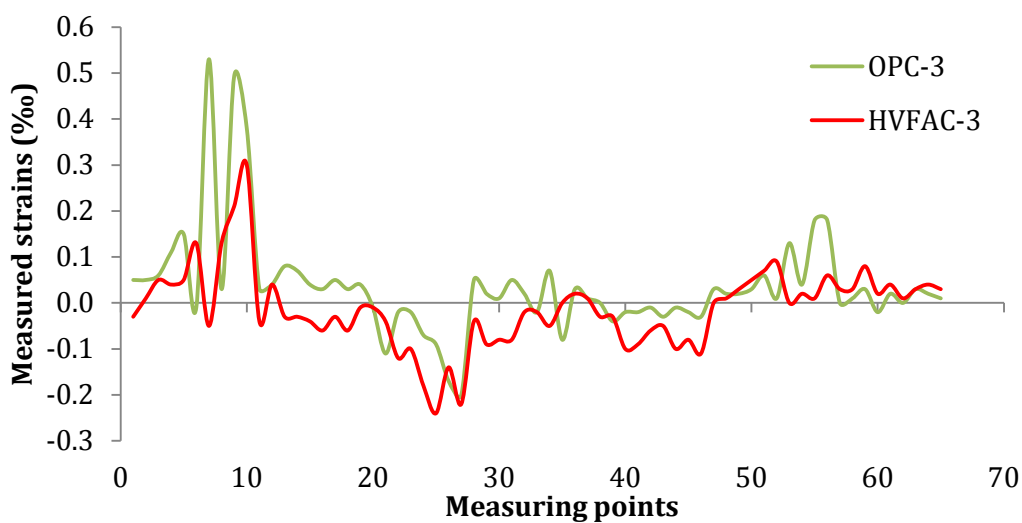


Figure 4.274 Measured values of strains in the first loading step for the OPC-3 and HVFAC-3 beams

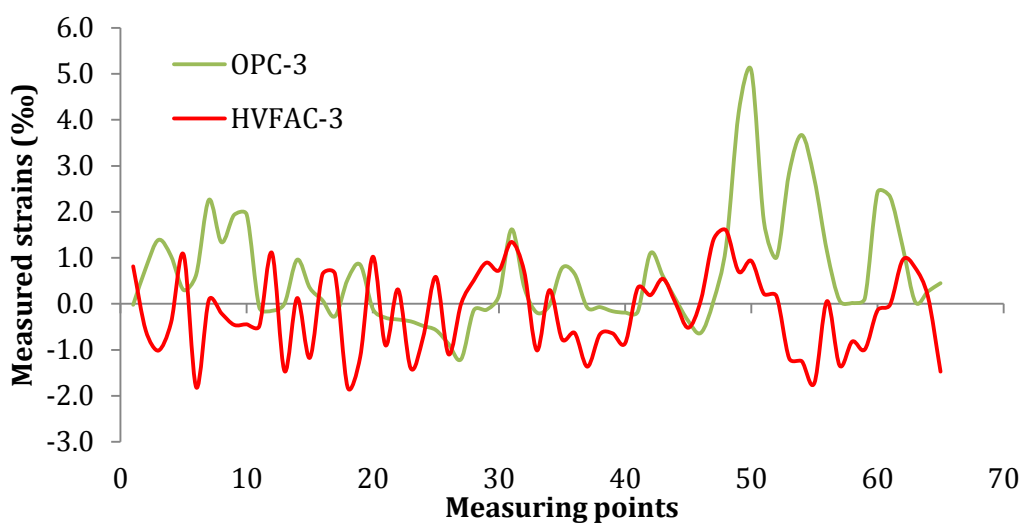


Figure 4.275 Measured values of strains in the last loading step for the beams OPC-3 and HVFAC-3

4. Experimental program and test results

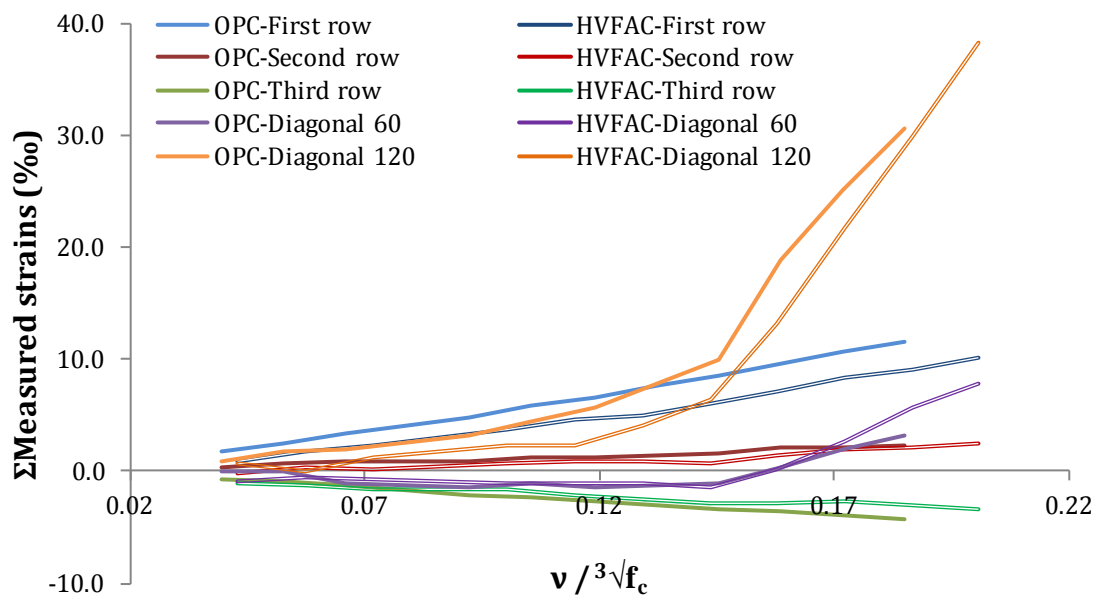


Figure 4.276. Sum of all measured strains in OPC-3 and HVFAC-3 beams versus normalized shear stress

The difference between OPC-3 and HVFAC-3 measured strains was greater than in the previous cases. Figures 4.274 and 4.275 show higher tension strains and lower compression strains in the OPC-3 beam. It can be seen that strains measured in the OPC-3 beam in the first row and in the 120° direction were higher compared with corresponding strain in the HVFAC-3 beam. This difference can be a consequence of different failure modes. No specific conclusions regarding measured strains can be obtained due to different crack patterns that developed in different beams.

Strain measurements were not performed up to failure, but only up to 75% of the ultimate beam capacity and the principal strains were presented for loads from 100 kN to 280 kN. Difference in failure mode between the OPC-3 and HVFAC-3 beams was also noticed in the principal strain measurements in shear span. More flexural cracks developed in the OPC-3 beam in the part of the shear span closer to the beam midpoint. This was the reason why the principal tension strains were approximately horizontal in that zone in the OPC-3 beam. The difference between the OPC-3 and HVFAC-3 beams was noticed in the middle part of the shear span and closer to the beams' midpoint.

4. Experimental program and test results

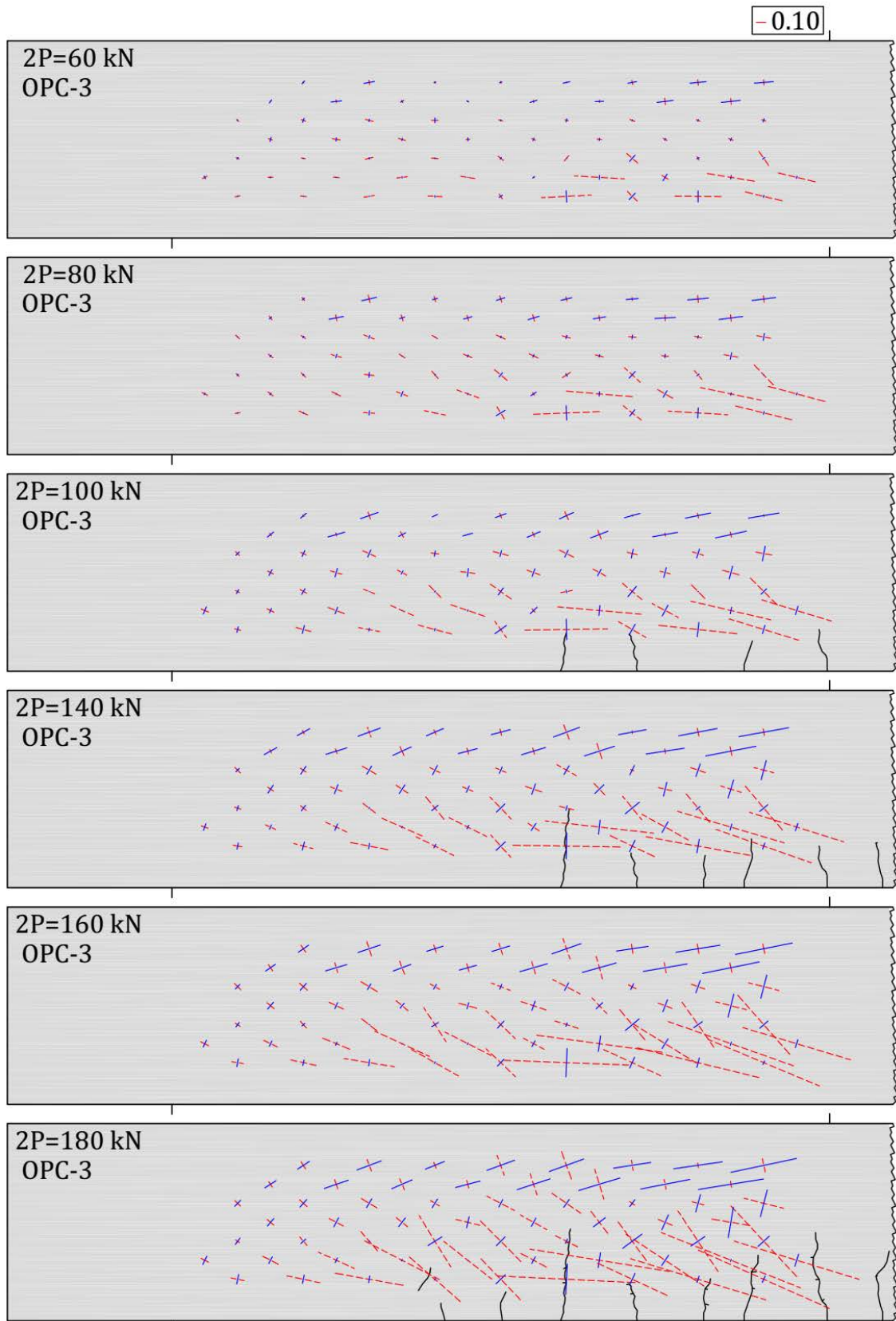


Figure 4.277 Principal strains and crack patterns in the OPC-3 beam up to the loading level of 180 kN

4. Experimental program and test results

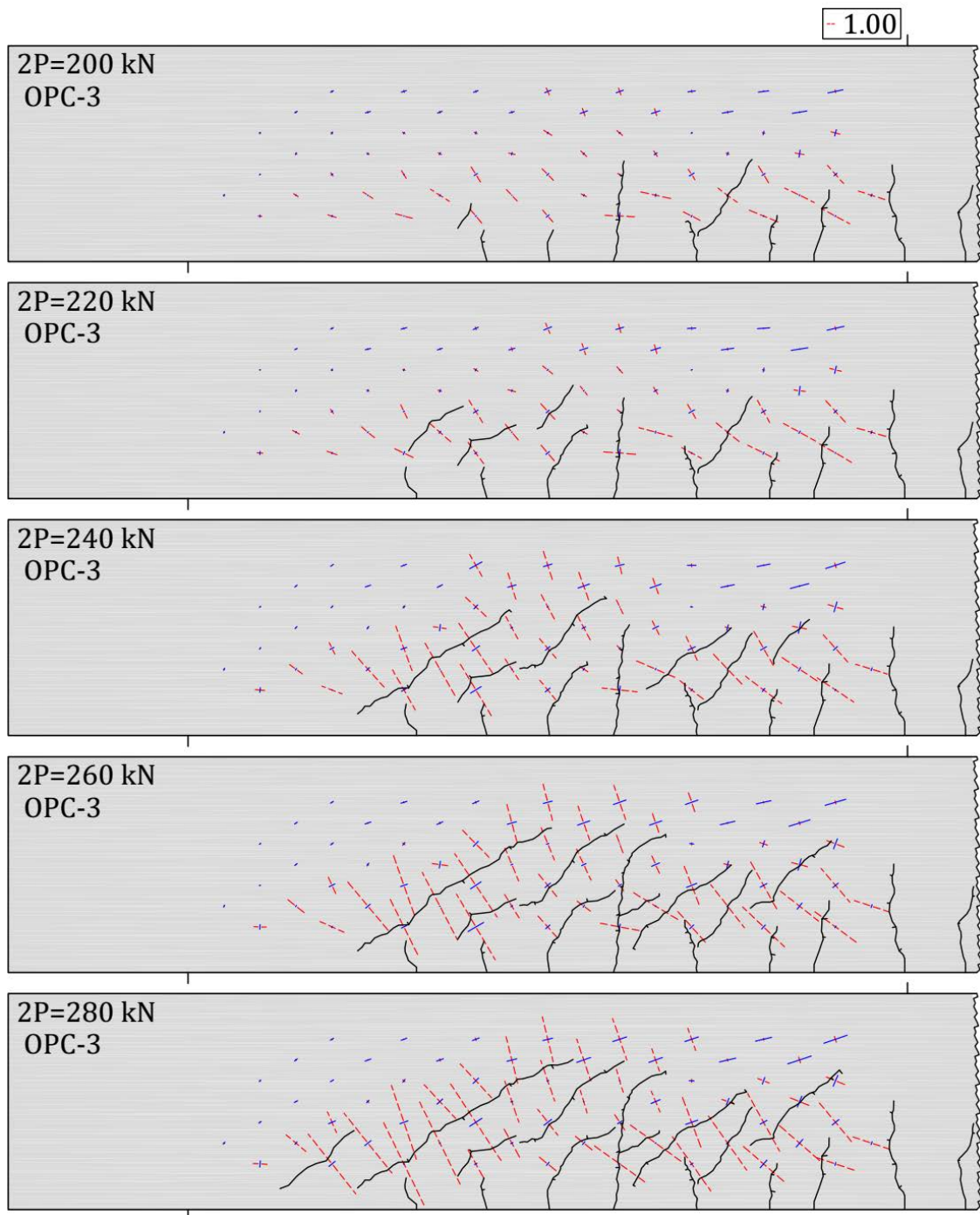


Figure 4.278 Principal strains and crack patterns in the OPC-3 beam up to the loading level of 280 kN

4. Experimental program and test results

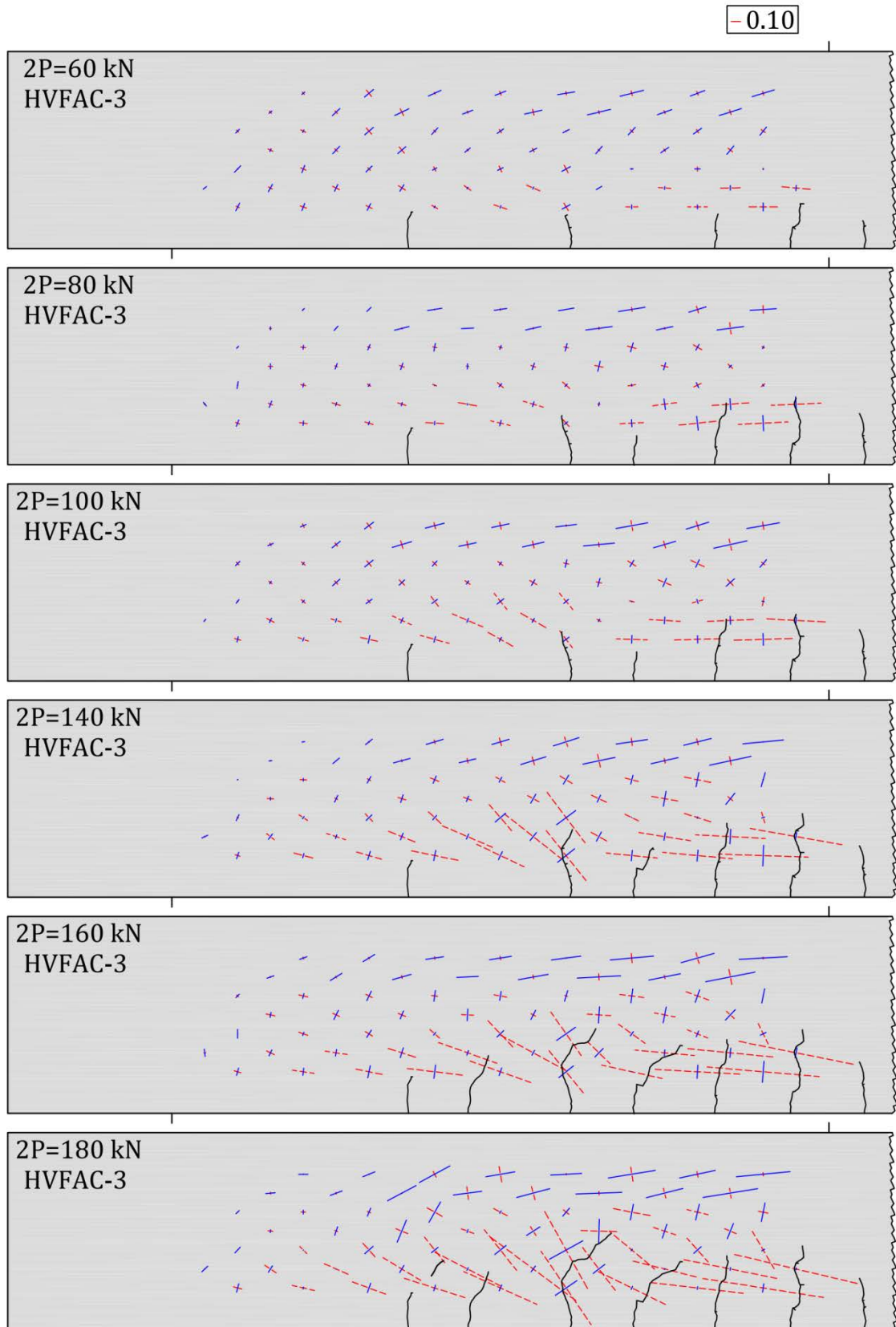


Figure 4.279 Principal strains and crack patterns in the HVFAC-3 beam up to the loading level of 180 kN

4. Experimental program and test results

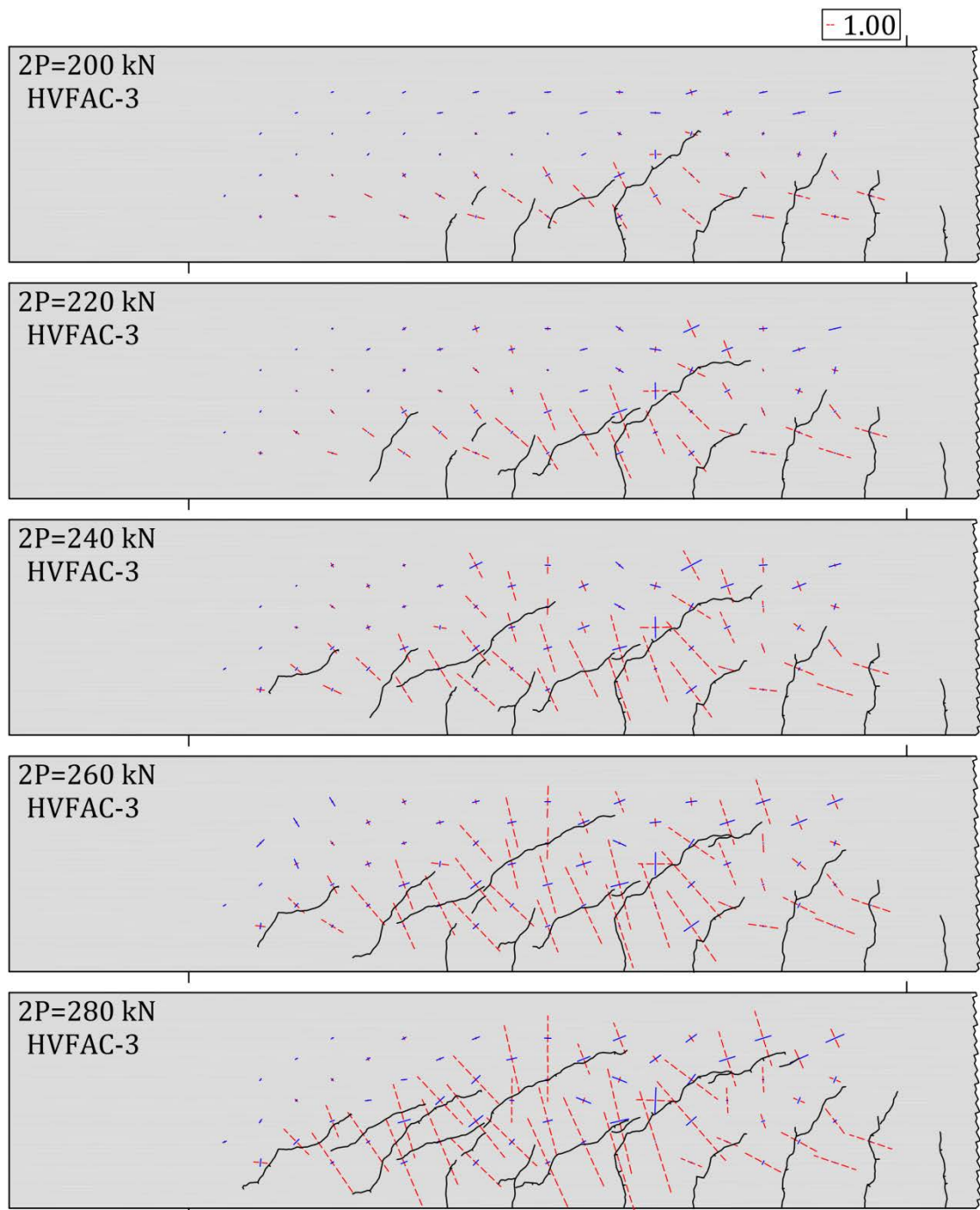


Figure 4.280 Principal strains and crack patterns in the HVFAC-3 beam up to the loading level of 280 kN

The principal strain angle was more inclined in the HVFAC-3 beam indicating shear cracking. In the part of the beams close to the support, no significant differences were noticed between the OPC-3 and HVFAC-3 beams.

4. Experimental program and test results

Table 4.36 Principal strains and stresses in the first shear cracking zone in the OPC-3 beam

2P (kN)	60	80	100	140	160	180	200	220	280
$v/\sqrt[3]{f_c}$	0.040	0.053	0.066	0.092	0.106	0.119	0.132	0.145	0.185
ε_1 (‰)	0.08	0.10	0.13	0.17	0.21	0.27	0.50	0.83	4.35
ε_2 (‰)	0.02	0.05	0.00	-0.01	0.01	-0.01	-0.04	-0.08	-0.49
σ_1 (MPa)	3.80	4.82	5.57	7.10	9.04	11.61	21.32	35.43	184.11
σ_2 (MPa)	1.40	3.15	1.02	0.88	2.05	1.91	2.60	3.74	16.61

Table 4.37 Principal strains and stresses in the first shear cracking zone in the HVFAC-3 beam

2P (kN)	60	80	100	140	160	180	200	220	280
$v/\sqrt[3]{f_c}$	0.043	0.057	0.072	0.100	0.115	0.129	0.143	0.158	0.201
ε_1 (‰)	0.09	0.10	0.23	0.67	0.58	0.95	1.53	3.05	5.53
ε_2 (‰)	-0.07	-0.05	-0.09	-0.24	-0.16	-0.28	-0.42	-0.69	-1.01
σ_1 (MPa)	2.50	3.00	6.79	20.24	17.78	29.10	47.13	95.02	173.70
σ_2 (MPa)	-1.72	-0.92	-1.57	-3.55	-1.35	-3.01	-3.83	-2.68	3.14

Regardless of the failure mode, the OPC-3 beam developed a similar shear crack pattern like the HVFAC-3 beam so the same analysis of principal strains was performed for both beams.

Tables 4.36 and 4.37 show that the maximum strain value of 0.10‰ is exceeded after 80 kN load for both beams. This indicates that the shear crack was formed between 80 kN and 100 kN for both beams. This was more than two times lower than the value of 180 kN when the shear crack was first noticed.

The development of the principal strains in the shear crack zone was similar in both beams before shear cracking. Higher values of principal strains in the HVFAC-3 beam were noticed after the shear crack formation indicating higher shear crack width in the HVFAC-3 beam and.

4. Experimental program and test results

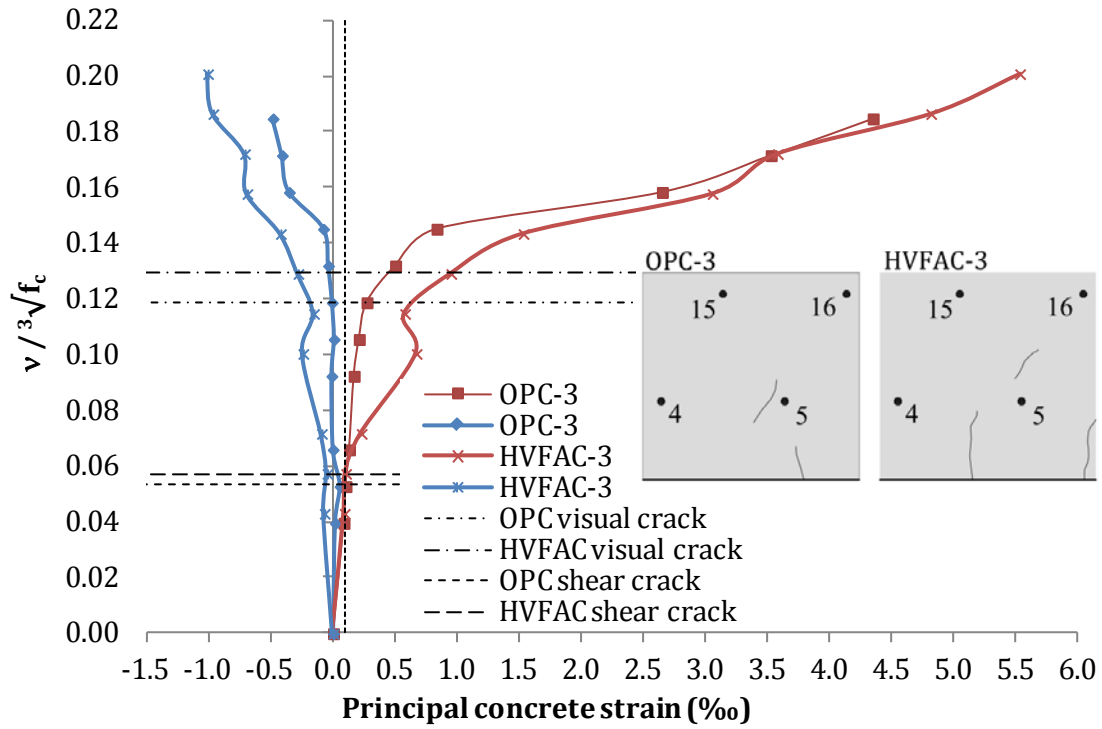


Figure 4.281 Principal concrete strain developments for beams OPC-3 and HVFAC-3

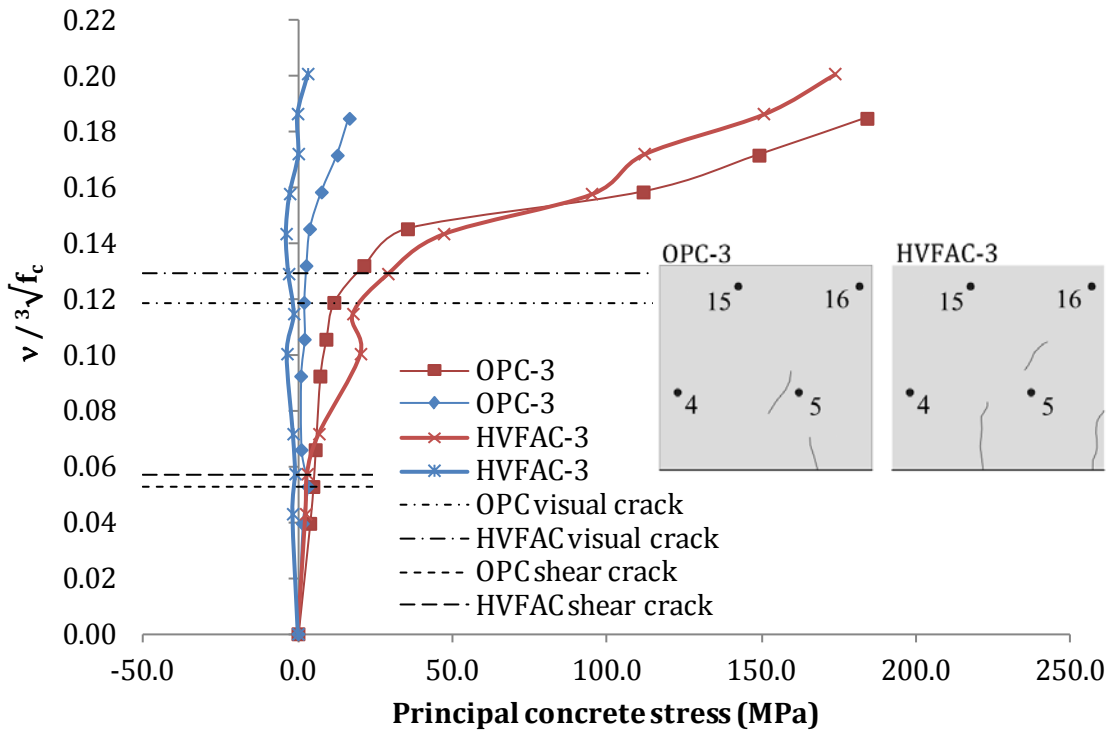


Figure 4.282 Principal concrete stress developments for beams OPC-3 and HVFAC-3

The principal stress development was similar in both beams with lower difference between values obtained for the OPC-3 and HVFAC-3 beams due to higher modulus of elasticity of beam OPC-3. The first shear cracking occurred at the principal

4. Experimental program and test results

tensile stresses in the range from 4.8 MPa to 5.6 MPa in the OPC-3 beam and in the range from 3.0 MPa to 6.8 MPa in the HVFAC-3 beam.

4.4.14. Conclusions

In the first part of the beams' shear behavior testing, fresh and hardened concrete properties of selected HVFAC and OPCC were tested.

- The test results showed that HVFAC mixture C200_F200 had up to 6% lower fresh and hardened concrete density compared with the OPC_S mixture. Workability of the mixtures was similar and corresponded to the slump class S3 according to the EN 206 standard;
- The 90-day compressive strength of OPC_S was 10% higher compared with the C200_F200 samples cured in water. The difference was higher for specimens cured the same as beams—up to 22%;
- HVFAC and OPCC samples cured the same like beams had, on average, 2% and 8% higher compressive strengths compared with the samples cured in water, respectively;
- For samples cured the same like beams, the splitting tensile strength was up to 30% lower and the flexural tensile strength up to 42% lower in HVFAC mixture compared with the OPCC;
- It can be concluded that different curing regime had higher influence on the tensile strength compared with the compressive strength;
- The modulus of elasticity was higher in the OPC_S concrete mixture compared with the C200_F200 after both 28 and 90 days, and especially for the samples cured in the same way as the beams where the difference was 24%.

All beam specimens without and with stirrups experienced shear failure, except the OPC-3 beam made with a higher than minimum shear reinforcement that failed in flexure. Flexural failure was located at the midpoint of the beam caused by the crushing of the concrete at the compression zone due to the fact that the actual concrete strength was lower than the designed strength. The crack propagation in all beams began with the flexural cracks formation in the middle part of the beam. The behavior of beams with shear reinforcement was similar to the behavior of

4. Experimental program and test results

beams without stirrups up to the point of the first shear crack formation at 50-60% of the ultimate shear loading. Both OPCC and HVFAC beams specimens exhibited linear-elastic behavior approximately until the formation of the shear crack. The ultimate shear stress was higher for the HVFAC beams compared with the OPCC beams in groups 1, 2 and 3 for 2%, 11% and 6%, respectively.

All beams with shear reinforcement showed a significant bearing capacity after the shear cracking until failure. The OPCC beams showed a more ductile behavior, except in the case of beams with the minimum shear reinforcement ratio. The difference between OPCC and HVFAC beams falls within the 10% margin.

The maximum deflection under service loading was not significantly different in the OPCC and HVFAC beams for the first and the second group of beams. In beams with higher shear reinforcement, the maximum deflection was approximately 14% higher in the OPC-3 beam compared with the HVFAC-3 beam. This was mostly a consequence of different failure modes of beams. No significant difference in the stiffness of HVFAC and OPCC beams was noticed. The inclination of the linear-elastic part of the deflection-stress relationship was up to 10% higher for all HVFAC beams compared with the OPCC ones.

Reinforcement strains developed in the same way for both OPC-1 and HVFAC-1 beams without shear reinforcement until the first flexural cracks appeared. After that point in all three sections, the OPC-1 beam had higher strains for the same normalized shear stress. The maximum strain values in each measured section showed that the difference between the OPC-1 and HVFAC-1 beams was within the 10% margin. Reinforcement strains developed in the same way for all four beams with shear reinforcement until flexural cracks appeared. After that point, the OPCC beams had higher strains for the same normalized shear stress with the difference being within the 20% margin. In both types of beams with shear reinforcement, as a general trend, higher stirrups strains are shown in the HVFAC beams compared with the OPCC ones.

Concrete compressive strains at failure were higher in OPCC beams compared with the HVFAC ones. The concrete compressive strains were, on average, 12%, 19% and 31% higher in the OPC-1, OPC-2 and OPC-3 beams compared with the

4. Experimental program and test results

corresponding HVFAC beams, respectively. The distribution of strains along the beams' height was linear for all tested beams. The height of the concrete compression zone was similar in all HVFAC and OPCC corresponding cross sections. It can be concluded that no significant difference between the OPCC and HVFAC beams compressed concrete shear component existed.

The number, maximum vertical length and width of flexural cracks were higher in HVFAC beams compared with the OPCC beams in both service and the ultimate loading stage.

- The maximum flexural crack length at the service load level was, on average, 30% higher in HVFAC beams compared with the OPCC ones. This difference decreased to 25% at the ultimate loading level;
- The maximum crack widths were generally higher in HVFAC beams compared with the OPCC ones;
- The sum of all cracks at the service loading stage was, on average, 27% lower in OPCC beams compared with the HVFAC ones.

The analysis of measured concrete strains in the shear web showed similar trend in all tested OPCC and HVFAC beams, without any significant difference before shear cracking. The only difference between OPCC and HVFAC measured strains was seen in the beams with higher shear reinforcement ratio. Higher tension strains and lower compression strains in the OPC-3 beam were noticed compared with the corresponding HVFAC beam. The maximum difference was approximately up to 30-45%. This difference was most likely the consequence of different failure modes of the OPC-3 and HVFAC-3 beams. No specific conclusions regarding measured strains can be obtained due to different crack patterns that developed in different beams.

The first shear cracking appeared at similar normalized shear stress levels in corresponding OPCC and HVFAC beams. For OPC-1, OPC-2, HVFAC-1 and HVFAC-2 beams, the principal tension strains indicated shear cracking at the loading between 120 kN and 140 kN. In beams with higher shear reinforcement ratios, the shear cracking appeared at approximately 30% lower normalized shear stress

4. Experimental program and test results

compared with the beams from other two groups. The first shear cracking occurred at the principal tensile stress levels in the following range:

- 3.0 - 5.4 MPa in the OPC-1 beam;
- 1.8 - 7.6 MPa in the HVFAC-1 beam;
- 2.1 - 8.2 MPa in the OPC-2 beam;
- 1.9 - 7.6 MPa in the HVFAC-2 beam;
- 4.8 - 5.6 MPa in the OPC-3 beam;
- 3.0 - 6.8 MPa in the HVFAC-3 beam.

It can be seen that the shear cracking generally occurred at lower principal stress levels in the HVFAC beams that had lower modulus of elasticity. The development of the principal strains in the shear cracking zone was similar in both types of beams before shear cracking occurred. Higher values of principal strains in the HVFAC beams were noticed after the shear crack formation indicating higher shear crack widths compared with the OPCC beams. The principal stress development was also similar in both types of beams with lower difference between values obtained for OPCC and HVFAC beams due to the 25% higher modulus of elasticity in the OPCC beams.

5. ANALYSIS AND DISCUSSION OF RESULTS

5. Analysis and discussion of results

5.1. INTRODUCTION

This chapter is divided in two parts and it presents the analysis of HVFAC material and structural properties.

In the first part, the analysis of HVFAC mechanical properties was done. The database of available HVFAC mixtures tested for basic mechanical properties was made and analyzed. The application of code predictions defining the mechanical properties of OPCC defined in EN 1992-1-1 was evaluated for HVFAC mixtures from the database. All proposals for modification of those predictions which were found in literature were re-evaluated using the collected HVFAC database. Own proposal for FA efficiency factor (k) was made as the function of FA chemical and physical properties. This analysis was also done on own HVFAC experimental results.

In the second part, the analysis of flexural and shear behavior of full-scale HVFAC beams was done. First, the variation of the HVFAC compressive strength based on the database of own experimental results of HVFAC samples was analyzed. The analysis of the flexural and shear behavior of full-scale beams was done based on own experimental results and the HVFAC beams database collected from current literature. Evaluation of the equations defined in BAB '87 (Faculty of Civil Engineering 1995), European Standard EN 1992-1-1 (CEN 2004), American Standard ACI 318 (ACI 2008) and *fib* Model Code 2010 (*fib* 2010a; b) in designing HVFAC beams was analyzed on the OPCC and HVFAC beams databases.

5.2. ANALYSIS OF HVFAC MATERIAL PROPERTIES

Analysis of HVFAC material properties was done by comparing the HVFAC and OPCC mechanical properties and by analyzing the possible application of available code predictions defined for OPCC on HVFAC. This analysis was done in two stages.

In the first stage, the database of all adequate HVFAC experimental results found in literature was made to evaluate the following relations defined for OPCC:

- Empirical equation for 28-day compressive strength determination;

5. Analysis and discussion of results

- Compressive strength development over time defined in EN 1992-1-1;
- Modulus of elasticity and compressive strength relation defined in EN 1992-1-1;
- Development of modulus of elasticity over time defined in EN 1992-1-1;
- Splitting tensile and compressive strength relation defined in EN 1992-1-1.

In the second stage, the analysis of own HVFAC material properties testing experimental results was done—HVFAC mixtures presented in Tables 4.7, 4.9 and 4.10. Comparison with the European Standard EN 206-1 and EN 1992-1-1 equations and already proposed models for HVFAC was done for ten HVFAC mixtures presented in section 4.2.5. of this thesis. In addition to the relations analyzed in the first stage of this section, evaluation of the *k-value concept* defined in European Standard EN 206-1 (CEN 2011a) was also done on own experimental results.

5.2.1. Analysis of HVFAC mechanical properties based on a literature review

The use of HVFAC is not yet defined with adequate standards, so it is not a surprise that research regarding HVFAC material, durability and structural properties are still very important. One of the starting assumptions regarding FA is that it is a by-product which is not additionally processed and therefore, its chemical and physical properties are not always the same. Its quality lies in the fact that it is a waste material that is now used as a raw material in the concrete production. That quality is also a big shortcoming due to the chemical and physical heterogeneity of FA produced from different types of coal. In order to draw some general conclusions regarding the mechanical properties of HVFAC, a systematic analysis of the experimental results found in the literature is necessary. For that purpose, the database of adequate experimental results from the literature is made in order to analyze the basic mechanical properties of HVFAC.

The experimental results were collected from available research papers, technical reports, master and doctoral theses. The first step was the collection of all available studies on FA concrete that had own experimental results of basic

5. Analysis and discussion of results

mechanical properties. The selection of the results was done based on the following two criteria:

- only studies with class F FA were selected;
- the amount of FA in CM was chosen in the range between 40% and 75%.

In the selected studies that did not have the ASTM C618 (ASTM C618 2015) classification of FA, classification was made based on the available chemical and physical properties of FA. For each collected publication, the analysis in order to determine the relevance of presented results was performed. After this, the database of 66 research papers, project reports and theses was yielded (Alaka and Oyedele 2016; Atis 2002, 2003a; b, 2005; Balakrishnan and Awal 2014; Berndt 2009; Bilodeau and Malhotra 2000; Bortz 2008; Bouzoubaâ et al. 2000, 2001; Bouzoubaâ and Fournier 2003; Bouzoubaa and Lachemi 2001; Bouzoubaa and Malhotra 2001; Burden 2006; Carette et al. 1993; Construction 1998; Dinakar et al. 2008, 2013; Duran-Herrera et al. 2011; Filho et al. 2013; Hannesson G. 2010; Ho and Lewis 1985; Huang et al. 2013; Hung 1997; Inderpreet Kaur 2005; Jiang et al. 2000; Jiang and Malhotra 2000; Kayali and Sharfuddin Ahmed 2013; Keith 2011; Kou and Poon 2013; Lam et al. 1998; Langan et al. 1990; Langley et al. 1989; Li and Zhao 2003; Lima et al. 2013; Malhotra 1986, 1990, 1999; Malhotra et al. 2000; Mardani-Aghabaglou et al. 2013; Mathur et al. 2005; McCarthy and Dhir 2005; Mittal et al. 2006; Mukherjee et al. 2013; Naganathan et al. 2017; Naik et al. 1991; Nath 2010; Obla et al. 2003; Ortega 2012; Poon et al. 2000; Proske et al. 2014; Quan and Kasami 2013; Rao et al. 2011; Ravina and Mehta 1988; Şahmaran et al. 2009; Siddique 2004; Sivasundaram et al. 1990, 1991; Soman and K. Sobha 2014; Tokyay 1999; Yoo et al. 2015; Yoon et al. 2014; Younsi et al. 2011; Zhao et al. 2016, 2015). All the presented studies were carried out in the period of 31 years, from 1986 to 2017, with the total of 563 different RCC and HVFAC mixtures tested for different mechanical properties. In order to carry out the comprehensive analysis of the available results, important parameters were selected to describe the concrete component materials (cement, FA, aggregate and water reducing admixtures), concrete mixtures, physical and mechanical properties of concretes (compressive strength, tensile splitting strength and modulus of elasticity) at

5. Analysis and discussion of results

different ages. The results regarding the following parameters are collected in the database for each study:

- 1) Cement type;
- 2) Cement class (28-day compressive strength);
- 3) Cement early age strength (S, N, R);
- 4) % of SiO₂ in cement (CEM SiO₂);
- 5) % of Al₂O₃ in cement (CEM Al₂O₃);
- 6) % of Fe₂O₃ in cement (CEM Fe₂O₃);
- 7) % of CaO in cement (CEM CaO);
- 8) Cement specific surface - Blain method (CEM Blaine, cm²/g);
- 9) Cement specific gravity (γ_{CEM} , kg/m³);
- 10) % of SiO₂ in FA (FA SiO₂);
- 11) % of Al₂O₃ in FA (FA Al₂O₃);
- 12) % of Fe₂O₃ in FA (FA Fe₂O₃);
- 13) % of CaO in FA (FA CaO);
- 14) LOI in FA (FA LOI, %);
- 15) FA fineness expressed through residue on 45 μ m sieve (Fineness >45 μ m, %);
- 16) FA specific surface - Blaine method (FA Blaine, cm²/g);
- 17) FA specific gravity (γ_{FA} , kg/m³);
- 18) Coarse aggregate type;
- 19) Fine aggregate type;
- 20) Maximum aggregate size (mm);
- 21) Plasticizer type;
- 22) Plasticizer amount expressed as a percentage of plasticizer mass to total CM mass (m_{pl}/CM , %);
- 23) FA mass in total CM (FA/CM, %);
- 24) Referent CEM mass (Ref. Cem., kg/m³);
- 25) Total cementitious materials mass (CM, kg/m³);
- 26) Water mass (m_{w} , kg/m³);
- 27) W/CM ratio;
- 28) Curing type;

5. Analysis and discussion of results

- 29) Slump (mm);
- 30) Compressive strength - Sample type and size;
- 31) - 42) Compressive strength results at 1, 3, 7, 14, 28, 56, 90, 180, 365, 1095, 1825 and 3650 days;
- 43) Splitting tensile strength - Sample type and size;
- 44) - 50) Splitting tensile strength at 1, 3, 7, 28, 56, 90, 365 days;
- 51) Modulus of elasticity - Testing procedure;
- 52) Modulus of elasticity - Sample type and size;
- 53) - 59) Modulus of elasticity at 3, 7, 14, 28, 90, 180, 365 days.

Although all selected studies did not provide all necessary data, information regarding concrete design properties and results of some mechanical properties were available in all of them. Among all selected studies, 55 of them had RCC mixture, while in other 11 studies only HVFAC mixtures were analyzed. Only 172 of total 432 HVFAC mixtures had the same W/CM ratio in RCC and HVFAC. When analyzing HVFAC, the term RCC is often used for concrete that has the same component materials and cement mass that is partially replaced with FA in HVFAC. A variety of methodologies for RCC preparation were found in the presented studies which made it difficult to draw conclusions about HVFAC by simply comparing it to RCC. The term "RCC" - *referent cement concrete* was mostly used because of the tendency to define FA concrete with the percentage of cement replacement in the OPCC with FA. This was mostly done because the necessary relations defining physical and mechanical properties of HVFAC were not quantitatively determined. When this methodology of HVFAC evaluation is used, special focus should be placed on the RCC and HVFAC mix design parameters. The replacement of FA can be done by mass or by volume of cement. The specific density of FA can be significantly lower compared with the cement and, if the mass replacement was done, it is necessary to compensate the difference in volume by reducing the amount of total aggregate or only fine aggregates mass. Both methods were used in the literature, and the particle size distribution and packing of aggregate and FA can affect the compressive strength enough to corrupt the conclusion making process if not addressed systematically. The second problem

5. Analysis and discussion of results

noticed in designing of concrete mixtures in the literature was the W/CM ratio in FA concrete and RCC. In some cases, they were not the same. Some experimental programs included the reduction of the W/CM ratio in FA concrete compared with the RCC. In this way, concrete compressive strength was influenced by both FA addition and the reduction of W/CM ratio.

In a large number of concrete mixtures (469), the used cement type was OPC, ASTM Type I or CEM I. Other types of cement like ASTM Type II, ASTM Type IP, EN 197-1, CEM II or PPC were also used in some studies. The cement class refers to the standard 28-day compressive strength measured according to the adequate standard for cement classification–EN 197-1 (CEN 2011b) and ASTM C150 and C595 (ASTM 2014, 2017). The early age strength is defined by the strength increase rate in the cement classification. It is usually presented with S, N or R referring to slow, normal or rapid strength gain, respectively (CEN 2011b). Figure 5.1 shows the number of concrete mixtures that had available/not available data regarding cement classification.

It can be seen that the least data was found regarding the cement class and the cement early age strength. In most studies, the chemical composition of cement was available with cement physical properties available in a smaller number of the collected research. The availability of the chemical and physicals properties of FA are graphically presented in Figure 5.2. A wide range of chemical and physical properties of FA and cement used in the selected studies is shown in Table 5.1.

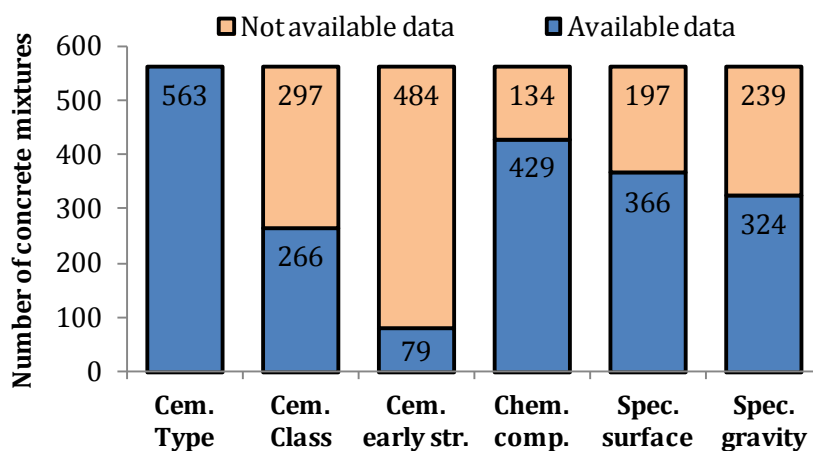


Figure 5.1 Number of concrete mixtures regarding cement properties

5. Analysis and discussion of results

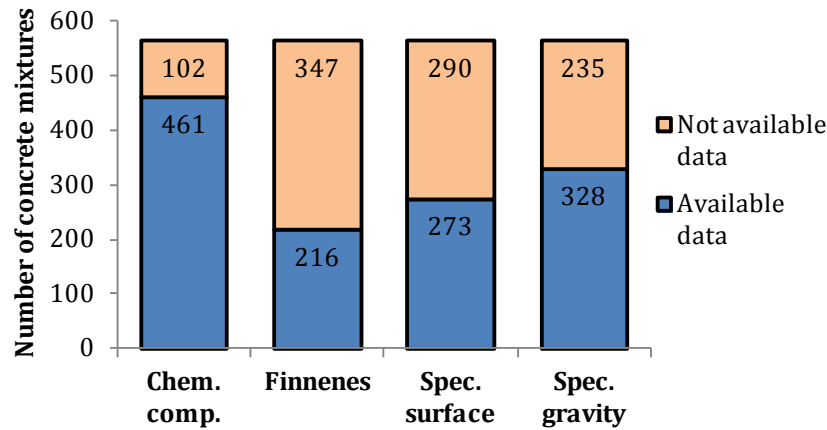


Figure 5.2 Number of concrete mixtures regarding FA properties

Class F FA was used in all studies, but the dispersion of FA chemical and physical properties was still relatively high. The availability of data regarding the aggregate type was summarized and shown in the following figures: general aggregate type in Figure 5.3, aggregate stone type in Figure 5.4, and maximum aggregate size in Figure 5.5.

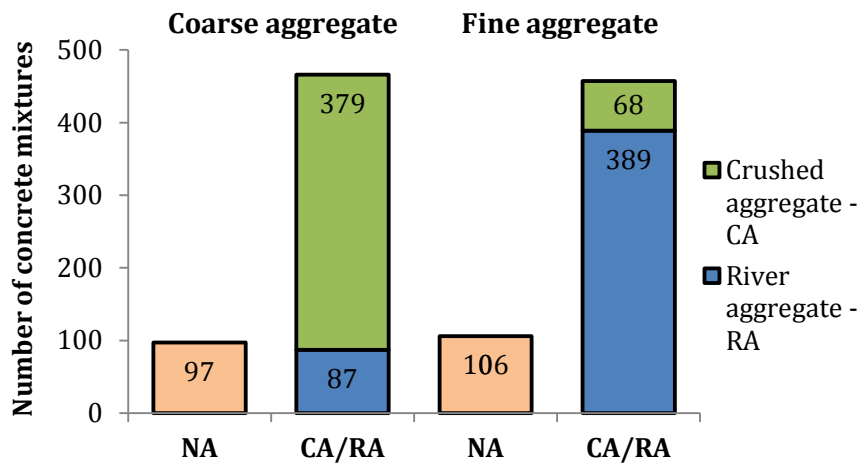
Table 5.1 Chemical and physical properties of FA and cement

Chemical properties	FA	Cement
SiO_2 (%)	36.8 - 68.4	17.1-39.1
Al_2O_3 (%)	11.1 - 32.5	3.1-10.3
Fe_2O_3 (%)	2.7 - 39.7	1.9-6.2
CaO (%)	0.3 - 20.3	45.7-65.9
LOI (%)	0.17 - 9.7	-
Physical properties	FA	Cement
Fineness (>45 mm, %)	0.1 - 35.9	-
Specific surface area (cm^2/g)	1874 - 6780	2890-5790
Specific gravity (kg/m^3)	1900 - 2960	2890-3230

The most frequently used aggregate type was crushed coarse (CA) and river sand aggregate (RA) with maximum aggregate size ranging from 10 mm to 32 mm. Different types of plasticizer were used in most of the studies in different amounts ranging from no plasticizer to 16% (percent of total CM mass) in some studies. The number of studies with different plasticizer amounts is shown in Figure 5.6.

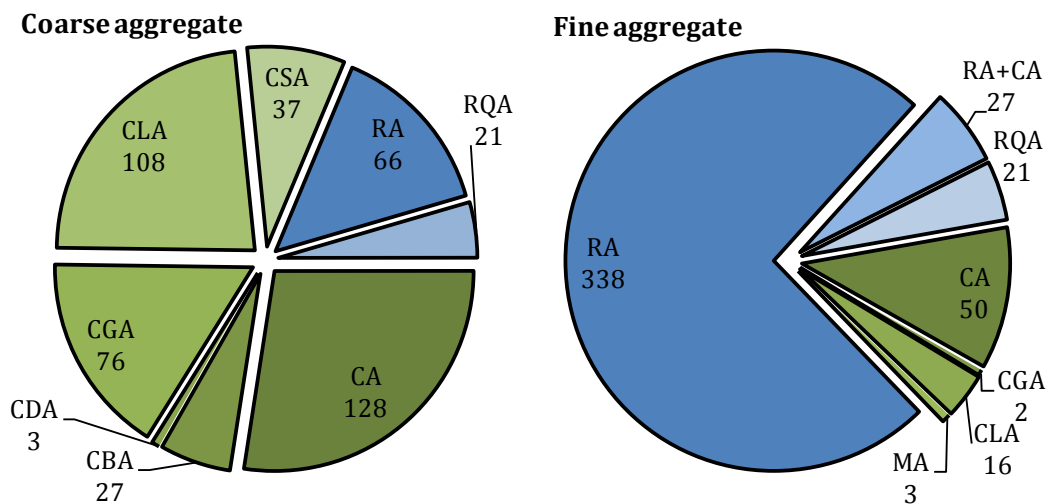
5. Analysis and discussion of results

Different types of plasticizer were used but mostly carboxylic, melanine, naphtaline and sulphonated-naphtaleme-formaldehyd based.



* NA - Not available data

Figure 5.3 Number of concrete mixtures regarding coarse and fine aggregate type



CBA - crushed basalt aggregate

RA - river aggregate

CDA - crushed diorite aggregate

RQA - river quartzite aggregate

CGA - crushed granite aggregate

MA - marine aggregate

CLA - crushed limestone aggregate

CA - undefined crushed

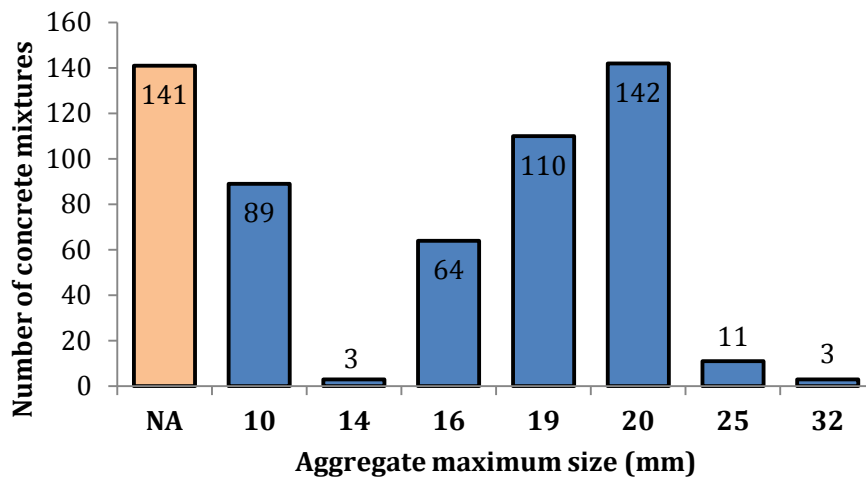
CSA - crushed sandstone aggregate

aggregate

Figure 5.4 Number of concrete mixtures regarding coarse and fine aggregate stone

type

5. Analysis and discussion of results



* NA - Not available data

Figure 5.5 Number of concrete mixtures regarding the aggregate maximum size

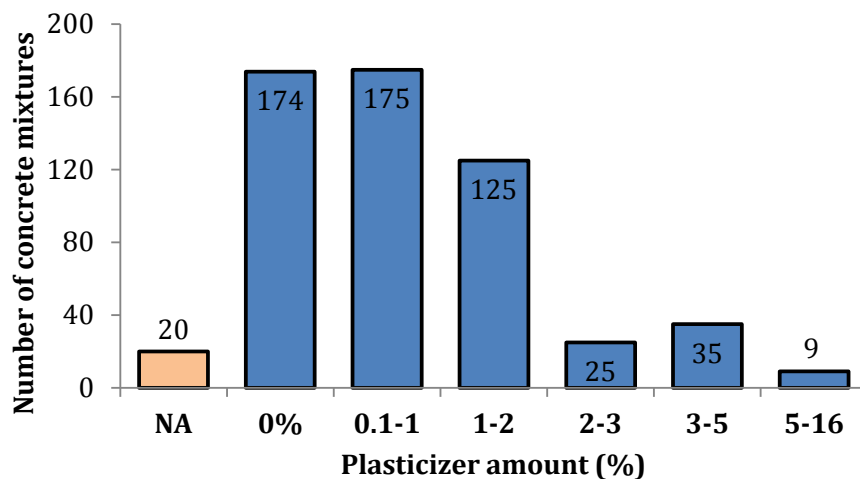


Figure 5.6 Number of concrete mixtures regarding plasticizer amount

Figure 5.7 shows FA content in CM mass in all selected studies and, as it can be seen, in most studies (345 studies) FA makes 40-60% of the total CM. The curing of samples was done in different ways but mostly by standard moist curing (SMC) or standard water curing (SWC). Air curing (AC) of samples was done in only two studies (Malhotra 1986; Malhotra et al. 2000). The number of concrete mixtures regarding the curing type is shown in Figure 5.8. The workability of concrete mixtures was available in most of the concrete mixtures - 472 of total 563 mixtures had available information of slump/flow values.

5. Analysis and discussion of results

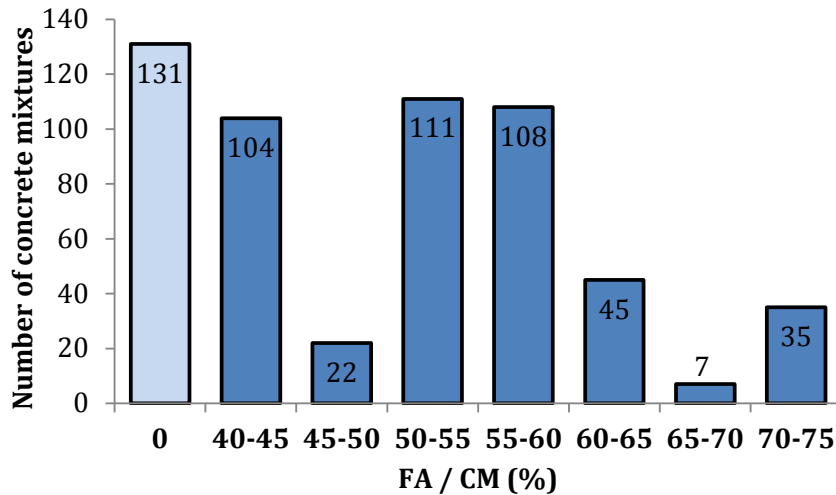
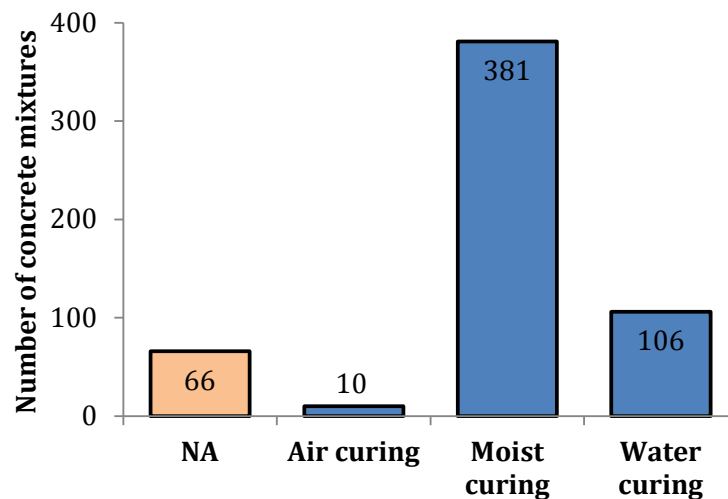


Figure 5.7 Number of concrete mixtures regarding FA amount in CM



* NA - Not available results

Figure 5.8 Number of concrete mixtures regarding sample curing type

The testing of compressive, splitting tensile strength and modulus of elasticity was done on different samples in different studies. In order to compare these results, all compressive and splitting tensile strength results were recalculated on 150-300 mm cylinders using scaling factors found in the literature (Neville 1981; Zabihi 2012a). Similar sample sizes were treated with the same factors and they are all listed in Tables 5.2 and 5.3. In different studies, analyzing modulus of elasticity, different testing methods and cylinder sizes were used. No corresponding factors for modulus of elasticity results recalculation were found in the literature, so this effect was neglected during this research. All modulus of elasticity testing results were used as presented in the selected study.

5. Analysis and discussion of results

Table 5.2 Scaling factors for recalculating compressive strength results

Sample size and dimension	Scaling factor
Cylinder 150 · 300 mm	1.00
Cylinder 152 · 305 mm	1.00
Cylinder 100 · 200 mm	0.975
Cylinder 102 · 204 mm	0.975
Prism 100 · 100 · 200 mm	0.975
Cylinder 110 · 220 mm	0.975
Cylinder 76 · 152 mm	0.915
Cube 150 · 150 · 150 mm	0.850
Cube 100 · 100 · 100 mm	0.750
Prism 100 · 100 · 500 mm	0.750

Table 5.3 Scaling factors for recalculating splitting tensile strength results

Sample size and dimension	Scaling factor
Cylinder 150 · 300 mm	1.00
Cylinder 152 · 305 mm	1.00
Cylinder 102 · 204 mm	0.91
Cylinder 150 · 150 mm	1.00
Cube 150 · 150 · 150 mm	1.00
Cube 100 · 100 · 100 mm	0.90

The compressive, splitting tensile strength and modulus of elasticity were tested at different ages in different studies. The number of concrete mixtures tested at a certain age regarding compressive and splitting tensile strength and modulus of elasticity are presented in Figures 5.9 – 5.11, respectively. In most of the studies, testing was done at the age of 28 days for all mechanical properties.

The 28-day compressive strength was tested on 416 HVFAC mixtures from different studies, but only 172 of them had the same W/CM ratio like in RCC. The 28-day splitting tensile strength was tested on 65 HVFAC mixtures with only 27 of them with the same W/CM ratio like in RCC.

5. Analysis and discussion of results

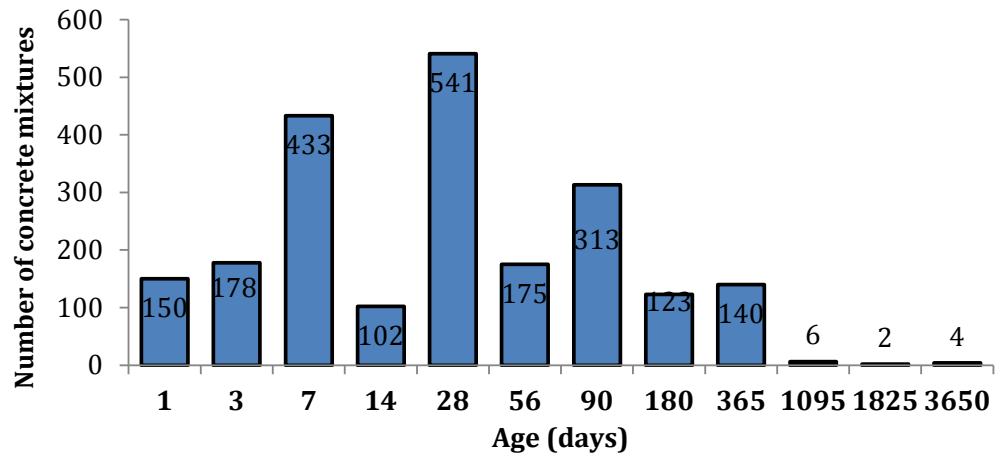


Figure 5.9 Number of concrete samples tested for different age compressive strength

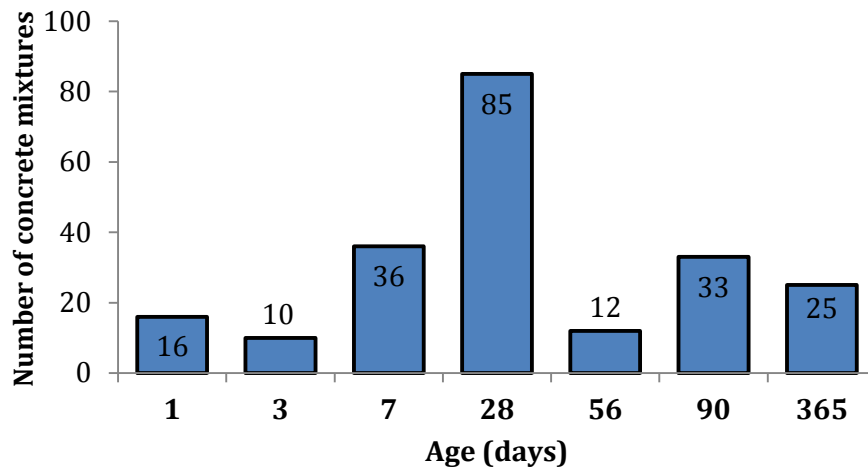


Figure 5.10 Number of concrete samples tested for different age splitting tensile strength

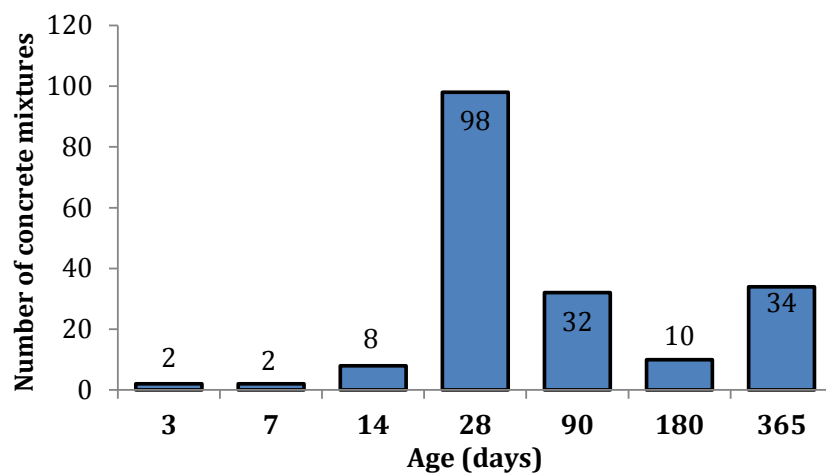


Figure 5.11 Number of concrete samples tested for different age modulus of elasticity

5. Analysis and discussion of results

Similar as for splitting tensile strength, 77 HVFAC mixtures were tested for a 28-day modulus of elasticity with only 27 of them with the same W/CM ratio like in RCC. Different target compressive strengths were set in different studies and the number of concrete mixtures regarding the compressive strength is shown in Figure 5.12.

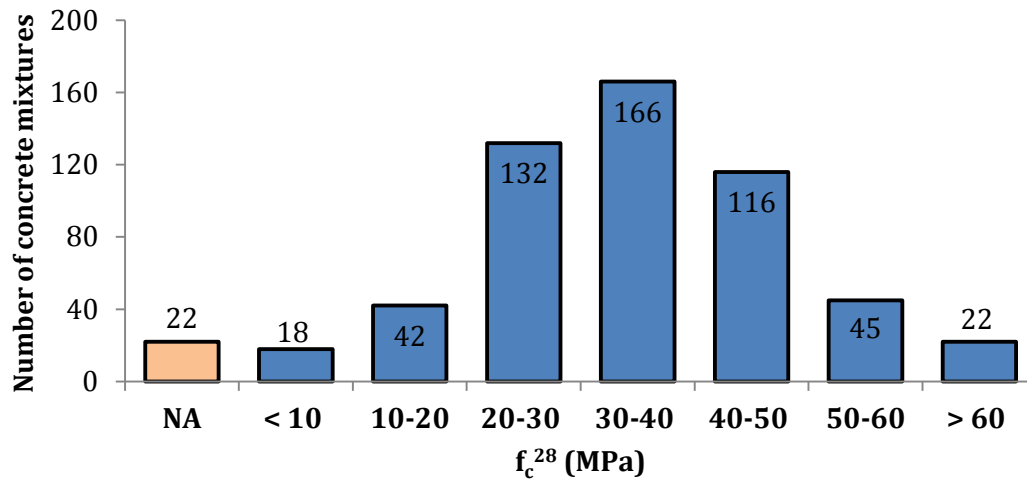


Figure 5.12 Number of concrete mixtures regarding 28-day compressive strength test results

5.2.1.1. Comparison of HVFAC and OPCC compressive strength

A simple comparison of HVFAC compressive strength results with RCC ones cannot lead to the quantification of the FA content influence on the compressive strength. As it was previously mentioned, the methodology of the concrete mix design was not the same in all selected studies. All HVFAC mixtures that had RCC were selected and analyzed (300 HVFAC mixtures from 46 different studies). W/CM was not the same in all selected HVFAC and RCC mixtures. The HVFAC to RCC 28-day compressive strength ratios compared with the W/CM ratio and FA/CM ratio are shown in Figures 5.13 and 5.14, respectively.

Results presented in this way can only serve as a starting impression of the influence of FA content in total CM on the compressive strength. It can be seen that 21% of the results presented in Figures 5.13 and 5.14 have equal or greater HVFAC compressive strength compared with the RCC. These results were mostly related

5. Analysis and discussion of results

to the lower FA content or the lower W/CM ratio in HVFAC. A group of results presented in Figures 5.13 and 5.14 were normally distributed according to the Anderson-Darling goodness-of-fit test ($A^*=0.409 < A_{0.05}^2=0.752$).

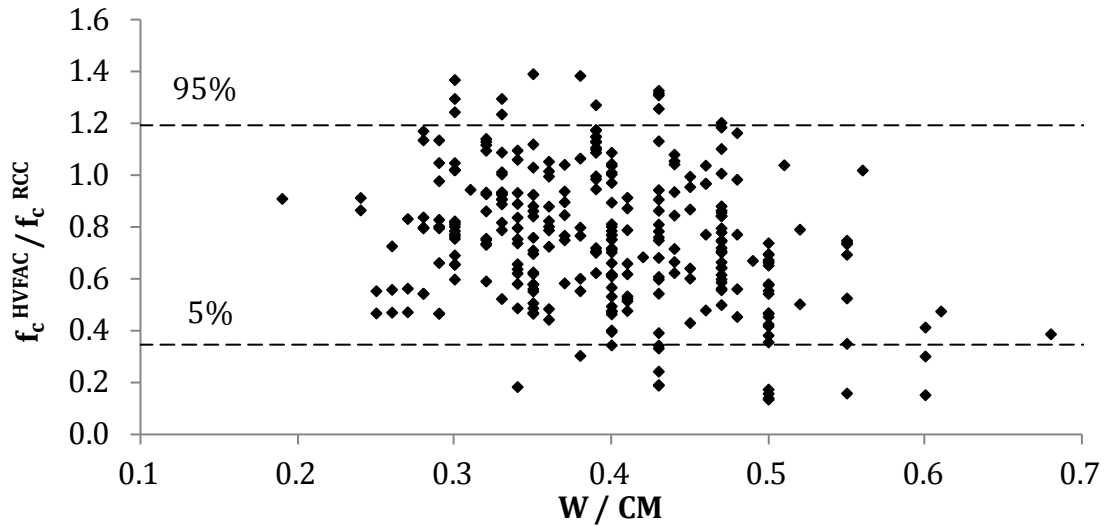


Figure 5.13 The ratio of HVFAC and RCC 28-day compressive strength compared with the W/CM ratio

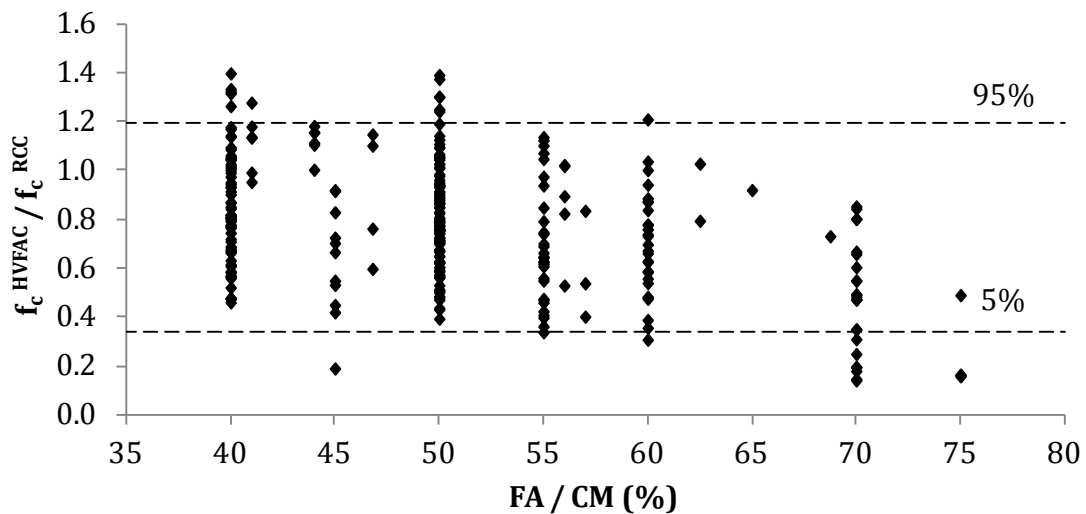


Figure 5.14 The ratio of HVFAC and RCC 28-day compressive strength compared with the FA/CM ratio

The horizontal lines represent the 5–95% interval around the mean value ($\mu \pm 1.645 \cdot \sigma$). As expected, the 5-95% interval shown in Figures 5.13 and 5.14 is relatively wide due to the large range of parameters taken into account. The figures show no clear correlation between the HVFAC to RCC compressive strength ratio compared with the W/CM and FA/CM ratios.

5. Analysis and discussion of results

Descriptive statistical analysis parameters of the presented data for different FA/CM ratios are shown in Table 5.4. It can be seen that the standard deviation for all cement replacement levels is rather high and the coefficient of variation (CoV) is between 26.2% and 47.1%. It can also be seen that the mean values are decreasing with the increase of FA content.

Table 5.4 Important statistical parameters for the data presented in Figure 2.23

f_c^{HVFAC} / f_c^{RCC}	FA / CM (%)					
	40%	45%	50%	55%	60%	70%
Sample No.	76	20	104	36	27	25
Mean value	0.876	0.862	0.809	0.701	0.688	0.480
St. Error	0.026	0.054	0.021	0.041	0.042	0.045
St. Deviation	0.229	0.243	0.218	0.244	0.217	0.226
CoV (%)	26.18	28.16	27.90	34.87	31.53	47.11
Minimum	0.458	0.417	0.391	0.336	0.305	0.139
Maximum	1.396	1.180	1.389	1.135	1.207	0.851
Lower bound (5%)	0.499	0.463	0.451	0.299	0.331	0.108
Upper bound (95%)	1.254	1.262	1.168	1.103	1.044	0.853

*CoV - coefficient of variation

Figure 5.15 shows the mean values of the HVFAC and RCC compressive strength ratios plotted with standard deviations.

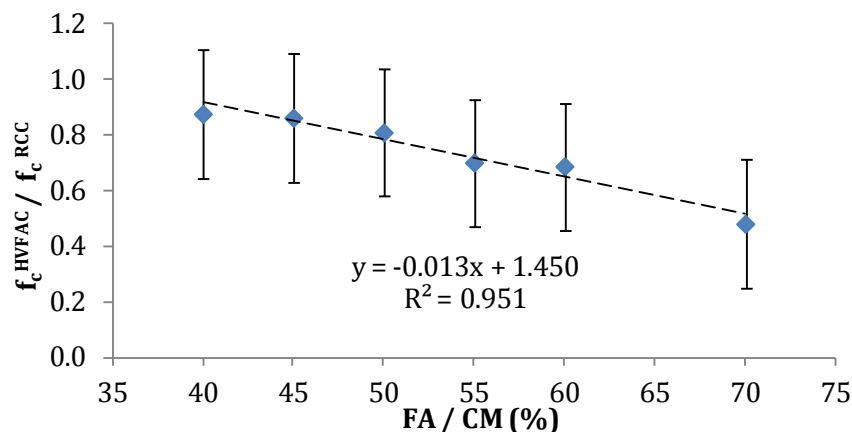


Figure 5.15 Mean values of the HVFAC and RCC compression strength ratio versus FA/CM ratio

5. Analysis and discussion of results

It is clear that HVFAC compressive strength decreases with the increase of FA amount regardless of the combined effect of a great number of factors (different W/CM ratios, physical and chemical properties of FA, different types of cement and aggregate used in the studies, etc). Figure 5.15 showed a great scatter of results and, therefore, a more detailed analysis of the concrete mixtures available in the database should be done.

5.2.1.2. HVFAC 28-day compressive strength evaluation

First, the relationship between the compressive strength and W/CM ratio already established for OPCC was evaluated. The cement type strongly affects the concrete strength and therefore, only commonly used types of cement were selected for the analysis. The aggregate type and size as well as the curing conditions affect the compressive strength, so most commonly used types were selected for the analysis. High FA content in concrete usually requires plasticizers for achieving good workability and it is not surprising that 67% of the concrete mixtures from the database contained plasticizers. The influence of the plasticizer on physical and mechanical properties of HVFAC is not fully known. It is considered that the usual amount of plasticizer up to 2-3% (Neville 1981) will not influence the compressive strength in RCC. Having all this in mind, the following HVFAC mixtures were selected from the database:

- Concrete mixtures with cement conforming to ASTM type I/II and CEM I/II;
- Mixtures with crushed coarse aggregate and maximum size ranging from 10 mm to 25 mm;
- Mixtures made and cured under standard water and moist curing conditions;
- Mixtures with up to 3% of plasticizer.

The application of these filters to the database yielded 198 results of the HVFAC and 37 results of the RCC 7-day compressive strength; 250 HVFAC and 68 RCC results of the 28-day compressive strength and 147 HVFAC and 43 RCC mixtures with the results of the 90-day compressive strength. Figures 5.16 – 5.18 show the compressive strength of HVFAC and RCC compared with the W/CM ratio tested at the age of 7 days, 28 days and 90 days, respectively.

5. Analysis and discussion of results

The selected concrete mixtures had FA and cement with different properties and the results were plotted in three series regarding the FA/CM ratio (40-50%, 50-60% and 60-70%). It can be concluded that the FA amount has a significant influence on the HVFAC compressive strength, separating the series of results regarding the FA/CM ratio with good correlation.

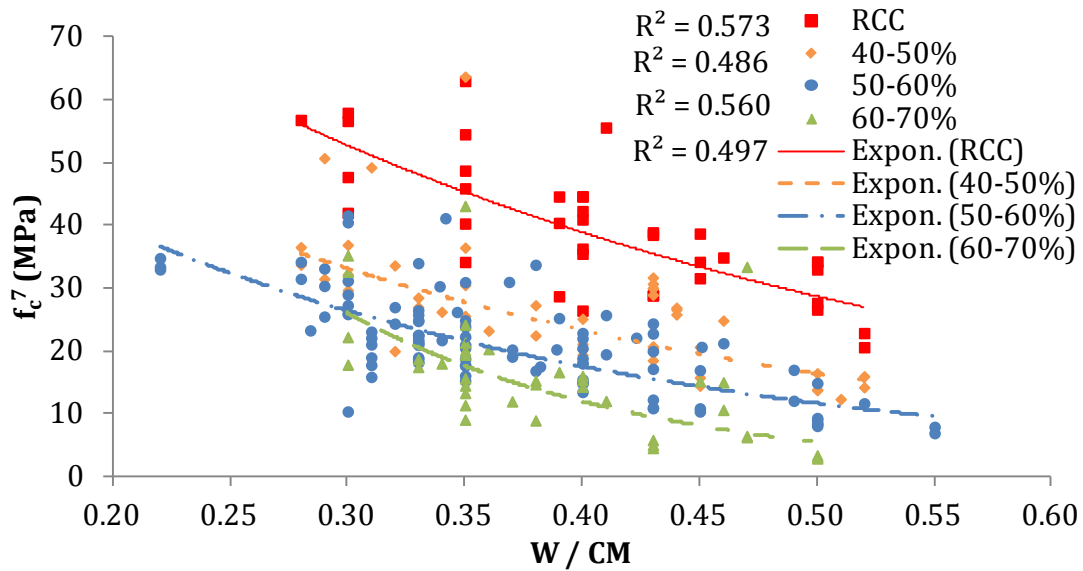


Figure 5.16 7-day compressive strength of the HVFAC and RCC versus the W/CM ratio

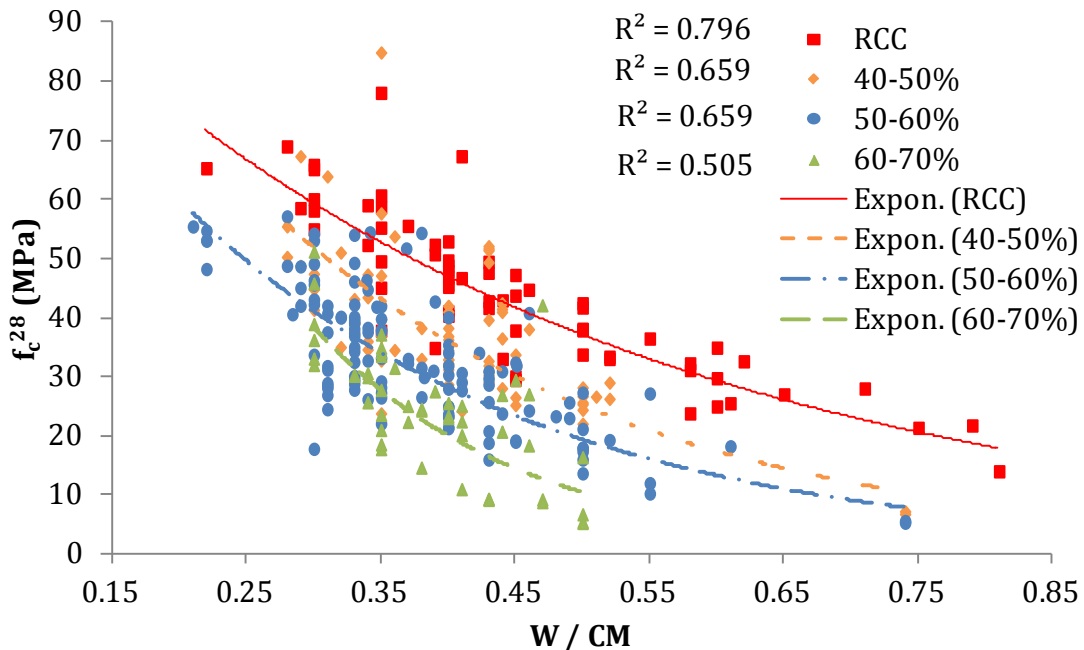


Figure 5.17 28-day compressive strength of the HVFAC and RCC versus the W/CM ratio

5. Analysis and discussion of results

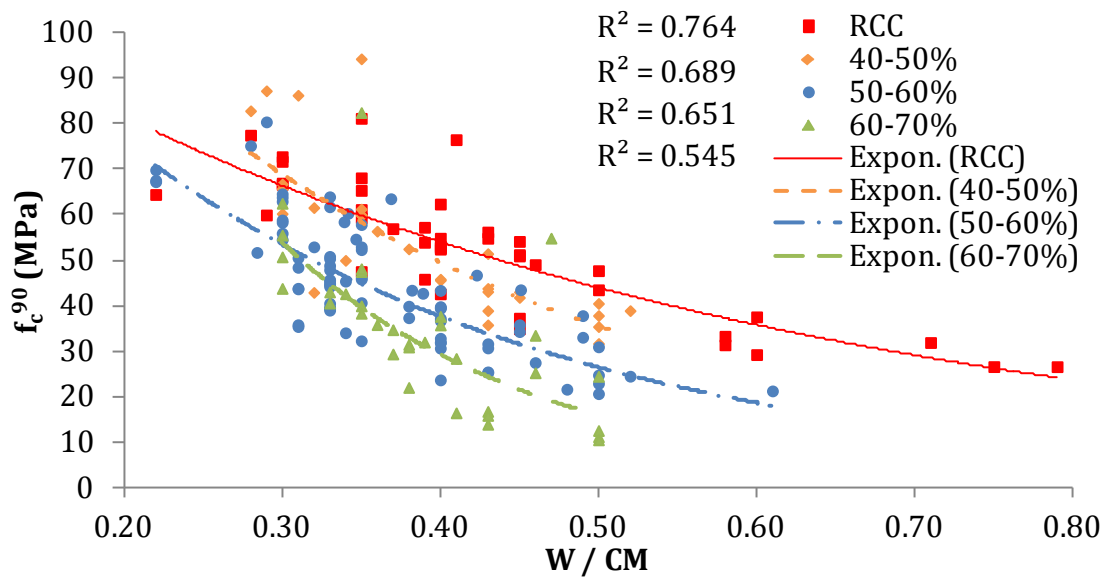


Figure 5.18 90-day compressive strength of the HVFAC and RCC versus the W/CM ratio

The presented results were evaluated through the determination coefficient (R^2) based on the correlation coefficient (R) that represent the degree of the relationship between two variables. The correlation coefficient was equal or greater than 0.7 (Figures 5.16 – 5.18) for all concrete series, indicating that there is a good correlation between the compressive strength and the W/CM ratio (Silva et al. 2016). A relatively big scatter of the results was a consequence of different cement and FA types used in different concrete mixtures. The relations shown in Figures 5.16 – 5.18 indicate that the HVFAC compressive strength at the age of 7 days, 28 days and 90 days has a strong correlation to the W/CM ratio ($R^2=0.486$ – 0.689), but weaker than in the case of RCC ($R^2=0.573$ – 0.796). This means that the correlation between the HVFAC compressive strength and the W/CM ratio can be defined in a similar way like in OPCC with needed alterations, taking into account more parameters regarding the FA amount and properties.

In order to establish an adequate relationship between the HVFAC compressive strength and the W/CM ratio, the FA efficiency factor k is often used. This concept was first proposed by Smith in 1967. (Smith, 1967). He defined the FA efficiency factor in such a way that the RCC compressive strength to the W/CM ratio relation

5. Analysis and discussion of results

was also valid for FA concrete introducing the effective W/CM ratio, given as $W/(C+k \cdot FA)$.

In a more general way, the FA efficiency factor can be defined as a portion of cement mass that could be replaced by one part of FA without changing the studied property (Babu and Rao 1996). There is a significant amount of research done regarding the evaluation of the mechanical and physical properties of HVFAC, but there is a lack of the quantitative representation of the FA influence on concrete properties.

The efficiency of FA is influenced by many factors, but mostly by the amount, the physical and mechanical properties of FA and cement, the age of concrete and curing conditions (Babu and Rao 1993, 1996; Hwang et al. 2004; Papadakis et al. 2002; Yildirim et al. 2011). The list of relevant research papers regarding the FA efficiency is shown in Table 5.5 along with all parameters analyzed in these studies. According to the results from the literature, it is clear that the FA efficiency is increasing over time and k factor is therefore calculated for different concrete ages. It is important to find an easy quantitative way to determine the FA efficiency and predict the HVFAC compressive strength based on the empirical equations, similar as in the case of RCC. In this way, the practical application of HVFAC would be increased. To better understand the efficiency of FA, proposed predications for k factor found in the literature were re-evaluated for HVFAC results collected from the literature.

One of the first research regarding the efficiency of CM (FA, silica fume and ground granulated blast-furnace slag) defined by k factor was performed by Babu (Babu 1995; Babu and Kumar 2000; Babu and Rao 1993, 1994, 1996). A detailed explanation of this concept was given by Babu and Rao (Babu and Rao 1993). Researchers assumed that the FA efficiency is mostly influenced by the W/CM ratio, FA replacement level and age.

They re-evaluated the results from previous studies and defined the FA efficiency at different ages - 7, 28 and 90 days for FA replacement levels from 15% to 75%.

5. Analysis and discussion of results

Table 5.5 Relevant research proposals regarding k factor

Study	FA class	FA/CM (%)	Parameters	Efficiency factor k
(Babu and Rao 1996)	F / C	15-75	FA/CM ratio (p), concrete age.	$k_7 = 2.67 \cdot p^2 - 3.75 \cdot p + 1.45$ $k_{28} = 2.78 \cdot p^2 - 3.80 \cdot p + 1.64$ $k_{90} = 2.50 \cdot p^2 - 3.59 \cdot p + 1.73$
(Papadakis et al. 2002)	F / C	10-20	Activity index (AI), active silica content in FA (γ_S), silica content in C and FA, concrete age, W/C ratio.	$k = 1 + 4 \cdot (AI - 1)/(1 - 0.5a)$ a - parameter depending on time and curing; $k = \gamma_S \cdot \frac{f_{S,P}}{f_{S,C}} \cdot \left(1 - a \frac{W}{C}\right)$ $f_{S,P}$ - weight fraction of SiO ₂ in FA; $f_{S,C}$ - weight fraction of SiO ₂ in C.
(Hwang et al. 2004)	-	10-49	FA fineness (Blaine method), FA/C ratio, concrete age.	$k_7 = 0.21 \cdot \exp\left(-0.43 \times \frac{FA}{C}\right) \cdot \alpha_2$ $k_{28} = 0.42 \cdot \exp\left(-0.72 \times \frac{FA}{C}\right) \cdot \alpha_2$ $k_{90} = 0.85 \cdot \exp\left(-1.36 \times \frac{FA}{C}\right) \cdot \alpha_2$ $\alpha_2 = 1.14 \cdot 10^{-4}(\text{Blaine} - 2500) + 1$
(Rajamane et al. 2007)	F	10-80	FA/CM percentage (P), concrete age.	$k_7 = 0.9 - 0.1 \cdot \log_e P$ $k_{28} = 1.2 - 0.14 \cdot \log_e P$
(Kuder et al. 2012)	C	60-90	CaO, SiO ₂ , Al ₂ O ₃ content in FA and cement (C, S, A), concrete age.	$k(t) = H(t) \cdot \frac{C}{S + A}$ $H(t)$ - 0.4; 0.5; 0.6; 0.7; 0.8; 0.8; 0.8 for 7, 14, 28, 56, 84, 112 and 168 days respectively.
(Yeh 2016)	-	10-70	FA /CM ratio (p), concrete age (t).	$k_t = 1.25 + 0.14 \cdot \log_e t - 3.90 \cdot p + 2.75 \cdot p^2$

5. Analysis and discussion of results

The selection of the results was done in the way that only OPCC mixtures with maximum aggregate size of 20 mm, plasticizer amount less than 2%, cured under normal conditions were used for the evaluation. The evaluation of the efficiency was done using Δw concept (Figure 5.19) that attempts to bring the FA concrete W/CM ratio closer to the W/C₀ ratio of RCC ($\Delta w \rightarrow 0$) by applying the k factor at any strength presented as:

$$\Delta w = \frac{W}{C_0} - \frac{W}{C + k \cdot FA} \quad \text{Eq. 5.1}$$

where:

W water mass (kg/m³);

C cement mass in FA concrete (kg/m³);

C₀ cement mass in RCC concrete (kg/m³);

FA FA mass (kg/m³).

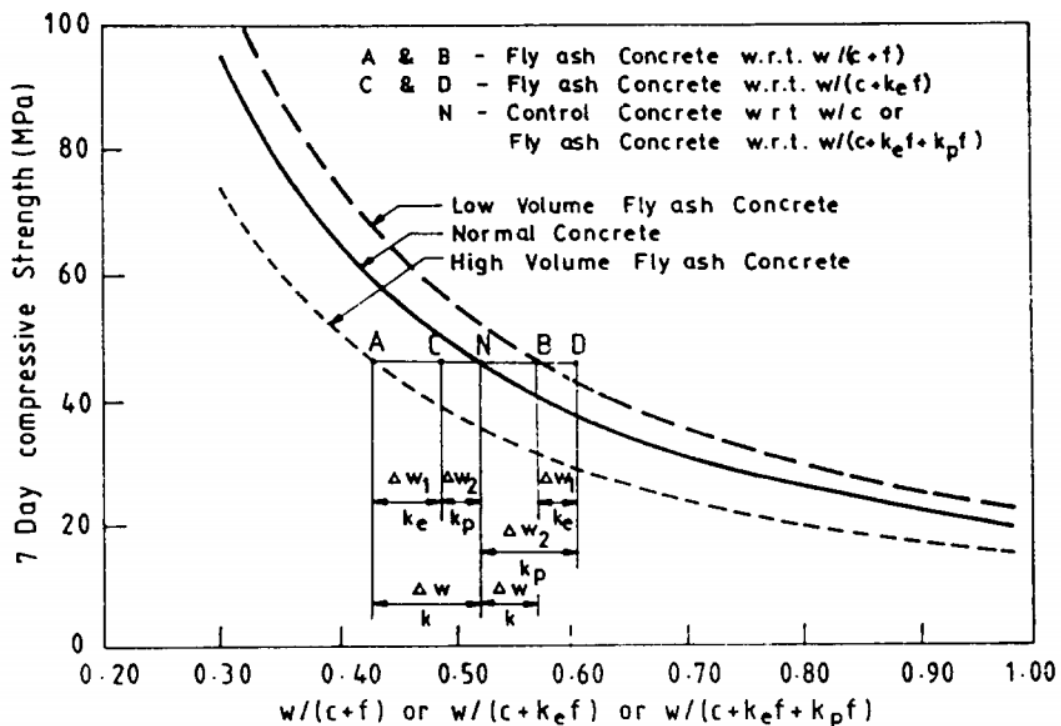


Figure 5.19 Conceptual diagram showing the effect of efficiency factor (Babu and Rao 1994)

The type of FA in selected studies was ASTM class C or F and conforming to the characteristics specified by ASTM C618 (ASTM C618 2015). The efficiency of FA

5. Analysis and discussion of results

was defined with two factors ($k = k_e + k_p$), the general efficiency factor k_e and the percentage efficiency factor k_p .

The researchers found that the best fit for general efficiency factors were values $k_e = 0.3, 0.5$ and 0.6 for 7, 28 and 90 days respectively. These values were chosen as the ones that brought the FA concrete compressive strength closest to the RCC compressive strength using the same values for all FA percentage ratios. This procedure was not explained in detail in the evaluated papers. The remaining difference between the FA concrete and the RCC strength was used to determine the percentage efficiency factor proposed as:

$$k_p = 2.54 \cdot p^2 - 3.62 \cdot p + 1.13 \quad \text{Eq. 5.2}$$

where:

p FA replacement.

The total efficiency factor $k = k_e + k_p$ was then proposed as shown in Table 5.5. For the FA concretes with 50% of FA in CM, the total efficiency factors were 0.24, 0.44 and 0.56 for 7, 28 and 90 days, respectively.

The evaluation of the proposed efficiency factors was done on the selected results from the database. It can be noted that similar criteria for the selection of the results from the database were applied as in the study done by Babu and Rao (Babu and Rao 1993). Figures 5.20–5.22 show the relationship between 7-day, 28-day and 90-day compressive strength of RCC and HVFAC experimental values compared with the $W/(C+FA)$ ratio (HVFAC_{k=1}) and with the $W/(C+k \cdot FA)$ ratio with k values (HVFAC_k) proposed by Babu and Rao (Babu and Rao 1993). As it can be seen, the R^2 for experimental results (HVFAC_{k=1}) was lower compared with the RCC for all ages. The correlation improved significantly by applying the FA efficiency factor (HVFAC_k) proposed by Babu and Rao (Babu and Rao 1993) at the same or similar value as for RCC. It can be concluded that the proposed values for k factor showed a good fit between the HVFAC and RCC compressive strengths dependence on the W/CM ratio, for all ages. A higher scatter of results was noticed for the 7-day compressive strength due to the fact that this strength is mostly influenced by the cement and its properties and the amount and not the FA (Babu

5. Analysis and discussion of results

and Rao 1994). The results presented in Figures 5.20 – 5.22 also show that the efficiency of FA increases over time in a more pronounced way in mixtures with low W/CM ratio (lower than 0.3).

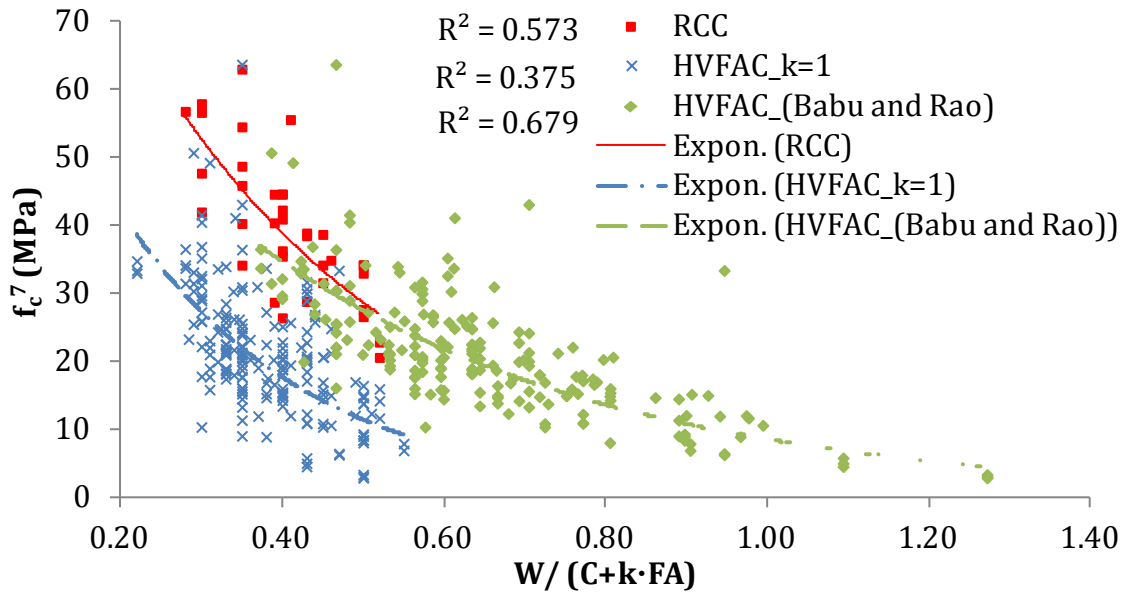


Figure 5.20 Relationship between 7-day compressive strength and $W/(C+k \cdot FA)$ (Babu and Rao 1993)

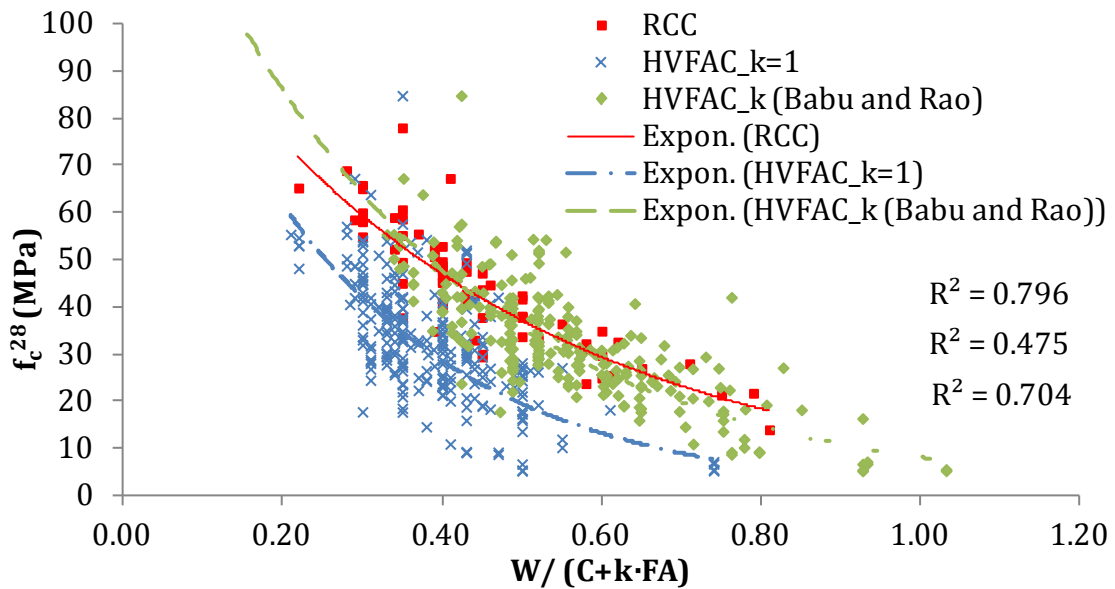


Figure 5.21 Relationship between 28-day compressive strength and $W/(C+k \cdot FA)$ (Babu and Rao 1993)

5. Analysis and discussion of results

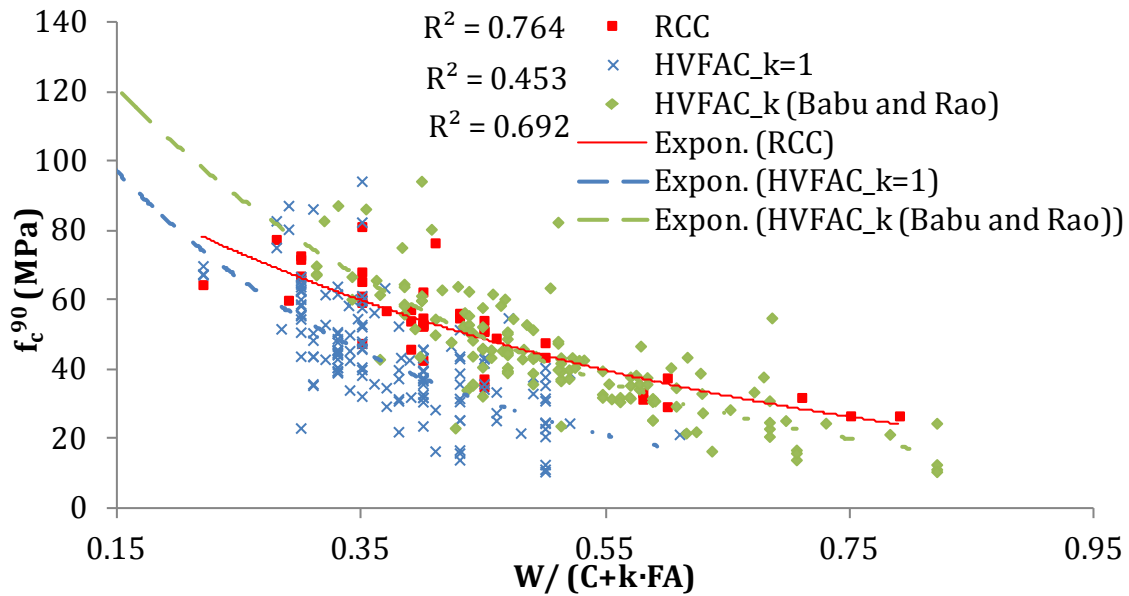


Figure 5.22 Relationship between 90-day compressive strength and $W/(C+k \cdot FA)$
(Babu and Rao 1993)

Other researchers also recognized the FA amount as an important parameter influencing the compressive strength of FA concrete. In the research conducted by Rajamane et al. (Rajamane et al. 2007), the prediction of the HVFAC compressive strength that was made by replacing the portion of sand was presented. The concrete mixtures made with 10–80% of FA in CM and different sand amount were analyzed. Researchers re-evaluated the Bolomey's equation (Bolomey 1935) defined for OPCC based on own experimental results obtained for FA concretes. As a result, they proposed the FA efficiency factor as a function of the FA amount and concrete age, as shown in Table 5.5. The results showed satisfactory compressive strength estimation further evaluated on the results from the literature. A similar estimation for the FA efficiency factor was also proposed by Yeh (Yeh 2016) as shown in Table 5.5. Predictions proposed by Yeh (Yeh 2016) were made based on the database of concretes made with 10-80% of FA in CM with maximum aggregate size up to 20 mm. Predictions given by Rajamane et al. (Rajamane et al. 2007) and Yeh (Yeh 2016) for the FA efficiency factor at different ages are shown in Figures 5.23–5.27.

It can be seen that both Rajamane et al. (2007) and Yeh (2016) predictions for k factor improved the correlation between the RCC and HVFAC. Lower scattering of the results was noticed for prediction proposed by Yeh (2016).

5. Analysis and discussion of results

Regardless of the criteria proposed for the selection of the results, there were still some limitations regarding this analysis. The selected results from the literature included different types and classes of FA and cement that were not taken into account—FA and cement’s physical, mineralogical and chemical properties were not considered. It can be concluded that more parameters defining FA and cement properties should be analyzed.

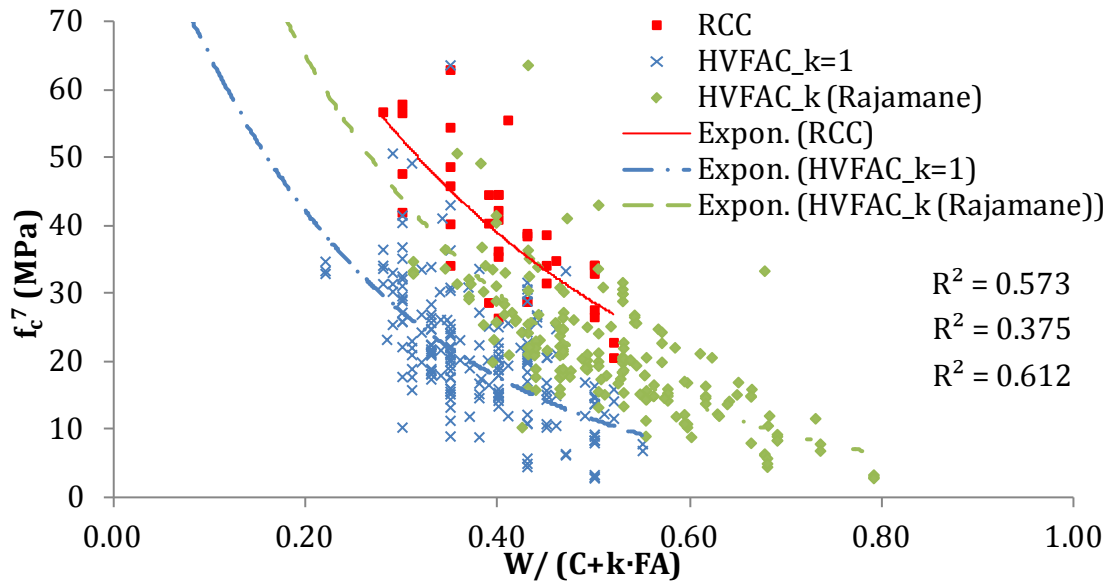


Figure 5.23 7-day compressive strength versus $W/(C+k \cdot FA)$ (Rajamane et al. 2007)

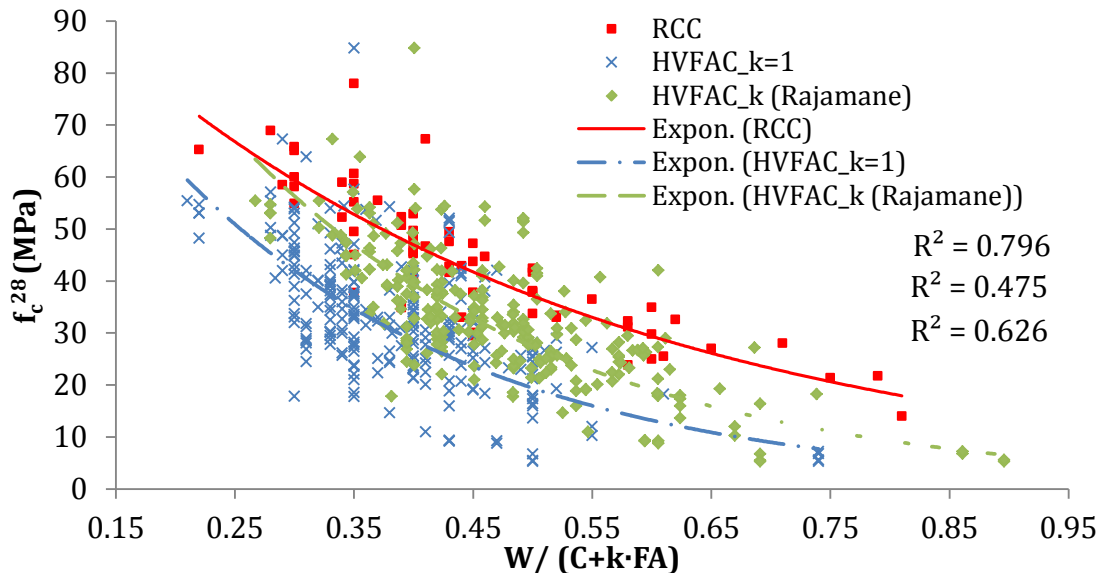


Figure 5.24 28-day compressive strength versus $W/(C+k \cdot FA)$ (Rajamane et al. 2007)

5. Analysis and discussion of results

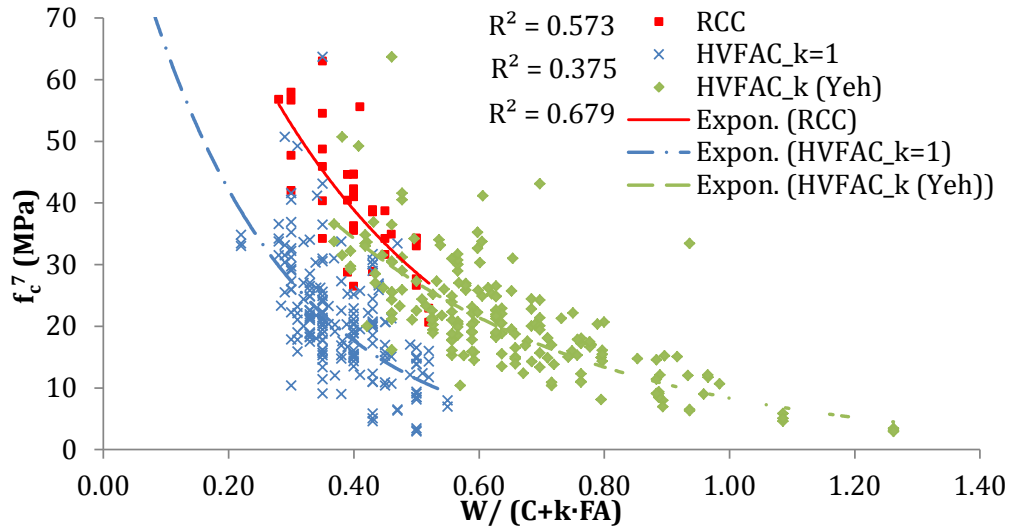


Figure 5.25 7-day compressive strength versus $W/(C+k \cdot FA)$ (Yeh 2016)

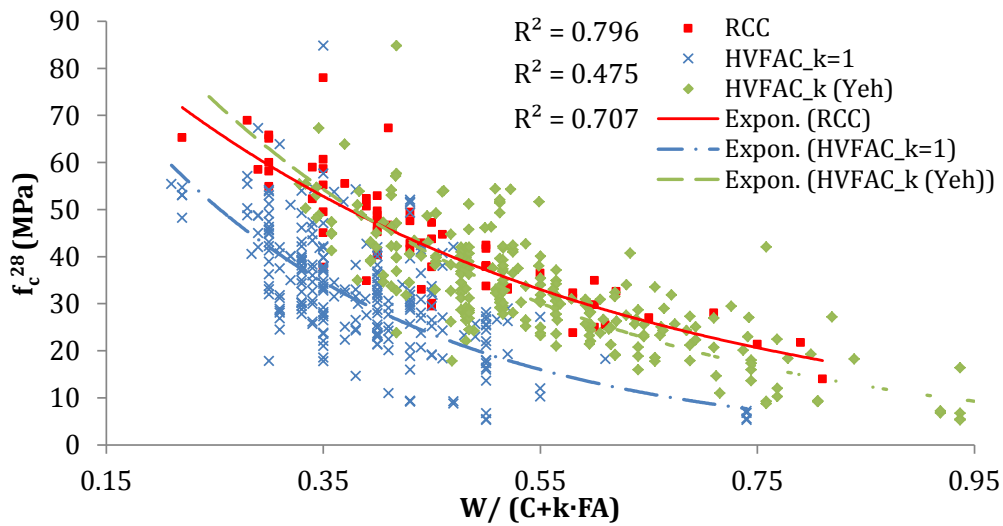


Figure 5.26 28-day compressive strength versus $W/(C+k \cdot FA)$ (Yeh 2016)

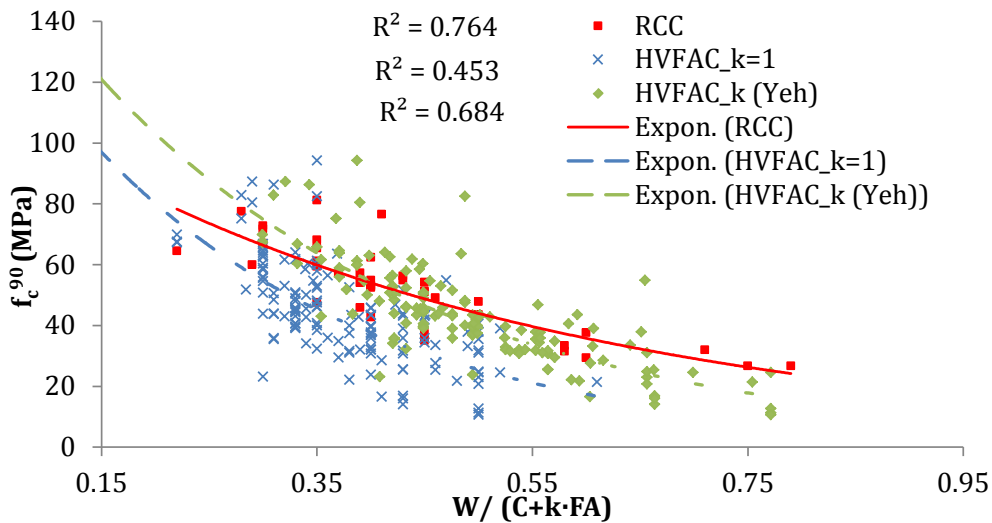


Figure 5.27 90-day compressive strength versus $W/(C+k \cdot FA)$ (Yeh 2016)

5. Analysis and discussion of results

Papadakis investigated the influence of active silica (active SiO₂) in FA on the efficiency of FA in concrete (Papadakis 1999, 2000; Papadakis et al. 2002; Papadakis and Tsimas 2002). According to Papadakis et al. (2002) the activity of CM was greatly influenced by the amount of active SiO₂ in FA and cement and the FA activity index. According to the defined procedure, given in EN 450-1 (CEN 2012), the FA activity index is being tested on mortars made with 25% of FA in CM mass. Papadakis et al. (2002) analyzed the influence of these two parameters on the efficiency of FA in concrete mixtures made with 10% to 20% of FA in CM. Two different predictions for *k* factor were proposed by the authors, as shown in Table 5.5, but their application in HVFAC was not discussed. The predictions proposed by Papadakis et al. (2002) were not re-evaluated in this study due to the lack of available results regarding FA and cement active silica content and the FA activity index.

Another important parameter influencing the FA efficiency is its fineness, especially at the early ages (Babu and Rao 1996; Papadakis et al. 2002). A study conducted by Hwang et al. (2004) evaluated the efficiency of FA as the function of the FA content, Blaine specific surface area and concrete age. The authors highlighted that the FA efficiency is strongly influenced by the FA and cement amount ratio, but suggested that the effect of the FA fineness should also be evaluated. In order to re-evaluate the *k* factor proposed by Hwang et al. (Table 5.5) selected RCC and HVFAC mixtures from the database were analyzed. Only the studies with available results of FA Blaine specific surface area were chosen for the analysis. These criteria yielded 152 results for the 7-day compressive strength (131 HVFAC and 21 RCC concrete), 192 results for the 28-day compressive strength (157 HVFAC and 35 OPC concrete) and 124 results for the 90-day compressive strength (100 HVFAC and 24 OPC concrete). The relationships between the RCC and HVFAC compressive strength results at different age compared with the $W/(C+k \cdot FA)$ ratio proposed by Hwang et al. (2004) are shown in Figures 5.28–5.30. The strong correlation shown in Figures 5.28–5.30 indicates that the Blaine specific surface area is an important factor influencing FA at all tested ages. The Blaine method is widely used for the characterization of the

5. Analysis and discussion of results

cement fineness and it is defined in the EN 196-6 (CEN 2008). However, this method is not included in the EN 450-1 for the use of FA in concrete (CEN 2012).

One of the basic assumptions regarding the Blaine method testing is that the material particles are mostly spherical with no particles that are highly irregular in shape (Arvaniti et al. 2015).

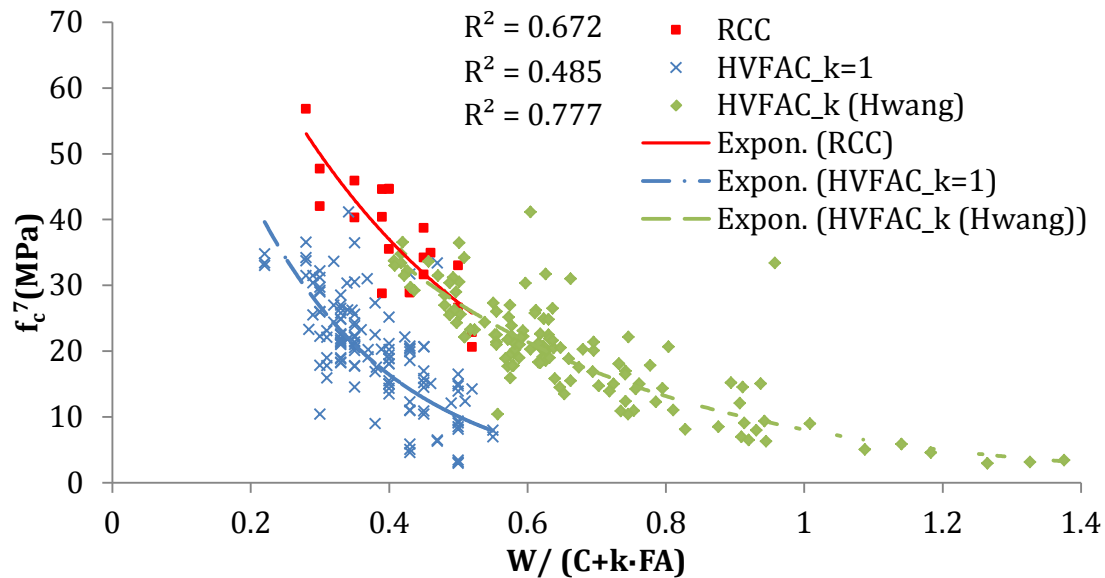


Figure 5.28 7-day compressive strength versus $W/(C+k \cdot FA)$ (Hwang et al. 2004)

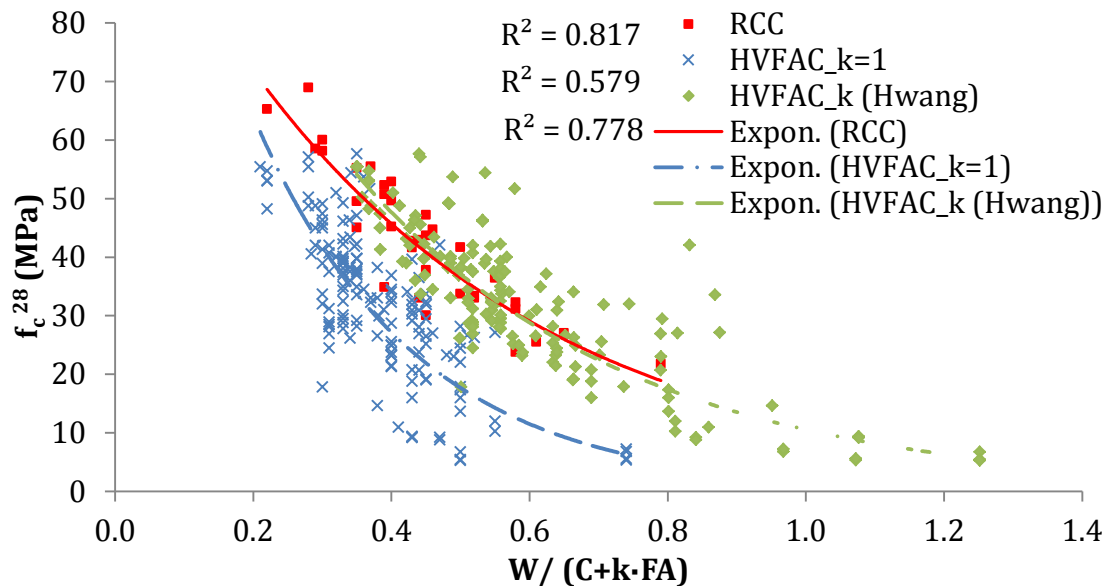


Figure 5.29 28-day compressive strength versus $W/(C+k \cdot FA)$ (Hwang et al. 2004)

5. Analysis and discussion of results

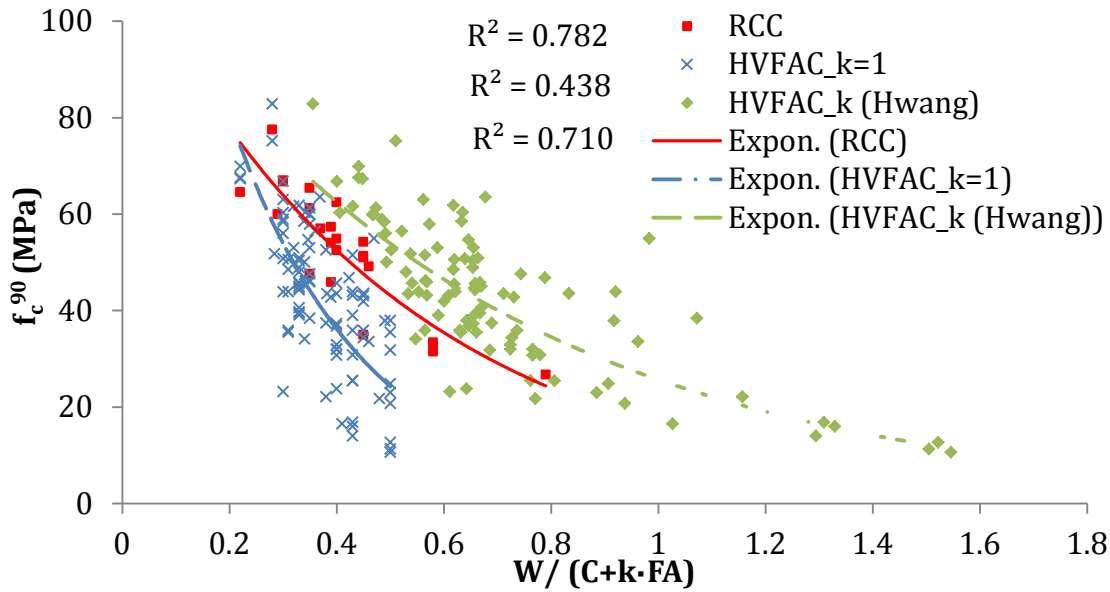


Figure 5.30 90-day compressive strength versus $W/(C+k \cdot FA)$ (Hwang et al. 2004)

As it was already mentioned, FA particles can be irregular in shape with a certain number of unburned coal residues and inter-particle heterogeneity. Hence, a special attention is needed during the selection of measuring technologies developed for cement in the characterization of FA (Arvaniti et al. 2014, 2015). This can be a disadvantage of the FA efficiency method proposed by Hwang et al. (Hwang et al. 2004). Nevertheless, fineness, particularly that of its glassy phase, is considered to be an important factor influencing the FA efficiency (Wesche 2004).

The amount of reacted FA greatly depends on its glassy phase - reactive SiO_2 and Al_2O_3 content and on the amount of available $Ca(OH)_2$ present in the concrete matrix. Hannesson (2010) conducted research in order to determine the FA efficiency as a function of FA and cement chemical composition. He concluded that the amount of CaO , SiO_2 and Al_2O_3 in the cement and FA was an important factor influencing the FA concrete compressive strength. Since these three chemical compounds are important for both early and long-term strength, the FA efficiency was presented as the function of the CaO mass to the sum of SiO_2 and Al_2O_3 mass ratio in total CM for different concrete age using the following definition:

$$\frac{C}{S + A} = \frac{CaO^{cement} + CaO^{FA}}{SiO_2^{cement} + SiO_2^{FA} + Al_2O_3^{cement} + Al_2O_3^{FA}} \quad Eq. 5.3$$

5. Analysis and discussion of results

In a paper published by Kuder et al. (2012), the summary of the research done by Hannesson (2010) was presented. The evaluation of the FA and granulated blast furnace slag efficiency in different concrete mixtures was done. The proposed efficiency factor was re-evaluated in this study on the selected results from the database using solely the class F FA mixtures. Out of all available results in the database, only the ones with available data of CaO, SiO₂ and Al₂O₃ content in cement and FA were used for the analysis. After applying these filters to the database, 358 concrete mixtures (273 HVFAC and 85 RCC mixtures) were selected for further analysis.

The relationships between the 7-day, 28-day and 90-day compressive strength compared with the $W/(C+k \cdot FA)$ ratio are shown in Figures 5.31–5.33 for Kuder et al. (2012) k factor predictions.

Good correlation between the RCC and HVFAC compressive strength results was obtained at all evaluated concrete ages (Figures 5.31 – 5.33). It can be concluded that all proposed predications for the FA efficiency gave similar improvements to RCC and HVFAC compressive strength relations.

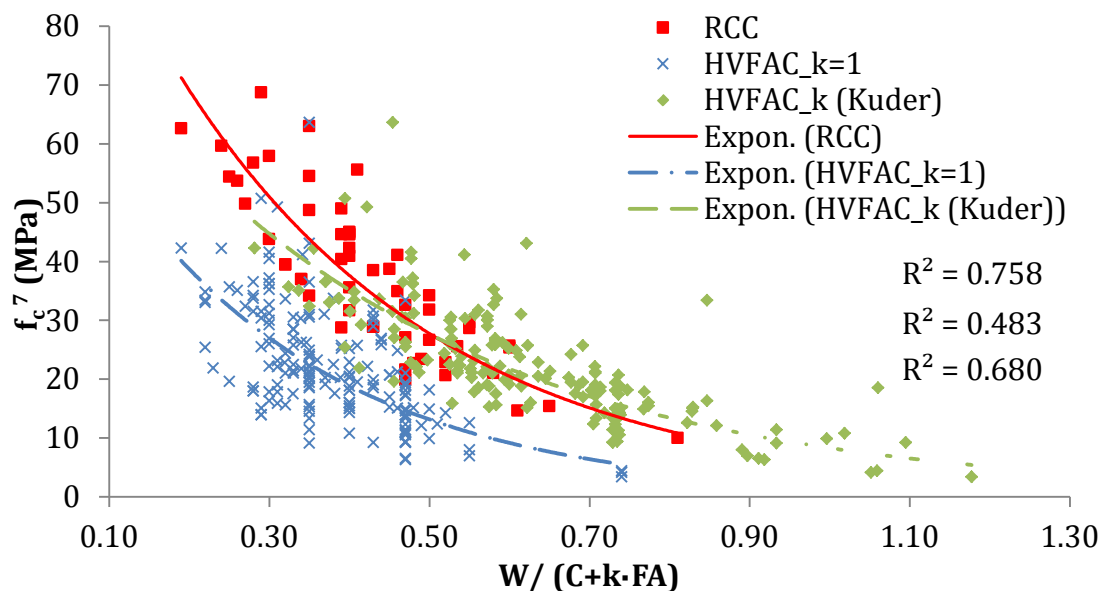


Figure 5.31 7-day compressive strength versus $W/(C+k \cdot FA)$ (Kuder et al. 2012)

5. Analysis and discussion of results

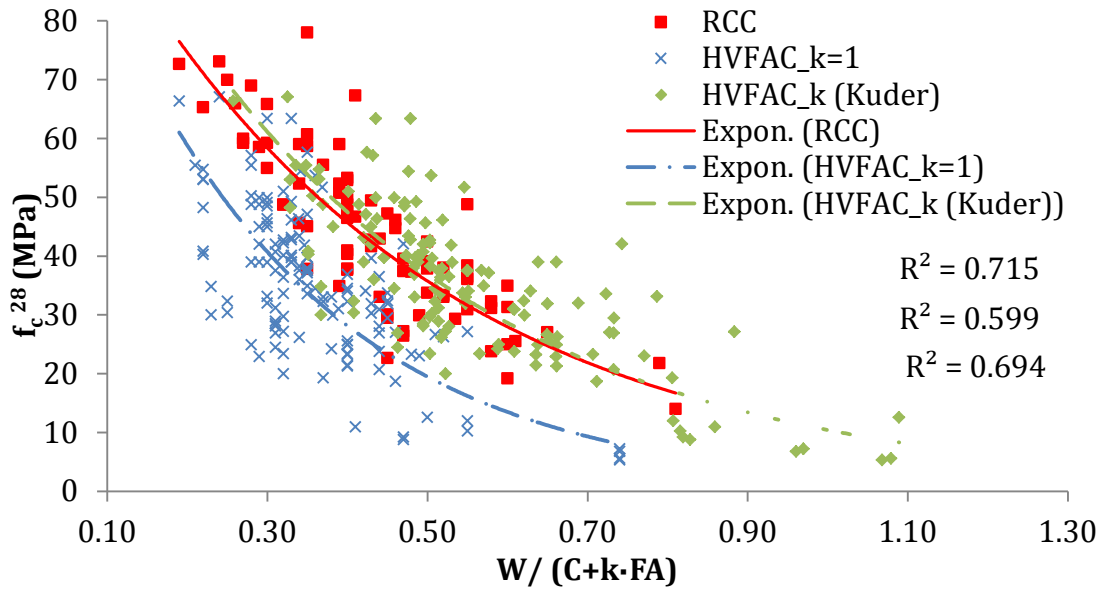


Figure 5.32 28-day compressive strength versus $W/(C+k \cdot FA)$ (Kuder et al. 2012)

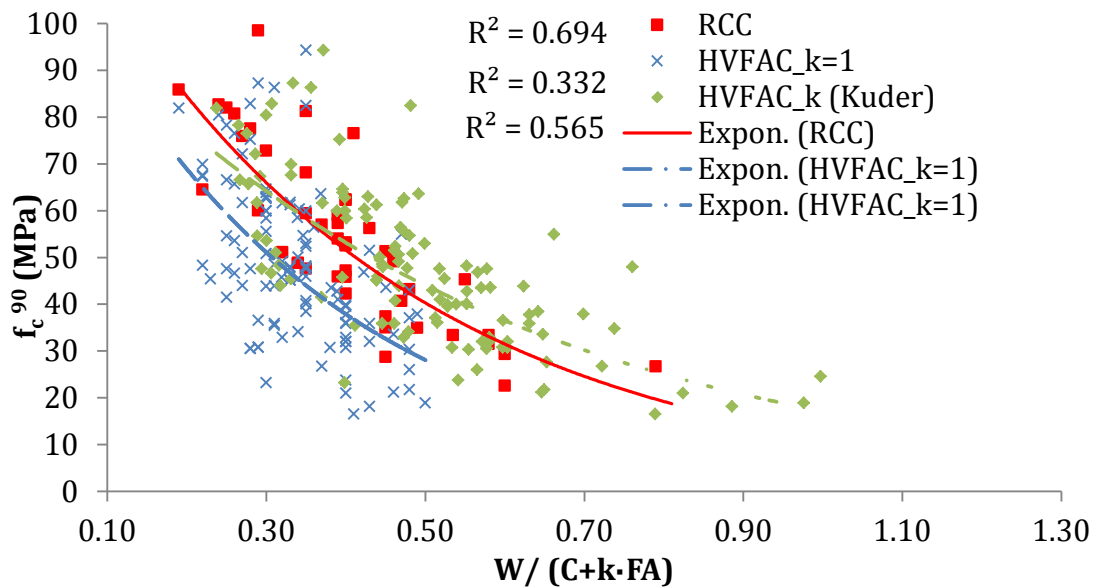


Figure 5.33 90-day compressive strength versus $W/(C+k \cdot FA)$ (Kuder et al. 2012)

The previous analysis showed that HVFAC can be defined with the same type of compressive strength and W/CM ratio relationship with needed alterations of the FA efficiency factor. It was also shown that some of the parameters influencing the FA efficiency in concrete are the amount of FA in CM, concrete age, FA fineness and the FA and cement chemical composition.

The next step in the FA efficiency analysis was to calculate the experimental values of the FA k factors for the selected HVFAC mixtures from the database using the

5. Analysis and discussion of results

available OPCC compressive strength and W/CM ratio equations. The following procedure was applied for that purpose:

- 1) Evaluation of the selected empirical equations defining the relationship between the compressive strength and W/CM ratio of OPCC;
- 2) Calculation of necessary coefficients for the use of these equations;
- 3) Calculation of the experimental k factor values for the HVFAC from the database;
- 4) Selection of the best equation for k factor calculation;
- 5) Evaluation of the important parameters influencing FA efficiency.

One of the main reasons for analyzing the FA efficiency was the need to use the empirical equations for compressive strength predictions in order to determine the concrete mix design and component material proportion. There are few empirical equations used for the compressive strength prediction of OPCC and they are all the function of the W/CM ratio accounting different parameters of influence. The most commonly used empirical equations are Abrams, Bolomey, Feret and Baljejev (Abrams 1918; Bolomey 1935; Feret 1892; Gopalan and Haque 1985; Muravljev 2007; Oner et al. 2005; Rajamane and Ambily 2012; Yeh 2006). These equations usually give significantly different compressive strength values for the same concrete mixtures, so the three of them were chosen for further analysis. In this study Bolomey, Baljejev and Feret equations were selected for evaluation in the following forms:

Bolomey equation:

$$f_c = A \cdot \left(\frac{1}{\frac{W}{(C + k \cdot FA)}} - 0.5 \right) \quad \text{Eq. 5.4}$$

where:

W water mass (kg/m³);

C cement mass (kg/m³);

FA FA mass (kg/m³);

5. Analysis and discussion of results

k FA efficiency factor;

A coefficient defining cement strength and aggregate type.

Baljejev equation:

$$f_c = \frac{B}{\left(\frac{W}{C + k \cdot FA}\right)^{1.5}} \quad \text{Eq. 5.5}$$

where:

B coefficient defining cement strength and aggregate type.

Feret equation:

$$f_c = \frac{K}{\left(1 + \frac{W}{C + k \cdot FA} \cdot \frac{\gamma_{sc}}{\gamma_w}\right)^2} \quad \text{Eq. 5.6}$$

where:

K parameter depending on the cement class;

γ_{sc} specific gravity of cement;

γ_w specific gravity of water.

The empirical coefficients A, B and K in Bolomey, Baljejev and Feret equations were calculated based on the experimental results of the RCC made with the same cement, aggregate and plasticizer type and cured under the same conditions as the HVFAC. In this way, it was further possible to compare the compressive strength results of the RCC and HVFAC regardless of these properties. Out of all available results in the database, only the ones with available data regarding physical and chemical properties of the FA and cement, RCC concrete and available 28-day compressive strength were selected. After applying these filters to the database, 358 concrete mixtures remained for further analysis. The selected concrete mixtures were divided into two groups, HVFAC mixtures (273) and RCC mixtures (85). The coefficients A, B and K in Bolomey, Baljejev and Feret equations were calculated for each RCC in each study using the following equations:

5. Analysis and discussion of results

$$A_i = \frac{f_c^{RCC}}{C/W - 0.5} \quad \text{Eq. 5.7}$$

$$B_i = f_c^{RCC} \cdot \left(\frac{W}{C}\right)^{1.5} \quad \text{Eq. 5.8}$$

$$K_i = f_c^{RCC} \cdot \left(1 + \frac{W}{C} \cdot \frac{\gamma_{sc}}{\gamma_w}\right)^2 \quad \text{Eq. 5.9}$$

where:

i number of different studies;

f_c^{RCC} experimental 28-day compressive strength of RCC (MPa);

C, W cement and water mass in RCC;

γ_{sc} specific gravity of cement, if not available taken as 3150 kg/m³;

$\gamma_w = 1000$ kg/m³.

In some studies, more than one RCC mixture was used and in that case A_i , B_i and K_i coefficients were taken as the mean values of all RCC mixtures in that study. This procedure was justified given that all RCC in one study were made with the same cement and aggregate type. In order to evaluate this method, the compressive strength for all RCC mixtures was calculated using coefficients A_i , B_i and K_i . The results are plotted in Figure 5.34. It can be seen that all three equations gave excellent predictions for all RCC, as expected.

The next step was the calculation of the FA efficiency factor (k^{EXP}) from the experimental HVFAC compressive strength results using Bolomey, Baljejev and Feret equations (Eq. 5.7, 5.8 and 5.9, respectively) with $k=k^{EXP}$. The results of the calculated k^{EXP} for all 273 HVFAC mixtures (sample number ranging from 1 to 273) are shown in Figure 5.35. It can be seen that the Bolomey and Baljejev equations gave similar k^{EXP} values while the Feret equation yielded slightly higher k^{EXP} values. The most probable reason for different Feret equation predictions was the assumption of the cement specific gravity that may have been different in some cases. Nevertheless, all three equations predicted similar values of k^{EXP} showing that this method of evaluation of the FA efficiency in HVFAC was correct. The

5. Analysis and discussion of results

calculations of k^{EXP} done with the Bolomey equation were adopted for further FA efficiency evaluation.

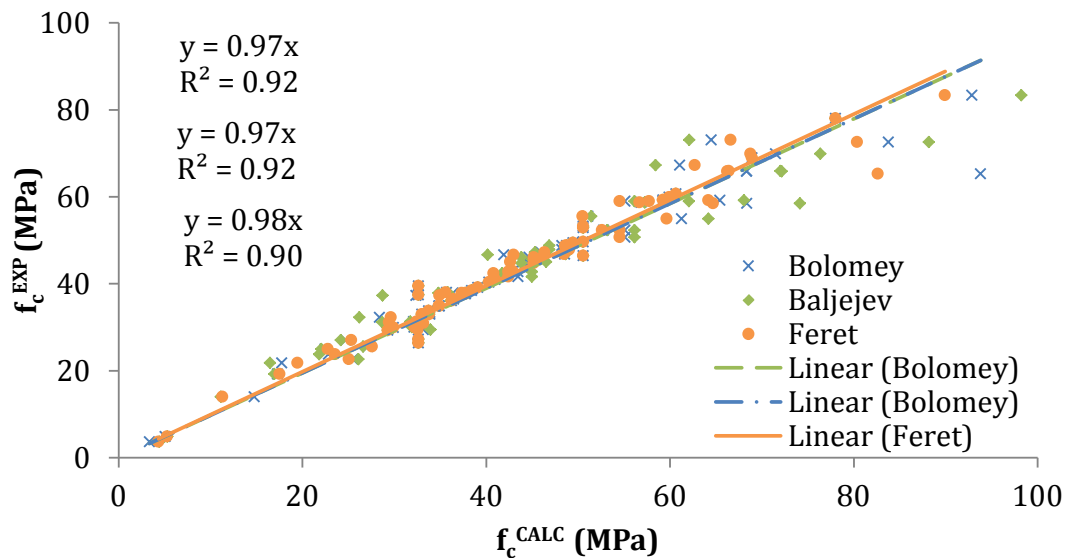


Figure 5.34 Experimental and calculated RCC compressive strength

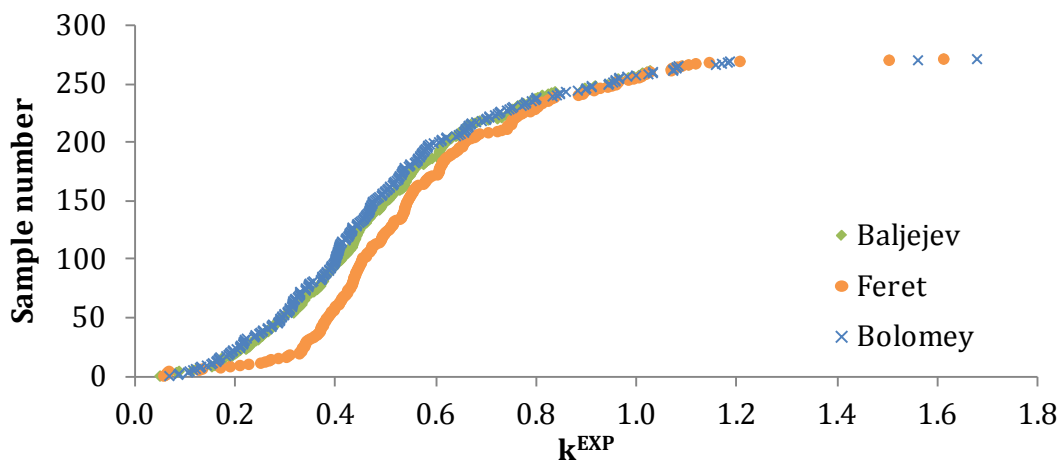


Figure 5.35 Experimental values of k factor for all 273 HVFAC mixtures

The next step was the evaluation of the important parameters influencing the FA efficiency. The calculated k^{EXP} factors are plotted versus the FA/CM ratio, C/(S+A) ratio, and specific gravity of FA and Blain specific surface in Figures 5.36–5.39, respectively.

It can be seen that k^{EXP} generally decreases with the increase of the FA amount in CM. No clear correlation between other parameters and k^{EXP} can be made, but a general increasing trend of FA efficiency with the increase of the C/(S+A) ratio, FA specific gravity and Blaine specific surface can be noticed.

5. Analysis and discussion of results

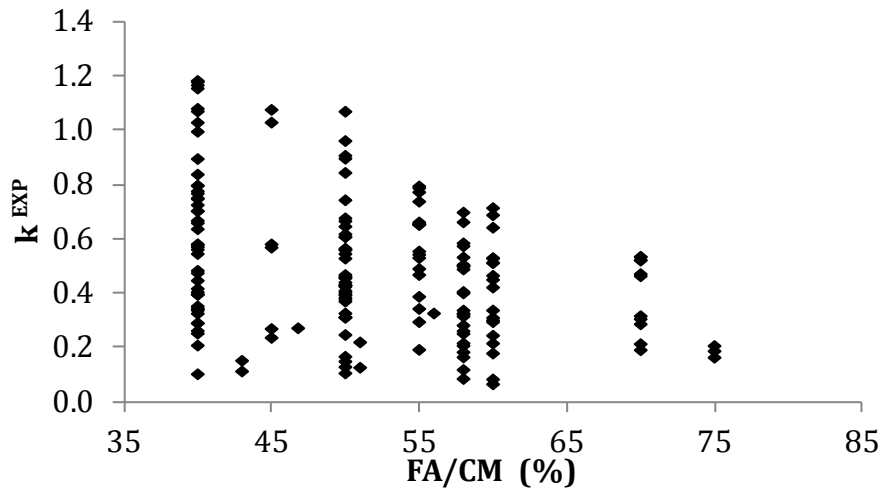


Figure 5.36 Calculated k^{EXP} factor versus FA/CM ratio

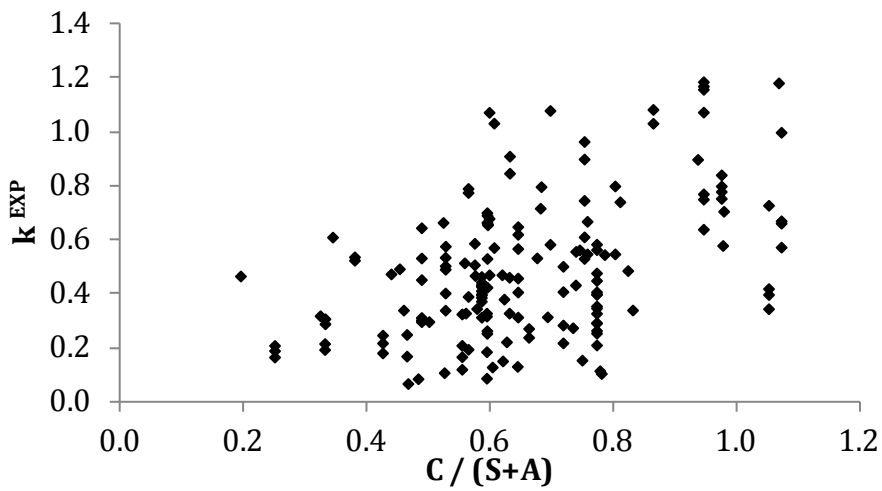


Figure 5.37 Calculated k^{EXP} factor versus $C/(S+A)$ ratio

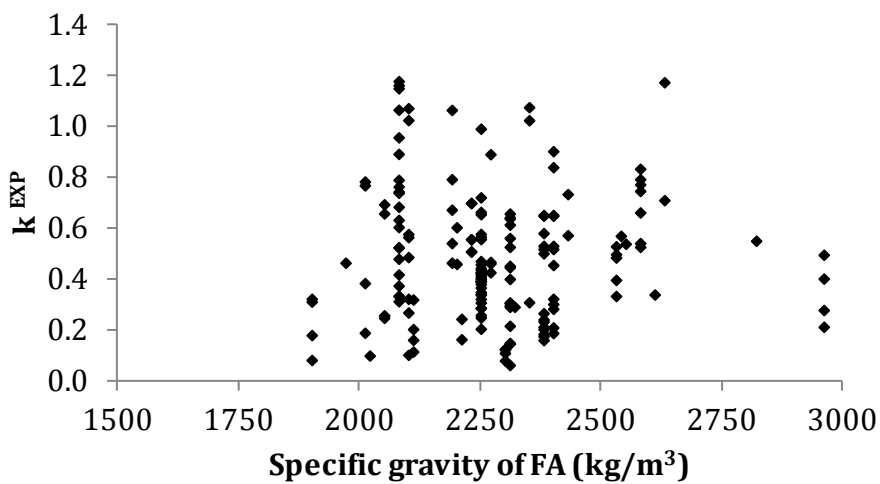


Figure 5.38 Calculated k^{EXP} factor versus FA specific gravity

5. Analysis and discussion of results

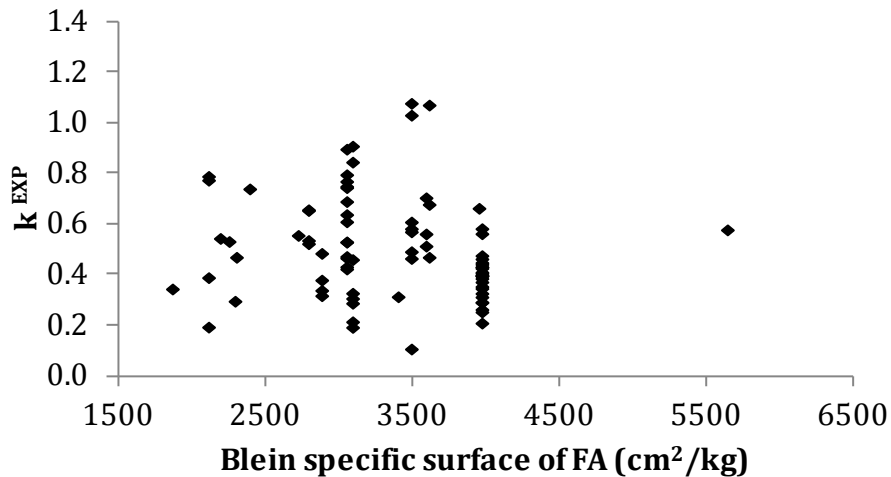


Figure 5.39 Calculated k^{EXP} factor versus Blain specific surface of FA

The best correlation was noticed for the $C/(S+A)$ ratio that has been evaluated by Kuder et al. (2012) as already described. After everything previously discussed, it was concluded that the FA fineness should be taken into account in some way in the FA efficiency predictions. The specific gravity of FA was chosen for that purpose. The correlation between the k^{EXP} and FA specific gravity was not clearly expressed (Figure 5.38), but this parameter was chosen because it is commonly used in the FA characterization as the fineness indicator. Further evaluation was done on selected studies from the database that had available FA specific gravity data (175 HVFAC mixtures). The aim of the analysis was to propose the modification of the $C/(S+A)$ ratio by incorporating the FA specific gravity. The best fit for the k factor plotted versus $\gamma \cdot C/(S+A)$ was obtained for the following modified $C/(S+A)$ ratio (Figure 5.40):

$$k = \gamma \cdot \frac{C}{S+A} = \frac{\gamma_{FA}}{3150} \cdot \frac{C}{S+A} \quad Eq. 5.10$$

where:

γ_{FA} FA specific gravity (kg/m^3).

The compressive strength of the selected HVFAC mixtures was calculated using the Bolomey equation and the previously proposed modification of the k factor defined by Kuder et al. (2012) and plotted versus the experimental strength in Figure 5.41. It can be seen that the incorporation of the FA specific gravity improved the

5. Analysis and discussion of results

compressive strength prediction ($R^2=0.74$) compared with the k factor proposed by Kuder et al. (2012) ($R^2=0.55$).

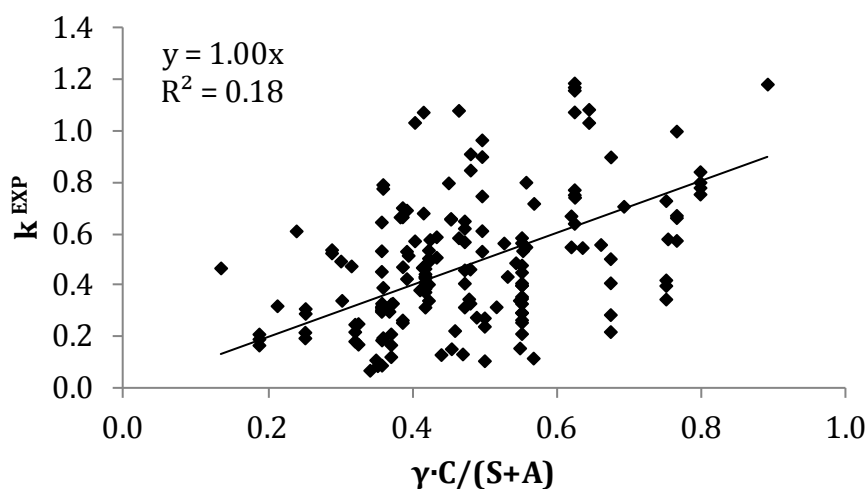


Figure 5.40 Calculated k^{EXP} factor versus modified $C/(S+A)$ ratio

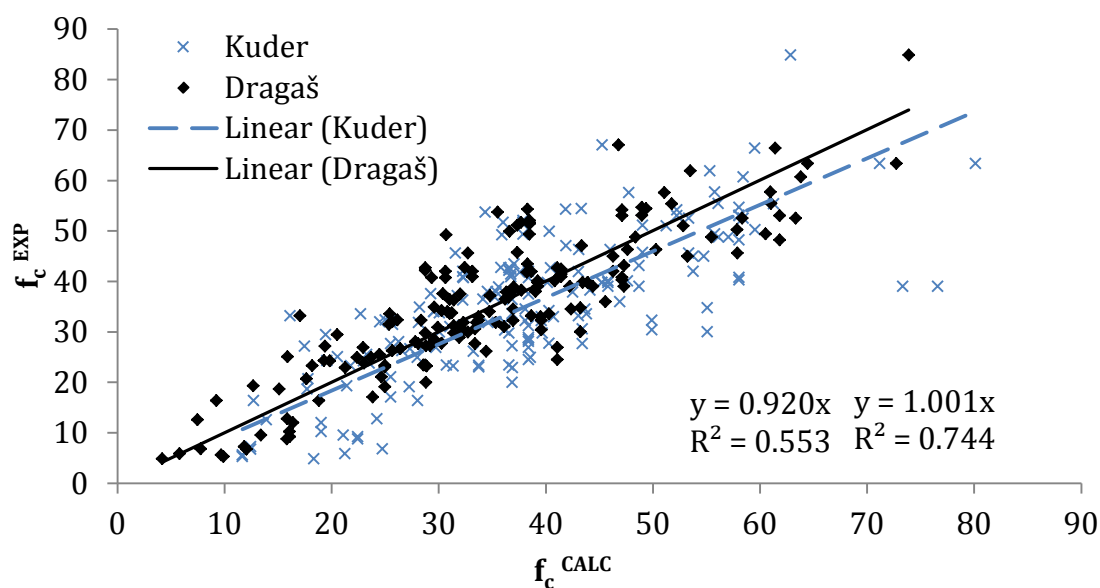


Figure 5.41 HVFAC compressive strength calculated using different k factor values

The mean value of the calculated-to-experimental compressive strength ratio was 1.02 and 1.18 for the k factor calculated using own proposal for k factor (Eq. 5.10) and the k factor proposed by Kuder et al. (2012), respectively. A relatively large CoV of the calculated-to-experimental compressive strength ratio was noticed in the application of both k factor predictions. However, a significantly lower CoV was noticed for the application of Eq. 5.10 (23.8%) compared with the k factor proposed by Kuder et al. (41.0%). It can be concluded that the incorporation of the

5. Analysis and discussion of results

FA specific gravity in the k factor proposed by Kuder et al. (2012) led to the improvement of the compressive strength prediction. This analysis showed that the FA efficiency factor can be defined using both physical and chemical FA and cement properties. It is possible that these factors may be altered by future findings; however, this analysis and the k factor proposal are based on the current state of knowledge.

The previous analysis showed that the available empirical equations defined for OPCC can be used to predict the 28-day compressive strength of HVFAC using the FA efficiency factor. This factor can be determined based on the experimental testing, by treating the k factor as an empirical constant determined from the trial RCC and HVFAC mixtures or by applying one of the previously proposed methods.

5.2.1.3. Compressive strength development over time

In order to understand the HVFAC compressive strength development over time, all available results from the database were selected. The relationship between the experimental 28-day compressive strength and the strength at the age of 1, 7, 14, 56, 90, 180 and 365 days is shown in Figures 5.42–5.49, respectively. It can be seen that the HVFAC compressive strength development was carried out in a similar way as in the RCC. This indicates that the same relationship types can be used to predict the compressive strength development over time for both RCC and HVFAC.

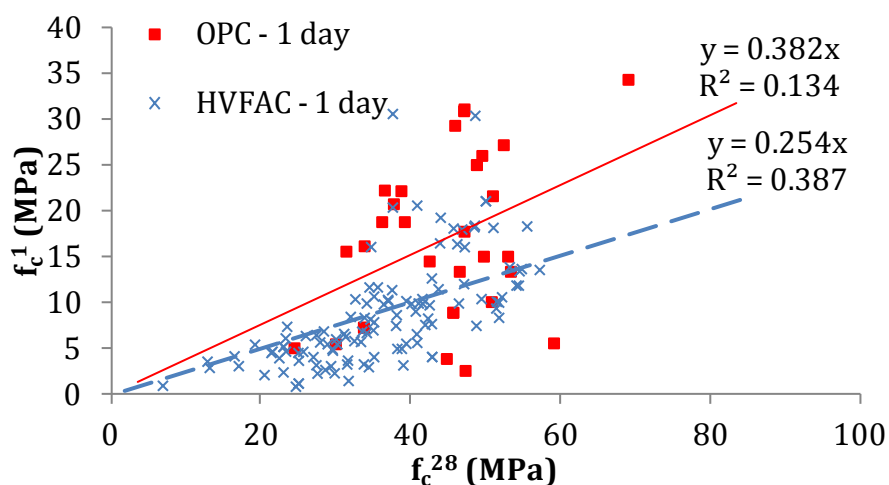


Figure 5.42 1-day HVFAC compressive strength

5. Analysis and discussion of results

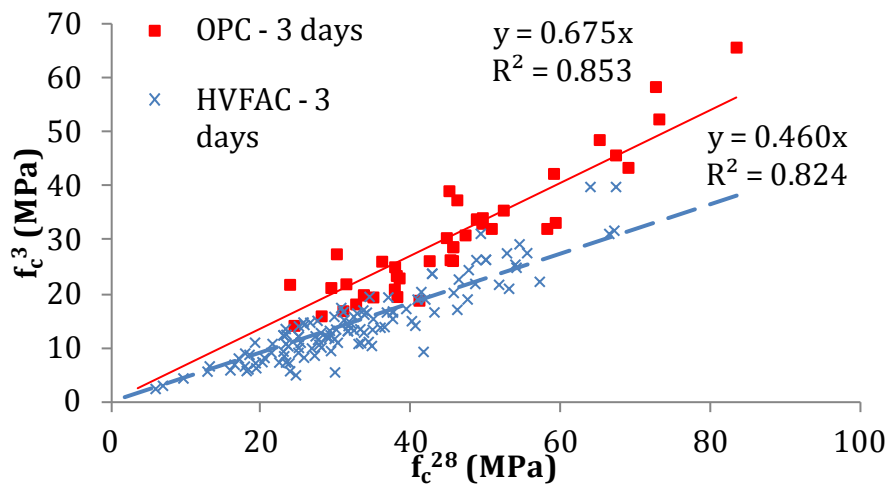


Figure 5.43 3-day HVFAC compressive strength

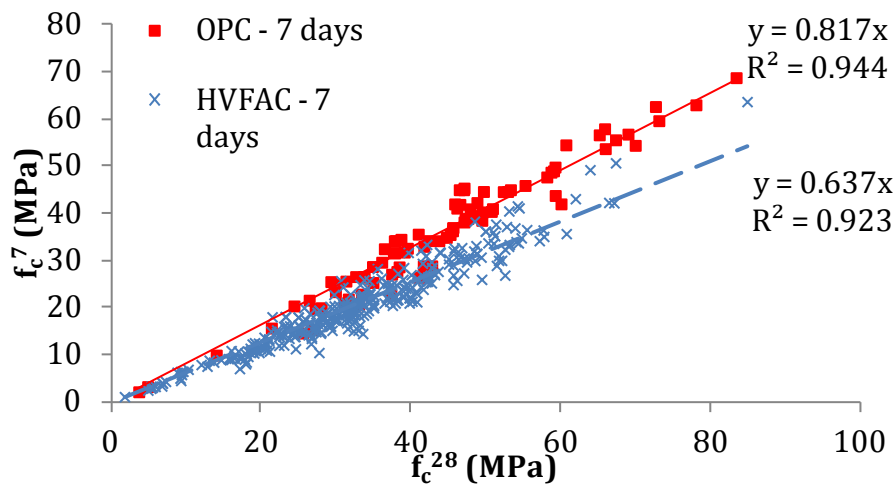


Figure 5.44 7-day HVFAC compressive strength

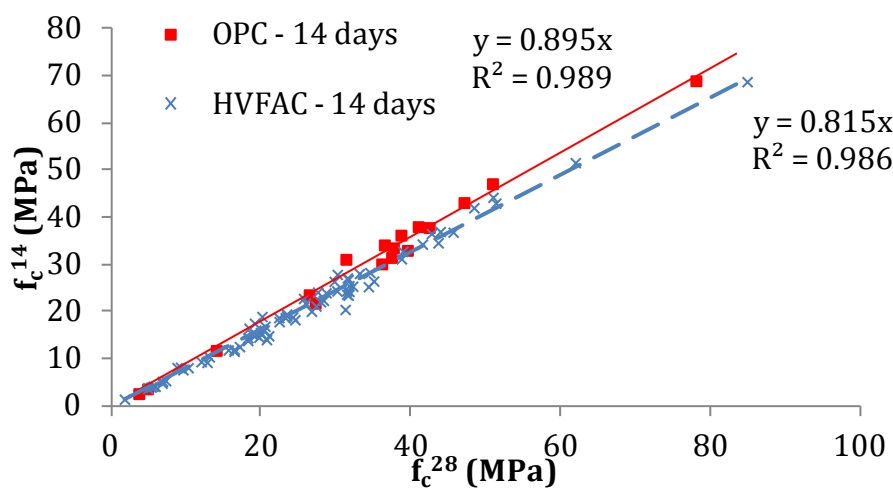


Figure 5.45 14-day HVFAC compressive strength

5. Analysis and discussion of results

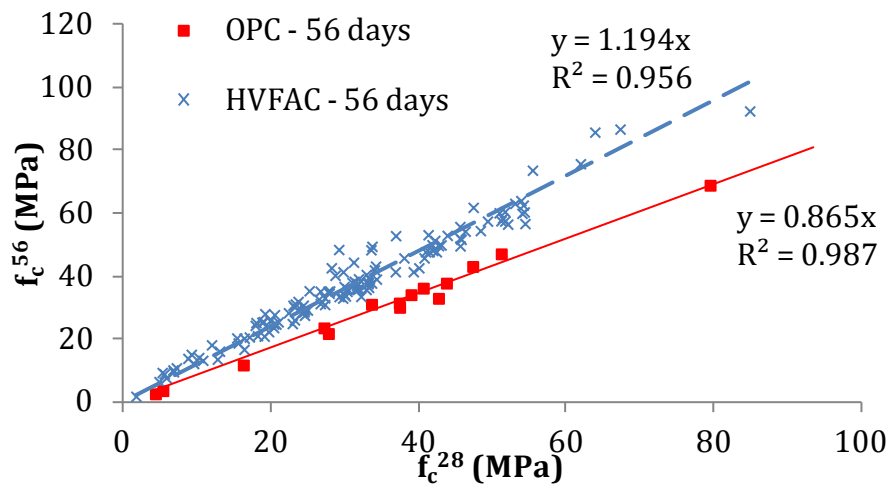


Figure 5.46 56-day HVFAC compressive strength

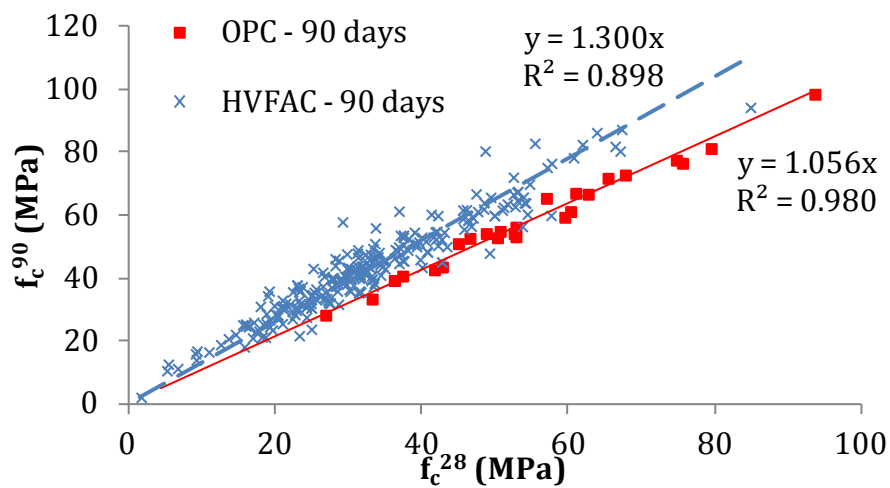


Figure 5.47 90-day HVFAC compressive strength

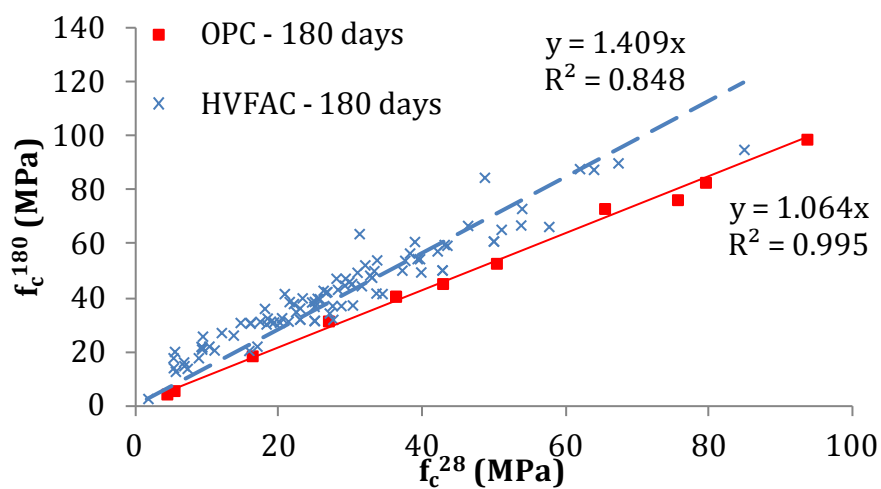


Figure 5.48 180-day HVFAC compressive strength

5. Analysis and discussion of results

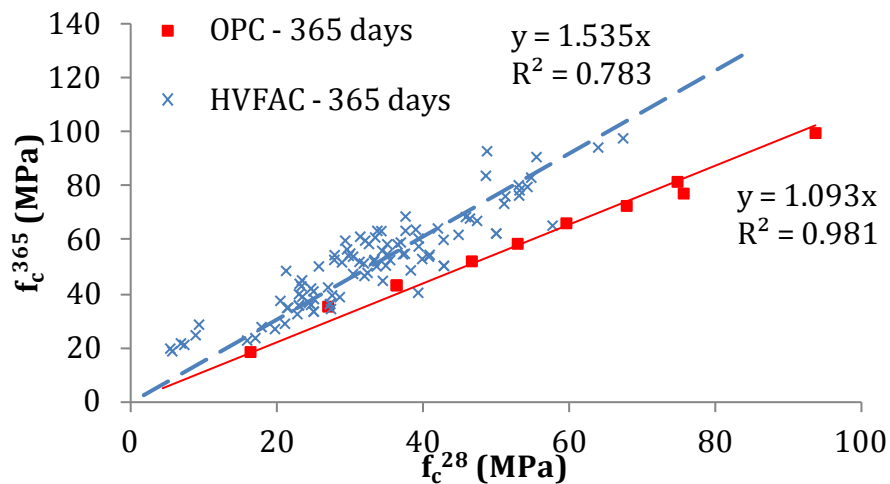


Figure 5.49 365-day HVFAC compressive strength

It can also be concluded that the HVFAC early age compressive strengths ($t < 28$ days) relative to the 28-day compressive strength were, in general, lower than in the RCC. On the other hand, the HVFAC compressive strengths at later ages ($t > 28$ days) relative to the 28-day compressive strength were higher than in the RCC. European Standard EN 1992-1-1 (CEN 2004) defines the following equation for the compressive strength development for cement concrete:

$$f_{cm}(t) = f_{cm}(28) \cdot \beta_{cc}(t) = f_{cm}(28) \cdot EXP \left\{ s \cdot \left(1 - \sqrt{\frac{28}{t}} \right) \right\} \quad Eq. 5.11$$

where:

$f_{cm}(28)$ 28-day compressive strength;

t days;

s constant depending on the cement type and class.

The coefficient s is defined for three groups of cement as:

- 0.2 - cement strength classes CEM 42.5 R, CEM 52.5 N and CEM 52.5 R;
- 0.28 - cement strength classes CEM 32.5 R, CEM 42.5 N;
- 0.38 - cement strength classes CEM 32.5 N.

The cement early age strength was defined in only 14% of the total concrete mixtures in the database which disabled the HVFAC strength gain analysis. In

5. Analysis and discussion of results

order to overcome this lack of data, the s coefficient was calculated from the experimental values of different age compressive strengths for all RCC mixtures. Similar to the FA efficiency analysis, the fact that the same cement was used in the RCC and corresponding HVFAC in the same study gave a possibility to compare the strength gain in RCC and HVFAC mixtures. First, the s coefficient was calculated for all RCC mixtures tested at all ages in each study. The s coefficient was calculated using the Eq. 5.11 and the experimental values of RCC compressive strengths at different ages. Furthermore, the mean value of all calculated s coefficients from one study was chosen as the s coefficient for the evaluation of all concretes in that study. In this way, one s value was defined for each study in the database conducted using one cement type. This analysis yielded the s coefficients in the range from 0.15 to 0.47. The correlation between the RCC compressive strength calculated with calculated s value and corresponding experimental compressive strength is shown in Figure 5.50. It can be seen that this methodology gave good correlation between calculated and measured RCC compressive strengths for all concrete ages.

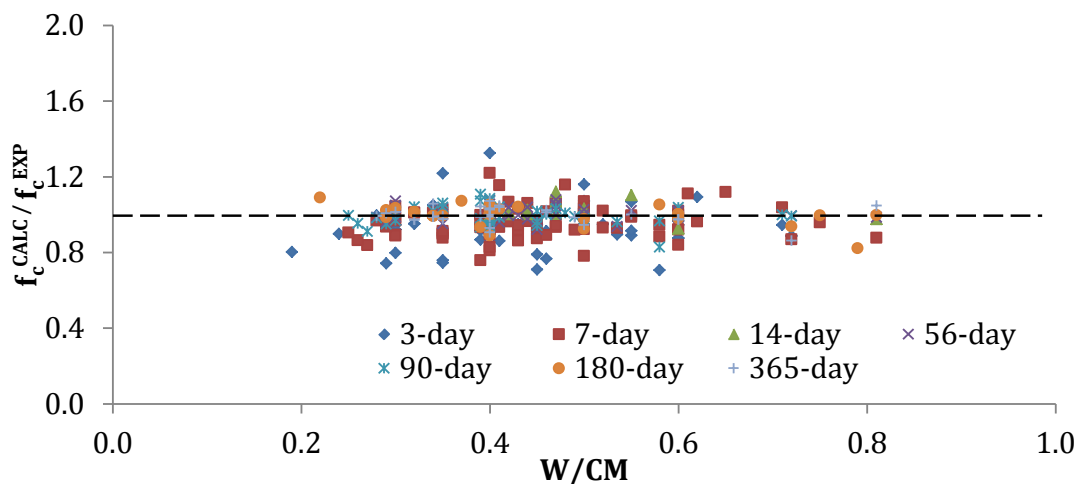


Figure 5.50 Relationship between calculated and experimental RCC compressive strength

The coefficients s calculated in this way were then used to calculate the compressive strength development of HVFAC. The experimental versus the calculated HVFAC compressive strengths for 3-14 days and 56-365 days are shown in Figures 5.51 and 5.52, respectively. The HVFAC compressive strength was also calculated using $s=0.38$ (cement class S) as proposed by Bamforth et al. (2008) for

5. Analysis and discussion of results

concretes with more than 35% of FA in total CM. Figures 5.51 and 5.52 show good prediction of the HVFAC compressive strength at different ages calculated with previously determined s coefficients. However, values calculated in this way overestimated the early age compressive strength (slope is 1.191) and underestimated the compressive strength after 28 days (slope is 0.835).

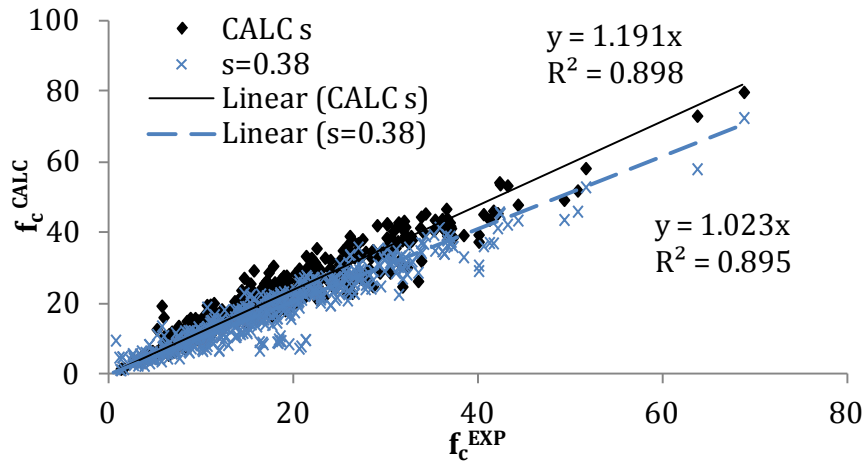


Figure 5.51 3-14 days HVFAC compressive strength calculated using $s=0.38$ and calculated s coefficients

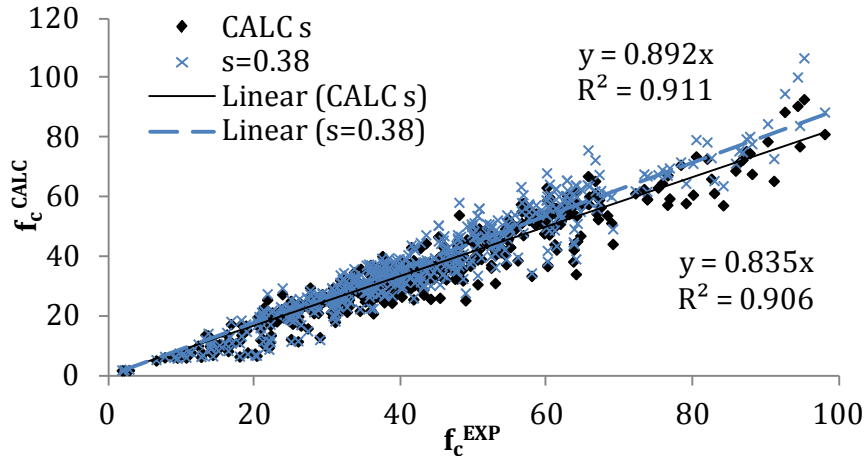


Figure 5.52 56-365 days HVFAC compressive strength calculated using $s=0.38$ and calculated s coefficients

When using the coefficient $s=0.38$, the early age compressive strengths (Figure 5.51) showed good correlation with the experimental results, but the difference was still significant for later ages (Figure 5.52). It can be concluded that the HVFAC compressive strength development over time requires some modification of the Eq. 5.11 defined in EN 1992-1-1 (CEN 2004) by modifying the s coefficient.

5. Analysis and discussion of results

The evaluation of the HVFAC compressive strength development was done by Yoon et al. (2014) by analyzing the HVFAC made with 50% and 60% of class F FA and different W/CM ratios. The researchers concluded that the W/CM ratio is also an important factor influencing the strength gain, especially in high FA content concrete made with low water amount. They proposed the modified s coefficients for different FA amount and W/CM ratios as follows:

- $s = 0.57 \pm 0.08$ for FA/CM=0.5 for all W/CM;
- $s = 0.56 \pm 0.02$ for FA/CM=0.6 for and W/CM = 0.3;
- $s = 0.89 \pm 0.05$ for FA/CM=0.6 for all other W/CM.

In order to re-evaluate these predictions, a selection of the HVFAC results with 45% to 65% of FA in CM was done yielding 178 HVFAC mixtures. The selected HVFAC mixtures were divided in three groups:

- The first group of HVFAC mixtures: 45%-53% of FA in CM mass;
- The second group of HVFAC mixtures: 54%-65% of FA in CM mass and W/CM ratio from 0.21 to 0.35;
- The third group of HVFAC mixtures: 54%-65% of FA in CM mass and W/CM ratio from 0.36 to 0.60.

The s coefficients were calculated for all selected HVFAC mixtures using the experimental values of the compressive strength at different ages. Tables 5.6, 5.7 and 5.8 show the results of the descriptive statistical analysis of the calculated s values for these three groups presented for each concrete age. The average values of the s coefficient for all ages were 0.57, 0.55 and 0.61 for the first, the second and the third group of HVFAC, respectively. It can be seen that the results from the first two groups were in good correlation with the values proposed by Yoon et al. (2014). The average value of the third group was significantly lower compared with the value proposed by Yoon et al. (2014).

A relatively big scatter of the results was noticed in all groups of HVFAC implying that the other parameters which were not taken into account during this analysis have a significant influence on the HVFAC strength increase over time. All concrete

5. Analysis and discussion of results

mixtures tested by Yoon et al. (2014) were made with one cement and FA type neglecting their properties in their prediction for the s coefficient.

Table 5.6 Descriptive statistics analysis of coefficient s for HVFAC mixtures from the first group

Age (days)	1	3	7	14	56	90	180	365
Sample No.	17	29	95	31	57	56	18	23
Mean value	0.36	0.38	0.48	0.60	0.74	0.64	0.71	0.62
St. Error	0.03	0.02	0.01	0.02	0.05	0.05	0.10	0.09
St. Deviation	0.13	0.10	0.13	0.13	0.39	0.34	0.43	0.41
CoV (%)	36.14	26.29	26.94	22.09	52.88	52.11	60.81	66.54
Minimum	0.16	0.27	0.17	0.28	0.15	0.11	0.27	0.24
Maximum	0.57	0.57	0.79	0.93	1.96	1.55	1.63	1.84

Table 5.7 Descriptive statistics analysis of coefficient s for HVFAC mixtures from the second group

Age (days)	1	3	7	14	56	90	180	365
Sample No.	48	34	79	14	17	67	9	41
Mean value	0.38	0.45	0.48	0.52	0.57	0.63	0.69	0.69
St. Error	0.02	0.02	0.01	0.03	0.05	0.02	0.05	0.03
St. Deviation	0.16	0.12	0.08	0.12	0.22	0.16	0.14	0.16
CoV (%)	42.61	26.93	17.05	23.75	38.07	25.27	20.02	23.92
Minimum	0.05	0.30	0.28	0.29	0.14	0.23	0.50	0.39
Maximum	1.03	0.81	0.78	0.71	1.13	1.14	0.92	1.00

Table 5.8 Descriptive statistics analysis for HVFAC mixtures from the third group

Age (days)	1	3	7	14	56	90	180	365
Sample No.	19	26	43	10	19	40	26	14
Mean value	0.38	0.43	0.48	0.45	0.73	0.69	0.85	0.84
St. Error	0.02	0.01	0.02	0.07	0.10	0.04	0.05	0.09
St. Deviation	0.09	0.07	0.12	0.22	0.42	0.25	0.27	0.32
CoV (%)	24.66	15.38	25.52	48.69	57.20	35.85	32.03	38.07
Minimum	0.22	0.33	0.17	0.18	0.08	0.23	0.26	0.41
Maximum	0.58	0.55	0.75	0.83	1.70	1.23	1.37	1.58

5. Analysis and discussion of results

Figure 5.53 shows the mean values for all three groups of HVFAC and indicates that the s coefficient could be different for concrete age before and after 28 days.

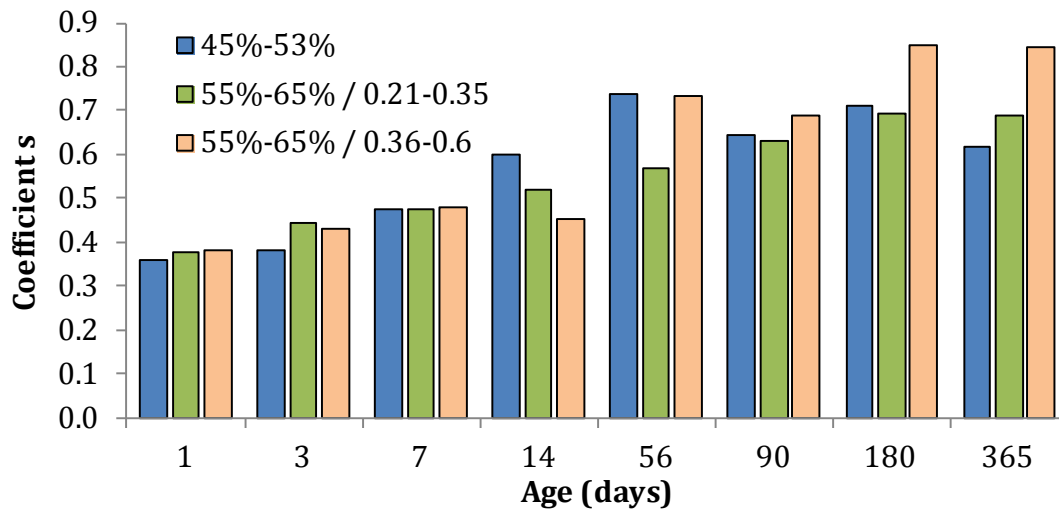


Figure 5.53 Mean values of the s coefficient for three groups of HVFAC

Chen et al. (2017) presented their research regarding the long-term properties of concretes containing CM and presented three time-dependent models for the compressive strength, modulus of elasticity and creep. They proposed the modification of the s coefficient depending on the $C/(S+A)$ ratio, mentioned before, as follows:

$$s \cdot \beta_{cc} \left(\frac{C}{S+A} \right) = \begin{cases} s \cdot \left(-0.38 \cdot \frac{C}{S+A} + 2.12 \right), & t < 28 \text{ days} \\ s \cdot \left(-1.15 \cdot \frac{C}{S+A} + 3.70 \right), & t > 28 \text{ days} \end{cases} \quad \text{Eq. 5.12}$$

where:

s coefficient defined in EN 1992-1-1 (CEN 2004).

They concluded that the $C/(S+A)$ ratio influenced the compressive strength development in a different way for the ages before and after 28 days. As they concluded, the increase of $C/(S+A)$ ratio led to the increase of the compressive strength before 28 days, and the decrease of strength after 28 days (Chen et al. 2017). This can be explained by the fact that the cement hydration is dominant at the early ages when more CaO is favorable. At later ages, the pozzolanic reaction takes place and more SiO₂ and Al₂O₃ is needed. In order to re-evaluate these

5. Analysis and discussion of results

findings, the proposed modification was used to calculate the s coefficient for the HVFAC mixtures from the database. Only the HVFAC mixtures with available data regarding FA and cement chemical composition and compressive strength at different age were selected (294 HVFAC mixtures). The coefficient s was calculated for each of 294 HVFAC mixtures from the database using Eq. 5.12. The results are presented using descriptive statistics parameters and shown in Table 5.9. It can be seen that the mean values of the coefficient s were significantly higher compared with the EN 1992-1-1 (CEN 2004). The evaluation of the obtained results was done by comparing the calculated and experimental values of the compressive strength for the ages before and after 28 days as shown in Figure 5.54.

Table 5.9 Descriptive statistics analysis for the HVFAC s coefficients

	Sample No.	Mean Values	St. Error	St. Deviation	CoV (%)	Min	Max
$t < 28$ days	294	0.55	0.01	0.25	44.77	0.15	1.95
$t > 28$ days	294	0.88	0.02	0.40	44.98	0.27	3.17

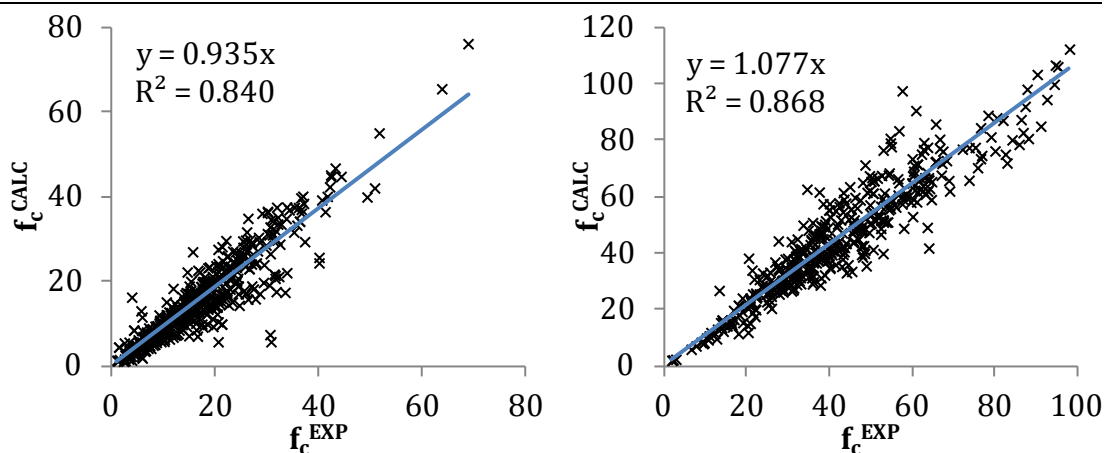


Figure 5.54 Relationship between the experimental and calculated (Chen et al. 2017) compressive strength for ages from a) 3-28 days and b) 28-365 days

It can be seen that the prediction of the compressive strength development was improved by the introduction of the FA and cement chemical composition into the s coefficient. The compressive strengths at a later age (after 28 days) expressed very good correlation to the experimental values. The early age compressive strengths were significantly improved with this modification but slightly overestimated. The previous analysis showed that the correlation between the

5. Analysis and discussion of results

compressive strength development and the C/(S+A) ratio was very good and that it gave significant improvements for the HVFAC strength development determination.

It can finally be concluded that the compressive strength development is lower at the early age and higher at the later age for HVFAC compared with OPCC. The Eq. 5.11 defined in EN 1992-1-1 (CEN 2004) can be used to predict the compressive strength development with modifications proposed by Yoon et al. (2014) or Chen et al. (2017). The results obtained by the application of the Chen et al. (2017) prediction gave better results compared with Yoon et al. (2014), as it can be seen in Figure 5.55.

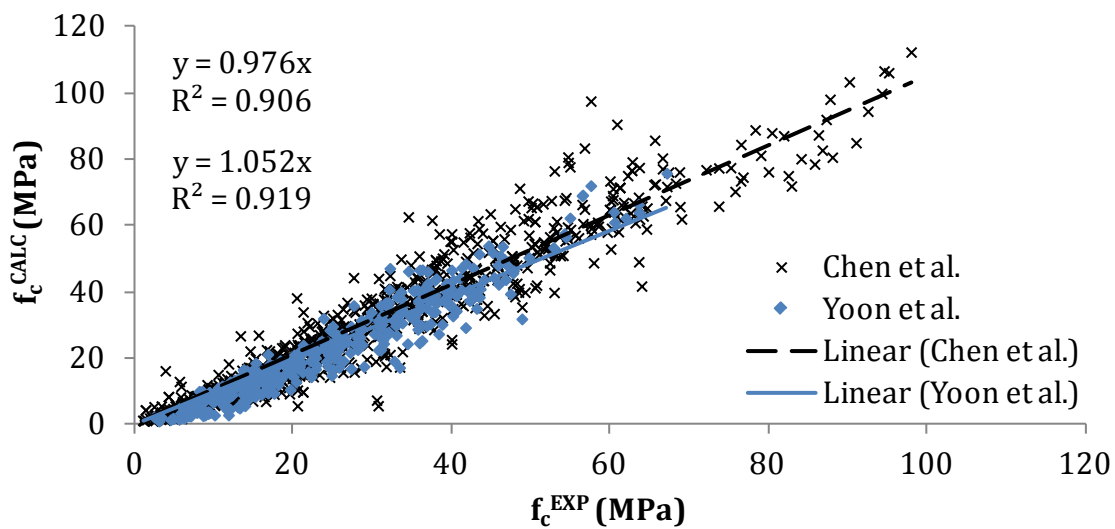


Figure 5.55 Relationship between the experimental and calculated compressive strength for all ages (Chen et al. 2017; Yoon et al. 2014)

5.2.1.4. Modulus of elasticity

The modulus of elasticity is mostly influenced by the concrete age, cement (binder) paste, aggregate type, interfacial transition zone and the porosity of concrete (Neville 1981). The analysis of the HVFAC modulus of elasticity was done based on the selected studies from the literature. Available results from different studies, analyzing modulus of elasticity, were obtained on cylindrical samples 100·200 mm or 150·300 mm. Different strength rates were used, but all up to 40% of the

5. Analysis and discussion of results

ultimate strength. The influence of the sample size and strength rate was neglected in this discussion.

European standard EN 1992-1-1 (CEN 2004) defines the modulus of elasticity prediction as a function of the compressive strength. The secant 28-day modulus of elasticity for quartzite aggregate is defined as follows:

$$E_c = 22 \cdot \left(\frac{f_c}{10}\right)^{0.3} \quad \text{Eq. 5.13}$$

where:

f_c mean 28-day compressive strength (MPa).

Having in mind that the concrete elastic deformation is mostly influenced by the aggregate type, different recommendations for Eq. 5.13 modification are given in EN 1992-1-1 (CEN 2004):

- for limestone aggregates modulus should be reduced by 10%;
- for sandstone aggregates modulus should be reduced by 30%;
- for basalt aggregates modulus should be increased by 20%.

In order to re-evaluate this equation, studies with the experimental results of the HVFAC modulus of elasticity were selected from the database (21 RCC and 77 HVFAC mixtures). Figure 5.56 shows the relationship between the compressive strength and the modulus of elasticity of HVFAC mixtures made with 40-70% of FA in CM and granite, limestone and sandstone aggregates. The general trend of a higher HVFAC modulus of elasticity compared with RCC was noticed. The correlation between the HVFAC and RCC was similar, but with much greater scattering of the results presented in HVFAC mixtures. It can be concluded that the same modulus of elasticity and compressive strength relationship type can be used for the HVFAC as in RCC.

The application of the EN 1992-1-1 (CEN 2004) equation (Eq. 5.13) with modifications regarding the aggregate type on the selected HVFAC mixtures from the database was done. Moreover, a possible application of the modification found in the literature was also evaluated.

5. Analysis and discussion of results

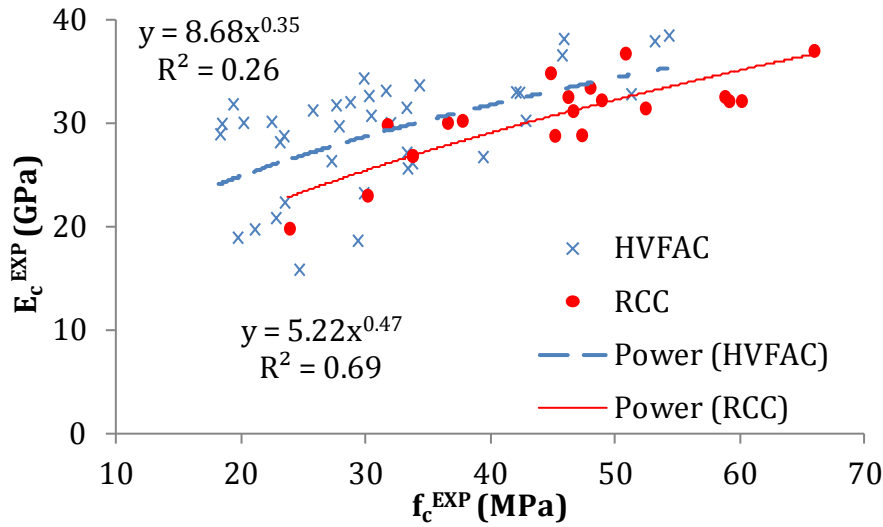


Figure 5.56 Relationship between experimental values of modulus of elasticity and compressive strength

Yoon et al. (2014) analyzed the HVFAC modulus of elasticity and proposed the following modification of the EN 1992-1-1 (CEN 2004) equation:

- for HVFAC with 50% of FA in CM:

$$E_c = (17 \pm 0.08) \cdot \left(\frac{f_c}{10}\right)^{(0.45 \pm 0.10)} \quad \text{Eq. 5.14}$$

- for HVFAC with 60% of FA in CM:

$$E_c = (21.7 \pm 0.77) \cdot \left(\frac{f_c}{10}\right)^{(0.29 \pm 0.08)} \quad \text{Eq. 5.15}$$

The modulus of elasticity was calculated using the EN 1992-1-1 (CEN 2004) equation taking into account different aggregate types. The Yoon et al. (2014) proposal was evaluated for the lower, average and upper values of proposed coefficients. The HVFAC modulus of elasticity was calculated for these four values of the coefficients and shown in Table 5.10 as the calculated-to-experimental modulus ratio using descriptive statistical parameters.

The evaluation of Yoon et al. (2014) modification was done on the HVFAC mixtures with 45%-55% of FA in CM using the modification proposed for 50% of FA in CM and for HVFAC mixtures with 55%-65% of FA in CM using the modification proposed for 60% of FA in CM. It can be seen that the mean values of the calculated

5. Analysis and discussion of results

to experimental modulus of elasticity ratios were similar for EN 1992-1-1 (CEN 2004) and Yoon et al. (2014) modification (average). A better prediction with slightly lower CoV was obtained using the EN 1992-1-1(CEN 2004) equation taking into account the aggregate type. It can be concluded that the EN 1992-1-1 (CEN 2004) equation gives good estimation for the HVFAC modulus of elasticity if the aggregate type is taken into account. This is not a surprise having in mind that aggregate is the main parameter influencing concrete elastic behavior.

Table 5.10 Descriptive statistical parameters for HVFAC modulus of elasticity evaluation

	EN 1992-1-1	Yoon et al.		
	aggregate type	Lower	Average	Upper
<i>Sample No.</i>	77	67	67	67
<i>Mean Value</i>	1.00	0.87	0.98	1.13
<i>St. Error</i>	0.02	0.02	0.02	0.02
<i>St. Deviation</i>	0.16	0.16	0.18	0.20
<i>CoV (%)</i>	15.72	18.42	17.94	17.75
<i>Minimum</i>	0.76	0.72	0.77	0.82
<i>Maximum</i>	1.42	1.59	1.75	1.97

The development of the modulus of elasticity over time can be estimated using the equation given in EN 1992-1-1 (CEN 2004) as:

$$E_c(t) = \left(\frac{f_c(t)}{f_c} \right)^{0.3} \cdot E_c \quad \text{Eq. 5.16}$$

where:

$E_c(t), f_c(t)$ modulus of elasticity and compressive strength at the age t .

In order to evaluate the possible application of these equations on the results from the database, studies with available experimental results of HVFAC modulus of elasticity were selected (21 OPC and 77 HVFAC mixtures). Figure 5.57 shows the relationship between the 28-day modulus of elasticity and modulus at different age for RCC and HVFAC mixtures with known aggregate type. As it can be seen, a small

5. Analysis and discussion of results

amount of results was available for the modulus of elasticity at ages different from 28 days.

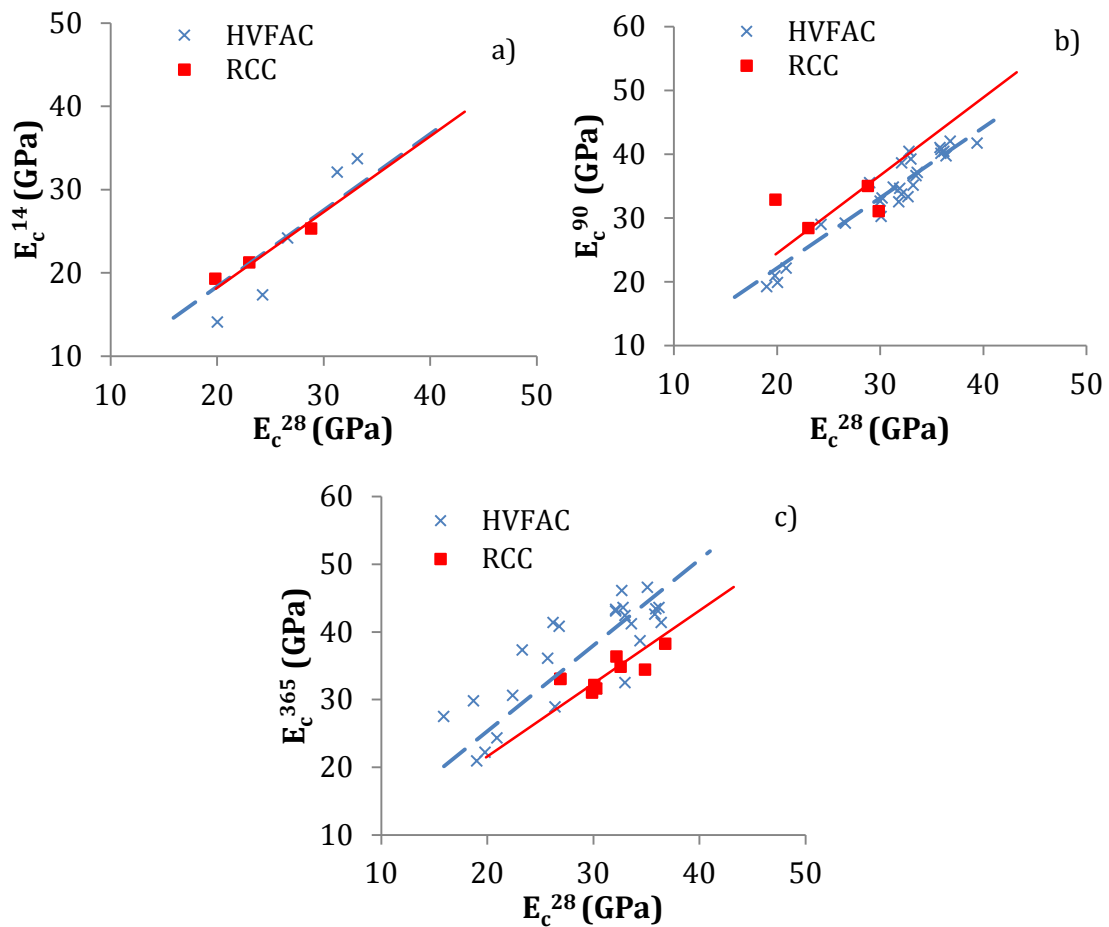


Figure 5.57 RCC and HVFAC modulus of elasticity at a) 14 days, b) 90 days and c) 365 days

As it can be seen, the correlation of these two variables was similar for the RCC and HVFAC mixtures at all evaluated ages, indicating that the same relationship type can be used to define them. The modulus of elasticity development over time was calculated using the EN 1992-1-1 (CEN 2004) equation (Eq. 5.16) and the experimental values of the s coefficients previously calculated for each HVFAC mixture. The s coefficients were calculated using the Eq. 5.11 and experimental values of RCC compressive strengths at different ages. The results are presented as the calculated to experimental modulus ratio in Table 5.11 using the descriptive statistical parameters. Chen et al. (2017) proposed the modification of the EN

5. Analysis and discussion of results

1992-1-1 (CEN 2004) equation (Eq. 5.11) as a function of the previously described coefficient $C/(S+A)$ as follows:

$$E_{cm}(t) = E_{cm} \cdot \beta_{cc}(t)^{0.3} = E_{cm} \cdot \left\{ EXP \left[s \cdot \left(1 - \sqrt{\frac{28}{t}} \right) \cdot \left(-1.60 \cdot \frac{C}{S+A} + 5.26 \right) \right] \right\}^{0.3}$$

Eq. 5.17

These results are also presented as the calculated to experimental modulus ratio in Table 5.11 using descriptive statistical parameters.

Table 5.11 Descriptive statistical parameters for HVFAC modulus of elasticity development over time

	Sample No.	Mean Values	St. Error	St. Deviation	CoV (%)	Min	Max
<i>EN 1992-1-1</i>	56	0.93	0.02	0.12	12.49	0.75	1.39
<i>Chen et al.</i>	56	1.11	0.01	0.11	9.89	0.80	1.34

It can be seen that EN 1992-1-1 (CEN 2004) was, in average, underestimating the HVFAC modulus of elasticity. The Chen et al. (2017) proposal provided the estimation that was higher than the experimental values with lower scattering of the results compared with the EN 1992-1-1 (CEN 2004) proposal. The graphical representation of the results is shown in Figure 5.58. It can be seen that the values predicted using Chen et al. (2017) were, in most cases, higher compared with the EN 1992-1-1 (CEN 2004) prediction.

The previously conducted analysis showed that Chen et al. (2017) proposal overestimated the modulus of elasticity, which is not on the safety side. The EN 1992-1-1 prediction provided similar accuracy of the modulus of elasticity development over time and yielded slightly conservative results. It can be concluded that the use of the EN 1992-1-1 prediction for the modulus of elasticity development over time would be more appropriate compared with the Chen et al. (2017) proposal.

5. Analysis and discussion of results

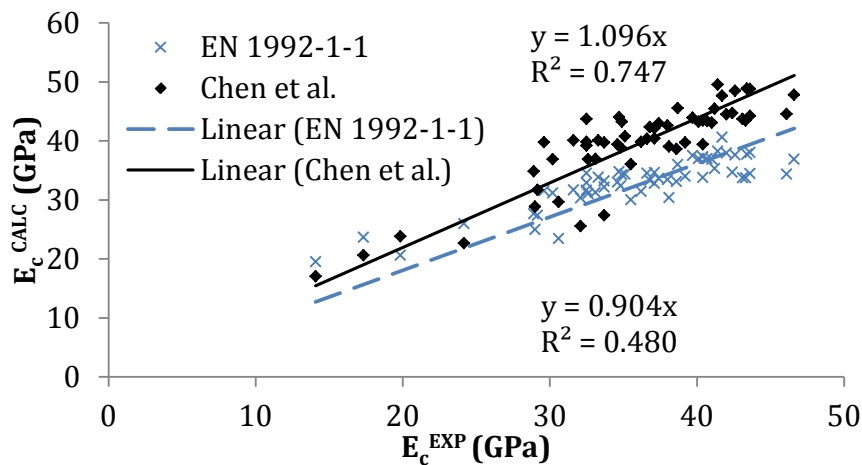


Figure 5.58 HVFAC modulus of elasticity experimental versus calculated values

5.2.1.5. Splitting tensile strength

Concrete splitting tensile strength is an important parameter in both the serviceability and ultimate state. It is used in stress analysis, the determination of crack width and spacing, deflection, minimum reinforcement, shear strength etc. Splitting tensile strength is usually defined in relation to the compressive strength. European Standard EN 1992-1-1 (CEN 2004) defines the splitting tensile strength of concrete as follows:

$$f_{ct} = 0.3 \cdot \sqrt[3]{f_c^2} \quad \text{Eq. 5.18}$$

where:

f_{ct} axial tensile strength of concrete.

Axial tensile strength is rarely determined by testing, but it can be determined based on the splitting tensile strength using the equation given in EN 1992-1-1 (CEN 2004) as follows:

$$f_{ct} = 0.9 \cdot f_{ct,sp} \quad \text{Eq. 5.19}$$

where:

f_{ct} axial tensile strength;

$f_{ct,sp}$ splitting tensile strength.

5. Analysis and discussion of results

In order to evaluate the possibility to apply these equations on the HVFAC, concrete mixtures with available data regarding splitting tensile strength were selected from the database (16 RCC and 34 HVFAC). The specimen size and shape have a big influence on the splitting tensile strength of concrete (Modr and Kadlecěk 2002; Rocco et al. 1999; Zabihi 2012b). Different specimen size and shape were used in different studies and the size effect was taken into account based on the recommendations from the literature as described in Table 5.3 of this chapter.

The relationship between the 28-day compressive and splitting tensile strength for the selected HVFAC and RCC mixtures is shown in Figure 5.59. As it can be seen, the correlation between these two variables is similar for the RCC and HVFAC mixtures indicating that the same relationship type can be used to define them both.

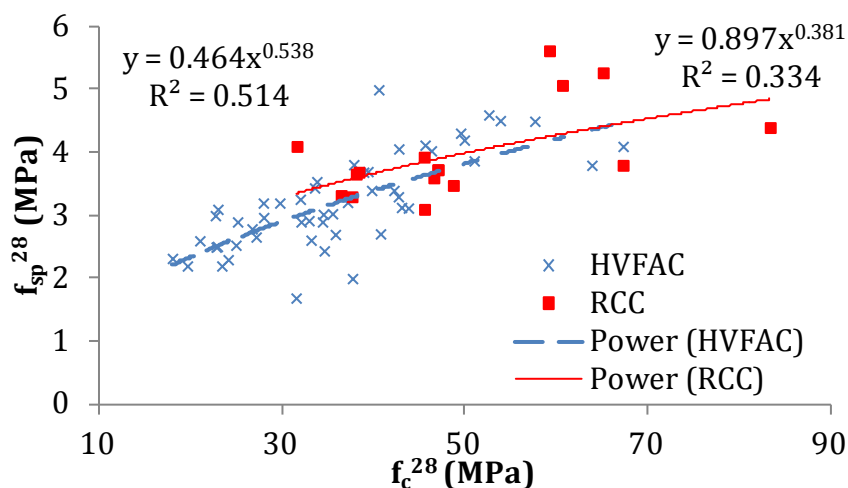


Figure 5.59 Relationship between 28-day compressive and splitting tensile strength

Splitting tensile strength was then calculated for the HVFAC and RCC mixtures from the database using the EN 1992-1-1 equation (Eq. 5.18). The results are shown in Table 5.12 as the calculated to experimental splitting tensile strength ratio using the descriptive statistical parameters. The experimental versus calculated splitting tensile strengths are also shown in Figure 5.60.

It can be concluded that the EN 1992-1-1 (CEN 2004) equation can be used to predict the HVFAC splitting tensile strength with similar accuracy as in the RCC.

5. Analysis and discussion of results

Other predictions regarding splitting tensile strength were not found in the literature.

Table 5.12 Descriptive statistical parameters for HVFAC and RCC splitting tensile strength evaluation using EN 1992-1-1 prediction

	Sample No.	Mean Values	St. Error	St. Deviation	CoV (%)	Min	Max
HVFAC	34	1.04	0.03	0.18	17.47	0.71	1.77
RCC	16	1.02	0.04	0.16	15.88	0.73	1.31

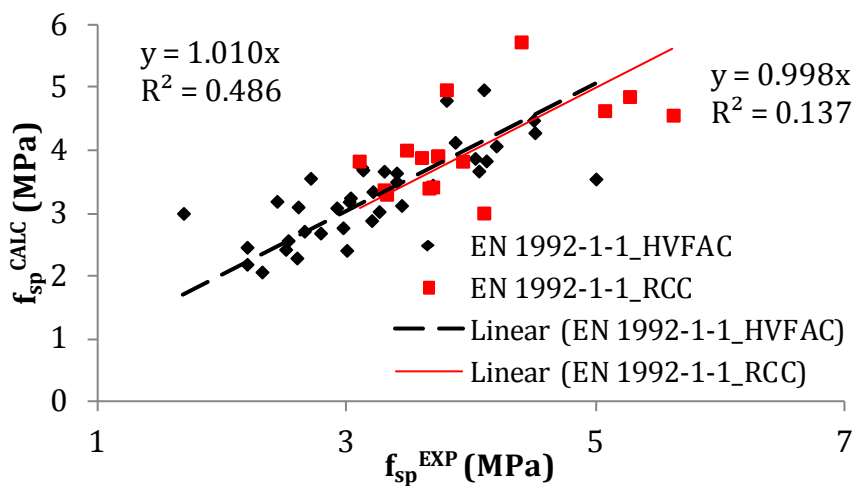


Figure 5.60 HVFAC and RCC splitting tensile strength experimental values versus calculated values

5.2.2. Analysis of HVFAC mechanical properties based on own experimental results

A comparison of obtained HVFAC experimental results to standard code predictions for OPCC (EN 206-1 (CEN 2011a), EN 1992-1-1 (CEN 2004)) was carried out in this section. Ten HVFAC mixtures from the second stage of material testing were selected for evaluation (Table 4.7, 4.9 and 4.10).

5.2.2.1. k-value concept

In order to predict compressive strength of HVFAC using the *k-value concept* according to EN 206-1 (CEN 2011a), Bolomey, Baljejev and Feret empirical

5. Analysis and discussion of results

equations (Eq. 5.4, 5.5, and 5.6) were used. All compressive strengths evaluated in this section were calculated using all three equations and presented as their average value. The parameters depending on the cement class and aggregate type were taken as following:

- In Bolomeys equation (Eq. 5.4) coefficient A defining aggregate type and cement strength was taken as equal to $0.65 \cdot 42.5$;
- In Baljejev equation (Eq. 5.5) coefficient B defining aggregate type and cement strength was taken as equal to $4 \cdot 42.5$;
- In Feret equation (Eq. 5.6) coefficient K defining cement strength was taken as equal to 320.

According to the k -value concept, a $W/(C+k \cdot FA)$ ratio was used in the equations Eq. 5.4, 5.5, and 5.6 instead of the W/C ratio. Besides, a maximum mass of FA that can be taken into account in the calculation of this ratio is 33% of the mass of Portland cement CEM I according to EN 206-1 (CEN 2011a). Since CEM II was used in this research, only the mass of cement clinker was taken into account (about 80% of the cement mass for CEM II 42.5R). The value of the k factor was chosen as 0.4 as recommended for CEM I 42.5. For the first group of HVFAC, the $W/(C+k \cdot FA)$ ratio was constant and calculated as 0.88, and for the second group as 1.10. The W/C ratio was also constant for the first group ($=0.98$) and for the second group ($=1.22$). Results of experimental and calculated compressive strength are presented in Figure 5.61.

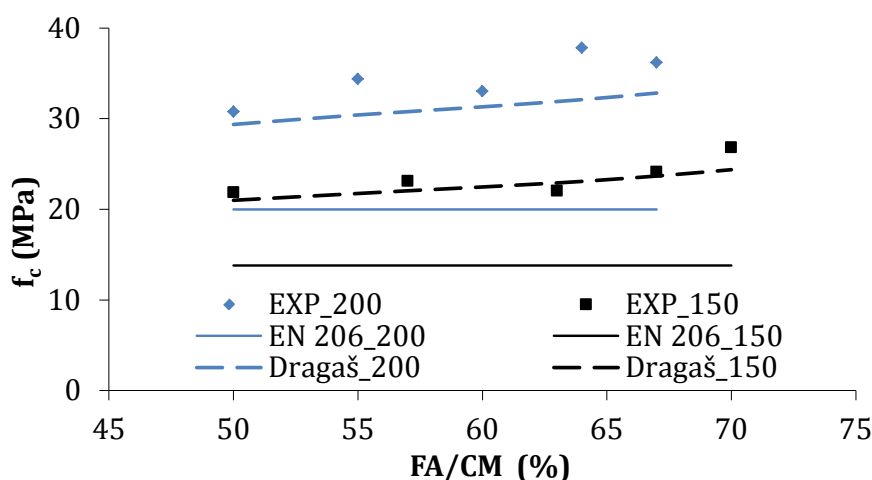


Figure 5.61 Compressive strength of HVFAC versus the amount of FA

5. Analysis and discussion of results

The experimentally obtained compressive strength of all HVFAC mixtures (converted to a 200 mm cube) was more than 30% higher compared with predicted values with the difference increasing with increasing FA content. Compressive strength prediction obtained using own proposal for the k value (Eq. 5.10), calculated for HVFAC mixtures of both groups, are also plotted in Figure 5.61. In this case the total mass of FA was taken into account while calculating the $W/(C+k \cdot FA)$ ratio. It can be seen that this prediction gives a good correlation with experimental results, especially for HVFAC with 150 kg/m³ of cement.

5.2.2.2. Compressive strength development over time

The EN 1992-1-1 (CEN 2004) equation for estimating the development of compressive strength (Eq. 5.11) of OPCC over time was tested against the HVFAC experimental results. All ten HVFAC mixtures in the second stage had a similar logarithmic trend of strength increase over time. For clarity, the test results of only two concrete mixtures (C200F200_049 and C200F350_036) are plotted against the predictions for cement concrete according to Eq. 5.11 in Figure 5.62. Test results of HVFAC compressive strength (Table 4.9) were multiplied by 0.75 to get corresponding compressive strength for 150 · 300 mm cylinders used in EN 1992-1-1 (CEN, 2004). For comparison, ordinary cement concrete with a 28-day compressive strength equal to the tested 28-day HVFAC compressive strength was chosen as equivalent. It is evident that the EN 1992-1-1 (CEN 2004) Eq. 5.11 overestimates the compressive strength of HVFAC at early ages and underestimates the compressive strength after approximately 28 days in this case. This is in accordance with *fib* Model Code 2010 (*fib* 2010a; b) remarks regarding the compressive strength increase over time for concrete with a high content of FA. The predictions obtained according to Yoon et al. (2014) and Kuder et al. (2012) proposals are also plotted in Figure 5.62.

Average values of Yoon et al. proposal for HVFAC made with 50% and 60% of FA in CM were used: $s=0.57$ and $s=0.89$, respectively. It can be seen that these predictions gave satisfactory results for C200F200_0.49 concrete mixture but underestimated the early age strength, and overestimated the later compressive

5. Analysis and discussion of results

strength in C200F350_0.36 concrete mixture (Figure 5.62). Tested against own experimental results, the proposal by Kuder et al. (2012) seems to provide satisfactory results for both early and later ages and both HVFAC mixtures.

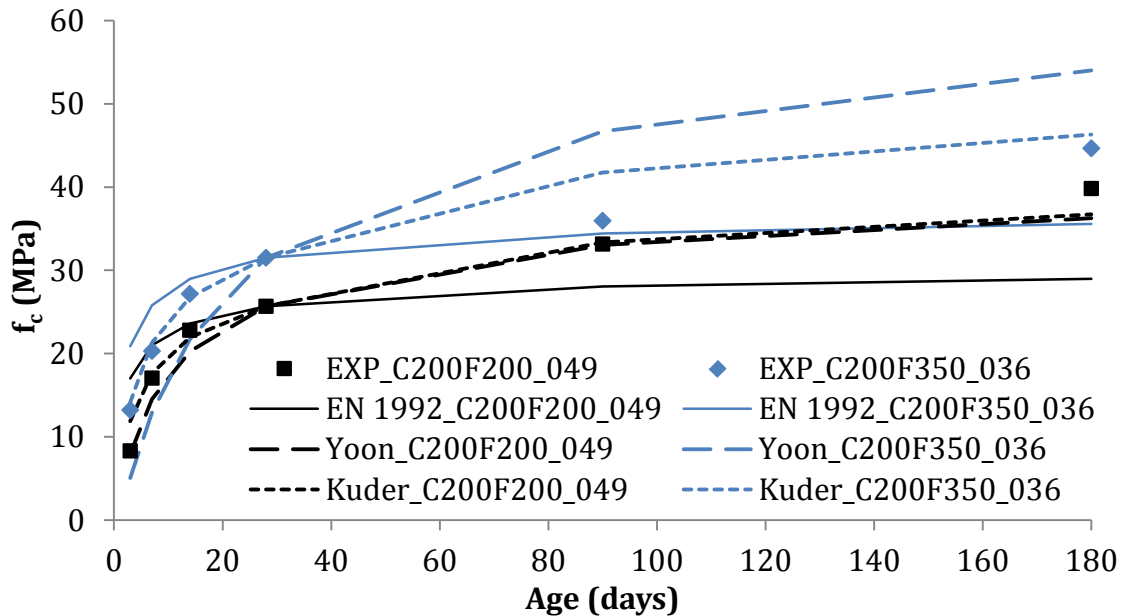


Figure 5.62 Development of HVFAC compressive strength over time

5.2.2.3. Modulus of elasticity

Experimental HVFAC results were compared with EN 1992-1-1 (CEN 2004) provisions for the modulus of elasticity of cement concrete (Eq. 5.13). Figure 5.63 shows that test values of all HVFAC 28-day modulus of elasticity are higher than the values of modulus of elasticity calculated according to Eq. 5.13 for equivalent OPCC. However, the trend of increase is similar to the EN 1992-1-1 (CEN 2004) prediction. Figure 5.63 also shows the modulus of elasticity prediction proposed by Yoon et al. (2014) for HVFAC with 50% and 60% cement replacement with FA. It can be seen in Figure 5.63 that these predictions (using the mean values for coefficients) show a poor correlation with own experimental results. The development of the HVFAC modulus of elasticity over time (experimental values) was tested against the EN 1992-1-1 (CEN 2004) equation for cement concrete (Eq. 5.16). The test values of the modulus of elasticity development over time for two HVFAC mixtures and for equivalent OPCC (with the modulus of elasticity after 28

5. Analysis and discussion of results

days equal to the measured HVFAC value after 28 days) calculated according to Eq. 5.16 are shown in Figure 5.64.

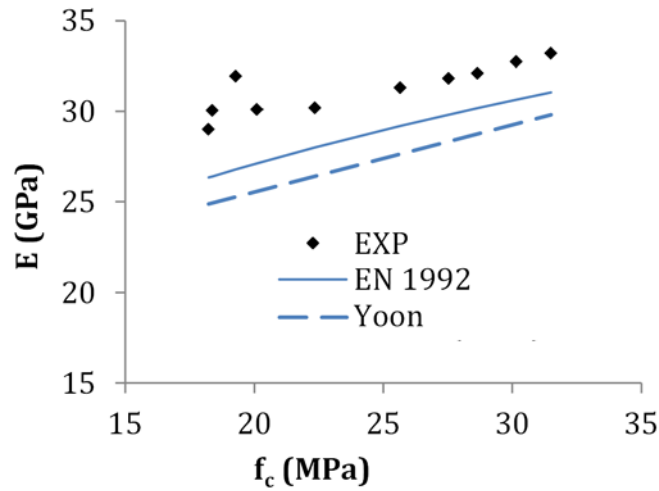


Figure 5.63 Relationship between the 28-day modulus of elasticity and the compressive strength of HVFAC

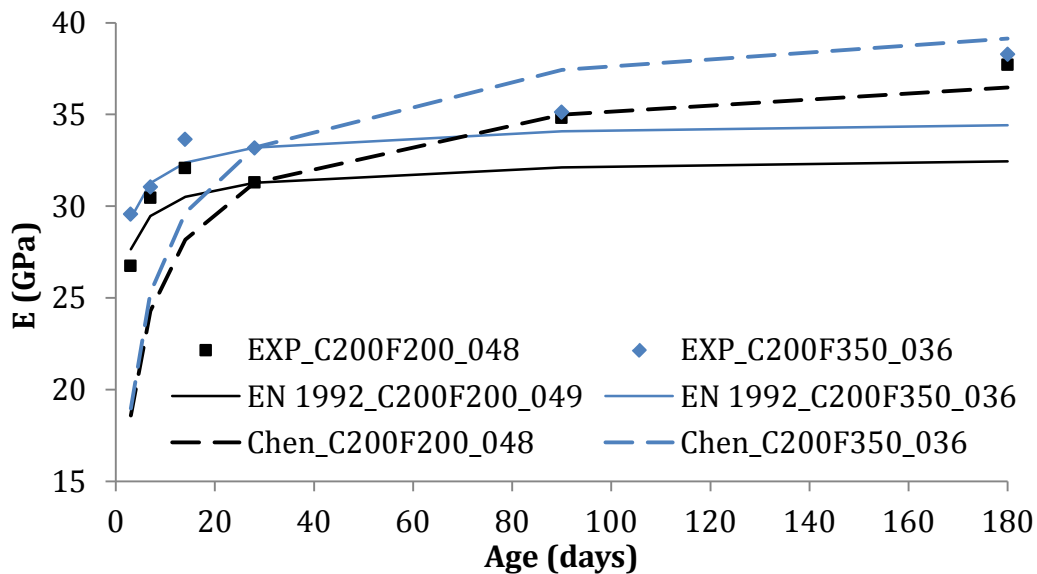


Figure 5.64 Development of the HVFAC modulus of elasticity over time

The EN 1992-1-1 Eq. 5.16 underestimates the modulus of elasticity of HVFAC at all ages. The increase of the modulus of elasticity of both HVFAC mixtures is similar to the logarithmic increase of compressive strength with a faster rate after 28 days compared with predicted modulus of elasticity according to EN 1992-1-1 (CEN 2004). The prediction of the HVFAC modulus of elasticity development over time, if the Chen et al. (2017) proposal was applied in Eq. 5.16 is also shown in Figure

5. Analysis and discussion of results

5.64. The correlation for ages after 28 days is better compared with EN 1992-1-1 Eq. 5.16, but still the modulus of elasticity is underestimated at early ages.

5.2.2.4. Splitting tensile strength

As already mentioned, splitting tensile strength results of HVFAC indicate a large scatter. The expression used to determine splitting tensile strength of OPCC in EN 1992-1-1 (CEN 2004) (Eq. 5.18) is tested against the HVFAC experimental results. Figure 5.65 shows splitting tensile strength versus 28-day compressive strength of HVFAC (test values) and the same relationship for equivalent ordinary cement concrete calculated according to Eq. 5.18. No clear correlation can be seen between the HVFAC measured results and those obtained using Eq. 5.18. However, experimental HVFAC values of splitting strength are, all except two, higher than EN 1992-1-1 (CEN 2004) predictions for the same compressive strength.

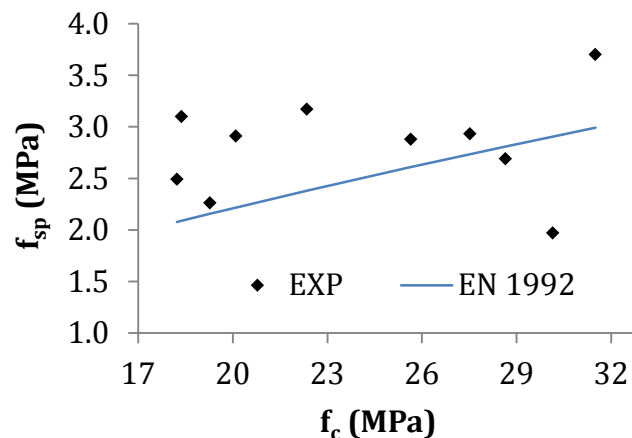


Figure 5.65 Relationship between the splitting tensile and compressive strength of HVFAC

5.2.3. Conclusions

The analysis of available HVFAC material properties results showed that the extensive amount of research has been done so far. The collected results are certainly not the only ones, but the ones that were available during this research. However, due to the great variety of FA physical and mechanical properties comprehensive analysis of HVFAC mechanical properties was not found in the literature. Having that in mind, the database of 432 HVFAC and 131 RCC mixtures

5. Analysis and discussion of results

selected from literature was made and analyzed. After the analysis of all parameters influencing the mechanical properties of HVFAC, the following conclusions can be made:

- HVFAC compressive strength decreased with the increase of FA amount regardless of the combined effect of a great number of factors (different W/CM ratios, physical and chemical properties of FA, different types of cement and aggregate used in the studies, etc);
- HVFAC can be defined with the same type of compressive strength and W/CM ratio relationship with needed alterations using the FA efficiency factor;
- the most important parameters influencing the FA efficiency are the amount of FA in CM, FA fineness and the FA and cement chemical composition;
- Own proposal for FA efficiency (k factor value) as the function of FA chemical composition and its' specific gravity (Eq. 5.10) showed good correlation to the experimental results. HVFAC compressive strength was calculated using the Bolomey (Eq. 5.4) equation and own proposal for k factor value (Eq. 5.10). The calculated-to-experimental compressive strength ratio was 1.02 with CoV of 23.8%;
- The compressive strength development of HVFAC was lower at the early age and higher at the later age for HVFAC compared with OPCC;
- The equation defined in EN 1992-1-1 (Eq. 5.11) can be used to predict the compressive strength development with modifications proposed by Yoon et al. (2014) or Chen et al. (2017);
- The EN 1992-1-1 equation (Eq. 5.13) gives good estimation for the HVFAC modulus of elasticity if the aggregate type is taken into account;
- The EN 1992-1-1 prediction (Eq. 5.16) provided similar accuracy of the HVFAC modulus of elasticity compared with the OPCC development over time and yielded slightly conservative results. The Chen et al. (2017) proposal overestimated the modulus of elasticity development over time.
- It can be concluded that the EN 1992-1-1 equation (Eq. 5.18) can be used to predict the HVFAC splitting tensile strength with similar accuracy as in the OPCC.

5. Analysis and discussion of results

Previously obtained conclusions were confirmed on own experimental results. The additional conclusion that can be made based on the analysis conducted on own experimental results is the following:

- HVFAC compressive strength predicted with the empirical equations (Bolomey, Baljejev and Feret) using the *k-value concept* defined in EN 260-1 was significantly lower compared with experimental obtained results. The experimentally obtained compressive strength of all HVFAC mixtures was more than 30% higher compared with predicted values with the difference increasing with increasing FA content.

Based on the analysis showed in this section, it can generally be concluded that by adapting code provisions for OPCC adequate predictions for HVFAC mechanical properties can be obtained.

5. Analysis and discussion of results

5.3. ANALYSIS OF HVFAC STRUCTURAL PROPERTIES

Analysis of HVFAC structural properties was done by comparing the HVFAC and OPCC flexural and shear behavior and by analyzing the possible application of available code predications defined for OPCC on HVFAC. The analysis was conducted in three parts.

In the first part the variation of HVFAC compressive strength was evaluated based on own experimental results.

In the second part the analysis of HVFAC beams flexural behavior was done. The flexural behavior of OPCC and HVFAC beams was compared and discussed based on the collected HVFAC beams database from current literature. During this analysis, the following parameters were evaluated: flexural strength; cracking moment; beams' yielding moment; beams' deflection at yielding and the ultimate deflection; beams' ductility; number, average spacing and crack width. Possible application of available code provisions was also evaluated for own experimental results in more detail and, afterwards, for the collected HVFAC beams database. Prediction of the cracking moment (BAB '87, EN 1992-1-1 and ACI 318) and the ultimate flexural strength (BAB '87, EN 1992-1-1, ACI 318 and MCFT analysis) was evaluated.

In the third part the analysis of HVFAC beams shear behavior was done. The shear behavior of OPCC and HVFAC beams was compared and discussed based on the collected HVFAC beams database from current literature. During this analysis, the following parameters were evaluated: shear strength, shear cracking stress, beams' ductility, and shear crack angle. Possible application of available code provisions was also evaluated for own experimental results in more detail and, afterwards, for the collected HVFAC beams database. Prediction of the shear strength (BAB '87, EN 1992-1-1, *fib* Model Code, ACI 318 and MCFT analysis) and shear crack angle (*fib* Model Code) was analyzed. Finally, comparison of the shear strength predictions obtained using EN 1992-1-1, ACI 318 and *fib* Model Code 2010 between the HVFAC beams database and the Reineck et al. (2013, 2014) OPCC beams database was done.

5. Analysis and discussion of results

A different number of parameters influence each design property evaluated in this section. In order to have a consistent analysis, the following assumptions were used in both flexural and shear design evaluations:

- The geometry of beam elements was measured during testing and it was considered as a known parameter;
- The beams' self-weight was calculated using the measured concrete density and reinforcement weight and included in the analysis where needed;
- The weight of the steel girder and load press were also measured and included in the experimental values of flexural and shear strength;
- The experimental cracking moment was taken as the moment when the first flexural cracks were noticed by the naked eye as described in Section 4.3 by taking into account the addition of the beams' self-weight, steel girder and the load press mass;
- The experimental inclined strut angle in beams failed in shear was determined based on the crack patterns as described in Section 4.3;
- The measured values of steel reinforcement properties were used in the analysis with all safety factors taken as equal to one;
- The measured values of mechanical concrete properties of samples cured in the same way as the tested beams were used in the analysis with all safety factors taken as equal to one.

5.3.1. Evaluation of HVFAC strength variation

The analysis of the HVFAC beams' flexural and shear behavior implies the evaluation of the applicability of models proposed in different standards for OPCC on HVFAC members. During this analysis, all safety factors regarding loads and member geometry can be set equal to one having in mind the same variation of these variables, regardless of concrete type. The safety factors referring to the material properties are also set equal to one assuming that the variation of compressive strength of HVFAC is in the same range as for OPCC. A typical value of the CoV for OPCC compressive strength is 15% (Faber 2007). In order to analyze the variation of HVFAC compressive strength, a database of own experimental

5. Analysis and discussion of results

results of HVFAC samples made in the last 4 years was made. The database consists of 577 different HVFAC samples that have been tested. Samples in the database were tested for compressive strength, f_c (cube sample), splitting tensile strength, f_{sp} (cylinder sample), flexural tensile strength, f_{fl} (prismatic sample) and modulus of elasticity, E (cylinder sample). The number of samples regarding a specific test is shown in Figure 5.66.

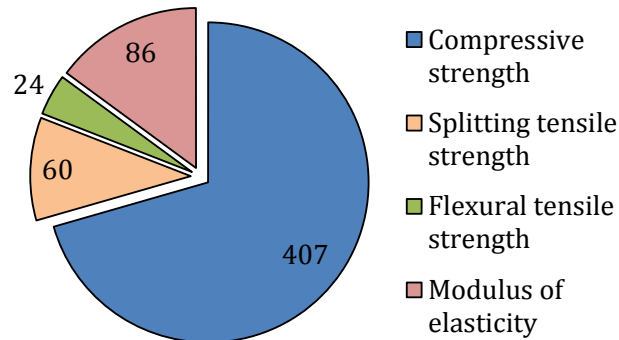


Figure 5.66 Number of tested HVFAC samples

As can be seen, the majority of samples were tested for compressive strength at different ages. All samples were prepared and tested in the Laboratory for Materials and Structures at the Faculty of Civil Engineering in Belgrade. Preparation of samples was done in different concrete mixers and not always with the same mixing procedure. Samples were made during different seasons but the variation of temperature and humidity in the Laboratory was not significant. Fine and coarse aggregates used for the sample preparation were both river and crushed aggregate obtained from different suppliers (Figure 5.67a). The aggregate particle size distribution varied from one batch to another but the aggregate mixture used for concrete preparation was always in the limits defined by the appropriate standard. The aggregate was used in a dry state or with natural moisture content that was taken into account during the concrete mixture preparation. Cement used in all mixtures was from the same supplier but obtained at different times. Most of the concrete mixtures were made with 150 and 200 kg/m³ of cement (Figure 5.67e) but the cement content varied from 150 to 384 kg/m³. All concrete samples were made with 26 different HVFAC mixtures (Figure 5.67d). Most of the samples were made with the same batch of FA obtained from

5. Analysis and discussion of results

the "Nikola Tesla B" power plant and kept in paper bags. A new batch of FA was obtained from the same power plant three years after the first one.

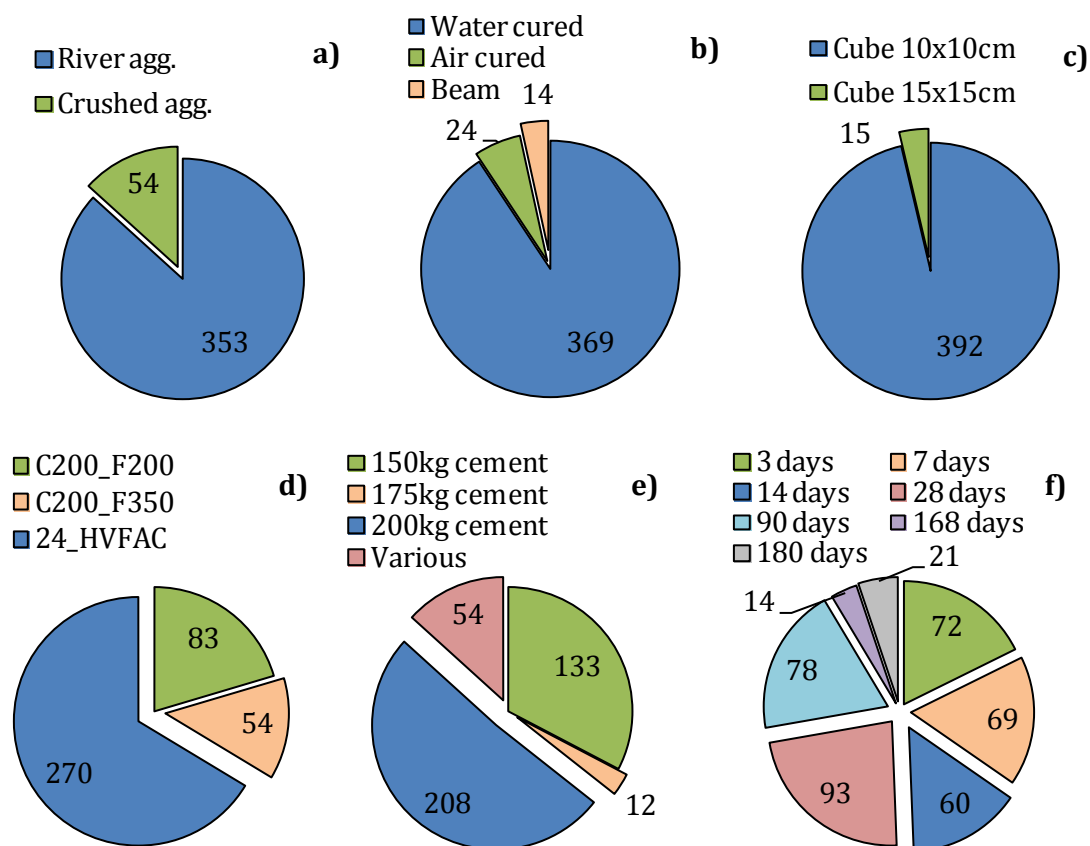


Figure 5.67 Number of samples tested for HVFAC compressive strength regarding a) aggregate type, b) curing type, c) sample size, d) HVFAC mixture type, e) cement amount and f) sample testing age

Different types of superplasticizers were used in HVFAC preparation. The amount of FA was in the range from 150 to 400 kg/m³ in all mixtures. Tap water was used for concrete preparation.

The compacting of samples was always done on a vibrating table except for the core samples drilled from the beams that have been compacted using a vibrating needle. The different curing regimes were applied for different samples. The majority of samples was first cured under wet burlap for the first 24 h and then in a water tank until testing. Some samples were air-cured or cured in the same way as beams made for testing (Figure 5.67b). All samples tested for compressive strength were 100 or 150 mm cube samples (Figure 5.67c). Compressive strength

5. Analysis and discussion of results

was tested at different ages, unlike the other properties that have been tested after 28 and 90 days (Figure 5.67f). Testing of HVFAC properties was not always done by the same person and in exactly the same way, as it is common in practice.

The database made in this way consists of different HVFAC mechanical property test results taking into account various but usual variations in aggregate and cement type, environmental conditions during mixing and curing, compacting and curing techniques, and variations in concrete testing.

For each property that has been tested three or more samples were made and tested. The CoV was calculated for each group of samples made from the same concrete design mixture, from the same component materials, cured in the same way, and tested at the same age. All samples from one group were not made from the same batch. The CoVs for these groups were then calculated and presented in Table 5.13. The number of samples represents the total amount of samples tested for a certain concrete property but not necessarily belonging to the same group. Minimum, maximum and the average CoVs were calculated for all CoVs for separate groups. The average value of compressive strength CoV was significantly lower compared with the typical value used as a limit for OPCC (15%). The maximum value of 20.3% exceeds this limit, but only two CoV results were actually higher than 15%.

Table 5.13 CoV for the results of own HVFAC testing

	f_c	f_{sp}	f_n	E
<i>Number of samples</i>	407	60	24	86
<i>Min CoV (%)</i>	0.1	1.7	1.7	1.1
<i>Max CoV (%)</i>	20.3	23.0	34.6	11.2
<i>AvgCoV (%)</i>	6.6	10.0	15.6	7.0

This leads to a conclusion that HVFAC results presented in this database have lower CoV than a typical value accepted for OPCC. Variation of the modulus of elasticity results was similar as for the compressive strength with a lower maximum value of the CoV. As expected, tensile strength results showed a higher variation compared with compressive strength results. For both splitting and

5. Analysis and discussion of results

flexural tensile strength results, the average CoV was similar or lower than 15% but with a significantly higher maximum value. In order to further evaluate the HVFAC mixtures used in this study in the preparation of beams, more detailed results are given in Table 5.14.

Table 5.14 CoV of C200_F200 and C200_F350 tested mechanical concrete properties

	$f_{c,3}$	$f_{c,7}$	$f_{c,14}$	$f_{c,28}$	$f_{c,90}$	$f_{c,168}^*$	$f_{sp,28}$	$f_{fl,28}$	E_{28}	E_{90}
C200_F200										
No. of samples	9	12	9	12	21	14	15	9	9	6
CoV (%)	8.5	8.3	8.2	7.2	11.1	7.1	21.4	34.6	6.6	9.4
C200_F350										
No. of samples	9	9	9	9	15	-	12	3	9	9
CoV (%)	8.6	13.7	6.9	13.2	11.9	-	14.2	22.2	7.7	10.5
Avg CoV (%)	8.5	11.0	7.5	10.2	11.5	7.1	17.8	28.4	7.1	10.0

* Cylindrical core samples (100 · 200 mm) drilled from beams tested for shear

It can be seen that the compressive strength CoV is lower than 15% for all ages for both HVFAC mixtures. Only a small number of samples tested for flexural tensile strength were available, but the results are still in accordance with conclusion obtained for the entire database. The average value of the CoV for splitting tensile and flexural tensile strength was higher than the average obtained for the entire database. Higher variation in tensile strength is common for OPCC so it is not surprising for HVFAC. Variation up to 30% is considered as acceptable. The modulus of elasticity expressed a relatively small average and maximum values of CoV for both C200_F200 and C200_F350 HVFAC mixtures.

This short analysis was done in order to evaluate the correctness of the assumption that all safety factors regarding concrete material properties can be set to one for HVFAC in further analyses. It can be concluded that there was no significant difference in mechanical properties variation between HVFAC and OPCC mixtures tested in this study. Furthermore, this conclusion enables the use of concrete properties obtained on samples cured and tested in the same way as beams.

5. Analysis and discussion of results

5.3.2. HVFAC beams flexural behavior – HVFAC beams database

In order to compare the OPCC and HVFAC flexural behavior, a database of all available results was made. Only a few researchers investigated the flexural strength of HVFAC beams (Arezoumandi et al. 2015a; Putte Gowda B. et al. 2013; Srinivas and Rao 2015; Thangaraj and Thenmozhi 2016; Yoo et al. 2015) and all important parameters and results from their research are shown in Table B-1 in the Appendix B. Detailed overview of the selected studies was given in the Section 2.5.2 of these thesis.

The HVFAC-to-OPCC ultimate bending moment (M_u) ratios are plotted against the longitudinal reinforcement ratio (ρ), effective beam depth (d) and concrete compressive strength (f_c) in Figures 5.68, 5.69 and 5.70, respectively. Results of the flexural strength ratios presented in these figures show a relatively small scatter of the results with the HVFAC-to-OPCC ultimate bending moment values ranging from 0.84 to 1.15. The average value of this ratio indicated that the flexural strengths of HVFAC and referent OPCC beams were very similar in the presented studies and, on average, had the same strength. Own experimental results corresponded well to the results from literature as shown in Figures 5.68, 5.69, and 5.70. No correlation can be found between the HVFAC-to-OPCC flexural strength ratios and any of the parameters: longitudinal reinforcement ratio, beams' effective depth or concrete compressive strength.

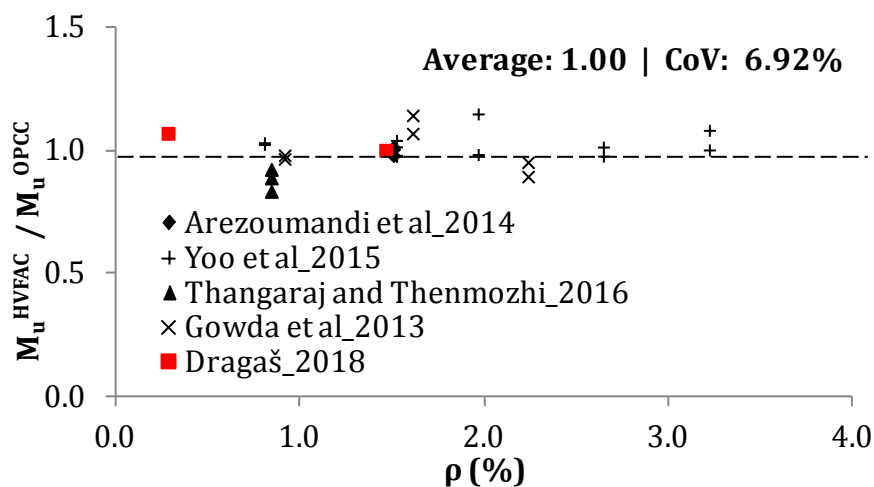


Figure 5.68 Ultimate bending moment of the HVFAC and OPCC beams compared with the longitudinal reinforcement ratio

5. Analysis and discussion of results

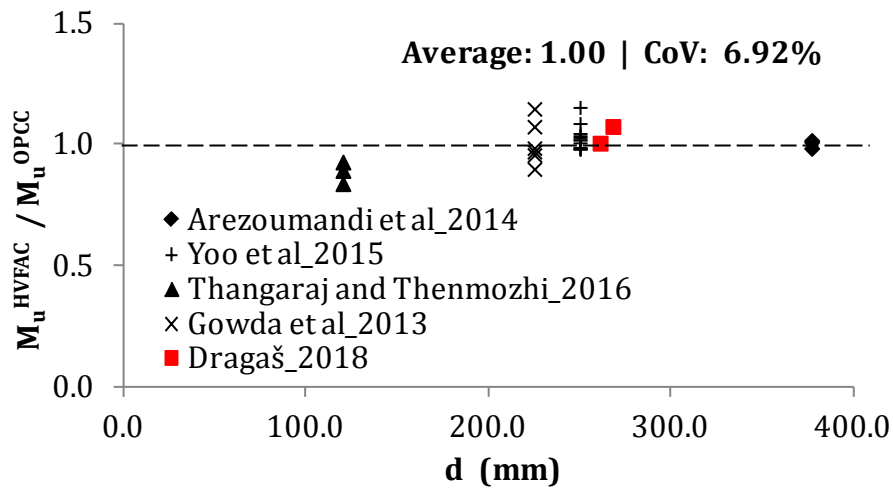


Figure 5.69 Ultimate bending moment of the HVFAC and OPCC beams compared with the beam's effective depth

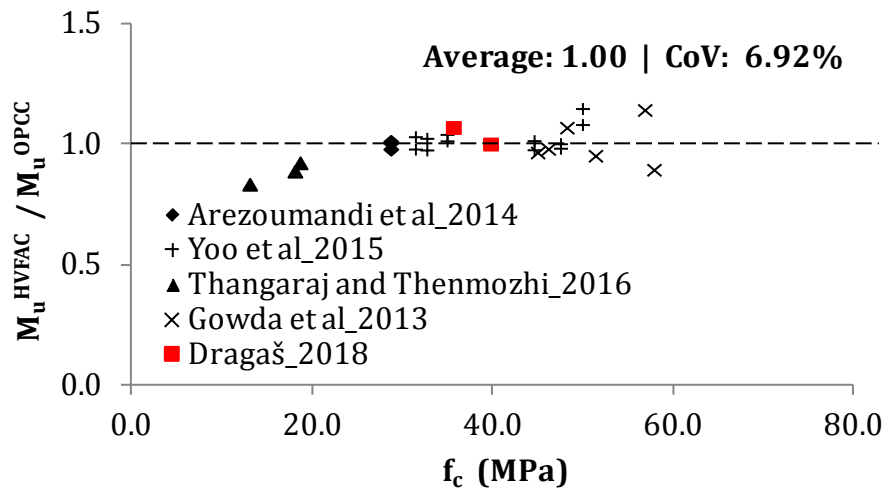


Figure 5.70 Ultimate bending moment of the HVFAC and OPCC beams compared with the concrete compressive strength

Previous conclusion indicated that the flexural strength of HVFAC and OPCC beams could be predicted with the model incorporating these three parameters with the same accuracy in the complete range of the parameters' values (Tošić et al. 2016). All further relationships regarding the flexural behavior of beams are shown in relation to the longitudinal reinforcement ratio.

The cracking moment results found in literature were also evaluated (Arezoumandi et al. 2015a; Putte Gowda B. et al. 2013; Yoo et al. 2015). In all selected studies, experimental cracking moments were taken as the values when the first flexural cracks were noticed on tested beams. The results presented in

5. Analysis and discussion of results

Figure 5.71 show that the HVFAC-to-OPCC cracking moment ratio is in the range from 0.43 to 1.72 with an average value of 0.95. The scatter of the results was higher than in the case of the ultimate bending moment. Presented results showed that the cracking moment was, on average, 5% lower for HVFAC beams compared with the OPCC beams. Own experimental results correspond well to the presented results with lower values of HVFAC beams cracking moment.

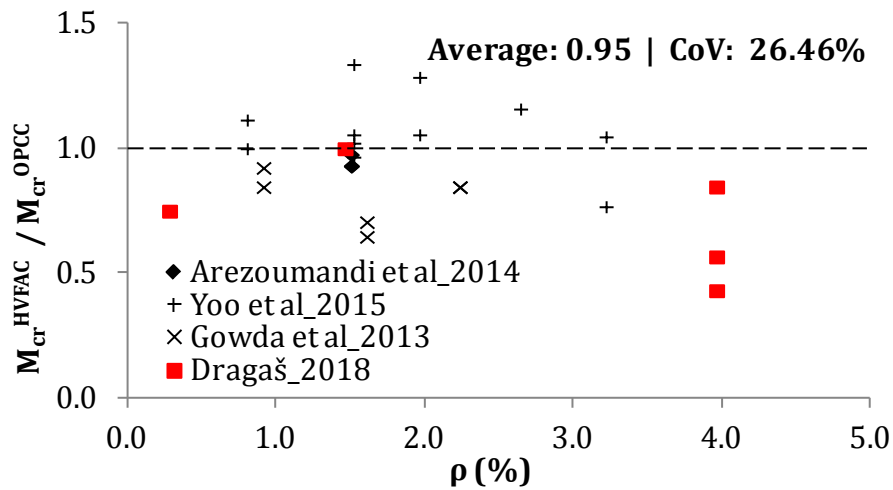


Figure 5.71 Cracking moment of the HVFAC and OPCC beams compared with the longitudinal reinforcement ratio

Another important parameter that was evaluated is the beams' yielding moment as an indicator of the beams' ductility. Only few studies found in literature had available data regarding beams' yielding moment determined based on the load-deflection curves of the tested beams. Available results from literature that are presented in Figure 5.72 show relatively small scatter of the results with values ranging from 0.78 to 1.14, similar as for the ultimate bending moment. The average value of HVFAC-to-OPCC beams' yielding moment indicated a similar behavior of HVFAC and OPCC beams. Own experimental results correspond well to the presented results.

Available results from literature regarding beams short-term deflection were also evaluated. The HVFAC-to-OPCC beams deflection ratios at the yielding point (a_y) and at failure (a_u) are shown in Figures 5.73 and 5.74, respectively. A relatively large scatter of the results can be seen with the beams' deflection at yielding ratio ranging from 0.57 to 1.50 and the beams ultimate deflection ratio from 0.52 to

5. Analysis and discussion of results

1.87. The average values showed that the HVFAC beams' deflection at yielding was 7% lower compared with the corresponding OPCC beams. At the same time, obtained results indicated that the ultimate deflection was on average 2% higher in HVFAC beams compared with the OPCC beams. Own experimental results were higher than the average value of beams' deflection at yielding and corresponded well with the ultimate beams' deflection.

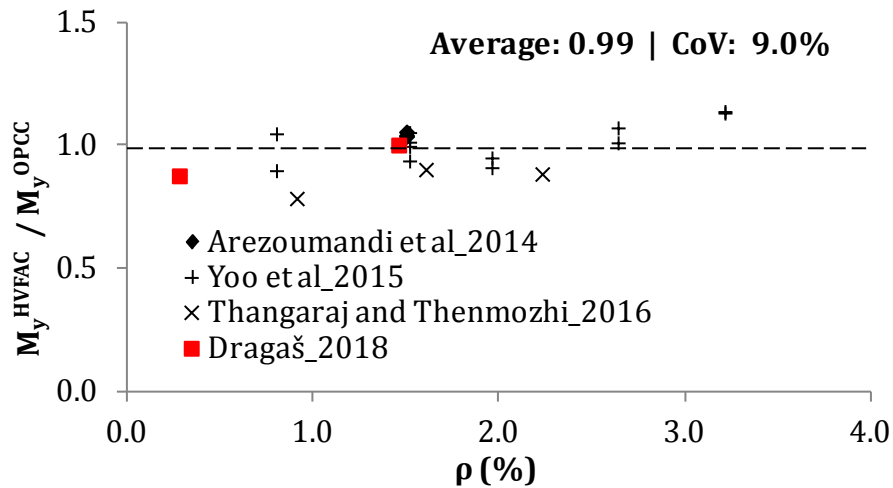


Figure 5.72 Bending moment at yielding of the HVFAC and OPCC beams compared with the longitudinal reinforcement ratio

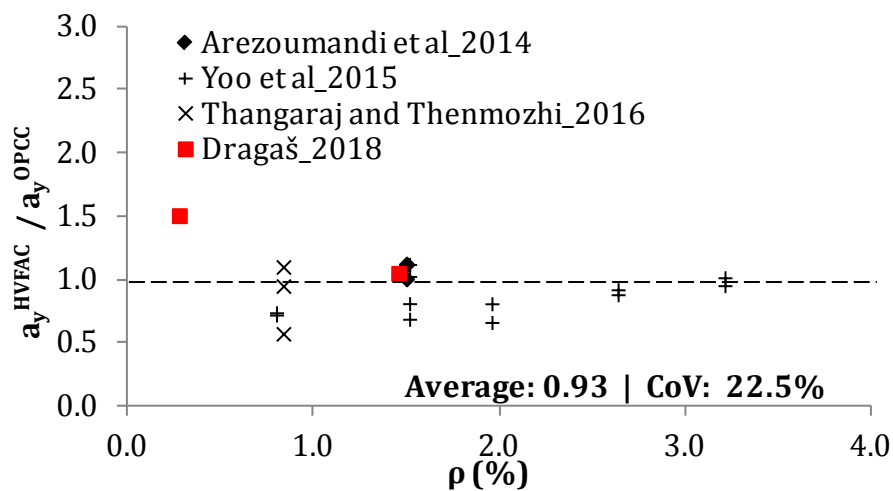


Figure 5.73 Ratio of beam's deflection at yielding for HVFAC and OPCC beams compared with the longitudinal reinforcement ratio

5. Analysis and discussion of results

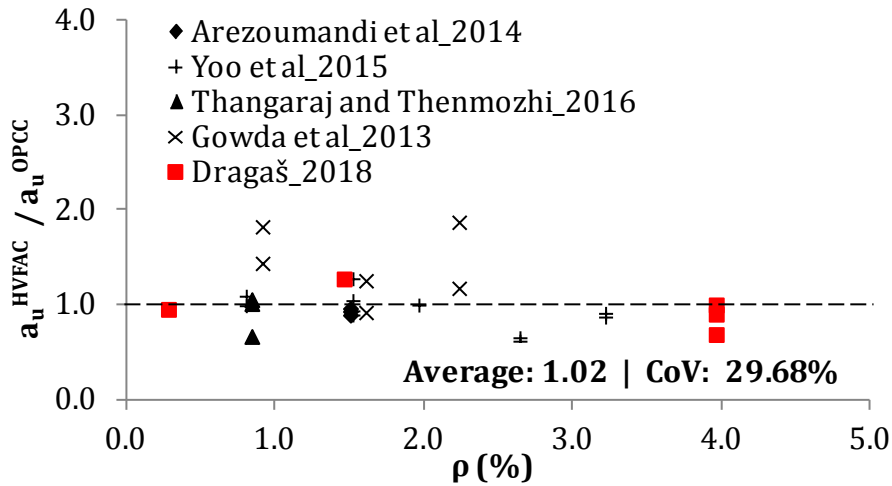


Figure 5.74 Ratio of beam's deflection at failure for HVFAC and OPCC beams compared with the longitudinal reinforcement ratio

Another parameter describing the ductility of beams is the yielding-to-ultimate deflection ratio (a_y/a_u). Available results from literature show that this ratio is on average 2% higher for HVFAC beams compared with the OPCC beams (Figure 5.75).

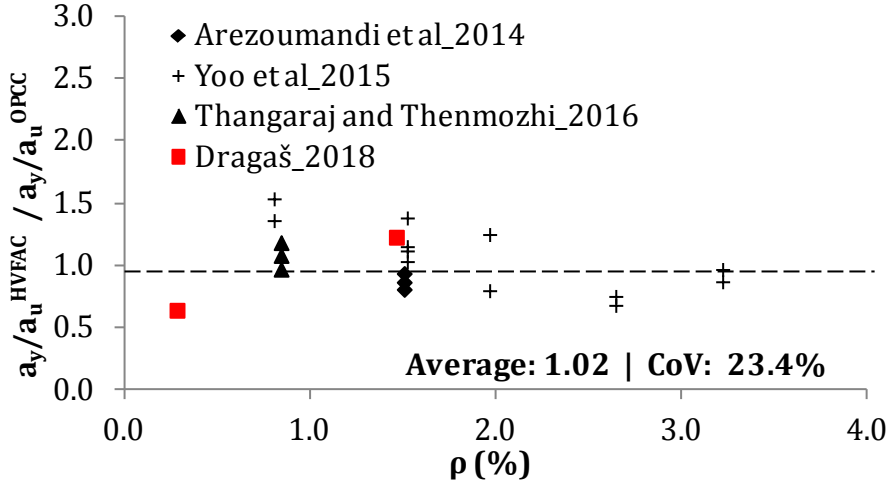


Figure 5.75 The HVFAC to OPCC beams ductility ratio compared with the longitudinal reinforcement ratio

Again, a relatively large scatter of the results can be seen with the a_y/a_u ratio ranging from 0.64 to 1.53. Own experimental results regarding deflection had a good fit with the results from literature.

5. Analysis and discussion of results

Measurement and analysis of cracks in HVFAC beams was done only in one study found in literature (Putte Gowda B. et al. 2013) and these results were compared with the own experimental work. Comparisons of the number of cracks, average spacing and width at the serviceability and ultimate loading state were done and shown in Figures 5.76 and 5.77.

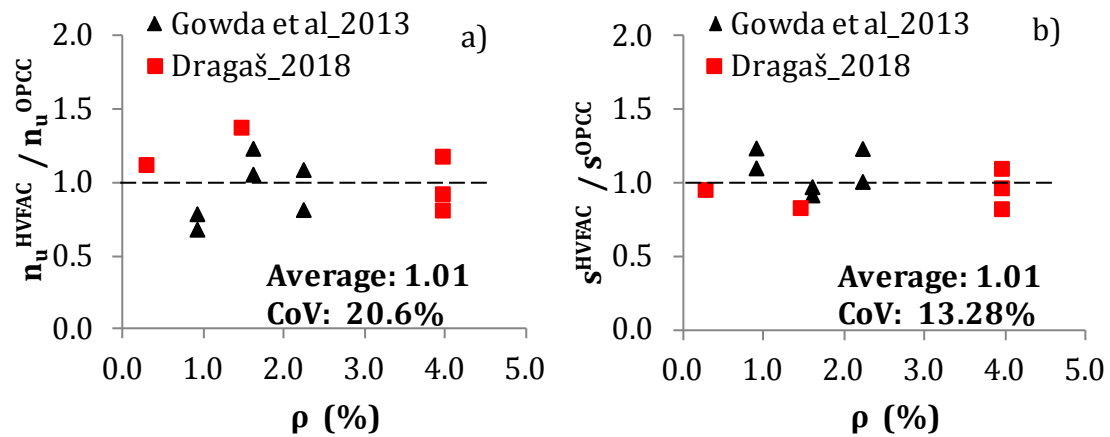


Figure 5.76 a) The HVFAC-to-OPCC beams crack number ratio and b) the HVFAC-to-OPCC average spacing ratio compared with the longitudinal reinforcement ratio at the ultimate loading state

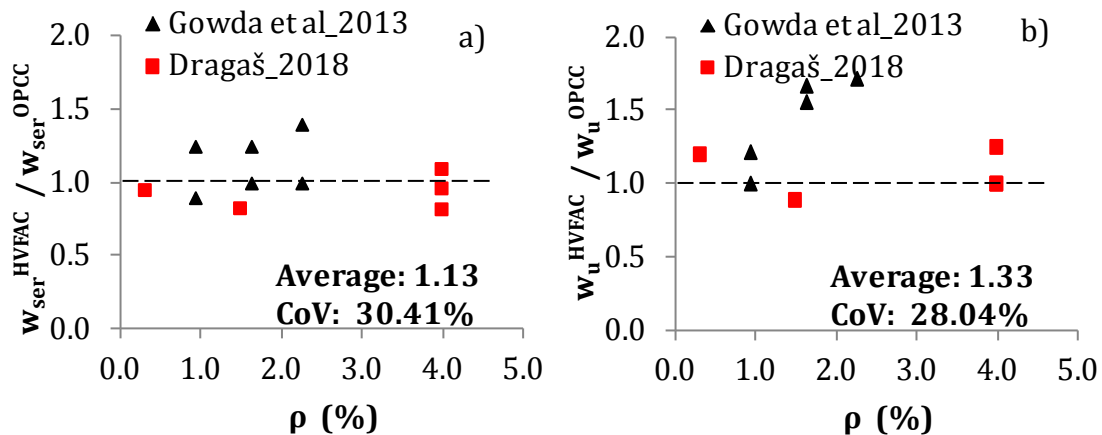


Figure 5.77 a) The HVFAC-to-OPCC beams crack width at serviceability and b) the ultimate loading state compared with the longitudinal reinforcement ratio

Only a small number of the results were available with a relatively large scatter, as shown in Figures 5.76 and 5.77. It can be concluded, based on these results that the HVFAC beams developed similar number and average spacing between cracks but larger crack widths compared with the corresponding OPCC beams. The maximum

5. Analysis and discussion of results

crack widths were 13% and 33% higher in HVFAC beams compared with the OPCC beams for the service and ultimate loading state, respectively. Even though this was a small sample to provide any general conclusions, it indicated that the HVFAC beams had in some extent higher crack widths compared with the OPCC beams. These issues need more comprehensive research to provide reliable and quantitative general conclusions.

After analyzing all these parameters it can be concluded that own experimental results regarding HVFAC beams' flexural behavior correspond well with the existing results from literature. Based on all evaluated results from the HVFAC beams database it can be concluded that the flexural strength of HVFAC and OPCC beams showed no significant differences. The only significant differences that need more attention and research are HVFAC beams crack and deflection evolution.

5.3.2.1. Application of standards on own flexural test results

5.3.2.1.1. Cracking moment

All standards defining the behavior of RC beams take into account the cracking of concrete elements that normally occurs in RC structures at the service load level. Determination of the cracking moment in beams is therefore one of the first steps in designing RC beams. Equations defining the cracking moment were given in Chapter 3, showing that it depends on the geometry of the cross-section and the flexural tensile strength of concrete. The geometry of the cross-section can be easily determined in each case but the results regarding flexural tensile strength require a brief analysis. Flexural tensile strength used for the cracking moment calculation can be obtained in three ways: directly from three point bending tests on prismatic samples, recalculating from the compressive strength or splitting tensile strength. Having in mind a large scatter of the results regarding concrete tensile strength, an analysis of different ways to obtain flexural tensile strength was performed. Flexural tensile strength was calculated in different ways using BAB '87 (Faculty of Civil Engineering 1995), EN 1992-1-1 (CEN 2004) and ACI 318

5. Analysis and discussion of results

(ACI Committee 318 2014) equations (Eq. 3.1, 3.5, and 3.9) and using measured 90-day splitting tensile strength (f_{sp}) and 90-day compressive strength (f_c).

The flexural tensile strength and the cracking moment were evaluated for both beams tested for flexural and shear behavior. Flexural tensile strength results calculated using BAB '87 (BAB), EN 1992-1-1 (EC2) and ACI 318 (ACI) are shown in Figures 5.78, 5.79 and 5.80, respectively. Measured 90-day flexural tensile strength (f_n) was also used for evaluation and shown in Figures 5.78, 5.79 and 5.80.

The highest values of the flexural tensile strength for all beams and all three standards are measured values, obtained using the direct three point bending test. They were on average higher by 48%, 38% and 44% for OPCC compared with the other calculated values using BAB '87, EN 1992-1-1 and ACI 318, respectively. For HVFAC mixtures, the measured values of flexural tensile strength were on average higher by 31%, 19% and 26% compared with the other calculated values using BAB '87, EN 1992-1-1 and ACI 318, respectively.

Correlation between the calculated and measured flexural tensile strength was better for HVFAC mixtures compared with the OPCC ones. The difference was lower for HVFAC mixtures by, on average, 20%.

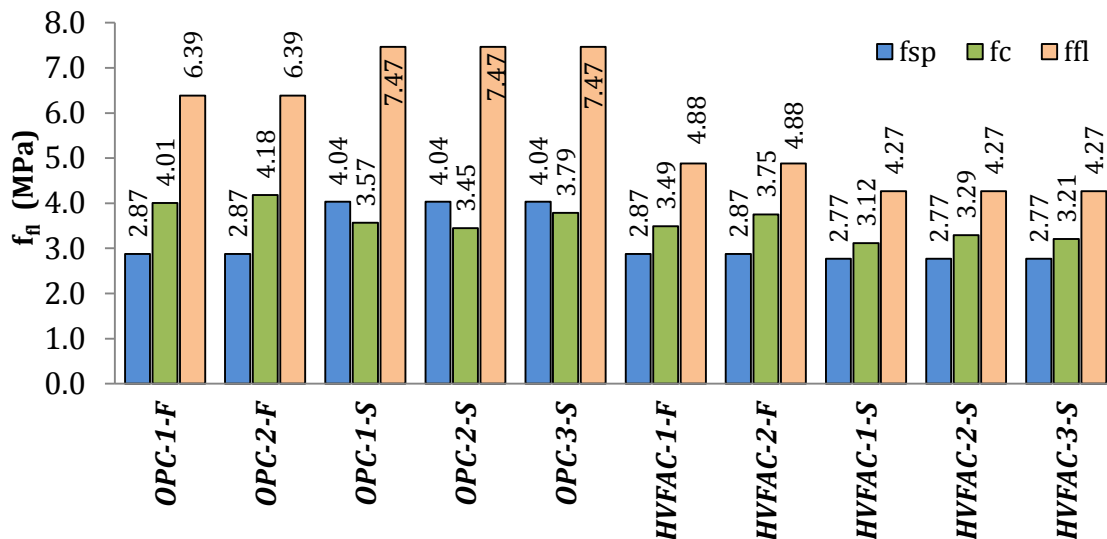


Figure 5.78 Flexural tensile strength calculated according to BAB '87

5. Analysis and discussion of results

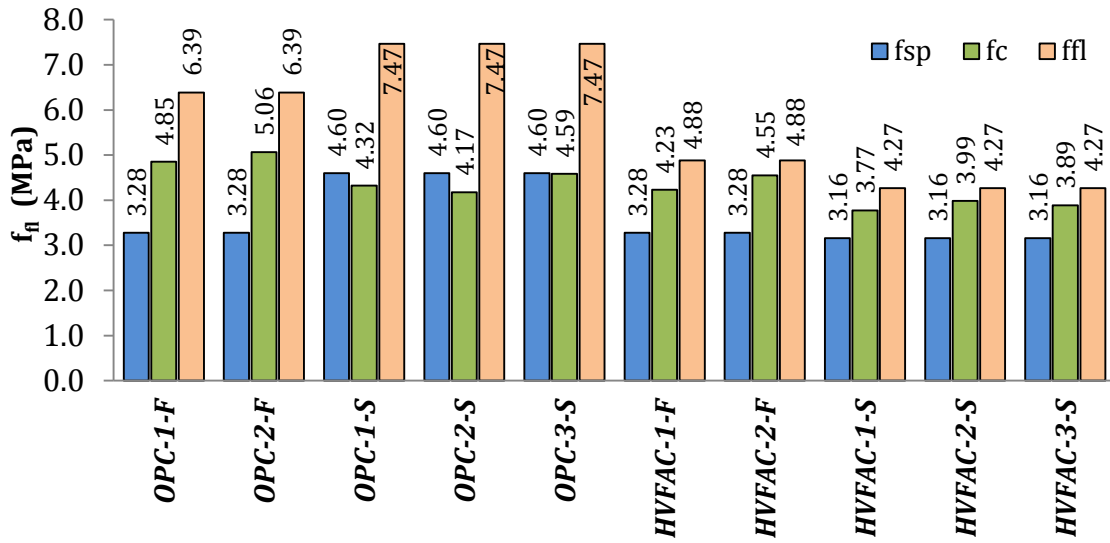


Figure 5.79 Flexural tensile strength calculated according to EN 1992-1-1

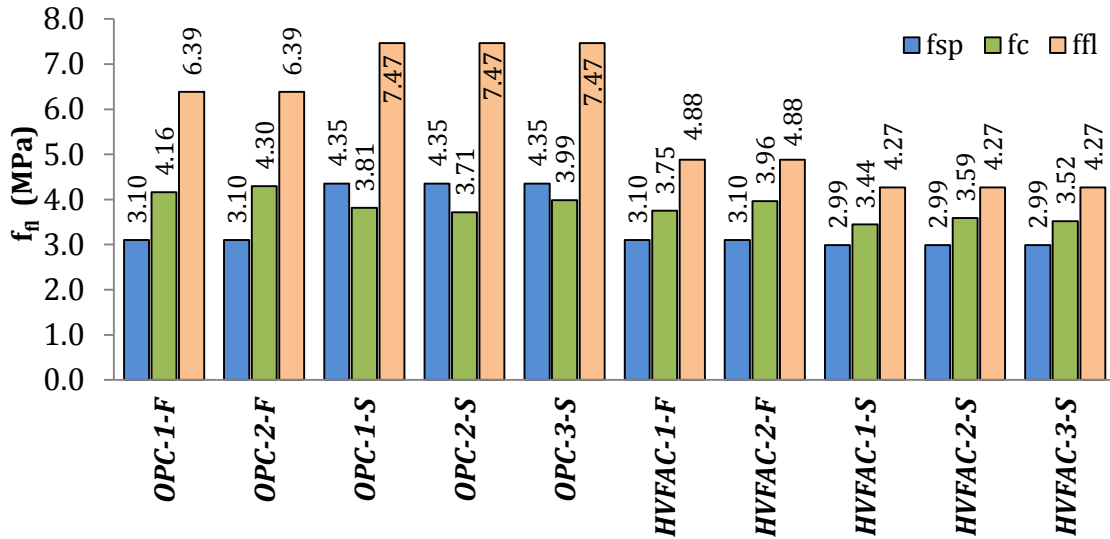


Figure 5.80 Flexural tensile strength calculated according to ACI 318

The smallest values of the flexural tensile strength were obtained by using the splitting tensile strength of samples, except in the case of OPCC beams tested for shear behavior. Similar trend was noticed for all tested standards. Having in mind a generally large scatter of tensile strength results, this shows a certain reliability of the obtained tensile strength results.

The cracking moment was calculated using the experimental value of the flexural tensile strength ($M_{cr,fl}$), and the calculated values with the splitting tensile strength ($M_{cr,sp}$) and compressive strength ($M_{cr,c}$). The results calculated using BAB '87, EN

5. Analysis and discussion of results

1992-1-1 and ACI 318 for beams tested for flexural (OPC-1-F, OPC-2-F, HVFAC-1-F and HVFAC-2-F) and shear (OPC-1-S, OPC-2-S, OPC-3-S, HVFAC-1-S, HVFAC-2-S and HVFAC-3-S) behavior are shown in Table 5.15.

Table 5.15 Calculated values of the cracking moment

	BAB '87			EN 1992-1-1			ACI 318		
	$M_{cr, sp}$	$M_{cr, c}$	$M_{cr, fl}$	$M_{cr, sp}$	$M_{cr, c}$	$M_{cr, fl}$	$M_{cr, sp}$	$M_{cr, c}$	$M_{cr, fl}$
OPC-1-F	9.04	12.61	20.10	9.83	14.56	19.17	9.30	12.48	19.17
OPC-2-F	10.19	14.82	22.64	9.83	15.19	19.17	9.30	12.89	19.17
OPC-1-S	15.24	13.46	28.19	13.81	12.96	22.40	13.06	11.44	22.40
OPC-2-S	15.24	13.00	28.19	13.81	12.52	22.40	13.06	11.14	22.40
OPC-3-S	15.24	14.29	28.19	13.81	13.76	22.40	13.06	11.96	22.40
HVFAC-1-F	9.04	10.98	15.35	9.83	12.69	14.64	9.30	11.25	14.64
HVFAC-2-F	10.19	13.30	17.30	9.83	13.64	14.64	9.30	11.88	14.64
HVFAC-1-S	11.13	12.51	17.13	9.48	11.32	12.80	8.97	10.33	12.80
HVFAC-2-S	11.13	13.22	17.13	9.48	11.96	12.80	8.97	10.77	12.80
HVFAC-3-S	11.13	12.88	17.13	9.48	11.66	12.80	8.97	10.56	12.80

Experimental values of the cracking moment corresponding to the first flexural crack formation were taken into account with the applied load, beams' self-weight and the weight of steel beam and the load press. The experimental-to-calculated cracking moment ratios are shown in Figures 5.81, 5.82, and 5.83.

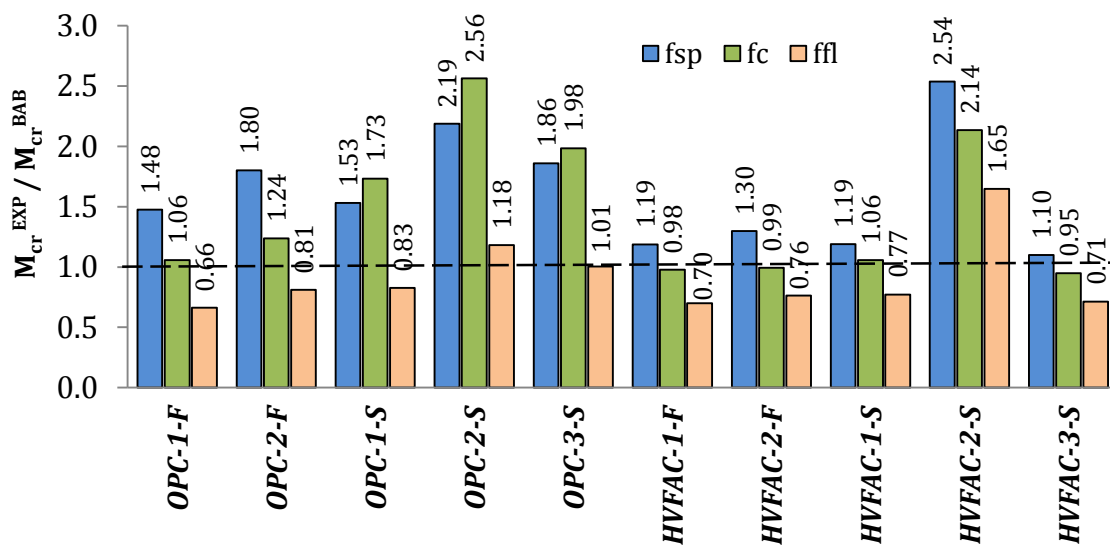


Figure 5.81 Experimental-to-calculated values of the cracking moment -BAB '87

5. Analysis and discussion of results

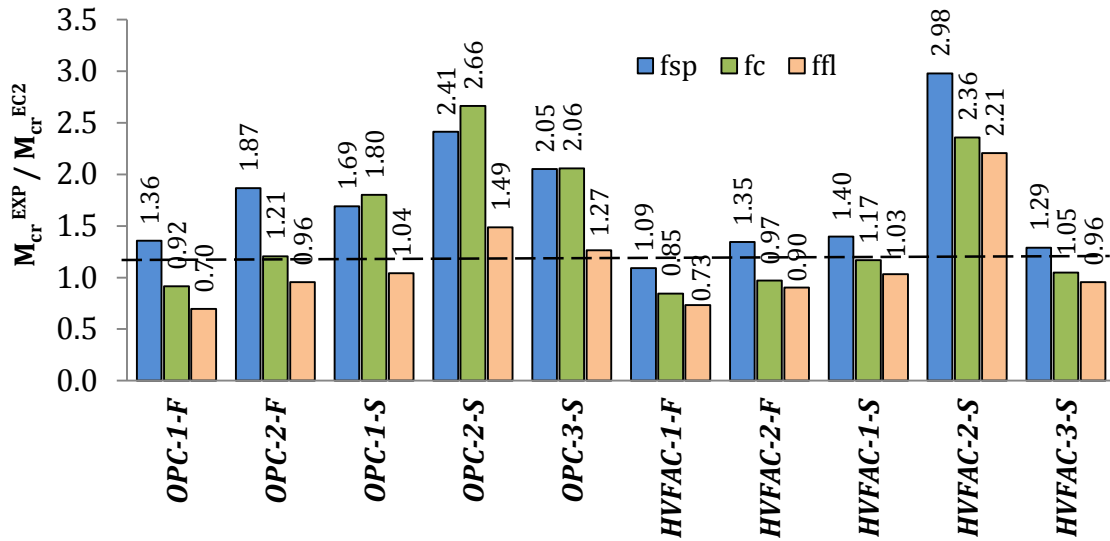


Figure 5.82 Experimental-to-calculated values of the cracking moment -EN 1992-1-1

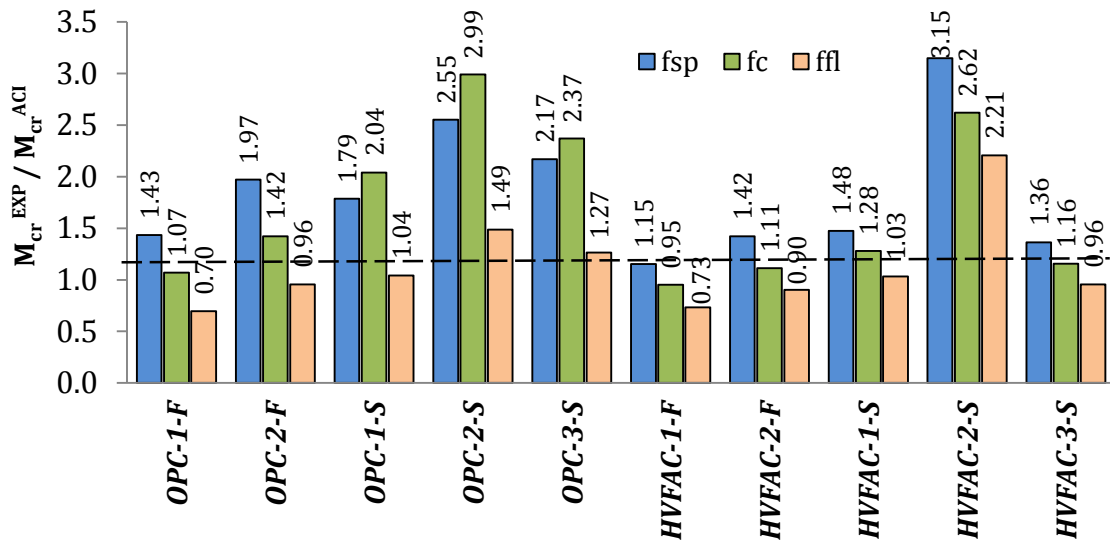


Figure 5.83 Experimental-to-calculated values of the cracking moment -ACI 318

The highest calculated values of the cracking moment were obtained using the flexural tensile strength obtained from the three point bending test. The experimental-to-calculated cracking moment ratio varied from 0.66 to 3.15 for all three standards in a similar way. The most conservative values were obtained for the lowest flexural tensile strength calculated using the splitting tensile strength. In order to compare the cracking moment predictions for OPCC and HVFAC, average values of the experimental-to-calculated cracking moment ratios are shown in Table 5.16. It can be seen that the HVFAC cracking moment predictions were less conservative compared with the OPCC mixtures for all standards, except

5. Analysis and discussion of results

when the calculation was done using measured values of the flexural tensile strength.

Table 5.16 Experimental-to-calculated values of the cracking moment

	M_{EXP}/M_{BAB}^{fsp}	M_{EXP}/M_{BAB}^{fc}	M_{EXP}/M_{BAB}^{ffi}	M_{EXP}/M_{EC2}^{fsp}	M_{EXP}/M_{EC2}^{fc}	M_{EXP}/M_{EC2}^{ffi}	M_{EXP}/M_{ACI}^{fsp}	M_{EXP}/M_{ACI}^{fc}	M_{EXP}/M_{ACI}^{ffi}
AVG^{OPCC}	1.77	1.72	0.90	1.88	1.73	1.09	1.98	1.98	1.09
AVG^{HVFAC}	1.46	1.22	0.92	1.62	1.28	1.17	1.71	1.42	1.17
CoV^{OPCC}	14.5	31.4	20.0	18.9	35.9	24.8	18.9	34.4	24.8
CoV^{HVFAC}	37.0	37.4	39.7	42.4	43.1	45.4	42.4	42.6	45.4
AVG^{HVFAC}/AVG^{OPC}	0.83	0.71	1.02	0.86	0.74	1.07	0.86	0.72	1.07
	$AVG^{BAB}=0.85$			$AVG^{EC2}=0.89$			$AVG^{ACI}=0.88$		

HVFAC cracking moment predictions were less conservative compared with the OPCC beams for up to 15% on average. The obtained conclusions were similar for all evaluate standards. This implies that the cracking of HVFAC beams occurred at lower calculated moment levels compared with OPCC beams, as shown in the experiment. The cracking moment predictions were still higher than the experimental ones for 28% on average.

5.3.2.1.2. Ultimate bending moment

For members predominantly under bending, bearing capacity is usually defined by the ultimate bending moment. Flexural strength, i.e., ultimate bending moment depends on the members cross-section dimensions, reinforcement ratio and type, concrete compressive strength and concrete stress-strain relationship. In this part of the study experimental ultimate bending moments were compared with the predictions given by different standards (Chapter 3). The calculation was done using the measured values of the concrete and steel properties with different concrete stress-strain models proposed by different standards. For the application of BAB '87 and EN 1992-1-1 for the concrete stress-strain relation the parabola-rectangle diagram was chosen. American standard ACI 318 prescribes the use of a

5. Analysis and discussion of results

block diagram for the concrete stress–strain relationship. For the reinforcement steel, in all cases, the stress–strain relation in the form of an idealized bi-linear diagram with a horizontal top branch was selected. The ultimate bending moment was also calculated using the Response-2000 program with the stress-strain relationship proposed by Popovics, Thorenfeldt and Collins (Collins and Mitchell 1991). Experimental values of the ultimate bending moment presented here took into account the contribution of the beams' self-weight and the weights of the steel beam and hydraulic press.

Calculated values of the ultimate bending moment are shown in Table 5.17 and in Figure 5.84. The experimental-to-calculated ultimate bending moment ratios are shown in Figure 5.85. It can be seen that all evaluated standards gave similar ultimate bending moment predictions for beams with the same longitudinal reinforcement ratio for both OPCC and HVFAC beams. The difference between corresponding OPCC and HVFAC beams was up to 6% for both groups of tested beams and all standards. This was expected having in mind the same or similar concrete compressive strength and the applied concrete stress-strain relationship for OPCC and HVFAC beams. It can be seen that all analyzed models gave conservative values of the ultimate bending moments but the least conservative for the OPC-1 beam.

Table 5.17 Experimental and calculated values of the ultimate bending moment

	EXP	BAB	EC2	ACI	MCFT	M_{EXP}/M_{BAB}	M_{EXP}/M_{EC2}	M_{EXP}/M_{ACI}	M_{EXP}/M_{MCFT}
OPC-1	28.7	26.3	27.1	27.0	28.5	1.09	1.06	1.06	1.01
HVFAC-1	30.5	26.1	26.7	26.6	28.6	1.17	1.14	1.15	1.07
OPC-2	115.1	102.8	101.7	100.6	101.9	1.12	1.13	1.14	1.14
HVFAC-2	115.6	100.8	99.2	97.7	100.6	1.15	1.16	1.18	1.16
Average					OPCC	1.11	1.09	1.10	1.07
					HVFAC	1.16	1.15	1.17	1.11
CoV (%)					OPCC	3.42	3.87	3.86	2.79
					HVFAC	1.19	1.47	1.68	1.00
AVG^{HVFAC}/AVG^{OPC}						1.05	1.05	1.06	1.04

5. Analysis and discussion of results

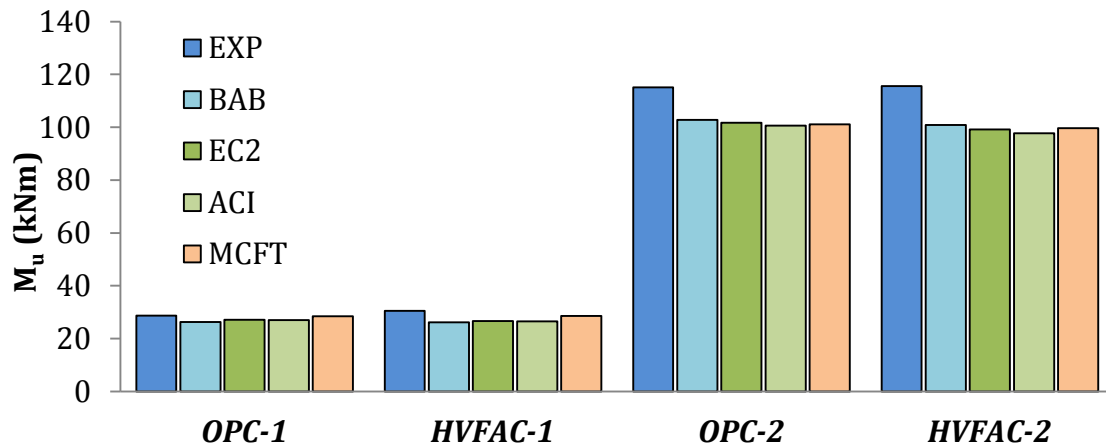


Figure 5.84 Experimental and calculated values of the ultimate bending moment

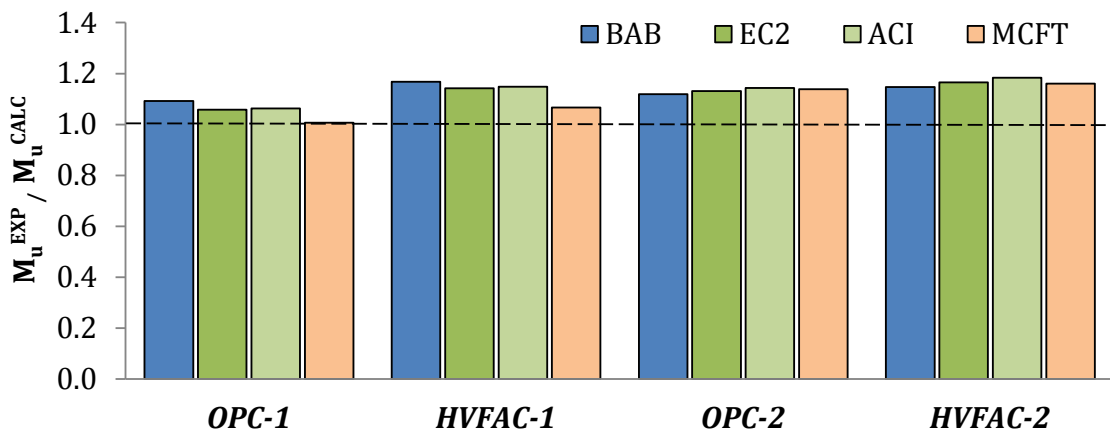


Figure 5.85 The experimental-to-calculated ultimate bending moment ratios

For beams OPC-2, HVFAC-1 and HVFAC-2 the ratio of experimental-to-calculated ultimate bending moment was in the range of 1.12 to 1.18. Predicted values of the ultimate bending moment were not significantly different between different standards. The average experimental-to-calculated ratio between different standards was in the range of 1.06 to 1.17 for the first group of beams and 1.12 to 1.18 for the second group. The calculations done using the Response-2000 (MCFT) gave slightly better predictions compared with the BAB '87, EN 1992-1-1 and ACI 318.

It can be seen that the existing models for ultimate bending moment calculations proposed in BAB '87, EN 1992-1-1, ACI 318, and Response-2000 gave, on average, 9% and 15% higher ultimate bending moments compared with the experimental values obtained for OPCC and HVFAC beams, respectively. The presented results

5. Analysis and discussion of results

showed that the used prediction models from different standards gave more conservative results for HVFAC beams compared with the OPCC beams for up to 6%.

5.3.2.2. Application of standards on flexural test results -HVFAC beams database

Results from literature were also used to evaluate the flexural strength predictions given in BAB '87, EN 1992-1-1, and ACI 318. Only studies from the HVFAC database with all available data needed for calculations were used in this evaluation. The experimental-to-calculated flexural strength ratios calculated using BAB '87, EN 1992-1-1 and ACI 318 for the OPCC and HVFAC beams are shown in Figures 5.86 – 5.91.

The scatter of presented results was similar in all OPCC and HVFAC flexural strength predictions with up to a 2% higher scatter in HVFAC beams. The average values of the experimental-to-calculated flexural strength ratios were similar or the same for all evaluated standards. More importantly, no significant difference between predictions for OPCC and HVFAC beams was observed. Beside practically the same average values, the experimental-to-calculated flexural strength ratio was in the range from 0.67 to 1.37 and from 0.70 to 1.46 for OPCC and HVFAC beams, respectively.

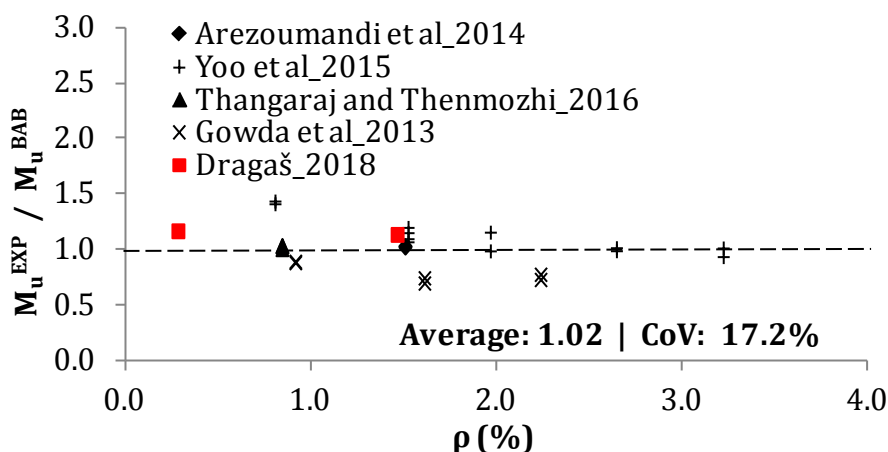


Figure 5.86 BAB '87 flexural strength predictions for HVFAC beams compared with the longitudinal reinforcement ratio

5. Analysis and discussion of results

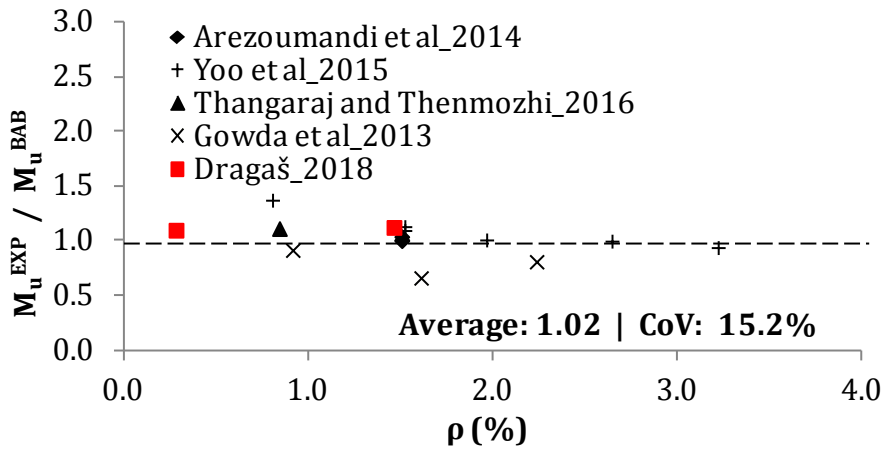


Figure 5.87 BAB '87 flexural strength predictions for OPCC beams compared with the longitudinal reinforcement ratio

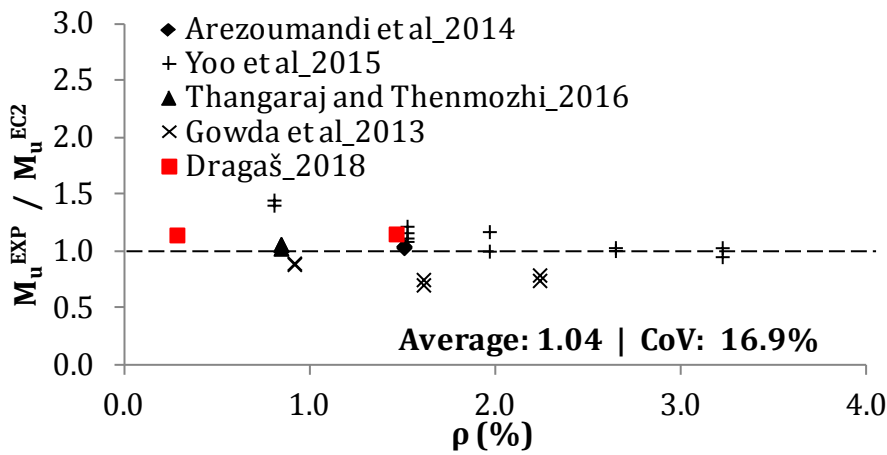


Figure 5.88 EN 1992-1-1 flexural strength predictions for HVFAC beams compared with the longitudinal reinforcement ratio

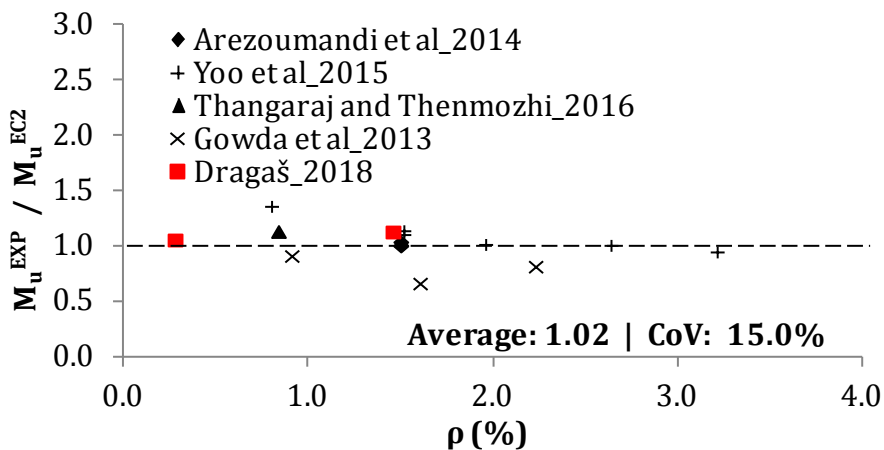


Figure 5.89 EN 1992-1-1 flexural strength predictions for OPCC beams compared with the longitudinal reinforcement ratio

5. Analysis and discussion of results

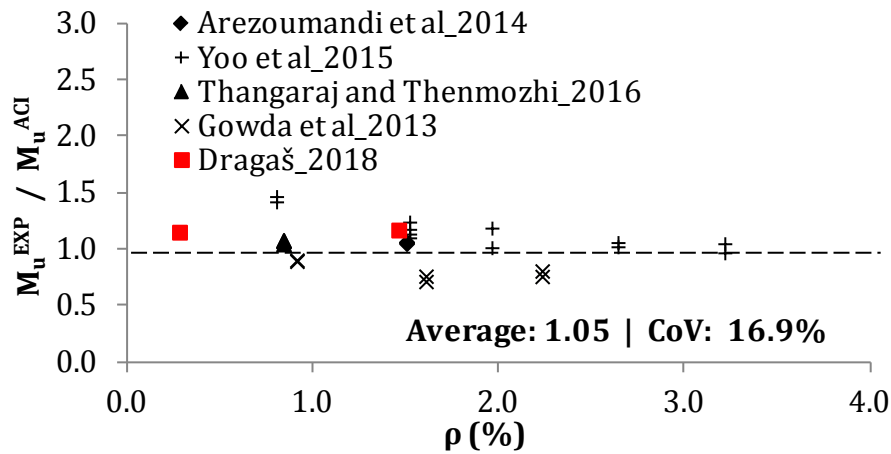


Figure 5.90 ACI 318 flexural strength predictions for HVFAC beams compared with the longitudinal reinforcement ratio

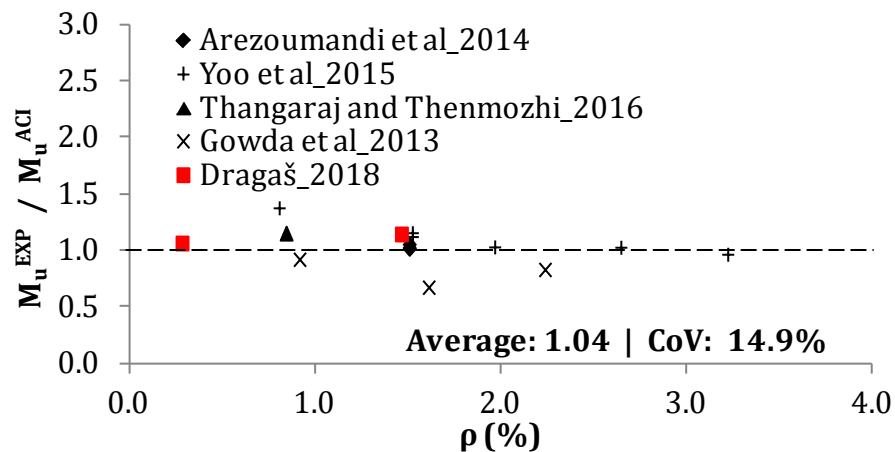


Figure 5.91 ACI 318 flexural strength predictions for OPCC beams compared with the longitudinal reinforcement ratio

Similar average values and scatter of the results for HVFAC and OPCC beams showed that there was no significant difference in the applicability of BAB '87, EN 1992-1-1 and ACI 318 standards for the prediction of HVFAC beams ultimate bending moment compared with the OPCC beams.

After everything previously stated, it can be concluded that the existing prediction models for OPCC given in standards can be used for the prediction of the ultimate bending moment of HVFAC beams.

5. Analysis and discussion of results

5.3.3. HVFAC shear behavior – HVFAC beams database

The comparison of OPCC and HVFAC beams shear behavior was done next based on the HVFAC beams database collected from literature and own experimental results. Only a few researchers have investigated the shear strength of HVFAC beams (Alghazali and Myers 2017; Arezoumandi et al. 2013b, 2015b; Arezoumandi and Volz 2013; Lisantono et al. 2017; Ortega 2012; Rao et al. 2011; Sadati et al. 2016) and all important parameters and results from their research are shown in Table B-2 in the Appendix B. Detailed overview of the selected studies was given in Chapter 2 of these thesis. Comparison of own results with the results from literature was done separately for beams without and beams with shear reinforcement. Shear strength was presented with normalized shear stress calculated using Eq. 4.3.

5.3.3.1. Database of HVFAC beams made without shear reinforcement

The HVFAC-to-OPCC shear stress ratio at failure for beams without shear reinforcement is presented versus the longitudinal reinforcement ratio in Figure 5.92. The results show relatively large scatter with values ranging from 0.48 to 1.52. The average value of this ratio indicated that the failure shear stresses for HVFAC and OPCC beams were very similar in the presented studies with HVFAC beams having on average 2% lower shear stress at failure. Own experimental results correspond well to the results from literature as shown in Figure 5.92.

Shear force which induces the first shear cracks is important from the point of view of a beam's ductility, and needs to be evaluated for HVFAC beams. This value is related to the moment of the first shear crack formation noticed by the naked eye and determined from the beams load-deflection curve. Not many results regarding the first shear cracking were found in literature, but those presented in Figure 5.93 show that the HVFAC-to-OPCC shear cracking stress ratio is in the range from 0.65 to 1.18 with an average value of 0.92. The scatter of the results was lower than in the case of the ultimate shear force but this can be attributed to the lower sample size. The presented results showed that the diagonal shear

5. Analysis and discussion of results

cracking appeared at, on average, 8% lower shear stress in HVFAC beams compared with the OPCC beams.

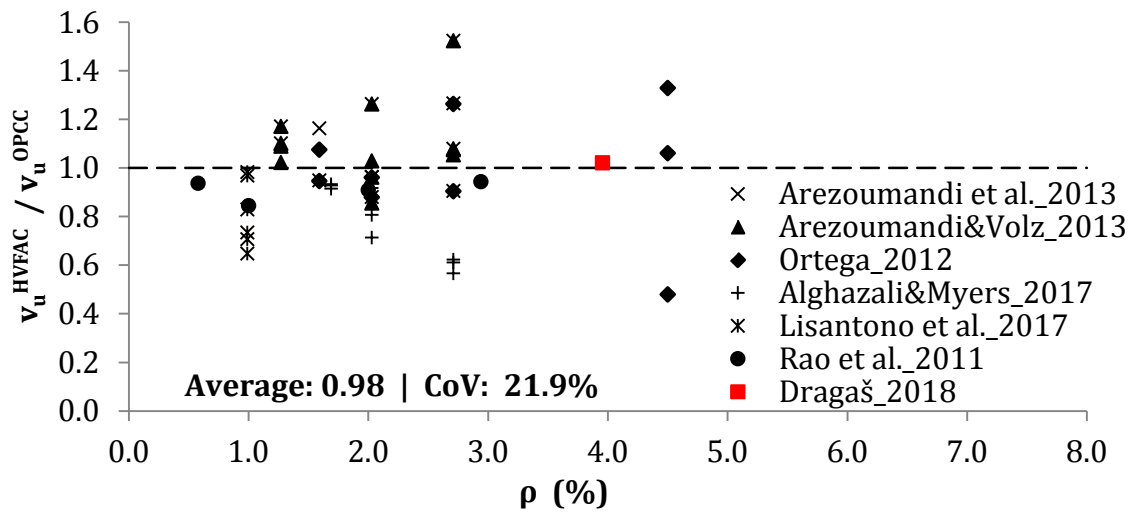


Figure 5.92 The HVFAC-to-OPCC beam normalized ultimate shear stress ratio—beams without shear reinforcement

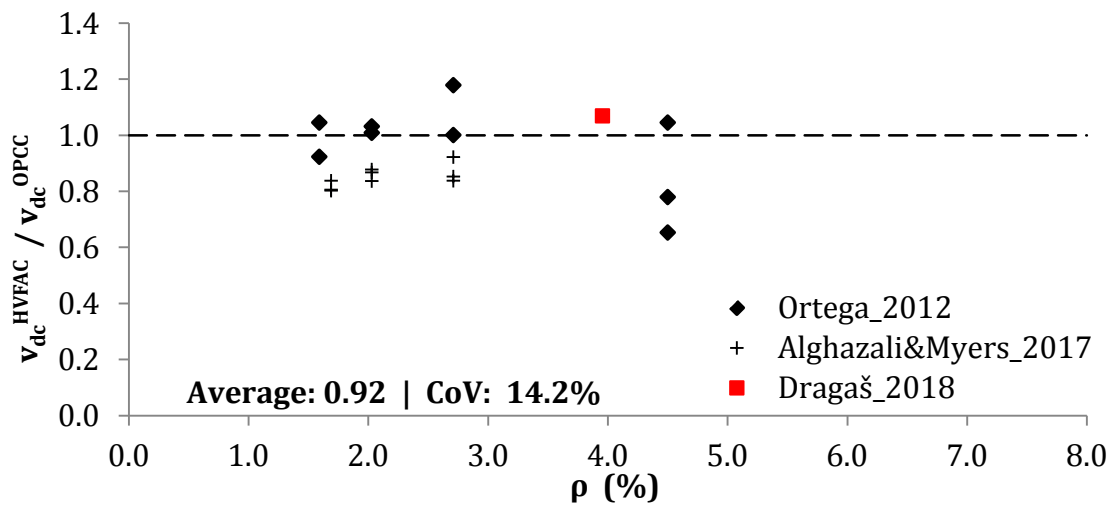


Figure 5.93 The HVFAC-to-OPCC beam diagonal crack formation normalized shear stress ratio – beams without shear reinforcement

In order to have a second look at the beams' ductility behavior, the ratio of normalized shear stress at failure to the shear cracking stress was taken as an indicator of ductility and plotted in Figure 5.94. As can be seen, the average ductility ratio is 0.98, indicating only a 2% less ductile behavior of HVFAC beams. Own experimental results correspond well to the results from literature.

5. Analysis and discussion of results

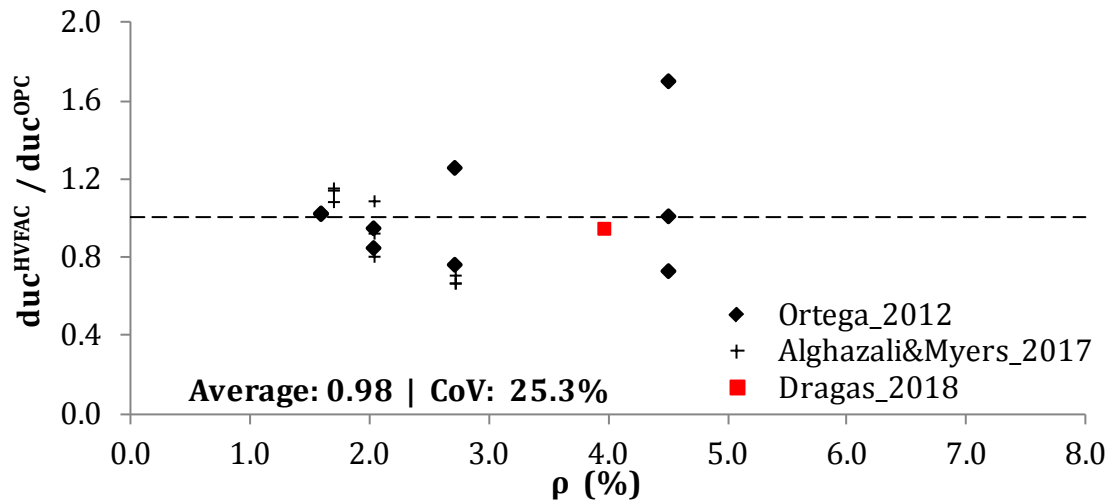


Figure 5.94 The HVFAC-to-OPCC beams' ductility ratio – beams without shear reinforcement

Another parameter available in literature explaining the beams' shear behavior is the angle of the inclined strut – shear crack angle. The HVFAC-to-OPCC inclined strut angle ratio versus the longitudinal reinforcement ratio is plotted in Figure 5.95. The average value of this ratio was similar or the same as in the previous data sets (Figures 5.91–5.94) indicating a consistent conclusion based on the selected data. Having in mind only a 2% lower average strut angle, it can be concluded that HVFAC and OPCC beams without shear reinforcement expressed similar behavior under shear loading.

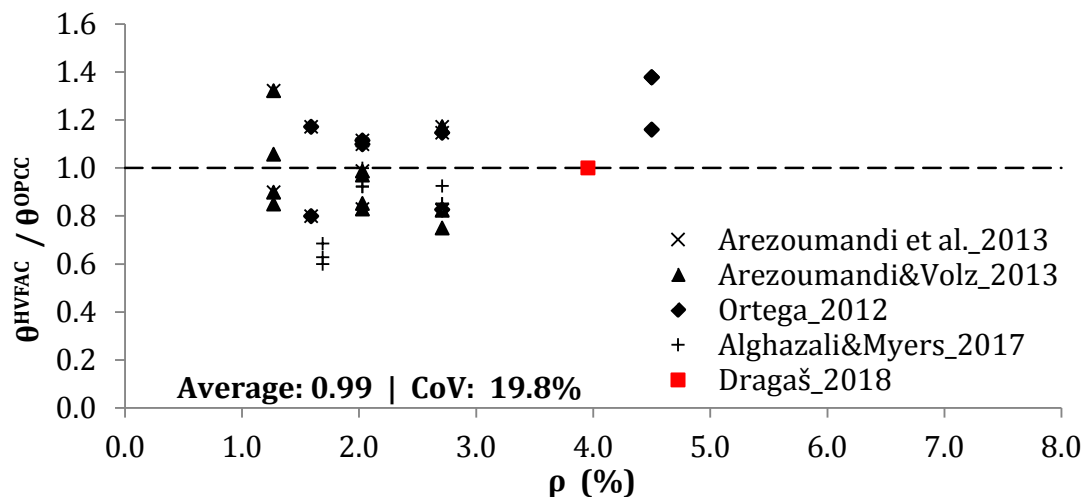


Figure 5.95 The HVFAC-to-OPCC beams' strut angle ratio – beams without shear reinforcement

5. Analysis and discussion of results

After analyzing all these parameters it can be concluded that own experimental results obtained on HVFAC beams without shear reinforcement corresponded well with the existing results from literature. supporting the fact that the shear behavior of HVFAC and OPCC beams shows no significant differences.

5.3.3.2. Database of HVFAC beams made with shear reinforcement

The same analysis was done for beams with shear reinforcement (vertical stirrups in all studies) with appropriate diagrams plotted in Figures 5.96–5.99. The ultimate shear stress ratios presented in Figure 5.96 show a lower scatter than in the case of beams without shear reinforcement with average values ranging from 0.78 to 1.19. The average value of this ratio was similar as in beams without stirrups with HVFAC beams having, on average, 3% lower failure shear stress. Own experimental results were 10% and 20% higher than this average value but correspond well to the results from literature as shown in Figure 5.96.

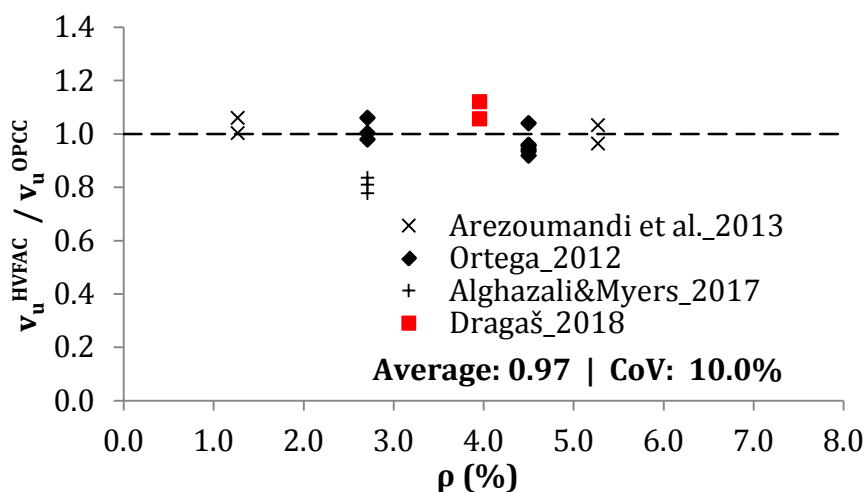


Figure 5.96 The HVFAC-to-OPCC beam normalized ultimate shear stress ratio—beams with shear reinforcement

Only a small number of shear cracking results were found in literature, and the ones presented in Figure 5.97 show the HVFAC-to-OPCC ratio ranging from 0.70 to 1.10 with the average value of 0.87. The results also showed that the diagonal shear cracking appeared in HVFAC beams at, on average, 13% lower shear stress compared with OPCC beams.

5. Analysis and discussion of results

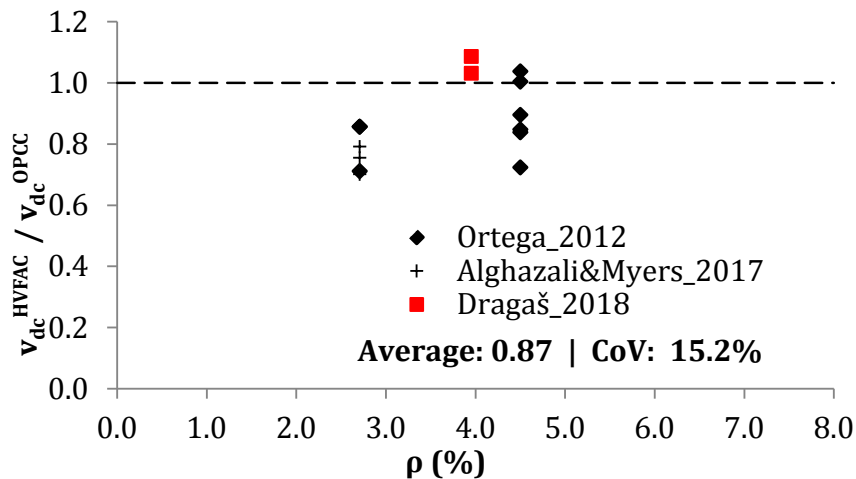


Figure 5.97 The HVFAc-to-OPCC beam diagonal crack formation normalized shear stress ratio—beams without shear reinforcement

The ratio of normalized shear stress at failure and at shear cracking stress for HVFAc and OPCC beams is plotted in Figure 5.98.

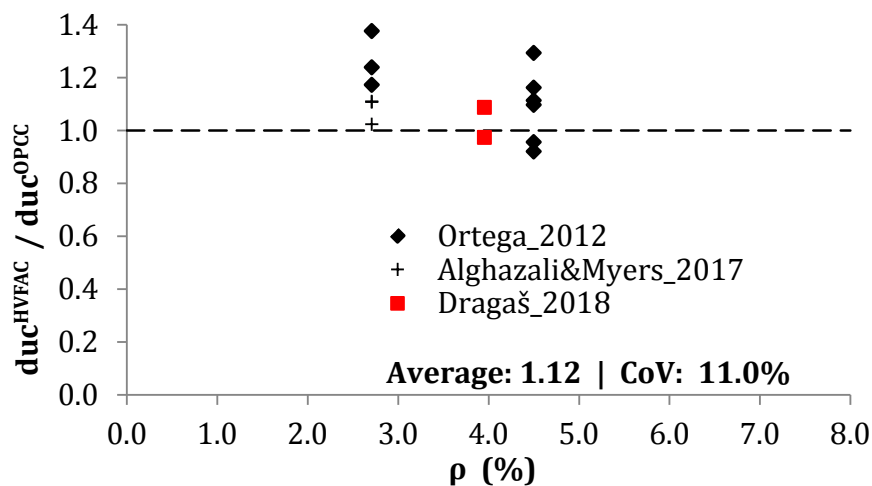


Figure 5.98 The HVFAc-to-OPCC beams' ductility ratio—beams with shear reinforcement

As can be seen, the average ductility ratio is 1.12 indicating a 12% higher ductile behavior of HVFAc beams. Own experimental results correspond well to the results presented from literature. The angle of the inclined strut is plotted as the HVFAc-to-OPCC beams' angle ratio compared with the longitudinal reinforcement ratio in Figure 5.99. The average value of this ratio, 0.91, was similar to the one in previous data sets, indicating a consistent conclusion based on the selected data. Having in mind a 9% lower average strut angle, it can be concluded that HVFAc and OPCC beams with shear reinforcement had similar behavior under shear.

5. Analysis and discussion of results

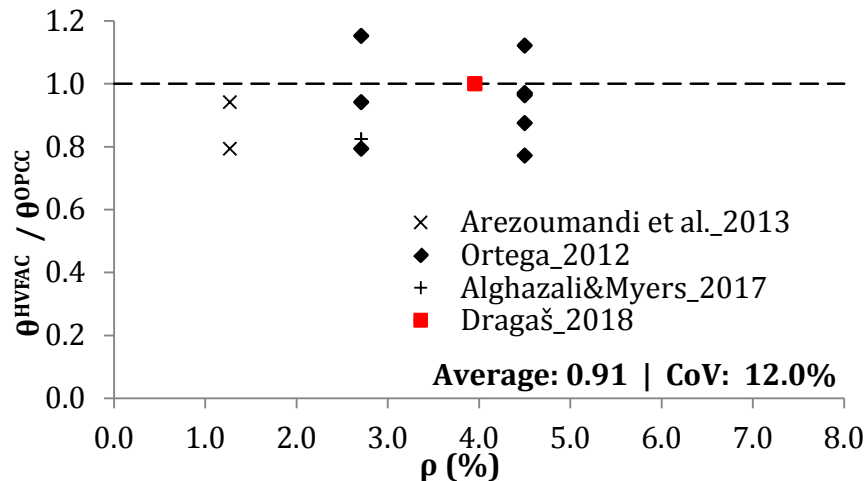


Figure 5.99 The HVFAC-to-OPCC beams' strut angle ratio–beams with shear reinforcement

After analyzing all these parameters it can be concluded that own experimental results regarding HVFAC beams with shear reinforcement correspond well with existing results from literature. Based on all evaluated results from the HVFAC beams database it can be concluded that the shear strength of HVFAC and OPCC beams showed no significant differences.

5.3.3.3. Application of standards on own shear test results

In order to evaluate the application of well-known standards defining reinforced OPCC members' behavior, shear strength was calculated using BAB '87 (Faculty of Civil Engineering 1995), EN 1992-1-1 (CEN 2004), ACI 318 (ACI Committee 318 2014) and *fib* Model Code 2010 (*fib* 2010b). Experimental values (EXP) and calculated shear strength using BAB '87 (BAB), EN 1992-1-1 (EC2), ACI 318 (ACI), *fib* Model Code 2010 LoA III (MC) and the results obtained using the Response-2000 program (MCFT) are shown in Table 5.18. Experimental values of the shear strength are shown with the addition of the beams' self-weight and the weight of additional equipment loading the beams during testing.

It can be seen from Table 5.18 that predicted shear strengths for both beams without and with shear reinforcement are lower compared with the experimentally obtained values. In order to get a better understanding of the

5. Analysis and discussion of results

mutual relationship between different predictions, calculated values are plotted in Figures 5.100 and 5.101.

In the case of beams with a minimum reinforcement (OPC-2 and HVFAC-2) the shear reinforcement capacities calculated using EN 1992-1-1 were lower than the concrete shear strength, so the concrete shear strength was chosen as the relevant value. Figures 5.100 and 5.101 show that the most precise shear strength predictions for beams without shear reinforcement were obtained using Response-2000 (MCFT) and *fib* Model Code 2010 and the least precise using the BAB '87 predictions for both OPCC and HVFAC beams.

Table 5.18 Shear strength predictions

	EXP	BAB	EC2	ACI	MC	MCFT
<i>OPC-1</i>	229.3	119.8	143.6	127.6	156.6	175.0
<i>OPC-2</i>	323.2	179.2	142.4	166.1	191.9	198.6
<i>OPC-3</i>	388.4	253.7	221.3	221.5	265.2	289.4
<i>HVFAC-1</i>	217.9	105.7	134.2	118.2	145.0	153.8
<i>HVFAC-2</i>	350.8	174.5	139.2	163.2	188.4	191.6
<i>HVFAC-3</i>	377.4	235.2	221.3	210.7	253.4	278.6

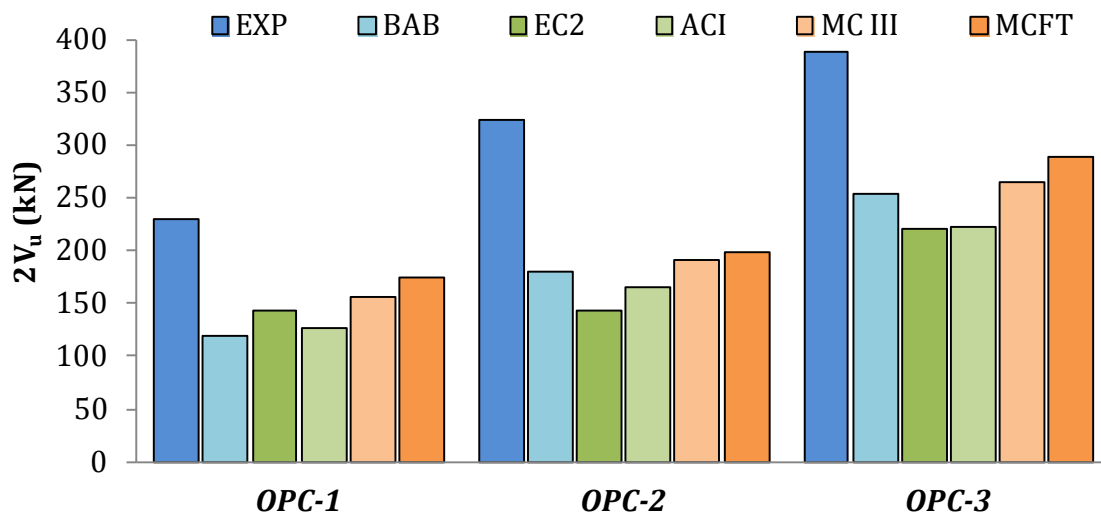


Figure 5.100 Experimental and calculated values of the OPCC beams' shear strength using different standards

5. Analysis and discussion of results

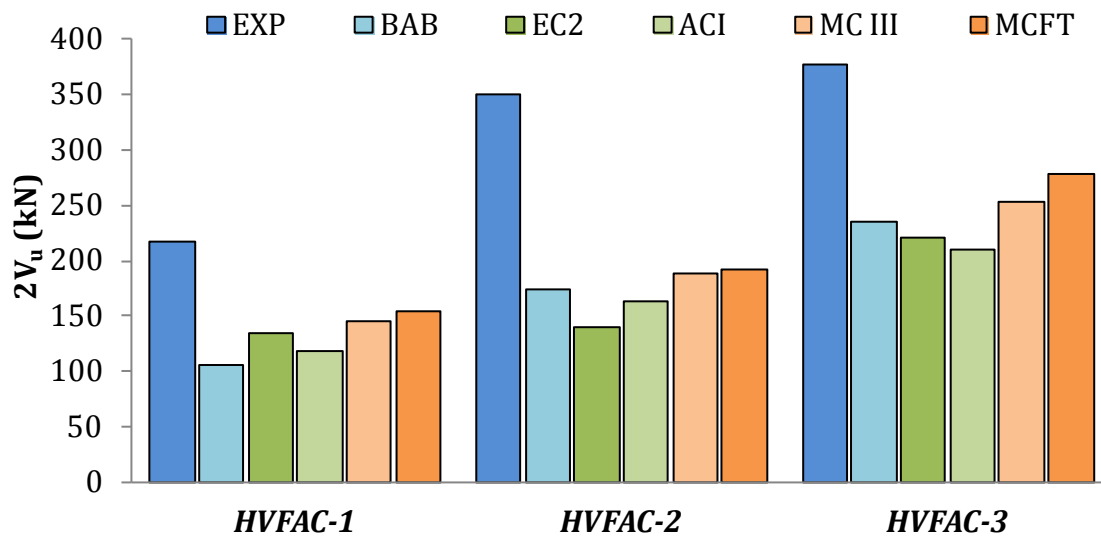


Figure 5.101 Experimental and calculated values of HVFAC beams' shear strength using different standards

For all beams with shear reinforcement the most precise predictions were obtained using Response-2000 (MCFT), *fib* Model Code 2010 and BAB '87 predictions. Table 5.19 shows the experimental-to-calculated shear strengths ratios along with their average values and CoVs.

Table 5.19 The experimental-to-predicted shear strength ratios

		V_{EXP} / V_{BAB}	V_{EXP} / V_{EC2}	V_{EXP} / V_{ACI}	V_{EXP} / V_{MC}	V_{EXP} / V_{MCFT}
	OPC-1	1.91	1.60	1.80	1.46	1.31
	OPC-2	1.80	2.27	1.95	1.68	1.63
	OPC-3	1.53	1.76	1.75	1.46	1.34
	HVFAC-1	2.06	1.62	1.84	1.50	1.42
	HVFAC-2	2.01	2.52	2.15	1.86	1.83
	HVFAC-3	1.60	1.71	1.79	1.49	1.35
Average	OPCC	1.75	1.87	1.83	1.54	1.43
	HVFAC	1.89	1.95	1.93	1.62	1.53
CoV (%)	OPCC	9.19	15.33	4.50	6.75	10.00
	HVFAC	10.81	20.76	8.21	10.67	13.78
AVG^{HVFAC} / AVG^{OPCC}		1.08	1.04	1.05	1.05	1.08

5. Analysis and discussion of results

For beams without shear reinforcement the experimental-to-calculated shear strength ratio was similar in both types of beams ranging between 1.31 and 1.91 for OPCC and 1.42 and 2.06 for HVFAC beams. It can also be noticed that the experimental-to-calculated shear strength ratios for HVFAC beams were higher compared with the OPCC beams, differing by not more than 9%. All standards underestimated the shear strength of beams without shear reinforcement but the Response-2000 (MCFT) did so the least, by approximately 30%. This was not a surprise having in mind the influence of cracked concrete taken into account using the MCFT and more realistic concrete and steel stress–strain behavior models. The second best prediction was obtained by using the *fib* Model Code 2010 equation for the concrete shear strength calculation. Shear strength calculated using EN 1992-1-1 and ACI 318 predictions were approximately 1.60 to 2.84 times lower than the experimental ones for both OPCC and HVFAC beams. The BAB '87 standard gave the most conservative predictions of shear strength.

The shear strength predictions regarding beams with shear reinforcement were generally more conservative compared with the beams without shear reinforcement for EN 1992-1-1, ACI 318, *fib* Model Code 2010 and Response-2000 (MCFT) predictions, and less conservative for BAB '87 predictions. Predictions for beams with higher shear reinforcement were less conservative compared with beams with a minimum shear reinforcement ratio in all cases. The experimental-to-predicted shear strength ratio was in the range of 1.34–2.27 and 1.42–2.52 for the OPCC and HVFAC beams, respectively. The best predictions were obtained by using Response-2000 (MCFT) and *fib* Model Code 2010 provisions with the experimental-to-predicted shear strength ratio between 1.34 and 1.86. The CoV was lower than 20% for all evaluated standards except EN 1992-1-1 where the CoV was around 21%. HVFAC beams had, in general, higher experimental-to-calculated shear strength ratio by up to 13% compared with the OPCC beams. The shear strength predictions calculated for beams with a minimum reinforcement ratio were the most conservative ones for all standards.

5. Analysis and discussion of results

After this analysis it can be concluded that the application of available standards on HVFAC beams, tested in these study, yielded more conservative shear strength predictions compared with the OPCC beams.

5.3.3.4. Application of standards on shear test results - HVFAC beams database

The HVFAC beams database was also used to evaluate the shear design predictions given in EN 1992-1-1, ACI 318 and *fib* Model Code 2010. Evaluation was done separately for beams without and with shear reinforcement and for HVFAC and OPCC beams from the selected studies.

5.3.3.4.1. HVFAC beams made without shear reinforcement

The experimental shear strength-to-calculated shear strength ratios calculated using EN 1992-1-1 for HVFAC and OPCC beams from the selected studies are shown in Figures 5.102 and 5.103, respectively. Similar scatter of the results for both HVFAC and OPCC beams indicated similar applicability of the EN 1992-1-1 equation (Eq. 3.23) for shear strength prediction for the beams without stirrups. The average values of 1.13 and 1.17 for HVFAC and OPCC beams showed that EN 1992-1-1 standard underestimates the shear strength of beams without stirrups for both HVFAC and OPCC beams in a similar way.

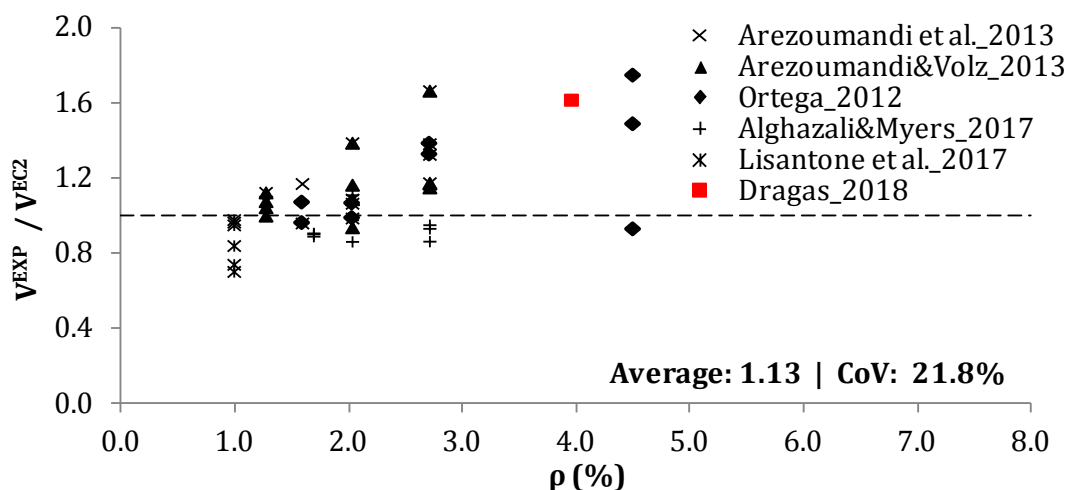


Figure 5.102 EN 1992-1-1 shear strength predictions for the HVFAC beams without shear reinforcement

5. Analysis and discussion of results

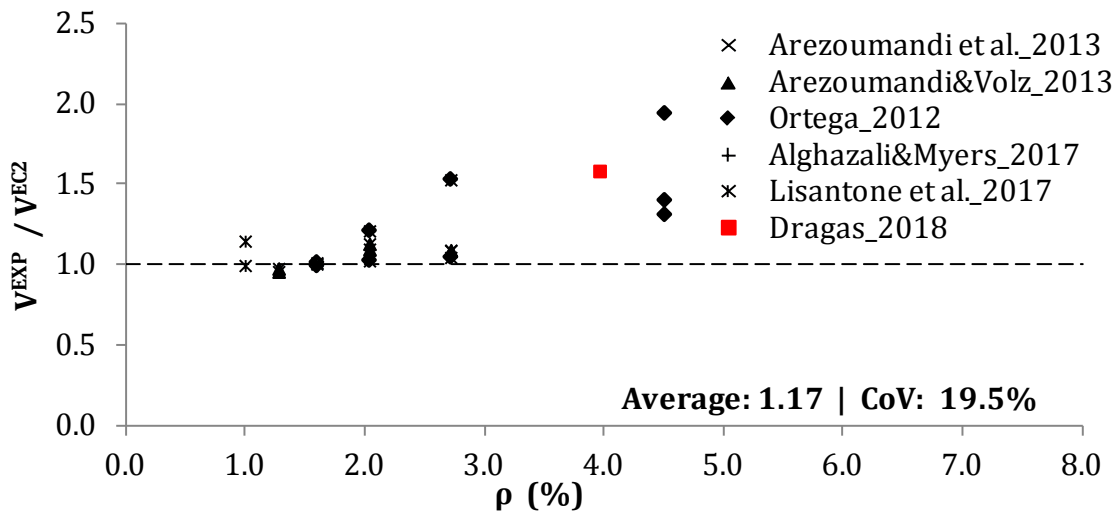


Figure 5.103 EN 1992-1-1 shear strength predictions for the OPCC beams without shear reinforcement

Own experimental results were higher than the average values obtained for the selected results from literature. Nevertheless, they fit well with the presented results. The experimental shear strength-to-calculated shear strength ratios determined using ACI 318 for HVFAC and OPCC from the selected studies are shown in Figures 5.104 and 5.105, respectively. The average values of 1.30 and 1.34 for HVFAC and OPCC beams showed that ACI 318 standard underestimated the shear strength of beams without stirrups for both HVFAC and OPCC beams in a similar way. Similar scatter of the results for HVFAC and OPCC beams indicates similar applicability of the ACI 318 prediction (Eq. 3.45).

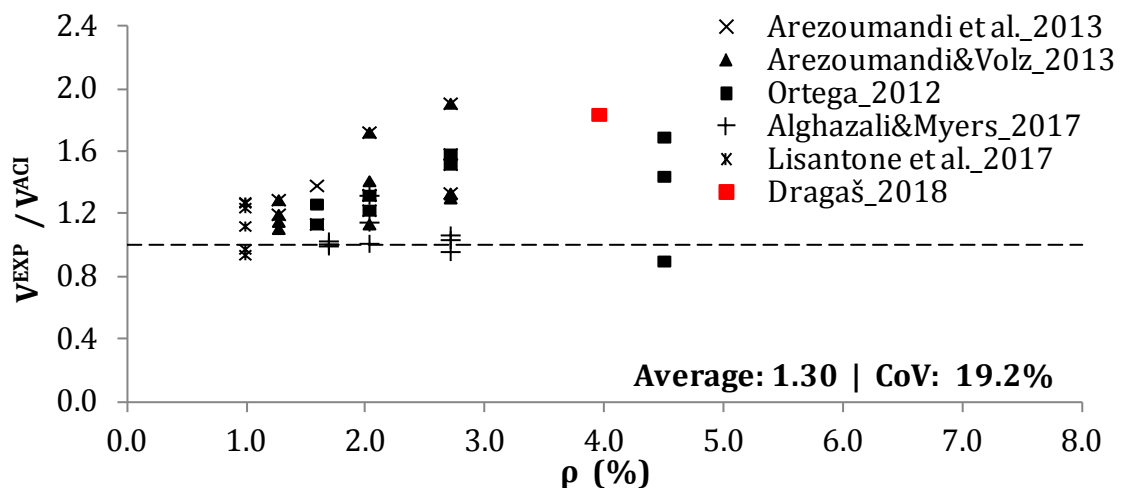


Figure 5.104 ACI 318 shear strength predictions for the HVFAC beams without shear reinforcement

5. Analysis and discussion of results

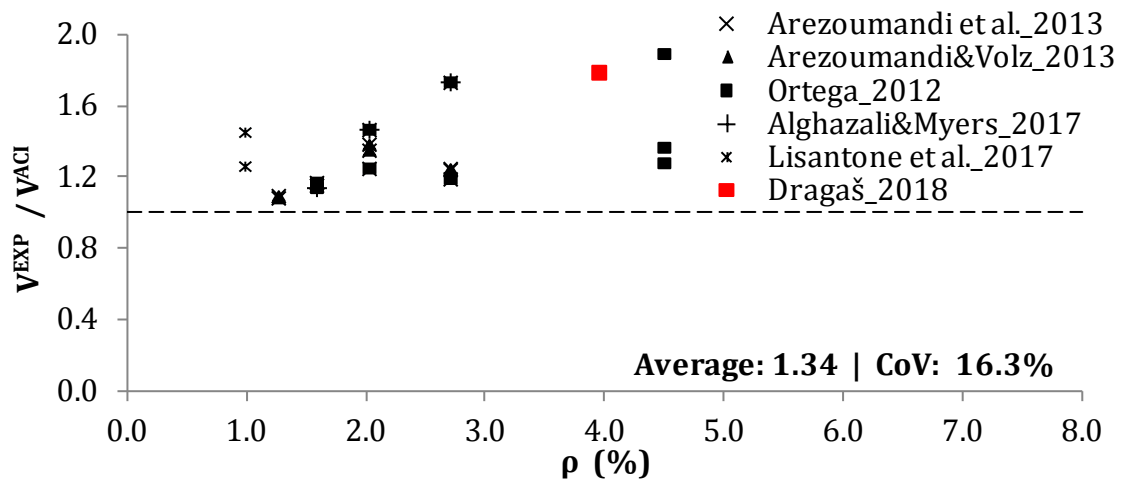


Figure 5.105 ACI 318 shear strength predictions for the OPCC beams without shear reinforcement

Own experimental results were higher than the average values but within the range of the presented results from literature. These average values were higher compared with the EN 1992-1-1 prediction indicating more conservative approach defined in ACI 318 for both OPCC and HVFAC beams.

The experimental-to-calculated shear strength ratios determined using *fib* Model Code 2010 for HVFAC and OPCC beams from the selected studies are shown in Figures 5.106 and 5.107.

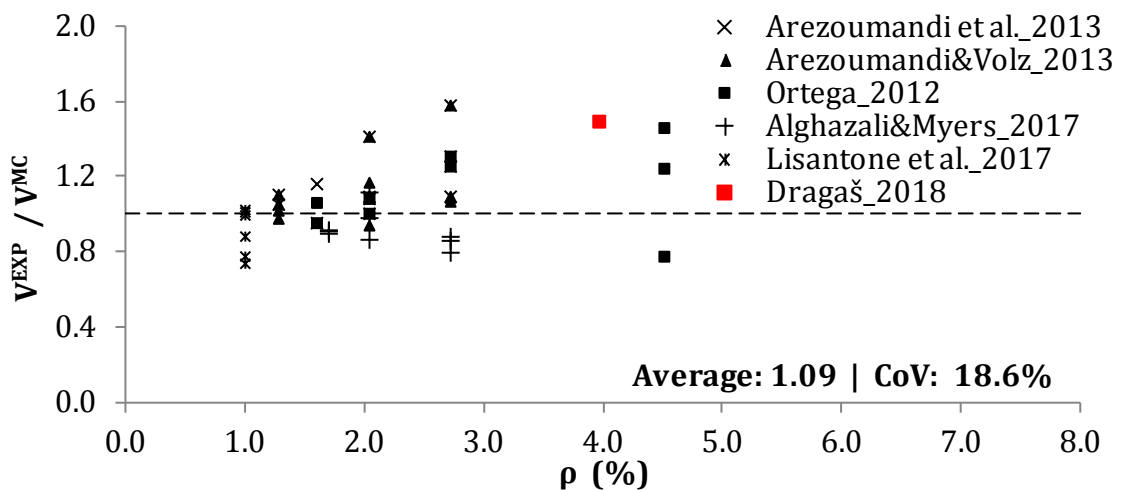


Figure 5.106 *fib* Model Code 2010 shear strength predictions for the HVFAC beams without shear reinforcement

5. Analysis and discussion of results

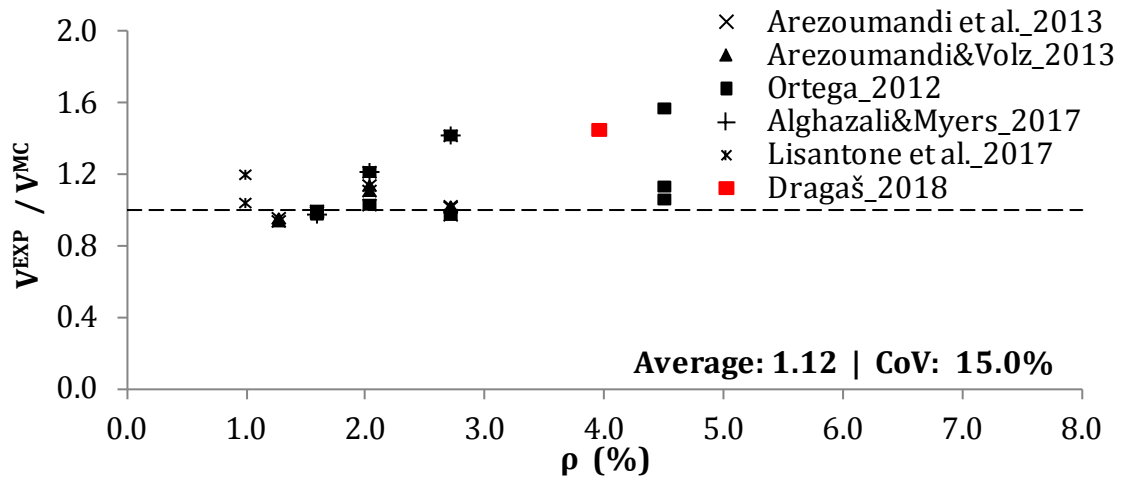


Figure 5.107 *fib Model Code 2010 shear strength predictions for the OPCC beams without shear reinforcement*

The average values of 1.09 and 1.12 for HVFAC and OPCC beams showed that *fib Model Code 2010* prediction for shear strength of beams without stirrups gave good results for both HVFAC and OPCC beams. Own experimental results were in good agreement with the presented results.

The *fib Model Code 2010* equation for inclined strut angle prediction (Eq. 3.27) in beams loaded in shear was also evaluated. The experimental-to-calculated strut angle ratios are shown in Figures 5.108 and 5.109. Scattering of the results was similar as for the shear strength predictions.

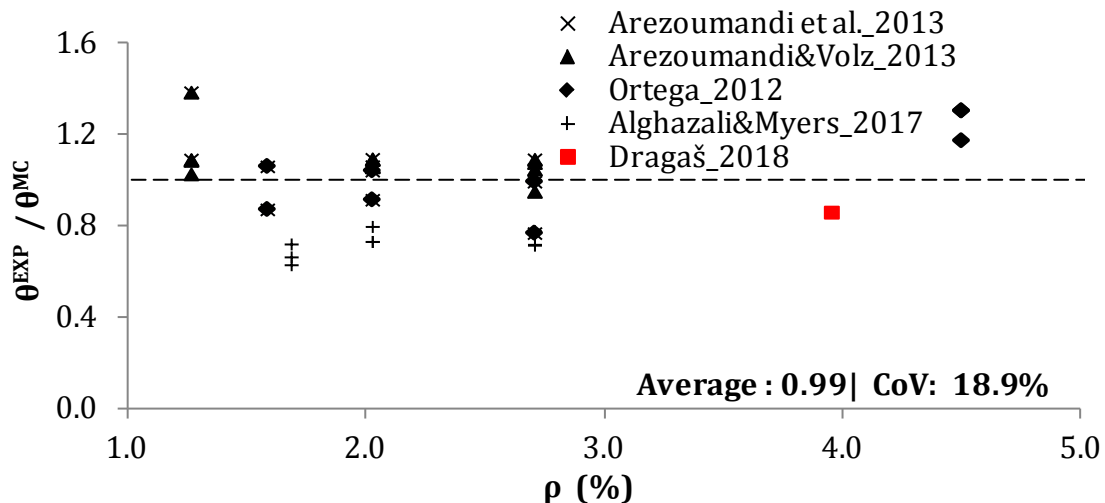


Figure 5.108 *fib Model Code 2010 strut angle predictions for the HVFAC beams without shear reinforcement*

5. Analysis and discussion of results

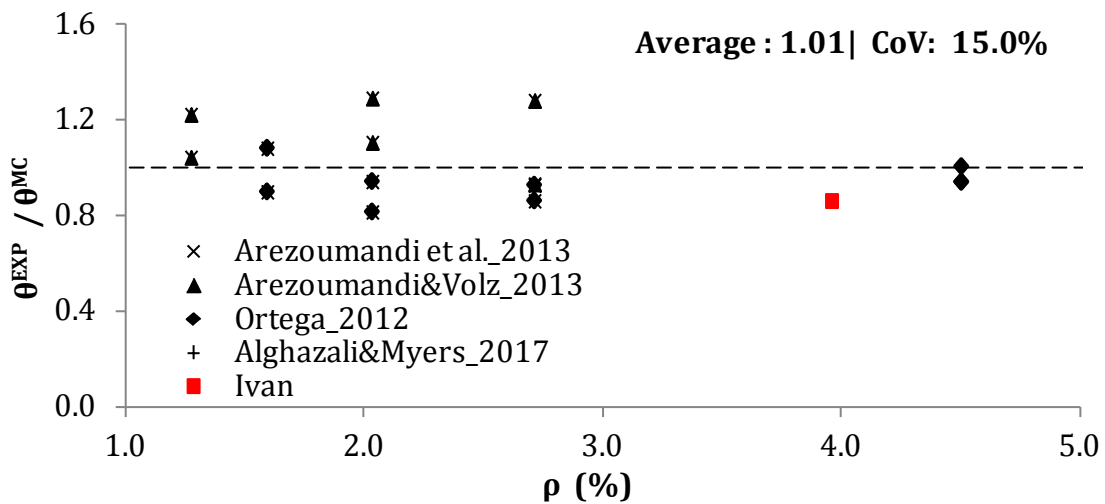


Figure 5.109 *fib* Model Code 2010 strut angle predictions for the OPCC beams without shear reinforcement

The average values for HVFAC and OPCC beams indicated that the *fib* Model Code 2010 equation (Eq. 3.27) can be used to predict the strut angle for both HVFAC and OPCC beams with similar accuracy. Own experimental-to-predicted strut angles were up to 15% lower than the average values obtained for all the results from literature.

Previously conducted analysis showed that there were no significant differences between the predicted and experimental shears strength and strut angles for OPCC and HVFAC beams without shear reinforcement. The difference between OPCC and HVFAC beams predictions was only up to 5% for all results from the database. It can be concluded that the application of EN 1992-1-1, ACI 318 and *fib* Model Code 2010 predictions can be used with similar accuracy for both OPCC and HVFAC beams without shear reinforcement.

5.3.3.4.2. HVFAC beams made with shear reinforcement

The experimental-to-calculated shear strength ratios calculated using EN 1992-1-1, ACI 318 and *fib* Model Code 2010 for HVFAC and OPCC beams with shear reinforcement are shown in Figures 5.110 – 5.105 (Alghazali and Myers 2017; Arezoumandi et al. 2013a; Ortega 2012). The average values of the experimental-to-calculated ratios for EN 1992-1-1 were 1.26 and 1.32 for HVFAC and OPCC beams with stirrups. Predictions for own beams with a minimum shear

5. Analysis and discussion of results

reinforcement were higher than the results found in literature for both OPCC and HVFAC beams.

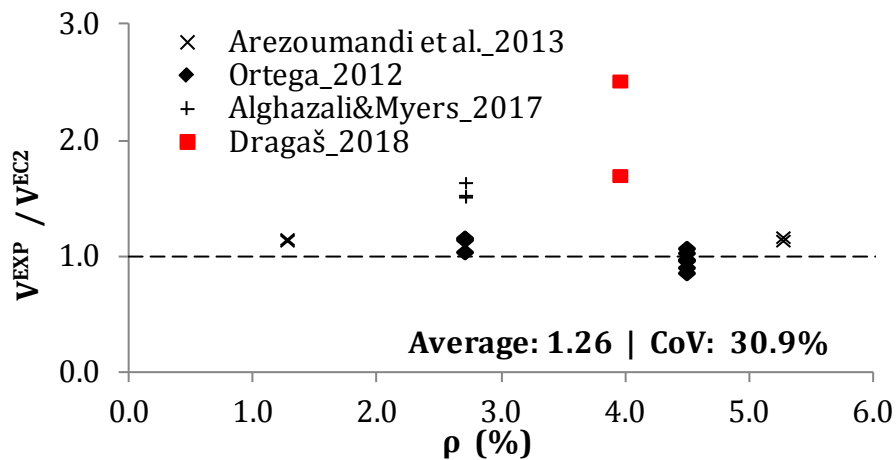


Figure 5.110 EN 1992-1-1 shear strength predictions for the HVFAC beams with shear reinforcement

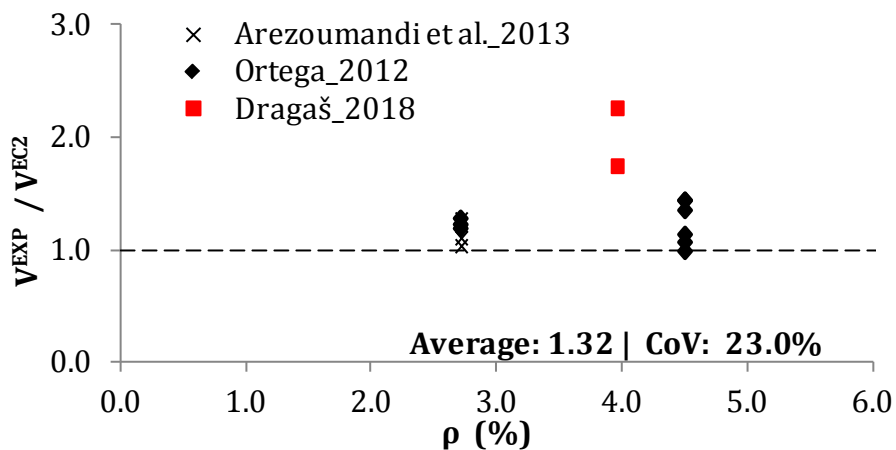


Figure 5.111 EN 1992-1-1 shear strength predictions for the OPCC beams with shear reinforcement

The ACI 318 provisions for shear strength of beams with stirrups were in worse agreement with experimental results compared with the EN 1992-1-1 ones with average values of 1.37 and 1.44 for HVFAC and OPCC beams (Figures 5.112 and 5.113). Similar scatter of the results for HVFAC and OPCC beams indicated similar applicability of the equation for shear strength prediction of beams with stirrups defined in ACI 318. The predictions obtained for own beams were more conservative compared with the results found in literature.

5. Analysis and discussion of results

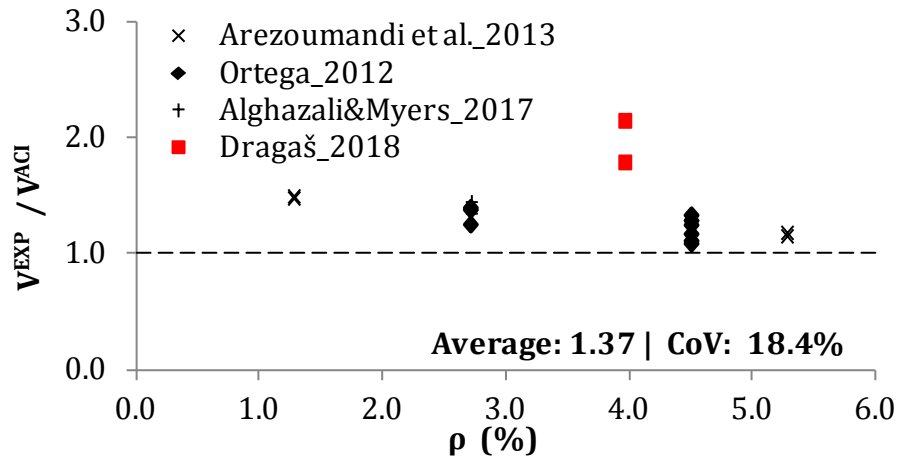


Figure 5.112 ACI 318 shear strength predictions for the HVFAC beams with shear reinforcement

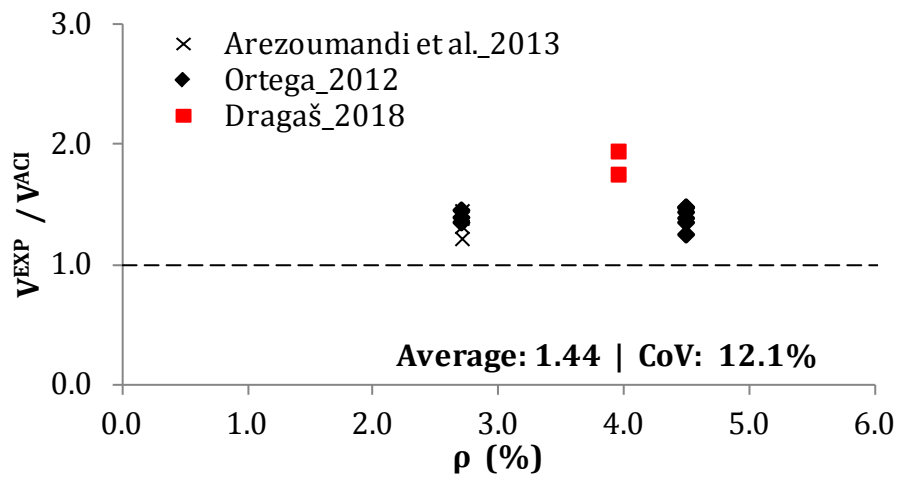


Figure 5.113 ACI 318 shear strength predictions for the OPCC beams with shear reinforcement

The best agreement with experimental results was obtained using the *fib* Model Code 2010 equations (Figures 5.114 and 5.115), as expected. The average values of 1.17 and 1.21 for HVFAC and OPCC beams with stirrups showed that *fib* Model Code 2010 also underestimated the actual shear strength, but is the least conservative of all the evaluated standards. The shear strength predictions obtained for own beams were higher than the average values obtained for all beams from literature.

Evaluation of the *fib* Model Code 2010 equation for the inclined strut angle was also done. The experimental-to-calculated strut angle ratios are shown in Figures 5.116 and 5.117. Scattering of the results was similar as in the case of shear

5. Analysis and discussion of results

strength predictions and the average values for HVFAC and OPCC beams were 0.93 and 0.98, respectively. It can be concluded that *fib* Model Code 2010 slightly overestimated the values of the inclined strut angle for HVFAC beams with stirrups. Own experimental results were in good agreement with the presented results.

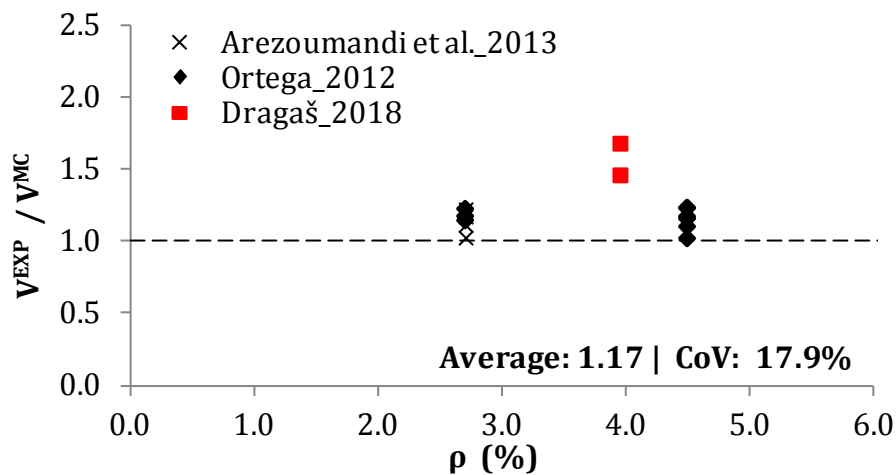


Figure 5.114 *fib* Model Code 2010 shear strength predictions for the HVFAC beams with shear reinforcement

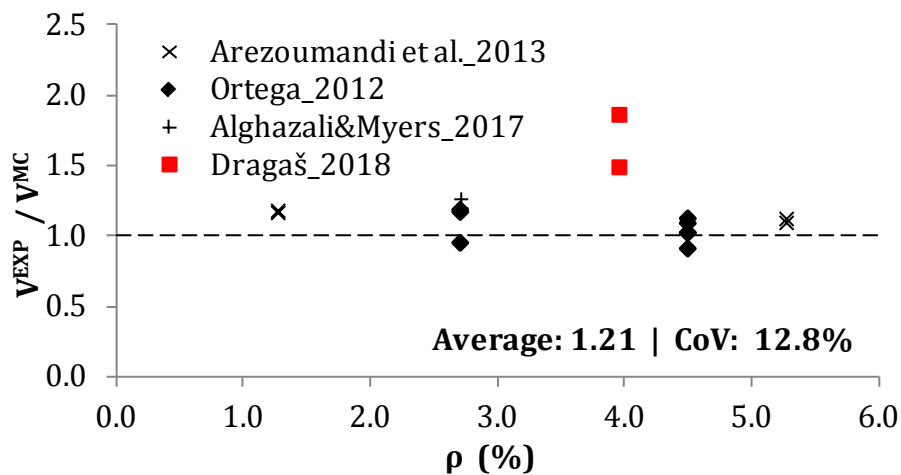


Figure 5.115 *fib* Model Code 2010 shear strength predictions for the OPCC beams with shear reinforcement

Previously conducted analysis of the results from available literature showed that EN 1992-1-1, ACI 318 and *fib* Model Code 2010 predictions for shear strength of beams with stirrups gave conservative values for both OPCC and HVFAC beams. The difference between OPCC and HVFAC beams predictions was up to 5% for all

5. Analysis and discussion of results

results from the database with more conservative values predicted for OPCC beams. This difference for own OPCC and HVFAC beams was up to 10% with more conservative values predicted for HVFAC beams.

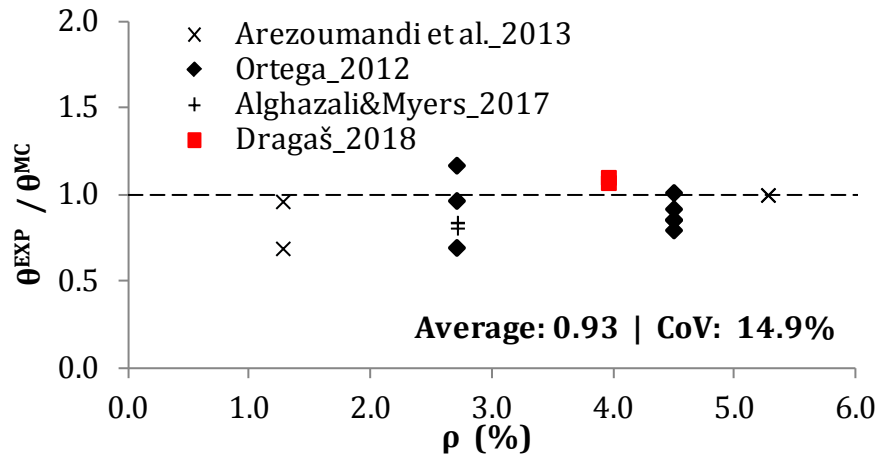


Figure 5.116 fib Model Code 2010 strut angle predictions for the HVFAC beams with shear reinforcement

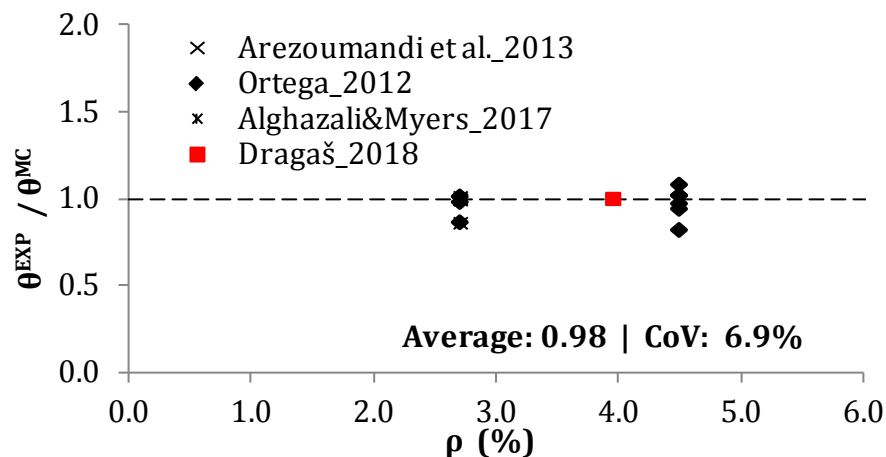


Figure 5.117 fib Model Code 2010 strut angle predictions for the OPCC beams with shear reinforcement

5. Analysis and discussion of results

5.3.3.5. Application of standards on shear test results – Reineck database

In order to further evaluate the shear strength of HVFAC beams, OPCC shear databases from literature (Reineck et al. 2013, 2014; Tošić et al. 2016) were selected and analyzed.

5.3.3.5.1. HVFAC and OPCC beams made without shear reinforcement

For beams without shear reinforcement, the database compiled by Reineck et al. (Reineck et al. 2013) was selected. Selected studies from this database included beam members tested for shear with beam width in the range from 50 to 1000 mm; beam height from 76.2 to 2000 mm; shear span-to-effective depth ratio from 2.4 to 8.1; longitudinal reinforcement ratio from 0.14% to 5.00% and the concrete compressive strength from 12.9 to 60.8 MPa. Selected OPCC results are shown in figures as "*OPCC database*". On the same diagrams selected results of HVFAC beams tested for shear are presented as "*HVFAC database*" (Alghazali and Myers 2017; Arezoumandi et al. 2013b; Arezoumandi and Volz 2013; Lisantono et al. 2017; Ortega 2012). Own experimental results are shown as "*Dragaš_2018_OPCC*" and "*Dragaš_2018_HVFAC*" for the OPCC and HVFAC beams respectively. Normalized shear stress versus the shear span-to-effective depth ratio, longitudinal reinforcement ratio, beams' effective depth and the compressive strength are shown in Figures 5.118–5.121, respectively.

It can be seen that all HVFAC beams test results fall within the main portion of the data from the OPCC database and follow the same general trend of increasing shear strength as a function of the longitudinal reinforcement ratio and decreasing shear strength as a function of the shear span-to-effective depth ratio and the beams' effective depth.

In order to further evaluate the obtained conclusions regarding HVFAC beams shear strength predictions, shear strength was calculated for all OPCC mixtures from the database using EN 1992-1-1, ACI 318 and *fib* Model Code 2010 equations for shear strength of beams without shear reinforcement.

5. Analysis and discussion of results

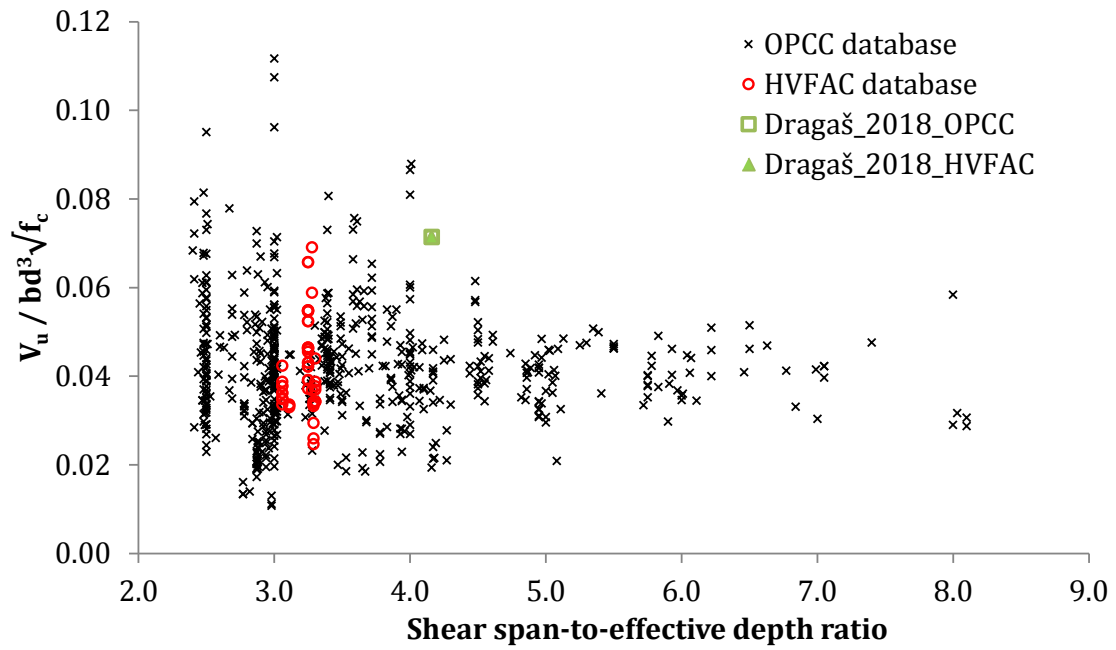


Figure 5.118 Shear strength of beams without shear reinforcement versus the shear span-to-effective depth ratio

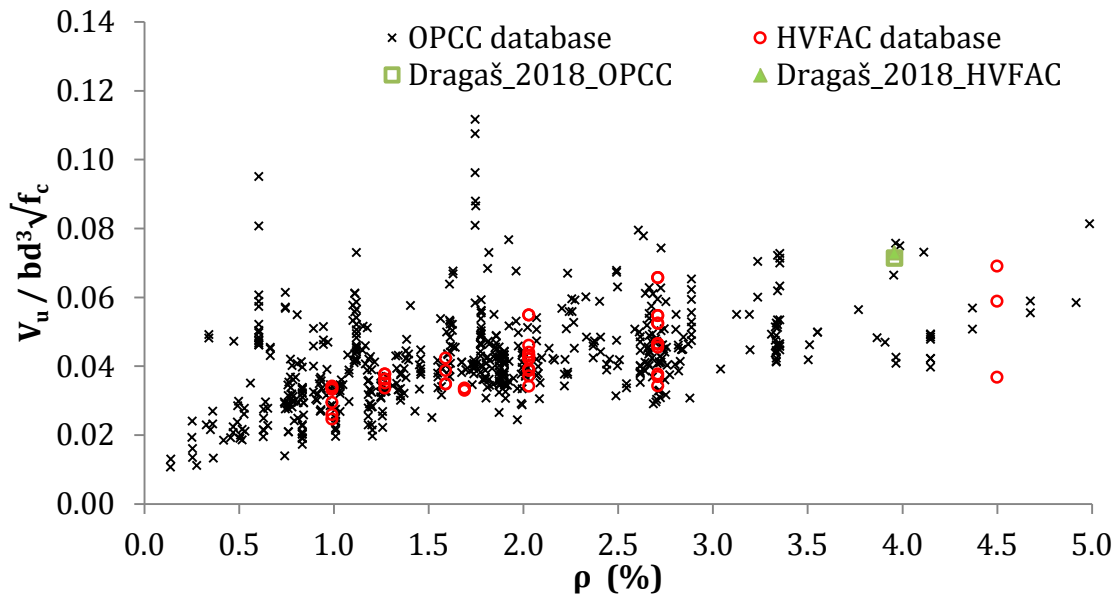


Figure 5.119 Shear strength of beams without shear reinforcement versus the longitudinal reinforcement ratio

5. Analysis and discussion of results

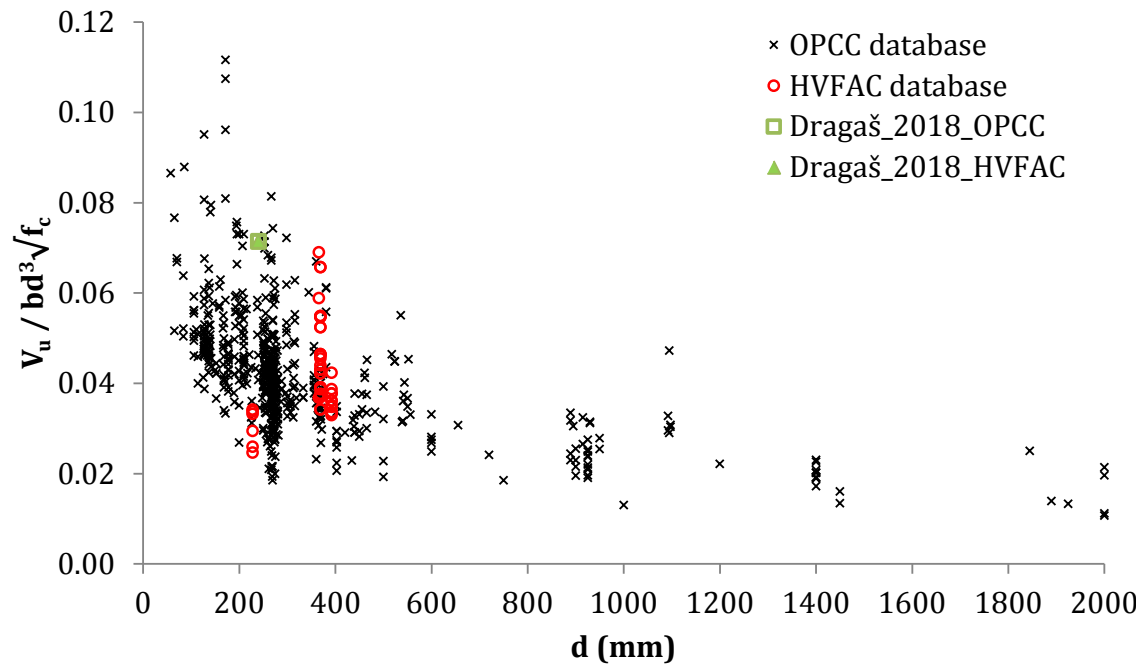


Figure 5.120 Shear strength of beams without shear reinforcement versus the beams' effective depth

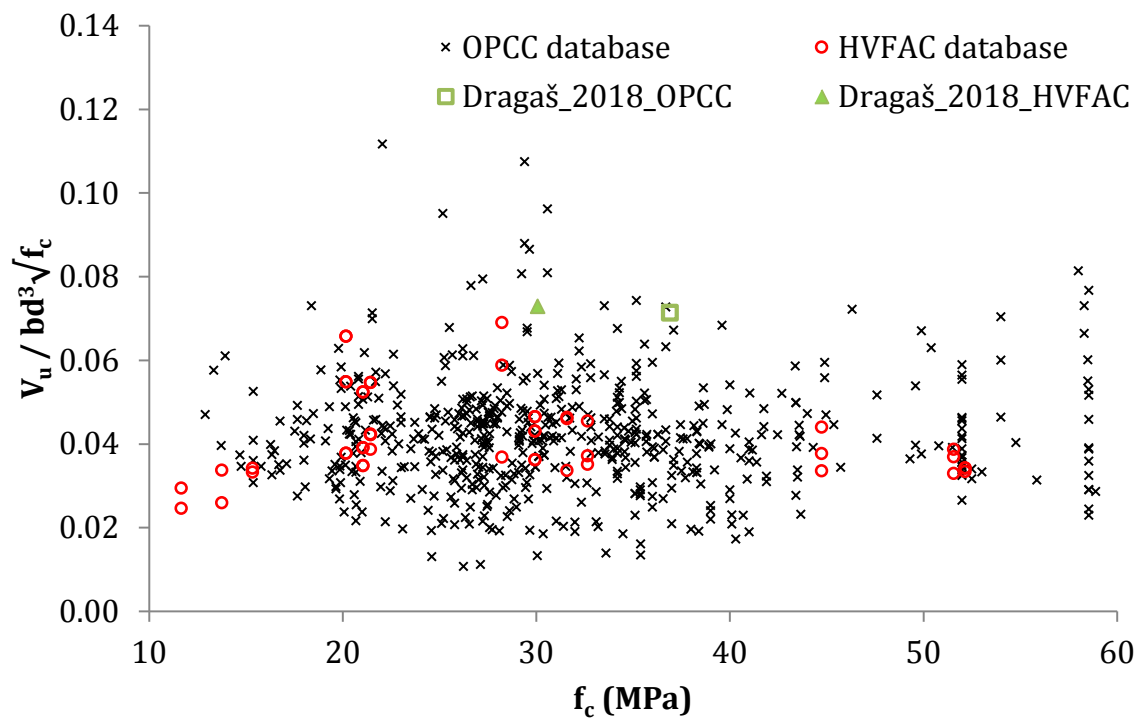


Figure 5.121 Shear strength of beams without shear reinforcement versus the concrete compressive strength

5. Analysis and discussion of results

Experimental-to-calculated shear strength ratio obtained using the EN 1992-1-1 prediction are plotted versus the shear span-to-effective depth ratio, longitudinal reinforcement ratio, beams' effective depth and the compressive strength in Figures 5.122 – 5.125.

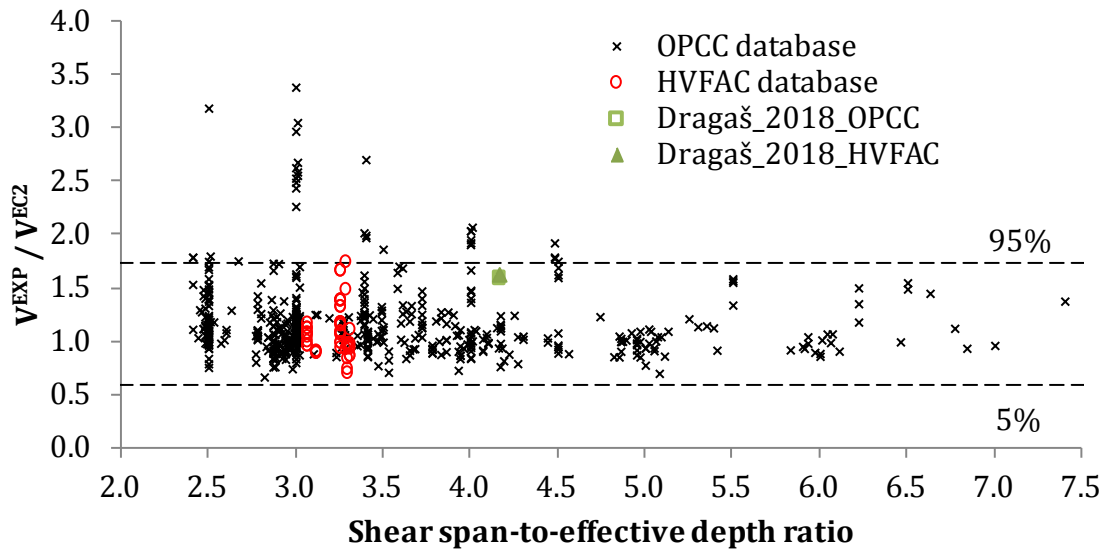


Figure 5.122 EN 1992-1-1 shear strength predictions for beams without shear reinforcement versus the shear span-to-effective depth ratio

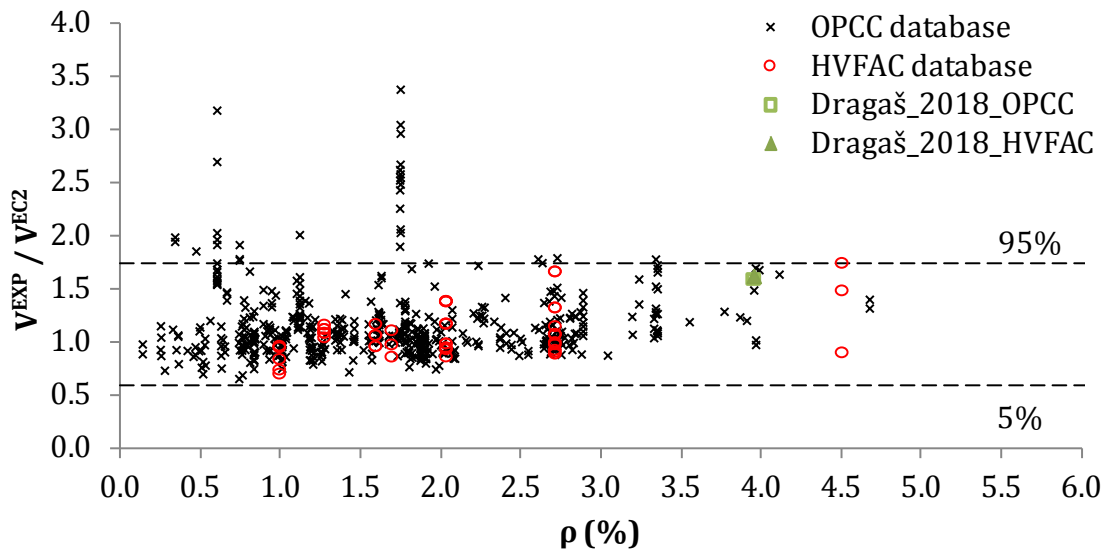


Figure 5.123 EN 1992-1-1 shear strength predictions for beams without shear reinforcement versus the longitudinal reinforcement ratio

5. Analysis and discussion of results

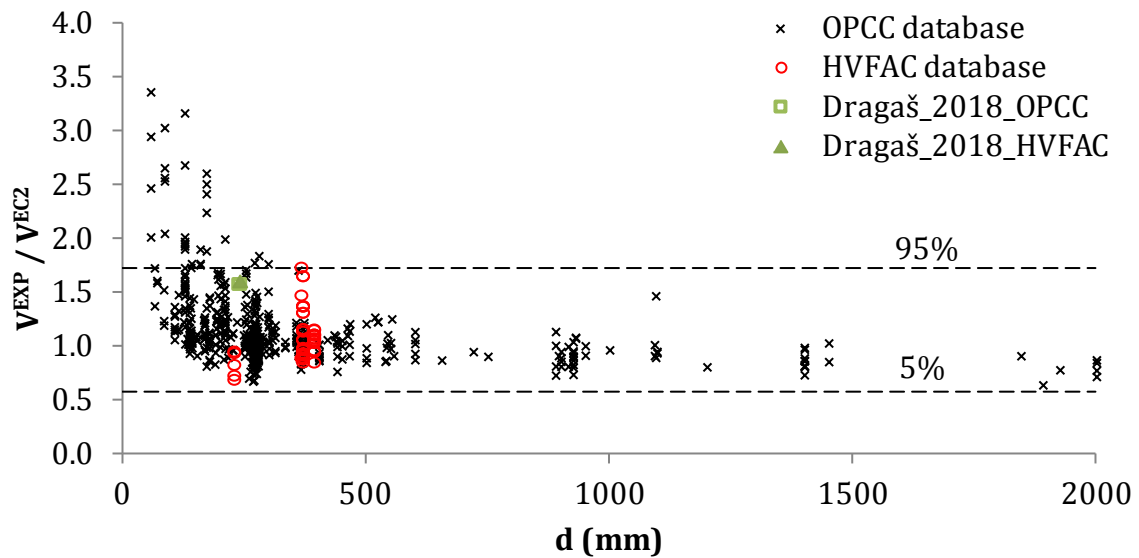


Figure 5.124 EN 1992-1-1 shear strength predictions for beams without shear reinforcement versus the beams' effective depth

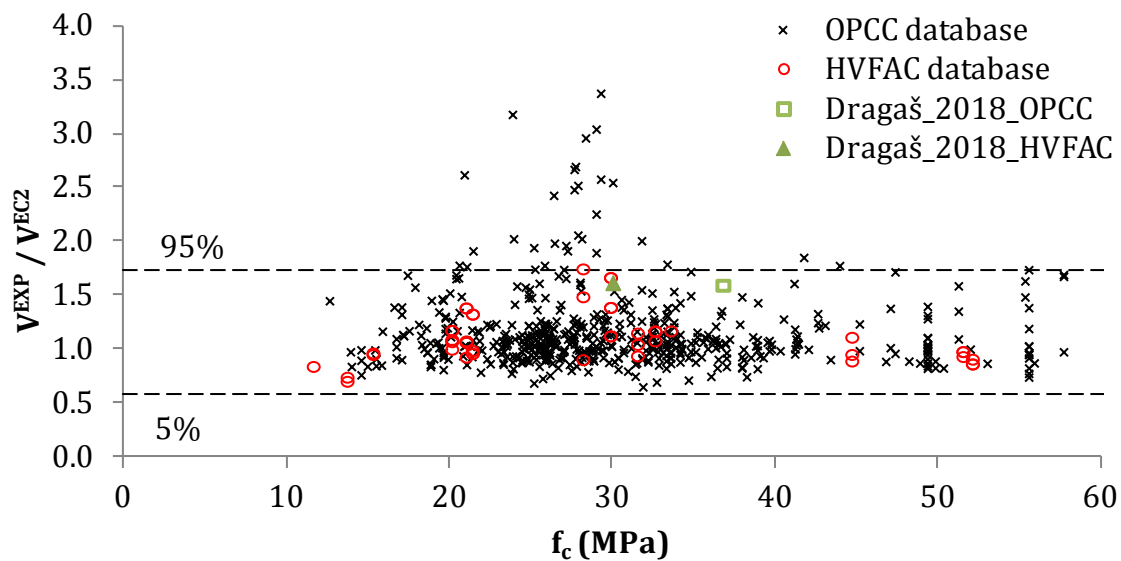


Figure 5.125 EN 1992-1-1 shear strength predictions for beams without shear reinforcement versus the compressive strength

Experimental-to-calculated shear strength using the ACI 318 prediction are plotted versus the shear span-to-effective depth ratio, longitudinal reinforcement ratio, beams' effective depth and the compressive strength in Figures 5.126–5.129, respectively.

5. Analysis and discussion of results

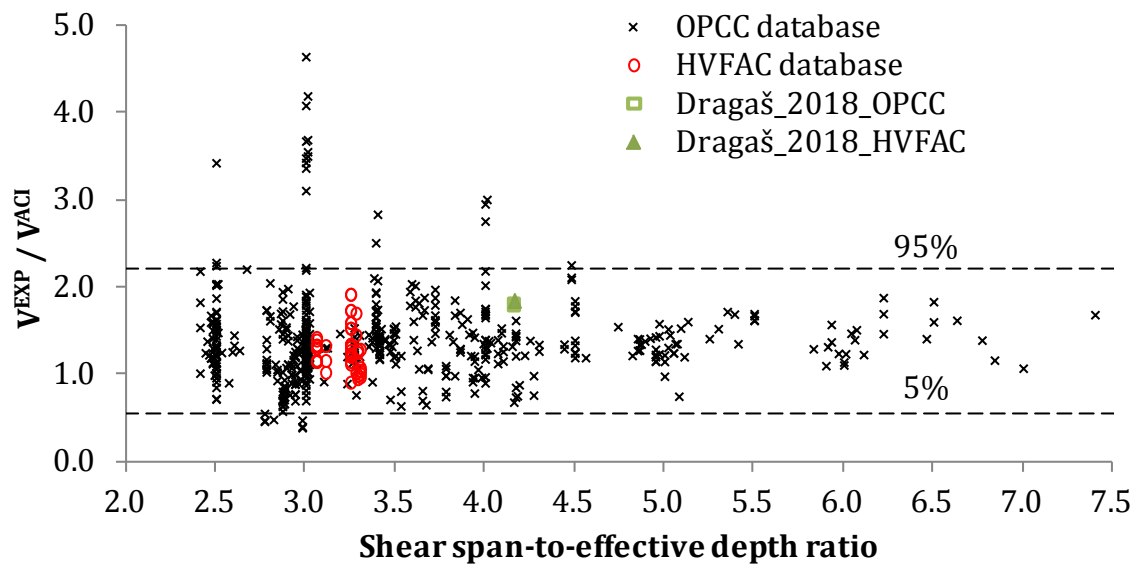


Figure 5.126 ACI 318 shear strength predictions for beams without shear reinforcement versus the shear span-to-effective depth ratio

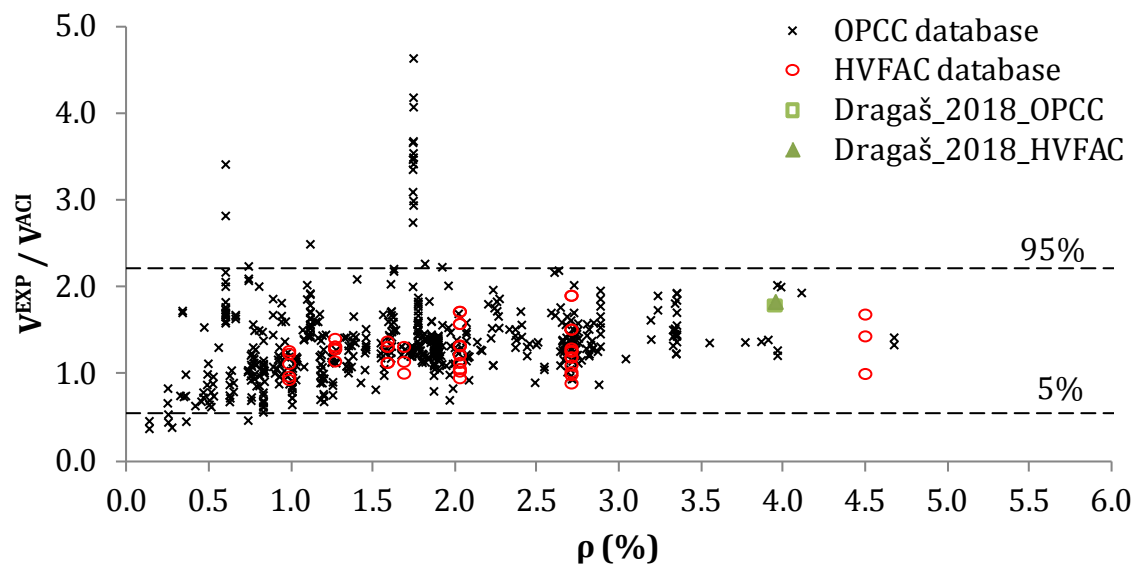


Figure 5.127 ACI 318 shear strength predictions for beams without shear reinforcement versus the longitudinal reinforcement ratio

5. Analysis and discussion of results

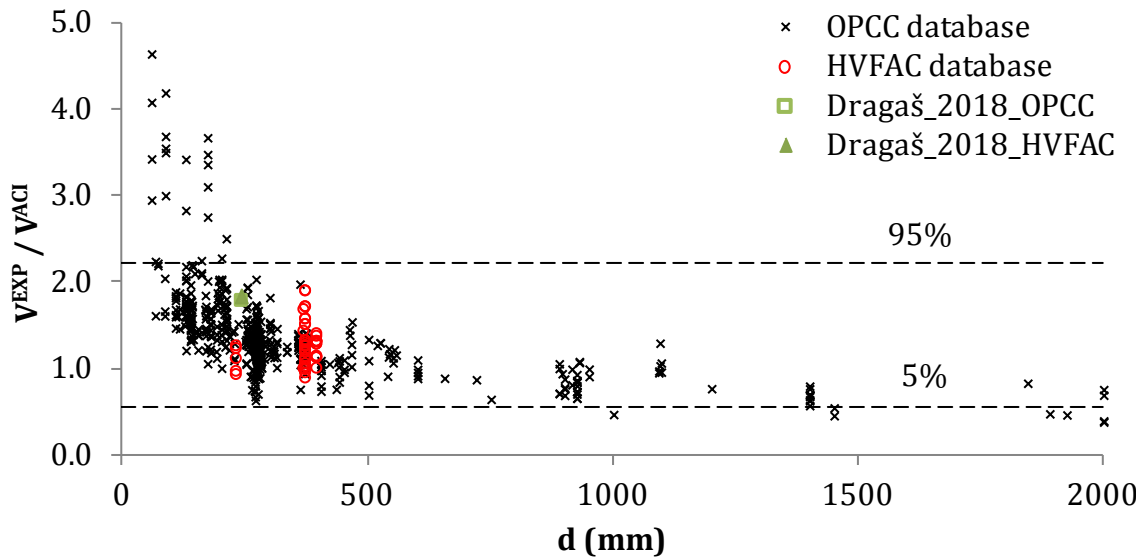


Figure 5.128 ACI 318 shear strength predictions for beams without shear reinforcement versus the beams' effective depth

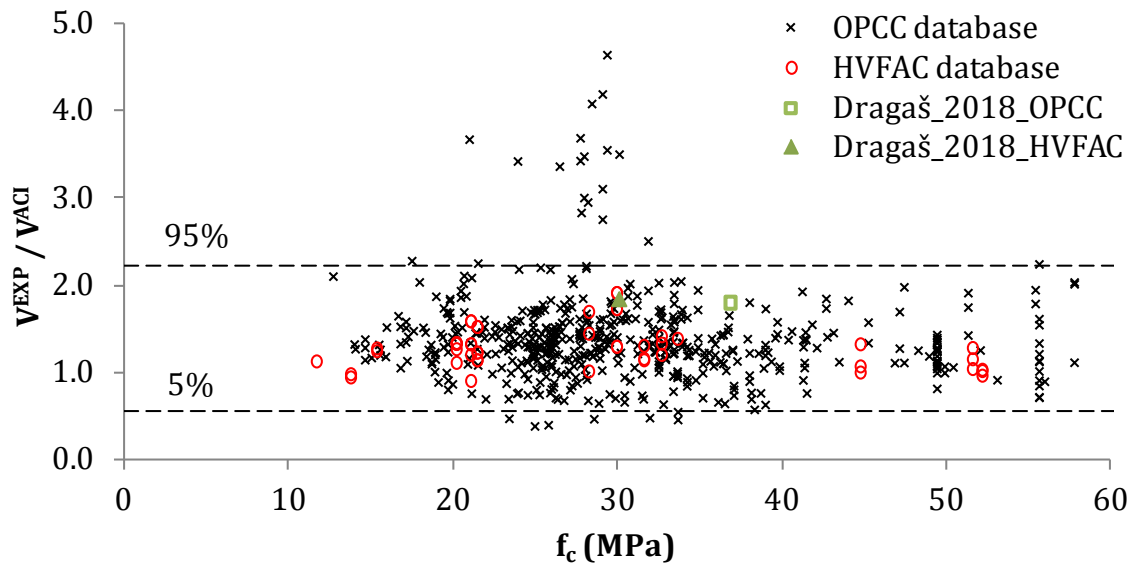


Figure 5.129 ACI 318 shear strength predictions for beams without shear reinforcement versus the compressive strength

Experimental-to-calculated shear strength using the *fib* Model Code 2010 prediction are plotted versus the shear span-to-effective depth ratio, longitudinal reinforcement ratio, beams' effective depth and the compressive strength in Figures 5.130 – 5.133, respectively.

5. Analysis and discussion of results

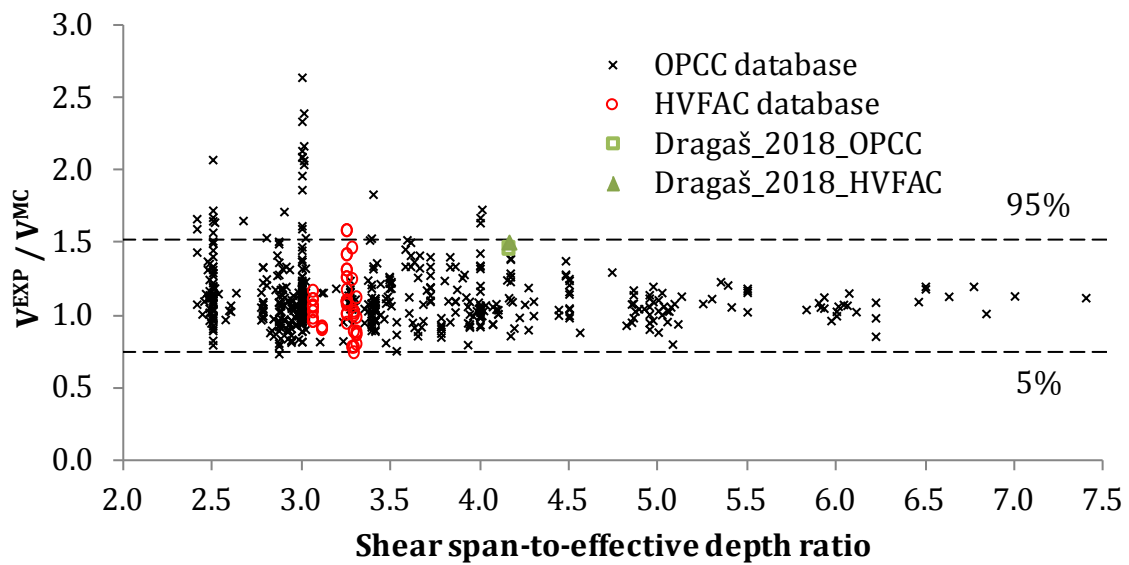


Figure 5.130 fib Model Code 2010 shear strength predictions for beams without shear reinforcement versus the shear span-to-effective depth ratio

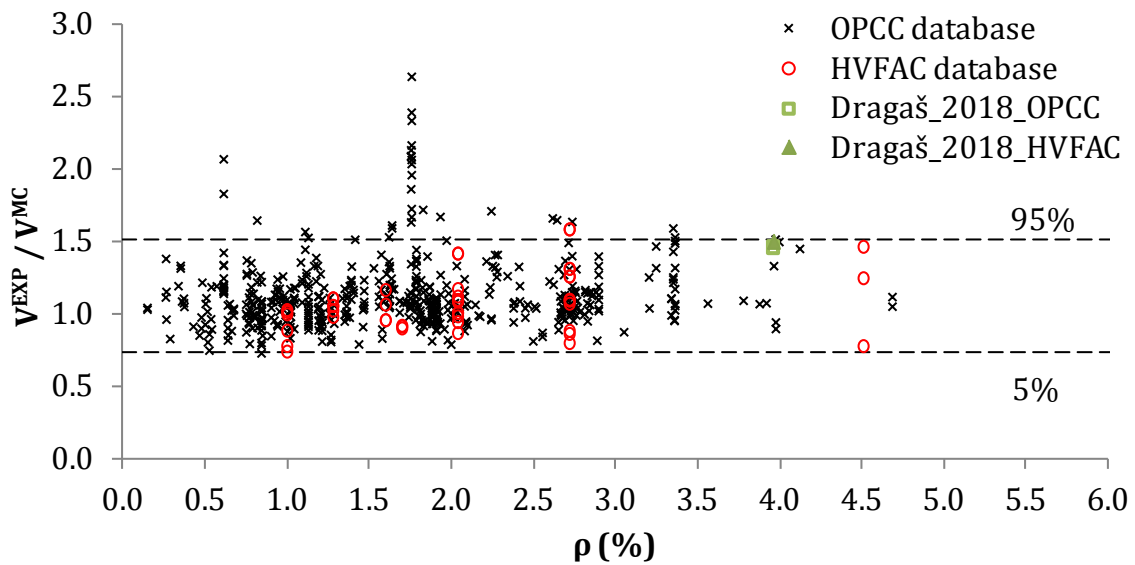


Figure 5.131 fib Model Code 2010 shear strength predictions for beams without shear reinforcement versus the longitudinal reinforcement ratio

5. Analysis and discussion of results

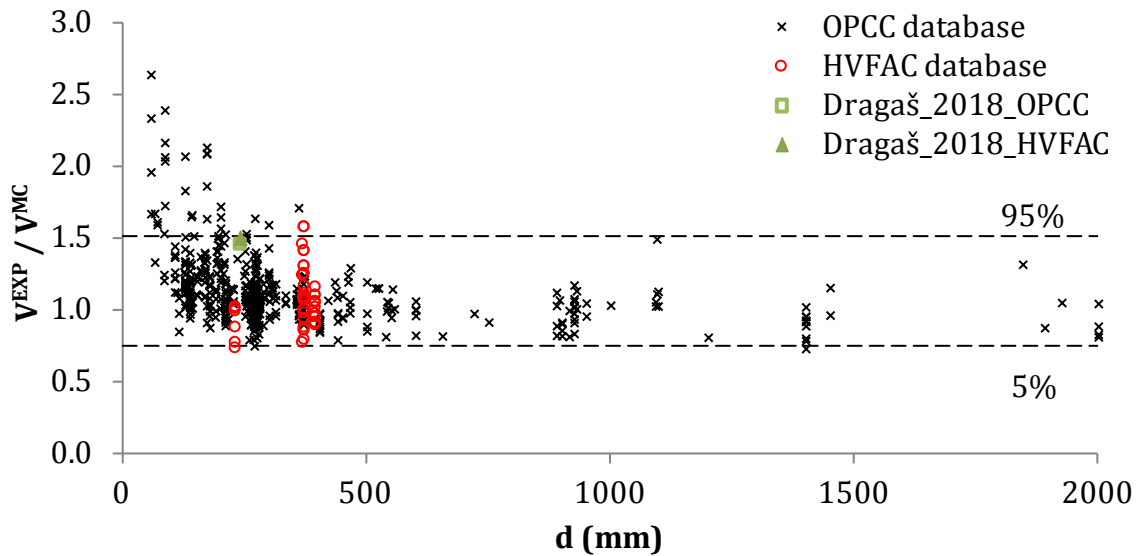


Figure 5.132 *fib Model Code 2010 shear strength predictions for beams without shear reinforcement versus the beams' effective depth*

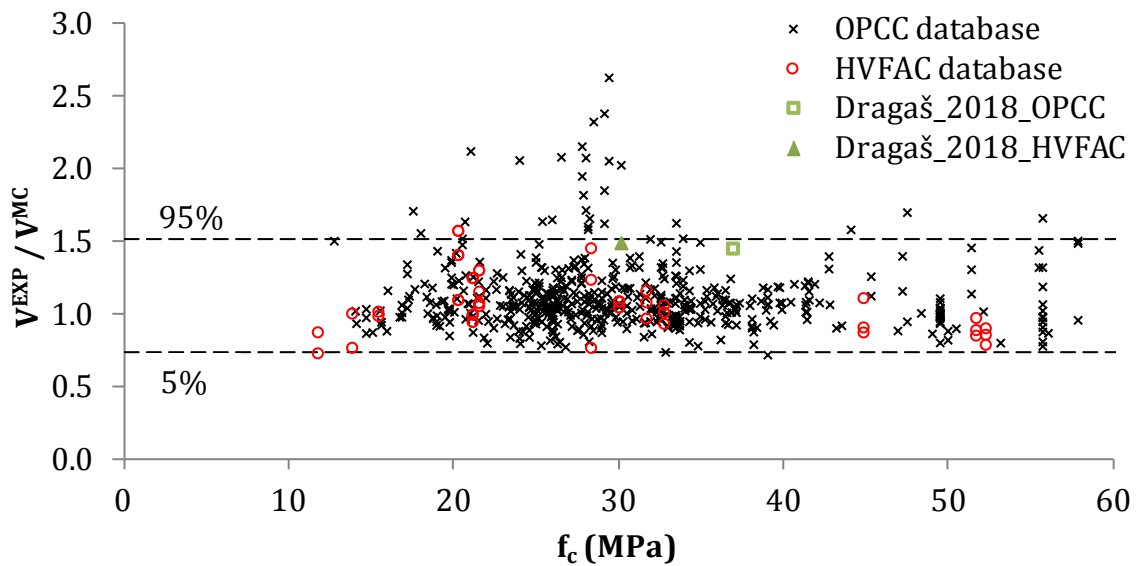


Figure 5.133 *fib Model Code 2010 shear strength predictions for beams without shear reinforcement versus the compressive strength*

It can be seen that the most of the results corresponding to HVFAC beams fell within the 5-95% confidence interval for all evaluated standards with only one result outside this interval in *fib Model Code 2010* evaluation. The average values and CoVs of the experimental-to-calculated shear strength ratios using all standards are summed up in Table 5.20. In addition to the results obtained for EN 1992-1-1, ACI 318 and *fib Model Code 2010* predictions application, results

5. Analysis and discussion of results

presented by Sigrist et al. (2013) were also used for evaluation. The presented average value and CoV refer to the experimental-to-calculated shear strength ratios obtained using *fib* Model Code 2010 LoA II on the collected OPCC beams database (Sigrist et al. 2013). It can be seen that the difference between the OPCC and HVFAC beams shear strength prediction was only up to 6% for all evaluated standards. Scattering of the results was lower for HVFAC beams compared with the OPCC beams. Similar average values for *fib* Model Code 2010 prediction were obtained in own analysis and in the analysis conducted by Sigrist et al. (2013).

Table 5.20 Experimental-to-calculated shear strength ratios for beams without shear reinforcement

	EN 1992-1-1		ACI 318		<i>fib</i> Model Code 2010		
	OPCC	HVFAC	OPCC	HVFAC	OPCC	HVFAC	OPCC*
<i>Average</i>	1.16	1.13	1.38	1.30	1.13	1.09	1.15
<i>CoV (%)</i>	30.1	21.8	36.7	19.2	20.9	18.6	10.6

**fib Model Code 2010 LoA II (Sigrist et al. 2013)*

All previously concluded indicates similar applicability of EN 1992-1-1, ACI 318 and *fib* Model Code 2010 predictions for shears strength of beams without shear reinforcement for both OPCC and HVFAC beams.

5.3.3.5.2. HVFAC and OPCC beams made with shear reinforcement

The same analysis was done for beams with stirrups using a different OPCC shear database compiled by Reineck et al. (Reineck et al. 2014; Tošić et al. 2016). The selected studies from this database included beam members tested for shear with beam width in the range from 100 to 457.2 mm; beam height from 250 to 1250 mm; shear span-to-effective depth ratio from 2.5 to 7.1; longitudinal reinforcement ratio from 0.5% to 5.0% and the concrete compressive strength from 15.7 to 61.6 MPa. Normalized shear stress versus the shear span-to-effective depth ratio, longitudinal reinforcement ratio, beams' effective depth, compressive strength and the shear reinforcement ratio (ρ_w) are shown in Figures 5.134–5.138, respectively.

5. Analysis and discussion of results

It can be seen that all HVFAC beams test results fall within the main portion of the data from the OPCC database and follow the same general trend as in OPCC beam test results.

In order to evaluate the obtained conclusions regarding shear strength predictions, EN 1992-1-1, ACI 318 and *fib* Model Code 2010 were chosen for further evaluation on the OPCC shear database. Shear strength was calculated for all OPCC mixtures from the database using the EN 1992-1-1, ACI 318 and *fib* Model Code 2010 predictions for shear strength of beams with shear reinforcement.

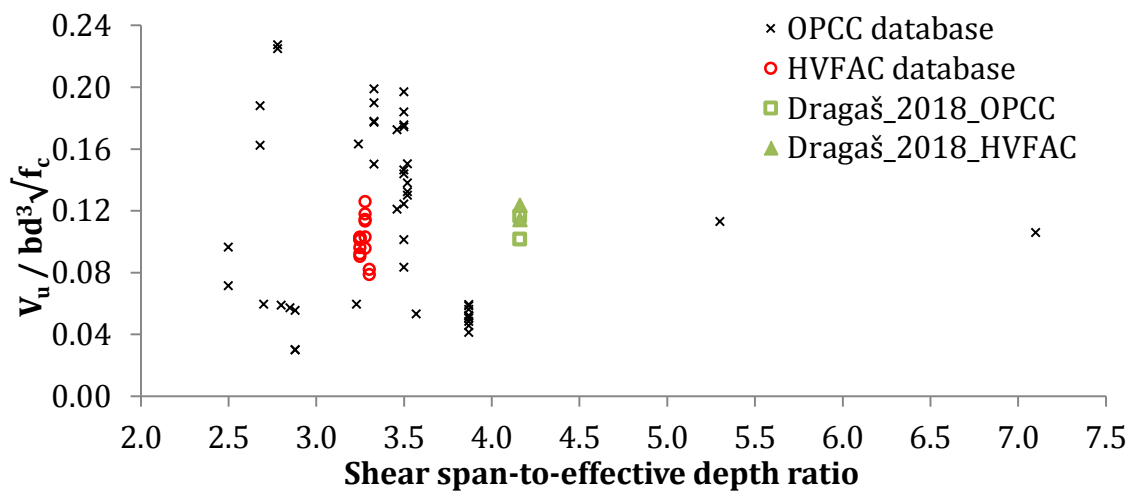


Figure 5.134 Shear strength of beams with stirrups versus the shear span-to-effective depth ratio

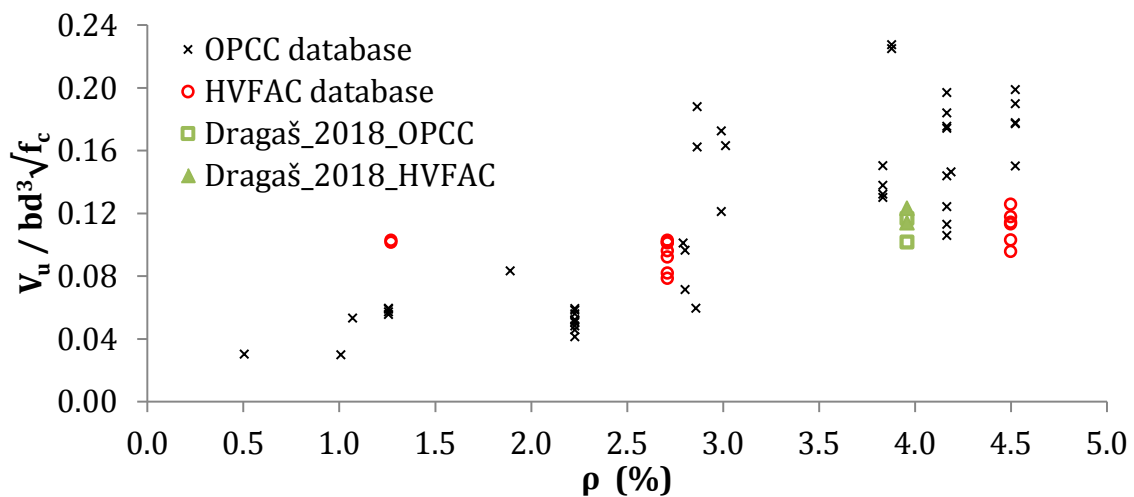


Figure 5.135 Shear strength of beams with stirrups versus the longitudinal reinforcement ratio

5. Analysis and discussion of results

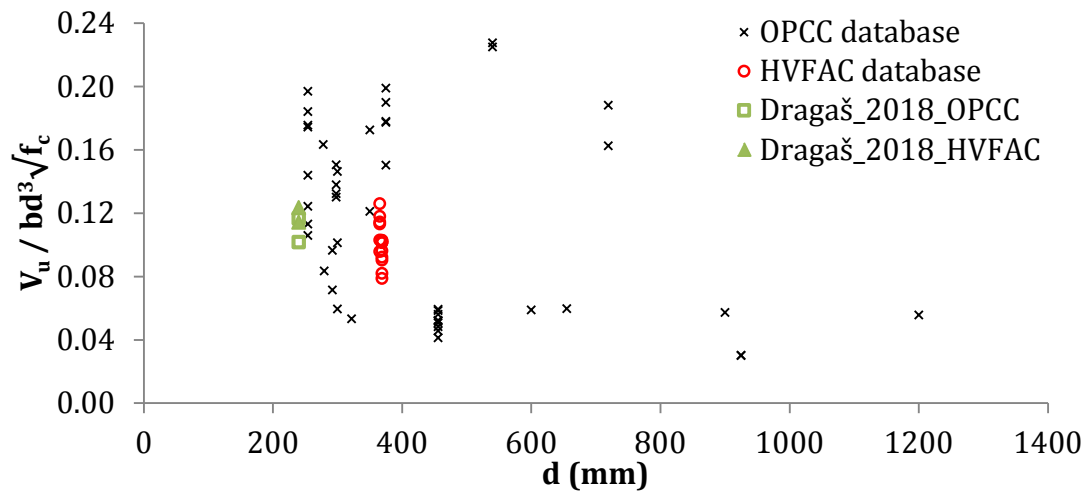


Figure 5.136 Shear strength of beams with stirrups versus the beams' effective depth

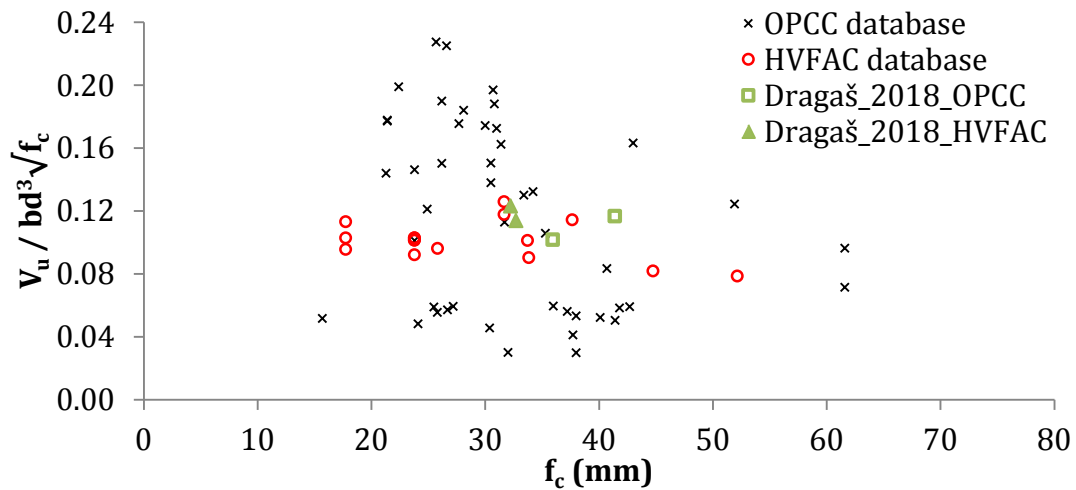


Figure 5.137 Shear strength of beams with stirrups versus concrete compressive strength

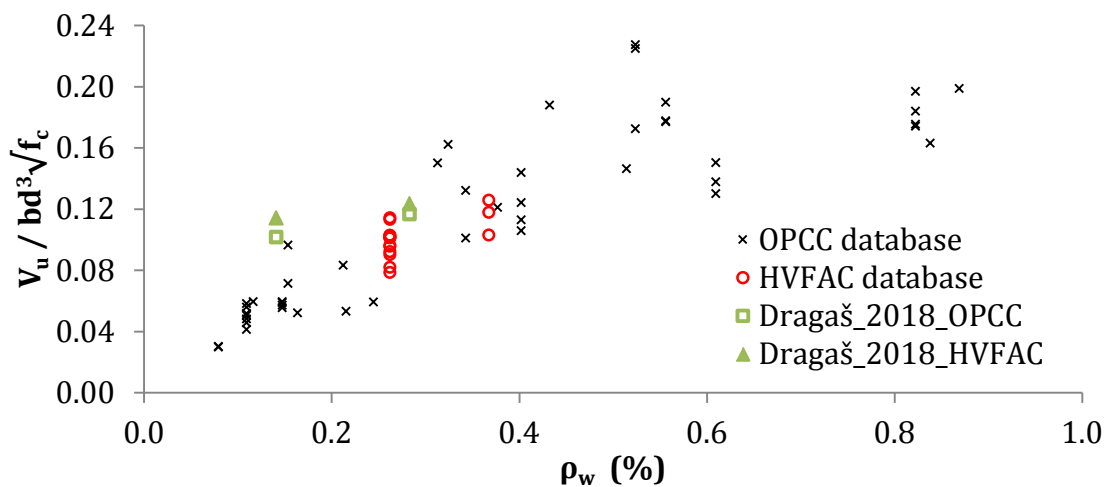


Figure 5.138. Shear strength of beams with stirrups versus the shear reinforcement ratio

5. Analysis and discussion of results

Experimental-to-calculated shear strength ratios are plotted for all standards versus the shear span-to-effective depth ratio, longitudinal reinforcement ratio, beams' effective depth, compressive strength and the shear reinforcement ratio in Figures 5.139–5.153, respectively. It can be seen that the most of the results corresponding to HVFAC beams fell within the 5-95% confidence interval for all evaluated standards with up to five OPCC and three HVFAC results outside this interval.

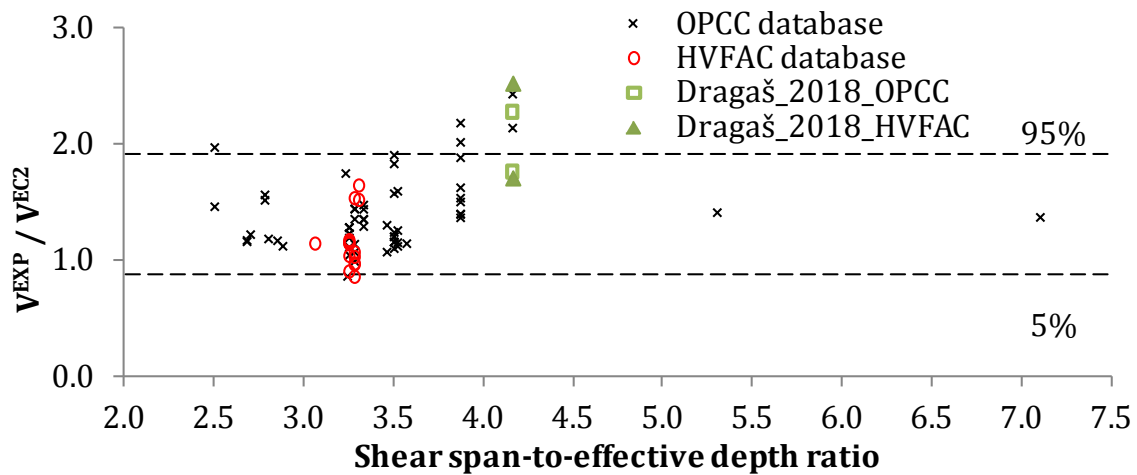


Figure 5.139 EN 1992-1-1 shear strength predictions for beams with shear reinforcement versus the shear span-to-effective depth ratio

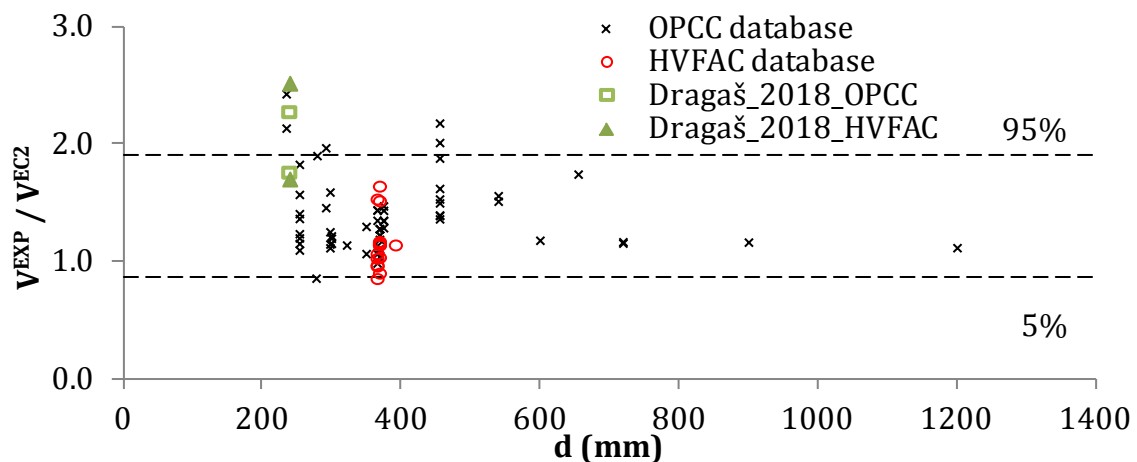


Figure 5.140 EN 1992-1-1 shear strength predictions for beams with shear reinforcement versus the beams' effective depth

5. Analysis and discussion of results

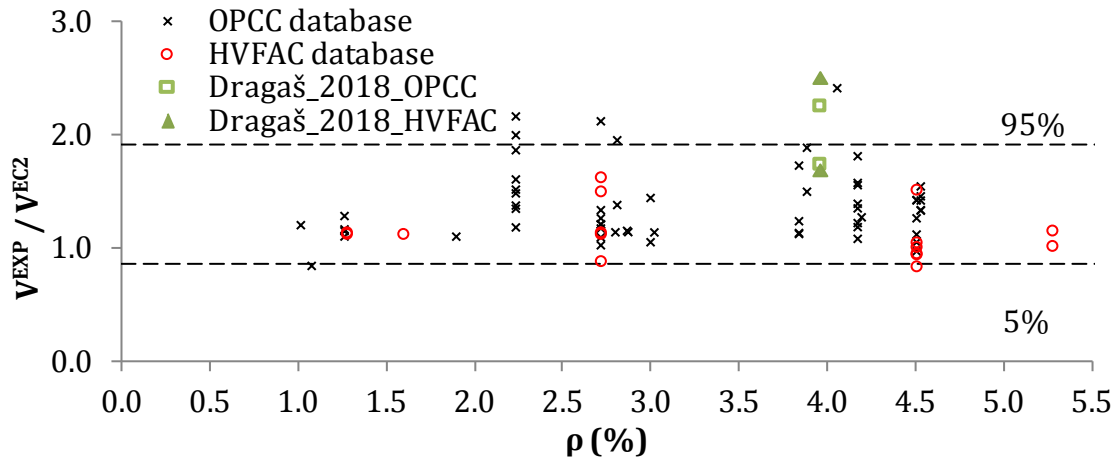


Figure 5.141 EN 1992-1-1 shear strength predictions for beams with shear reinforcement versus the longitudinal reinforcement ratio

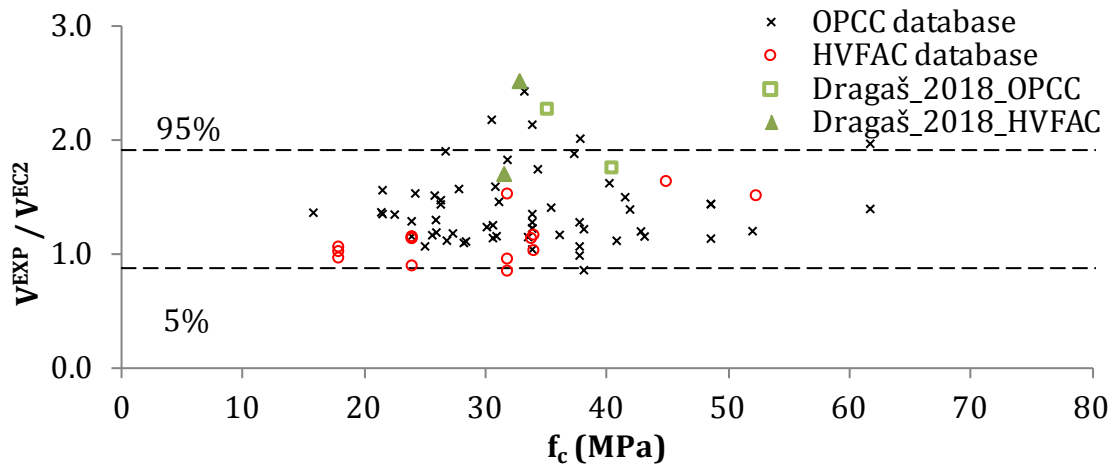


Figure 5.142 EN 1992-1-1 shear strength predictions for beams with shear reinforcement versus the compressive strength

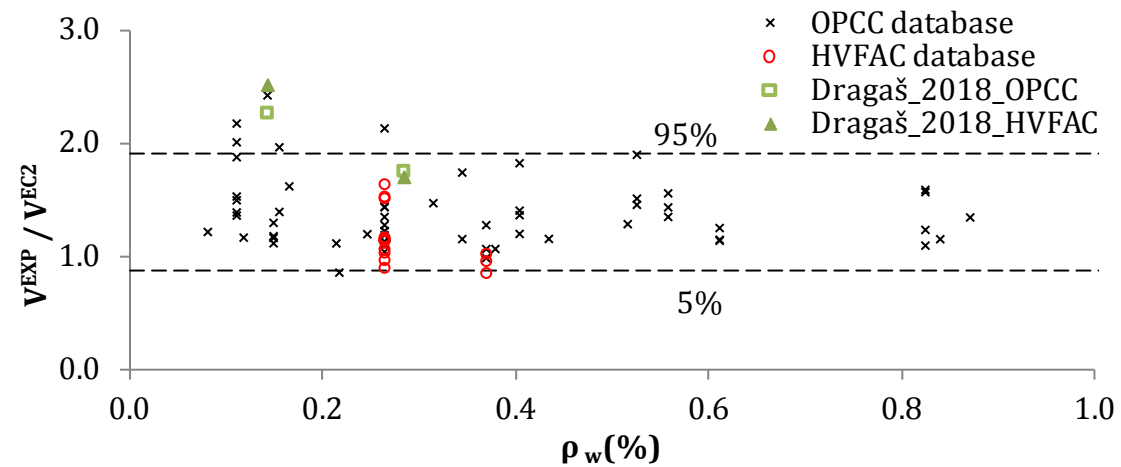


Figure 5.143 EN 1992-1-1 shear strength predictions for beams with shear reinforcement versus the shear reinforcement ratio

5. Analysis and discussion of results

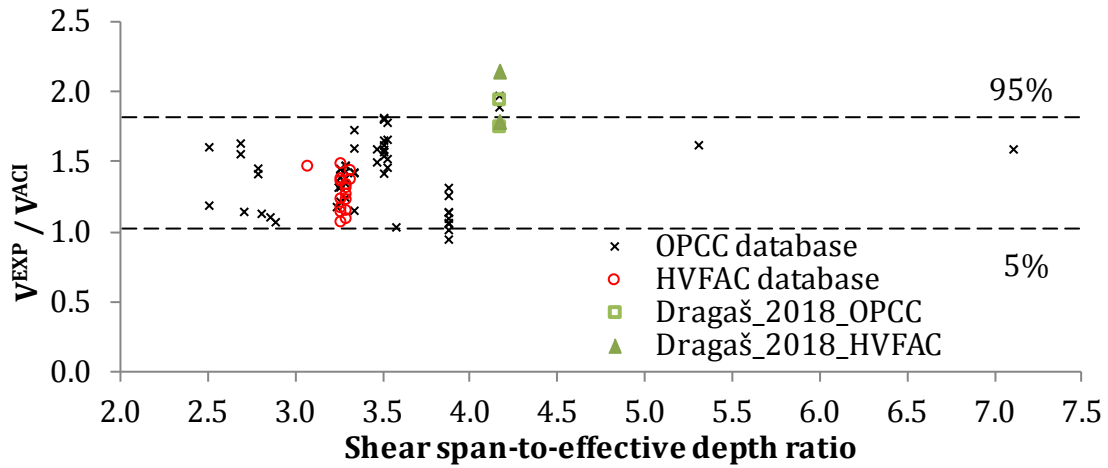


Figure 5.144 ACI 318 shear strength predictions for beams with shear reinforcement versus the shear span-to-effective depth ratio

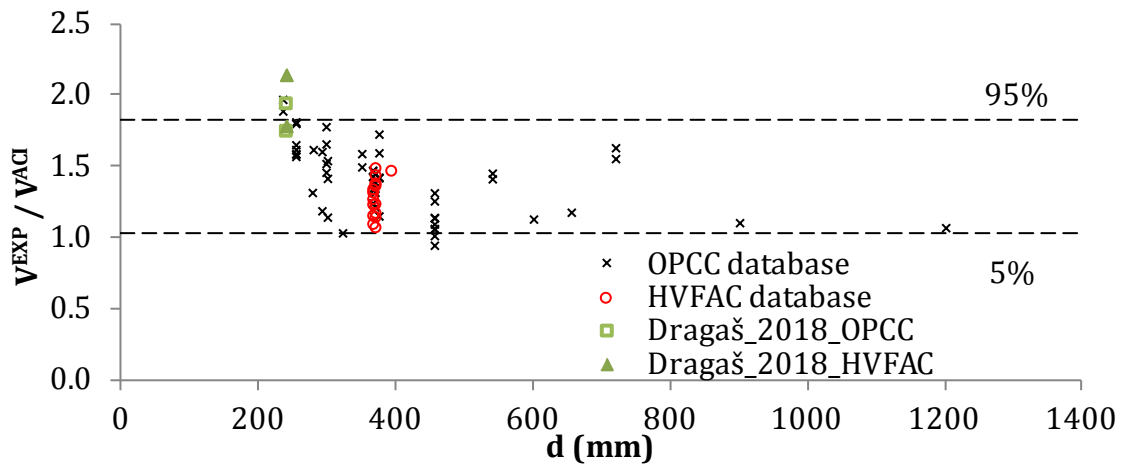


Figure 5.145 ACI 318 shear strength predictions for beams with shear reinforcement versus the beams' effective depth

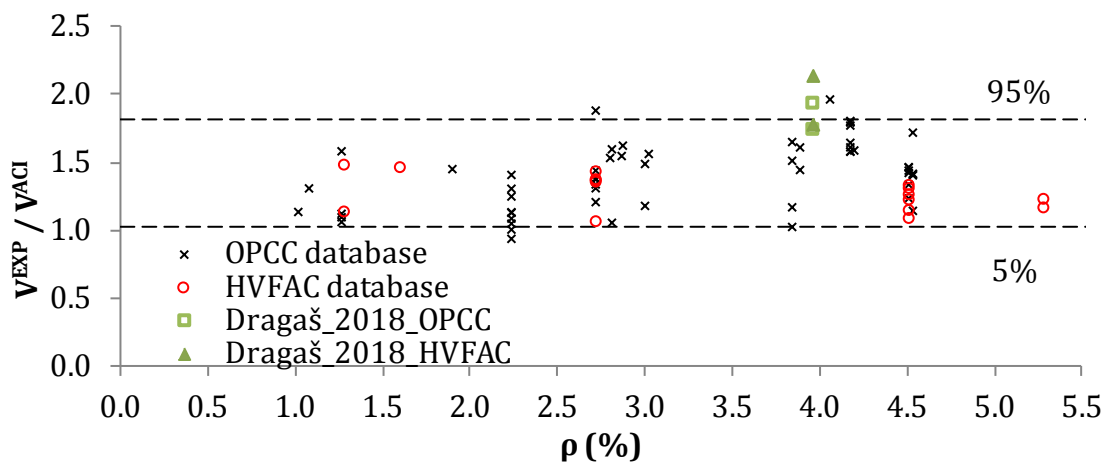


Figure 5.146 ACI 318 shear strength predictions for beams with shear reinforcement versus the longitudinal reinforcement ratio

5. Analysis and discussion of results

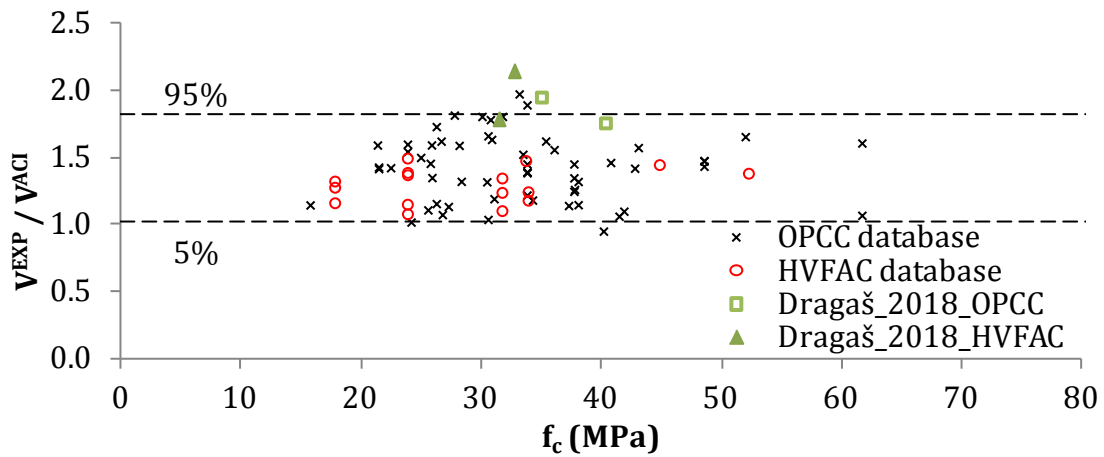


Figure 5.147 ACI 318 shear strength predictions for beams with shear reinforcement versus the compressive strength

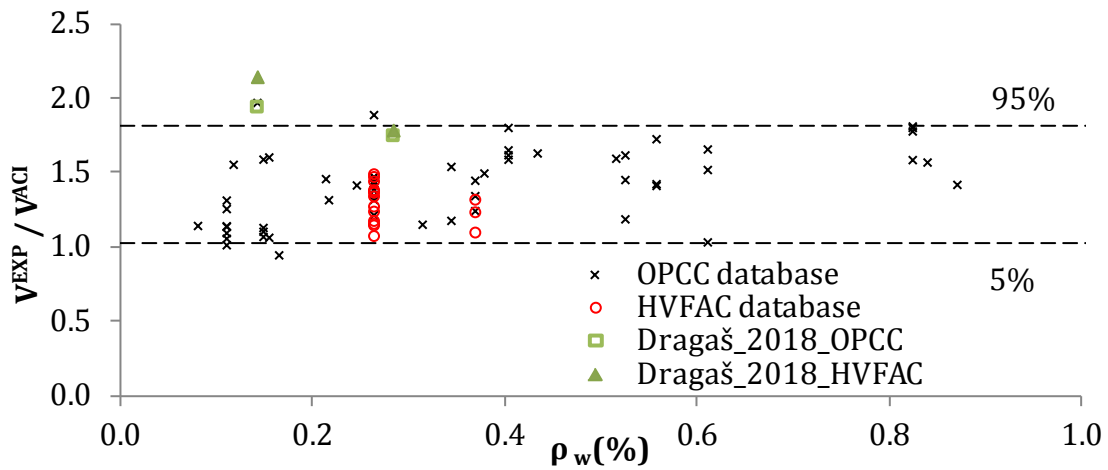


Figure 5.148 ACI 318 shear strength predictions for beams with shear reinforcement versus the shear reinforcement ratio

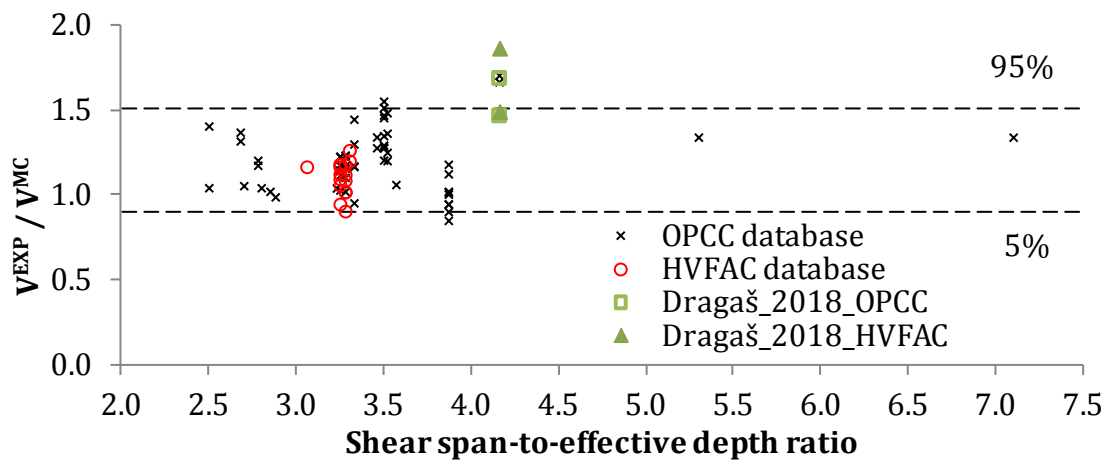


Figure 5.149 fib Model Code 2010 shear strength predictions for beams with shear reinforcement versus the shear span-to-effective depth ratio

5. Analysis and discussion of results

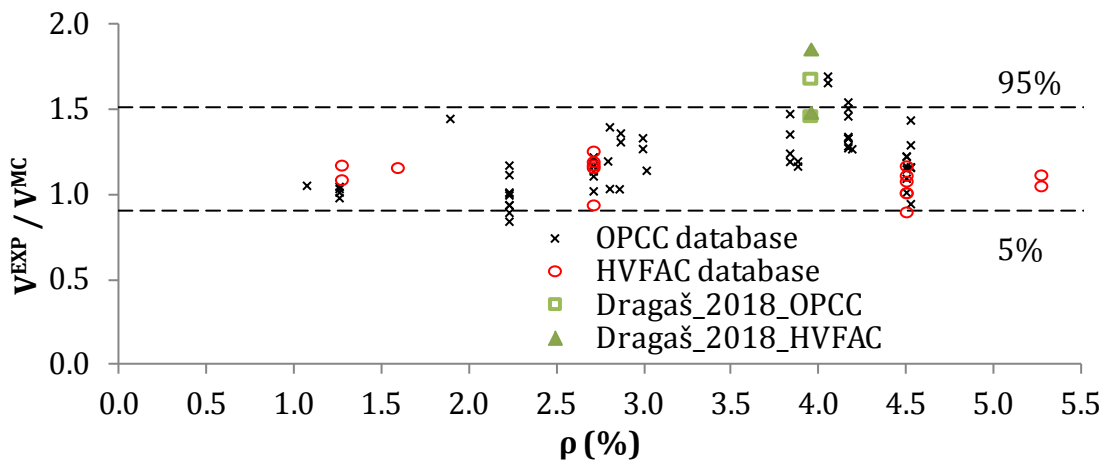


Figure 5.150 fib Model Code 2010 shear strength predictions for beams with shear reinforcement versus the longitudinal reinforcement ratio

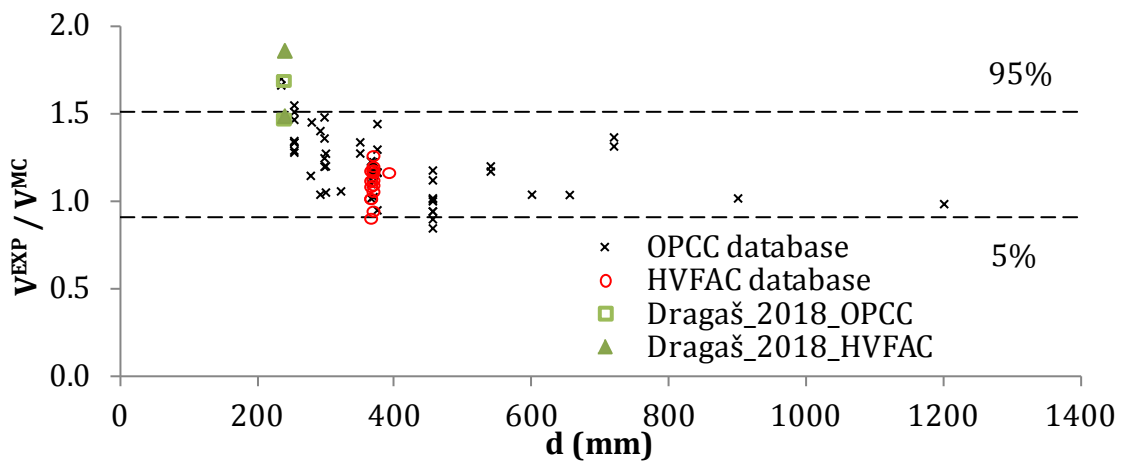


Figure 5.151 fib Model Code 2010 shear strength predictions for beams with shear reinforcement versus the beams' effective depth

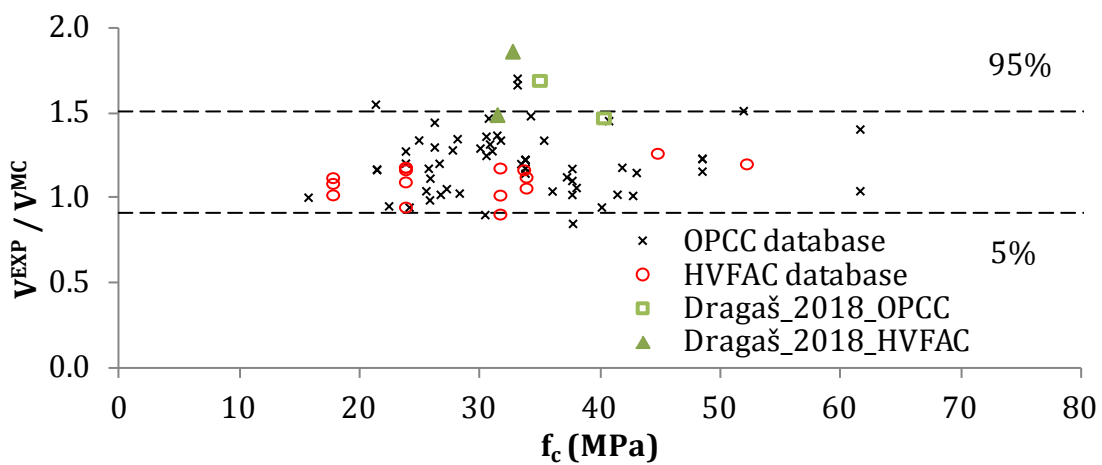


Figure 5.152 fib Model Code 2010 shear strength predictions for beams with shear reinforcement versus the compressive strength

5. Analysis and discussion of results

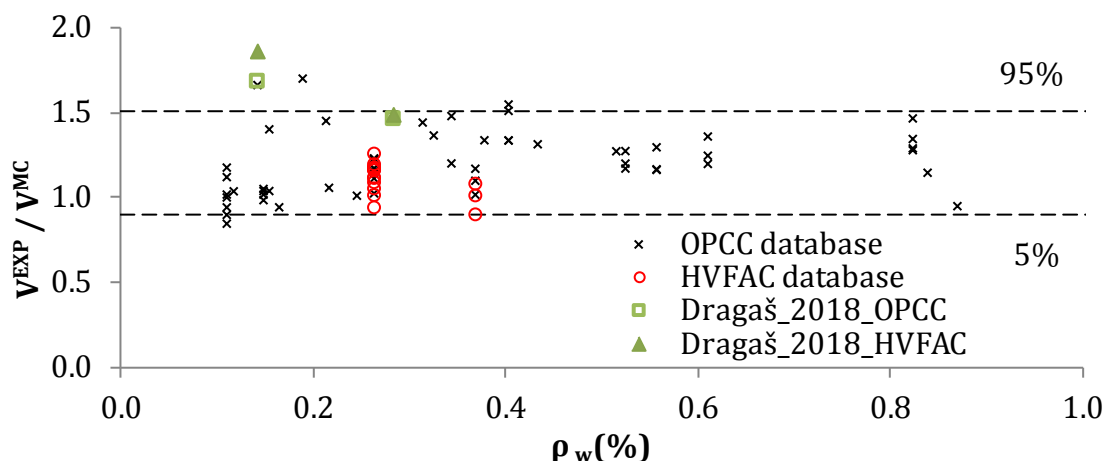


Figure 5.153 *fib Model Code 2010 shear strength predictions for beams with shear reinforcement versus the shear reinforcement ratio*

The average values and CoVs of the experimental-to-calculated shear strength ratios obtained using all standards are summed up in Table 5. 21. In addition to the results obtained for EN 1992-1-1, ACI 318 and *fib Model Code 2010* predictions application, results presented by Sigrist et al. (2013) were also used for evaluation. The presented average value and CoV refer to the experimental-to-calculated shear strength ratios obtained using *fib Model Code 2010* LoA III on the collected OPCC beams database of beams made with stirrups (Sigrist et al. 2013).

Table 5.21 *Experimental-to-calculated shear strength ratios for beams with shear reinforcement*

	EN 1992-1-1		ACI 318		fib Model Code 2010		
	OPCC	HVFAC	OPCC	HVFAC	OPCC	HVFAC	OPCC*
Average	1.39	1.26	1.42	1.37	1.21	1.17	1.20
CoV (%)	22.7	30.9	17.0	18.4	15.2	17.9	13.0

**fib Model Code 2010* LoA III (Sigrist et al. 2013)

It can be seen that the difference between OPCC and HVFAC beams predictions was up to 10%, 4% and 4% for EN 1992-1-1, ACI 318 and *fib Model Code 2010*, respectively. Scattering of the results was generally higher for HVFAC beams compared with the OPCC beams. Similar average values for *fib Model Code 2010* prediction were obtained in own analysis and in the analysis conducted by Sigrist

5. Analysis and discussion of results

et al. (2013). OPCC and HVFAC beams experimental-to-calculated shear strength ratios obtained in own experimental work fell in the upper part of the 5-95% interval except OPCC and HVFAC beams with a minimum reinforcement ratio that were higher than the 95% limit. This was noticed for all evaluated standards and in both OPCC and HVFAC beams with higher overestimation of shear strength for HVFAC beam. Previously described effect can be attributed to the low beams' effective depth and shear reinforcement ratio having in mind that it occurred in both OPCC and HVFAC beams. The difference between the OPCC and HVFAC beams experimental-to-calculated shear strength ratio was in the 10% margin for all evaluated standards indicating that the concrete type was not the main reason for the obtained results outside the 95% limit. Everything previously concluded can indicate similar applicability of EN 1992-1-1, ACI 318 and *fib* Model Code 2010 predictions for shears strength of beams with shear reinforcement for both OPCC and HVFAC beams.

5.3.4. Conclusions

A previously conducted analysis showed that the variation of HVFAC compressive strength was in the same range as for OPCC mixtures. The analysis that was conducted on own experimental results (577 different HVFAC samples) led to the conclusion that no significant differences in the compressive strength variation between HVFAC and OPCC mixtures existed. The CoV of HVFAC compressive strength test results was lower compared with a typical value of the CoV for OPCC compressive strength of 15% (Faber 2007).

After the analysis of HVFAC beams flexural behavior that was based on the HVFAC beams database collected from literature, the following conclusions can be made:

- The flexural strength of HVFAC and OPCC beams from the database was, on average, the same, with relatively small variation of the results;
- Presented results showed that the cracking moment was, on average, 5% lower for HVFAC beams compared with the OPCC beams;
- The average value of the HVFAC-to-OPCC beams' yielding moment indicated a similar behavior of HVFAC and OPCC beams;

5. Analysis and discussion of results

- The average value of the HVFAC-to-OPCC beams deflection ratio at yielding was 7% lower compared with the corresponding OPCC beams. At the same time, obtained results indicated that the ultimate deflection was on average 2% higher in HVFAC beams compared with the OPCC beams;
- The yielding-to-ultimate deflection ratio was, on average, 2% higher for HVFAC beams compared with the OPCC beams;
- Only a small number of available results regarding crack evolution in HVFAC beams were available in the literature. Based on these results, it can be concluded that the HVFAC beams developed a similar number and average spacing between cracks but larger crack widths compared with the corresponding OPCC beams;
- The maximum crack widths were 13% and 33% higher in HVFAC beams compared with the OPCC beams for the service and ultimate loading state, respectively.

Application of standards on HVFAC beams' cracking moment and flexural strength was first done based on own experimental results. After that analysis, the following conclusions can be made:

- HVFAC cracking moment predictions were similar for all evaluated standards (BAB '87, EN 1992-1-1 and ACI 318) and less conservative compared with the OPCC beams for up to 15%, on average;
- The cracking moment predictions for HVFAC beams were higher than the experimental ones for 28% on average;
- The existing models for ultimate flexural strength calculations proposed in BAB '87, EN 1992-1-1, ACI 318, and Response-2000 gave, on average, 9% and 15% higher ultimate bending moments compared with the experimental values obtained for OPCC and HVFAC beams, respectively;
- The analysis of the ultimate flexural strength results showed that the used prediction models from different standards gave more conservative results for HVFAC beams compared with the OPCC beams for up to 6%.

5. Analysis and discussion of results

Application of standards on HVFAC beams' flexural strength was also done based on the HVFAC beams database. After that analysis, the following conclusion can be made:

- Similar average values and scatter of the results for HVFAC and OPCC beams showed that there was no significant difference in the applicability of BAB '87, EN 1992-1-1 and ACI 318 standards for the prediction of HVFAC beams ultimate bending moment compared with the OPCC beams. HVFAC beams exhibited up to 2% more conservative results.

After the analysis of HVFAC beams shear behavior that was based on the HVFAC beams database collected from literature, the following conclusions can be made:

- The average value of the HVFAC-to-OPCC shear stress ratio indicated only 2% and 3% lower shear stress at failure for HVFAC beams without and with shear reinforcement, compared with the OPCC beams from the database;
- The presented results showed that the diagonal shear cracking appeared at 8% and 13% lower shear stress, on average, in HVFAC beams without and with shear reinforcement compared with the OPCC beams from the database;
- The average ductility ratio indicated a 2% less ductile behavior of HVFAC beams without shear reinforcement and 12% higher ductility for beams with shear reinforcement;
- The average value of the HVFAC-to-OPCC strut angle was 1% and 9% lower for HVFAC beams without and with shear reinforcement compared with the OPCC beams.

Application of standards of HVFAC beams' shear strength was first done based on own experimental results. After that analysis, the following conclusions can be made:

- The experimental-to-calculated shear strength ratios (BAB '87, EN 1992-1-1, ACI 318, *fib* Model Code and Response-2000) were up to 9% higher for HVFAC beams compared with the OPCC beams;
- The most precise predictions were obtained using the MCFT approach and the Response-2000 program.

5. Analysis and discussion of results

Application of standards on HVFAC beams' shear strength was done based on the HVFAC beams database. After that analysis the following conclusion can be made:

- The shear strength predictions of HVFAC beams without and with shear reinforcement were up to 4% and 5% less conservative compared with the OPCC beams;
- The ratio of the experimental-to-calculated strut angle was 2% and 5% lower for HVFAC beams without and with shear reinforcement compared with the corresponding OPCC beams.

Application of standards on HVFAC beams' shear strength was also evaluated by comparing the HVFAC beams shear strength predictions with the Reineck et al. OPCC beams shear database. After that analysis, the following conclusion can be made:

- All shear strength results from the HVFAC beams database fall within the main portion of the data from the OPCC database;
- The difference between shear strength predictions for OPCC and HVFAC beams without shear reinforcement was up to 3%, 6% and 4% for EN 1992-1-1, ACI 318 and *fib* Model Code 2010, respectively. The scattering of results was lower for HVFAC beams compared with the OPCC beams.
- It can be seen that the difference between shear strength predictions for OPCC and HVFAC beams with shear reinforcement was up to 10%, 4% and 4% for EN 1992-1-1, ACI 318 and *fib* Model Code 2010, respectively. The scattering of results was generally higher for HVFAC beams compared with the OPCC beams.

6. SUMMARY, CONCLUSIONS AND RECOMENDATIONS FOR FUTURE RESEARCH

6. Summary, conclusions and recommendations for future research

6.1. SUMMARY OF PRESENTED THESIS

HVFAC has become one of the most promising sustainable alternatives to conventional concrete. However, much research is still needed for its safe application in the construction industry as structural concrete. In order to overcome the low early age strength of HVFAC and the lack of reliable predictions for HVFAC mechanical properties as well as other questions and problems, more research is necessary. Predictions of HVFAC mechanical properties defined in adequate standards will encourage the use of HVFAC in everyday construction practice. To date, the most research considered the evaluation of HVFAC physical, mechanical and durability properties and only a limited amount of research was focused on full-scale structural elements made with HVFAC.

The main purpose of this research was to evaluate HVFAC as concrete for structural application. The first aim was to design, test and evaluate the HVFAC mixtures made with more than 50% of class F FA in CM. Suitable workability, early age strengths and 28-day compressive strength were set as the parameters for HVFAC structural evaluation. Furthermore, the intention was to evaluate the current guidelines defined for cement concrete mechanical properties and to determine their applicability to HVFAC. The second goal was to manufacture, test, and evaluate the HVFAC beams for flexural and shear behavior. The main question that was addressed in this study was how flexural and shear strength compared between HVFAC and RCC. The application of different standards defining flexural and shear strength for cement concrete was evaluated for their applicability to HVFAC beams.

This chapter contains the main findings obtained in each section of this thesis and conclusions regarding the mechanical properties of HVFAC, and the flexural and shear behavior of HVFAC beams. In the end, recommendations for future research are also presented.

6. Summary, conclusions and recommendations for future research

6.1.1. Literature review

The analysis of available results of the HVFAC mechanical properties testing found in literature showed that it is possible to make HVFAC with more than 50% of FA in CM that has similar or higher compressive strength compared with the RCC, if properly designed.

The analysis of available results regarding the bond, flexural and shear strength of HVFAC beams was also done. A clear conclusion regarding the HVFAC bond strength cannot be made based on the available research found in literature. However, based on the conclusion obtained by Wolfe (2011) and Arezoumandi et al. (2015a), it can be expected that the HVFAC with the same compressive strength will have comparable bond strength as in the RCC.

Only four research papers investigating the flexural strength of HVFAC beams were found in literature. These studies were mostly done on the HVFAC beams made with class C FA (Arezoumandi et al. 2015c) or on relatively small beam samples (Srinivas and Rao 2015; Thangaraj and Thenmozhi 2016). Only one research investigating the flexural behavior of HVFAC beams made with up to 50% of class F FA was found (Yoo et al. 2015). The authors concluded that the structural behavior of HVFAC beams was similar to that of RCC beams. The presented results did not provide enough conclusions regarding the HVFAC beams flexural crack propagation and the maximum width and length compared with the RCC beams.

More research investigating shear strength of HVFAC beams was found in literature compared with the flexural behavior. Nevertheless, this database consisted of only eight studies investigating mostly class C HVFAC beams (Alghazali and Myers 2017; Arezoumandi et al. 2013, 2015b; Arezoumandi and Volz 2013; Ortega 2012; Sadati et al. 2016). The other two studies were performed on relatively small beam samples (Rao et al. 2011) or on HVFAC and OPCC beams made with different compressive strengths (Lisantonio et al. 2017). The presented results indicated that the ultimate shear strength of the OPCC and HVFAC beams was not significantly different.

6. Summary, conclusions and recommendations for future research

Analysis done in this chapter led to the conclusion that more research regarding the flexural and shear strength of HVFAC beams made with 50% and more than 50% of class F FA in CM is necessary for its safe application in practice.

6.1.2. Testing of HVFAC physical and mechanical properties

This chapter consisted of own experimental work done in order to define the process of developing HVFAC mix design using a class F FA from one power plant in Serbia. The experimental program consisted of seventeen HVFAC and 2 OPCC mixtures.

The presented results showed that HVFAC suitable for structural use can be made with FA amount equal or higher than 50% of total CM mass. Satisfactory early age and 28-day compressive strengths were obtained with adequate workability of HVFAC mixtures. Since these requirements were met in HVFAC mixtures with different FA and CM amount, mixtures with highest FA amount fulfilling requirements of the structural testing phase were chosen for further evaluation. It was shown that concrete mixtures with 200 kg/m³ of cement, 350 kg/m³ of class F FA and up to 2% of commercially available superplasticizer could be used to produce structural grade HVFAC.

6.1.3. Testing of reinforced concrete beams' flexural behavior

To address the question of the HVFAC beams flexural behavior, an experimental program was designed to give comparative results of the HVFAC and OPCC beams flexural behavior. Two groups of beams were made and tested. The first group was made with a minimum reinforcement ratio and the second with a five times higher longitudinal reinforcement ratio. First, the mechanical properties of selected mixtures were tested on different concrete samples. The 90-day compressive strength of HVFAC and OPCC samples cured in water was different by not more than 3% but the difference was higher for specimens cured the same as beams—up to 19%. The splitting tensile strength showed similar results for both types of concrete. On the other hand, flexural tensile strength of OPCC was 24% higher compared with the HVFAC mixture.

6. Summary, conclusions and recommendations for future research

Furthermore, all beams were tested until failure and presented similar behavior in all steps until failure. The crack propagation in the beams began with the appearance of flexural cracks in the maximum moment region. The first flexural cracks appeared at lower loading levels for HVFAC beams compared with the OPCC ones: 25% lower for beams with a minimum reinforcement ratio and 16% lower for beams with a higher reinforcement ratio. Before the first flexural crack formation, all of the beams showed similar linear-elastic behavior. After the additional load was applied, the longitudinal steel yielded. With further load increase, compressed concrete crushed and the beams failed. In the beams with the minimum longitudinal reinforcement ratio, failure occurred after the crushing of concrete and braking of the longitudinal reinforcement. The difference between the OPCC and HVFAC ultimate loading levels was not significant.

The analysis of the ductility of beams showed that the HVFAC-1 beam had around 40% lower ductility compared with the OPC-1 beam and the HVFAC-2 beam 20% higher ductility compared with the OPC-2 beam.

The comparative analysis of the longitudinal reinforcement strains in the HVFAC and OPCC beams showed no significant difference between the load-strain curves of different concrete beams prior to flexural cracking. The reinforcement strains in HVFAC beams were generally higher compared with the strains in the OPCC beams after cracking. In the first group of beams, the reinforcement strains were higher in HVFAC beams for 35% and in the second group for 70% compared with the OPCC beams. Having in mind the big influence of crack vicinity to the measuring place on the reinforcement strains values, no specific conclusions can be made. The concrete compressive strains at failure were higher in HVFAC beams compared with the OPCC, but the difference was only up to 9% for all measured sections.

The maximum deflections of HVFAC beams at the service load level were higher compared with the OPCC beams, especially in the beams with a minimum reinforcement ratio. This difference decreased as the ultimate loading level approached. The analysis of load-deflection curves showed that the stiffness of the tested HVFAC beam with a minimum reinforcement ratio was lower than the

6. Summary, conclusions and recommendations for future research

stiffness of the OPCC beam, differing by not more than 11%. This difference was relatively small in beams with a higher than minimum reinforcement ratio.

The first flexural cracks appeared at 25% and 33% lower loading level for HVFAC-1 and HVFAC-2 beams compared with the corresponding OPCC beams. A higher number of flexural cracks, higher crack lengths and widths, and more cracks branching developed in HVFAC beams compared with the corresponding OPCC beams. These effects were more pronounced in the beams with the minimum longitudinal reinforcement ratio.

6.1.4. Testing of reinforced concrete beams' shear behavior

To address the concern of the shear strength of HVFAC beams compared with the OPCC, full-scale shear tests were performed on six beams. All beams in this part of the study had the same longitudinal reinforcement and different shear reinforcement ratios. The first group of beams was made without shear reinforcement in the tested shear span; the second group was made with a minimum shear reinforcement ratio; the third group of beams was made with twice the minimum shear reinforcement. First, the mechanical properties of selected mixtures were tested on different concrete samples. The 90-day compressive strength of the OPCC was 10% higher compared with the HVFAC samples cured in water. The difference was higher for specimens cured the same as beams—up to 22%. For samples cured the same like beams, the splitting tensile strength was up to 30% lower and the flexural tensile strength up to 42% lower in HVFAC mixture compared with the OPCC. The modulus of elasticity was 24% higher in the OPCC mixture for samples cured the same as the beams.

The difference between the OPCC and HVFAC ultimate shear stress levels was not significant. In beams without shear reinforcement, the crack progression began with flexural cracks occurring in the beams' maximum moment region close to the location of applied load points. As the load increased, the number of flexural cracks increased in the middle part of the beam and in the shear span. At a point of approximately 75% of the ultimate load short diagonal shear crack began to appear in the middle part of the shear region. Failure of both OPCC and HVFAC

6. Summary, conclusions and recommendations for future research

beams occurred in a brittle manner when the diagonal crack reached the loading point. Both OPCC and HVFAC beam specimens exhibited linear-elastic behavior approximately until the formation of the diagonal crack.

All beam specimens with stirrups experienced the shear failure, except the OPCC beam made with a higher than minimum shear reinforcement that failed in flexure. Flexural failure was located at the midpoint of the beam caused by the crushing of the concrete at the compression zone due to the fact that the actual concrete strength was lower than the designed strength. The behavior of beams with shear reinforcement was similar to the behavior of beams without stirrups up to the point of first shear crack formation at 50-60% of the ultimate shear load. All beams with shear reinforcement showed a significant bearing capacity after diagonal crack formation until failure. The ultimate shear stress was higher for the HVFAC beams in groups 1, 2 and 3 for 2%, 11% and 6%, respectively.

All beams with shear reinforcement showed a significant bearing capacity after the shear cracking until failure. The OPCC beams showed a more ductile behavior, except in the case of beams with a minimum shear reinforcement ratio. The difference between OPCC and HVFAC beams falls within a 10% margin.

Reinforcement strains developed in the same way for both OPC-1 and HVFAC-1 beams without shear reinforcement until the first flexural cracks appeared. After that point in all three sections, the OPC-1 beam had higher strains for the same normalized shear stress. The maximum strain values in each measured section showed that the difference between the OPC-1 and HVFAC-1 beams was in the 10% margin. Reinforcement strains developed in the same way for all four beams with shear reinforcement until flexural cracks appeared. After that point, the OPCC beams had higher strains for the same normalized shear stress with the difference being within the 20% margin. In both types of beams with shear reinforcement, a general trend is showing higher stirrups strains in the HVFAC beams compared with the OPCC ones.

Concrete compressive strains at failure were higher in OPCC beams compared with the HVFAC ones. The ultimate concrete strains ranged from 2.68‰ to 3.98‰. Concrete compressive strains at failure were higher in OPCC beams compared with

6. Summary, conclusions and recommendations for future research

the HVFAC ones. The concrete compressive strains were, on average, 12%, 19% and 31% higher in the OPC-1, OPC-2 and OPC-3 beams compared with the corresponding HVFAC beams, respectively. It was noticed that the distribution of strains along the beams height was linear with practically the same compressed concrete zone height in all beams which failed in shear.

The maximum deflection under service loading was not significantly different in OPCC and HVFAC beams for the first and the second group of beams. In beams with higher shear reinforcement, the maximum deflection was approximately 14% higher in the OPCC beam compared with the HVFAC beam. This was mostly a consequence of different failure modes of the OPC-3 and HVFAC-3 beams. No significant difference in the stiffness of HVFAC and OPCC beams was noticed. The inclination of the linear-elastic part of the deflection-stress relationship was up to 10% higher for all HVFAC beams compared with the OPCC ones.

The number and vertical length of flexural cracks were higher in HVFAC beams compared with the OPCC beams in both service and the ultimate loading state. Higher flexural and shear crack widths were also noticed in the HVFAC beams compared with the OPCC beams.

The first shear cracking appeared at similar principal stress levels in both OPCC and HVFAC beams. The shear cracking generally occurred at lower principal stress levels in the HVFAC beams that had lower modulus of elasticity compared with the OPCC beams. The development of principal strains in the shear cracking zone was similar in both types of beams before shear cracking occurred. Higher values of principal strains in the HVFAC beams were noticed after the shear crack formation. The principal stress development was also similar in both types of beams with lower difference between values obtained for OPCC and HVFAC beams due to 25% higher modulus of elasticity in the OPCC beams.

6.1.5. Analysis and discussion of results

The analysis conducted in this chapter was divided in two parts. In the first part the analysis of HVFAC material properties was done by comparing the HVFAC and OPCC mechanical properties and by analyzing the possible application of available

6. Summary, conclusions and recommendations for future research

code predications defined for OPCC on HVFAC. In the second part, the analysis of flexural and shear behavior of HVFAC beams was done.

In the first part, the database of all adequate HVFAC experimental results found in literature was made to evaluate the following relations defined for OPCC:

- Empirical equation for 28-day compressive strength determination;
- Compressive strength development over time defined in EN 1992-1-1;
- Modulus of elasticity and compressive strength relation defined in EN 1992-1-1;
- Development of modulus of elasticity over time defined in EN 1992-1-1;
- Splitting tensile strength and compressive strength relation defined in EN 1992-1-1.

The database of HVFAC mixtures consisted of 131 RCC and 432 HVFAC mixtures made with 40-75% of class F FA in CM mass. The results of compressive and splitting tensile strength and modulus of elasticity tested at different ages were collected. The most of the results from the database was obtained by testing at the age of 28 days: 541 results of compressive strength, 85 results of splitting tensile strength and 98 results of modulus of elasticity testing. The analysis of HVFAC and RCC mixtures from the database showed that the correlation between HVFAC compressive strength and W/CM ratio can be defined in the same form like in OPCC. Furthermore, it was concluded that the available empirical equations used in practice to predict OPCC 28-day compressive strength (Bolomey, Baljejev, and Feret) can be used in the HVFAC strength prediction using adequate FA efficiency (k factor) values. Modification of the k factor defined by Kuder et al. (2012) using the FA specific gravity was proposed and evaluated. The experimental-to-calculated compressive strength ratios obtained using Bolomey equation and own proposal for k factor (Eq. 5.10) was 1.02 (CoV=24%).

Available OPCC mechanical properties predictions given in 1992-1-1 were evaluated for the use in HVFAC. It was concluded that the equation defined in EN 1992-1-1 for compressive strength development can be used to predict these properties in HVFAC using modifications proposed by Yoon et al. (2014) or Chen et al. (2017). The analysis of EN 1992-1-1 predictions for calculation of modulus of elasticity and its development provided good estimation for the HVFAC if the

6. Summary, conclusions and recommendations for future research

aggregate type was taken into account. The splitting tensile strength equation given in EN 1992-1-1 can be used to predict the HVFAC splitting tensile strength with similar accuracy as in the OPCC.

The conclusions previously obtained from the HVFAC database regarding code predictions were applied on own HVFAC experimental results. Comparison with EN 206-1 and EN 1992-1-1 equations and already proposed models for HVFAC was done for ten HVFAC mixtures. In addition to the relations analyzed in the first phase of this section, evaluation of the *k-value concept* defined in the European Standard EN 206-1 (CEN 2011a) was also done on own experimental results.

Based on the analysis of own HVFAC mixtures additional conclusion that can be made is that the HVFAC compressive strength predicted with the empirical equations (Bolomey, Baljejev and Feret) using the *k-value concept* defined in EN 206-1 was significantly lower compared with experimental results. The experimentally obtained compressive strength of all HVFAC mixtures was more than 30% higher compared with predicted values with the difference increasing with increasing FA content.

The analysis of the HVFAC beams flexural and shear behavior implies the evaluation of the applicability of models proposed in different standards for OPCC on HVFAC members. During this analysis, all safety factors regarding loads, member geometry and material properties were set equal to one assuming that the variation of compressive strength of HVFAC was in the same range as for OPCC. The analysis that was conducted on own experimental results (577 different HVFAC samples) led to a conclusion that no significant differences in the compressive strength variation between HVFAC and OPCC mixtures existed. The CoV of HVFAC compressive strength test results was lower compared with a typical value of the CoV for OPCC compressive strength of 15% (Faber 2007).

The analysis of HVFAC beams' flexural and shear strength was done through the following parts:

- 1) The comparison of the flexural and shear behavior of HVFAC and OPCC beams based on the HVFAC beams database collected from literature. This analysis

6. Summary, conclusions and recommendations for future research

implied the evaluation of the following parameters: cracking moment, ultimate flexural strength, ultimate shear strength, beams' yielding moment, ductility of beams, number and average spacing of flexural cracks, maximum flexural crack width, diagonal shear cracking stress and shear crack inclination angle.

- 2) The discussion of the application of available code predictions defining flexural and shears strength of OPCC beams on HVFAC beams based on own experimental results. The application of the equations defined in BAB '87, EN 1992-1-1, ACI 318 and *fib* Model Code 2010 in designing HVFAC beams was done. The calculation of the ultimate flexural and shear strength was also done by applying the MCFT analysis using the Response-2000 program. The evaluation of the following parameters was performed: cracking moment, ultimate flexural strength, and ultimate shear strength.
- 3) The evaluation of available code predictions defining flexural and shears strength of OPCC beams was done on the HVFAC beams database made from results collected from literature. The application of the equations defined in EN 1992-1-1, ACI 318 and *fib* Model Code 2010 in designing HVFAC beams was done. The evaluation of the following parameters was performed: cracking moment, ultimate flexural strength, ultimate shear strength, and shear crack inclination angle.
- 4) The comparison of the shear strength predictions obtained using EN 1992-1-1, ACI 318 and *fib* Model Code 2010 between the HVFAC beams database and the Reineck et al. (2013, 2014) OPCC beams database.

The HVFAC beams database consisted of all available studies collected from the literature regarding HVFAC beams and their referent OPCC beams tested for flexural and shear behavior and own experimental results obtained in this study. Three groups of beams were incorporated in the HVFAC beams database: 26 beams tested for flexural behavior, 37 beams without stirrups and 16 beams with stirrups tested for shear behavior (Appendix B). The comparison between HVFAC and OPCC beam behavior was done based on the HVFAC-to-OPCC ratio determined for each evaluated property. Findings that were obtained in this part of the study are presented in the following text.

6. Summary, conclusions and recommendations for future research

- 1) The results obtained from the HVFAC beams database showed that the HVFAC-to-OPCC cracking moment ratio was in the range from 0.43 to 1.72 with, on average, 5% lower values for HVFAC beams compared with the OPCC beams. A relatively high scatter of the results was noticed (CoV=26.46%).

The results of the flexural strength ratios showed a relatively small scatter of the results (CoV=6.92%) with the HVFAC-to-OPCC ultimate bending moment values ranging from 0.84 to 1.15. The results also showed that the HVFAC and OPCC beams had, on average, the same flexural strength.

The average values of the HVFAC-to-OPCC beams' yielding moment (=0.99), deflection at yielding (=0.93) and the ductility ratio (=1.02) indicated similar behavior of HVFAC and OPCC beams. Based on the available results, similar short-term loading deflection at failure was also noticed—the average HVFAC-to-OPCC ratio was 1.02.

Only two studies from the HVFAC beams database had experimental results regarding the flexural crack development. It was shown, based on those results, that the HVFAC and OPCC beams had a similar crack number (HVFAC-to-OPCC ratio=1.01) and the average spacing between cracks (HVFAC-to-OPCC ratio =1.01) at the ultimate loading. However, the conducted analysis showed that the HVFAC beams developed flexural cracks with higher widths both at service (HVFAC-to-OPCC ratio=1.33) and the ultimate loading (HVFAC-to-OPCC ratio=1.13).

The average values of the HVFAC-to-OPCC shear strength ratios were very similar in all studies from the HVFAC beams database. The average values of the ultimate HVFAC-to-OPCC shear stress ratios were 0.98 and 0.97 for beams without and with shear reinforcement, respectively.

Not many results regarding the first shear cracking were found in the HVFAC beams database, but the available results showed that the HVFAC-to-OPCC shear cracking stress ratio was, on average, 0.92 and 0.87 for beams without and with shear reinforcement respectively. The presented results indicated

6. Summary, conclusions and recommendations for future research

that the diagonal shear cracking appeared at a lower shear stress in the HVFAC beams compared with the OPCC beams.

Another parameter defining the beams' shear behavior that was evaluated is the angle of the inclined strut. The average values of the HVFAC-to-OPCC shear crack inclination angle ratios were 0.99 and 0.91 for HVFAC beams without and with shear reinforcement, respectively.

- 2) A possible application of the available code predictions on own experimental results was evaluated next. In beams tested for flexural and shear behavior, the experimental-to-calculated cracking moment ratio varied from 0.66 to 3.15 for BAB '87, EN 1992-1-1 and ACI 318 in a similar way. The average values of the experimental-to-calculated cracking moment ratio for the HVFAC and OPCC beams were 0.85, 0.89 and 0.88 for BAB '87, EN 1992-1-1 and ACI 318, respectively. It was shown that the HVFAC cracking moment predictions were less conservative compared with the OPCC mixtures but still higher than the experimental ones.

The evaluation of the flexural strength predictions defined in different standards was done next. All evaluated standards gave similar ultimate bending moment predictions for beams with the same longitudinal reinforcement ratio for both OPCC and HVFAC beams. The experimental-to-calculated ultimate bending moment ratios calculated using BAB '87, EN 1992-1-1, ACI 318, and Response-2000 were, 1.11, 1.09, 1.10 and 1.07 for OPCC beams, and 1.16, 1.15, 1.17 and 1.11 for HVFAC beams, respectively. It was shown that the HVFAC beams flexural strength predictions were up to 6% more conservative for the HVFAC beams compared with the OPCC beams.

The evaluation of well-known predictions defining OPCC beams shear strength on HVFAC beams was done next. The experimental-to-calculated shear strength ratios obtained using BAB '87, EN 1992-1-1, ACI 318, *fib* Model Code 2010 and Response-2000 were 1.75, 1.87, 1.83, 1.54 and 1.43 for OPCC beams, and 1.89, 1.95, 1.93, 1.62 and 1.53 for HVFAC beams respectively. The predictions obtained for the HVFAC beams were up to 8% more conservative compared with the OPCC beams.

6. Summary, conclusions and recommendations for future research

- 3) The evaluation of the flexural strength code predictions was done for the second time based on the HVFAC beams database. The evaluation was done by comparing the experimental-to-calculated shear strength ratios between HVFAC beams and their referent OPCC beams from the database. The experimental-to-calculated flexural strength ratios calculated using BAB '87, EN 1992-1-1, and ACI 318, were 1.02, 1.02, and 1.04 for OPCC beams, and 1.02, 1.04, and 1.05 for HVFAC beams, respectively.

The evaluation of the shear strength code predictions was also done for the second time based on the HVFAC beams database in the same way as the flexural strength. The experimental-to-calculated shear strength ratios for beams without shear reinforcement calculated using EN 1992-1-1, ACI 318, and *fib* Model Code 2010 were 1.17, 1.34, and 1.12 for OPCC beams, and 1.13, 1.30, and 1.09 for HVFAC beams, respectively. The experimental-to-calculated shear strength ratios for beams with shear reinforcement calculated using EN 1992-1-1, ACI 318, and *fib* Model Code 2010 were 1.32, 1.44, and 1.21 for OPCC beams, and 1.26, 1.37, and 1.17 for HVFAC beams, respectively.

The shear crack angle was evaluated using the *fib* Model Code 2010 prediction. The experimental-to-calculated shear crack inclination angle for beams without and with shear reinforcement was 1.01 and 0.98 for OPCC beams, and 0.99 and 0.93 for HVFAC beams, respectively.

- 4) In order to further evaluate the shear strength of HVFAC beams Reineck et al. (2013, 2014) OPCC beams databases were selected and analyzed. It was shown that all HVFAC beams test results from the database fell within the main portion of the data from the OPCC database and followed the same general trend as in the OPCC beam test results for both beams without and with shear reinforcement. Furthermore, the EN 1992-1-1, ACI 318, and *fib* Model Code 2010 shear strength predictions were evaluated for the third time on the HVFAC beams database and the Reineck et al. (2013, 2014) OPCC beams databases for beams without and with stirrups. The experimental-to-calculated shear strength ratios for all standards are shown in Table 6.1.

6. Summary, conclusions and recommendations for future research

Table 6.1 Experimental-to-calculated shear strength ratios for the HVFAC beams database and the Reineck et al. (2013, 2014) OPCC beams databases

Experimental-to-calculated shear strength ratio	EN 1992-1-1		ACI 318		fib Model Code 2010	
	OPCC	HVFAC	OPCC	HVFAC	OPCC	HVFAC
<i>Beams without stirrups</i>	1.16	1.13	1.38	1.30	1.13	1.09
<i>Beams with stirrups</i>	1.39	1.26	1.42	1.37	1.21	1.17

The analysis showed that the most of the results regarding the HVFAC beams without shear reinforcement fell within the 5-95% confidence interval with only one result outside this interval. The scattering of the results was lower for the HVFAC beams compared with the OPCC beams. The obtained conclusions indicated similar applicability of EN 1992-1-1, ACI 318, and fib Model Code 2010 predictions for the shear strength of beams without shear reinforcement for the OPCC and HVFAC beams. The same analysis was done for beams with stirrups. It was shown that the most of the results corresponding to the HVFAC beams fell within the 5-95% confidence interval for all evaluated standards with up to five OPCC and three HVFAC results outside this interval. The scattering of the results was generally higher for the HVFAC beams compared with the OPCC beams. The OPCC and HVFAC beams experimental-to-calculated shear strength ratios obtained in own experimental work fell in the upper part of the 5-95% interval, except the OPCC and HVFAC beams with the minimum reinforcement ratios that were higher than the 95% limit. The difference between own OPCC and HVFAC beams experimental-to-calculated shear strength ratio was in the 10% margin for all evaluated standards, indicating that the concrete type was not the main reason for the obtained results outside the 95% limit. All previous conclusions indicated similar applicability of EN 1992-1-1, ACI 318 and fib Model Code 2010 predictions for shear strength of beams with shear reinforcement for OPCC and HVFAC beams. More research ought to be carried out on the HVFAC and referent OPCC beams with different shear reinforcement ratios to make more reliable conclusions.

6. Summary, conclusions and recommendations for future research

6.2. CONCLUSIONS

Based on the obtained results and conducted analyses, two general conclusions can be drawn from this research:

- 1) No significant differences between OPCC and HVFAC beam flexural and shear strengths exist.
- 2) Available code predictions defining the flexural and shear strength of OPCC structural elements can be applied in HVFAC elements design with the same accuracy.

Based on the analysis of available results from the literature regarding HVFAC physical, mechanical and structural properties, the following specific conclusions can be drawn:

- HVFAC can be defined with the same type of compressive strength and W/CM ratio relationship with needed alterations using the FA efficiency factor;
- Own proposal for FA efficiency (k factor value) as the function of FA chemical composition and its' specific gravity (Eq. 5.10) shows good correlation to the experimental results. HVFAC compressive strength can be calculated using the Bolomey equation and own proposal for k factor value. The calculated-to-experimental compressive strength ratio obtained on the HVFAC mixture database collected from literature is 1.02 with CoV of 23.8%;
- The EN 1992-1-1 equation gives good estimation for the HVFAC modulus of elasticity if the aggregate type is taken into account;
- The EN 1992-1-1 prediction provides similar accuracy of the HVFAC modulus of elasticity compared with the OPCC development over time with slightly conservative results;
- The EN 1992-1-1 equation can be used to predict the HVFAC splitting tensile strength with similar accuracy as in the OPCC.

Based on own experimental results of the HVFAC physical and mechanical properties the following specific conclusions can be drawn:

- HVFAC made with more than 50% of class F FA in total CM mass can be produced to have 3-day compressive strength higher than 20 MPa and 28-day strength higher than 40 MPa with adequate workability;

6. Summary, conclusions and recommendations for future research

- HVFAC is more sensitive to the change in superplasticizer amount compared with the OPCC;
- When 50% of cement is replaced with class F FA, the compressive strength decreases to 44% and 75% at the age of 3 days and 28 days compared with the RCC, respectively;
- The additional replacement of 30% of sand (together with 50% of cement replacement) in the HVFAC mixtures led to 7% and 13% increase in compressive strength at the age of 7 and 28 days compared with the corresponding HVFAC mixture without the additional sand replacement;
- By increasing the FA content (FA/CM ratio 50–70%), in concrete with constant cement and water mass, the HVFAC compressive strength increases by 22% on average at all tested ages, but the viscosity and effect of thixotropy of the fresh concrete also increases;
- The variation of the HVFAC compressive strength analyzed on own experimental results (CoV=6.6%) is lower compared with the typical value used as a limit for OPCC (CoV=15%). HVFAC and OPCC mixtures have comparable variation of the splitting and flexural tensile strength and modulus of elasticity with the variation of results up to 16%;

The following specific conclusions can be drawn based on own experimental work regarding the flexural behavior of OPCC and HVFAC beams:

- Tested HVFAC and OPCC beams show similar flexural behavior in all steps until failure, with similar ultimate flexural strengths differing by not more than 10%;
- No significant differences between the HVFAC and corresponding OPCC load-deflection curves exist;
- The longitudinal reinforcement strains develop in the same way for the OPCC and HVFAC beams with, on average, 40% higher values in the HVFAC beams;
- The maximum concrete strain values are, on average, 7% higher in the HVFAC beams compared with the OPCC beams;
- The distribution of strains across the cross section height is linear for all tested beams with no significant difference in the compressed concrete height between the HVFAC and OPCC beams;

6. Summary, conclusions and recommendations for future research

- At the service load level, the maximum deflection is, on average, 30% higher in the HVFAC beam compared with the OPCC beams;
- At the service load level 48% more flexural cracks develop in the HVFAC beams compared with the OPCC beams. The flexural cracks are, on average, 45% longer with 40% higher maximum crack widths in the HVFAC beams compared with the OPCC beams. The sum of all flexural cracks is, on average, 55% higher in HVFAC beams with 20% lower average crack spacing compared with the corresponding OPCC beams.

The following, specific conclusions can be drawn based on own experimental work regarding the shear behavior of the OPCC and HVFAC beams:

- HVFAC and OPCC beams tested for shear behavior show similar behavior in all steps until failure, with similar ultimate shear stresses differing by not more than 10%;
- No significant differences between the HVFAC and corresponding OPCC load-deflection curves exist;
- The longitudinal reinforcement strains develop in the same way for the OPCC and HVFAC beams, with up to 20% higher values in the OPCC beams;
- Higher shear reinforcement strains develop in the HVFAC beams compared with the OPCC beams;
- The maximum concrete strain values are, on average, 20% higher in the OPCC beams compared with the HVFAC beams;
- The distribution of strains across the cross section height is linear for all tested beams with no significant difference in the compressed concrete height between the HVFAC and OPCC beams;
- No significant difference between the OPCC and HVFAC beams deflection at the service load level can be found;
- At the service load level 20% more flexural cracks develop in the HVFAC beams compared with the OPCC beams. The flexural cracks are, on average, 30% longer with 40% higher maximum crack width in the HVFAC beams compared with the OPCC beams. The sum of all cracks at the service loading level is, on average,

6. Summary, conclusions and recommendations for future research

27% higher in HVFAC beams with 15% lower average crack spacing compared with the corresponding OPCC beams.

- No significant difference in the normalized shear stress levels at the first shear cracking exists between the OPCC and HVFAC beams.
- The development of the principal strains in the shear cracking zone is similar in both OPCC and HVFAC beams before shear cracking. Higher values of principal strains in the HVFAC beams are noticed after the shear crack formation.
- The difference between HVFAC and OPCC beams crack development is higher for beams tested for flexural behavior (C200F350 mixture with 350 kg/m³ of FA) compared with the beams tested for shear behavior (C200F200 mixture with 200 kg/m³ of FA)—28% higher number of flexural cracks, 28% higher sum of all crack widths and 14% higher maximum crack length develop in beams with higher FA amount compared with the difference existing between C200F200 and the corresponding OPCC beams.

The following, specific conclusions can be drawn regarding flexural and shear behavior of the OPCC and HVFAC beams based on the HVFAC beams database:

- No significant differences between the OPCC and HVFAC beams with regard to the ultimate bending moment exist;
- The cracking moment is, on average, 5% lower for the HVFAC beams compared with the OPCC beams;
- The shear strength results of the HVFAC and OPCC beams without and with shear reinforcement show no significant difference;
- The concrete shear cracking first appears in the HVFAC beams at 10% lower shear stress, on average, compared with the OPCC beams without and with shear reinforcement;
- The angle of the shear crack inclination in the HVFAC beams is similar to the shear crack angle in the OPCC beams without shear reinforcement and it is, on average, 9% lower in beams with shear reinforcement;
- The ductility of the HVFAC beams is, on average, 10% higher compared with the OPCC beams;

6. Summary, conclusions and recommendations for future research

- The maximum flexural crack widths are higher in the HVFAC beams compared with the OPCC beams for 13 - 33% at service and the ultimate loading level;

The following, specific conclusions can be drawn regarding the application of code predictions defined for OPCC on the HVFAC beams database:

- The HVFAC cracking moment code predictions are, on average, 15% less conservative compared with the OPCC mixtures;
- The application of BAB '87, EN 1992-1-1, and ACI 318 on the flexural strength prediction calculation shows that the available code provisions for the OPCC members can be applied for the ultimate bending moment prediction of HVFAC members with equal accuracy;
- The application of EN 1992-1-1, ACI 318, and *fib* Model Code 2010 on the shear strength prediction calculation shows no significant difference between the OPCC and HVFAC beams. The difference between the OPCC and HVFAC beams shear strength prediction is up to 6% and 9% for beams without and with shear reinforcement, respectively.
- All evaluated code provisions seem to have sensitivity to low shear reinforcement ratios and low beams' effective depth. Own experimental results for the HVFAC and OPCC beams with the minimum shear reinforcement ratios displayed the most inconsistent results when compared with the results obtained on OPCC beams from literature.

6.3. RECOMMENDATIONS FOR FUTURE RESEARCH

Based on the obtained findings and conclusions, the following recommendations for future research regarding HVFAC are presented:

- The heterogeneity of FA is still a big shortcoming disabling its greater use in HVFAC. There is a need for a more detailed categorization of FA regarding its properties influencing the physical and mechanical properties.
- Reliable predictions for the HVFAC mechanical properties incorporated in code provisions are still lacking. Their development is crucial for further HVFAC application in practice. The variability of the HVFAC material properties still

6. Summary, conclusions and recommendations for future research

requires more research to be fully determined and incorporated in code provisions.

- The durability of HVFAC has been extensively researched in the past few years. Further research is still necessary to fully understand all the deterioration mechanisms that occur in HVFAC. Only after the specific conclusions, can HVFAC be used as the sustainable alternative to the cement concrete.
- More research regarding the long-term behavior of HVFAC is needed to provide the specific conclusions regarding the HVFAC creep and shrinkage influence on the RC elements long-term deflection.
- No research regarding pre-stressed HVFAC can be found in available literature. Low early-age strength is one of the reasons for this lack of testing. However, promising results regarding the use of low water amounts and various super-plasticizers in HVFAC yielded the possibility to obtain satisfactory early-age strengths.
- Based on the available results found in literature, no specific conclusions can be made regarding the HVFAC short-term deflection and crack development. More research analyzing crack widths and the energy needed for their development is needed.
- More research regarding the HVFAC tension softening and tension stiffening is needed in order to provide the full understating of the HVFAC RC elements behavior under the flexural and shear loading. Furthermore, the HVFAC compression softening is also a parameter that needs additional research to be fully defined.
- The stress-strain relationship in HVFAC is one of the fundamental parameters that require more research in order to establish the HVFAC as the structural concrete.
- More research is still lacking in order to define the specific conclusions regarding the reinforcement bond strength in HVFAC.
- The current conclusions regarding the flexural and shear behavior of HVFAC beams are made on a small sample of available results. More research with the variation of different parameters influencing the flexural and shear behavior of is necessary in order to obtain reliable conclusions.

REFERENCES

References

- Abrams, D., 1918. Design of Concrete Mixures. Chicago.
- ACI, 2014. ACI Committee 232.3R-14: Report on High-Volume Fly Ash Concrete for Structural Applications. Farmington Hills, Michigan, USA.
- ACI, 2013. ACI Committee E-701: Education Bulletin E3-013 - Cementitious Materials for Concrete. Farmington Hills, Michigan, USA.
- ACI, 2008. ACI 318-08: Building Code Requirements for Structural Concrete. Farmington Hills, Michigan, USA. [https://doi.org/10.1016/0262-5075\(85\)90032-6](https://doi.org/10.1016/0262-5075(85)90032-6)
- ACI, 2002. ACI Committee 232.3R-96: Use of Fly Ash in Concrete. Farmington Hills, Michigan, USA.
- ACI, 2000. ACI Committee 116R-00: Cement and Concrete Terminology. Farmington Hills, Michigan, USA.
- ACI-ASCE 445, 1998. Recent Approaches to Shear design of Structural Concrete, Journal of Structural Engineering. [https://doi.org/10.1061/\(ASCE\)0733-9445\(1998\)124:12\(1375\)](https://doi.org/10.1061/(ASCE)0733-9445(1998)124:12(1375))
- ACI Committee 318, 2014. Building Code Requirements for Structural Concrete and Commentary ACI 318-14.
- Aggarwal, Y., Siddique, R., 2014. Microstructure and properties of concrete using bottom ash and waste foundry sand as partial replacement of fine aggregates. Constr. Build. Mater. 54, 210–223.
- Alaka, H.A., Oyedele, L.O., 2016. High volume fly ash concrete: The practical impact of using superabundant dose of high range water reducer. J. Build. Eng. 8, 81–90. <https://doi.org/10.1016/j.job.2016.09.008>
- Alghazali, H.H., Myers, J.J., 2017. Shear behavior of full-scale high volume fly ash-self consolidating concrete (HVFA-SCC) beams. Constr. Build. Mater. 157, 161–171. <https://doi.org/10.1016/j.conbuildmat.2017.09.061>
- Antiohos, S.K., Papadakis, V.G., Tsimas, S., 2014. Rice husk ash (RHA) effectiveness in cement and concrete as a function of reactive silica and fineness. Cem. Concr. Res. 61–62, 20–27. <https://doi.org/10.1016/j.cemconres.2014.04.001>

References

- Antiohos, S.K., Tsimas, S., 2006. Reactive silica of fly ash as an indicator for the mechanical performance of blended cements, in: Maria S. Konsta-Gdoutos (Ed.), *Measuring, Monitoring and Modeling Concrete Properties - An International Symposium Dedicated to Professor Surendra P. Shah*. Springer, Dordrecht, Northwestern University, U.S.A., pp. 403–409.
- Aponte, D.F., Barra, M., Vázquez, E., 2012. Durability and cementing efficiency of fly ash in concretes. *Constr. Build. Mater.* 30, 537–546.
- Arezoumandi, M., Looney, T.J., Volz, J.S., 2015a. Effect of fly ash replacement level on the bond strength of reinforcing steel in concrete beams. *J. Clean. Prod.* 87, 745–751. <https://doi.org/10.1016/j.jclepro.2014.10.078>
- Arezoumandi, M., Ortega, C. a., Volz, J.S., 2015b. Flexural Behavior of High-Volume Fly Ash Concrete Beams. *Transp. Res. Rec. J. Transp. Res. Board* 2508, 22–30. <https://doi.org/10.3141/2508-03>
- Arezoumandi, M., Ph, D., Asce, M., Volz, J.S., Ortega, C.A., Myers, J.J., Asce, F., 2015c. Shear Behavior of High-Volume Fly Ash Concrete versus Conventional Concrete : Experimental Study. *J. Struct. Eng.* 141, 1–11.
- Arezoumandi, M., Smith, A., Volz, J.S., Khayat, K.H., 2015d. An experimental study on flexural strength of reinforced concrete beams with 100% recycled concrete aggregate. *Eng. Struct.* 88, 154–162.
- Arezoumandi, M., Smith, A., Volz, J.S., Khayat, K.H., 2014. An experimental study on shear strength of reinforced concrete beams with 100% recycled concrete aggregate. *Constr. Build. Mater.* 53, 612–620.
- Arezoumandi, M., Volz, J.S., 2014. Shear Strength of Chemically Based Self-Consolidating Concrete Beams: Fracture Mechanics Approach versus Modified Compression Field Theory. *J. Mater. Civ. Eng.* 26, 713–720.
- Arezoumandi, M., Volz, J.S., 2013a. Effect of fly ash replacement level on the fracture behavior of concrete. *Front. Struct. Civ. Eng.* 7, 411–418. <https://doi.org/10.1007/s11709-013-0228-4>
- Arezoumandi, M., Volz, J.S., 2013b. Effect of fly ash replacement level on the shear

References

- strength of high-volume fly ash concrete beams. *J. Clean. Prod.* 59, 120–130.
<https://doi.org/10.1016/j.jclepro.2013.06.043>
- Arezoumandi, M., Volz, J.S., Ortega, C.A., 2013a. Effect of High-Volume Fly Ash on Shear Strength of Concrete Beams. *Adv. Civ. Eng. Mater.* 2, 20120052.
<https://doi.org/10.1520/ACEM20120052>
- Arezoumandi, M., Volz, J.S., Ortega, C.A., 2013b. Effect of Fly Ash on the Shear Strength of Concrete Beams Without Shear Reinforcement. *Adv. Civ. Eng. Mater.* 2, 20120052. <https://doi.org/10.1520/ACEM20120052>
- Arezoumandi, M., Volz, J.S., Ortega, C.A., Myers, J.J., 2013c. Effect of total cementitious content on shear strength of high-volume fly ash concrete beams. *Mater. Des.* 46, 301–309.
- Arezoumandi, M., Wolfe, M.H., Volz, J.S., 2013d. A comparative study of the bond strength of reinforcing steel in high-volume fly ash concrete and conventional concrete. *Constr. Build. Mater.* 40, 919–924.
- Arvaniti, E.C., Juenger, M.C.G., Bernal, S.A., Duchesne, J., Courard, L., Leroy, S., Provis, J.L., Klemm, A., De Belie, N., 2015. Physical characterization methods for supplementary cementitious materials. *Mater. Struct.* 48, 3675–3686.
<https://doi.org/10.1617/s11527-014-0430-4>
- Arvaniti, E.C., Juenger, M.C.G., Bernal, S.A., Duchesne, J., Courard, L., Leroy, S., Provis, J.L., Klemm, A., De Belie, N., 2014. Determination of particle size , surface area , and shape of supplementary cementitious materials by different techniques. *Mater. Struct.* 48, 3687–3701. <https://doi.org/10.1617/s11527-014-0431-3>
- ASCE-ACI Committee 426, 1973. The shear strength of reinforced concrete members. *ASCE Journal of the Structural Division*, 99(6), pp.1091–1187.
- ASTM, 2017. ASTM C150/C150M - 17: Standard Specification for Portland Cement. West Conshohocken, Pennsylvania.
- ASTM, 2014. ASTM C595/C595M-14: Standard Specification for Blended Hydraulic Cements. West Conshohocken, Pennsylvania.

References

- ASTM, 2010. ASTM: Standard Specification for Coal Fly Ash and Raw or Calcined Natural Pozzolan for Use. Annu. B. ASTM Stand. 3–6. West Conshohocken, Pennsylvania.
- ASTM C204, 2016. Standard Test Methods for Fineness of Hydraulic Cement by Air-Permeability Apparatus. West Conshohocken, Pennsylvania.
- ASTM C618, 2015. Standard Specification for Coal Fly Ash and Raw or Calcined Natural Pozzolan for Use in Concrete. West Conshohocken, Pennsylvania.
- Atis, C.D., 2005. Strength properties of high-volume fly ash roller compacted and workable concrete, and influence of curing condition. *Cem. Concr. Res.* 35, 1112–1121. <https://doi.org/10.1016/j.cemconres.2004.07.037>
- Atis, C.D., 2003a. High-Volume Fly Ash Concrete with High Strength and Low Drying Shrinkage. *J. Mater. Civ. Eng.* 15, 153–156.
- Atis, C.D., 2003b. Accelerated carbonation and testing of concrete made with fly ash. *Constr. Build. Mater.* 17, 147–152.
- Atis, C.D., 2002. Heat evolution of high-volume fly ash concrete. *Cem. Concr. Res.* 32, 751–756. [https://doi.org/10.1016/S0008-8846\(01\)00755-4](https://doi.org/10.1016/S0008-8846(01)00755-4)
- Aubert, J.E., Husson, B., Vaquier, A., 2004. Use of municipal solid waste incineration fly ash in concrete. *Cem. Concr. Res.* 34, 957–963.
- Babu, K.G., 1995. Efficiency of silica fume in concrete. *Cem. Concr. Res.* 25, 1273–1283.
- Babu, K.G., Kumar, V.S.R., 2000. Efficiency of GGBS in concrete. *Cem. Concr. Res.* 30, 1031–1036.
- Babu, K.G., Rao, G.S.N., 1996. Efficiency of fly ash in concrete with age. *Cem. Concr. Res.* 26, 465–474.
- Babu, K.G., Rao, G.S.N., 1994. Early strength behaviour of fly ash concretes. *Cem. Concr. Res.* 24, 277–284.
- Babu, K.G., Rao, G.S.N., 1993. Efficiency of fly ash in concrete. *Cem. Concr. Compos.* 15, 223–229.

References

- Balakrishnan, B., Awal, A.S.M.A., 2014. Durability Properties of Concrete Containing High Volume Malaysian Fly Ash. *Int. J. Res. Eng. Technol.* 3, 529–533.
- Bamforth, P., Chisholm, D., Gibbs, J., Harrison, T., 2008. Properties of Concrete for use in Eurocode 2, A cement and concrete industry publication.
- Bapat, J., 2013. Mineral Admixtures in Cement and Concrete. Teylor and Fransis Group.
- Barazzetti, L., Scaioni, M., 2010. Development and implementation of image-based algorithms for measurement of deformations in material testing. *Sensors* 10, 7469–7495. <https://doi.org/10.3390/s100807469>
- Bažant, Z.P., Kim, J.K., Pfeiffer, P.A., 1986. Nonlinear fracture properties from size effect tests. *ASCE J. Struct. Eng.* 112, 289–307.
- Bažant, Z.P., Yu, Q., 2005. Designing Against Size Effect on Shear Strength of Reinforced Concrete Beams Without Stirrups: II. Verification. *J. Struct. Eng.* 131, 1886–1897.
- Bentz, D.P., Ferraris, C.F., Galler, M.A., Hansen, A.S., Gynn, J.M., 2012. Influence of particle size distributions on yield stress and viscosity of cement-fly ash pastes. *Cem. Concr. Res.* 42, 404–409.
- Bentz, E.C., 2000. Sectional analysis of reinforced concrete members. University of Toronto.
- Bentz, E.C., Vecchio, F.J., Collins, M.P., 2006. Simplified modified compression field theory for calculating shear strength of reinforced concrete elements. *ACI Struct. J.* 103, 614–624. <https://doi.org/10.14359/16438>
- Berndt, M.L., 2009. Properties of sustainable concrete containing fly ash, slag and recycled concrete aggregate. *Constr. Build. Mater.* 23, 2606–2613. <https://doi.org/10.1016/j.conbuildmat.2009.02.011>
- Bilodeau, A., Malhotra, V.M., 2000a. High-volume fly ash system: Concrete solution for sustainable development. *ACI Struct. J.* 97, 41–48.
- Bilodeau, A., Malhotra, V.M., 2000b. High-Volume Fly Ash System: Concrete Solution for Sustainable Development. *ACI Mater. J.* 41–47.

References

- Bingöl, A.F., Tohumcu, I., 2013. Effects of different curing regimes on the compressive strength properties of self compacting concrete incorporating fly ash and silica fume. *Mater. Des.* 51, 12–18.
- Blaber, J., Adair, B., Antoniou, A., 2015. Ncorr: Open-Source 2D Digital Image Correlation Matlab Software. *Exp. Mech.* 55, 1105–1122.
- Bolomey, J., 1935. Granulation et prévision de la résistance probable des bétons. *Bull. Tech. la Suisse Rom.* 62, 73–78.
- Borges, P.H.R., Costa, J.O., Milestone, N.B., Lynsdale, C.J., Streatfield, R.E., 2010. Carbonation of CH and C-S-H in composite cement pastes containing high amounts of BFS. *Cem. Concr. Res.* 40, 284–292.
- Bortz, B.S., 2008. Salt-scaling Durability of Fly Ash Concrete. Thesis. Kansas State University.
- Bouzoubaâ, N., Fournier, B., 2003. Optimization of fly ash content in concrete Part I: Non-air-entrained concrete made without superplasticizer. *Cem. Concr. Res.* 33, 1029–1037. [https://doi.org/10.1016/S0008-8846\(03\)00004-8](https://doi.org/10.1016/S0008-8846(03)00004-8)
- Bouzoubaâ, N., Fournier, B., 2003. Current Situation of SCMs in Canada, in: *Materials Technology Laboratory Report. MTL/CANMET*, p. 55.
- Bouzoubaa, N., Lachemi, M., 2001. Self-compacting concrete incorporating high volumes of class F fly ash Preliminary results. *Cem. Concr. Res.* 31, 413–420.
- Bouzoubaa, N., Malhotra, V.M., 2001. Performance of Lab-Produced High-Volume Fly Ash Cements in Concrete. *Concr. Int.* 23, 31–35.
- Bouzoubaâ, N., Zhang, M.H., Malhotra, V.M., 2001. Mechanical properties and durability of concrete made with high-volume fly ash blended cements using a coarse fly ash. *Cem. Concr. Res.* 31, 1393–1402.
- Bouzoubaâ, N., Zhang, M.H., Malhotra, V.M., 2000. Laboratory-produced high-volume fly ash blended cements: compressive strength and resistance to the chloride-ion penetration of concrete. *Cem. Concr. Res.* 30, 1037–1046.
- Britannica, T.E. of E., 2016. Pozzolana - Hydraulic Cement [WWW Document]. *Encycl. Br. Online*. URL <https://www.britannica.com/technology/pozzolana>

References

- (accessed 1.1.17).
- Brown, M.D., 2005. Design for Shear in Reinforced Concrete Using Strut-and-Tie and Sectional Models. Univ. Texas Austin 7.
- Burden, D., 2006. The Durability of Concrete Containing High Levels of Fly Ash. The University of New Brunswick.
- Cabrera, J.G., Hopkins, C.J., Woolley, G.R., Lee, R.E., Shaw, J., Plowman, C., Fox, H., 1986. Evaluation of the properties of British pulverized fuel ashes and their influence on the strength of concrete, in: In Proceedings of the Second International Conference on the Use of Fly Ash, Silica Fume, Slag and Other Mineral Byproducts in Concrete. pp. 115–144.
- Cao, C., Sun, W., Qin, H., 2000. The analysis on strength and fly ash effect of roller-compacted concrete with high volume fly ash. *Cem. Concr. Res.* 30, 71–75.
- Carette, G., Bilodeau, A., Chevrier, R.L., Malhotra, V.M., 1993. Mechanical Properties of Concrete Incorporating High Volumes of Fly Ash From Sources in the U.S. *Mater. J.* 90, 535–544.
- Celik, K., Meral, C., Petek Gursel, A., Mehta, P.K., Horvath, A., Monteiro, P.J.M., 2015. Mechanical properties, durability, and life-cycle assessment of self-consolidating concrete mixtures made with blended portland cements containing fly ash and limestone powder. *Cem. Concr. Compos.* 56, 59–72. <https://doi.org/10.1016/j.cemconcomp.2014.11.003>
- CEN, 2014. Technical report 16639: Use of k-value concept, equivalent concrete performance concept and equivalent performance of combinations concept. European Committee for Standardization, Brussels.
- CEN, 2012. EN 450-1: Fly ash for concrete — Part 1: Definition, specifications and conformity criteria. European Committee for Standardization, Brussels.
- CEN, 2011a. EN 197-1: Cement - Part 1: Composition, specifications and conformity criteria for common cements. European Committee for Standardization, Brussels.
- CEN, 2011b. EN 206-1: Concrete – Part 1: Specification performance, production

References

- and conformity. European Committee for Standardization, Brussels.
- CEN, 2010. EN 12620:2010. Aggregates for concrete. Brussels, Belgium.
- CEN, 2009a. EN 12390-3 Testing hardened concrete - Part 3: Compressive strength of test specimens. p. 19. Brussels, Belgium.
- CEN, 2009b. EN 12390-6 Testing hardened concrete - Part 6: Tensile splitting strength of test specimens. p. 10. Brussels, Belgium.
- CEN, 2009c. EN 12390-13 Testing hardened concrete - Part 13: Determination of secant modulus of elasticity in compression. p. 14. Brussels, Belgium.
- CEN, 2009d. EN 12350-6 Testing fresh concrete - Part 6: Density. p. 10. Brussels, Belgium.
- CEN, 2009e. EN 12350-2: Testing fresh concrete - Part 2: Slump. p. 9. Brussels, Belgium.
- CEN, 2009f. EN 12390-7 Testing hardened concrete - Part 7: Density of hardened concrete. p. 10. Brussels, Belgium.
- CEN, 2009g. EN 12390-5 Testing hardened concrete - part 5: Flexural strength of test specimens. p. 11. Brussels, Belgium.
- CEN, 2008. EN 196-1: Methods of testing cement - Part 1: Determination of strength. European Committee for Standardization, Brussels.
- CEN, 2005. EN 450-2: Fly ash for concrete - Part 2: Conformity evaluation. European Committee for Standardization, Brussels.
- CEN, 2004. EN 1992-1-1: Design of concrete structures - Part 1-1: General rules and rules for buildings. European Committee for Standardization, Brussels.
- Chen, J., Kuder, K.G., Lehman, D., Roeder, C.W., 2017. Creep modeling of concretes with high volumes of supplementary cementitious materials and its application to concrete-filled tubes. *Mater. Struct.* 50, 1–20.
- Chen, Y.Y., Tuan, B.L.A., Hwang, C.L., 2013. Effect of paste amount on the properties of self-consolidating concrete containing fly ash and slag. *Constr. Build. Mater.* 47, 340–346. <https://doi.org/10.1016/j.conbuildmat.2013.05.050>

References

- Choi, Y.S., Kim, J.G., Lee, K.M., 2006. Corrosion behavior of steel bar embedded in fly ash concrete. *Corros. Sci.* 48, 1733–1745.
- Chowdhury, S., Maniar, A., Suganya, O.M., 2014. Strength development in concrete with wood ash blended cement and use of soft computing models to predict strength parameters. *J. Adv. Res.* 6, 907–913.
- Collins, M.P., Mitchell, D., 1991. *Prestressed Concrete Structures*. New Jersey.
- Construction, G., 1998. *Concrete Admixture Use with High Volume Fly Ash - Technical Bulletin TB-0113*.
- Da Silva, P.R., De Brito, J., 2015. Experimental study of the porosity and microstructure of self-compacting concrete (SCC) with binary and ternary mixes of fly ash and limestone filler. *Constr. Build. Mater.* 86, 101–112. <https://doi.org/10.1016/j.conbuildmat.2015.03.110>
- Deo, S. V, Pofale, A.D., 2015. Parametric Study for Replacement of Sand by Fly Ash for Better Packing and Internal Curing. *Open J. Civ. Eng.* 5, 118–130. <https://doi.org/10.4236/ojce.2015.51012>
- Destrebecq, J.F., Toussaint, E., Ferrier, E., 2011. Analysis of Cracks and Deformations in a Full Scale Reinforced Concrete Beam Using a Digital Image Correlation Technique. *Exp. Mech.* 51, 879–890.
- Dhir, R.K., El-Mohr, M.A.K., Dyer, T.D., Pomeroy, C.D., 1997. Developing chloride resisting concrete using PFA. *Cem. Concr. Res.* 27, 1633–1639. <https://doi.org/10.1017/CBO9781107415324.004>
- Dhir, R.K., Jones, M.R., 1999. Development of chloride-resisting concrete using fly ash. *Fuel* 78, 137–142. [https://doi.org/10.1016/S0016-2361\(98\)00149-5](https://doi.org/10.1016/S0016-2361(98)00149-5)
- Dinakar, P., Babu, K.G., Santhanam, M., 2008. Durability properties of high volume fly ash self compacting concretes. *Cem. Concr. Compos.* 30, 880–886. <https://doi.org/10.1016/j.cemconcomp.2008.06.011>
- Dinakar, P., Kartik Reddy, M., Sharma, M., 2013. Behaviour of self compacting concrete using Portland pozzolana cement with different levels of fly ash. *Mater. Des.* 46, 609–616. <https://doi.org/10.1016/j.matdes.2012.11.015>

References

- Dragaš, J., Tošić, N., Ignjatović, I., Marinković, S., 2016. Mechanical and time-dependent properties of high-volume fly ash concrete for structural use. *Mag. Concr. Res.* 68, 632–645. <https://doi.org/10.1680/jmacr.15.00384>
- Dunstan, M.R.H., 1983. Development of high fly ash content concrete, in: *Proceedings of the Institution of Civil Engineers.* pp. 495–513. <https://doi.org/10.1680/iicep.1983.1407>
- Duran-Herrera, A., Juarez, C., Valdez, P., Bentz, D., 2011. Evaluation of sustainable high-volume fly ash concretes. *Cem. Concr. Compos.* 33, 39–45.
- Dutton, M., 2012. Digital image correlation for evaluating structural engineering materials. Queen's University, Kingston, Ontario, Canada. [https://doi.org/10.1016/S1369-7021\(10\)70235-2](https://doi.org/10.1016/S1369-7021(10)70235-2)
- Dutton, M., 2012. Digital image correlation for evaluating structural engineering materials. Queen's University Kingston, Ontario, Canada.
- Duxson, P., Fernández-Jiménez, a., Provis, J.L., Lukey, G.C., Palomo, a., Deventer, J.S.J., 2006. Geopolymer technology: the current state of the art. *J. Mater. Sci.* 42, 2917–2933. <https://doi.org/10.1007/s10853-006-0637-z>
- EPS (Electric Power Industry of Serbia), 2011. Technical Report for 2011. Electric Power Industry of Serbia. (accessed 15/01/2017). [http://www.eps.rs/Godisnjilzvestaji/%0AGodisnjak EPS 2011_sr_web.pdf](http://www.eps.rs/Godisnjilzvestaji/%0AGodisnjak%20EPS%202011_sr_web.pdf)
- Faber, M.H., 2007. Risk and safety in civil engineering (Lectur Notes). *Lect. Notes, Inst. Struct. Eng.* 335. <https://doi.org/10.3929/ethz-a-004230964>
- Faculty of Civil Engineering, 1995. *Beton i armirani beton prema BAB '87-Priručnik.* Belgrade.
- Fayyad, T.M., Lees, J.M., 2017. Experimental investigation of crack propagation and crack branching in lightly reinforced concrete beams using digital image correlation. *Eng. Fract. Mech.* 182, 487–505.
- Fenwick, R.C., T., P., 1968. Mechanisms of shear resistance of concrete beams. *ASCE J. Struct. Eng.* 94, 2325–2350.
- Feret, R., 1892. Sur la compacite des mortiers hydrauliques. *Ann. des ponts*

References

- chaussées 4, 5–164.
- Ferraris, C.F., Obla, K.H., Hill, R., 2001. The influence of mineral admixtures on the rheology of cement paste and concrete. *Cem. Concr. Res.* 31, 245–255. [https://doi.org/10.1016/S0008-8846\(00\)00454-3](https://doi.org/10.1016/S0008-8846(00)00454-3)
- Ferreira, C., Ribeiro, A., Ottosen, L., 2003. Possible applications for municipal solid waste fly ash. *J. Hazard. Mater.* 96, 201–216. [https://doi.org/10.1016/S0304-3894\(02\)00201-7](https://doi.org/10.1016/S0304-3894(02)00201-7)
- fib, 2010a. *Fib Bulletin 66: Model Code 2010 Volume 2*.
- fib, 2010b. *Fib Bulletin 65: Model Code 2010 Volume 1*.
- Filho, J.H., Medeiros, M.H.F., Pereira, E., Helene, P., Isaia, G.C., 2013. High-Volume Fly Ash Concrete with and without Hydrated Lime: Chloride Diffusion Coefficient from Accelerated Test. *J. Mater. Civ. Eng.* 25, 411–418. [https://doi.org/10.1061/\(ASCE\)MT.1943-5533.0000596](https://doi.org/10.1061/(ASCE)MT.1943-5533.0000596)
- Ganesan, K., Rajagopal, K., Thangavel, K., 2008. Rice husk ash blended cement: Assessment of optimal level of replacement for strength and permeability properties of concrete. *Constr. Build. Mater.* 22, 1675–1683. <https://doi.org/10.1016/j.conbuildmat.2007.06.011>
- Gastebled, O., May, I., 2001. Fracture mechanics model applied to shear failure of reinforced concrete beams without stirrups. *ACI Struct. J.* 98, 184–190. <https://doi.org/10.14359/10186>
- Gebler, S.H., Klieger, P., 1986. Effect of Fly Ash on the Durability of Air-Entrained Concrete, in: *Proceedings of the 2nd International Conference on Fly Ash, Silica Fume, Slag, and Other Natural Pozzolans in Concrete*. American Concrete Institute, Farmington Hills, MI, pp. 483–519.
- Givi, A.N., Rashid, S.A., Aziz, F.N.A., Salleh, M.A.M., 2010. Assessment of the effects of rice husk ash particle size on strength, water permeability and workability of binary blended concrete. *Constr. Build. Mater.* 24, 2145–2150. <https://doi.org/10.1016/j.conbuildmat.2010.04.045>
- Golewski, G.L., Sadowski, T., 2014. An analysis of shear fracture toughness K_{IIc} and

References

- microstructure in concretes containing fly-ash. *Constr. Build. Mater.* 51, 207–214. <https://doi.org/10.1016/j.conbuildmat.2013.10.044>
- Gopalan, M.K., Haque, M.N., 1985. Design of fly ash concrete. *Cem. Concr. Res.* 15, 694–702.
- Gu, X., Jin, X., Zhou, Y., 2015. *Basic Principles of Concrete Structures*. Springer.
- Hannesson, G., Kuder, K., Shogren, R., Lehman, D., 2012. The influence of high volume of fly ash and slag on the compressive strength of self-consolidating concrete. *Constr. Build. Mater.* 30, 161–168.
- Hannesson G., 2010. *Mechanical Properties of High-Volume SCM Concretes*. University of Washington Graduate School.
- Hardjito, D., 2005. *Studies on Fly Ash-Based Geopolymer Concrete*. Curtin University of Technology.
- Hawkins, N.M., Kuchma, D.A., Mast, R.F., Marsh, M.L., Reineck, K., 2005. *Simplified Shear Design of Structural Concrete Members*.
- Hemalatha, T., Ramaswamy, A., 2017. A review on fly ash characteristics – Towards promoting high volume utilization in developing sustainable concrete. *J. Clean. Prod.* 147, 546–559.
- Ho, D.W.S., Lewis, R.K., 1985. Effectiveness of fly ash for strength and durability of concrete. *Cem. Concr. Res.* 15, 793–800.
- Hopkins, D.S., Thomas, M.D.A., Oates, D.B., Girn, G., Munro, R., 2001. York University uses High-Volume Fly Ash Concrete for Green Building. *Proceedings- Can. Soc. Civ. Eng.* 1–7.
- Huang, C.H., Lin, S.K., Chang, C.S., Chen, H.J., 2013. Mix proportions and mechanical properties of concrete containing very high-volume of Class F fly ash. *Constr. Build. Mater.* 46, 71–78. <https://doi.org/10.1016/j.conbuildmat.2013.04.016>
- Hung, H.-H., 1997. *Properties of High Volume Fly Ash Concrete*. Faculty of Engineering, University of Sheffield.
- Hwang, K., Noguchi, T., Tomosawa, F., 2004. Prediction model of compressive

References

- strength development of fly-ash concrete. *Cem. Concr. Res.* 34, 2269–2276. <https://doi.org/10.1016/j.cemconres.2004.04.009>
- Ignjatović, I.S., Marinković, S.B., Tošić, N., 2017. Shear behaviour of recycled aggregate concrete beams with and without shear reinforcement. *Eng. Struct.* 141, 386–401. <https://doi.org/10.1016/j.engstruct.2017.03.026>
- Inderpreet Kaur, 2005. Mechanical properties of high volume fly ash (hvfa) concrete subjected to elevated temperatures up to 120oc. Deemed University.
- ISO, 2006. Environmental Management - Life Cycle Assessment, Set of International standards: ISO 14040-14043. International Organization for Standardization, Geneva.
- Jiang, L., Lin, B., Cai, Y., 2000. A model for predicting carbonation of high-volume fly ash concrete. *Cem. Concr. Res.* 30, 699–702. [https://doi.org/10.1016/S0008-8846\(00\)00227-1](https://doi.org/10.1016/S0008-8846(00)00227-1)
- Jiang, L.H., Malhotra, V.M., 2000. Reduction in water demand of non-air-entrained concrete incorporating large volumes of fly ash. *Cem. Concr. Res.* 30, 1785–1789. [https://doi.org/10.1016/S0008-8846\(00\)00397-5](https://doi.org/10.1016/S0008-8846(00)00397-5)
- Jiménez-Quero, V.G., León-Martínez, F.M., Montes-García, P., Gaona-Tiburcio, C., Chacón-Nava, J.G., 2013. Influence of sugar-cane bagasse ash and fly ash on the rheological behavior of cement pastes and mortars. *Constr. Build. Mater.* 40, 691–701. <https://doi.org/10.1016/j.conbuildmat.2012.11.023>
- Kani, G.N.J., 1967. How Safe Are Our Large Reinforced Concrete Beams? *ACI Journal, Proc.* 64, 128–141.
- Kani, G.N.J., 1964. The Riddle of Sshear Failure and Its Solution. *J. ACI* 441–468. <https://doi.org/10.14359/7791>
- Kartini, K. (University of T.M., 2011. *International Journal of Applied Science and Technology.* Rice Husk Ash-Pozzolanic Mater. *Sustain.* 1, 169–178. <https://doi.org/10.5958/2322-0465.2014>
- Kayali, O., Sharfuddin Ahmed, M., 2013. Assessment of high volume replacement fly ash concrete – Concept of performance index. *Constr. Build. Mater.* 39, 71–76.

References

- <https://doi.org/10.1016/j.conbuildmat.2012.05.009>
- Kayyali, O.A., Haque, M.N., 1988. Chloride penetration and the ratio of cl^-/oh^- in the pores of cement paste. *Cem. Concr. Res.* 18, 895–900.
- Keith, K.P., 2011. Characterization of the Behavior of High Volume Fly Ash Concrete. Auburn University.
- Khunthongkeaw, J., Tangtermsirikul, S., Leelawat, T., 2006. A study on carbonation depth prediction for fly ash concrete. *Constr. Build. Mater.* 20, 744–753. <https://doi.org/10.1016/j.conbuildmat.2005.01.052>
- Kiattikomol, K., Jaturapitakkul, C., Songpiriyakij, S., Chutubtim, S., 2001. A study of ground coarse fly ashes with different finenesses from various sources as pozzolanic materials. *Cem. Concr. Compos.* 23, 335–343.
- Kim, H.K., 2015. Utilization of sieved and ground coal bottom ash powders as a coarse binder in high-strength mortar to improve workability. *Constr. Build. Mater.* 91, 57–64. <https://doi.org/10.1016/j.conbuildmat.2015.05.017>
- Kim, H.K., Jeon, J.H., Lee, H.K., 2012. Flow, water absorption, and mechanical characteristics of normal- and high-strength mortar incorporating fine bottom ash aggregates. *Constr. Build. Mater.* 26, 249–256.
- Kim, J.H., Noemi, N., Shah, S.P., 2012. Effect of powder materials on the rheology and formwork pressure of self-consolidating concrete. *Cem. Concr. Compos.* 34, 746–753. <https://doi.org/10.1016/j.cemconcomp.2012.02.016>
- Kokovic, V., 2016. Ultimate strength of hollow core slabs supporting connection. University of Belgrade.
- Komljenović, M., Bašćarević, Z., Bradić, V., 2010. Mechanical and microstructural properties of alkali-activated fly ash geopolymers. *J. Hazard. Mater.* 181, 35–42. <https://doi.org/10.1016/j.jhazmat.2010.04.064>
- König, G., Fischer, J., 1995. Model Uncertainties concerning Design Equations for the Shear Capacity of Concrete Members without Shear Reinforcement, CEB Bulletin 224.
- Kou, S.C., Poon, C.S., 2013. Long-term mechanical and durability properties of

References

- recycled aggregate concrete prepared with the incorporation of fly ash. *Cem. Concr. Compos.* 37, 12–19.
- Kuchma, D.A., Collins, M.P., 1998. Advances in understanding shear performance of concrete structures. *Prog. Struct. Eng. Mater.* 1, 360–369.
- Kuder, K., Lehman, D., Berman, J., Hannesson, G., Shogren, R., 2012. Mechanical properties of self consolidating concrete blended with high volumes of fly ash and slag. *Constr. Build. Mater.* 34, 285–295.
- Küntz, M., Jolin, M., Bastien, J., Perez, F., Hild, F., 2006. Digital image correlation analysis of crack behavior in a reinforced concrete beam during a load test. *Can. J. Civ. Eng.* 33, 1418–1425. <https://doi.org/10.1139/106-106>
- Kwan, A.K.H., Chen, J.J., 2013. Adding fly ash microsphere to improve packing density, flowability and strength of cement paste. *Powder Technol.* 234, 19–25. <https://doi.org/10.1016/j.powtec.2012.09.016>
- Lam, L., Wong, Y.L., Poon, C.S., 2000. Degree of hydration and gel/space ratio of high-volume fly ash/cement systems. *Cem. Concr. Res.* 30, 747–756. [https://doi.org/10.1016/S0008-8846\(00\)00213-1](https://doi.org/10.1016/S0008-8846(00)00213-1)
- Lam, L., Wong, Y.L., Poon, C.S., 1998. Effect of fly ash and silica fume on compressive and fracture behaviors of concrete. *Cem. Concr. Res.* 28, 271–283.
- Lane, R.O., 1983. Effect of fly ash on freshly mixed concrete. *Concr. Int.* 5, 50–52.
- Langan, B.W., Joshi, R.C., Ward, M.A., 1990. Strength and durability of concretes containing 50% Portland cement replacement by fly ash and other materials. *Can. J. Civ. Eng.* 17, 19–27.
- Langley, W.S., Carette, G.G., Malhotra, V.M., 1989. Structural Concrete Incorporating High Volumes of ASTM Class Fly Ash. *Mater. Lett.* 86, 507–514.
- Lecompte, D., Vantomme, J., Sol, H., 2006. Crack Detection in a Concrete Beam using Two Different Camera Techniques. *Struct. Heal. Monit.* 5, 59–68. <https://doi.org/10.1177/1475921706057982>
- Lee, S.H., Kim, H.J., Sakai, E., Daimon, M., 2003. Effect of particle size distribution of

References

- fly ash-cement system on the fluidity of cement pastes. *Cem. Concr. Res.* 33, 763–768. [https://doi.org/10.1016/S0008-8846\(02\)01054-2](https://doi.org/10.1016/S0008-8846(02)01054-2)
- Li, G., Zhao, X., 2003. Properties of concrete incorporating fly ash and ground granulated blast-furnace slag. *Cem. Concr. Compos.*
- Liang, M. Te, Huang, R., Jheng, H.Y., 2010. Revisited to the relationship between the free and total chloride diffusivity in concrete. *J. Mar. Sci. Technol.* 18, 442–448. [https://doi.org/10.1016/S0008-8846\(01\)00664-0](https://doi.org/10.1016/S0008-8846(01)00664-0)
- Lima, C., Caggiano, A., Faella, C., Martinelli, E., Pepe, M., Realfonzo, R., 2013. Physical properties and mechanical behaviour of concrete made with recycled aggregates and fly ash. *Constr. Build. Mater.* 47, 547–559. <https://doi.org/10.1016/j.conbuildmat.2013.04.051>
- Lisantono, A., Wigroho, H.Y., Purba, R.A., 2017. Shear Behavior of High-volume Fly Ash Concrete as Replacement of Portland Cement in RC Beam. *Procedia Eng.* 171, 80–87. <https://doi.org/10.1016/j.proeng.2017.01.312>
- Liu, B., Xie, Y., Li, J., 2005. Influence of steam curing on the compressive strength of concrete containing supplementary cementing materials. *Cem. Concr. Res.* 35, 994–998. <https://doi.org/10.1016/j.cemconres.2004.05.044>
- MacGregor, J., 1997. *Reinforced Concrete: Mechanics and Design* 3rd Edition. Prentice Hall, Englewood Cliffs, NJ.
- Malhotra, V.M., 1999. Making concrete “greener” with fly ash. *Concr. Int.* 61–66.
- Malhotra, V.M., 1993. Fly ash, slag, silica fume, and rice-husk ash in concrete. A review. *Concr. Int.* 15, 23-28.
- Malhotra, V.M., 1990. Durability of concrete incorporating high-volume of low-calcium (ASTM Class F) fly ash. *Cem. Concr. Compos.* 12, 271–277. [https://doi.org/10.1016/0958-9465\(90\)90006-J](https://doi.org/10.1016/0958-9465(90)90006-J)
- Malhotra, V.M., 1986. Superplasticized fly ash concrete for structural application. *Concr. Int.* 8, 28–31.
- Malhotra, V.M., Mehta, P.K., 2005. *High-Performance, High-Volume Fly Ash Concrete for Building Sustainable and Durable Structures*, Third Edit. ed.

References

- Supplementary Cementing Materials for Sustainable Development Inc., Ottawa, Canada.
- Malhotra, V.M., Zhang, M.-H., Read, P.H., Ryell, J., 2000. Long-Term Mechanical Properties and Durability Characteristics of High-Strength/High-Performance Concrete Incorporating Supplementary Cementing Materials under Outdoor Exposure Conditions. *ACI Mater. J.* 518–525.
- Mandal, K.K., Thokchom, S., Roy, M., 2011. Effect of Na₂O Content on Performance of Fly ash Geopolymers at Elevated Temperature. *World Acad. Sci. Eng. Technol.* 91, 34–40.
- Mardani-Aghabaglou, A., Andiç-Çakir, Ö., Ramyar, K., 2013. Freeze-thaw resistance and transport properties of high-volume fly ash roller compacted concrete designed by maximum density method. *Cem. Concr. Compos.* 37, 259–266. <https://doi.org/10.1016/j.cemconcomp.2013.01.009>
- Marinković, S., Dragaš, J., Ignjatović, I., Tošić, N., 2017. Environmental assessment of green concretes for structural use. *J. Clean. Prod.* 154, 633–649. <https://doi.org/10.1016/j.jclepro.2017.04.015>
- Mathur, V.K., Verma, C.L., Gupta, B.S., Agarwal, S.K., Kumar, A., 2005. Use of high volume fly ash in concrete for building sector. Ottawa, Ontario.
- McCarthy, M.J., Dhir, R.K., 2005. Development of high volume fly ash cements for use in concrete construction. *Fuel* 84, 1423–1432.
- Mehta, P.K., GjØrv, O.E., 1982. Properties of portland cement concrete containing fly ash and condensed silica-fume. *Cem. Concr. Res.* 12, 587–595.
- Michel, de S., Bily, L., Beveridge, J., Fournier, B., Moore, A., Wojtarowicz, M., 2001. The EcoSmart concrete project Results from the Case Studies. Vancouver, Canada.
- Mittal, A., Kaisare, M.B., Rajenderakumar, S., 2006. Experimental study on use of fly ash in concrete [WWW Document]. URL https://www.sefindia.org/forum/files/experimental_study_on_use_of_fly_ash_in_concrete_by_mr_amit_mittal_136.pdf (accessed 1.22.18).

References

- Modr, S., Kadlecěk, V.I., 2002. Size effect of test specimens on tensile splitting strength of concrete : general relation 35, 28–34.
- Moosberg-Bustnes, H., Lagerblad, B., Forsberg, E., 2004. The function of fillers in concrete. *Mater. Struct.* 37, 74–81. <https://doi.org/10.1007/BF02486602>
- Mörsch E., 1909. *Concrete-Steel Construction: Der Eisenbetonbau*. Engineering News Publishing Co.
- Mukherjee, S., Mandal, S., Adhikari, U.B., Ash, F., 2013. Comparative Study on Physical and Mechanical Properties of High Slump and Zero Slump High Volume Fly Ash Concrete (HVFA). *Glob. NEST J.* 15, 578–584.
- Muravljev, M., 2007. *Building Materials*. Građevinska knjiga, Belgrade, Serbia.
- Muttoni, A., Fernández Ruiz, M., 2008. Shear strength in one- and two-way slabs according to the Critical Shear Crack Theory. *Taylor Made Concr. Struct.* 559–563.
- Muttoni, A., Schwartz, J., Thürlimann, B., 1997. *Design of Concrete Structures with Stress Fields*. Birkhäuser, Basel, Switzerland.
- Muttoni, A.R., Fernandez, M., 2012. Levels-of-Approximation Approach in Codes of Practice. *Struct. Eng. Int.* 22, 190–194.
- Naganathan, S., Nasional, U.T., Beddu, S., Nasional, U.T., Lau, J., Jin, Y., Nasional, U.T., Nair, S., Nasional, U.T., Kanadasan, J., 2017. Influence of curing on the properties of high volume fly ash concrete. *Int. J. Sci. Technol.* 3, 308–315.
- Naik, T., Sivasundaram, V., Singh, S.S., 1991. Use of high-volume class f fly ash for structural grade concrete. *Transp. Res. Rec.* 40–47.
- Naik, T.R., Singh, S.S., 1997. Influence of fly ash on setting and hardening characteristics of concrete systems. *ACI Mater. J.* 94, 355-360.
- Naik, T.R., Singh, S.S., 1994. Use of High-Calcium Fly Ash in Cement-Based Construction Materials, in: *5th International CANMET/ACI Conference on the Use of Fly Ash, Silica Fume, Slag, and Natural Pozzolans in Concrete*. Milwaukee, pp. 1–67.

References

- Narmluk, M., Nawa, T., 2011. Effect of fly ash on the kinetics of Portland cement hydration at different curing temperatures. *Cem. Concr. Res.* 41, 579–589. <https://doi.org/10.1016/j.cemconres.2011.02.005>
- Nath, P., 2010. Durability of Concrete Using Fly Ash as a Partial Replacement of Cement. Curtin University of Technology.
- Nehdi, M., Duquette, J., El Damatty, A., 2003. Performance of rice husk ash produced using a new technology as a mineral admixture in concrete. *Cem. Concr. Res.* 33, 1203–1210. [https://doi.org/10.1016/S0008-8846\(03\)00038-3](https://doi.org/10.1016/S0008-8846(03)00038-3)
- Nehdi, M., Pardhan, M., Koshowski, S., 2004. Durability of self-consolidating concrete incorporating high-volume replacement composite cements. *Cem. Concr. Res.* 34, 2103–2112.
- Neundorf, M., Haebler, R., 2000. High-Volume Fly Ash As a Supplementary Cementing Material: A case study: Arthur Erickson designed artist live / work studios. Vancouver, Canada.
- Neville, A.M., 1981. Properties of Concrete. Longman Scientific and Technical.
- Nikbin, I.M., Rahimi R., S., Allahyari, H., Damadi, M., 2016. A comprehensive analytical study on the mechanical properties of concrete containing waste bottom ash as natural aggregate replacement. *Constr. Build. Mater.* 121, 746–759. <https://doi.org/10.1016/j.conbuildmat.2016.06.078>
- Nilson, A.H., Darwin, D., Dolan, C.W., 2010. Design of concrete structures. McGraw-Hill.
- Obla, B.Y.K.H., Hill, R.L., Martin, R.S., 2003. HVFA Concrete – An Industry Perspective. *Concr. Int.* 29–34.
- Ogawa, K., Uchikawa, H., Takemoto, K., 1980. The mechanism of hydration in the system C3S-pozzolana. *Cem. Concr. Res.* 10, 683–696.
- Oikonomou, N.D., 2005. Recycled concrete aggregates. *Cem. Concr. Compos.* 27, 315–318. <https://doi.org/10.1016/j.cemconcomp.2004.02.020>
- Oner, A., Akyuz, S., Yildiz, R., 2005. An experimental study on strength development

References

- of concrete containing fly ash and optimum usage of fly ash in concrete. *Cem. Concr. Res.* 35, 1165–1171.
- Ortega, C.A., 2012. Shear and fracture behavior of high-volume fly ash reinforced concrete for sustainable construction. Missouri University of science and technology.
- Owens, P., 1979. Fly ash and its usage in concrete. *Concr. Soc. J.* 13, 21–26.
- Pacheco-Torgal, F., Castro-Gomes, J., Jalali, S., 2008. Alkali-activated binders: A review. Part 2. About materials and binders manufacture. *Constr. Build. Mater.* 22, 1315–1322. <https://doi.org/10.1016/j.conbuildmat.2007.03.019>
- Pacheco Torgal, F., Miraldo, S., Labrincha, J. a., De Brito, J., 2012. An overview on concrete carbonation in the context of eco-efficient construction: Evaluation, use of SCMs and/or RAC. *Constr. Build. Mater.* 36, 141–150.
- Pan, B., Qian, K., Xie, H., Asundi, A., 2009. Two-dimensional digital image correlation for in-plane displacement and strain measurement: a review. *Meas. Sci. Technol.* 20, 1–18.
- Papadakis, V.G., 2000. Effect of fly ash on Portland cement systems: Part II. High-calcium fly ash. *Cem. Concr. Res.* 30, 1647–1654.
- Papadakis, V.G., 2000. Effect of supplementary cementing materials on concrete resistance against carbonation and chloride ingress. *Cem. Concr. Res.* 30, 291–299.
- Papadakis, V.G., 1999. Effect of fly ash on Portland cement systems: Part I. Low-calcium. *Cem. Concr. Res.* 29, 1727–1736.
- Papadakis, V.G., Antiohos, S., Tsimas, S., 2002. Supplementary cementing materials in concrete Part II: A fundamental estimation of the efficiency factor. *Cem. Concr. Compos.* 32, 1533–1538.
- Papadakis, V.G., Tsimas, S., 2005. Greek supplementary cementing materials and their incorporation in concrete. *Cem. Concr. Compos.* 27, 223–230. <https://doi.org/10.1016/j.cemconcomp.2004.02.011>
- Papadakis, V.G., Tsimas, S., 2002. Supplementary cementing materials in concrete

References

- Part I : Efficiency and design. *Cem. Concr. Res.* 32, 1525–1532.
- Paterse, I., 2008. Nicola Valley Institute. Merrit, British Columbia Busby + associates architects inc. Waterloo, Canada.
- Paya, J., Monzo, J., Borrachero, M.V., Peris-Mora, E., 1995. Mechanical treatment of fly ashes. Part I: physico-chemical characterization of ground fly ashes. *Cem. Concr. Res.* 25, 1469–1479.
- Payá, J., Monzó, J., Borrachero, M. V., Peris-Mora, E., Amahjour, F., 2000. Mechanical treatment of fly ashes - Part IV. Strength development of ground fly ash-cement mortars cured at different temperatures. *Cem. Concr. Res.* 30, 543–551. [https://doi.org/10.1016/S0008-8846\(00\)00218-0](https://doi.org/10.1016/S0008-8846(00)00218-0)
- Peter, M.A., Muntean, A., Meier, S.A., Böhm, M., 2008. Cement and Concrete Research Competition of several carbonation reactions in concrete : A parametric study. *Cem. Concr. Res.* 38, 1385–1393.
- Poon, C.S., Kou, S.C., Lam, L., 2007. Influence of recycled aggregate on slump and bleeding of fresh concrete. *Mater. Struct.* 40, 981–988.
- Poon, C.S., Lam, L., Wong, Y.L., 2000. A study on high strength concrete prepared with large volumes of low calcium fly ash. *Cem. Concr. Res.* 30, 447–455. [https://doi.org/10.1016/S0008-8846\(99\)00271-9](https://doi.org/10.1016/S0008-8846(99)00271-9)
- Proske, T., Hainer, S., Rezvani, M., Graubner, C.-A., 2014. Eco-friendly concretes with reduced water and cement content – Mix design principles and application in practice. *Constr. Build. Mater.* 67, 413–421.
- Provis, J.L., van Deventer, J.S.J., 2014. Alkali-activated Materials. State-of-the-Art Report. RILEM TC 224-AAM
- Putte Gowda B., M, A., K, M., 2013. Experimental investigation on flexure behaviour of fly ash concrete beams. *Int. J. Adv. Sci. Tech. Res.* 2, 184–199.
- Quan, H., Kasami, H., 2013. Experimental Study on Effects of Type and Replacement Ratio of Fly Ash on Strength and Durability of Concrete. *Open Civ. Eng. J.* 93–100.
- Rafieizonooz, M., Mirza, J., Salim, M.R., Hussin, M.W., Khankhaje, E., 2016.

References

- Investigation of coal bottom ash and fly ash in concrete as replacement for sand and cement. *Constr. Build. Mater.* 116, 15–24.
- Rajamane, N.P., Ambily, P.S., 2013. Fly ash as a sand replacement material in concrete - A study. *Indian Concr. J.* 87, 11–17.
- Rajamane, N.P., Ambily, P.S., 2012. Modified Bolomey equation for strengths of lightweight concretes containing fly ash aggregates. *Magaz* 64, 285–293.
- Rajamane, N.P., Annie Peter, J., Ambily, P.S., 2007. Prediction of compressive strength of concrete with fly ash as sand replacement material. *Cem. Concr. Compos.* 29, 218–223. <https://doi.org/10.1016/j.cemconcomp.2006.10.001>
- Rao, R.M., Mohan, S., Sekar, S.K., 2011. Shear resistance of high volume fly ash reinforced concrete beams without web reinforcement 1, 986–993. <https://doi.org/10.6088/ijcser.00202010084>
- Ravina, D., Mehta, P.K., 1988. Compressive strength of low cement/high fly ash concrete. *Cem. Concr. Res.* 18, 571–583. [https://doi.org/10.1016/0008-8846\(88\)90050-6](https://doi.org/10.1016/0008-8846(88)90050-6)
- Ravina, D., Mehta, P.K., 1986. Properties of fresh concrete containing large amounts of fly ash. *Cem. Concr. Res.* 16, 227–238.
- Regan, P.E., 1993. Research on shear: a benefit to humanity or a waste of time? *Struct. Eng.* 71, 337–347.
- Reineck, K., 1991. Ultimate shear force of structural concrete members Without Transverse Reinforcement Derived From a Mechanical Model. *Struct. J.* 88, 592–602.
- Reineck, K.-H., Bentz, E.C., Fitik, B., Kuchma, D.A., Bayrak, O., 2013. ACI-DAfStb Database of Shear Tests on Slender Reinforced Concrete Beams without Stirrups. *Struct. J.* 110, 867–876.
- Reineck, K.H., 1991. Model for Structural Concrete Members without Transverse Reinforcement. Zurich, Switzerland.
- Reineck, K.H., Bentz, E., Fitik, B., Kuchma, D.A., Bayrak, O., 2014. ACI-DAfStb databases for shear tests on slender reinforced concrete beams with stirrups.

References

- ACI Struct. J. 111, 1147–1156. <https://doi.org/10.14359/51686819>
- Rocco, C., Guinea, G. V, Elices, M., 1999. Size effect and boundary conditions in the Brazilian test : Experimental verification 32, 210–217.
- Rodríguez De Sensale, G., 2006. Strength development of concrete with rice-husk ash. *Cem. Concr. Compos.* 28, 158–160.
- Roselló, J., Soriano, L., Santamarina, M.P., Akasaki, J.L., Monzó, J., Payá, J., 2017. Rice straw ashA potential pozzolanic supplementary material for cementing systems. *Ind. Crops Prod.* 103, 39–50.
- Sadati, S., Arezoumandi, M., Khayat, K.H., Volz, J.S., 2016. Shear performance of reinforced concrete beams incorporating recycled concrete aggregate and high-volume fly ash. *J. Clean. Prod.* 115, 284–293.
- Safiuddin, M., 2008. Development of Self-consolidating High Performance Concrete Incorporating Rice Husk Ash. University of Waterloo.
- Şahmaran, M., Yaman, İ.Ö., Tokyay, M., 2009. Transport and mechanical properties of self consolidating concrete with high volume fly ash. *Cem. Concr. Compos.* 31, 99–106. <https://doi.org/10.1016/j.cemconcomp.2008.12.003>
- Sarkhosh, R., 2014. Shear Resistance of Reinforced Concrete Beams without Shear Reinforcement under Sustained Loading. Faculty of Civil Engineering & Geosciences, Department of Structural Engineering, Concrete Structures.
- Schlaich, J., Schafer, K., Jennewein, M., 1987. Toward a Consistent Design of Structural Concrete. *PCI J.* 32, 74–150.
- Scrivener, K.L., Lothenbach, B., De Belie, N., Gruyaert, E., Skibsted, J., Snellings, R., Vollpracht, A., 2015. TC 238-SCM: hydration and microstructure of concrete with SCMs. *Mater. Struct.* 48, 835–862. <https://doi.org/10.1617/s11527-015-0527-4>
- Shioya, T., Iguro, M., Nojiri, Y., Akiayma, H., Okada, T., 1989. Shear strength of large reinforced concrete beams, fracture mechanics: Application to concrete. *ACI* 118, 259–279.
- Siddique, R., 2010. Use of municipal solid waste ash in concrete. *Resour. Conserv.*

References

- Recycl. 55, 83–91. <https://doi.org/10.1016/j.resconrec.2010.10.003>
- Siddique, R., 2008. Waste Materials and By-Products in Concrete. Springer. <https://doi.org/10.1007/978-3-540-74294-4>.
- Siddique, R., 2004. Performance characteristics of high-volume Class F fly ash concrete. *Cem. Concr. Res.* 34, 487–493.
- Siddique, R., 2003. Effect of fine aggregate replacement with Class F fly ash on the mechanical properties of concrete. *Cem. Concr. Res.* 33, 539–547. [https://doi.org/10.1016/S0008-8846\(02\)01000-1](https://doi.org/10.1016/S0008-8846(02)01000-1)
- Siddique, R., Aggarwal, P., Aggarwal, Y., 2012. Influence of water/powder ratio on strength properties of self-compacting concrete containing coal fly ash and bottom ash. *Constr. Build. Mater.* 29, 73–81.
- Siddique, R., Cachim, P., 2018. Waste and Supplementary Cementitious Materials in Concrete: Characterisation, Properties and Applications. Woodhead Publishing.
- Sigrist, V., 2011. Generalized Stress Field Approach for Analysis of Beams in Shear. *Struct. J.* 108, 479–487.
- Sigrist, V., Bentz, E., Ruiz, M.F., Foster, S., Muttoni, A., 2013. Background to the fib Model Code 2010 shear provisions - part I: beams and slabs. *Struct. Concr.* 14, 195–203. <https://doi.org/10.1002/suco.201200066>
- Silva, R.V., De Brito, J., Dhir, R.K., 2016. Establishing a relationship between modulus of elasticity and compressive strength of recycled aggregate concrete. *J. Clean. Prod.* 112, 2171–2186.
- Singh, M., Siddique, R., 2016. Effect of coal bottom ash as partial replacement of sand on workability and strength properties of concrete. *J. Clean. Prod.* 112, 620–630. <https://doi.org/10.1016/j.jclepro.2015.08.001>
- Singh, M., Siddique, R., 2015. Properties of concrete containing high volumes of coal bottom ash as fine aggregate. *J. Clean. Prod.* 91, 269–278. <https://doi.org/10.1016/j.jclepro.2014.12.026>
- Singh, M., Siddique, R., 2014. Strength properties and micro-structural properties

References

- of concrete containing coal bottom ash as partial replacement of fine aggregate. *Constr. Build. Mater.* 50, 246–256.
- Singh, M., Siddique, R., 2013. Effect of coal bottom ash as partial replacement of sand on properties of concrete. *Resour. Conserv. Recycl.* 72, 20–32. <https://doi.org/10.1016/j.resconrec.2012.12.006>
- Sisomphon, K., Franke, L., 2007. Carbonation rates of concretes containing high volume of pozzolanic material. *Cem. Concr. Res.* 37, 1647–1653.
- Sivasundaram, V., Carette, G.G., Malhotra, V.M., 1991. Mechanical Properties, Creep, and Resistance to Diffusion of Chloride Ions of Concretes Incorporating High Volumes of ASTM Class F Fly Ashes from Seven Different Sources. *ACI Mater. J.* 88, 407–416.
- Sivasundaram, V., Carette, G.G., Malhotra, V.M., 1990. Selected Properties of High-Volume Fly Ash Concretes. *Concr. Int.* 47-50.
- Soman, M., K. Sobha, 2014. Strength and Behaviour of High Volume Fly Ash Concrete. *Int. J. Innov. Res. Sci. Eng. Technol.* 3, 12416–12424.
- Srinivas, T., Rao, R., 2015. A Study on Flexural Behaviour of RCC Beams Containing High Volume Fly Ash. *J. Mech. Civ. Eng.* 12, 2278–1684. <https://doi.org/10.9790/1684-12453540>
- Sulapha, P., Wong, S.F., Wee, T.H., Swaddiwudhipong, S., 2003. Carbonation of Concrete Containing Mineral Admixtures. *J. Mater. Civ. Eng.* 15, 134–143. [https://doi.org/10.1061/\(ASCE\)0899-1561\(2003\)15:2\(134\)](https://doi.org/10.1061/(ASCE)0899-1561(2003)15:2(134))
- Tangchirapat, W., Saeting, T., Jaturapitakkul, C., Kiattikomol, K., Siripanichgorn, A., 2007. Use of waste ash from palm oil industry in concrete. *Waste Manag.* 27, 81–88. <https://doi.org/10.1016/j.wasman.2005.12.014>
- Taylor, H.P.J., 1974. The fundamental behavior of reinforced concrete beams in bending and shear. *ACI Spec. Publ.* 42, 43–78.
- Teixeira, E.R., Mateus, R., Camõesa, A.F., Bragança, L., Branco, F.G., 2016. Comparative environmental life-cycle analysis of concretes using biomass and coal fly ashes as partial cement replacement material. *J. Clean. Prod.* 112,

References

- 2221–2230. <https://doi.org/10.1016/j.jclepro.2015.09.124>
- Thangaraj, R., Thenmozhi, R., 2016. Experimental Study on RC Beams Using High Volume Fly Ash. *Int. J. Technol. Eng.* 3, 71–85.
- The Concrete Institute-ACI Education Bulletin E4-12, 2013. Chemical Admixtures for Concrete. Farmington Hills, Michigan, USA.
- Thomas, J.J., Chen, J.J., Allen, A.J., Jennings, H.M., 2004. Effects of decalcification on the microstructure and surface area of cement and tricalcium silicate pastes. *Cem. Concr. Res.* 34, 2297–2307.
- Thomas, M.D.A., 2007. Optimizing the Use of Fly Ash in Concrete. *Portl. Cem. Assoc.* 24.
- Thomas, M.D.A., Bamforth, P.B., 1999. Modelling chloride diffusion in concrete effect of fly ash and slag. *Cem. Concr. Res.* 29, 487–495. [https://doi.org/10.1016/S0008-8846\(98\)00192-6](https://doi.org/10.1016/S0008-8846(98)00192-6)
- Tokyay, M., 1999. Strength prediction of fly ash concretes by accelerated testing. *Cem. Concr. Res.* 29, 1737–1741. [https://doi.org/10.1016/S0008-8846\(99\)00160-X](https://doi.org/10.1016/S0008-8846(99)00160-X)
- Tošić, N., Marinković, S., Ignjatović, I., 2016. A database on flexural and shear strength of reinforced recycled aggregate concrete beams and comparison to Eurocode 2 predictions. *Constr. Build. Mater.* 127, 932–944. <https://doi.org/10.1016/j.conbuildmat.2016.10.058>
- Van Den Heede, P., De Belie, N., 2014. A service life based global warming potential for high-volume fly ash concrete exposed to carbonation. *Constr. Build. Mater.* 55, 183–193. <https://doi.org/10.1016/j.conbuildmat.2014.01.033>
- Van Den Heede, P., Furniere, J., De Belie, N., 2013. Influence of air entraining agents on deicing salt scaling resistance and transport properties of high-volume fly ash concrete. *Cem. Concr. Compos.* 37, 293–303.
- Van Tuan, N., Ye, G., Van Breugel, K., Fraaij, A.L.A., Bui, D.D., 2011. The study of using rice husk ash to produce ultra high performance concrete. *Constr. Build. Mater.* 25, 2030–2035. <https://doi.org/10.1016/j.conbuildmat.2010.11.046>

References

- Vasco, R., Brito, J. De, Neves, R., Dhir, R., 2015. Prediction of Chloride Ion Penetration of Recycled Aggregate Concrete. *Mater. Res.* 18, 427–440. <https://doi.org/http://dx.doi.org/10.1590/1516-1439.000214>
- Vecchio, F.J., Collins, M.P., 1986. The Modified Compression-Field Theory for Reinforced Concrete Elements Subjected to Shear. *ACI J. Proc.* 83, 219-231. <https://doi.org/10.14359/10416>
- Villain, G., Thiery, M., Platret, G., 2007. Measurement methods of carbonation profiles in concrete: Thermogravimetry, chemical analysis and gammadensimetry. *Cem. Concr. Res.* 37, 1182–1192.
- Villar-Cociña, E., Morales, E.V., Santos, S.F., Savastano, H., Frías, M., 2011. Pozzolanic behavior of bamboo leaf ash: Characterization and determination of the kinetic parameters. *Cem. Concr. Compos.* 33, 68–73. <https://doi.org/10.1016/j.cemconcomp.2010.09.003>
- Walraven, J.C., 1980. *Aggregate Interlock: a Theoretical and Experimental Analysis.* Delft University Press.
- Wang, A., Zhang, C., Sun, W., 2004. Fly ash effects: III. The microaggregate effect of fly ash. *Cem. Concr. Res.* 34, 2061–2066.
- Wang, A., Zhang, C., Sun, W., 2003. Fly ash effects: I. The morphological effect of fly ash. *Cem. Concr. Res.* 33, 2023–2029. [https://doi.org/10.1016/S0008-8846\(03\)00217-5](https://doi.org/10.1016/S0008-8846(03)00217-5)
- WBCSD, 2009. *The Cement Sustainability Initiative [WWW Document].* World Bus. Counc. Sustain. Dev.
- Wendner, R., Hubler, M.H., Bažant, Z.P., 2015. Optimization method, choice of form and uncertainty quantification of Model B4 using laboratory and multi-decade bridge databases. *Mater. Struct.* 771–796.
- Wesche, K., 2004. *Fly ash in concrete: Properties and Performance.* Taylor and Francis Group.
- Wolfe, M.H., 2011. *Bond strength of high-volume fly ash concrete.* Missouri University of science and technology.

References

- Xu, S., Zhang, X., Reinhardt, H.W., 2012. Shear capacity prediction of reinforced concrete beams without stirrups using fracture mechanics approach. *ACI Struct. J.* 109, 705–713.
- Yang, Y., 2014. Shear Behaviour of Reinforced Concrete Members without Shear Reinforcement. Delft University of Technology.
- Yeh, I., 2016. Modeling Efficiency Factor of Fly Ash in Concrete Using an Unification Approach Modeling Efficiency Factor of Fly Ash in Concrete Using an Unification Approach. *Int. J. Eng. Technol.* 5, 546–549.
- Yeh, I., 2006. Generalization of strength versus water – cementitious ratio relationship to age. *Cem. Concr. Res.* 36, 1865–1873.
- Yildirim, H., Sümer, M., Akyüncü, V., Gürbüz, E., 2011. Comparison on efficiency factors of F and C types of fly ashes. *Constr. Build. Mater.* 25, 2939–2947. <https://doi.org/10.1016/j.conbuildmat.2010.12.009>
- Yoo, S.W., Ryu, G.S., Choo, J.F., 2015. Evaluation of the effects of high-volume fly ash on the flexural behavior of reinforced concrete beams. *Constr. Build. Mater.* 93, 1132–1144. <https://doi.org/10.1016/j.conbuildmat.2015.05.021>
- Yoon, S., Monteiro, P.J.M., Macpheec, D.E., Glasser, F.P., Imbabi, M.S.-E., 2014. Statistical evaluation of the mechanical properties of high-volume class F fly ash concretes. *Constr. Build. Mater.* 54, 431–442.
- Younsi, A., Turcry, P., Rozire, E., Aït-Mokhtar, A., Loukili, A., 2011. Performance-based design and carbonation of concrete with high fly ash content. *Cem. Concr. Compos.* 33, 993–1000.
- Zabihi, N., 2012. Effect of Specimen Size and Shape on Strength of Concrete. Eastern Mediterranean University, Gazimağusa, North Cyprus.
- Zhang, M.H., 1995. Microstructure, crack propagation, and mechanical properties of cement pastes containing high volumes of fly ashes. *Cem. Concr. Res.* 25, 1165–1178. [https://doi.org/10.1016/0008-8846\(95\)00109-P](https://doi.org/10.1016/0008-8846(95)00109-P)
- Zhao, H., Sun, W., Wu, X., Gao, B., 2015. The properties of the self-compacting concrete with fly ash and ground granulated blast furnace slag mineral

References

admixtures. *J. Clean. Prod.* 95, 66–74.

Zhao, J., Cai, G., Yang, J., 2016. Bond-slip behavior and embedment length of reinforcement in high volume fly ash concrete. *Mater. Struct.* 49, 2065–2082. <https://doi.org/10.1617/s11527-015-0634-2>

Zhao, Q., Liu, X., Jiang, J., 2015. Effect of curing temperature on creep behavior of fly ash concrete. *Constr. Build. Mater.* 96, 326–333.

APPENDIX A

Appendix A

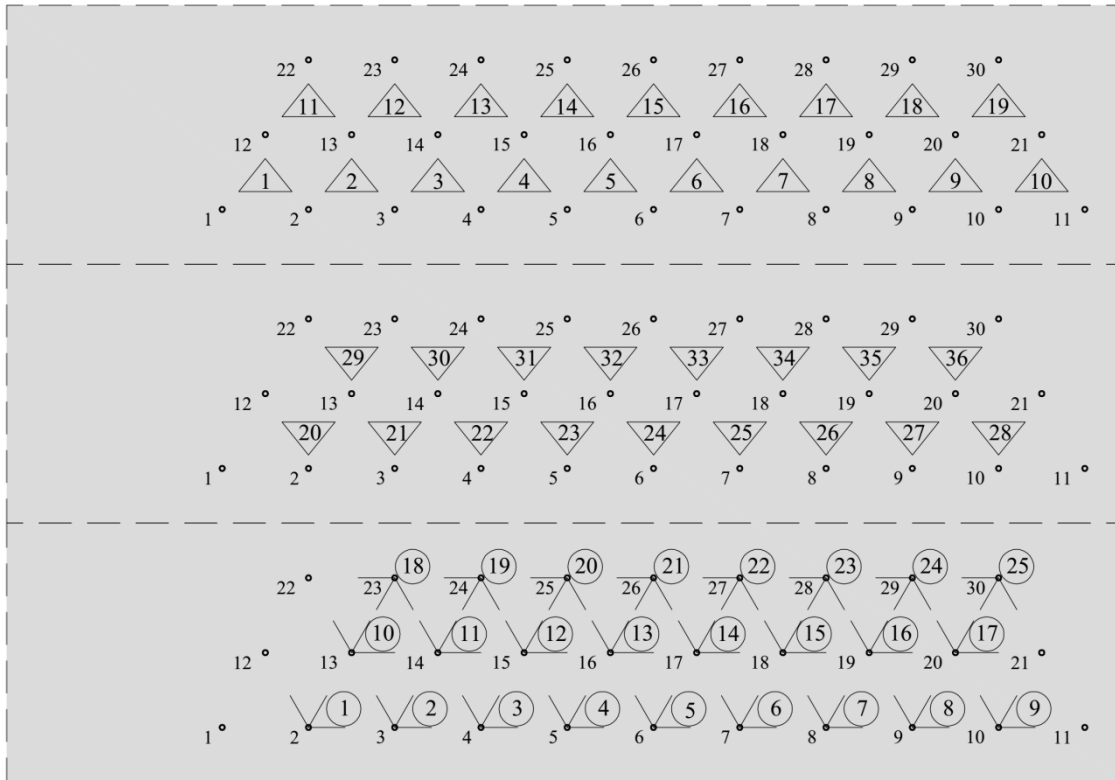


Figure A.1 Concrete strains measuring point notation

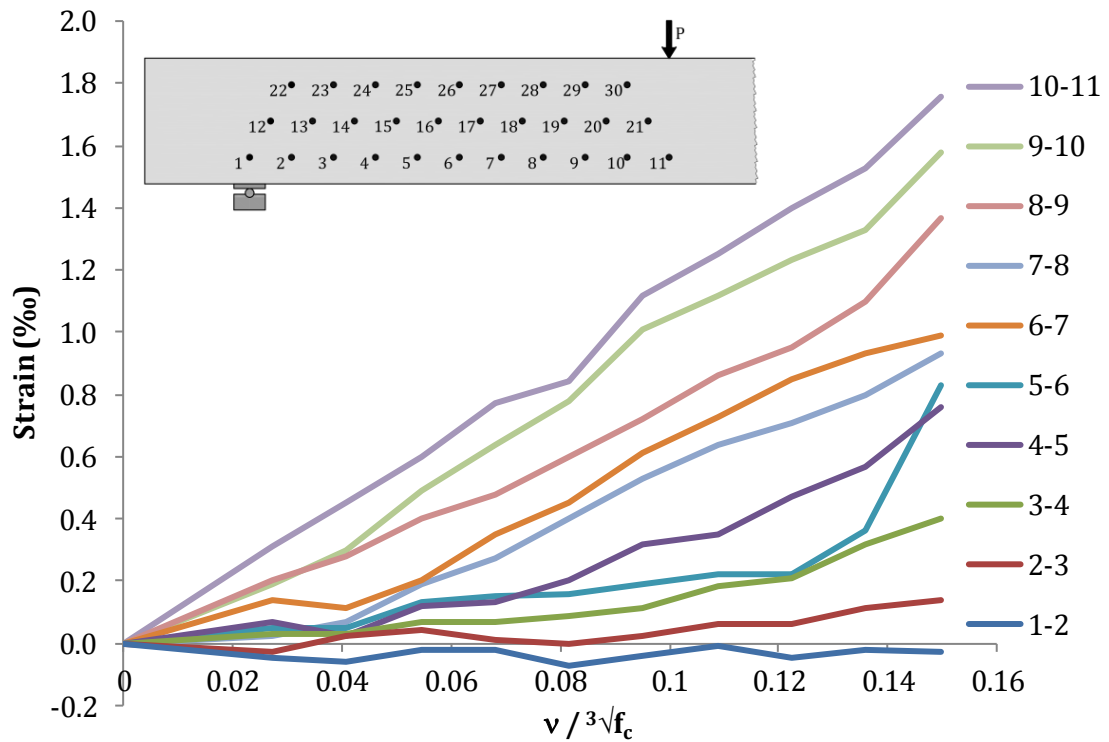


Figure A.2 Measured ϵ_0 strains in the first row for the OPC-1 beam

Appendix A

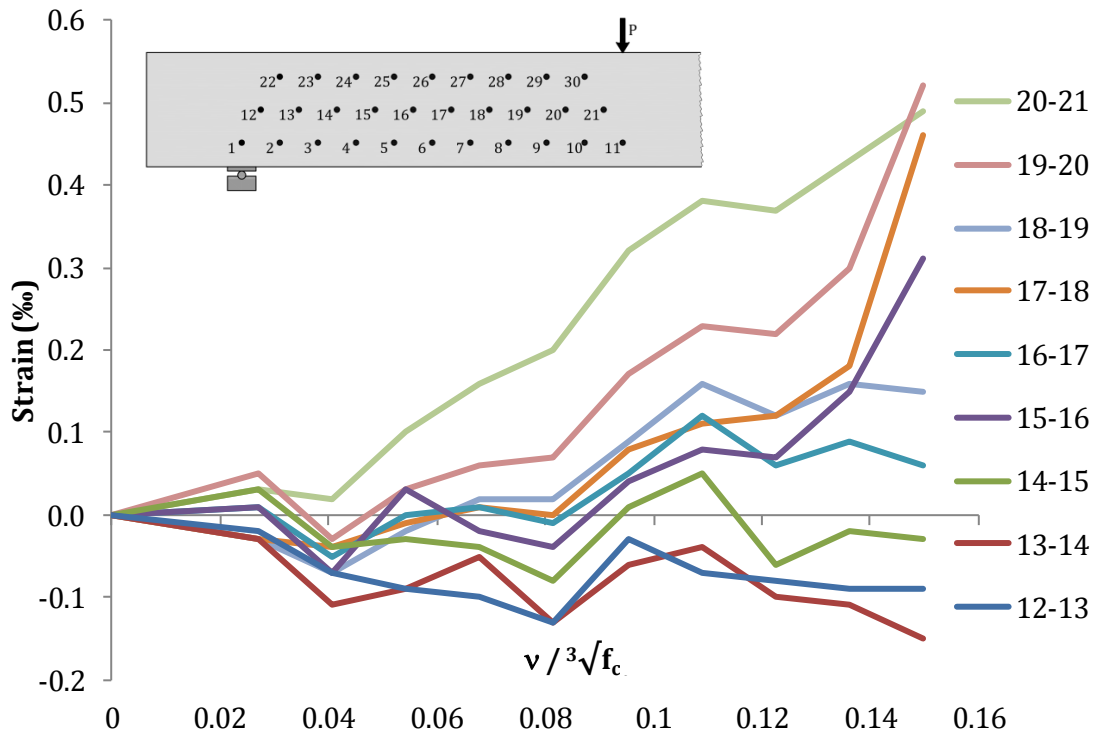


Figure A.3 Measured ϵ_0 strains in the second row for the OPC-1 beam

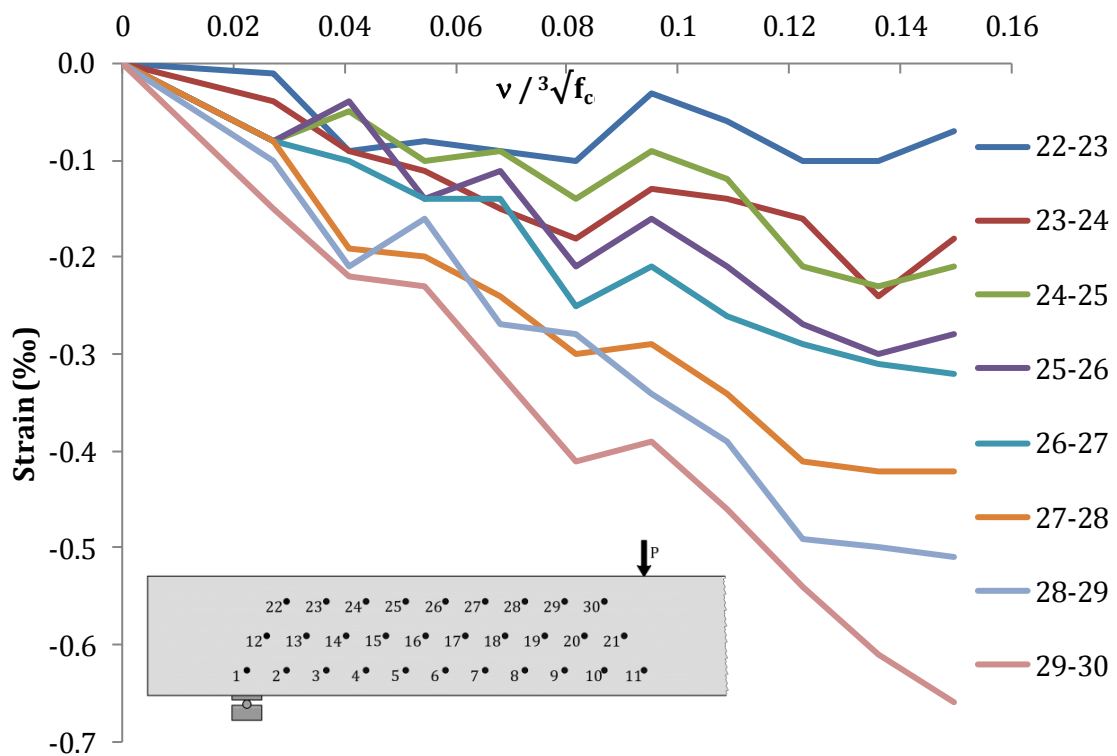


Figure A.4 Measured ϵ_0 strains in the third row for the OPC-1 beam

Appendix A

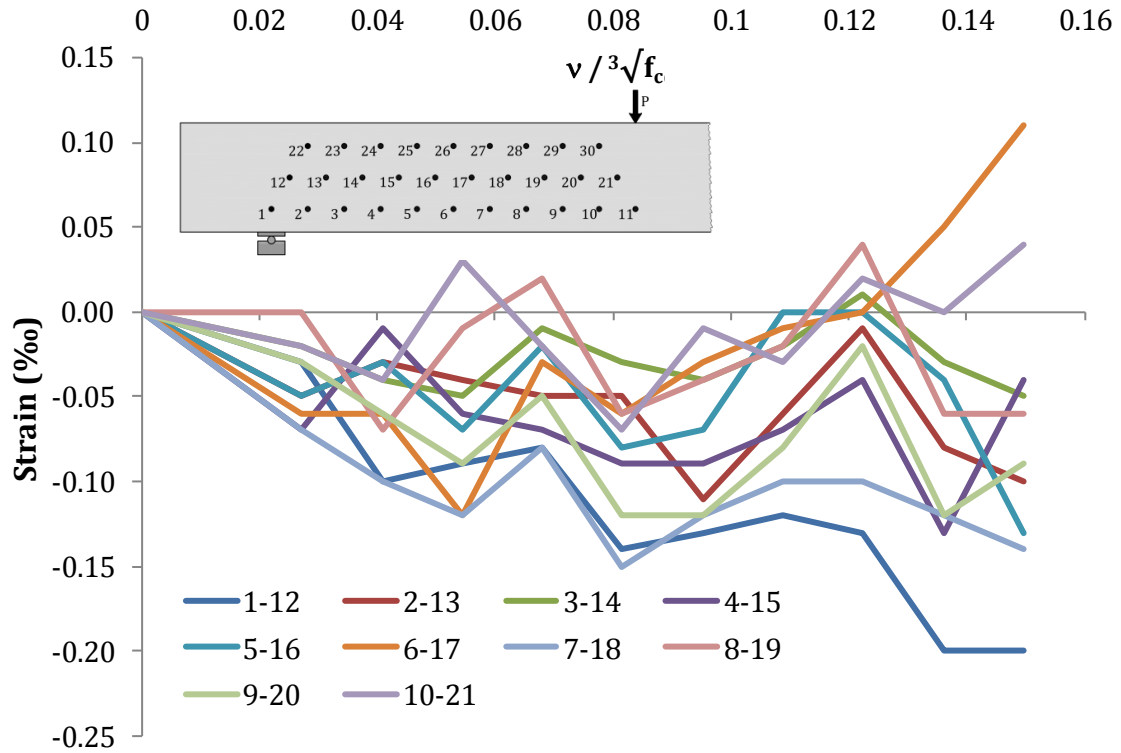


Figure A.5 Measured ε_{60} strains in the first row for the OPC-1 beam

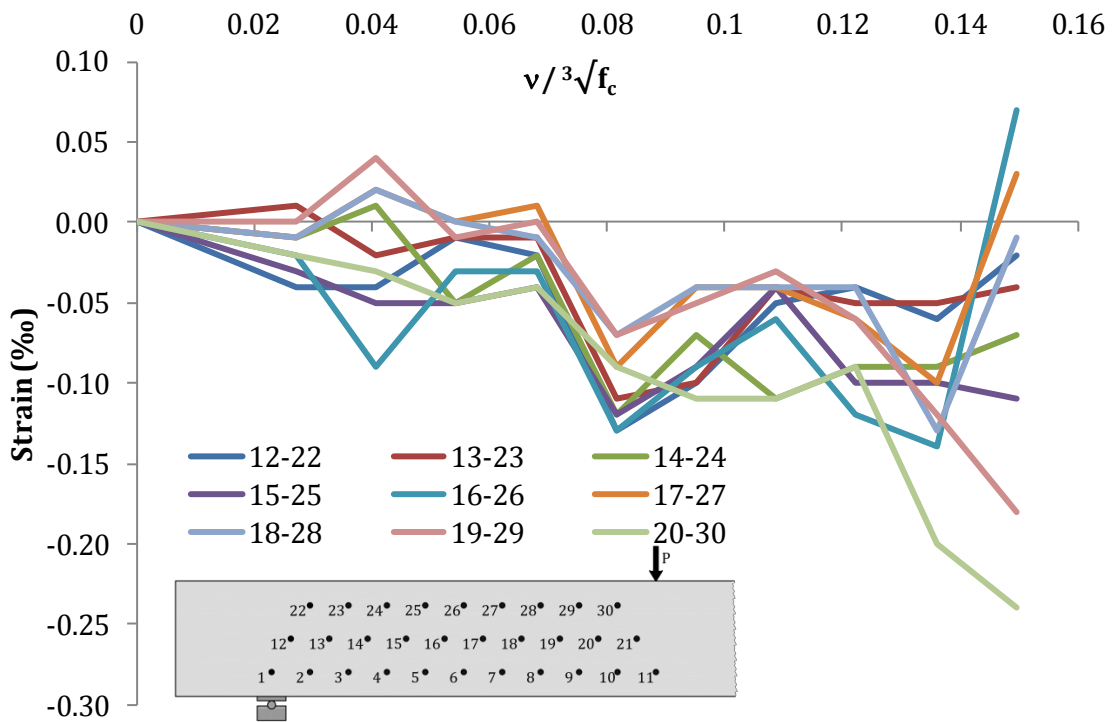


Figure A.6 Measured ε_{60} strains in the second row for the OPC-1 beam

Appendix A

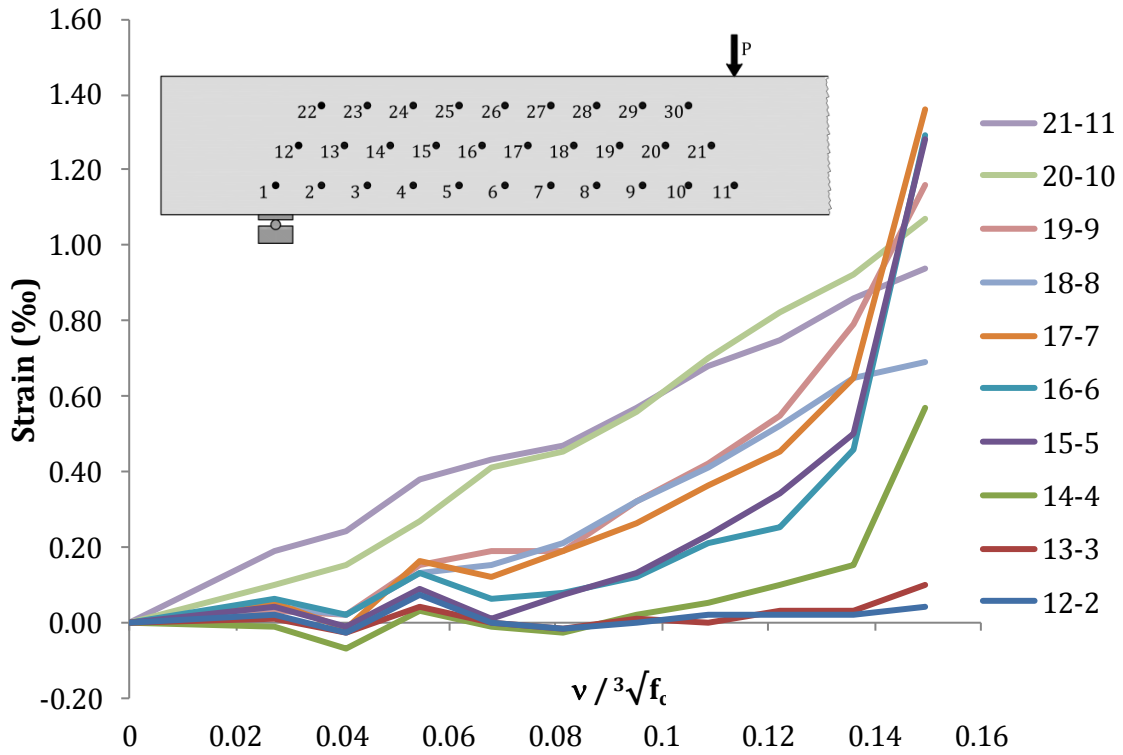


Figure A.7 Measured ε_{120} strains in the first row for the OPC-1 beam

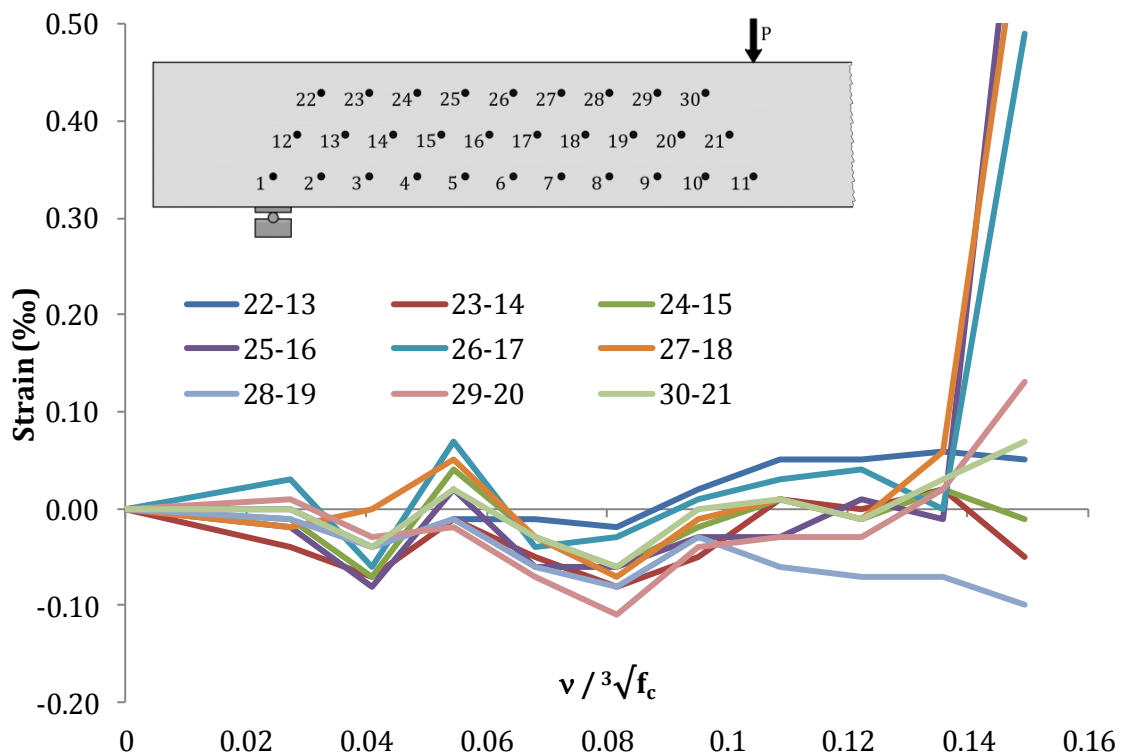


Figure A.8 Measured ε_{120} strains in the second row for the OPC-1 beam

Appendix A

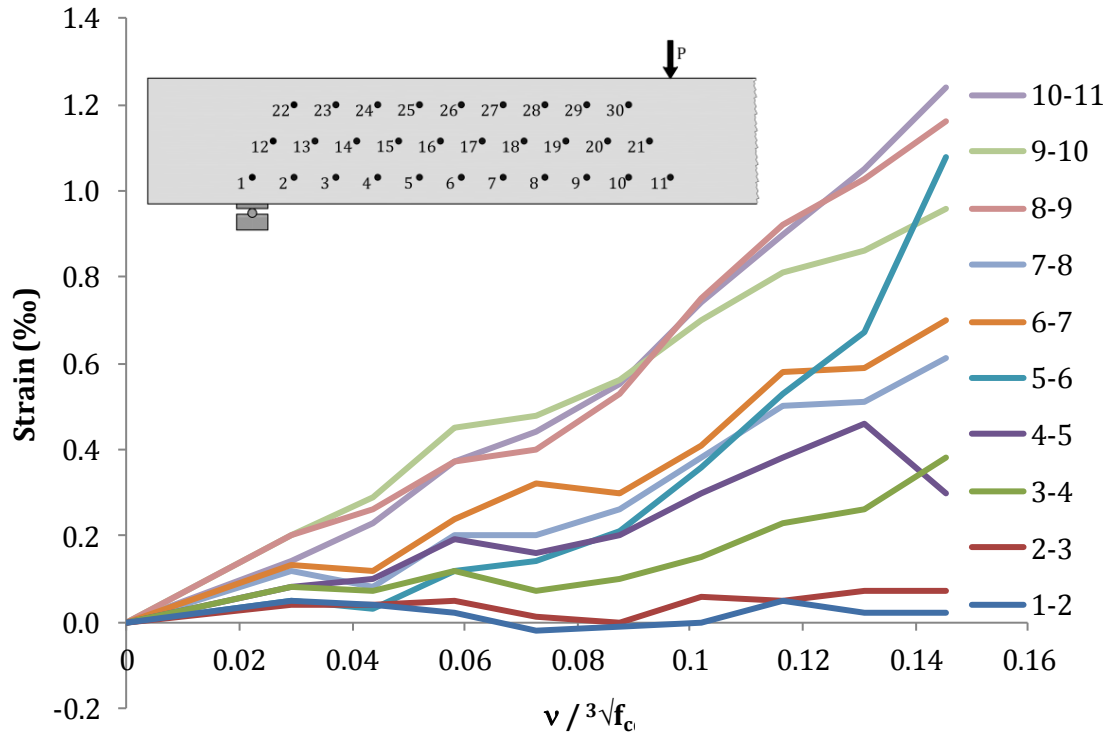


Figure A.9 Measured ε_0 strains in the first row for the HVFAC-1 beam

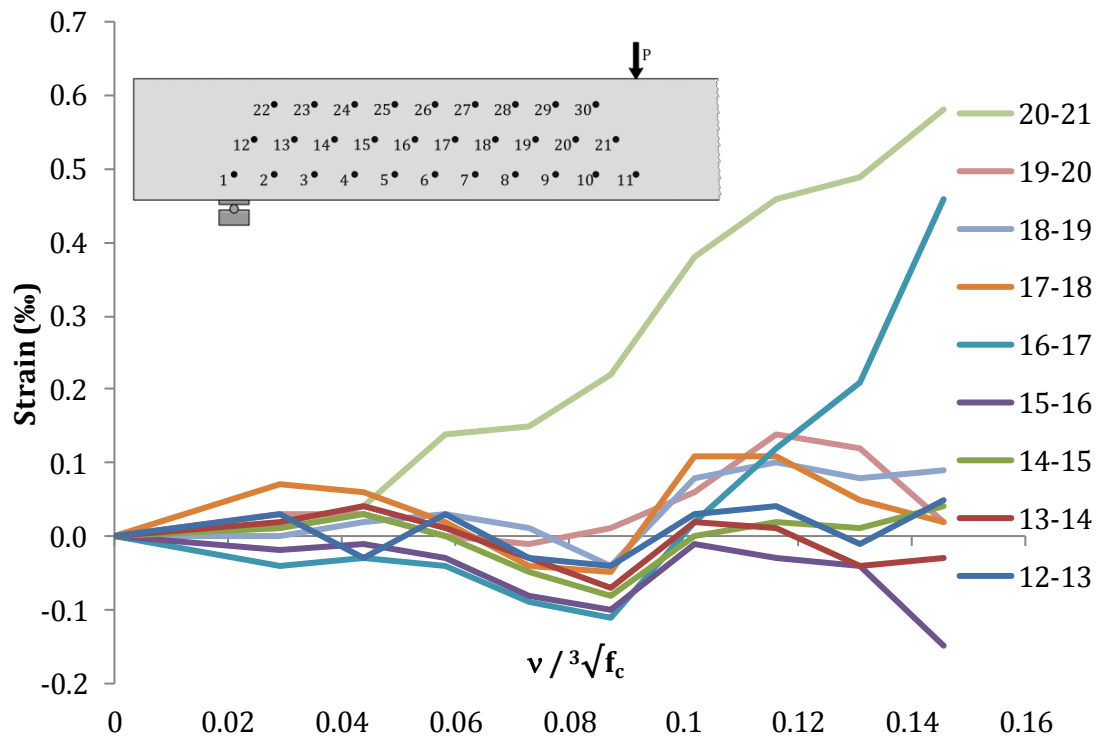


Figure A.10 Measured ε_0 strains in the second row for the HVFAC-1 beam

Appendix A

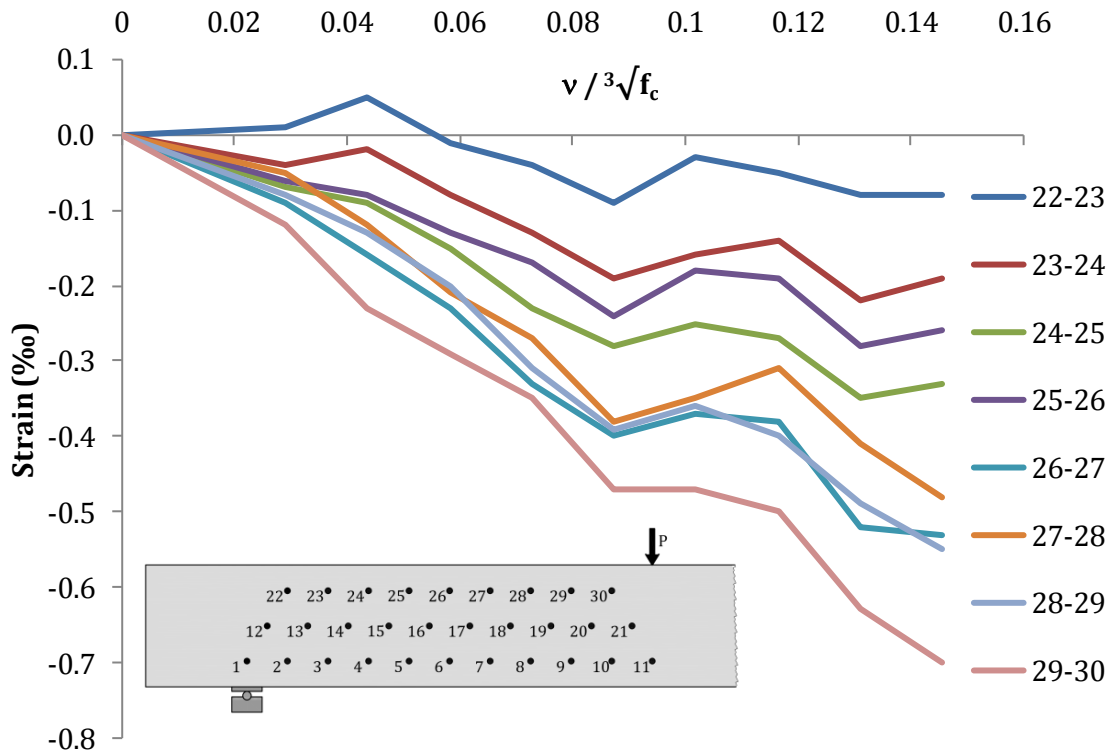


Figure A.11 Measured ε_0 strains in the third row for the HVFAC-1 beam

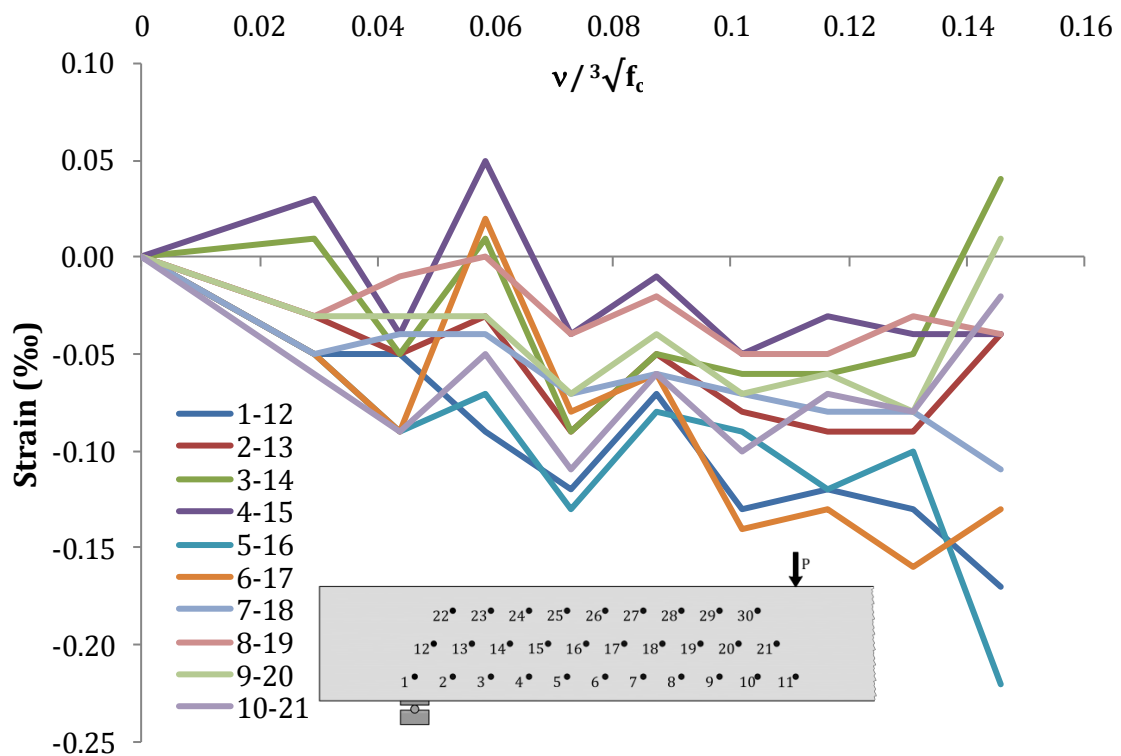


Figure A.12 Measured ε_{60} strains in the first row for the HVFAC-1 beam

Appendix A

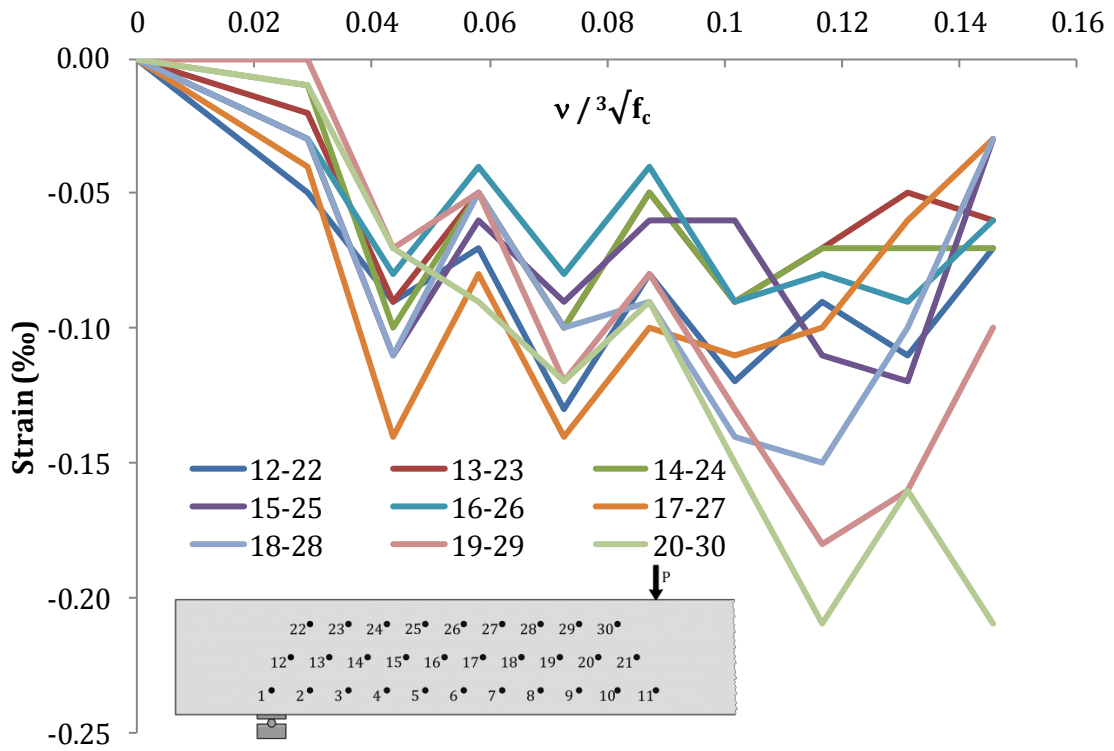


Figure A.13 Measured ε_{60} strains in the second row for HVFAC-1 beam

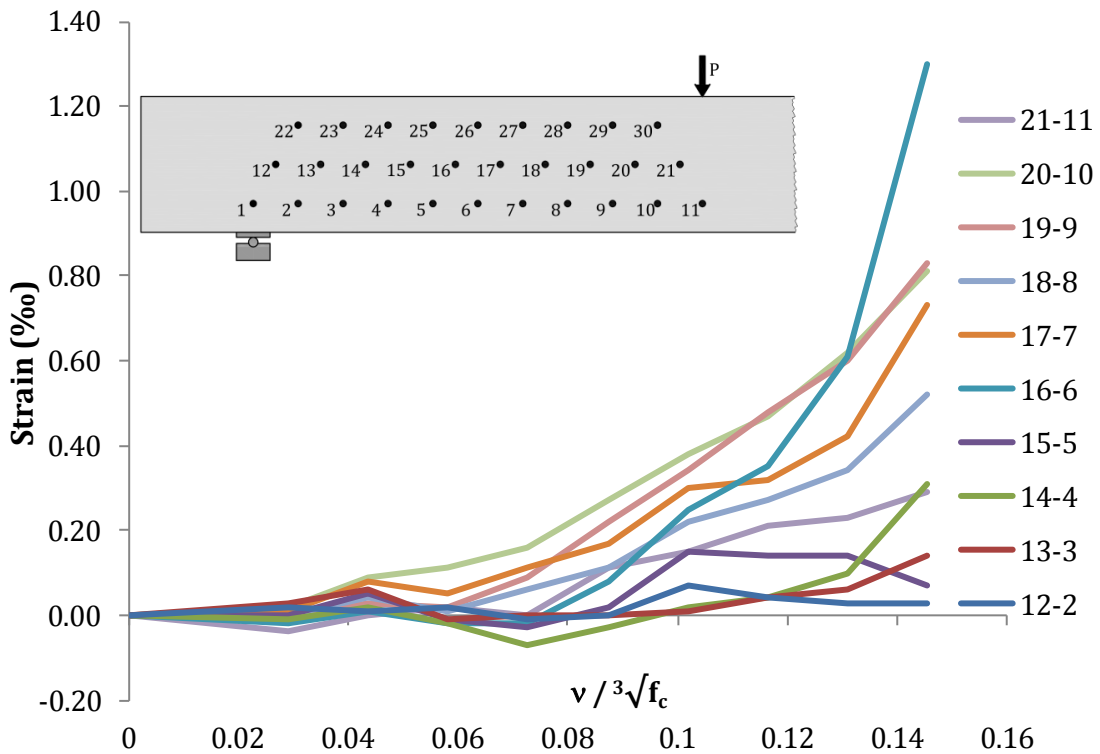


Figure A.14 Measured ε_{120} strains in the first row for the HVFAC-1 beam

Appendix A

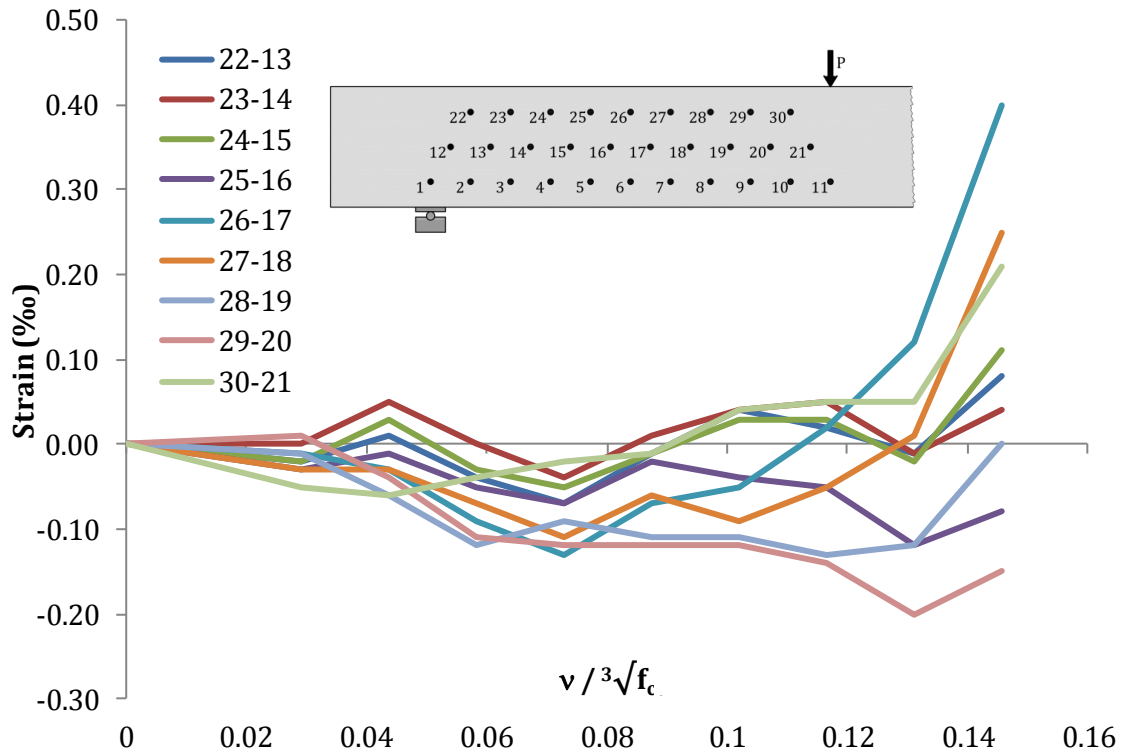


Figure A.15 Measured ε_{120} strains in the second row for the HVFAC-1 beam

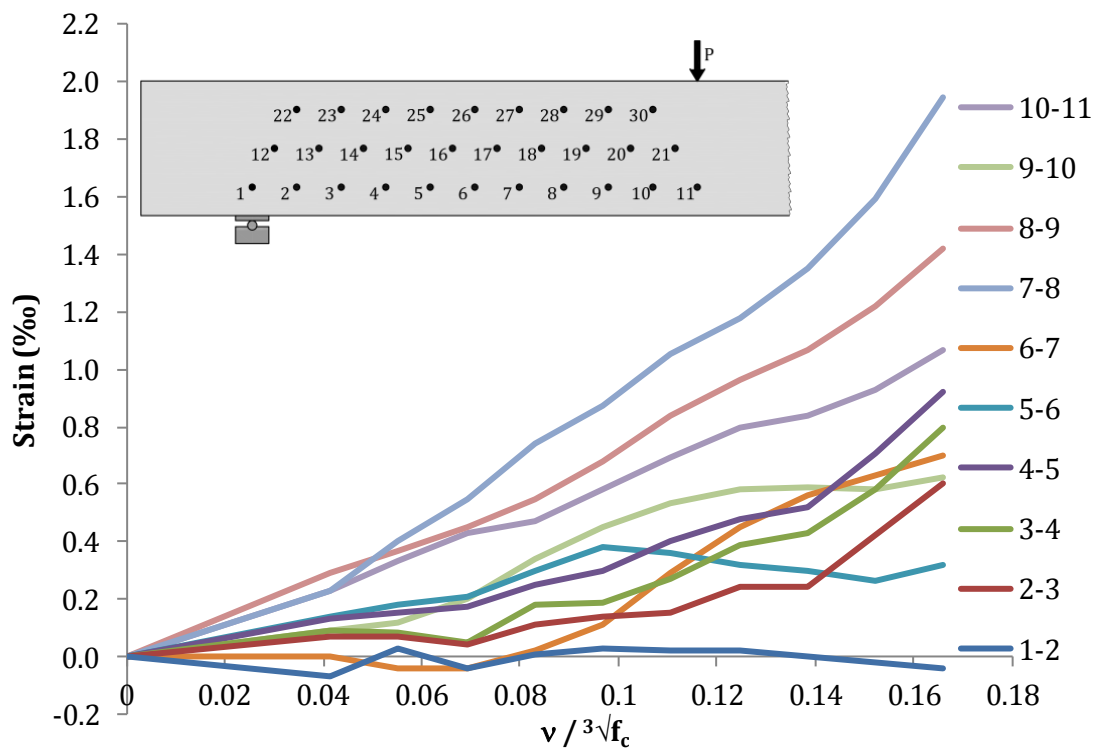


Figure A.16 Measured ε_0 strains in the first row for the OPC-2 beam

Appendix A

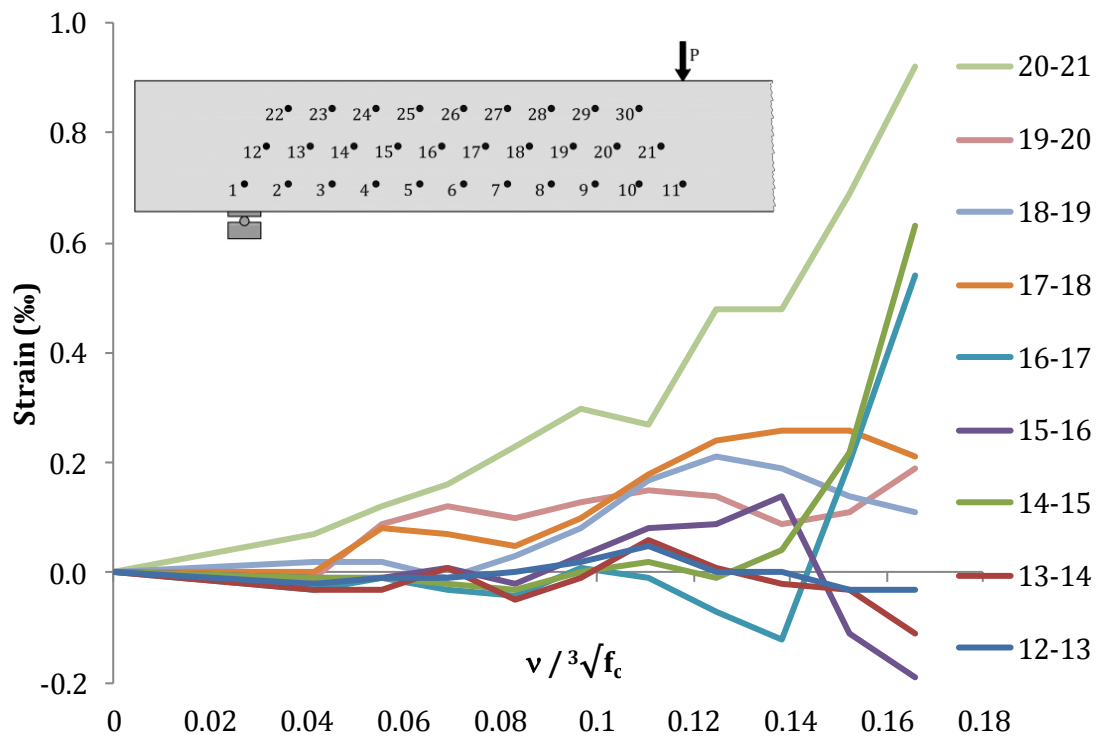


Figure A.17 Measured ϵ_0 strains in the second row for the OPC-2 beam

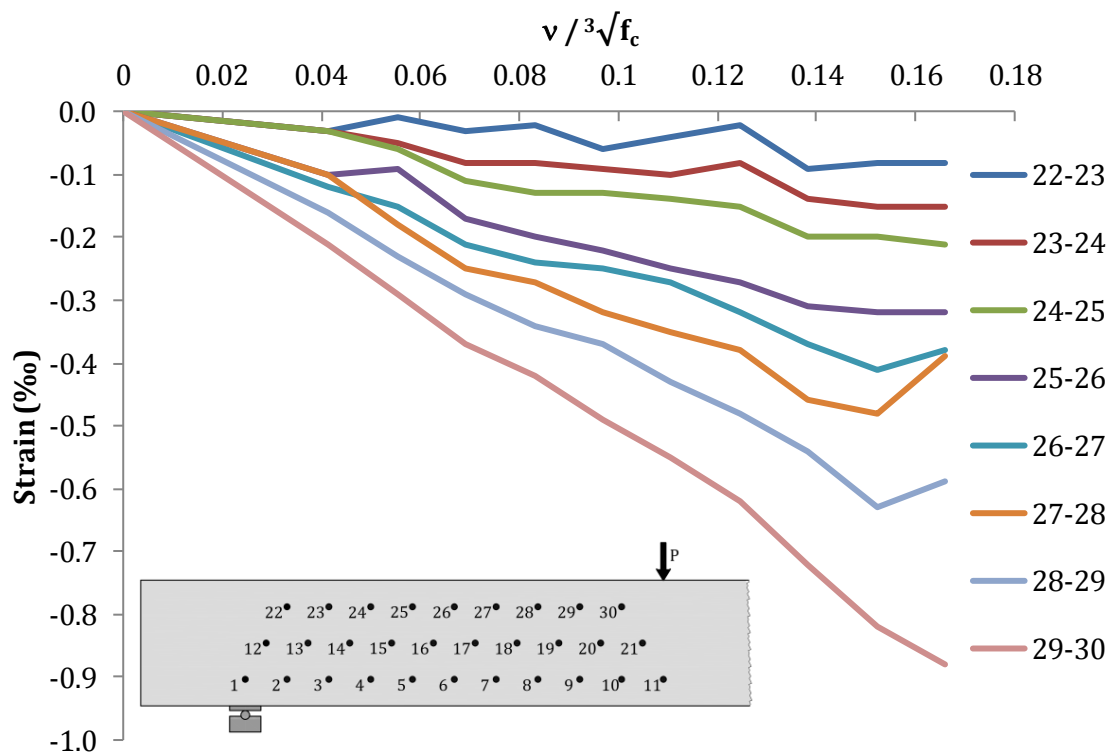


Figure A.18 Measured ϵ_0 strains in the third row for the OPC-2 beam

Appendix A

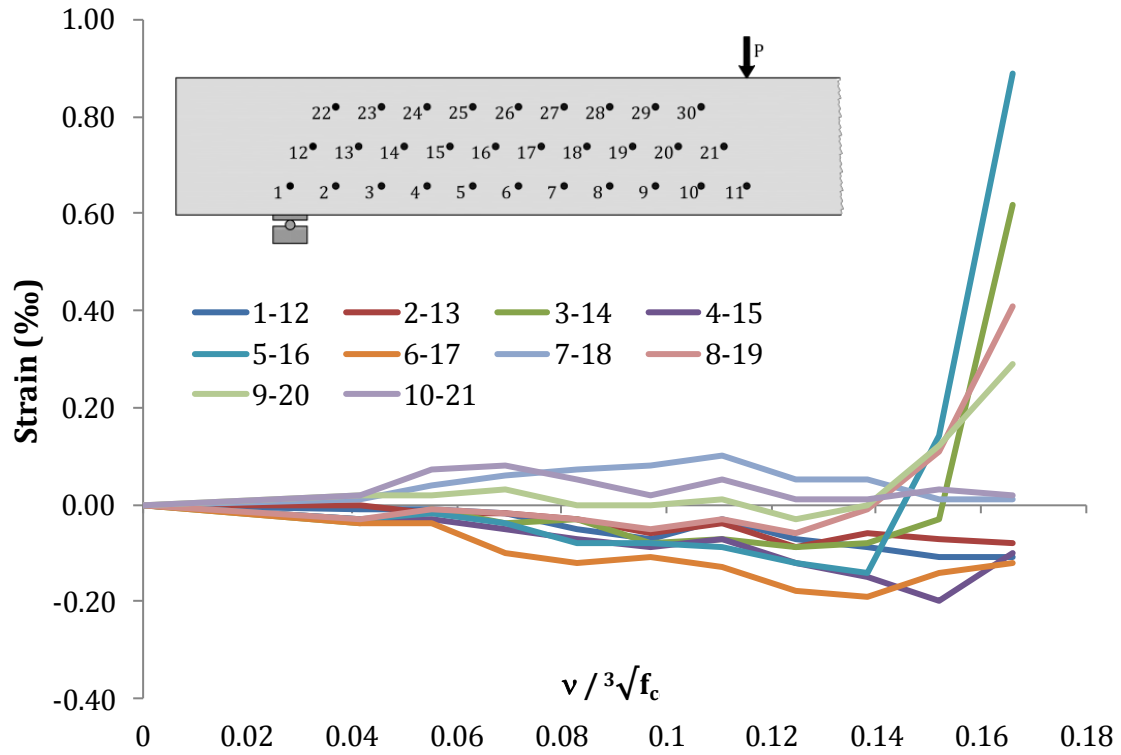


Figure A.19 Measured ϵ_{60} strains in the first row for the OPC-2 beam

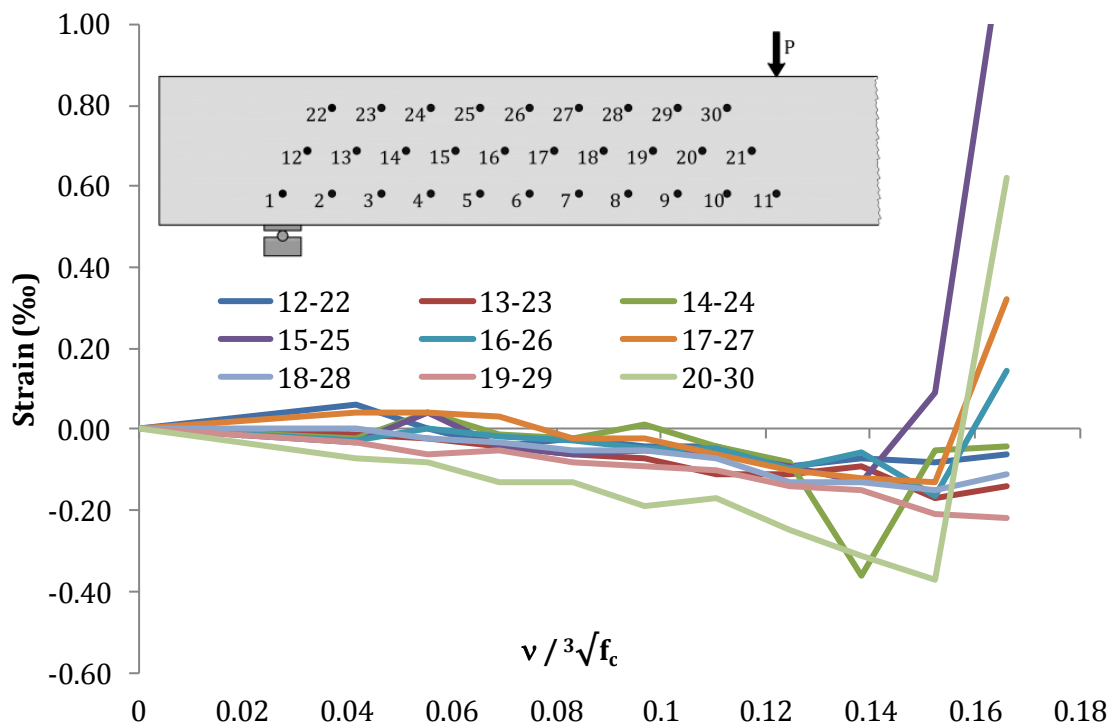


Figure A.20 Measured ϵ_{60} strains in the second row for the OPC-2 beam

Appendix A

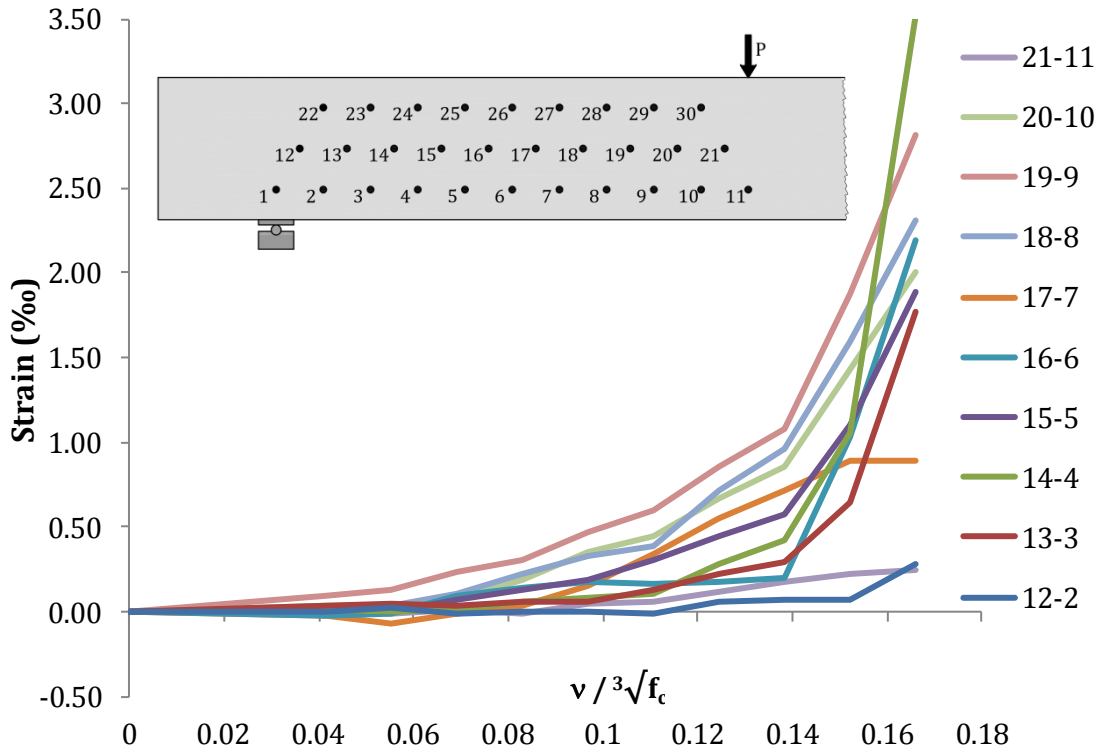


Figure A.21 Measured ϵ_{120} strains in the first row for the OPC-2 beam

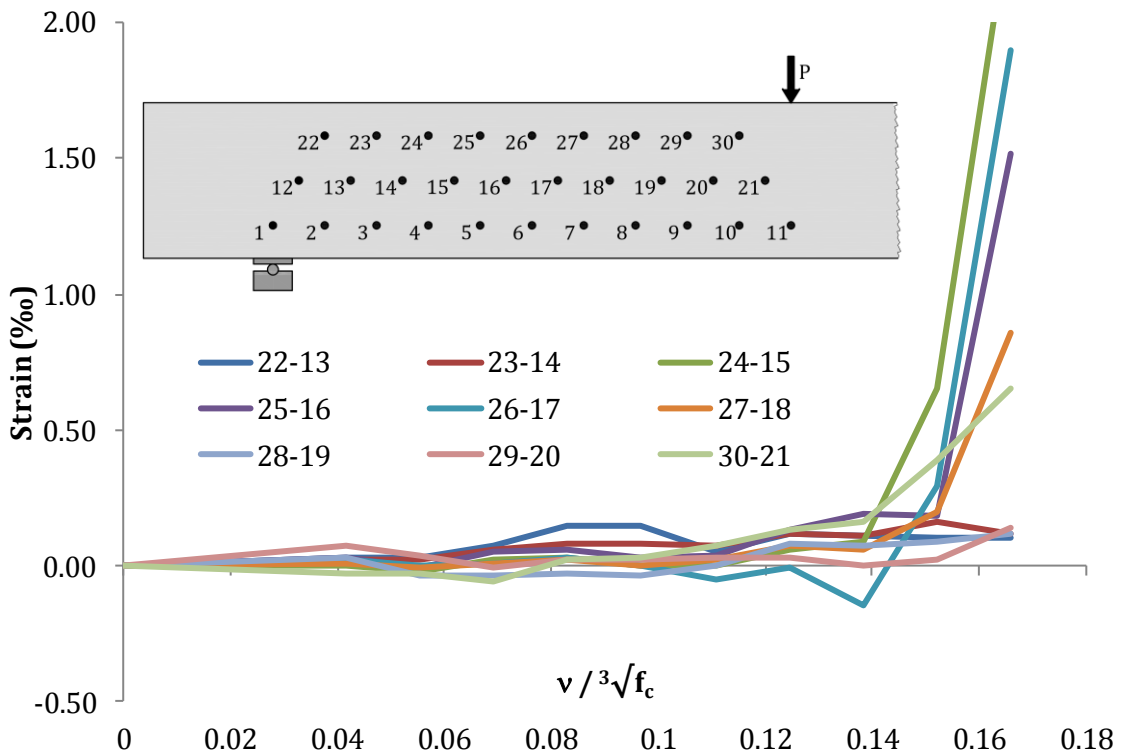


Figure A.22 Measured ϵ_{120} strains in the second row for the OPC-2 beam

Appendix A

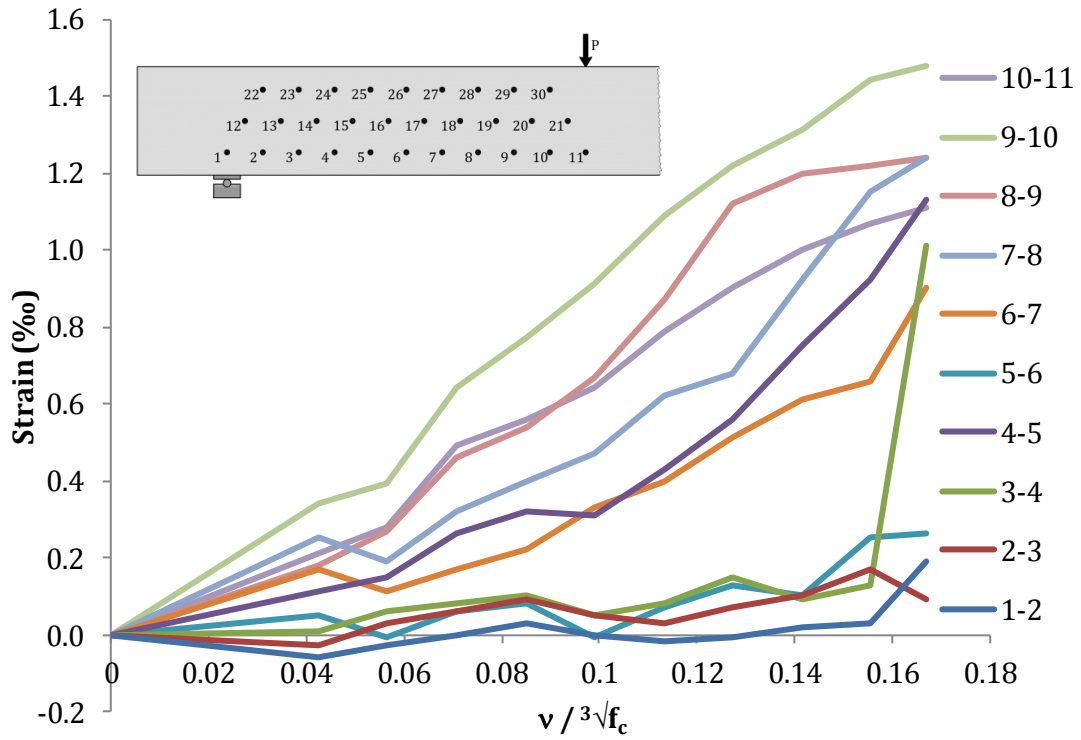


Figure A.23 Measured ε_0 strains in the first row for the HVFAC-2 beam

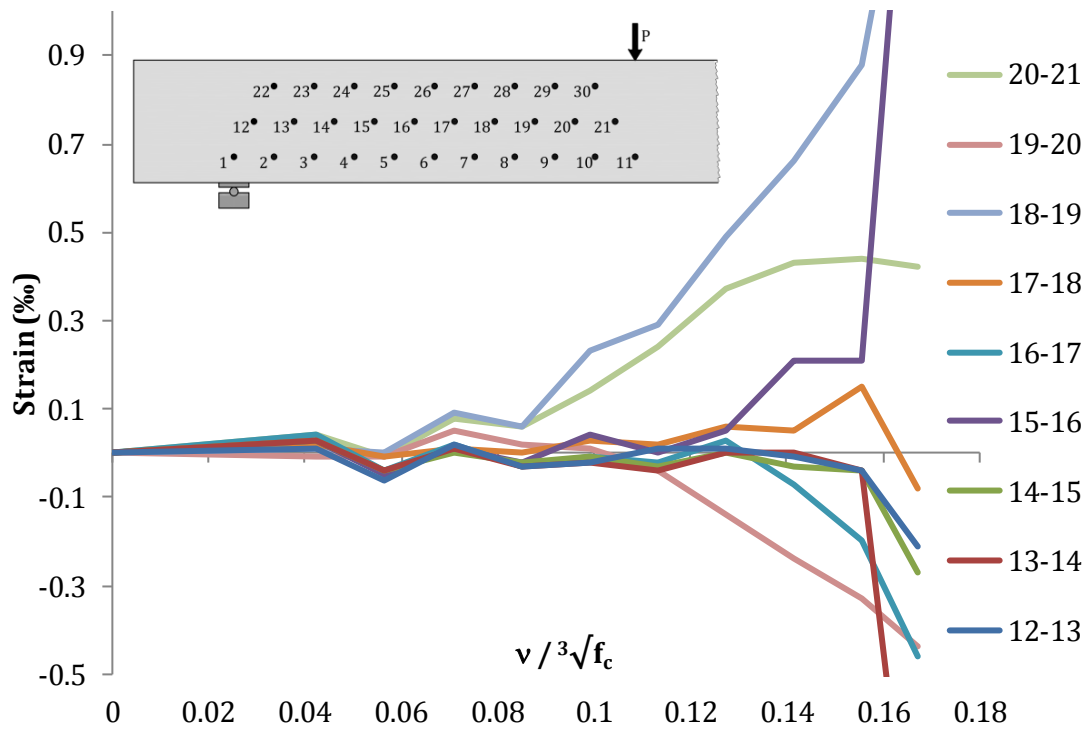


Figure A.24 Measured ε_0 strains in the second row for the HVFAC-2 beam

Appendix A

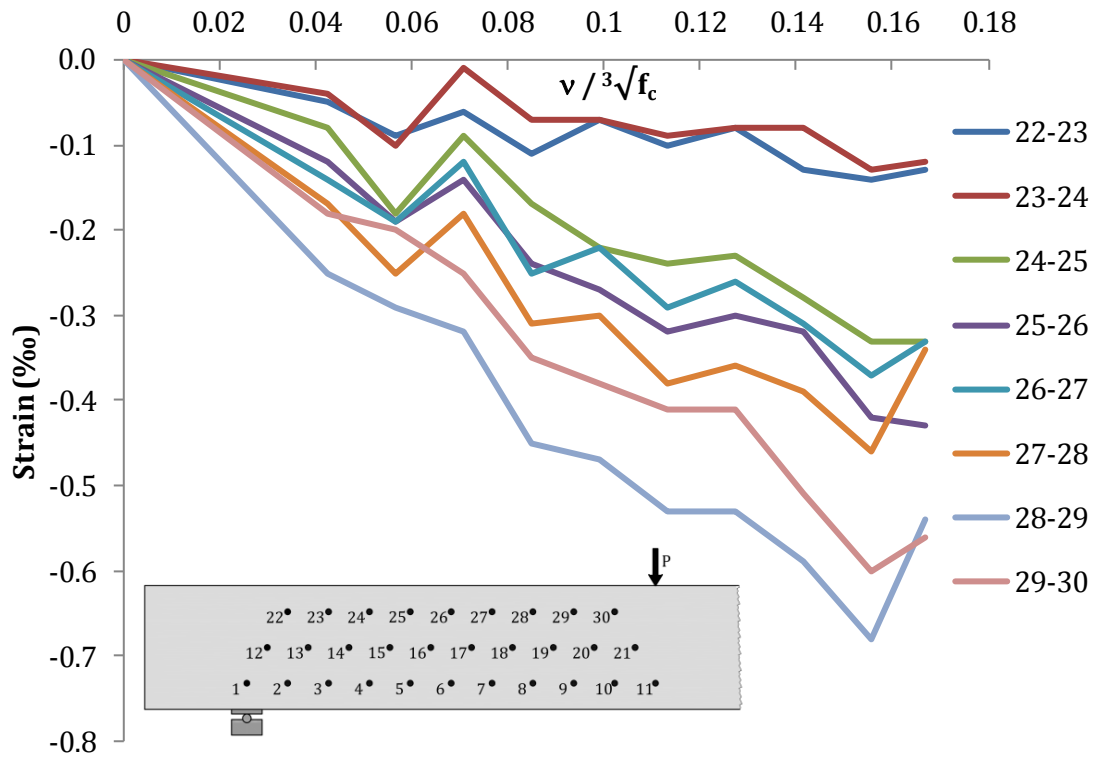


Figure A.25 Measured ϵ_0 strains in the third row for the HVFAC-2 beam

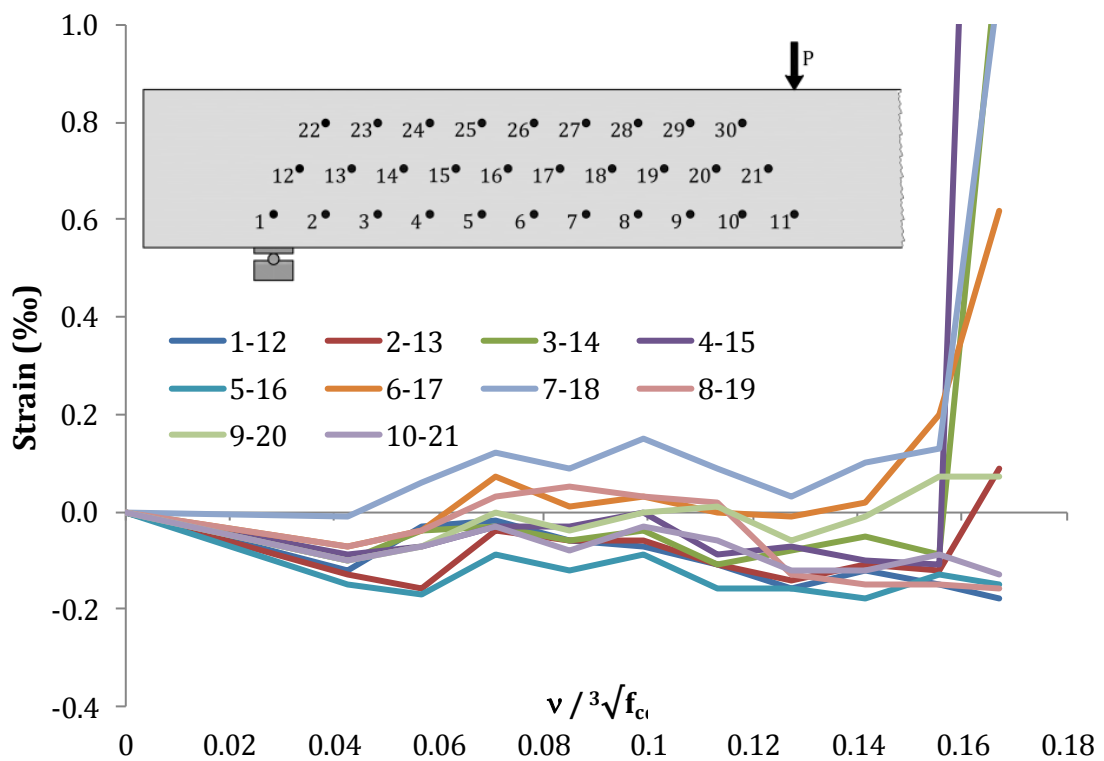


Figure A.26 Measured ϵ_{60} strains in the first row for the HVFAC-2 beam

Appendix A

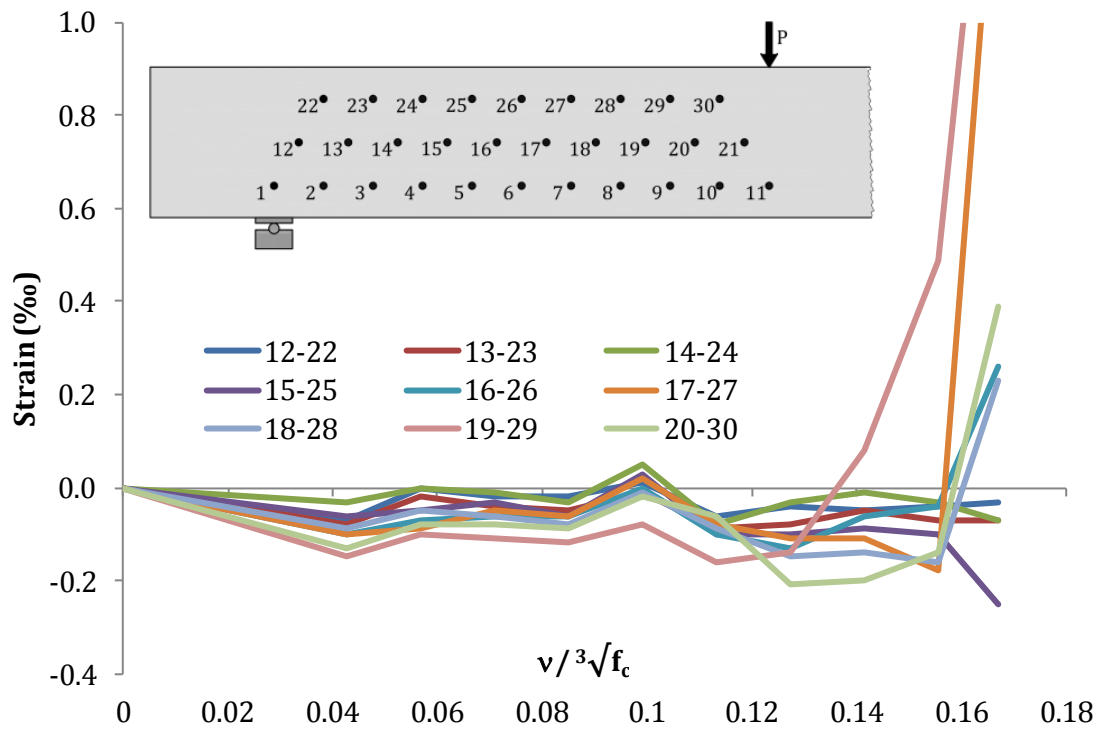


Figure A.27 Measured ϵ_{60} strains in the second row for the HVFAC-2 beam

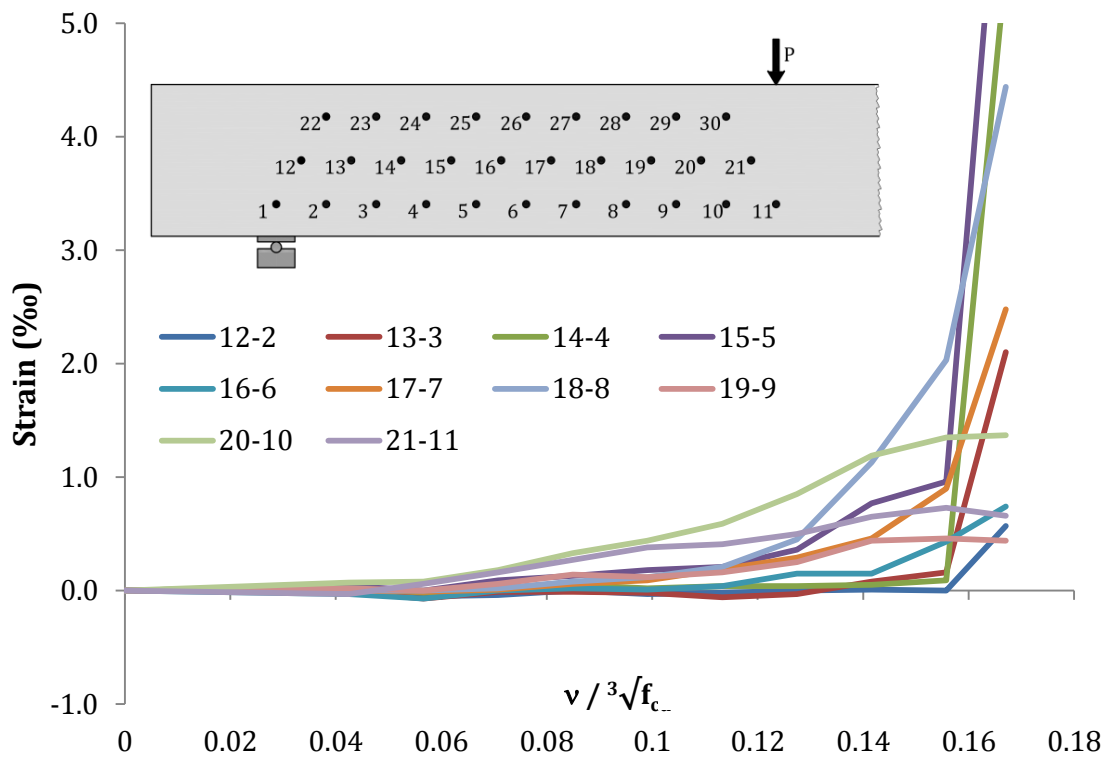


Figure A.28 Measured ϵ_{120} strains in the first row for the HVFAC-2 beam

Appendix A

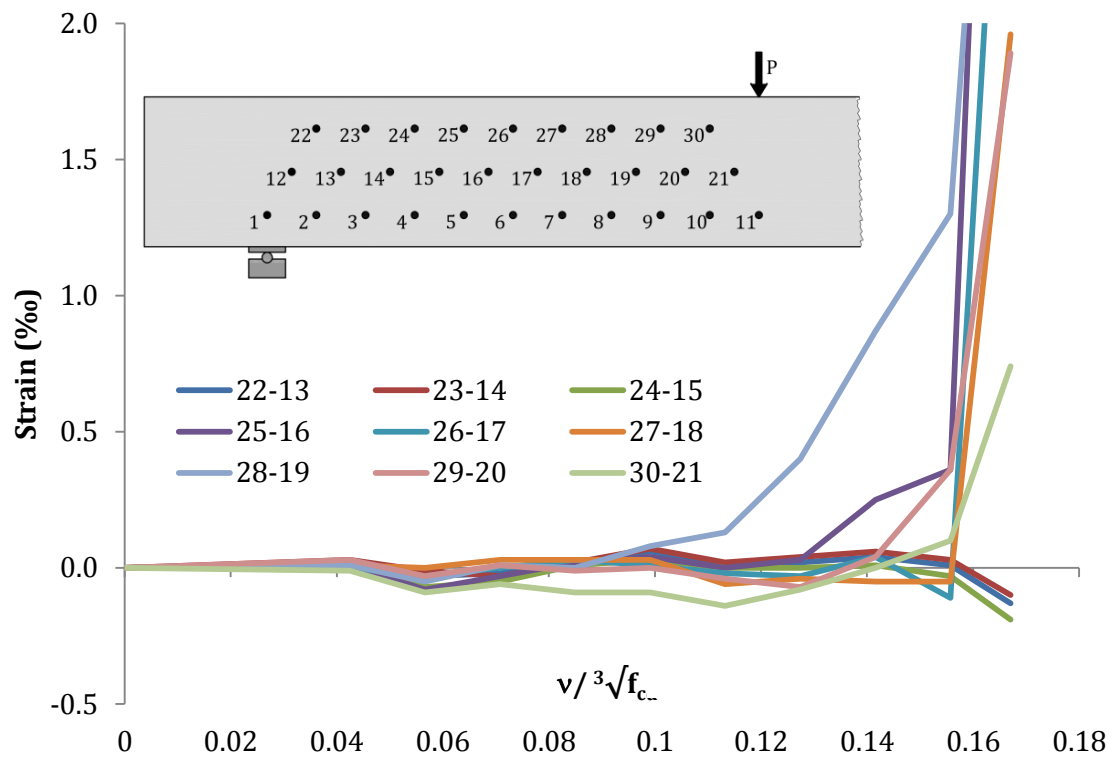


Figure A.29 Measured ε_{120} strains in the second row for the HVFAC-2 beam

APPENDIX B

Table B-1 The HVFAC beams database – flexural behavior

Notation	FA	FA/SCM	w/cm	b	h	l	f _c	E _c	A _{s1}	f _{ys,1}	E _{ys,1}	A _{s,2}	ρ _s	M _{EXP}	M _{Cr}	M _y	u _y	u _{max}
	class	%	-	mm	mm	mm	MPa	GPa	cm ²	MPa	GPa	cm ²	%	kNm	kNm	kNm	mm	mm
CC-1	-	0	0.45	300	460	3600	38.3	35.5	17.0	516	193	5.3	1.50	305	43.0	281.0	17.0	46.5
CC-2	-	0	0.45	300	460	3600	38.3	35.5	17.0	516	193	5.3	1.50	303	42.0	285.0	19.0	44.5
CC-3	-	0	0.45	300	460	3600	38.3	35.5	17.0	516	193	5.3	1.50	314	44.0	283.0	18.0	49.0
HVFAC-1	C	70	0.45	300	460	3600	29.5	32.0	17.0	516	193	5.3	1.50	310	40.0	292.0	19.0	44.7
HVFAC-2	C	70	0.45	300	460	3600	29.5	32.0	17.0	516	193	5.3	1.50	306	41.0	295.0	19.0	41.4
HVFAC-3	C	70	0.45	300	460	3600	29.5	32.0	17.0	516	193	5.3	1.50	309	41.0	298.0	20.0	43.7
00-20-L	-	0	0.56	200	300	3000	32.3	32.8	4.0	412	200	2.0	0.80	54	4.6	46.2	11.2	47.8
00-20-H	-	0	0.56	200	300	3000	32.3	32.8	7.6	412	200	3.8	1.52	78	6.7	69.8	13.8	55.5
00-40-L	-	0	0.45	200	300	3000	35.9	28.3	7.6	412	200	3.8	1.52	81	6.8	71.3	10.5	46.3
00-40-H	-	0	0.45	200	300	3000	35.9	28.3	13.2	412	200	6.6	2.64	118	8.0	101.7	12.8	68.9
00-60-L	-	0	0.35	200	300	3000	48.8	35.0	9.8	412	200	4.9	1.96	94	9.5	81.8	12.2	61.2
00-60-H	-	0	0.35	200	300	3000	48.8	35.0	16.1	412	200	8.0	3.22	137	15.9	111.2	11.2	46.0
35-20-L	F	35	0.44	200	300	3000	33.6	22.8	4.0	412	200	2.0	0.80	56	4.6	41.4	8.0	52.2
35-20-H	F	35	0.44	200	300	3000	33.6	22.8	7.6	412	200	3.8	1.52	77	8.9	65.3	9.4	52.0
35-40-L	F	35	0.35	200	300	3000	45.8	28.3	7.6	412	200	3.8	1.52	85	7.1	74.9	10.7	48.4
35-40-H	F	35	0.35	200	300	3000	45.8	28.3	13.2	412	200	6.6	2.64	120	9.3	108.7	11.2	45.0
35-60-L	F	35	0.30	200	300	3000	51.3	34.8	9.8	412	200	4.9	1.96	93	10.0	77.5	8.0	31.8
35-60-H	F	35	0.30	200	300	3000	51.3	34.8	16.1	412	200	8.0	3.22	138	12.2	125.6	10.6	41.9
50-20-L	F	50	0.40	200	300	3000	24.4	29.0	4.0	412	200	2.0	0.80	56	5.1	48.3	8.2	47.4
50-20-H	F	50	0.40	200	300	3000	24.4	29.0	7.6	412	200	3.8	1.52	76	6.5	69.5	11.1	49.6
50-40-L	F	50	0.48	200	300	3000	22.3	19.9	7.6	412	200	3.8	1.52	83	6.9	72.1	11.7	59.1
50-40-H	F	50	0.48	200	300	3000	22.3	19.9	13.2	412	200	6.6	2.64	116	13.8	102.6	11.7	42.5
50-60-L	F	50	0.33	200	300	3000	49.2	29.2	9.8	412	200	4.9	1.96	108	12.2	74.3	9.8	61.1
50-60-H	F	50	0.33	200	300	3000	49.2	29.2	16.1	412	200	8.0	3.22	148	16.6	126.3	11.3	40.1

Arzoumanidi et al 2014

Yoo et al 2015

T. T. 2016*	OPCC-P1	-	0	0.40	100	150	1300	23.6	-	1.0	-	-	1.0	0.84	6	-	5.5	2.7	3.6
	50%-P1	F	50	0.40	100	150	1300	22.9	-	1.0	-	-	1.0	0.84	6	-	5.0	2.5	3.7
	55%-P1	F	55	0.40	100	150	1300	16.6	-	1.0	-	-	1.0	0.84	5	-	4.9	2.9	3.8
	60%-P1	F	60	0.40	100	150	1300	12.4	-	1.0	-	-	1.0	0.84	5	-	4.3	1.5	2.4
Gowda et al. 2013	S1	-	0	0.31	125	250	1700	56.9	-	2.6	595	-	-	0.91	30	5.8	-	-	17.9
	S2	-	0	0.31	125	250	1700	61.0	-	2.6	595	-	-	1.61	36	5.8	-	-	23.7
	S3	-	0	0.31	125	250	1700	73.2	-	2.6	595	-	-	2.23	61	7.6	-	-	13.4
	S4	F	20	0.31	125	250	1700	58.4	-	4.5	593	-	-	0.91	29	4.9	-	-	32.6
	S5	F	20	0.31	125	250	1700	71.9	-	4.5	593	-	-	1.61	39	4.9	-	-	29.8
	S6	F	20	0.31	125	250	1700	65.0	-	4.5	593	-	-	2.23	55	5.3	-	-	15.8
	S7	F	35	0.31	125	250	1700	62.3	-	6.3	569	-	-	0.91	29	4.9	-	-	25.7
	S8	F	35	0.31	125	250	1700	73.7	-	6.3	569	-	-	1.61	42	5.3	-	-	21.8
	S9	F	35	0.31	125	250	1700	65.2	-	6.3	569	-	-	2.23	59	4.9	-	-	25.1
Dragas 2018	OPC-1	-	0	0.58	200	300	3000	58.5	33.0	1.5	666	202	1.01	0.28	51	20.0	40.0	12.0	128.0
	OPC-2	-	0	0.58	200	300	3000	62.4	33.0	7.6	560	200	1.01	1.46	224	30.0	210.0	23.0	45.2
	HVFAC-2	F	64	0.35	200	300	3000	47.6	27.6	1.5	666	202	1.01	0.28	55	15.0	35.0	18.0	122.0
	HVFAC-2	F	64	0.35	200	300	3000	53.1	27.6	7.6	560	200	1.01	1.46	225	30.0	210.0	24.0	57.6

Table B-2 The HVFAC beams database – shear behavior

Notation	FA class	FA/CM (%)	w/cm	b (mm)	h (mm)	a (mm)	a/d (-)	f _c (MPa)	d _g (mm)	A _s (mm ²)	n _s (-)	φ _s (mm)	ρ _s (%)	φ _w (mm)	s (mm)	ρ _w (%)	f _{yw} (MPa)	V _{EXP} (kN)
FH-NS-5-1	C	70	0.40	305	457	1200	3.06	21.5	19	1943.1	5	22	1.59	-	-	-	-	140.7
FH-NS-5-2	C	70	0.40	305	457	1200	3.06	21.1	19	1943.1	5	22	1.59	-	-	-	-	114.9
FH-NS-6-1	C	70	0.40	305	457	1200	3.25	21.5	19	2331.7	6	22	2.03	-	-	-	-	131.9
FH-NS-6-2	C	70	0.40	305	457	1200	3.25	21.1	19	2331.7	6	22	2.03	-	-	-	-	121.5
FH-NS-8-1	C	70	0.40	305	457	1200	3.25	21.5	19	3109.0	8	22	2.71	-	-	-	-	170.9
FH-NS-8-2	C	70	0.40	305	457	1200	3.25	21.1	19	3109.0	8	22	2.71	-	-	-	-	162.9
FH-S-8-1	C	70	0.40	305	457	1200	3.25	23.8	19	3109.0	8	22	1.27	10	178	0.262	432.0	328.6
FH-S-8-2	C	70	0.40	305	457	1200	3.25	23.8	19	3109.0	8	22	1.27	10	178	0.262	432.0	332.7
FL-NS-4-1	C	70	0.40	305	457	1200	3.06	29.9	19	1554.5	4	22	1.27	-	-	-	-	134.3

Arezoumandi, 2013

Appendix B

FL-NS-4-2	C	70	0.40	305	457	1200	3.06	20.2	19	1554.5	4	22	1.27	-	-	-	122.8
FL-NS-6-1	C	70	0.40	305	457	1200	3.25	29.9	19	2331.7	6	22	2.03	-	-	-	150.4
FL-NS-6-2	C	70	0.40	305	457	1200	3.25	20.2	19	2331.7	6	22	2.03	-	-	-	168.1
FL-NS-8-1	C	70	0.40	305	457	1200	3.25	29.9	19	3109.0	8	22	2.71	-	-	-	162.4
FL-NS-8-2	C	70	0.40	305	457	1200	3.25	20.2	19	3109.0	8	22	2.71	-	-	-	201.5
FL-S-8-1	C	70	0.40	305	457	1200	3.25	33.8	19	3109.0	8	22	5.27	10	178	0.262	432.0
FL-S-8-2	C	70	0.40	305	457	1200	3.25	33.8	19	3109.0	8	22	5.27	10	178	0.262	432.0
CL-NS-4-1	-	0	0.40	305	457	1200	3.06	28.3	19	1554.5	4	22	1.27	-	-	-	119.7
CL-NS-4-2	-	0	0.40	305	457	1200	3.06	25.8	19	1554.5	4	22	1.27	-	-	-	113.9
CL-NS-6-1	-	0	0.40	305	457	1200	3.25	28.3	19	2331.7	6	22	2.03	-	-	-	153.5
CL-NS-6-2	-	0	0.40	305	457	1200	3.25	25.8	19	2331.7	6	22	2.03	-	-	-	144.6
CL-NS-8-1	-	0	0.40	305	457	1200	3.25	28.3	19	3109.0	8	22	2.71	-	-	-	147.7
CL-NS-8-2	-	0	0.40	305	457	1200	3.25	25.8	19	3109.0	8	22	2.71	-	-	-	143.7
F1-NS-4-1	C	50	0.35	305	457	1200	3.06	31.6	19	1554.5	4	22	1.27	-	-	-	127.0
F1-NS-4-2	C	50	0.35	305	457	1200	3.06	32.7	19	1554.5	4	22	1.27	-	-	-	134.1
F1-NS-6-1	C	50	0.35	305	457	1200	3.25	31.6	19	2331.7	6	22	2.03	-	-	-	163.9
F1-NS-6-2	C	50	0.35	305	457	1200	3.25	32.7	19	2331.7	6	22	2.03	-	-	-	133.7
F1-NS-8-1	C	50	0.35	305	457	1200	3.25	31.6	19	3109.0	8	22	2.71	-	-	-	164.8
F1-NS-8-2	C	50	0.35	305	457	1200	3.25	32.7	19	3109.0	8	22	2.71	-	-	-	163.7
F2-NS-4-1	C	70	0.40	305	457	1200	3.06	29.9	19	1554.5	4	22	1.27	-	-	-	134.3
F2-NS-4-2	C	70	0.40	305	457	1200	3.06	20.2	19	1554.5	4	22	1.27	-	-	-	122.8
F2-NS-6-1	C	70	0.40	305	457	1200	3.25	29.9	19	2331.7	6	22	2.03	-	-	-	150.4
F2-NS-6-2	C	70	0.40	305	457	1200	3.25	20.2	19	2331.7	6	22	2.03	-	-	-	168.1
F2-NS-8-1	C	70	0.40	305	457	1200	3.25	29.9	19	3109.0	8	22	2.71	-	-	-	162.4
F2-NS-8-2	C	70	0.40	305	457	1200	3.25	20.2	19	3109.0	8	22	2.71	-	-	-	201.5
CL-NS-4-1	C	0	0.40	305	457	1200	3.06	28.3	19	1554.5	4	22	1.27	-	-	-	119.7
CL-NS-4-2	C	0	0.40	305	457	1200	3.06	25.8	19	1554.5	4	22	1.27	-	-	-	113.9
CL-NS-6-1	C	0	0.40	305	457	1200	3.25	28.3	19	2331.7	6	22	2.03	-	-	-	153.5
CL-NS-6-2	C	0	0.40	305	457	1200	3.25	25.8	19	2331.7	6	22	2.03	-	-	-	144.6
CL-NS-8-1	C	0	0.40	305	457	1200	3.25	28.3	19	3109.0	8	22	2.71	-	-	-	147.7
CL-NS-8-2	C	0	0.40	305	457	1200	3.25	25.8	19	3109.0	8	22	2.71	-	-	-	143.7
CH-NS-5-1	-	0	0.40	305	457	1200	3.06	33.6	19	1943.1	5	22	1.59	-	-	-	140.6
CH-NS-5-2	-	0	0.40	305	457	1200	3.06	31.2	19	1943.1	5	22	1.59	-	-	-	138.1
CH-NS-6-1	-	0	0.40	305	457	1200	3.25	33.6	19	2331.7	6	22	2.03	-	-	-	174.1
CH-NS-6-2	-	0	0.40	305	457	1200	3.25	31.2	19	2331.7	6	22	2.03	-	-	-	143.9
CH-NS-8-1	-	0	0.40	305	457	1200	3.25	33.6	19	3109.0	8	22	2.71	-	-	-	219.5
CH-NS-8-2	-	0	0.40	305	457	1200	3.25	31.2	19	3109.0	8	22	2.71	-	-	-	146.8

Arezoumandi&Volz_2013

15

Arezoumandi_20

Appendix B

CH-S-8-1	-	0	0.40	305	457	1200	3.25	33.7	19	3109.0	8	22	2.71	10	178	0.262	432.0	367.8
CH-S-8-2	-	0	0.40	305	457	1200	3.25	33.7	19	3109.0	8	22	2.71	10	178	0.262	432.0	352.5
CL-S-8-1	-	0	0.40	305	457	1200	3.25	28.3	19	3109.0	8	22	2.71	10	178	0.262	432.0	299.8
CL-S-8-2	-	0	0.40	305	457	1200	3.25	25.8	19	3109.0	8	22	2.71	10	178	0.262	432.0	319.8
CL-S-8-1	-	0	0.40	305	457	1200	3.25	28.3	19	3109.0	8	22	2.71	10	178	0.262	432.0	299.8
CL-S-8-2	-	0	0.40	305	457	1200	3.25	25.8	19	3109.0	8	22	2.71	10	178	0.262	432.0	319.8
C-NS-5-1	-	0	0.40	305	457	1200	3.06	33.6	19	1943.1	5	22	1.59	-	-	-	-	139.0
C-NS-5-2	-	0	0.40	305	457	1200	3.06	31.2	19	1943.1	5	22	1.59	-	-	-	-	138.4
C-NS-6-1	-	0	0.40	305	457	1200	3.25	33.6	19	2331.7	6	22	2.03	-	-	-	-	174.3
C-NS-6-2	-	0	0.40	305	457	1200	3.25	31.2	19	2331.7	6	22	2.03	-	-	-	-	144.2
C-NS-8-1	-	0	0.40	305	457	1200	3.25	33.6	19	3109.0	8	22	2.71	-	-	-	-	219.9
C-NS-8-2	-	0	0.40	305	457	1200	3.25	31.2	19	3109.0	8	22	2.71	-	-	-	-	147.0
C-NS-10-1	-	0	0.40	305	457	1200	3.28	49.2	19	5064.5	10	25	4.50	-	-	-	-	313.9
C-NS-10-2	-	0	0.40	305	457	1200	3.28	49.2	19	5064.5	10	25	4.50	-	-	-	-	212.4
C-NS-10-3	-	0	0.40	305	457	1200	3.28	49.2	19	5064.5	10	25	4.50	-	-	-	-	226.8
C-S-8-7-1	-	0	0.40	305	457	1200	3.25	33.7	19	3039.5	8	22	2.71	10	178	0.262	432.0	342.4
C-S-8-7-2	-	0	0.40	305	457	1200	3.25	33.7	19	3106.2	8	22	2.71	10	178	0.262	432.0	368.1
C-S-8-7-3	-	0	0.40	305	457	1200	3.25	33.7	19	3106.2	8	22	2.71	10	178	0.262	432.0	352.9
C-S-10-7-1	-	0	0.40	305	457	1200	3.28	48.5	19	5064.5	10	25	4.50	10	178	0.262	467.1	416.5
C-S-10-7-2	-	0	0.40	305	457	1200	3.28	48.5	19	5064.5	10	25	4.50	10	178	0.262	467.1	442.9
C-S-10-7-3	-	0	0.40	305	457	1200	3.28	48.5	19	5064.5	10	25	4.50	10	178	0.262	467.1	444.0
C-S-10-5-1	-	0	0.40	305	457	1200	3.28	37.6	19	5064.5	10	25	4.50	10	127	0.368	467.1	491.1
C-S-10-5-2	-	0	0.40	305	457	1200	3.28	37.6	19	5064.5	10	25	4.50	10	127	0.368	467.1	461.6
C-S-10-5-3	-	0	0.40	305	457	1200	3.28	37.6	19	5064.5	10	25	4.50	10	127	0.368	467.1	427.1
F-NS-5-1	C	70	0.40	305	457	1200	3.06	21.5	19	1943.1	5	22	1.59	-	-	-	-	128.6
F-NS-5-2	C	70	0.40	305	457	1200	3.06	21.1	19	1943.1	5	22	1.59	-	-	-	-	114.9
F-NS-6-1	C	70	0.40	305	457	1200	3.25	21.5	19	2331.7	6	22	2.03	-	-	-	-	131.9
F-NS-6-2	C	70	0.40	305	457	1200	3.25	21.1	19	2331.7	6	22	2.03	-	-	-	-	121.5
F-NS-8-1	C	70	0.40	305	457	1200	3.25	21.5	19	3109.0	8	22	2.71	-	-	-	-	170.9
F-NS-8-2	C	70	0.40	305	457	1200	3.25	21.1	19	3109.0	8	22	2.71	-	-	-	-	162.9
F-NS-10-1	C	70	0.40	305	457	1200	3.28	28.2	19	5064.5	10	25	4.50	-	-	-	-	125.0
F-NS-10-2	C	70	0.40	305	457	1200	3.28	28.2	19	5064.5	10	25	4.50	-	-	-	-	234.5
F-NS-10-3	C	70	0.40	305	457	1200	3.28	28.2	19	5064.5	10	25	4.50	-	-	-	-	199.8
F-S-8-7-1	C	70	0.40	305	457	1200	3.25	23.8	19	3106.2	8	22	2.71	10	178	0.262	432.0	298.2
F-S-8-7-2	C	70	0.40	305	457	1200	3.25	23.8	19	3106.2	8	22	2.71	10	178	0.262	432.0	328.6
F-S-8-7-3	C	70	0.40	305	457	1200	3.25	23.8	19	3106.2	8	22	2.71	10	178	0.262	432.0	332.8
F-S-10-7-1	C	70	0.40	305	457	1200	3.28	17.7	19	5064.5	10	25	4.50	10	178	0.262	467.1	278.3

Ortega_2012

Appendix B

F-S-10-7-2	C	70	0.40	305	457	1200	3.28	17.7	19	5064.5	10	25	4.50	10	178	0.262	467.1	329.2
F-S-10-7-3	C	70	0.40	305	457	1200	3.28	17.7	19	5064.5	10	25	4.50	10	178	0.262	467.1	299.4
F-S-10-5-1	C	70	0.40	305	457	1200	3.28	31.7	19	5064.5	10	25	4.50	10	127	0.368	467.1	444.1
F-S-10-5-2	C	70	0.40	305	457	1200	3.28	31.7	19	5064.5	10	25	4.50	10	127	0.368	467.1	415.8
F-S-10-5-3	C	70	0.40	305	457	1200	3.28	31.7	19	5064.5	10	25	4.50	10	127	0.368	467.1	370.2
C-NS-5-1	-	0	0.40	305	457	1200	3.06	33.6	19	1943.1	5	22	1.59	-	-	-	-	139.0
C-NS-6-1	-	0	0.40	305	457	1200	3.25	33.6	19	2331.7	6	22	2.03	-	-	-	-	174.3
C-NS-8-1	-	0	0.40	305	457	1200	3.25	33.6	19	3109.0	8	22	2.71	-	-	-	-	219.9
CH-NS-5-1	-	0	0.40	305	457	1200	3.06	33.6	19	1943.1	5	22	1.59	-	-	-	-	140.6
CH-NS-5-2	-	0	0.40	305	457	1200	3.06	31.2	19	1943.1	5	22	1.59	-	-	-	-	138.1
CH-NS-6-1	-	0	0.40	305	457	1200	3.25	33.6	19	2331.7	6	22	2.03	-	-	-	-	174.1
CH-NS-6-2	-	0	0.40	305	457	1200	3.25	31.2	19	2331.7	6	22	2.03	-	-	-	-	143.9
CH-NS-8-1	-	0	0.40	305	457	1200	3.25	33.6	19	3109.0	8	22	2.71	-	-	-	-	219.5
CH-NS-8-2	-	0	0.40	305	457	1200	3.25	31.2	19	3109.0	8	22	2.71	-	-	-	-	146.8
C-S-8-7-2	-	0	0.40	305	457	1200	3.25	33.7	19	3106.2	8	22	2.71	10	178	0.262	432.0	368.1
C-S-8-7-3	-	0	0.40	305	457	1200	3.25	33.7	19	3106.2	8	22	2.71	10	178	0.262	432.0	352.9
SCC50_NS-5-1	C	50	0.35	305	457	1220	3.11	44.6	19	1899.7	5	22	1.69	-	-	-	-	149.2
SCC50_NS-6-1	C	50	0.35	305	457	1220	3.30	44.6	19	2279.6	6	22	2.03	-	-	-	-	143.8
SCC50_NS-8-1	C	50	0.35	305	457	1220	3.30	44.6	19	3039.5	8	22	2.71	-	-	-	-	144.0
SCC50_S-8-1	C	50	0.35	305	457	1220	3.30	44.6	19	3039.5	8	22	2.71	10	178	0.262	324.0	330.5
SCC60_NS-5-1	C	60	0.34	305	457	1220	3.11	38.3	19	1899.7	5	22	1.69	-	-	-	-	142.5
SCC60_NS-6-1	C	60	0.34	305	457	1220	3.30	38.3	19	2279.6	6	22	2.03	-	-	-	-	175.7
SCC60_NS-8-1	C	60	0.34	305	457	1220	3.30	38.3	19	3039.5	8	22	2.71	-	-	-	-	150.6
SCC60_S-8-1	C	60	0.34	305	457	1220	3.30	38.3	19	3039.5	8	22	2.71	10	178	0.262	324.0	327.3
SCC70_NS-5-1	C	70	0.33	305	457	1220	3.11	44.1	19	1899.7	5	22	1.69	-	-	-	-	146.6
SCC70_NS-6-1	C	70	0.35	305	457	1220	3.30	44.1	19	2279.6	6	22	2.03	-	-	-	-	162.2
SCC70_NS-8-1	C	70	0.35	305	457	1220	3.30	44.1	19	3039.5	8	22	2.71	-	-	-	-	154.7
SCC70_S-8-1	C	70	0.35	305	457	1220	3.30	44.1	19	3039.5	8	22	2.71	10	178	0.262	324.0	354.1

Hyder_2017

Appendix B

<i>Lisitone_2017</i>																		
C-NS-12-1	-	0	0.62	150	260	750	3.29	20.4	20	339.1	3	12	0.99	-	65.1			
C-NS-12-2	-	0	0.62	150	260	750	3.29	20.4	20	339.1	3	12	0.99	-	74.9			
F50-NS-12-1	F	50	0.62	150	260	750	3.29	15.3	20	339.1	3	12	0.99	-	58.1			
F50-NS-12-2	F	50	0.62	150	260	750	3.29	15.3	20	339.1	3	12	0.99	-	56.4			
F60-NS-12-1	F	60	0.62	150	260	750	3.29	13.8	20	339.1	3	12	0.99	-	55.3			
F60-NS-12-2	F	60	0.62	150	260	750	3.29	13.8	20	339.1	3	12	0.99	-	42.5			
F70-NS-12-1	F	70	0.62	150	260	750	3.29	11.7	20	339.1	3	12	0.99	-	38.2			
F70-NS-12-2	F	70	0.62	150	260	750	3.29	11.7	20	339.1	3	12	0.99	-	45.6			
<i>Rao_2011</i>																		
C-NS-8	-	0	0.32	100	200	450	2.57	54.8	20	100.5	2	8	0.58	-	46.0			
C-NS-8+10	-	0	0.32	100	200	450	2.57	54.8	20	178.5	2+1	8+10	1.00	-	72.0			
C-NS-10+16	-	0	0.32	100	200	450	2.62	54.8	20	360.0	2+1	10+16	2.00	-	79.0			
C-NS-16+20	-	0	0.32	100	200	450	2.65	54.8	20	510.0	1+1	16+20	2.94	-	82.0			
F-NS-8	F	50	0.32	100	200	450	2.57	40.6	20	100.5	2	8	0.58	-	39.0			
F-NS-8+10	F	50	0.32	100	200	450	2.57	40.6	20	178.5	2+1	8+10	1.00	-	55.0			
F-NS-10+16	F	50	0.32	100	200	450	2.62	40.6	20	360.0	2+1	10+16	2.00	-	65.0			
F-NS-16+20	F	50	0.32	100	200	450	2.65	40.6	20	510.0	1+1	16+20	2.94	-	70.0			
<i>Drags_2018</i>																		
C-NS-5	-	0	0.62	200	300	1000	4.16	32.9	16	1900.0	5	22	3.95	-	114.1			
C-S-5-20	-	0	0.62	200	300	1000	4.16	35.0	16	1900.0	5	22	3.95	6	200	0.141	362	322.2
C-S-5-10	-	0	0.62	200	300	1000	4.16	40.4	16	1900.0	5	22	3.95	6	100	0.283	362	387.4
F50-NS-5	F	50	0.49	200	300	1000	4.16	24.9	16	1900.0	5	22	3.95	-	0	-	0	108.8
F50-S-5-20	F	50	0.48	200	300	1000	4.16	32.7	16	1900.0	5	22	3.95	6	200	0.141	362	350.5
F50-S-5-10	F	50	0.49	200	300	1000	4.16	31.4	16	1900.0	5	22	3.95	6	100	0.283	362	377.1

CURRICULUM VITAE

Jelena Dragaš was born on 14 May, 1986, in Belgrade, Serbia, where she completed her elementary and high school. She graduated at the University of Belgrade, Faculty of Civil Engineering obtaining the BSc. Degree in 2009 (average grade 9.35/10) and the MSc. Degree in 2010 (average grade 10.0/10) in the field of steel structures. She enrolled in the PhD programme at the same Faculty in 2010.

From 2010 to 2013, Ms. Dragaš worked as a civil engineer in a Belgrade-based steel construction company, working on the design and construction of numerous steel structures. Since 2013, she worked as a teaching assistant at the Faculty of Civil Engineering in Belgrade, participating in several courses in the field of concrete structures. Ms. Dragaš helped with the supervision of over twenty bachelor theses of students at the Department of Materials and Structures. She was one of the co-authors of the textbook for students enrolled in the Concrete Bridges course. Her research and study fields are concrete structures and new sustainable concrete materials with the main focus in the research of high volume fly ash concrete, alkali activated fly ash concrete and recycled aggregate concrete structures. Ms. Dragaš is a participant in the project TR 36017 (2014–2018), funded by the Serbian Ministry of Education, Science and Technological Development. She also participated in several international projects: Initiation of International Cooperation with Ruhr University Bochum and Ss. Cyril and Mehtodius University in Skopje (2018); Bilateral cooperation project 451-03-1924/2016-09/3 (2018–2019) with University of Lisbon; Multilateral project DS-2016-0060 (2017–2018) with Brno University of Technology and Technical University Vienna; COST Action TU 1301 (2014–2017) and SCOPES project (2013–2016) with ETH Zürich.

Ms. Dragaš has authored and co-authored over twenty scientific papers and book sections published in international and national journals and conferences, five of which were papers in journals listed in JCR. She is a member of the Association of Structural Engineers of Serbia. As a part of her professional work, she participated in the preparation of conceptual and major projects for different objects. She is fluent in written and spoken English.

Изјава о ауторству

Име и презиме аутора _____ Јелена Драгаш _____

Број индекса _____ 903/10 _____

Изјављујем

да је докторска дисертација под насловом

Гранична носивост армиранобетонских гредних носача од бетона са великим
садржајем летећег пепела

- резултат сопственог истраживачког рада;
- да дисертација у целини ни у деловима није била предложена за стицање друге дипломе према студијским програмима других високошколских установа;
- да су резултати коректно наведени и
- да нисам кршио/ла ауторска права и користио/ла интелектуалну својину других лица.

Потпис аутора

У Београду, 25.06.2018

Изјава о истоветности штампане и електронске верзије докторског рада

Име и презиме аутора Јелена Драгаш

Број индекса 903/10

Студијски програм Грађевинарство

Наслов рада Гранична носивост армиранобетонских гредних носача од бетона са
великим садржајем летећег пепела

Ментор Проф. др Снежана Маринковић

Изјављујем да је штампана верзија мог докторског рада истоветна електронској верзији коју сам предао/ла ради похрањена у **Дигиталном репозиторијуму Универзитета у Београду**.

Дозвољавам да се објаве моји лични подаци везани за добијање академског назива доктора наука, као што су име и презиме, година и место рођења и датум одбране рада.

Ови лични подаци могу се објавити на мрежним страницама дигиталне библиотеке, у електронском каталогу и у публикацијама Универзитета у Београду.

Потпис аутора

У Београду, 25.06.2018

Изјава о коришћењу

Овлашћујем Универзитетску библиотеку „Светозар Марковић“ да у Дигитални репозиторијум Универзитета у Београду унесе моју докторску дисертацију под насловом:

Гранична носивост армиранобетонских гредних носача од бетона са великим

садржајем летећег пепела

која је моје ауторско дело.

Дисертацију са свим прилозима предао/ла сам у електронском формату погодном за трајно архивирање.

Моју докторску дисертацију похрањену у Дигиталном репозиторијуму Универзитета у Београду и доступну у отвореном приступу могу да користе сви који поштују одредбе садржане у одабраном типу лиценце Креативне заједнице (Creative Commons) за коју сам се одлучио/ла.

1. Ауторство (CC BY)

2. Ауторство – некомерцијално (CC BY-NC)

3. Ауторство – некомерцијално – без прерада (CC BY-NC-ND)

4. Ауторство – некомерцијално – делити под истим условима (CC BY-NC-SA)

5. Ауторство – без прерада (CC BY-ND)

6. Ауторство – делити под истим условима (CC BY-SA)

(Молимо да заокружите само једну од шест понуђених лиценци.
Кратак опис лиценци је саставни део ове изјаве).

Потпис аутора

У Београду, 25.06.2018

1. **Ауторство.** Дозвољаваате умножавање, дистрибуцију и јавно саопштавање дела, и прераде, ако се наведе име аутора на начин одређен од стране аутора или даваоца лиценце, чак и у комерцијалне сврхе. Ово је најслободнија од свих лиценци.

2. **Ауторство – некомерцијално.** Дозвољаваате умножавање, дистрибуцију и јавно саопштавање дела, и прераде, ако се наведе име аутора на начин одређен од стране аутора или даваоца лиценце. Ова лиценца не дозвољава комерцијалну употребу дела.

3. **Ауторство – некомерцијално – без прерада.** Дозвољаваате умножавање, дистрибуцију и јавно саопштавање дела, без промена, преобликовања или употребе дела у свом делу, ако се наведе име аутора на начин одређен од стране аутора или даваоца лиценце. Ова лиценца не дозвољава комерцијалну употребу дела. У односу на све остале лиценце, овом лиценцом се ограничава највећи обим права коришћења дела.

4. **Ауторство – некомерцијално – делити под истим условима.** Дозвољаваате умножавање, дистрибуцију и јавно саопштавање дела, и прераде, ако се наведе име аутора на начин одређен од стране аутора или даваоца лиценце и ако се прерада дистрибуира под истом или сличном лиценцом. Ова лиценца не дозвољава комерцијалну употребу дела и прерада.

5. **Ауторство – без прерада.** Дозвољаваате умножавање, дистрибуцију и јавно саопштавање дела, без промена, преобликовања или употребе дела у свом делу, ако се наведе име аутора на начин одређен од стране аутора или даваоца лиценце. Ова лиценца дозвољава комерцијалну употребу дела.

6. **Ауторство – делити под истим условима.** Дозвољаваате умножавање, дистрибуцију и јавно саопштавање дела, и прераде, ако се наведе име аутора на начин одређен од стране аутора или даваоца лиценце и ако се прерада дистрибуира под истом или сличном лиценцом. Ова лиценца дозвољава комерцијалну употребу дела и прерада. Слична је софтверским лиценцама, односно лиценцама отвореног кода.